Investigations towards the Development and Biological Evaluation of Activity-based Protein Profiling (ABPP) of Flavin-dependent Oxidases

D I S S E R T A T I O N

zur Erlangung des akademischen Grades

DOCTOR RERUM NATURALIUM

(Dr. rer. nat.)

an der Technischen Universität Graz

vorgelegt

von **M. Sc. Joanna Maria Krysiak**

Angenommen aufgrund der Gutachten von:

Prof. Dipl.-Ing. Dr.rer.nat. R. Breinbauer

Prof. Mag. Dr.rer.nat. K. Gruber

Graz, 5th October 2012

EIDESSTATTLICHE ERKLÄRUNG

Ich erkläre an Eides statt, dass ich die vorliegende Arbeit selbstständig verfasst, andere als die angegebenen Quellen/Hilfsmittel nicht benutzt, und die den benutzten Quellen wörtlich und inhaltlich entnommene Stellen als solche kenntlich gemacht habe.

Graz, am ……………………………   …………………………………………………..
                                                                                    (Unterschrift)

Englische Fassung:

STATUTORY DECLARATION

I declare that I have authored this thesis independently, that I have not used other than the declared sources / resources, and that I have explicitly marked all material which has been quoted either literally or by content from the used sources.

……………………………   …………………………………………………..
          date   (signature)

To my family

Acknowledgments

First of all, I would like to thank Prof. Rolf Breinbauer for giving me the opportunity to work in his research group on such a fascinating project. I am enormously grateful for his belief in me and my abilities to cope with this highly interdisciplinary project. I also want to thank for his persistent support, countless new ideas, insightful advices and discussions throughout these all years as well as for providing the right mixture of enthusiastic motivation, scientific freedom and constructive criticism. Thank you Rolf!

I would like to express my gratitude to Prof. Karl Gruber for undertaking the role of the referee of this work and for the insightful evaluation of my thesis.

I would like to thank all the members of our research group: Jakov Ivkovic, Mario Leypold, Nicole Mayer, Martin Peters, Jakob Pletz, Jana Rentner, Hilmar Schroeder, Melanie Trobe, Xuepu Yu for the great atmosphere in the group and for help and support not only with the scientific issues. Especially, I would like to acknowledge Hilmar for his excellent scientific and technical assistance at the beginning of my PhD and for being a great labmate. I am also thankful to Jakov, who in a very short time became not only a supportive and helpful colleague, but also a good friend and a companion of countless coffee breaks. Moreover, I would like to thank my students Nathaniel Miska and Lukas Schafzahl for their help and enthusiasm during the work on the synthesis of new tool compounds. Lastly, I would like to thank all other students who worked at our group for creating an unforgettable atmosphere.

I am very thankful to Prof. Peter Macheroux and Prof. Albin Hermetter for valuable advices and support in designing and performing various biochemical experiments as well as for the possibility to work on a constant basis in their labs and use their equipment at the Institute of Biochemistry. I am also grateful to all members of their research groups for enormous help and patience in explaining me the complex world of biochemistry. Particularly, I would like to thank Venugopal Gudipati, Alexandra Binter, Karin Koch, Wolf-Dieter Lienhart, Bastian Daniel, Ute Stemmer, Bojana Stojcic and Lingaraju Marlingapla Halasiddappa for their great support and atmosphere at work. Thank you guys!

"Nothing in life is to be feared, it is only to be understood"

Maria Skłodowska-Curie

Physicist, double winner of the Nobel Prize, 1867-1934

Abstract

In recent years activity-based protein profiling (ABPP) has become a powerful chemoproteomic technology allowing the dissection of complex ligand-protein interactions in their native cellular environment and has enabled the identification and functional characterization of proteins involved in many physiological and pathological processes. However, one of the biggest challenges for ABPP is the extension of the proteome coverage.

In this thesis, the development and biological evaluation of a new ABPP strategy dedicated to monoamine oxidases (MAO) is presented. These enzymes are representative examples of flavin-dependent oxidases, playing a crucial role in the regulation of nervous system signaling. The methodology involves a 'tag-free' approach for *in situ* enzyme labeling within intact cells. Subsequent cell lysis followed by click chemistry resulted in the attachment of the fluorescent tag, which visualizes enzyme activities by gel electrophoresis and fluorescence scanning. LC-MS analysis and Western Blotting reveal finally the identity of target enzymes.

A small set of activity-based probes inspired by the structure of known irreversible MAO inhibitors along with biocompatible fluorescent tags were synthesized. The potential of the designed ABPP strategy was then examined using recombinant monoamine oxidases with respect to the scope of probes collection, selectivity and sensitivity of labeling as well as binding site of a probe to the enzyme. It could be shown that several probes efficiently labeled both isoforms of monoamine oxidase in a specific manner. These results stimulated further evaluation of the efficiency of the best probes in profiling MAO activity in far more complex biological samples (mouse tissues, human brain tumor cells). In addition, the protein target profile of the probes, including other flavin-dependent enzymes, was examined.

The results of this ABPP study revealed an outstanding selectivity of the probe molecules towards monoamine oxidases that is triggered by a unique labeling mechanism and that the covalently binding inhibitors pargyline and deprenyl act very cleanly with MAO A and B but with no other protein targets. Taken together, this work successfully demonstrates the first example of activity-based probes targeting a flavin-dependent oxidase.

Zusammenfassung

Activity-based protein profiling (ABPP) hat sich als nützliche chemische Proteommethode zur Analyse komplexer Ligand-Protein-Wechselwirkungen in nativer zellulärer Umgebung etabliert, mit der eine Identifikation und funktionelle Charakterisierung vieler in physiologischen und pathologischen Prozessen beteiligter Proteine gelang. Eine wichtige Herausforderung des ABPP ist jedoch die Abdeckung eines breiteren Proteombereichs.

In dieser Dissertation wird die Entwicklung und biologische Validierung einer neuen ABPP-Strategie für Monoaminooxidasen (MAO) präsentiert. Diese repräsentativen Flavin-abhängigen Oxidasen sind maßgeblich an der Regulation der Signaltransduktion im zentralen Nervensystem beteiligt. Es wurde ein markierungsfreier Ansatz für die *in situ* Enzymmarkierung in lebenden Zellen verwendet. Die anschließende Zelllyse, gefolgt von Click-Chemie führte zur Anheftung des Fluoreszenzmarkers, der die Visualisierung von Enzymaktivitäten mittels Gelelektrophorese und Fluoreszenz-Scanning ermöglichte. Die markierten Enzyme wurden dann mittels LC-MS Analyse und Western Blotting identifiziert.

Eine Gruppe neuer Aktivitätssonden auf Basis der bekannten irreversiblen MAO-Inhibitoren wurde zusammen mit bioorthogonalen Fluoreszenzmarkern synthetisiert. Dann wurde das Potential der ABPP-Strategie unter Verwendung rekombinanter Monoaminooxidasen hinsichtlich Sondenumfang, Selektivität und Sensitivität der Markierung, sowie die Art der Bindung untersucht. Die Experimente zeigten, dass einige Sonden effizient und spezifisch beide Isoformen der Monoaminooxidasen markierten. Dann wurde die Effizienz der besten Sonden in der Darstellung von MAO-Aktivität in komplexeren biologischen Proben (Mausgewebe, humane Hirntumorzellen) evaluiert. Außerdem wurde das Targetprofil der Sondenmoleküle einschließlich anderer Flavin-abhängiger Enzyme untersucht.

Die Ergebnisse zeigten eine hervorragende Selektivität der Sondenmoleküle gegenüber Monoaminooxidasen, bedingt durch den einzigartigen Markierungsmechanismus, und dass die kovalent bindenden Inhibitoren Pargylin und Deprenyl ausschließlich mit MAO A und B,

nicht aber mit anderen Zielproteinen reagieren. Zusammenfassend wurden die ersten auf Flavin-abhängige Oxidasen gerichteten Aktivitäts-basierten Sonden präsentiert.

TABLE OF CONTENT

1 Introduction

One of the greatest challenges in the post-genomic era facing the life science researchers is deciphering and understanding the emerging features of the sequenced genomes at the molecular level. The number of proteins encoded by the human genome[1] may greatly exceed one million of distinct entities due to processes such as alternative gene splicing or posttranslational modifications, thereby making the elucidation of their biological role both a daunting and exciting endavour. Profound spatiotemporal and quantitative knowledge about enzymes activity, ranging from cell to whole organism, would contribute not only to deeper understanding of complex biochemical pathways but would also provide a most desired and powerful tool in identification of viable therapeutic targets across all diseases. Ultimately, a long and disease lacking life is the primary goal of each human being.

There are many methods to investigate protein functions, both genomic and proteomic. Genomic strategies including chromosomal translocation, gene amplification, transcriptional profiling as well as siRNA-based gene silencing delivered significant insights into the role of proteins involved in cancer[2-3] and other (patho)physiological processes.[4-6] However, genomic signatures inherently depend on profiling and the manipulation of gene expression and therefore do not capture the myriad of posttranslational modifications (PTMs) that essentially regulate protein activity. On the other hand, classical proteomic methods as two-dimensional gel electrophoresis coupled with LC-MS based platforms for shotgun analysis, yeast two-hybrid assays, or protein microarrays provide information about protein expression levels[7] and interaction maps[8] as well as about their biochemical properties *in vitro*[9] but are not insufficient in reporting about their functional state. Thus, more direct methods to study enzyme activity, which apparently is rarely a simple function of its abundance but is tightly regulated by substrate co-localization, expression of endogenous inhibitors, post-translational modifications or allosteric control (Figure 1), are required.

Chemical biology, an increasingly expanding field pioneered by Stuart Schreiber, Peter Schultz and Herbert Waldmann, can be defined as the application of the enabling chemistry

toolbox to shed light on complex biological processes.[10] In this context, the synthetic chemistry toolkit was essential to establish a new approach dubbed Activity-Based Protein Profiling (ABPP) to tackle the challenge of profiling proteins with regard to their activity. At the heart of this powerful chemoproteomic technology, pioneered in the late 90's by the groups of Cravatt[11] and Bogyo[12] are selective covalent interactions between an active enzyme and small chemical molecules. The power and scope of this rapidly evolving method is continuously studied in great detail by several research groups with the ultimate aim to, along with metabolomic, biochemical and pharmacology methods, unravel the function of many uncharacterized protein products of the genome and fill the gaps on the proteome map.
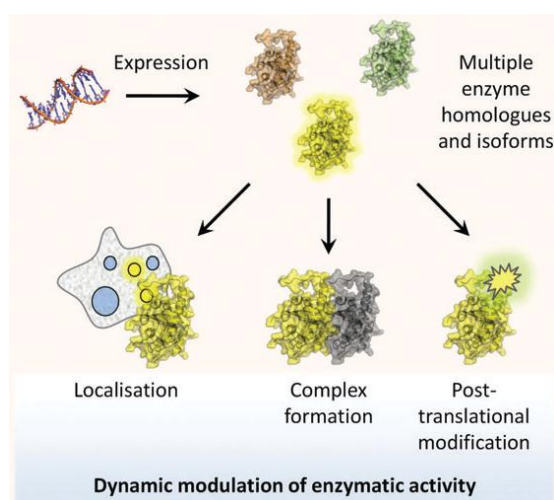
Figure 1. Complex regulation of enzyme activity *in vivo*. Picture taken from Ref. [13].

Also our research group undertook the encounter of developing new ABPP tools dedicated to flavin-dependent oxidases taking the advantage of expertise of two collaborating groups at the Institute of Biochemistry (Graz University of Technology): Prof. Macheroux's lab in the complex field of enzymology of flavoproteins as well as of Prof. Hermetter's group in the field of activity-based profiling of lipolytic enzymes.

This thesis deals mainly with the development and biological evaluation of novel activity-based probes designed for flavin-dependent oxidases, with a special focus on monoamine oxidases. Hence these two research topics are at heart of the theoretical background and the current state-of-the-art of ABPP and monoamine oxidase fields is discussed in detail.

2 State of the art

2.1 Activity-based Protein Profiling (ABPP)

2.1.1 Principles and aims of ABPP

Activity-based protein profiling (ABPP) has evolved in recent years into a mature chemoproteomic technology equipped with a sophisticated analytical and synthetic toolbox which allow the dissection of complex ligand-protein interactions in their native cellular environment.[13,14] The application of small molecule activity-based probes (ABPs) to interrogate enzyme activity on the cell level has led to the identification and functional characterization of proteins involved in cancer[15] and other severe human diseases, signaling pathways,[16] apoptosis,[17] microbial pathogenesis and virulence,[18] host-virus interactions[19] and many other physiological and pathological processes. Activity-based probes have been developed over the last decade for many enzyme classes, including serine hydrolases,[11,20] cysteine-[12,17] and threonine proteases,[21] glycosidases,[22] kinases,[16,23] phosphatases,[16,24] oxidoreductases[25] or transferases.[26] In recent years, as the ABPP field matured, there has been a significant expansion made from the relatively easy enzyme targets with well-established catalytic mechanisms and nucleophilic active-site residues participating in the formation of a covalent bond to activity-based probes toward enzymes that are intrinsically more demanding to address (less abundant or membrane-bound enzymes, enzymes without nucleophilic residues in their active site). However, the extension of the proteome coverage and introduction of new chemical probes to the ABPP toolbox is still a major challenge.

In a typical ABPP experiment, an activity-based probe is incubated with tissue or cell lysate *in vitro* or within living cells or animal *in vivo* to label a target enzyme or a group of mechanistically related enzymes. Subsequently, the labeled protein targets are separated, visualized or affinity-purified and identified *via* the appended reporter tag with an analysis system of choice: fluorescent SDS-PAGE, Western Blotting or LC-MS platforms. The ABPP workflow is schematically depicted in Figure 2.
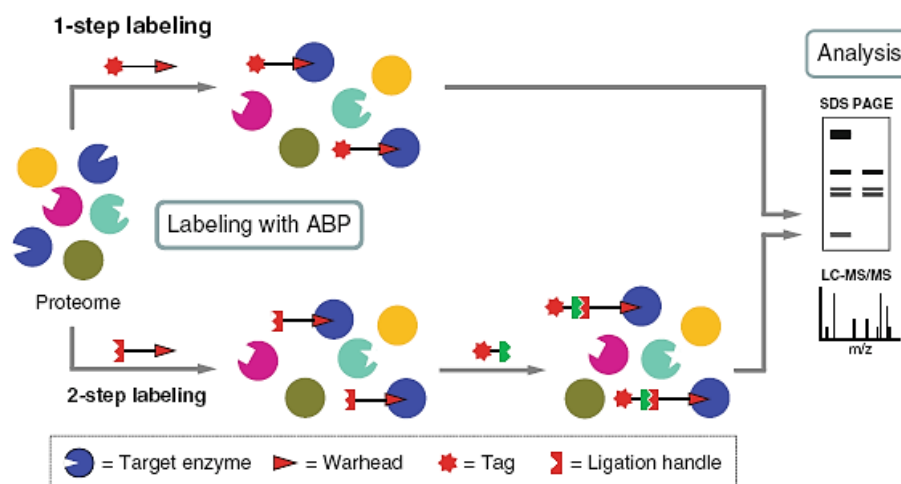
Figure 2. General outline of ABPP experiment workflow. Picture taken from Ref. [27].

Although the range of ABPP experimental setups is rapidly increasing, the main ABPP principle to profile enzyme activities remains very clear and simple and along with the rapid and straightforward readout methods make this technique so attractive and widely applicable not only in molecular and cellular biology but also in clinical research.

2.1.2 Activity-based probes

2.1.2.1 Key structural features

Activity-based probes (ABPs) utilize a wide range of chemical scaffolds (discussed further). However, all of them need to meet some specific requirements: First of all, an ABP should effectively form a stable covalent bond to the active site of a given enzyme or enzymes either by a direct alkylation of the specific nucleophilic residue at the catalytic site (e.g. Ser in serine hydrolases or Cys in cysteine proteases) or through enzymatic conversion of the ABP into a highly reactive intermediate (e.g. quinone methide) that can be nucleophically attacked by any proximal residue. Moreover, ABPs remain covalently linked to the active site of an enzyme, therby not only abolishing its catalytic activity in the same way as irreversible inhibitors but also conjugating it with the appropriate reporter tag. Further, ABPs should essentially target the active form of an enzyme, excluding the immature (zymogen) or inhibitor bound form. Finally, an ideal ABP would react with a large but managable number of

enzymes, which can be then distinguished from each other. The level of target promiscuity within the enzyme family must be however compensated by the limited cross-reactivity with other proteins.

Activity-based (ABP):   Peptide   Fluorophore
Electrophile   Clickable handle Biotin
Latent electrophile   PEG linker   Radioisotope
                              Cleavable

Affinity-based (A*f*BP):
Photocrosslinker
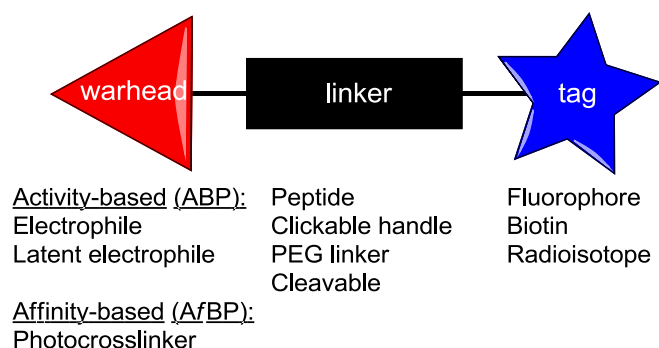
Figure 3. Schematic structural features of an activity-based probe.

The typical ABP (Figure 3) fulfilling all these requirements consists essentially of three structural elements: a reactive group (warhead) that covalently binds to the target enzyme, a reporter tag which allows the detection of the probe-bound enzyme and a linker (spacer) that stably connects these two elements together preventing the steric congestion as well as induce probe selectivity towards target proteins.

2.1.2.2 Activity vs. affinity

Depending on the mechanism by which the covalent connection between a protein and a warhead is formed, probes can be distinguished into: activity- (ABPs) and affinity-based probes (A*f*BP).[27] An activity-based probe achieves the labeling through a direct nucleophilic attack of the conserved active site residue on the electrophilic warhead of the probe. In contrast, the warhead of the affinity-based probe only guides the probe towards a specific site on a protein (not necessarily an active site) which is then followed by a non-specific covalent linkage event (Figure 4). In most cases, photochemical crosslinking of an aryl azide, benzophenone or aziridine moiety incorporated into the probe structure to any proximal amino acid residue upon UV iradiation establishes the stable link to an enzyme.
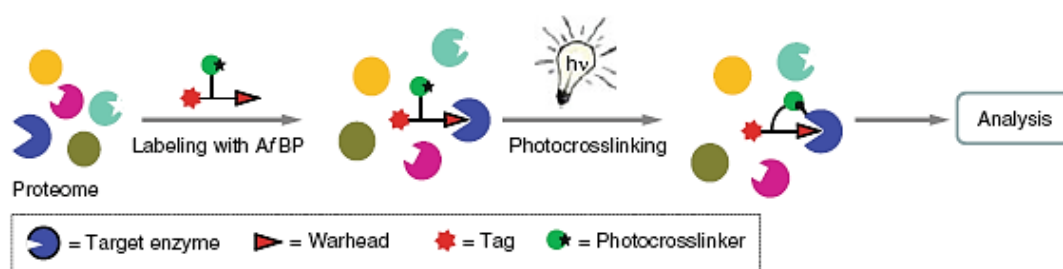
Figure 4. Photoaffinity labeling. Picture taken from Ref. [27].

Many affinity-based probes proved very useful to target enzymes that do not rely on a nucleophilic residue in their active site, which precludes the use of an electrophilic warhead, like metalloproteases,[28,29] histone deacetylases (HDACs)[30] (both of which employ a water molecule for their catalytic activity) or kinases.[31] For instance, the research group of Yao demonstrated recently the development of specific A*f*BPs towards Abelson tyrosine kinase (Abl) which is associated to cronic myelogenous leukemia (CML)[23c] as well as the application of photocrosslinker probes derived from potent kinase inhibitors such as staurosporine[23b] or Dasatinib[32] to identify their protein kinase targets in different cancer cell lines. Several prominent examples of such photocrosslinker probes are depicted in Figure 5.

Histone deacetylases (HDACs)

Kinases

Metalloproteases

P₁ a.a. = Leu, Ile, Val, Met, Phe, Gly, Thr, Lys, Glu
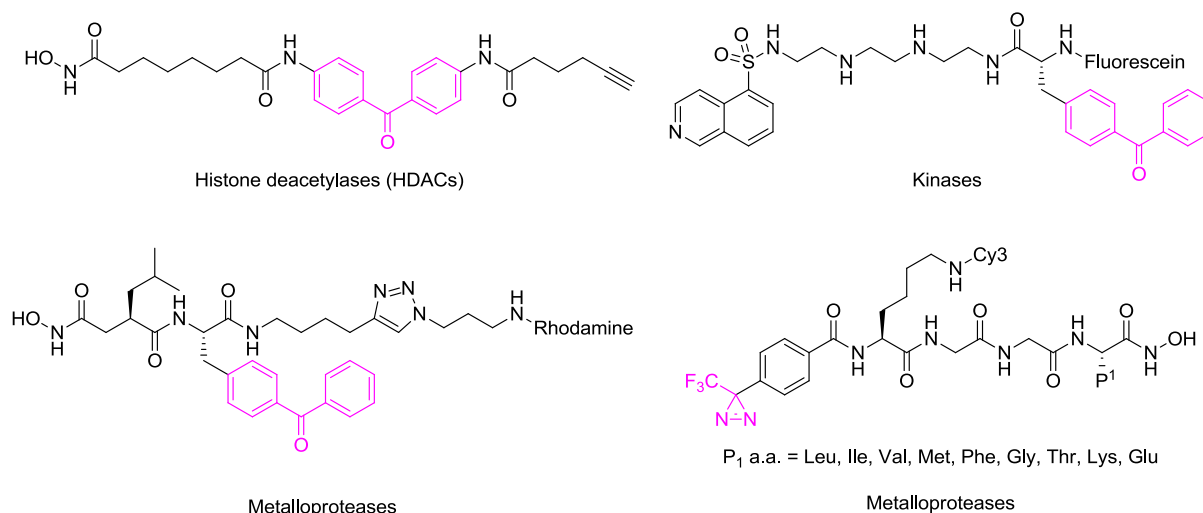
Metalloproteases

Figure 5. Photocrosslinker probes for histone deacetylases,[30] kinases,[31] and metalloproteases.[28,29] The photocrosslinking group is highlighted in purple.

2.1.2.3 Warheads

In the development of an activity-based probe the design of a warhead is the most crucial step which determines its reactivity and mechanism of action.

Many reactive groups are based on endogenous substrate mimics that are combined with an electrophilic trap which will covalently modify an essential nucleophilic residue in the enzyme active site. For instance, Cole and coworkers were able to selectively target diverse CoA acetyltransferases by incorporating the sulfoxycarbonyl CoA group into the probe (Figure 6 A) which mimicked a natural substrate acetyl CoA that is indispensable for the activity of those enzymes.[33] In another study, Zhang et al. prepared biotin- or rhodamine-derived probes (Figure 6 A) based on an α-bromobenzylphosphonate irreversible inactivator of protein tyrosine phosphatases (PTPs) that exclusively labeled those enzymes in cell lysates.[34] The structure of the inhibitory motif resembled very closely the phosphotyrosine ring that is present in the native substrate. A substrate mimicry approach was also used to target nitrilases[35] (Leu-Asp motif) and kinases[23d,36] (ATP mimetic).

Substrate scaffolds are also essential in another approach termed as substrate-directed ABPP or quinone (quinolimine) methide approach (Figure 6 B). In this strategy, substrate mimics (amino acid residue, peptide, sulfate, phosphate, sugar etc.) act as specificity regions which direct the ABP towards the enzyme active site. Following recognition of the substrate, the catalytic nucleophile cleaves the scissile bond in the probe (latent electrophile) in the proximity of the substrate scaffold inducing the facile rearrangement to a highly reactive electrophilic quinone methide which can react with an active site nucleophile resulting in the covalent attachment of the probe in a specific manner. The described approach was successfully applied to profile tyrosine phosphatases,[24a,37] glycosidases,[38] sulfatases,[39] and proteases.[40]
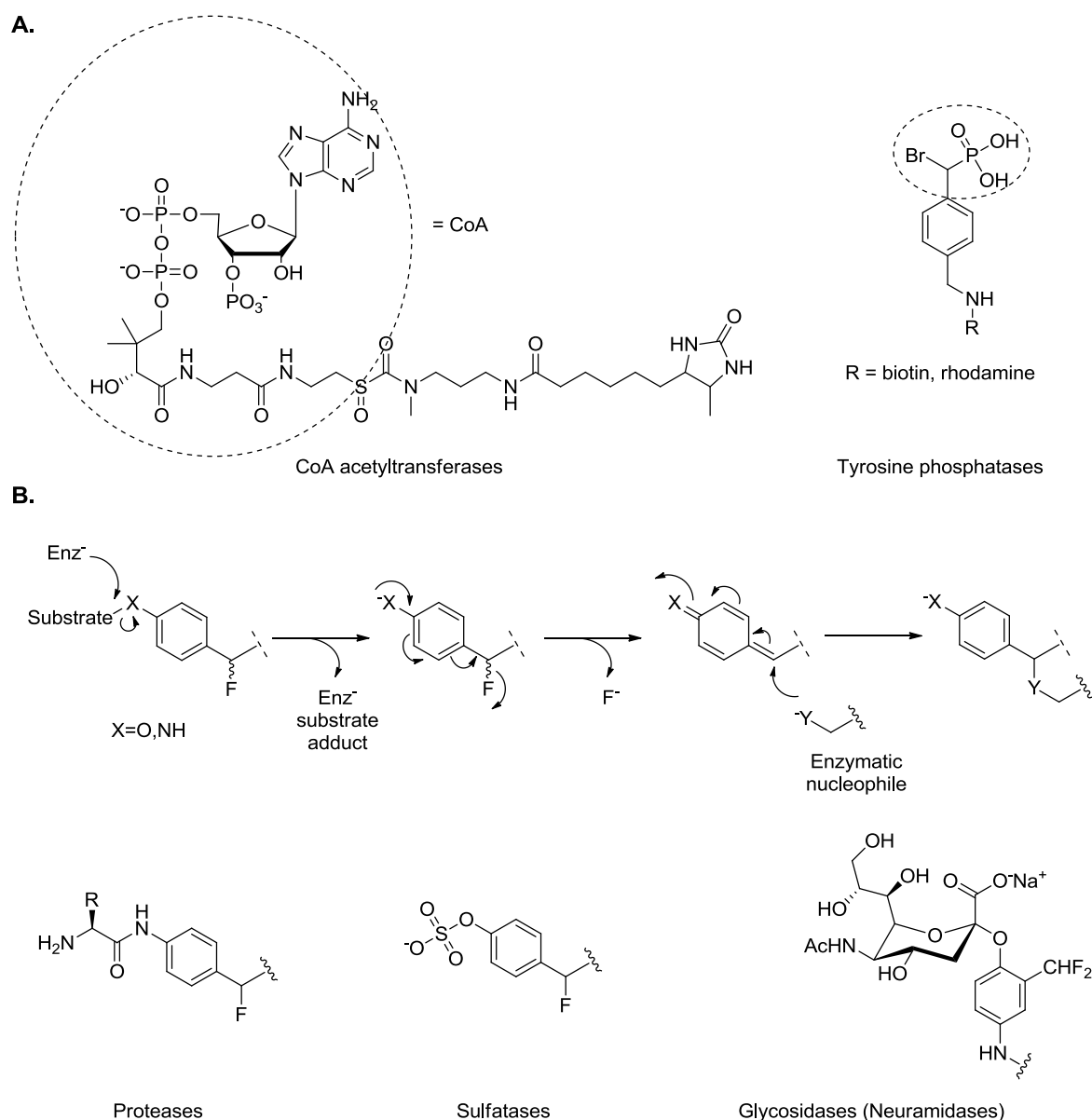
Figure 6. A. ABPs based on substrate mimicry approach. B. Quinone methide approach (top) and examples of reactive groups employed in substrate-based ABPP (bottom).

Another approach in ABP design is built on modification of irreversible mechanism-based enzyme inhibitors by introducing a reporter tag at a distant position to the inhibitory motif. The most prominent example of such ABPs are class-wide fluorophosphonate (FP) probes (Figure 7 A), introduced and diversified over the years by the Cravatt lab,[11,20a,20c] with the purpose to globally characterize the superfamily of serine hydrolases. Those powerful ABPs were based on simple fluorophosphonate reagents like diisopropyl fluorophosphate (DIFP) inhibitor (Figure 7 B), exploiting multiple conserved features of the serine hydrolase active site such as Ser-derived oxygen of increased nucleophilicity and an oxyanion hole that

stabilizes the enzyme-substrate tetrahedral intermediate, to achieve extraordinary specifity towards serine hydrolases and minimal cross-reactivity with other classes of hydrolases (cysteine-, aspartyl- or metalloproteases). The application of fluorophosphonate probes led to the identification of previously poorly characterized hydrolases such as KIAA1363,[41] monoacylglycerol lipase (MAGL),[42] or retinoblastoma-binding protein 9 (RBPP9),[43] which were found to be key players in regulating signaling of pro-tumorigenic ether lipids (monoalkylglycerol ethers MAGEs), controlling fatty acid pathways, or suppressing TGF-β-mediated antiproliferative sigaling in pancreatic carcinogenesis, respectively.

A.

FP-alkyl-biotin or **FP-alkyl-TAMRA**

R = Biotin, TAMRA

FP-PEG-biotin or **FP-PEG-TAMRA**

B.
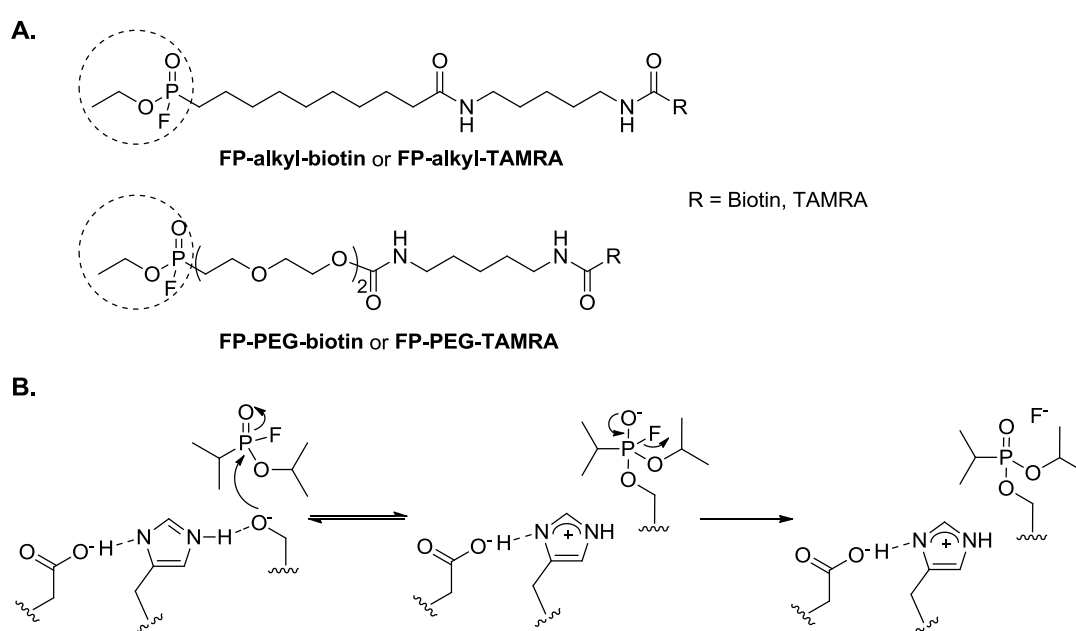
Figure 7. A. Fluorophosphonate probes (FP). The reactive group is designated in a dashed circle. B. Inactivation mechanism of a serine hydrolase by diisopropyl fluorophosphate (DIFP) inhibitor.

Other examples of mechanism-based ABPs are acyloxymethyl ketone (AOMK) probes for cysteine proteases (including caspases playing a crucial role in apoptosis) studied by the group of Bogyo,[17] 2-deoxy-2-fluoro glycoside probes for retaining exo- and endoglycosidases, reported by the groups of Bertozzi[44] and Withers[45], respectively or 2-ethynylnaphtalene (2EN) probes for cytochrome P450 enzymes developed by Cravatt and co-workers.[46] Also, the role of protein arginine deiminase 4 (PAD4), an enzyme implicated in rheumatoid arthritis was studied by the use of known haloacetamidine-based PAD4 inhibitors equipped with a rhodamine tag[47] (Figure 8).
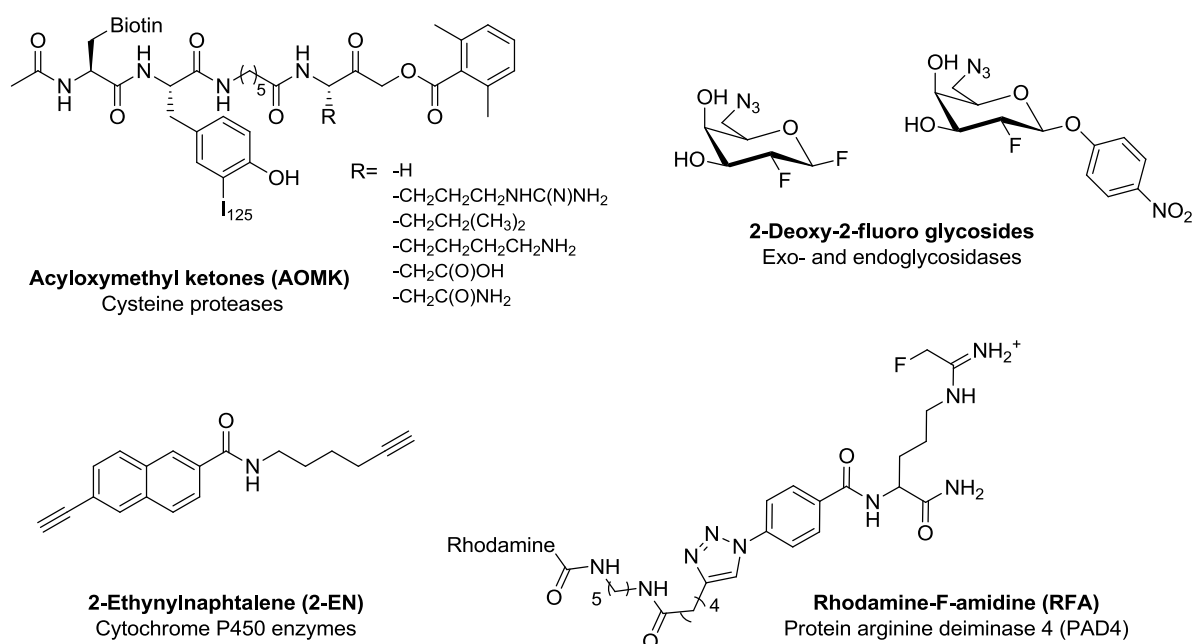
Figure 8. Mechanism-based ABPs.

Natural products are another group of privileged scaffolds in the ABP design due to their intrinsic reactivity towards protein targets resulting from their biosynthetic origin and biological purpose.[48-51] The variety of different electrophilic groups present in the natural products (Michael acceptors, epoxides, aziridines, cyclopropanes, β-lactones, β-lactams etc.), which form a stable covalent linkage with the target protein, along with complex core structure, modulate greatly their selectivity towards the corresponding cellular targets, which is of special interest in ABPP probe development. Several excellent overview articles about natural product-based ABPP probes have been recently published by the Sieber [52,53] as well as by our group.[54] However, it is worth to mention the most impressive examples of this approach.

Fungal metabolite E-64 containing an epoxysuccinyl motif was one of the first natural products equipped with an array of tags (biotin, radioisotope, BODIPY, clickable groups) to create an efficient probe for profiling the activity of cysteine proteases (especially cathepsins) in human tissues,[55] plants[56] and in infection model on macrophages with *Salmonella typhimurium*.[57] Syringolin A (α,β-unsaturated amide),[21b,58] lactacystin (bicyclic lactone)[59] and epoxomicin (epoxide)[21a] served as excellent scaffolds for ABPs to target specific subunits of the proteasome machinery, whereas a wortmannin-derived ABPP probe was

used to study cell signaling processes involving phosphoinositide 3-kinases (PI3K), PI3K related kinases (PIKK)[23f] and polo-like kinases (Plk 1 and 3).[23g] More recently, Sieber et al. showed the application of such natural products as vibralactone,[60] rugulactone[61] to investigate protein targets in pathogenic bacteria and duocarmycin SA[62] to study the role of aldehyde dehydrogenase 1 (ALDH1 A1) in cancer cells. Some examples of natural-product derived ABPP tools are collected in Figure 9.
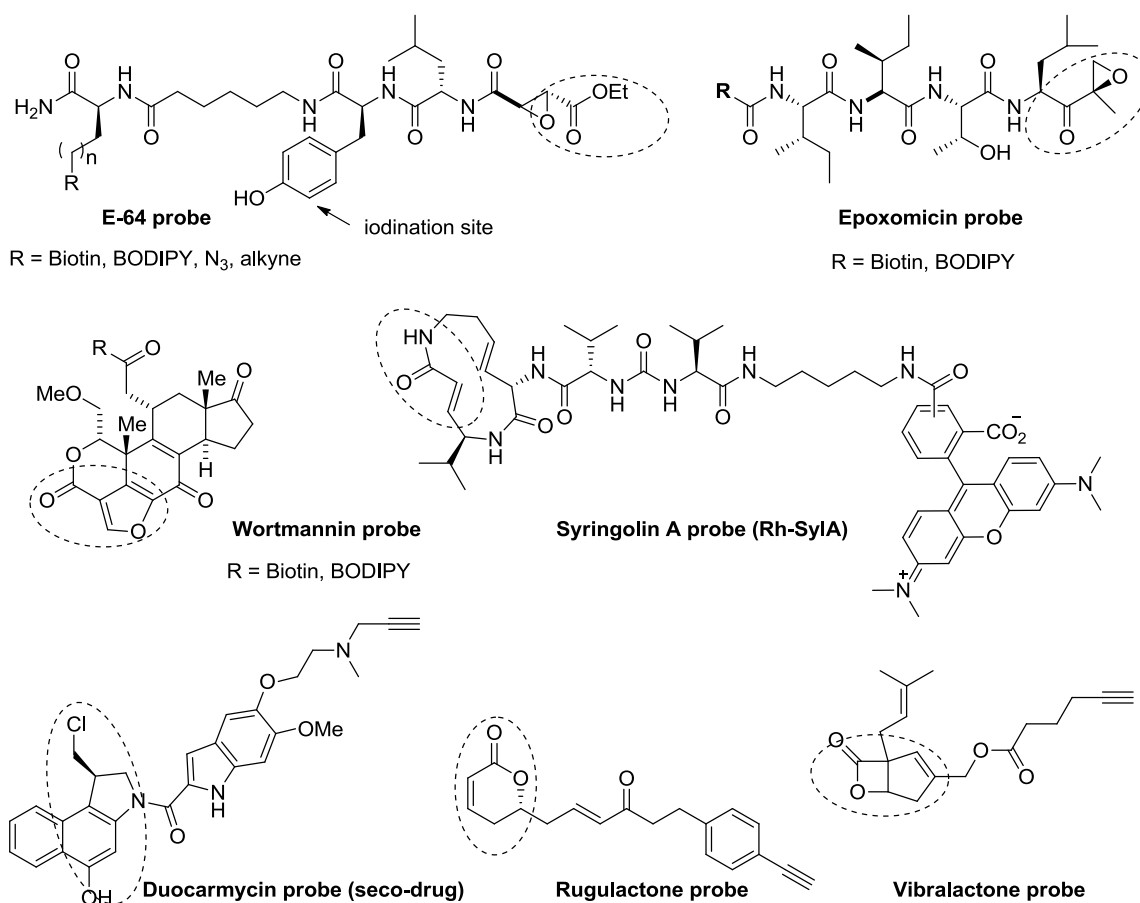
Figure 9. Natural products based ABPs. Reactive groups are indicated by a dashed circle.

The last group of chemical scaffolds used as wahrheads are general electrophiles such as vinyl sulfones, vinyl methyl esters or halomethylketones. Depending on the core structure to which such a general electrophilic group is appended, the selectivity toward particular protein targets can be fine-tuned. For instance, vinyl sulfones (VS) are known as excellent electrophiles modifying Cys containing enzymes. Attachment of the vinyl sulfone moiety to a peptide containing three leucines (Figure 10 A) modified by different tags resulted in a probe capable of profiling all subunits of the constitutive proteasome as well as the corresponding

immunoproteasome,[63] whereas tagging with ubiquitin (Ub) or ubiquitin-like (Ubl) peptide motifs (Figure 10 B) delivered probes to study ubiquitin conjugating machinery in cell lysates.[64]

A.

R = Dansyl, BODIPY, TAMRA, Cy3, Cy5   **R-Ahx₃L₃VS**

B.

R = Hemagglutinin

Ubiquitin-VS   **Ubiquitin-like-VS**
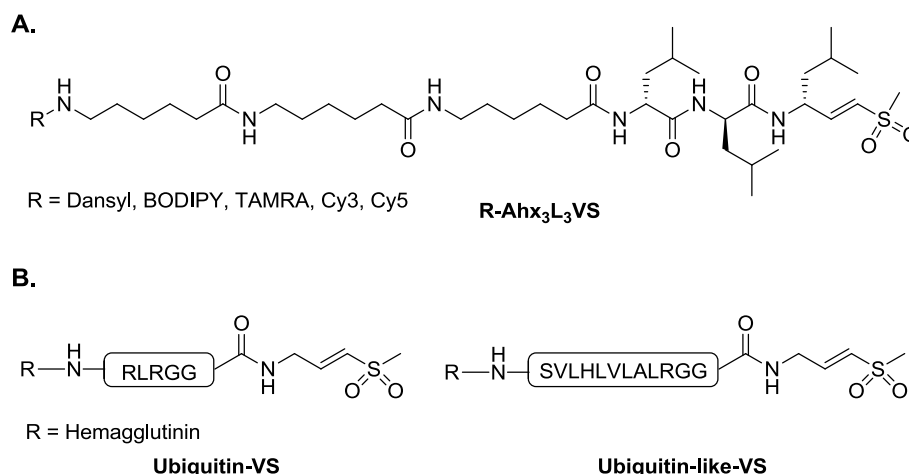
Figure 10. ABPs employing a vinyl sulfone warhead. A. Vinyl sulfone (R-Ahx₃L₃VS) for proteasome subunits. B. Vinyl sulfones for Ub- and Ubl-specific proteases (USPs).

With regard to the strategies for employing activity-based probes, one can distuinguish a *directed approach* in which ABPs incorporate well characterized and deliberately designed warheads (as presented above) to direct their reactivity towards enzymes sharing similar catalytic mechanisms or substrate selectivity. However, to extend application of ABPP to less predictable enzymes, also a *non-directed approach*[65] has been introduced, in which structurally diverse libraries of candidate probes bearing mild electrophilic groups (e.g. sulfonate esters) were screened against the proteomes for activity-dependent labeling events and allowed identification of some thiolases, NAD/NADP-dependent oxidoreductases, enoyl CoA hydratases or glutathione S-transferases.[26c]

2.1.2.4 Reporter tags used for ABPs

An efficient ABPP probe incorporates a reporter tag that provides the means to detect the targeted enzymes. Three major groups can be distinguished (Figure 11): fluorophores, (radio)isotopic labels, and affinity tags, used for visualization, detection and enrichment followed by purification of the ABP-bound proteins, respectively.[66] In many studies, the

reporter tags were incorporated into an ABP directly through a flexible linker region. However, the second approach dubbed tandem or 'tag-free' two-step labeling (Figure 2), employing a small surrogate tag, which enables the attachment of an analytical tag to a probe *via* highly specific bioorthogonal ligation chemistry methods, has recently been used more often due to the possibility of its application in *in vivo* studies.

A. Fluorophores

Fluorescein

R = H   Rhodamine
Me   TAMRA

NBD

Dansyl (DNS)

BODIPY

n = 1 Cy3
2 Cy5

B. Affinity tags

Biotin

Desthiobiotin

YPYDVPDYA—

Hemagglutinin

C. Isotope labels

^{125}I radiolabel (E-64 probe)

^{3}H label (Lactacystin probe)
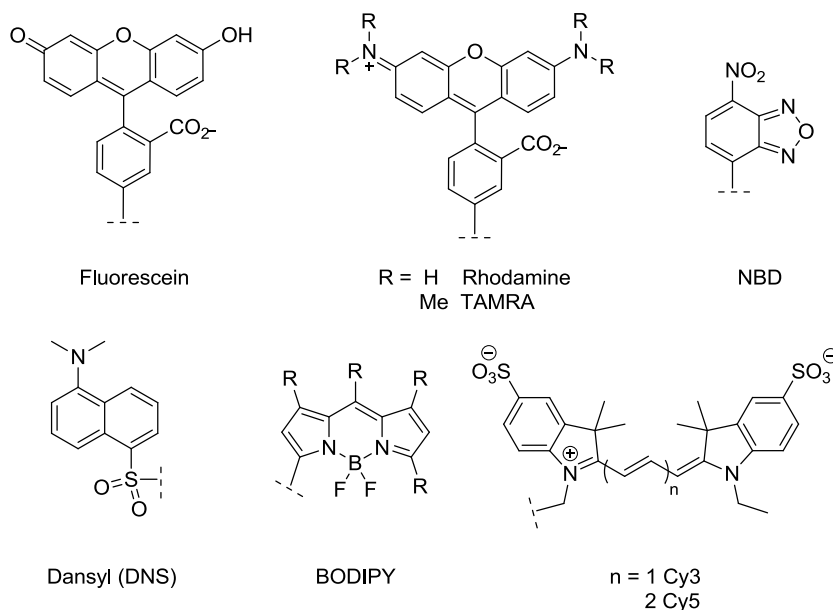
Figure 11. Reporter tags used in ABPP. A. Fluorophores. B. Affinity labels. C. Isotopes.

The most widely used tags are fluorophores due to the ease of their visualization by in-gel fluorescence scanning and their application in direct imaging of labeled protein targets by fluorescence microscopy. The most commonly applied fluorescent dyes in ABPP are fluorescein,[11,26b] rhodamine (Rh) and its tetramethyl- derivative (TAMRA), [18c,23g,34a] 4-chloro-

7-nitrobenzofurazan (NBD),[67] 5-dimethylaminonaphthalene-1-sulfonamide (dansyl, DNS),[68] boron-dipyrromethene (BODIPY),[21a,36,63b] and cyanines (Cy3, Cy5)[28,68] Fluorescein and rhodamine are relatively inexpensive, but suffer from relatively fast photo-bleaching and cell-impermeability, excluding them from direct *in vivo* applications and are rather used for lysate profiling. BODIPY and Cy-dyes have excellent photochemical properties and are hydrophobic and thus able to penetrate the cell membranes. However, their precursors are still very expensive and they are mostly used for *in vivo* studies.

Biotin is the most popular affinity tag in proteomics. Its strong binding affinity to (strept)avidin ($K_d \sim 10^{-15}$ M) makes it a powerful tool for the detection of the labeled proteins by blotting[23f] as well as for the enrichment and purification of the probe-bound enzymes by using avidin-coated beads.[28,60] However, low cell permeability limits its application for pull-down experiments to cell or tissue homogenates, if incorporated into the probe. Another drawback in biotin enrichment procedures is the high background due to the presence of endogenously biotinylated proteins in the cell or tissue extracts. Fortunately, these shortcomings can be overcome by a tandem strategy in which the purification tag can be attached after the labeling *via* bioorthogonal ligation or cleavable linkers that enable the specific release of probe-bound enzymes (discussed below). Sometimes, also, desthiobiotin[33] is used, which is a stable biotin precursor and binds to strept(avidin) resin with similar potency.

Other affinity tags, hemagglutinin (HA)[69] or rhodamine[70] can be detected by their corresponding specific antibodies, whereas peptide nucleic acid tags (PNA)[71] enable the isolation of the labeled targets on oligonucleotide microarrays, however, those methods are rarely employed.

The last group of tags embrace isotopic labels such as radioactive [125]I (E-64 probe) or [3]H (lactacystin probe), which have been used for a very sensitive detection of cysteine proteases[55b] and proteasome,[59] respectively. However, the use of isotopic labels has decreased markedly over the last years because of their limited half-lives and restriction to gel-based read-outs. Nevertheless, given the successful application of fluorescent probes to

non-invasive fluorescence imaging *in vivo*,[72] certainly it will be also possible to implement such isotopes as ^{19}F or ^{64}Cu to ABPs to report on enzyme activities in live organisms using positron electron tomography (PET). Very recently, Bogyo et al. demonstrated that acyloxymethyl ketone (AOMK) ABPs, that irreversibly modify the active site cysteine of papain family proteases, involving a 1,4,7,10-tetraazacyclododecane-1,4,7,10-tetraacetic acid (DOTA) tag for labeling with ^{64}Cu were suitable tools for biodistribution and microPET imaging studies in nude mice bearing subcutaneous tumors.[73a]

2.1.3 Bioorthogonal approaches for ABPP *in vivo*

Like many other biologically-imbricated fields, ABPP continuously strives to shift from *in vitro* to *in vivo* experimentation in order to accurately reflect enzyme activity within living organisms. A limitation encountered by traditional ABPP was that the reporter tag appended to the probe often disfavoured or even disallowed its use within the biologically active cell system. Reporter tags tend to be too bulky and/or chemically unfavorable for uptake across cell membranes and thus may prevent the probe from entering the active site and forming a specific linkage with the active site residue, so that ABPP has been limited mostly to *in vitro* studies. Great potential to overcome these limitations has been found in the development of a so called 'tag-free' two step or tandem labeling employing bioorthogonal ligation methods.

In this approach, an ABP is equipped with a small latent handle, innocent in a cellular environment and introducing only a minor structural change into the warhead. Following the labeling and cell lysis, the small tag can be derivatized in the second step with a reporter label.

The field of bioorthogonal ligation methods is rapidly developing providing a great benefit to ABPP as several "spring loaded" chemistries have been elaborated and are nowadays routinely applied in the ABPP field as Huisgen azide-alkyne 1,3-dipolar cycloaddition (click chemistry), Staudinger/Staudinger-Bertozzi ligation or Diels-Alder cycloaddition reviewed

recently by Willems et al.[73] An overview of the bioorthogonal reactions used in ABPP is presented in Figure 12.

Copper (I)-catalyzed azide-alkyne cycloaddition (CuAAC):
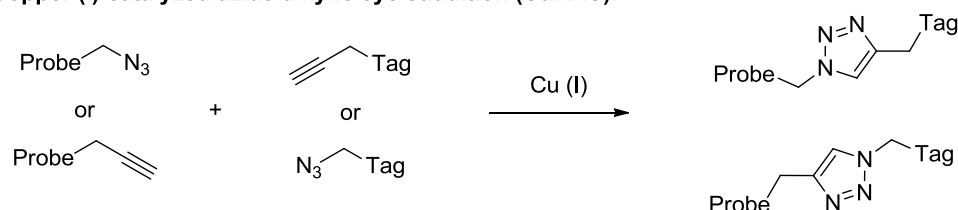
Strain-promoted azide-alkyne cycloaddition (SPAAC):
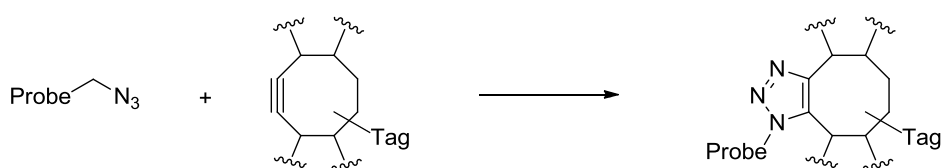
Staudinger-Bertozzi ligation:
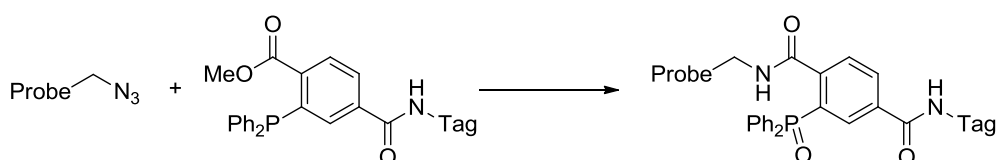
Diels-Alder cycloaddition:
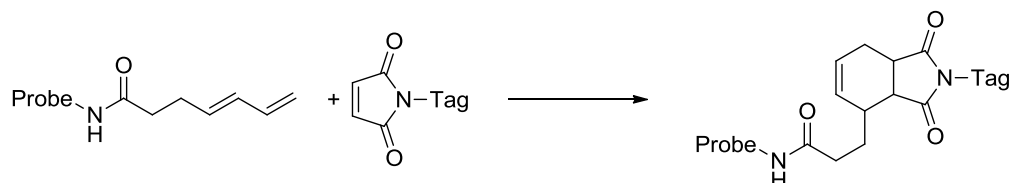
Inverse electron-demand Diels-Alder cycloaddition:
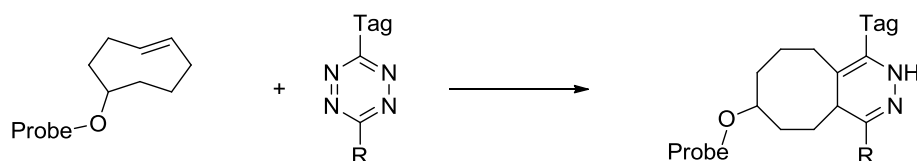
Figure 12. Bioorthogonal ligation reactions used in ABPP.

Copper(I)-catalyzed Huisgen 1,3-dipolar cycloaddition reaction between an azide and alkyne also known as click chemistry reaction (CC) was discovered independently by the groups of Sharpless[75] and Meldal[76] in 2002 and soon became a powerful tool for synthetic chemistry as well as for bioconjugation.[77,78] Click chemistry was introduced to ABPP by a very elegant study of Speers and Cravatt[79,80] and ever since has emerged as a 'spring loaded' strategy that allows efficient appending the reporter tag (fluorescent label, biotin) to an already

labeled enzyme under very mild conditions. Multiple ABPs bearing a small azide or alkyne handle have been prepared and successfully applied along with biocompatible fluorescent or affinity labels to profile enzyme activity *in vivo*.[81] Nevertheless, due to cell toxicity of the copper catalyst, CC can be only performed after the cell lysis and not in living systems. As an alternative to that caveat, a strain promoted version of CC has been developed employing a cyclooctyne as a biocompatible partner for an azide-derived fluorescent tag. Cyclooctyne tags were successfully coupled on cell-surface glycans.[82] However, in cell experiments with proteasome probes, biotinylated cyclooctynes showed remarkably higher background as compared to corresponding phosphanes used in Staudinger ligation[83] suggesting that these reagents need further optimization for future applications in ABPP.

The Staudinger ligation,[84] developed by the group of Bertozzi, makes use of a reaction between a phosphine to which an electrophilic trap is attached (typically methyl ester) and an azide leading to the formation of a stable amide bond upon rearrangement of an aza-ylide intermediate. In ABPP, a probe carries an azide group, whilst the fluorophore or biotin are coupled to a compatible phosphane. For instance, Overkleeft and coworkers demonstrated application of this method for the detection of active proteasome subunits in living cells[85,86] with vinyl sulfone or epoxomicin derived ABPs. Hang et al. used the Staudinger ligation for the analysis of cathepsins in macrophages.[57]

More recently, the Diels-Alder (DA) reaction has been used as a two-step bioorthogonal ligation strategy in ABPP. The group of Overkleeft prepared ABPs which were attached to a heptadienoyl group which was then reacted with a BODIPY-conjugated maleimide dienophile and demonstrated the utility of this cycloaddition reaction in detection of proteasome subunits and cathepsins.[87] The only disadvantage of this reaction in the complex protein sample is the need for cysteine residues capping prior to the reaction due to the intrinsic reactivity of the maleimide towards free thiols. However, an inverse-electron-demand DA reaction was developed to cope with that problem. Weissleder et al. used a norbornene- or trans-cyclooctene-modified antibody to tag live cells and subsequently, those dienophiles reacted with fluorophore-conjugated tetrazine allowing the imaging *in vivo*.[88] The same strategy was

also used to label and visualize *in vivo* microtubule structures with taxol-cyclooctene ABP, followed by the treatment with BODIPY-tetrazine fluorophore.[89]

2.1.4 Analytical platforms used in ABPP for identification of protein targets

Once an efficient ABP is developed, also an appropriate analytical platform is required in order to investigate the proteome of interest. There are several platforms available displaying distinct advantages and limitations that must be matched with the specific experimental problem to maximize the information content acquired in ABPP studies.

In the simplest gel-based methods (Figure 13), ABP-bound proteins are first resolved by one- or two dimensional polyacrylamide gel electrophoresis (1D- or 2D-SDS PAGE) and then visualized by in-gel fluorescence scanning for fluorescent probes or (strept)avidin blotting for biotinylated probes. However, a typical functional experiment would employ both modes of detection, first using fluorescent probes for rapid screening of proteomes and then applying biotinylated probes in combination with avidin enrichment and mass spectrometry analysis for the identification of labeled enzymes. The biggest limitation of gel based methods is the relatively low resolution. Nevertheless, the gel-based strategy is still widely used especially for preliminary screening of enzyme activities and rapid parallel comparative analysis of many proteomes due to its high throughput and robustness.
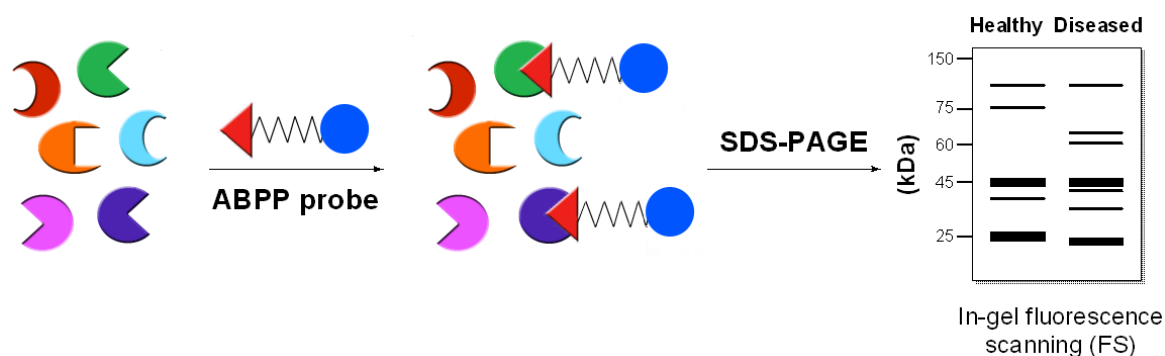
Figure 13. Gel electrophoresis based ABPP. Picture adopted from Ref. [14 b].

In order to overcome the low resolution of gel-based methods multiple liquid chromatography-mass spectrometry (LC-MS) strategies have been introduced to improve the information content obtained from ABPP experiments. Basically, these approaches can be divided into two categories.

First one analyzes the protein targets labeled by ABPs. In this strategy called ABPP–MudPIT (Multidimensional Protein Identification Technology) (Figure 14 A),[7b] labeled proteomes are incubated with affinity resins to enrich probe-labeled proteins (trifunctional biotin-fluorophore-probe or biotin-probe are typically used), which are subsequently digested with trypsin or chemically cleaved and subsequently analyzed by shotgun multidimensional LC-MS methods. The resulting MS data are searched using different algorithms such as SEQUEST[90] to identify the target protein. This method has proven capable to identify more than 100 enzyme activities in individual proteomes. However, this strategy does not allow straightforward identification of probe-labeled active-site residues. Fortunately, this caveat has been solved using the second LC-MS platform termed ABPP-ASPP (Active Site Peptide Profiling) (Figure 14 B).[91] This strategy involves digestion of the probe-labeled proteome with trypsin prior to enrichment on affinity resins. As a result, only active site labeled peptides are captured and then analyzed by LC-MS allowing direct identification of specific sites of probe labeling.
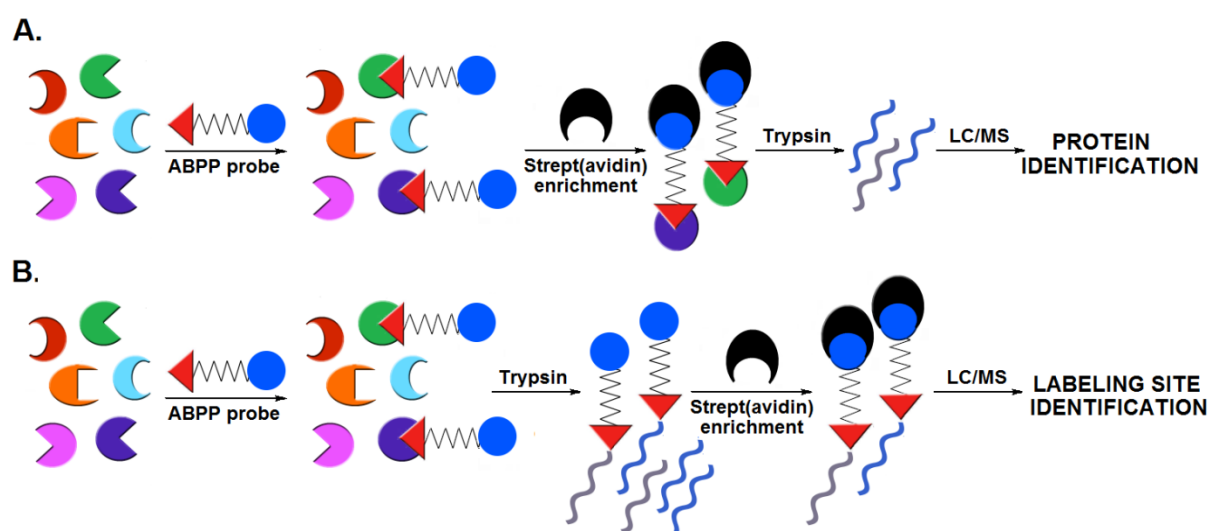
Figure 14. LC-MS based ABPP. A. ABPP-MudPIT (Multidimensional Protein Identification Technology). B. ABPP-ASPP (Active Site Peptide Profiling). Picture adopted from Ref. [14 b].

Also, the combination of these two methods has been successfully developed and it allows acquisition of both sets of information in a single ABPP experiment. In this strategy, termed Tandem Orthogonal Proteolysis ABPP (TOP-ABPP) (Figure 15),[92] a TEV protease cleavage site is introduced between the reactive group and analytical handle. The whole reporter tag can be conjugated to the already labeled proteome under CC conditions to avoid complications caused by the large size of the tag during the labeling. After enrichment, probe-bound proteins are subjected to on-bead trypsin digestion and subsequently bulk peptides are isolated by filtration from the active-site peptides captured on the avidin beads. Probe-bound peptides are then released from the beads by TEV protease digest. Then, trypsin and TEV digests are analysed by sequential MudPIT experiments to identify probe-labeled enzyme and site of probe modification, respectively.
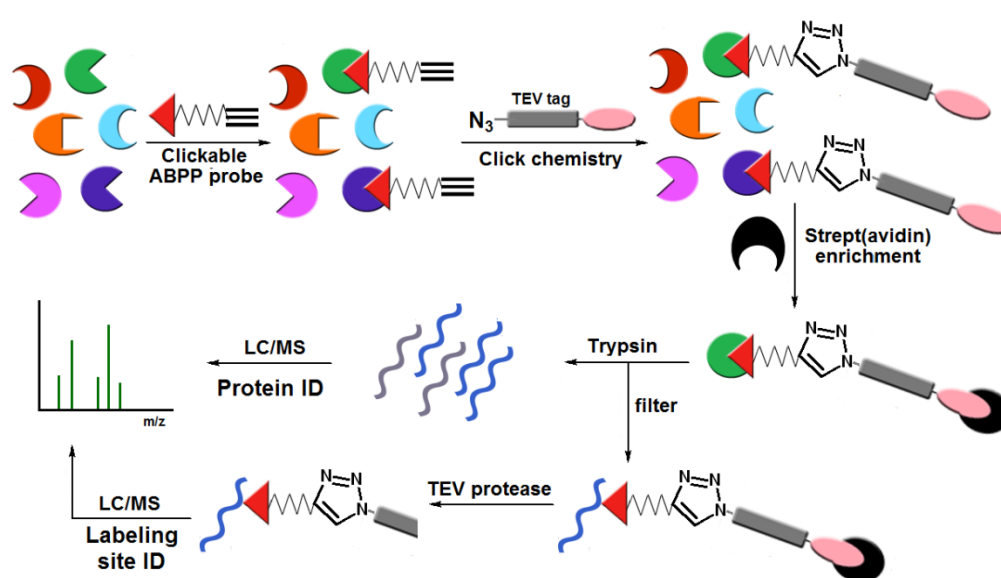
Figure 15. Tandem Orthogonal Proteolysis ABPP (TOP-ABPP). Picture adopted from Ref. [14 b].

Additionally, some alternatives such as capillary electrophoresis[70] or ABPP microarrays[93] have been introduced to diversify and extend the collection of analytical tools for ABPP.

2.1.5 Recent advancements in ABPP methods

In recent years, significant progress in ABPP methodology has been made with regard to high throughput inhibitor screening technologies, non-invasive *in vivo* imaging and

enrichment of probe-bound enzymes or quantification of active enzymes in proteomes. Several examples of the most prominent improvements will be described below.

2.1.5.1 Cleavable linkers

For unequivocal identification of a target protein labeled by an ABP, an efficient enrichment/purification from the rest of the proteome is required, followed by LC-MS analysis of the tryptically digested peptides. Typically, a biotin tag is incorporated into an ABPP probe or is attached *via* a bioorthogonal conjugation reaction, which enables a pull-down of probe-labeled proteins thanks to its strong binding affinity to streptavidin beads (Kd ~ 10^{-15} M). However, there are several weaknesses of the commonly used biotin-streptavidin system like harsh elution conditions, incomplete recovery of the proteins but mostly co-purification of unspecifically bound or endogenously biotinylated proteins which give rise to a high background and contamination of the samples. To overcome these issues, which are especially relevant in pull-downs of low abundant and instable proteins, a novel approach has been introduced which is based on cleavable linkers. The cleavable linker is introduced between the warhead and a biotin enrichment tag and once the labeled proteins are enriched it enables a specific elution of the probe-bound proteins upon chemical or enzymatic cleavage from the (strept)avidin beads, lowering the background levels as well as false positives. The cleavable linker approach is schematically depicted in Figure 16.

So far, several strategies have been elaborated, including the mild reduction of disulfide bonds,[94] the cleavage of (acyl)hydrazone,[95,96] diazobenzene,[97,98] or levulinolate ester[99] under very mild conditions. Apart of the chemical methods, also an enzymatic cleavage of TEV tag has been developed by the Cravatt group,[92] which involves a sequence specifically recognized by the TEV protease. On the other hand, Orth et al.[100] introduced a photolabile phenacyl ester linker, which can be easily cleaved upon UV light irradiation.

Many other examples of cleavable linkers used in chemical biology field including ABPP was comprehensively reviewed by Leriche et al.[101] underscoring the power of this strategy in ABPP applications.
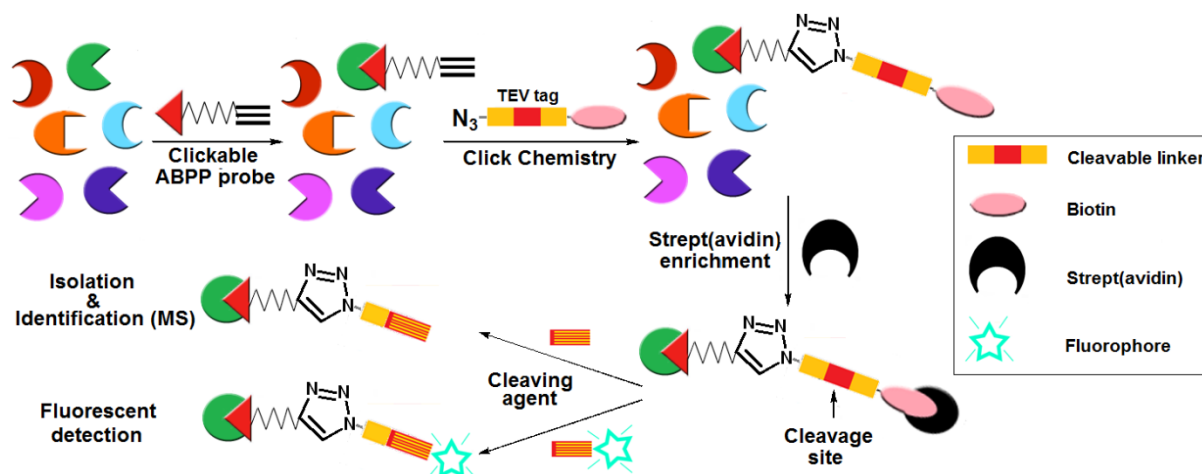
Figure 16. Schematic representation of cleavable linker approach. Picture adopted from Ref. [96].

Most prominent examples of cleavable linkers along with their corresponding cleavage methods are collected in Figure 17.
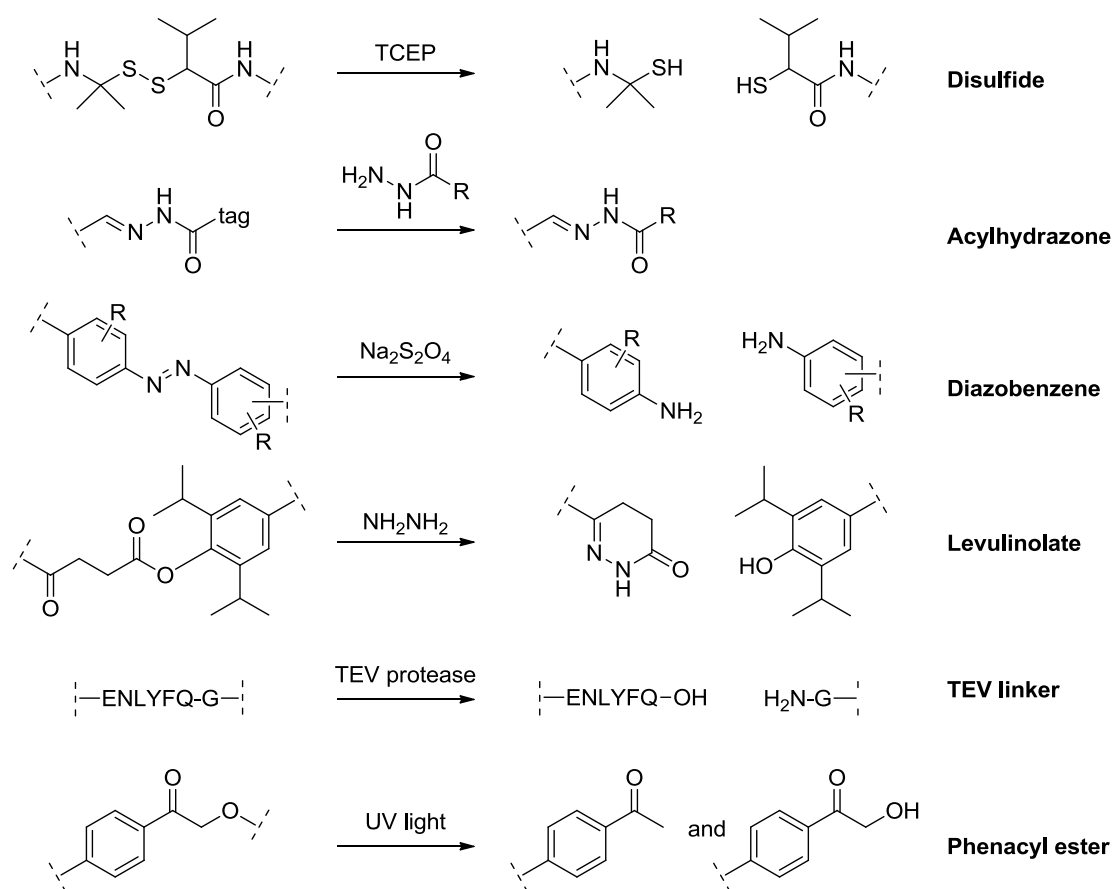
Figure 17. Cleavable linkers in ABPP and their cleavage mechanism.

2.1.5.2 Non-invasive *in vivo* imaging using ABPP

Non-invasive imaging of enzyme activity in living cells or whole organisms can provide essential information about its localization and interactions as well can serve as an excellent diagnostic tool enabling monitoring of disease progression associated to the activity of a particular enzyme (e.g. caspases in apoptosis and tumor growth). Precise and low background detection of protein activity changes in real time *in vivo* has become in high demand in Chemical Biology and multiple methods have been developed using fluorogenic substrates, GFP- or luciferase-based reporters but also fluorescent activity-based probes.[102]

The application of ABPs for *in vivo* imaging of different cysteine proteases has been pioneered by the group of Bogyo at Stanford University.[103] The biggest challenges in using ABPs for *in vivo* imaging is their intrinsic fluorescence giving rise to a low contrast between the specifically targeted enzymes and bulk unreacted probes freely diffusing in a cell or tissue until they get cleared or washed away and low cell permeability of a probe. An elegant method to overcome aforementioned limitations employs fluorescently quenched ABPs (qABPs) introduced by the group of Bogyo.[103,104] Such 'smart' ABP contains a reactive group coupled with a quencher which assures that a fluorophore remains dark until the quencher is cleaved off upon activity-dependent covalent modification of a specific protease. The probe becomes fluorescent only after its activation by a target protease thus allows its very specific real time monitoring in live systems (Figure 18).
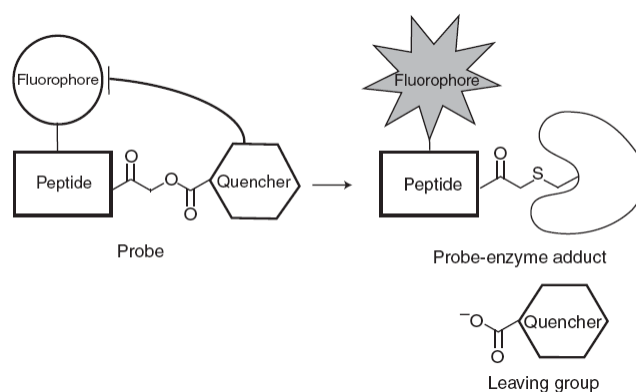
Figure 18. Schematic idea of labeling of a protease by fluorescently quenched ABP (qABP). Picture taken from Ref. [103].

The first study by Blum et al. demonstrated application of qABPs based on acyloxymethyl ketone warhead and its non-quenched counterpart to image the activity of cathepsins B and L in monolayer (NIH-3T3) as well as three dimensional (MCF-10A) cultured cells.[103] Essentially, qABP termed GB117 did not require extensive washing and fixing of cells as a non-quenched fluorescent probe GB111 did, allowing dynamic monitoring of cathepsins by fluorescence microscopy. In subsequent work, near infrared qABPs (GB137 (Cy5 and QSY21 quencher) and their non-quenched counterparts (GB123 (Cy5), GB138 (IR Dye 800CW)) were applied to whole-body non-invasive imaging of cathepsins in tumor xenografted nude mice[72] (Figure 19). Not surprisingly, quenched probe labeled tumor tissue in a specific manner with a maximum signal-to-noise ratio, which, not surprisingly, was achieved much faster when compared to the non-quenched probe.
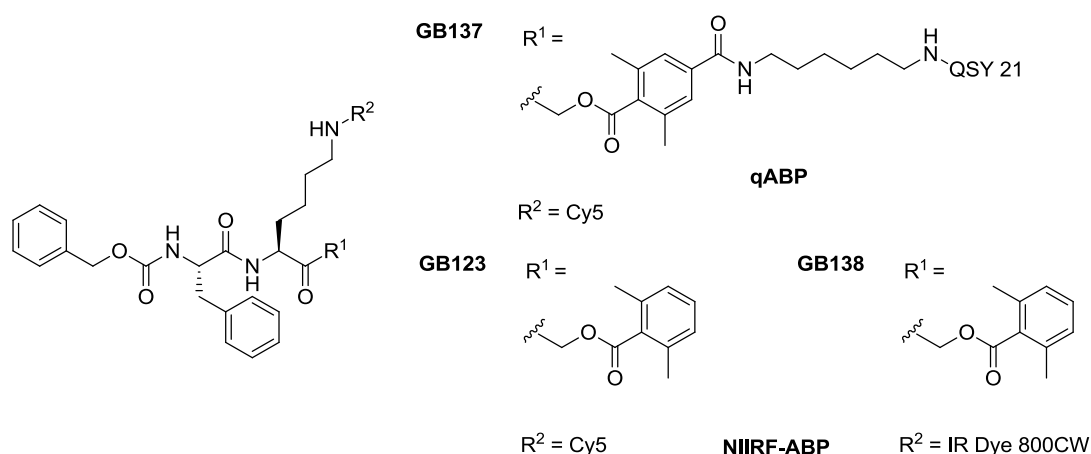
Figure 19. qABP GB137 and near infrared fluorescent ABPs (NIRF-ABP) based on an AOMK warhead to profile and image cathepsins *in vivo.*

Another near infrared AOMK probe was designed to selectively target caspases. Probe designated AB50-Cy5 (Figure 20 A bottom) was employed to monitor apoptosis in the thymi of mice treated with dexamethasone *ex vivo* (Figure 20 B) as well as in tumor-bearing mice treated with the apoptosis-inducing monoclonal antibody Apomab[104] (Figure 20 C). Additionally, this probe was equipped with a transporter peptide Tat (tAB50-Cy5) (Figure 20 A top) which significantly enhanced the uptake of the probe and a fluorescent signal only in apoptotic cells. These caspase ABPs allowed monitoring the kinetics of apoptosis in live mice in its early time points and could be useful tools in the future as apoptosis markers both

in preclinical and clinical applications. Near infrared ABPs have also been developed to show the localization of cathepsin B activity to caveolae of endothelial cells during tube formation,[105] to study the role of cathepsins in angiogenesis,[106] and to image legumain activity in tumor models[107] as well as to visualize the effects of expression of neutrophilic granule protein (NGP) in tumors.[108]
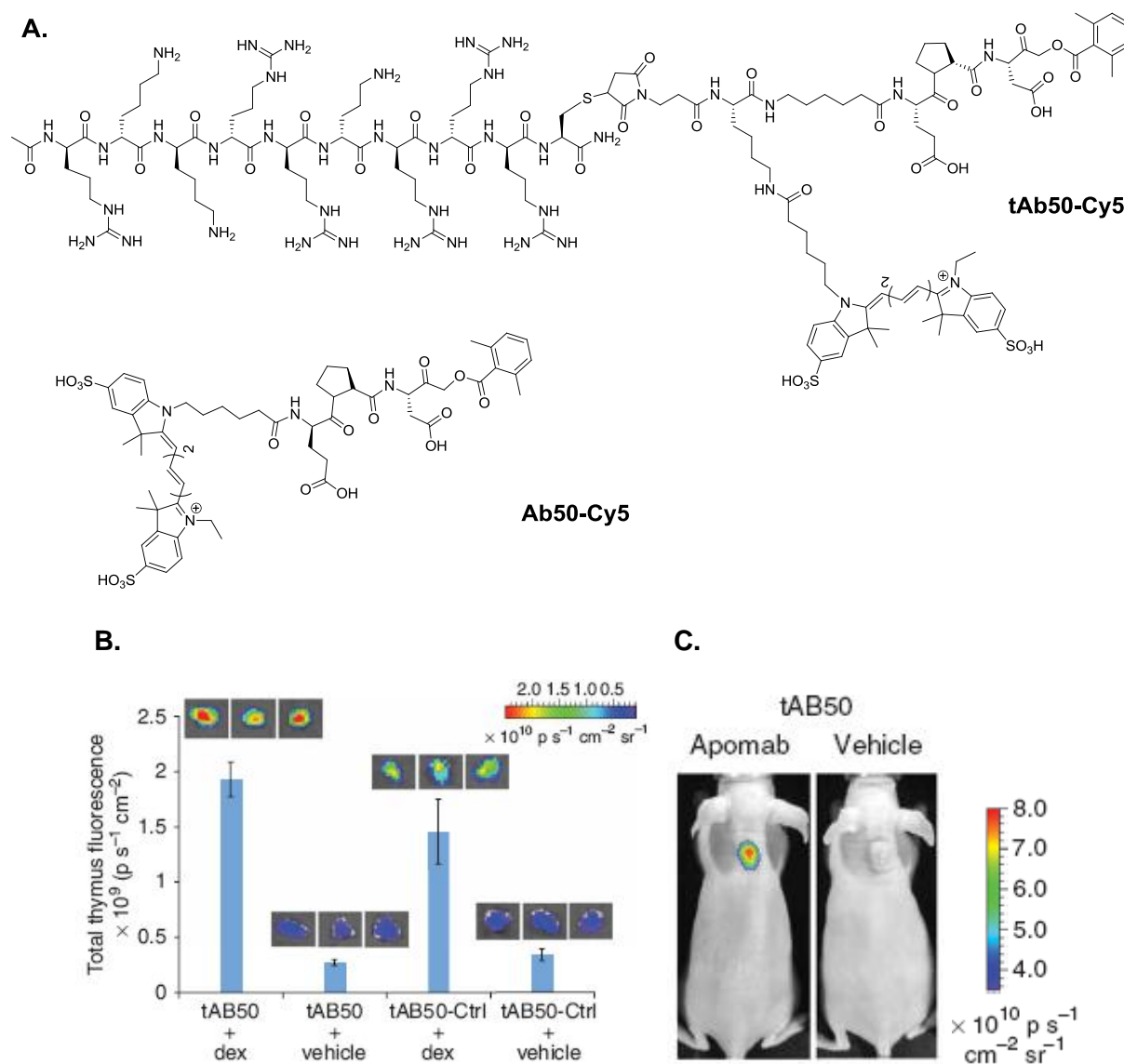
Figure 20. Labeling of tumor apoptosis using AB50-Cy5 and tAB50-Cy5 caspase ABPs. A. Structure of AB50-Cy5 (bottom) and tAB50-Cy5 (top). B. Imaging of thymi *ex vivo*. C. Imaging of tumor in mice *in vivo*. Picture taken from Ref. [104].

2.1.5.3 Inhibitor screening platforms in ABPP

Competitive ABPP has been successfully applied for the discovery of potent enzyme inhibitors, by performing experiments, in which inhibitors are detected by their ability to outcompete the labeling of enzyme by its selective ABP (Figure 21).
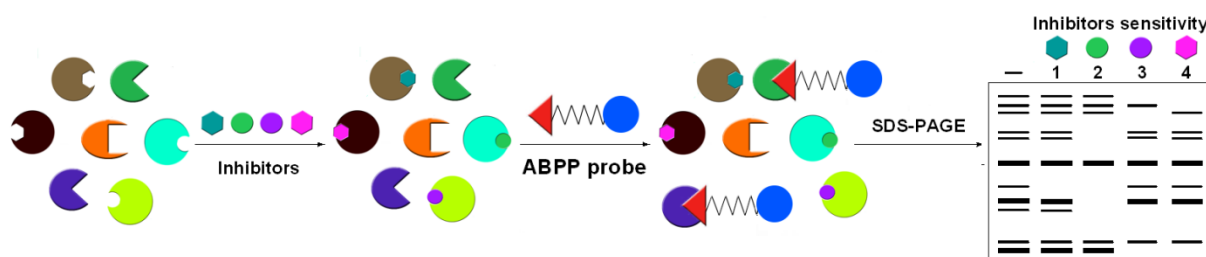
Figure 21. Competitive ABPP for inhibitor discovery. Picture adopted from Ref. [14 b].

This approach offers many advantages over traditional inhibitor screening methods. Firstly, inhibitors can be tested in complex protein samples (cell or tissue extracts or even live cells) so there is no need for tedious recombinant protein expression and purification. Also, a selective ABPP probe acts as a substrate surrogate and enables the inhibitor screening for poorly characterized enzymes with unknown endogenous substrates. Finally, testing of many enzymes in parallel in complex samples allows the assignment of selectivity and potency factors of the inhibitor candidates. This strategy has been used for identifying both irreversible[41a,109] and reversible potent inhibitors,[110] although reversible inhibitors need to be carefully tested under kinetically controlled conditions.[110] The biggest drawback of this screening method is relatively low throughput due to 1D-SDS PAGE read-out format, enabling screening of compounds libraries of only modest size (200-300 compounds).[109b]

To address this limitation, the group of Cravatt in 2009 developed a very innovative high throughput screening (HTS) technology for inhibitor discovery which combines ABPP with a fluorescence polarization read-out, which was dubbed fluopol-ABPP.[111] Fluopol-ABPP is based on a simple principle of variable velocity of molecular rotation of excited fluorophores, which is inversely propotional to their molecular volume. Hence, small fluorophores, excited with a plane-polarized light, will rotate quickly and tumble out of this plane in solution and will emit depolarized light (low polarization signal), while the attachment of a fluorophore to a

large biomolecule (e.g. protein) will greatly slow down the rotation, leading to the emission of highly polarized light (high polarization signal). In the fluopol-ABPP assay, a purified protein and a candidate inhibitor are dispensed into a 384- or 1536-well plate and incubated for a certain time interval. Subsequently, a fluorescent ABP is added to each well, which is able to efficiently label the target protein (e.g. FP for serine hydrolases). When the candidate inhibitor proves inactive, a fluorescent ABP labels the enzyme, resulting in the increase of the polarization signal, since the tumbling rate of probe-bound enzyme is much lower compared to the unbound probe. Conversely, if the enzyme is inhibited by a candidate compound, an ABP cannot bind to the enzyme and will remain unbound and freely rotating in the solution, leading to the drop in fluorescence polarization and identification of a 'hit' compound (Figure 22). In this way, the fluopol-ABPP can be employed to test for inhibitors of an enzyme, for which only a sensitive ABP is established, even if the natural substrate remains unknown.
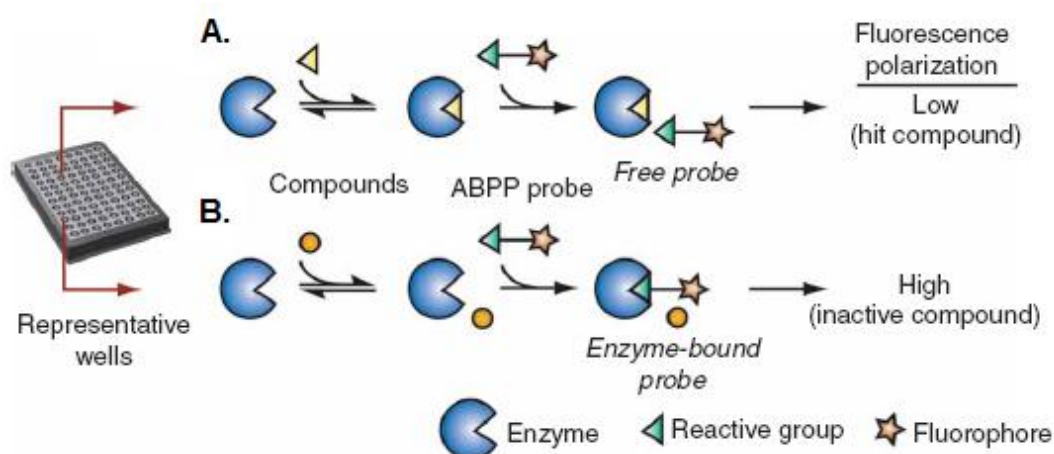
Figure 22. A schematic representation of the fluopol-ABPP assay. Picture taken from Ref. [111].

However, fluopol-ABPP can be used only for enzymes for which cognate activity-based probes have been developed (e.g. serine hydrolases or cysteine proteases). Also, a substantial amount of a purified target enzyme is required, which might be problematic for some proteins. Despite of these restrictions, fluopol-ABPP has been successfully applied to screening for inhibitors of such enzymes as poorly characterized serine hydrolase RBBP9[112] or prolyl endopeptidase like enzyme (PREPL),[113] for which no endogenous substrates are so far known. Using other than FP activity-based probes, potent inhibitors were identified in

fluopol-ABPP screens for such distinct enzymes like protein arginine deiminase 4 (PAD4),[114] glutathione S-transferase omega 1 (GSTO-1),[26a] protein arginine methyltransferase 1 (PRMT-1),[26b] or protein phosphatase methylesterase 1 (PME-1).[115] Fluopol-ABPP along with the development of new ABPs for other enzyme classes will be a very powerful tool for HTS of new inhibitors in the near future.

2.1.5.4 Quantitative reactivity profiling

Over the last few years, significant progress has been made in developing new techniques for ABPP that enable not only the identification and characterization of active enzymes in complex proteomes but also very precise quantification of protein levels and their activity in complex proteomes. Quantitative proteomics approaches embrace either stable isotope labeling (e.g. isotope-coded affinity tags (ICAT),[7c,116] stable isotope labeling of amino acids in cell culture (SILAC)[117,118]), and label-free MS-based methods as MudPIT,[7b] or TOP-ABPP.[92] They allow the relative or absolute quantification of protein levels and their modifications in various cells, tissues or comparison of protein expression under different conditions (healthy vs. diseased proteomes).

One of the challenges in ABPP is the development of methods for systematic identification and quantification of reactive amino acid residues, which are essential for the enzymatic catalysis or undergo posttranslational modifications, and therefore are indispensable for the enzyme activity and function.

Recently, Weerepana et al. combined the advantages of TOP-ABPP and quantitative proteomics and developed a strategy termed isoTOP-ABPP (isotopic TOP-ABPP) to quantitatively profile the intrinsic reactivity of cysteine residues *en masse* in native proteomes (Figure 23).[119] In this method, the robust alkyne iodoacetamide probe (IA) is used to label cysteines, to which either a heavy or light azido-TEV-biotin tag (with isotopically labeled valine) is attached under click chemistry conditions. After tandem on-bead digestion with trypsin and TEV protease, probe-bound peptides conjugated to isotopic tags are released

and analyzed by LC-MS/MS to identify and quantify IA-modified cysteines. The key assumption of the isotope-ABPP is that the cysteine functionality is reflected by the nucleophilicity and hence the 'hyperreactivity' of the cysteine residues with IA probe. Thus, hyper-reactive (and functional) cysteines will be labeled to completion with low IA concentrations (generating isotope-ABPP ratio R[light]:[heavy]~1), whereas less-reactive cysteines will show concentration-dependent labeling with IA probe (displaying isotope-ABPP ratio R[light]:[heavy]»1). Indeed, the isoTOP-ABPP experiments performed on human breast cancer cell line MCF7, identified over 800 IA-labeled cysteines in 522 proteins with various isotopic ratios. Interestingly, a small subset of cysteines (<10%) showed almost identical isotopic ratio of ~1 regardless the IA concentration applied and further investigations of those hyper-reactive cysteines revealed that a big fraction of them was annotated as active-site nucleophiles or redox-active residues susceptible to posttranslational modifications.
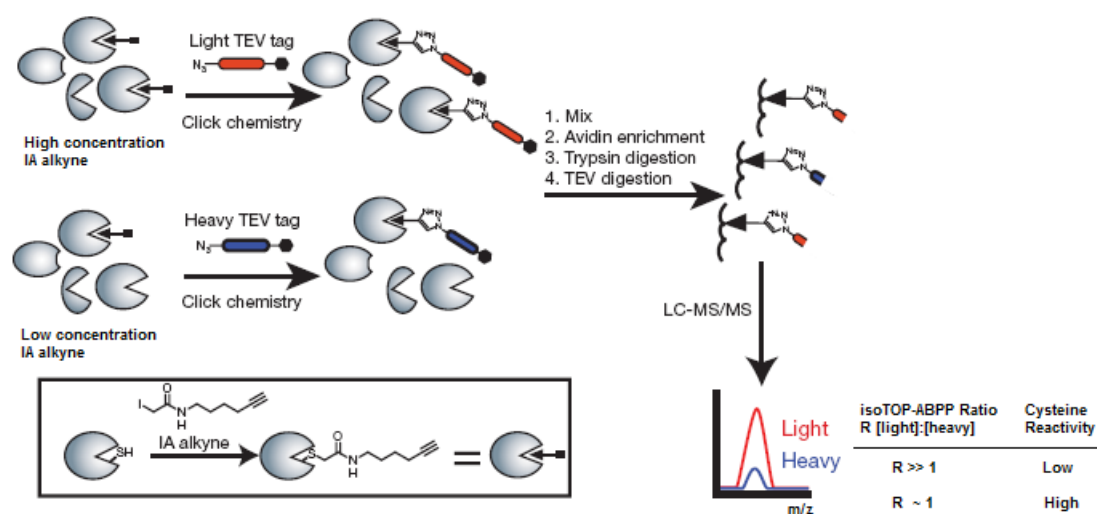
Figure 23. Schematic representation of isoTOP-ABPP approach to globally profile cysteine reactivity in proteomes. Picture taken from Ref. [119].

Despite of some limitations (steric hindrance to access some cysteines, regulation of cysteine reactivity by cofactors or endogenous substrates), the isoTOP-ABPP methodology for global profiling of reactive and thus functional cysteines proved very powerful and with a set of different electrophilic probes targeting specifically other residues (serine, threonine) or subsets of cysteine proteases its scope could be greatly extended.

2.1.6 Biological applications of ABPP

ABPP has matured in recent years as a unique and outstanding technology equipped with a broad array of powerful tools contributing to the great progress in Chemical Biology research. It has not only added to basic understanding of proteins and their functions in biological pathways, but also delivers tools for medicinal chemistry and pharmacology.

The original and still most common application of ABPP is the identification and annotation of enzyme activities in biological systems (target discovery) and elucidation of their role in complex biological processes as well as their comparative profiling throughout different cells, tissues, whole organisms. The typical experiment will compare two or more proteomes (e.g. healthy vs. diseased, diverse tissues or biopsies from different stages of disease or infection) in search for differing levels of enzyme activity. If the analysed proteomes in turn display different properties, particularly healthy versus diseased, the altered enzymes activities can be hypothesized to regulate these changes. Numerous target enzymes implicated in various physiological and pathological processes were identified by a wide range of activity-based probes (many of them discussed in the text above) showcasing the power of ABPP in unravelling the complex proteome and interactome map which yet is only poorly understood.

Additionally, many so far unknown (off) targets of clinically used drugs and antibiotics such as antiobesity drug Orlistat,[120] antibiotics vancomycin[121] or showdomycin,[18c] anticancer drugs imatinib,[122] dasatinib[32] or antiparkinsonian drug deprenyl[123] could be profiled across different disease models to give rise to understanding their mode of action and possible side effects resulting from interactions with other protein targets.

The second major application of ABPP is the discovery of enzyme inhibitors. Combination of high throughput screening technique fluopol-ABPP, competitive gel-based profiling of 'hit' compounds in complex biological samples (discussed in section 2.1.5.3), and conventional biochemical assays serve as a robust platform for medicinal chemistry and pharmacology. Chemoproteomic approaches have been used for development and optimization of many selective and potent inhibitors for serine hydrolases, cysteine proteases, kinases, histone

deacetylases, cytochrome P450 enzymes and many others, which is comprehensively discussed by Moellering and Cravatt in a recent review.[124]

The discovery of new kinase inhibitors is at heart of ATP-analogue based chemoproteomic platform called KiNativ developed by the groups of Gray and Kozarich in ActivX which aims to profile libraries of inhibitor candidates against set of over 200 kinases in native cell proteomes.[23d,125] This platform is a very useful tool for the discovery of potent and selective inhibitors interacting with the ATP-binding pocket. It does not require a recombinant or purified protein or knowledge about their natural substrates as it is based on competition between an inhibitor candidate and ATP-acylphosphate activity probe. Additionally, inhibitors display close to real cellular activity as the profiling is performed in a native proteome and strikingly, the authors found significant differences in inhibition profiles when compared to assays with recombinant enzymes, in particular, for Raf kinases.[125]

Imaging enzyme activity *in vivo* by employing fluorescent ABPs is another increasingly developing application of ABPP, which enables real time trafficking and localization studies of enzymes involved for instance in apoptosis and tumorigenesis. Imaging agents should be cell-permeable and selectively target enzymes of interest, but most importantly they should give maximum signal-to-background ratio shortly after injection (high contrast) and emit fluorescence signals not interfering with the auto-fluorescence background of the studied biological system. Significant contribution with regard to the development of efficient imaging probes meeting the above mentioned requirements has been made by the group of Bogyo. They developed many variants of fluorescently quenched ABPs (qABPs),[72,103] near infrared fluorescent ABPs,[104-108] which were discussed in detail in section 2.1.5.2. Very recently, also ^{64}Cu[73a] or ^{19}F[73b] isotopically labeled probes were developed allowing non-invasive PET imaging of proteases and hydrolases activity, respectively, *in vivo*.

Recently, the group of Yao presented a new class of qABPs based on quinone methide chemistry, which allows the modular design of probe scaffolds by combing different warheads (for distinct enzyme classes), fluorescent dyes (one- and two-photon fluorophores)

as well as tags as biotin or cell penetrating peptides.[126] This approach allowed preparation of several qABPs for caspases and phosphatases, which were used for sensitive imaging of active caspases 3 and 7 as well as protein tyrosine phosphatases in cell extracts and living cells. Additionally, these new qABPs did not deactivate the enzyme target, enabling amplification of the fluorescent signal through multiple enzyme turnovers.

Lastly, activity-based probes can be useful markers for diagnosis and prognosis of a series of diseases, which are associated with abnormal enzymatic activities, such as cancer, pathogenic and virus infections or metabolic diseases. For instance, BODIPY-cyclophellitol was used as an ultra-high sensitive marker for active glucocerebrosidase (GBA) enzyme whose deficiency underlies Gaucher disease, a common lysosomal storage disorder.[127] This probe can be a useful diagnostic tool for assessment of a type of Gaucher disease in patient material as well as for the development of effective chaperones for GBA. Another study by the group of Pezacki used FP-rhodamine probe to track the differential host enzyme activation during Hepatitis C virus (HCV) infection and identified carboxylesterase 1 (CES 1) as a key player in HCV propagation, which is a harfmful disease with still unclear pathogenesis.[128]

2.2 Flavin-dependent oxidases

Flavoenzymes are ubiquitous in nature as a family of colorful oxidoreductases, which contain either a FMN (flavin mononucleotide) or FAD (flavin adenine dinucleotide) cofactor.[129-131] To date, numerous flavin-dependent enzymes have been identified and characterized and it is estimated that approximately 1-3% of all genes in prokaryotic and eukaryotic genomes encode for flavin-containing enzymes. The outstanding chemical versatility of the flavin enables flavin-dependent enzymes to catalyze a diverse set of reactions encompassing oxidations, monooxygenations, reductions, dehydrogenations, halogenations and non-redox reactions, making them indispensable for many cellular processes (e.g. nucleotide biosynthesis,[132] protein folding,[133] apoptosis,[134] axon guidance,[135] chromatin remodelling,[136] or detoxification[137]).

Although flavoenzymes display a high level of structural and functional diversity, all of them intrinsically contain either a FAD or FMN cofactor derived from riboflavin (vitamin B_2)[138] (Figure 24). The cofactor is typically non-covalently bound to the apoprotein (90%).[139] However, a considerable number of flavoenzymes has the isoalloxazine ring covalently attached to the polypeptide chain *via* histidyl, tyrosyl, cysteinyl or threonyl linkage.[140]
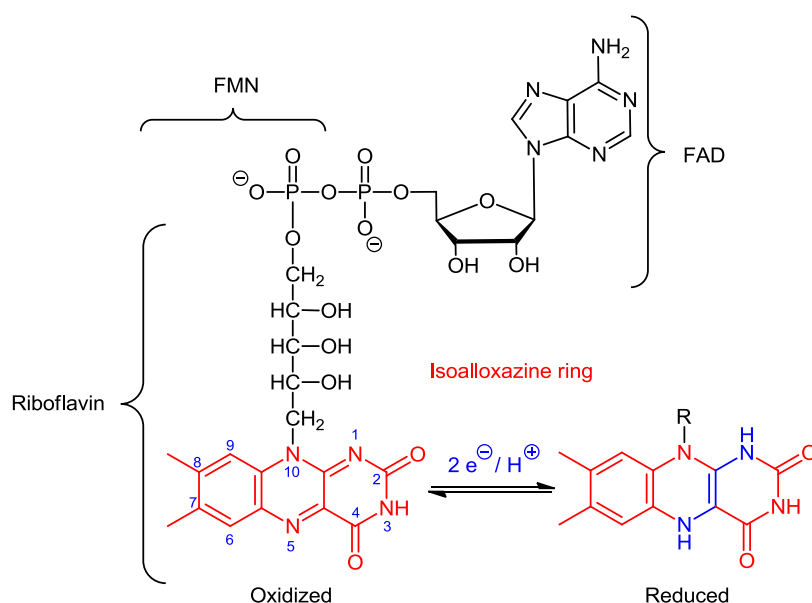
Figure 24. Chemical structure of the isoalloxazine ring and flavin cofactors. The redox active isoalloxazine ring is shown in its oxidized and two electron reduced state. Adopted from Ref.[140].

Covalent flavinylation is a post-translational and an autocatalytic process that adjusts the redox potential of the flavin and is beneficial for enzyme activity and stability. Recently, it was found that the flavin can be also attached by dual covalent linkage (e.g. *via* 6-*S*-cysteinyl and *N*1-histidyl linkages in glucooligosaccharide oxidase[141] or berberine bridge enzyme (BBE)[142]). Flavin cofactors are characterized by their well-defined spectroscopic properties, which are determined by the redox- (oxidized, one- or two-electron reduced form) and protonation state as well as by the nature of the protein environment (hydrogen bonds, hydrophobic interactions etc.).

Flavoenzyme catalytic reaction is comprised of two combined half-reactions by which the flavin alternates between oxidized and reduced state. In the reductive half-reaction a substrate is oxidized with concomitant reduction of the flavin cofactor whilst in the oxidative half-reaction - the flavin is re-oxidized by an electron acceptor (i.e. oxygen for oxidases) and depending on enzyme/substrate system proceeds *via* 'ping-pong' (electron acceptor reacts with free flavin after the product is released) or ternary complex mechanism (electron acceptor reacts with the flavin-product complex which is followed by the product release). These catalytic events are summarized in Figure 25.
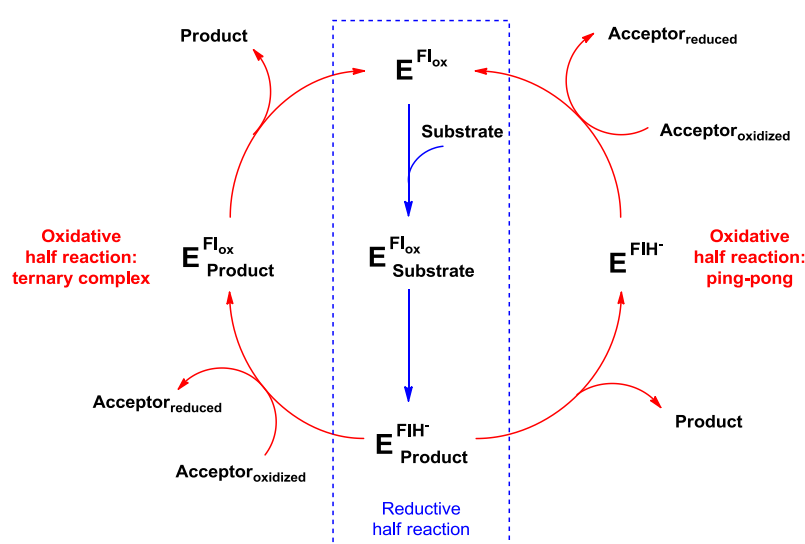
Figure 25. Catalytic cycle of flavoenzymes. Picture adopted from Ref. [142].

Oxidative flavoproteins embrace two classes: oxidases[143] and monooxygenases,[144] which are of particular interest for biocatalysis since they display high enantio- and regioselectivity

and are very efficient biocatalysts in oxyfunctionalization processes. These two classes differ in their intrinsic reactivity towards molecular oxygen. Flavin-dependent oxidases efficiently use dioxygen as an electron acceptor to produce hydrogen peroxide, whereas monooxygenases activate oxygen by forming the flavin C4a-(hydro)peroxide of the flavin, which is employed to insert an oxygen atom into the substrate (Figure 26). The initial step of the reaction (1) is the single electron transfer from the two-electron-reduced flavin (FlH$^-$) to molecular oxygen to generate a caged radical pair (semi-reduced flavin-superoxide anion). This radical pair can then follow different routes resulting in: the generation of hydrogen peroxide (in its deprotonated form) after second electron transfer (2) and (3 and 4) (in oxidases) either the insertion of an oxygen atom into a substrate *via* a peroxy-flavin intermediate (3 and 5) (in monooxygenases and hydroxylases) or the production of oxygen radicals after its dissociation (6).
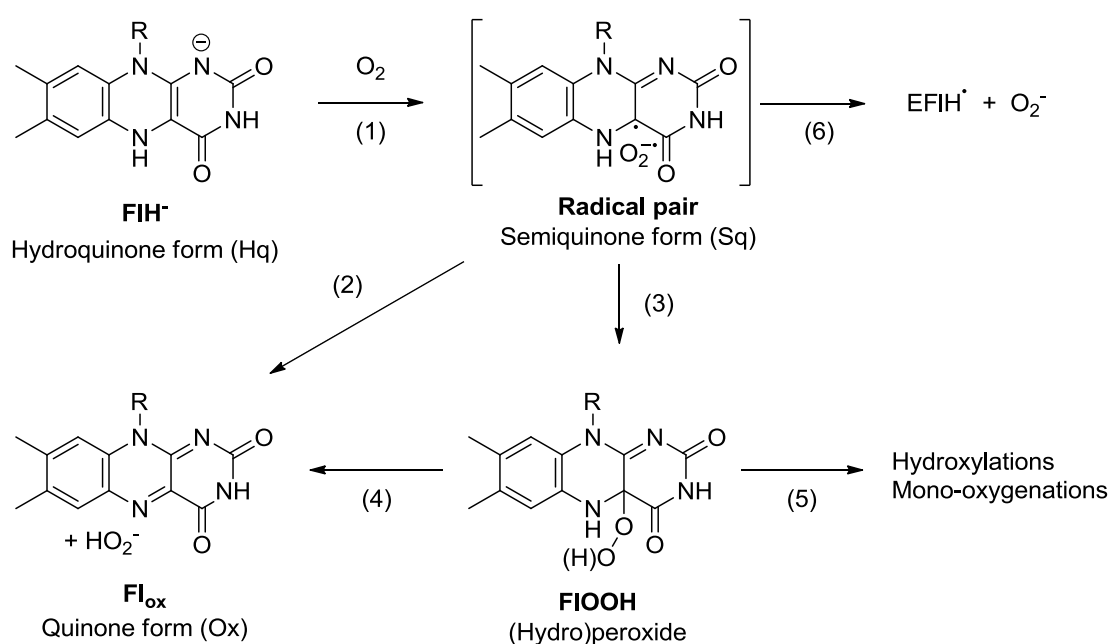
Figure 26. Pathways for the reactions with oxygen of the two-electron reduced flavin (FlH$^-$).

Flavin-dependent oxidases are a structurally and functionally diverse subclass of flavoenzymes converting their substrates with the concomitant reduction of molecular oxygen into hydrogen peroxide.[129,143] Analysis of redox potentials and kinetic properties of many flavin-dependent oxidases revealed that in most enzymes oxygen reacts with the flavin according to second-order kinetic behaviour (the reaction occurs via simple collision between

molecular oxygen and the protein-bound reduced cofactor). However reaction rate constants range from 1×10^6 M^{-1} s^{-1} to almost zero for protein-bound flavins compared to 2.5×10^2 M^{-1} s^{-1} for the free flavin, indicating that the oxygen reactivity is an adjustable and complex process regulated by combination of subtle factors such as dipole pre-organization, charge distribution, conformational dynamics and solvation in the enzyme active centre and cannot be predicted on the basis of the structural features or redox potentials.[143,145]

Commonly, flavin-dependent oxidases catalyze oxidation of a large variety of compounds including amines (e.g. mono- (MAO) and polyamine (PAO) oxidases, lysine specific demethylase 1 (LSD1)), aminoacids (e.g. glycine oxidase, L-tryptophan oxidase), alcohols (e.g. vanillyl alcohol oxidase (VAO), cholesterol oxidase), carbohydrates (e.g. glucooligosaccharide oxidase (GOOX), pyranose 2-oxidase, lactose oxidase), nitroalkanes (nitroalkane oxidase), and sulfides (sulfhydryl oxidases (SOX)). Some display narrow substrate specificity while the others are more substrate-tolerant. In conclusion, their intrinsic structural diversity, multiplicity of accepted substrates, and lack of conserved residues in the active-site make them elusive to functional annotation *via* established genomic, structural or proteomic analyses[139,146,147] and some alternative methods are still needed.

2.3 Monoamine oxidases (MAO)

Monoamine oxidases[148] (MAO, EC 1.4.3.4) are FAD containing enzymes, localized in the mitochondrial outer membrane, which catalyze the oxidative deamination of several important neurotransmitters and hormones in the central nervous system (CNS), including serotonin, dopamine, norepinephrine and adrenaline as well as exogenous dietary amines (e.g. tyramine) or xenobiotic amines (e.g. 1-methyl-4-phenyl-1,2,3,6-tetrahydropyridine (MPTP)). In humans, monoamine oxidases exist in two different isoforms designated MAO A and MAO B,[149] which are encoded by two distinct genes[150] located on the X chromosome and display unique substrate selectivities (MAO A oxidizes favorably serotonin, while MAO B prefers phenylethylamine) and inhibitor sensitivities[149] (MAO A is preferentially inhibited by clorgyline whereas MAO B by deprenyl) although they share a high level of sequence identity (70%).[150] Information about the organization of genes, overall structure and localization of human monoamine oxidases is compiled in Table 1.

Table 1. Structure, localization and gene properties of human MAO enzymes.[148]

Primary structure	MAO A: 527 aa (59.7 kDa)
	MAO B: 520 aa (58.8 kDa)
	Amino acid identity: 70% (hMAO A and hMAO B)
	3 highly conserved regions in all species (90% identity)
Crystal organization	MAO A: monomer
	MAO B: dimer
Membrane organization	MAO A: dimer
	MAO B: dimer
Cofactor	FAD covalently linked *via* 6-*S*-Cys (1 cofactor per subunit)
Subcellular localization	Outer mitochondrial membrane
Distribution	CNS and peripheral organs
Cell type	Neuronal (MAO A: catecholaminergic neurons, MAO B: serotonergic and histaminergic neurons, glial cells) and non-neuronal
Genes	Location: Chromosome X
	MAO A: Xp11.23-p11
	MAO B: Xp22.1
	Organization: 15 exons-14 introns (60-70 kb)
mRNA transcript	MAO A: 5 kb and 2 kb
	MAO B: 3kb

2.3.1 Crystal structures of human monoamine oxidases

The elucidation of the crystal structures of both isozymes MAO A[151] and MAO B[152] by the groups of Edmondson and Mattevi as well as Son and co-workers provided detailed insight into structural differences in their active sites accounting for distinct substrate and inhibitor specificities[151b,153] as well as into crucial features for enzyme activity. The X-ray structure for MAO B has been determined with many ligands (34 structures deposited in PDB) with the best resolution of 1.65 Å while human MAO A structure was assigned to 2.2 Å. Successful crystallization of both isoforms of MAO was facilitated by the development of high-level expression and purification system for the genes encoding for MAO A[154] and MAO B[155] using methylotrophic yeast *Pichia pastoris*. In addition, this system was also successfully applied for expressing MAO enzymes from rat[156] and zebrafish.[157]

2.3.1.1 Overall structure of human MAO A and MAO B

Human MAO A structure is comprised of 527 amino acid, while hMAO B contains 520 residues and both are folded into a compact structure that exhibits the same topology as L-amino acid oxidase (LAAO) and polyamine oxidase (PAO) assigned as "PHBH" fold (p-hydroxybenzoate hydroxylase).[158] (Figure 27).

While pulsed electron paramagnetic resonance-double electron-electron resonance (EPR-DEER) spectroscopic distance measurements clearly have shown that both isozymes exist in a dimeric form when bound to the membrane,[159] MAO A crystallizes as a monomer and MAO B as a dimer. However, rat MAO A (sharing 92% sequence identity with hMAO A), similarly to hMAO B crystallizes as dimer. It was suggested that responsible for this phenomenon is a selective Glu151Lys mutation that is unique to hMAOA among a wide variety of vertebrate MAOs.[160] Crystal structures of hMAO A show that Lys151 is situated on the protein surface far from the active site and interestingly, this location is proximal to a cluster of charged residues involved in monomer-monomer interactions contributing to the formation of the dimer in hMAOB and rMAOA. This hMAO A specific mutation destabilizes its

dimeric state, resulting in the observed monomeric crystal structure. In human MAO B contact surface between monomers is extensive and measures approx. 2095 $Å^2$ (~15% of the monomer accessible surface).

Human MAO A   Human MAO B
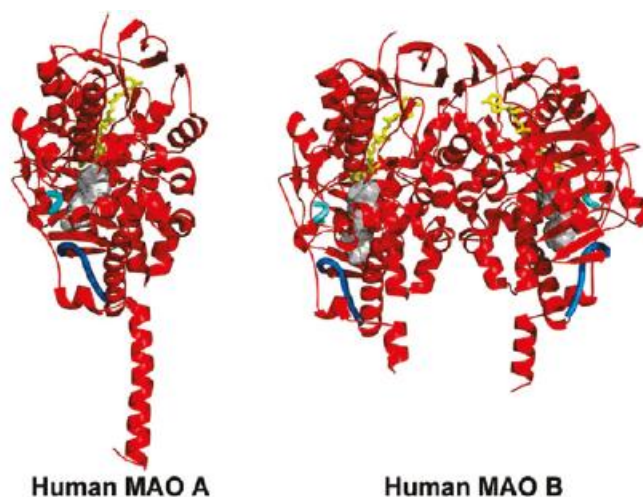
Figure 27. Ribbon diagram of the structures of MAO A and MAO B. All structures are oriented with the *C*-terminal transmembrane helices pointing downward. The FAD cofactor is presented as yellow balls and sticks. The active site cavity is drawn as a gray surface. The cavity-shaping loop is highlighted in cyan and the loop lining the entrance cavity space is blue. Picture taken from Ref. [148 b].

Both proteins are consisted of three conserved domains: *C*-terminal membrane region (residues 463-506 (MAO A) and 489-500 (MAO B)), FAD-binding domain (residues 13-88, 220-294, 400-462 (MAO A) and 4-79, 211-285, 391-453 (MAO B)) and the substrate-binding domain (residues 89-219, 295-399 (MAO A) and 80-210, 286-390, and 454-488 (MAO B)). Additionally, cavity-shaping loops (210-216 in MAO A, 201-207 in MAO B) exert a similar conformation.

2.3.1.2 Membrane binding region

The membrane binding region in both isozymes is formed by the *C*-terminal tail that first forms an extended polypeptide chain that traverses the monomer surface which is followed by an α-helix, establishing the predicted from previous biochemical studies[161,162] transmembrane helical segment inserted into the outer mitochondrial membrane. The helix of each monomer protrudes from the basal face of the dimer with the axis parallel to the

molecular two-fold axis. In addition to *C*-terminal helices also the other regions of the protein might be involved in membrane binding.[163] Interestingly, chimeric enzymes constructed from fragments of MAO A and MAO B show that interchanging of the respective *C*-terminal helices results in the loss of enzyme activity, especially in case of MAO B, suggesting that there are significant differences in specific membrane binding features between both isoforms.[161,162] A close-up of the membrane domain of hMAO B is depicted in Figure 28.
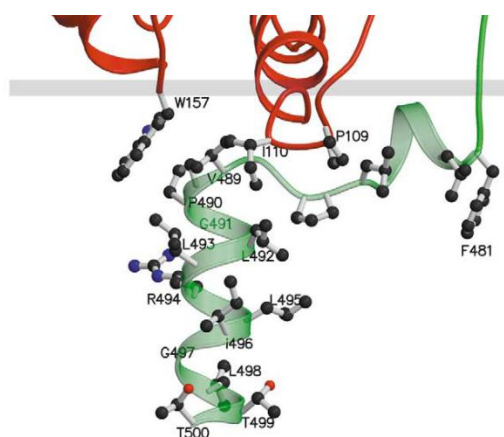
Figure 28. Close-up view of the membrane binding region in structure of human MAO B. Picture taken from Ref. [163].

In the membrane-bound conformations, MAO A and MAO B are both dimeric.[159] However, recent topological studies[164] demonstrated that MAO A localizes to the cytosolic face in intact rat liver mitochondria and in intact human placental mitochondria,[165] while MAO B resides in the intermembrane space,[164] which is in contrast to the topology of MAO A and MAO B exerted in the yeast *Pichia pastoris*.[164] This characteristic topology should be definitely studied in more detail in other tissues as it could provide a deeper insight into accessibility and permeability of the drugs across mitochondrial outer membrane (MOM) which very often is a complex process.[166]

2.3.1.3 Flavin-binding region

The protein structures around the FAD coenzyme are very similar between MAO A and MAO B. This region is comprised of four stranded parallel β-sheets sandwiched between three stranded antiparallel β-sheets and an α-helix.[151b] The crystal structure of MAO A and MAO B

confirmed previous degradation and sequence analysis studies[167] that have shown that the isoalloxazine ring of FAD cofactor is covalently bound to Cys406 (MAO A) or Cys397 (MAO B) *via* 8α-(S-cysteinyl)-riboflavin linkage.[151,152] The isoalloxazine ring is bent around N(5)-N(10) axis with an angle ~30° deviating from the planarity. As a consequence, the reactive centers of the flavin ring (N(5) and C(4a) atoms) can accommodate more sp^3 configuration than planar sp^2, which facilitates the formation of the covalent adducts at these positions with irreversible inhibitors. In addition, the peptide bonds between Cys406 and Tyr407 (MAO A) and Cys397 and Tyr398 (MAO B) are in a strained and less energetically favoured *cis* conformation, allowing however the formation of the "aromatic cage" in front of the flavin which is essential in positioning a substrate for the oxidation.[168] The extensive hydrogen bonding between the ribityl and ribose part of FAD and the protein as well as ionic interactions between the pyrophosphates and Arg residue and hydrophobic interactions between FAD and the enzyme residues play crucial role in the stabilization of the protein and FAD binding.[148a]

2.3.1.4 The active site of MAO A and MAO B and their differences influence on substrate and inhibitor selectivities

In human MAO A the active site is formed by a single cavity (ca. 550 Å^3) that extends from the flavin ring to the cavity-shaping loop (residues 210-216)[151] while the active site of human MAO B has a bipartite nature and is consisted of a 420 Å^3 hydrophobic flat 'substrate cavity' interconnected to an 'entrance cavity' (290 Å^3)[152] (Figure 29). The MAO A cavity is shorter in length and wider than the elongated and narrow cavity in MAO B. The substrate cavities in both isoforms are lined by a number of aromatic and aliphatic amino acids providing a highly hydrophobic environment. Additionally, hydrophobicity of the active site is supported by the flavin ring.

In human MAO B, the entrance cavity is a separate, smaller hydrophobic cavity, which is situated between the active site and the protein surface and is shielded from solvent by the

loop 99-112. Both cavities are separated by the following residues Tyr326, Ile199, Leu171 and Phe168. However, Ile199 proved essential in separating those two cavities and functions as a conformational 'gate keeper'. It can exist in either a "closed" or an "open" (two cavities fused with volume ~700 Å^3) conformation depending on the substrate approaching the active site. The corresponding residue in human MAO A would be Phe208. However it does not show any 'gating' function. The mutagenesis studies on MAO B in which Ile199 was mutated to Phe demonstrated that the bulky Phe residue abolished the conformational flexibility of the gating Ile residue, reduced the space of the entrance cavity and disallowed the binding of MAO B specific inhibitors, giving the evidence that Ile 199 serves as a structural determinant for the selective inhibition of human MAO B.[153]
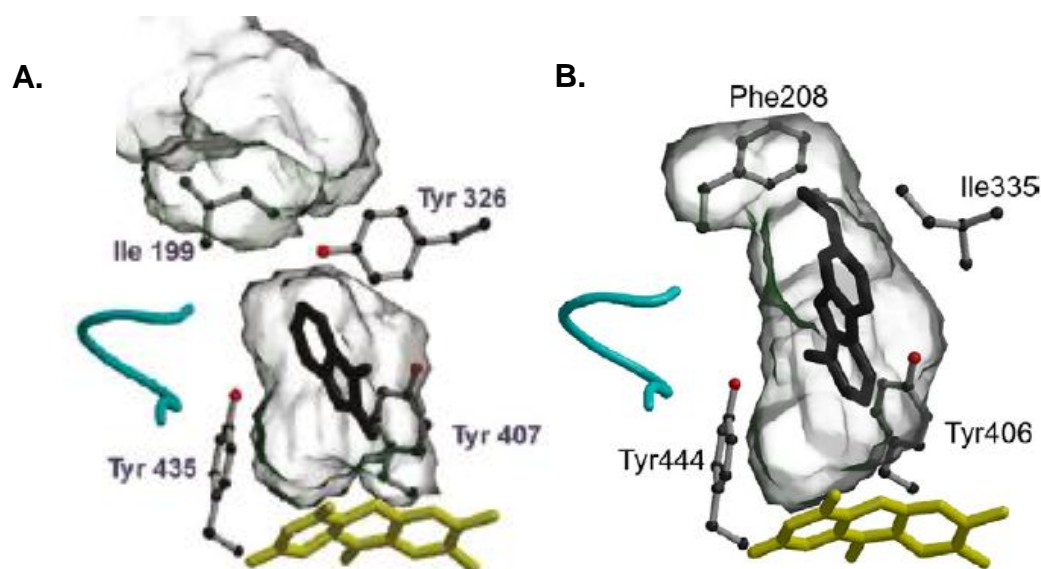
Figure 29. A. Active site structure for human MAO-B with isatin. (PDB Code 1OJA). Conformation of the Ile199 gating residue is in the closed conformation. B. Structure of the active site cavity of human MAO-A with harmine (PDB Code 2Z5X). Picture taken from Ref. [148 a].

Another pair of residues critical for substrate and inhibitor recognition is Ile335 in MAO A and the corresponding Tyr326 in MAO B. Tyr326 in MAO B is not directly involved in the separation of the two cavities. However, evaluation of the Tyr326Ala and Ile199Ala-Tyr326Ala MAO B mutants with respect to their binding properties with common substrates and inhibitors strikingly revealed loss of the specificity towards MAO B inhibitors and the demonstration of binding properties more similar to those of MAO A.[169] Conversely, displacement of Ile335 in MAO A to more bulky Phe would interfere with binding of the

specific substrate serotonin or the clorgyline inhibitor, but would allow binding of phenylethylamine and deprenyl.[170]

Other amino acid replacements (of the 20 residues constituting the active site, 7 residues are changed in identity) were found to be less significant regarding the substrate or inhibitor binding recognition. Figure 30 highlights residue differences in the active sites of MAO A and MAO B that affect substrate specificity.
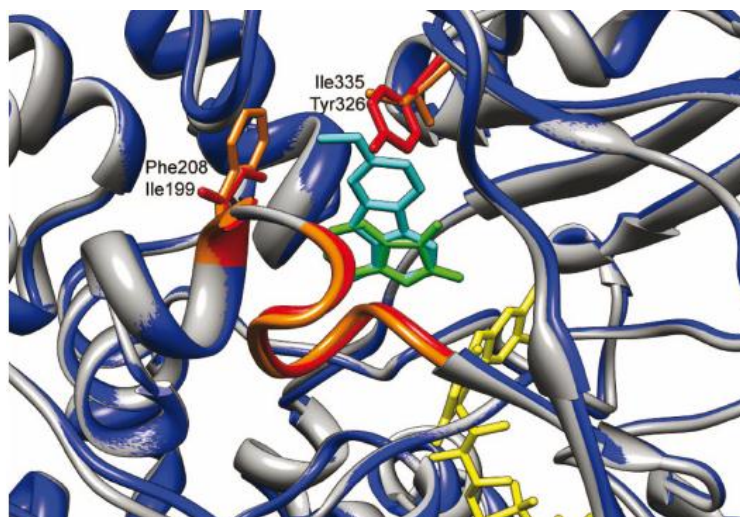
Figure 30. An overlay of the substrate-binding sites of hMAO B (PDB file 1OJA) and hMAO A (PDB file 2Z5X). MAO B is shown blue, and Ile199, residues 201-206, and Tyr326, are colored red; the inhibitor isatin is green. MAO A is shown in dark gray, with Phe208, residues 210-216, and Ile335 colored orange; the inhibitor harmine is cyan. The flavin cofactor is shown in yellow. Picture taken from Ref. [157].

On the other hand, highly conserved residues in both enzymes embrace the Tyr pair of the aromatic sandwich (Tyr407 and Tyr444 in hMAOA corresponding to Tyr398 and Tyr435 in hMAOB). These two tyrosines are situated on the re face of the isoalloxazine ring of the FAD in a perpendicular fashion, constituting a so called 'aromatic cage'. This region of the active sites of both enzymes is directly involved in the substrate oxidation, so this close similarity between MAO A and MAO B is consistent with the notion that both enzymes follow the same catalytic mechanism. The functional role of the 'aromatic cage' was investigated by kinetics and mutagenesis studies, which suggest that the aromatic cage has an important steric role in substrate positioning and its accessibility to the flavin as well as it facilitates polarization of the substrate increasing its nucleophilicity and hence susceptibility to efficient catalysis.[171]

Another conserved feature in the active site is the lysine residue hydrogen bonded *via* a water molecule to the N(5) atom of the flavin ring (Lys305 in MAO A and Lys296 in MAO B).

The substrate cavity lining loops 108-118 (MAO A) and 99-110 (MAO B) are also highly conserved in both enzymes, serving as a 'gating switch' and are situated close to the membrane binding region suggesting that the substrate must reach the active site from the protein surface oriented towards the membrane.

Overall, the active sites of MAO A and MAO B share a much conserved region in the proximity of the flavin cofactor enabling presumably the same catalytic mechanism for both isozymes. However, substrate and inhibitor recognition is highly controlled by 'gate keeper' residues, allowing entrance to the substrate cavity only for specific ligands.

2.3.2 Catalytic mechanism

Monoamine oxidases catalyze oxidative deamination of primary, secondary and tertiary amines to the corresponding imines, which are subsequently non-enzymatically hydrolyzed to the respective aldehydes or ketones with the release of ammonia or an amine. Molecular oxygen is consumed to re-oxidize the flavin cofactor with the concomitant formation of hydrogen peroxide (Scheme 1).

$$H_2O_2 \qquad O_2 + H^+$$

$$FAD \qquad FADH_2$$

$$RCH_2NR^1R^2 \longrightarrow RCHO + NHR^1R^2$$

$$MAO$$
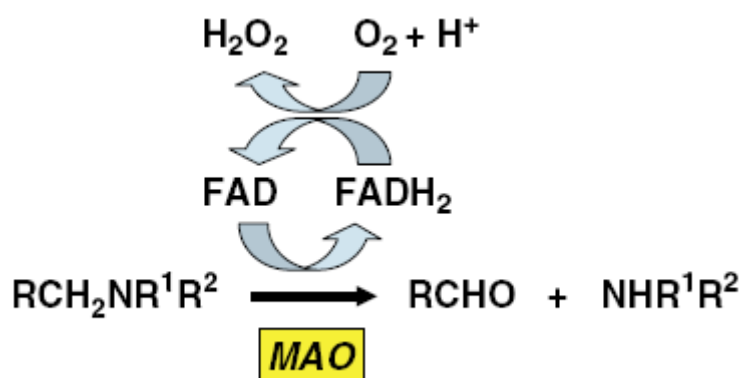
Scheme 1. Reaction catalyzed by MAO enzymes. Picture taken from Ref. [172]

In the reductive half reaction C_α-H bond of the amine substrate is cleaved with the transfer of the two reducing equivalents to the flavin which leads to the imine and flavin hydroquinone, respectively. In the oxidative half reaction O_2 is reduced to H_2O_2 on reaction with the flavin

hydroquinone. With most substrates, both enzymes follow this step *via* a ternary complex mechanism with the exception of MAO B with the phenylethylamine proceeding *via* ping-pong mechanism (Scheme 2).
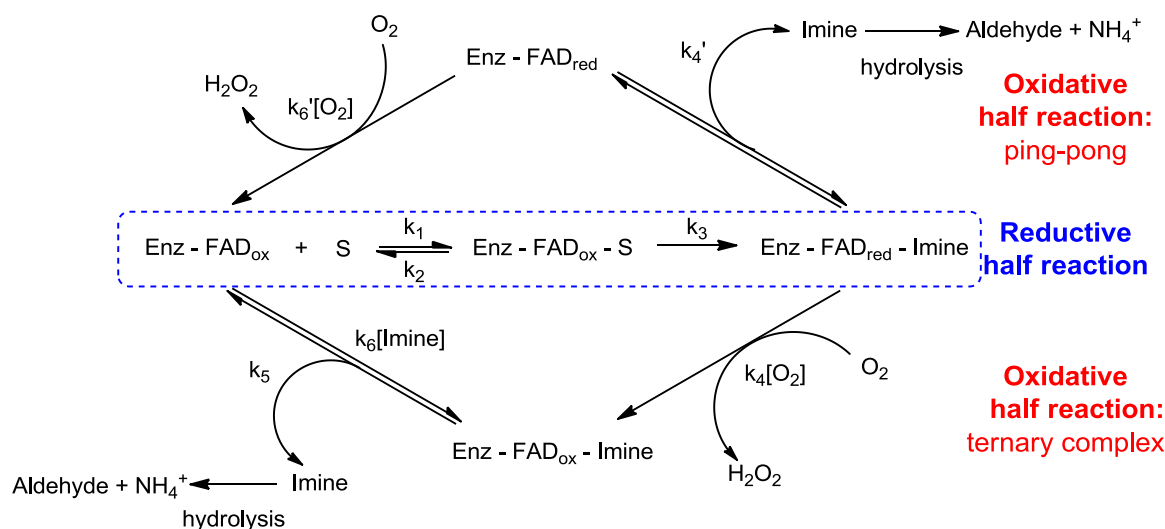
Scheme 2. General reaction scheme for MAO catalysis. Adopted from Ref. [147 b].

Stereospecifc removal of the pro-R hydrogen in the reductive half reaction could possibly occur by three different mechanisms: heterolytic hydride (H^-) transfer (1), heterolytic proton (H^+) abstraction (*via* single electron transfer (SET) (2a) or polar nucleophilic mechanism (2b) and hemolytic hydrogen atom ($H\bullet$) abstraction (3) (Figure 31).

Of these plausible mechanisms, the greatest controversy and extensive mechanistic studies are associated to single electron transfer (SET) mechanism postulated first by Silverman and co-workers[173] and polar nucleophilic mechanism proposed by Edmondson et al.[174]

In the SET mechanism the first step would be a reversible one-electron transfer from the lone pair on the amine nitrogen to oxidized flavin (Ox) to give an aminium cation radical and a flavin semiquinone (Sq) radical. Formation of the aminium radical results in a lowered pK_a of the α-C-H bond, which permits H^+ abstraction by an active site base in the catalytic site. Subsequent radical recombination with active site radical or second electron transfer to the flavin semiquinone would lead to the imine product and reduced flavin hydroquinone (Hq). However, the structural data on MAO B shows no amino acid residues in the catalytic site that could perform the role of an active site base.[152] Also, many other experiments designed

to probe this mechanism were not successful in providing unambiguous evidence for SET mechanism. Neither flavin radical intermediates could be detected using rapid-scanning or single wavelength stopped-flow absorbance spectroscopy measurements,[174-177] nor influence of magnetic field on the enzyme flavin reduction rate could be observed.[177] In addition, the thermodynamic barrier for single electron transfer is very high, with the high redox potential of amines (approx. 1.5 V)[178] making them unlikely to be oxidized by the flavin (+0.043 V for Ox/Sq and +0.037 V for Sq/Hq couple)[179] and no other apparent oxidant exists in the MAO active site.

(1) Hydride Transfer Mechanism

(2a) Single Electron Mechanism (SET)
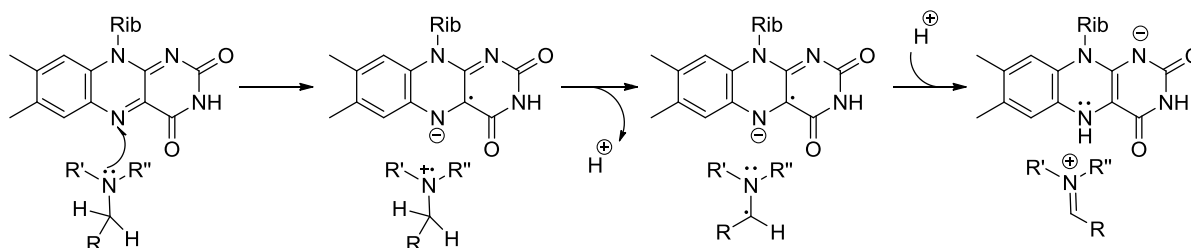
(2b) Polar Nucleophilic Mechanism
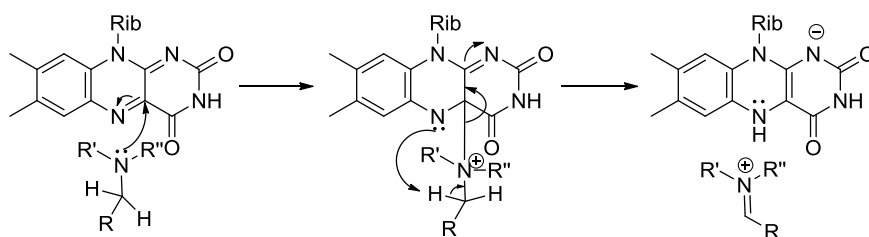
(3) Hydrogen Atom Transfer Mechanism
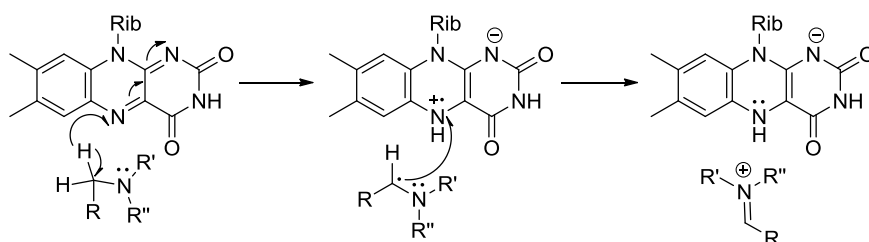
Figure 31. Mechanisms proposed for amine oxidation by MAO enzymes. Adopted from Ref. [158].

The major evidence used by Silverman to support SET mechanism was based on a chemical approach to detect radical intermediates, which were believed to be too short-lived or paired with another radical to be detected in spectral measurements. Silverman and coworkers[180,181] as well as Rimoldi et al.[182] prepared a wide range of chemical reporters based on cyclopropyl or cyclobutyl amines which inactivated MAO enzymes with subsequent ring opening, a reaction typical for radicals. Such reactive intermediates could be potentially trapped (by for instance Cys residues on the enzyme surface)[180] and analysed by MS delivering the support for this mechanism. However, these experiments do not provide sufficient evidence in favour of this mechanism.

Current mechanistic data support the polar nucleophilic mechanism proposed by Miller and Edmondson[174] and are based on QSAR steady-state and anaerobic stopped-flow kinetic studies on *p*-substituted benzylamines[174] and phenylethylamines[175] analogues reacted with human MAO A and *p*-substituted dimethylbenzylamine or *p*-substituted α-methylbenzylamine with MAO B.[183] These experiments along with large kinetic isotope effects (KIE) demonstrated that the α-C-H bond cleavage is the rate-limiting step in the MAO catalysis.

In this mechanism, the deprotonated amine functionality attacks nucleophilically the flavin coenzyme at the C(4a) position as the initial step in catalysis. The flavin is in a bent non-planar conformation[151,152] with N(5) atom close to sp^3 configuration which results in higher electron density at N(5) and lowered electron density on C(4a) (indicated by ^{15}N and ^{13}C NMR studies[184]), thus the formation of C(4a) adduct is facilitated. In addition, although deprotonated amines do not exhibit nucleophilicity to readily add to the C(4a) position, the necessity to approach the flavin through two tyrosyl residues activates the amine through interactions with dipole moments of the tyrosyl 'aromatic sandwich'.[171] On formation of such an adduct, the N(5) position of the flavin becomes a strong base (pKa ~ 25[185]), which exhibits sufficient basicity to abstract the α-pro-*R*- H from the substrate (pKa of the benzyl hydrogen is ~ 25[186]). This proton abstraction can be concerted with either the adduct or the product formation.[187] The proximity of the benzyl C-H bond with the N(5) of the flavin is consistent with the absolute stereochemistry exhibited for C-H transfer.

Interestingly, quantitative structure-activity relationship (QSAR) studies showed significant differences in factors influencing the substrate binding and enzyme reduction for MAO A[174] and MAO B.[176] MAO B affinity towards benzylamine analogues augmented with increasing hydrophobicity (π parameter) of the *p*-substituent and exhibited a small negative influence of van der Waals volume (V_W) on binding, suggesting a hydrophobic surrounding with steric constraints on *p*-substituent. On the other hand, the binding affinity of MAO A increased with the increasing van der Waals volume of the *p*-substituent, indicating a much more spacious binding pocket in the active site. The rate of flavin reduction in MAO B was not correlated with electronic effects (σ parameter), which is in contrast to MAO A, in which electron withdrawing substituents enhanced the rate of α-C-H bond cleavage by facilitating delocalization of electron density on the arene ring. This observation (positive ρ value ~2) is consistent with the notion of the negative charge developing at the α-carbon in the transition state, corresponding to a proton abstraction mechanism for α-C-H bond cleavage. These discrepancies can result from different mechanisms operative for both MAO isoforms (polar nucleophilic mechanism for MAO A (?) and non-concerted hydride transfer for MAO B (?),[188] or from the constrained orientation of the aromatic ring of benzylamine in MAO B which disallowed transmission of the electronic effects.

Recent nitrogen kinetic isotope effect studies[187] suggested that α-hydrogen abstraction is however not concerted with nitrogen atom rehybridization and preceeds or follows the partially rate-limiting nitrogen bond-change. Therefore, a concerted scenario, such as simultaneous hydride transfer, operational for instance for amino acid oxidases,[189] could be ruled out for MAO catalysis. However, this study could not unambiguously discriminate between the radical and polar mechanism for the reductive half reaction.

Also, several computational studies took lately the encounter of evaluation of the catalytic mechanisms postulated for monoamine oxidases[190-192] and their results are mostly in favour of polar nucleophilic mechanism.[191,192] However, they should be considered with caution as they cannot reflect the real catalytic or inhibition process. Doubtlessly, additional extensive experimental (NMR, EPR, stopped-flow kinetics, isotope labeling) and computational work is

required to dissipate all uncertainties and controversies and provide a clear image of MAO catalysis.

2.3.3 Biological role

Due to the involvement in complex metabolism of amine neurotransmitters in the central nervous system, [193,194] monoamine oxidases play an essential role in regulation of brain development and its functioning.[193,195] They also protect neurons from exogenous amines and regulate the intracellular redox state in neurons and other cells.[193,195] In peripheral tissues such as the intestine, liver, lungs and placenta MAOs have a neuro- and cardioprotective function by oxidizing various exogenous and dietary amines from the blood or by preventing their entry into the circulation.[195] The most famous example of these detrimental effects is the 'cheese effect', a hypertensive crisis caused by the absorption of sympathomimetic amines (e.g. tyramine) from fermented food (cheese, wine etc.), following the administration of MAO inhibitors.[196] Similarly, MAO B in the microvessels of the blood-brain barrier acts as a metabolic barrier.[195] The by-products of MAO activity, aldehydes, ammonia and hydrogen peroxide, might have regulatory and signaling functions[197] (the aldehydes derived from serotonin and noradrenaline are implicated in the regulation of sleep[198]), however, they are also cytotoxic, especially at higher concentrations.[199] Hydrogen peroxide is a potent oxidizer which can trigger formation of many reactive oxygen species (ROS) which in turn can induce permanent damage of neurons and glia.[199d]

Abnormal MAO activity, mostly due to disruption of MAO genes or age-related changes in their expression levels in different tissues, is associated with many behavioral, neurological, neurodegenerative and cardiological disorders.

For instance, it was found that MAO A deficiency caused by a spontaneous mutation in MAO A gene was responsible for a borderline mental retardation and impulsive aggressive and antisocial behavior in a large Dutch kindred.[200] Other studies have shown that people with low levels of MAO A are prone to aggressive behavior often to response to minor

stressors.[201] Similarly, MAO A knock-out mice[202] have demonstrated elevated aggressiveness,[202] reduction in exploratory activity,[203] maladaptive defensive behaviors[204] and low levels of depression-like behaviors, suggesting the crucial role of serotonin (5-HT) in these processes. Selective deletion of MAO B have not been reported in humans, to enable its correlation to any phenotypical outcomes. However, low platelets MAO B levels in patients (which exclusively contain MAO B) have been associated with broad spectrum of personality traits such as sensation- and novelty seeking, extraversion, impulsiveness and addictive behaviors (smoking, alcoholism and gambling).[205] MAO B knock-out mice[206] have shown traits of behavioral disinhibition and reduced anxiety-like behaviors.[207] However, also some discrepancies appeared when comparing mice behavior to personality traits in humans linked to MAO B deficiency,[208] indicating that the animal model is not always substantial in studying human disorders as these changes might be a result of different dopamine metabolism in humans and rodents.[209] Complete deletion of both MAO genes in humans[210] and mice[211] resulted in a range of severe abnormalities, including major developmental delay, mental retardation, anxiety-like behaviors, episodic hypotonia and stereotypical movements[210] clearly suggesting a critical role of MAO A and B in the earliest stages of brain development. A very recent example of a de novo Xp11.3 microdeletion exclusively encompassing MAO A and MAO B genes[212] in a male infant showcased a similar phenotype along with hallmarks of autism-spectrum disorder. But a personalized medicine approach to this patient strives to normalize his MAO-linked metabolites profile and prevent cardiovascular complications as well as gain a deeper insight in the role of MAO A and MAO B in the overall development.

On the other hand, age-related increases of expression levels of MAO A in the heart[213] and MAO B in neuronal tissue[214] have been associated with the development of cardiovascular[215] and neurodegenerative disorders,[216] respectively. Elevated levels of MAO B in the brain cause increased metabolism of dopamine and thus significantly diminish its levels in neuron tissue which may result in the loss of dopaminergic neurons in *substantia nigra,* which underlies neurodegenerative Parkinson's disease (PD).[216] Additionally, higher activity of MAO B results in increased levels of the catalytic reaction products, dopanal and

hydrogen peroxide. Dopanal has been implicated in α-synuclein accumulation involved in the etiology of PD,[217] whereas elevated amounts of H_2O_2 in neurons, involved in ROS generation, can promote apoptotic signaling events leading to the damage of dopamine producing cells thus to the development of PD.[216] Moreover, MAO B activates oxidation of MPTP to MPP^+, which is a known parkinsonogenic neurotoxin.[218] Collectively, these observations suggest a very complex role of MAO enzymes in neurodegenerative diseases. On the other hand, increased levels of MAO A in the heart are indicated to underlie enhanced apoptosis and necrosis of cardiac cells due to elevated levels of reactive oxygen species generated from hydrogen peroxide,[213] which might be one of the major factors contributing to heart failure and ischemia/reperfusion injury.[215]

2.3.4 MAO inhibitors and their therapeutical application

Involvement of monoamine oxidases in a variety of pathological processes and severe diseases resulted in the intensive development of MAO inhibitors (MAOI). Since the serendipitous discovery of the first hydrazine MAO inhibitor (isoniazid) which exhibited anti-depressant properties in tuberculosis patients[219] the field of investigations for potent MAO inhibitors underwent a long way including the fall after identification of severe side-effects and hepatotoxicity of many non-selective irreversible MAO used for the treatment of depression (e.g. iproniazid, tranylcypromine) and the spectacular recurrence after discovery of positive effects of selective MAO B inhibitors (deprenyl, rasagiline) in the treatment of Parkinson´s disease. Currently, several MAO inhibitors are clinically used for the treatment of depression, Parkinson's disease, anxiety disorders (obsessive-compulsive disorder) and are under clinical investigations for the treatment of other mental and neurological diseases.[172,195,220] Also, several very effective MAO inhibitors are only used as chemical or pharmacological tools due to their severe side effects or unsuccessful clinical trials.

The first generation of MAO inhibitors embraced non-selective and irreversible inhibitors based on hydrazine structure (Figure 32 A), which were used as antidepressant and

psychotropic drugs. After isoniazid (Laniazid®),[219] many other hydrazine compounds were developed such as iproniazid (Marsilid®), phenelzine (Nardil®), isocarboxazid (Marplan®), nialamide (Niamid®), pheniprazine (Catron®), and octamoxin (Ximaol®). The hydrazine moiety is a very reactive group, which undergoes MAO mediated oxidation followed by the formation of a covalent adduct with the N(5) atom of the flavin ring.[221] Despite of their high potency in handling depressive diseases, the chronic treatment with these drugs led to the impairment of the patient metabolism and liver toxicity (mainly due to the inhibition of cytochrome P450 enzymes),[222] thus they were withdrawn from the clinics. Currently, only phenelzine (Nardil®) is sporadically used in the treatment of atypical depression and anxiety disorders.[223]

Hydrazine MAO inhibitors were replaced later by the unselective and covalent antidepressant drug tranylcypromine (Parnate®) (*trans*-2-phenylcycloprropylamine, Figure 32 B), which is a mechanism-based inhibitor forming a covalent adduct to C(4a) atom of the flavin cofactor.[152a] Tranylcypromine was indeed devoid of hepatotoxicity side effect, but it was causing hypertensive crisis[196,224] ('cheese effect') in many patients leading even to their death, so it was removed from the market in the 1960's. However, similar to phenelzine, tranylcypromine was reintroduced in the clinics and is still applied in the treatment of major depressive disorder or post-traumatic stress disorder, however under strict diet conditions to prevent cardiovascular complications.[225]
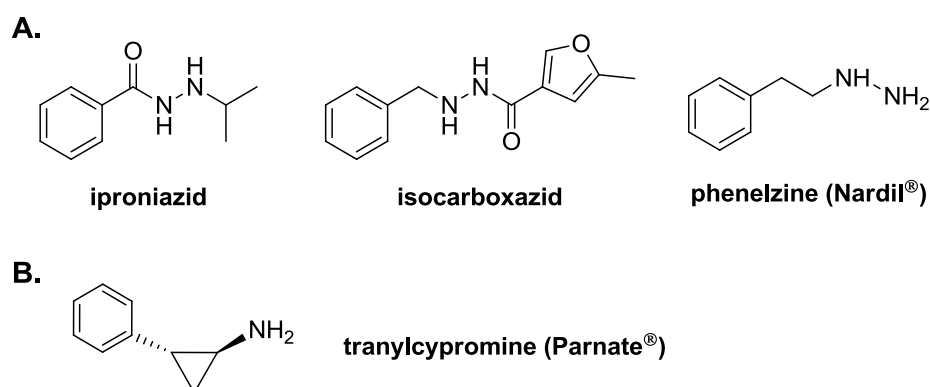
Figure 32. First generation of antidepressant MAO inhibitors. A. Hydrazine-based non-selective irreversible MAO inhibitors. B. Non-selective irreversible MAO inhibitor tranylcypromine.

These severe side effects caused by non-selective MAO inhibitors stimulated the search for other antidepressive drugs such as tricyclic antidepressants or selective-serotonin re-uptake inhibitors (SSRI), and MAO inhibitors were removed from the clinical spotlight, however the medical research on new MAO inhibitors was still pursued.

The next generation of MAO inhibitors included selective irreversible compounds featuring a propargylamine moiety (Figure 33). While pargyline (Eutonyl®) was still an unselective MAO inhibitor,[226] clorgyline and selegiline have been historically used to distinguish between the two isozymes being MAO A- and MAO B-selective, respectively.[148,227] Clorgyline revealed antidepressant properties,[228] however, due to its side effects (mostly 'cheese reaction') it was only used as research tool.[172] Selegiline known also as deprenyl (Deprenyl®, Eldepryl®) was and still is used in the treatment of Parkinson's disease as monotherapy[229] in the early stadium of the disease or as an adjuvant to L-DOPA[230] treatment by increasing levels of dopamine and 2-phenylethylamine in the brain but also by serving a putative neuroprotective and anti-apoptotic role which is not correlated to MAO B inhibition. Deprenyl in the form of a transdermal patch[231] (Emsam®) is also used to treat major depressive disorder. More recently, another compound belonging to this group, rasagiline, was introduced and similar to deprenyl is used in the treatment of Parkinson's disease, even with higher efficacy and without the neurotoxic effects of deprenyl as it is not degraded to amphetamine.[232,233] All propargylic MAO inhibitors form a stable covalent N(5) flavocyanine adduct, different from those formed by hydrazine compounds or tranylcypromine and which was unambiguously defined from several crystal structures of MAO with those inhibitors.[151,152,234]

**pargyline
(MAO A/B)** **clorgyline
(MAO A)** **L-deprenyl (Eldepryl®)
(MAO B)** **rasagiline (Azilect®)
(MAO B)**
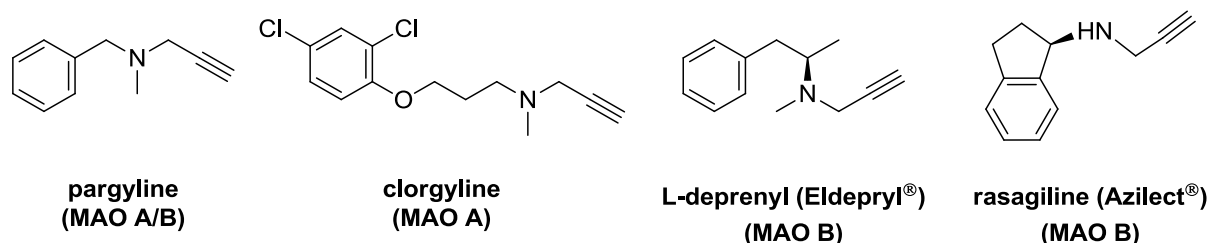
Figure 33. Irreversible acetylenic MAO inhibitors.

The most recent class of MAO inhibitors includes selective and reversible MAO A (RIMA) (Figure 34 A) and MAO B inhibitors (Figure 34 B) comprising structurally diverse compounds such as piperidylbenzofurans, morpholinobenzamides, oxazolidinones and others. Moclobemide (Aurorix®), toloxatone (Humoryl®), brofaromine (Consonar®) or pirlindole (Lifril®) are only few examples of selective MAO A inhibitors clinically used in the treatment of depression and anxiety.[235,236] Lazabemide (Pakio®), safinamide and zonisamide (Zonegran®) are MAO B reversible inhibitors, which are already used or are still under investigation as antiparkinsonian drugs.[237-239] Additionally, zonisamide is used as an antiepileptic agent.[239]
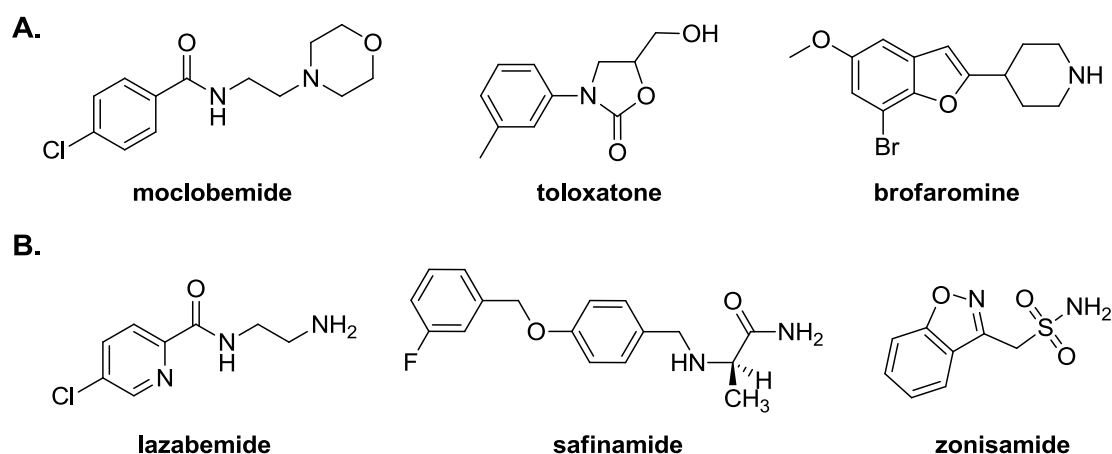
Figure 34. MAO reversible inhibitors. A. MAO A selective inhibitors. B. MAO B selective inhibitors.

Another interesting group of inhibitors are bifunctional inhibitors combining pharmacophores for MAO enzymes and acetylcholinesterase (AChE), which can be used as potential drugs in the treatment for Alzheimer's disease and diffuse Lewy Body disease like ladostigil[240] or the newly developed compound named ASS234.[241] Another example of such dual inhibitor would be M30 which combines pharmacophore for MAO inhibition with iron-chelating activity to be used as active agent against increased oxidative stress in brain[242] (Figure 35).
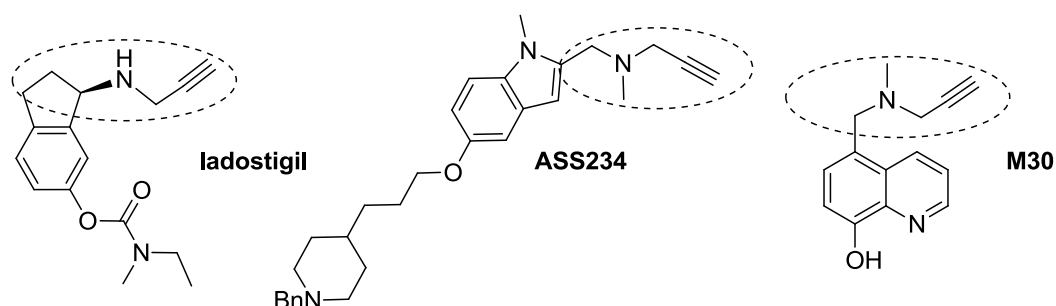
Figure 35. Structure of bifunctional inhibitors comprising a MAO pharmacophore (highlighted as dashed circle).

In addition to these purposely developed MAO inhibitors, a number of environmental and food molecules were discovered to bind non- or highly selectively to MAO enzymes. For instance, farnesol, isatin, 1,4-diphenyl-2-butene or 8-(3-chlorostyryl)-caffeine are potent and selective reversible MAO B inhibitors[153,243] (Figure 36 A), whereas methylene blue, harman or pirindole exhibit selective and reversible MAO A inhibition[244] (Figure 36 B).
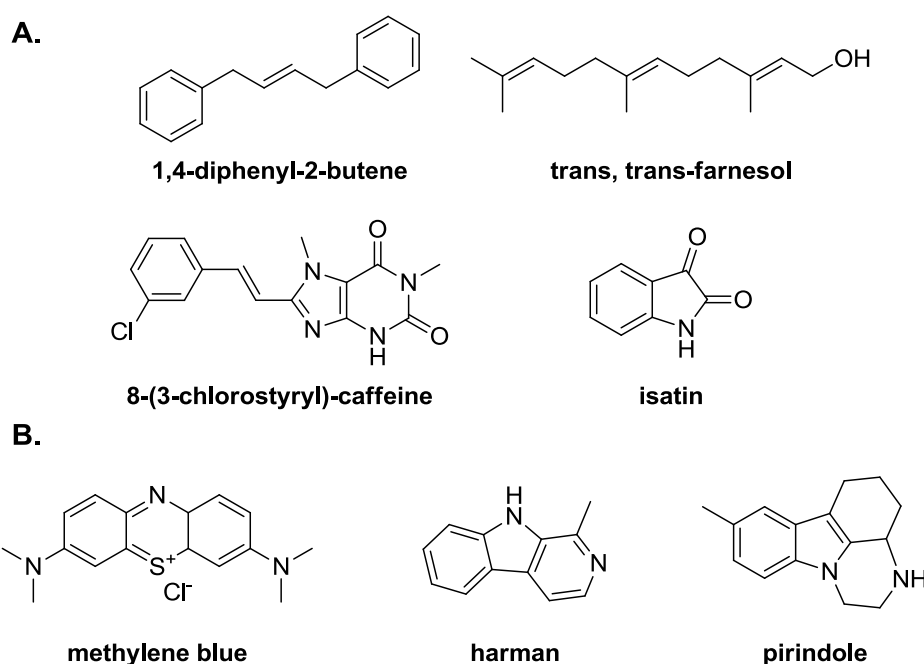
Figure 36. Environmental selective MAO inhibitors. A. MAO B selective. B. MAO A selective.

Also, very extensive computational[245] and experimental work[246] is being pursued in many research groups to design, synthesize and evaluate new potent and selective MAO inhibitors, which eventually could enter the clinics and help in the treatment of numerous disorders connected to MAO enzyme activity.

3 Aims of work

Elucidation of the biochemical and physiological functions of enzymes is one of the utmost endeavors for researchers in a post-genomic era. Profound spatiotemporal and quantitative understanding of proteins activity on the molecular level could not only aid deciphering complex biochemical pathways but also would provide the most wanted means for identifying important therapeutical targets across different pathological processes and diseases. In this way, the basic research would enter into the clinics, unifying everybody in the inevitable ambition of leading a healthy and long life.

Among a wide array of genomic and proteomic methods, Activity-Based Protein Profiling (ABPP) has emerged as a very efficient and direct strategy to study the functional state of enzymes by using small molecule probes.[13,14] To date, a great number of activity-based probes were prepared to interrogate the activity of many enzymes in a specific manner. However, one of the most challenging aspects of ABPP is expanding the pool of probes towards enzymes with more complex activities or which are very low abundant in the proteome or display low stability.

Hence, one of the major goals of this work was the development of new activity-based probes which would be dedicated to enzymes so far not addressed by ABPP. We decided to take the challenge of developing ABPP strategy towards flavin-dependent oxidases. This complex subclass of flavoenzymes oxidizing a wide range of substrates, exhibit a very low level of sequence identity as well as do not possess conserved motifs and nucleophilic residues in the active site that makes the annotation of these enzymes a very difficult task. In contrast, ABPP could serve as a simple alternative for global profiling of these enzymes.

We envisioned that new activity probes could be based on binding affinity of a probe activated through its oxidation by the enzyme, towards a flavin cofactor, which is intrinsically involved in the catalytic mechanism and is the only common feature across the whole family of these enzymes (Figure 37).
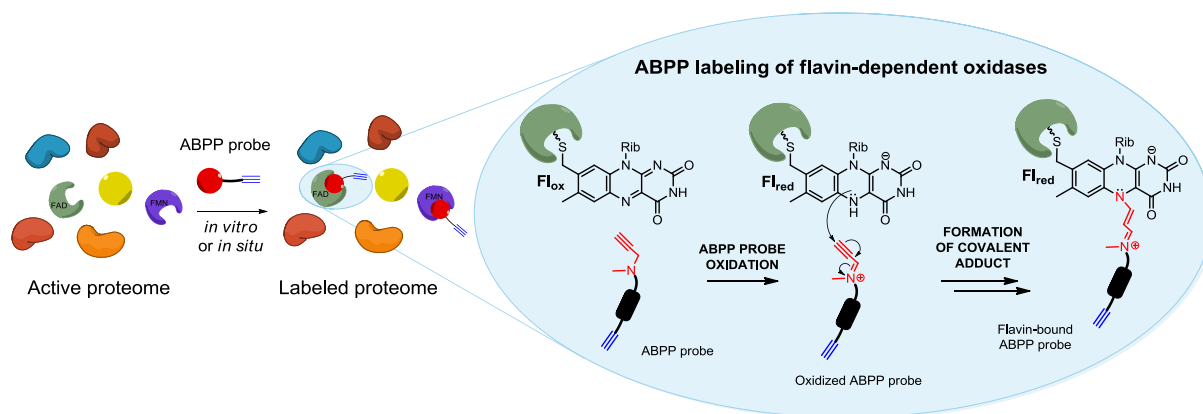
Figure 37. The concept for ABPP labeling of flavin-dependent oxidases.

To accomplish this challenging task, the first aim was to design a general core structure of a probe, including the selection of the warhead, and to develop a synthetic methodology, which would allow the robust and easy preparation of activity-based probes.

As the family of flavin-dependent oxidases is very complex, we decided to focus our efforts on monoamine oxidases (MAO), which are representative enzymes belonging to this group of flavoenzymes. Beyond their biological and therapeutical significance, we considered an extensive research towards elucidating their structure, catalytic mechanism and finding selective and potent inhibitors very useful for our purposes. This knowledge should help us to design the effective activity-based probes inspired by MAO inhibitors and validate the novel labeling mechanism on a well-known and studied protein target.

Successively, the next goal was the preparation of fluorescent tags compatible with 'tag free' click chemistry approach, which was selected to be applied to append the tag onto the probe. We planned to use for this purpose inexpensive and commonly used NBD- and TAMRA-based fluorescent tags.

Subsequently, our aim was to establish optimal conditions for enzyme labeling and evaluate the potential of developed ABPP strategy *in vitro* using *Pichia pastoris* membrane preparations overexpressing human monoamine oxidase in terms of the scope of probes collection, enzyme target selectivity as well as sensitivity of labeling and binding site of the probe to the enzyme. Moreover, we planned to screen other available flavin-dependent

enzymes using the developed ABPP system to check its range for profiling other protein targets.

Furthermore, it was of utmost interest to investigate the applicability of the established ABPP system in native biological systems both *in vitro* and *in vivo*. We were very interested to evaluate the potency and selectivity of the best probes in profiling of monoamine oxidases in far more complex biological samples (tissue lysates, live cells). In addition, we wanted to find out if these probes are able to target other flavin-dependent enzymes, including off-targets of drugs deprenyl and pargyline, which served as parent structure for the designed activity-based probes.

Finally, we aimed in finding a practical application of the ABPP system. We estimated that very specific probes for monoamine oxidases could serve as efficient tools for the discovery platform (competitive ABPP or fluopol-ABPP) for new potent and specific irreversible MAO inhibitors. Additionally, the probes could be efficiently used for imaging of active enzymes and localization studies in a real disease model, in which MAO enzymes are implicated as key players. Moreover, the MAO specific probes could be used as tool compounds for rapid evaluation of expression levels of monoamine oxidases in the live *Pichia pastoris* cells.

4 Results and Discussion

4.1 Design and synthesis of activity-based probes for monoamine oxidases

4.1.1 Design of ABPP probes inspired by irreversible MAO inhibitors

Each activity-based probe (ABP) contains three structural elements: a warhead, a binding group or a linker and a reporter tag. The careful design of these three elements is essential in providing a satisfactory selectivity towards target enzymes and an efficient visualization method of the labeled enzymes.

The design of ABPs for monoamine oxidases, which were chosen as demonstrative examples of flavin-dependent oxidases, was greatly facilitated by the accessibility to the crystal structures of both isozymes[151,152] and the extensive investigations on selective and potent MAO inhibitors.[219,225-231,235-242]

Several irreversible MAO inhibitors form stable covalent adducts with the flavin cofactor and their existence has been unambiguously assigned by spectral studies and crystal structures of MAO with phenelzine (N(5) adduct),[221] tranylcypromine[152a] (C(4a) adduct) and with acetylenic inhibitors such as deprenyl,[152] clorgyline,[151] or rasagiline[234] (all N(5) adduct) (Figure 38). Hence, we selected the *N*-propargylamine group to serve as a warhead of the designed ABPs, which will form a stable covalent bond to the active site of MAOs.
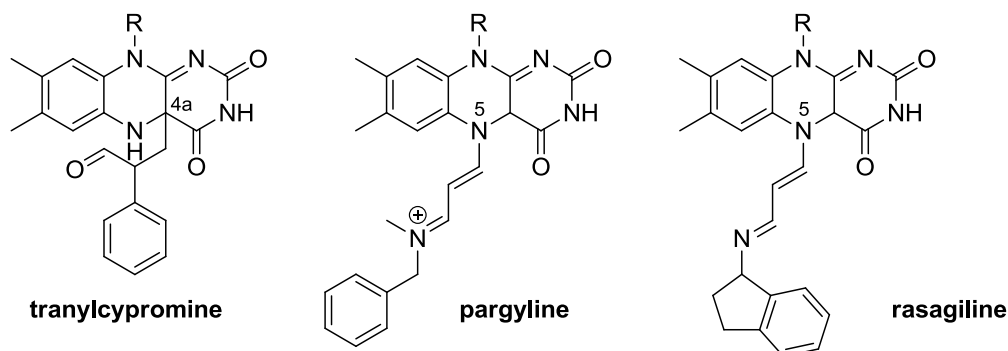
Figure 38. Covalent adducts of MAO inhibitors with the flavin cofactor.

This reactive group is essentially involved in the irreversible inhibition of monoamine oxidases. In the initial step of this 'suicide' inhibition mechanism, the amine group undergoes catalytic oxidation to an iminium cation mediated through the FAD cofactor. This provides a reactive intermediate resembling a Michael acceptor, which can be nucleophilically attacked by the N(5) atom of the isoalloxazine ring leading to the formation of the covalent adduct. We anticipated that activity-based probes built on these inhibitors will employ the same labeling mechanism (Figure 39).
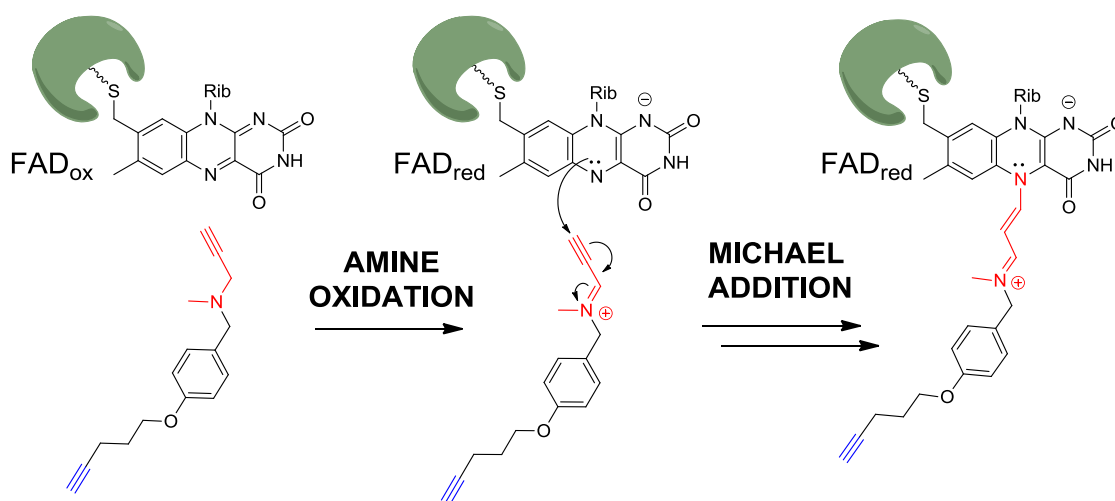
Figure 39. Labeling of activity-based probes dedicated to monoamine oxidases.

The highly hydrophobic environment of the major part of the active site cavity of both MAOs[151,152] favors a tight binding of apolar molecules due to possible hydrophobic interactions. Therefore, a binding group should be hydrophobic and aromatic or heteroaromatic rings are preferential structures, which are very frequently found in a wide range of MAO substrates and inhibitors. Hydrophilic substituents could be positioned only in the proximity of the reactive group of the ABP since the only hydrophilic region in MAOs is situated near the flavin ring and is required for recognition and directionality of the substrate amine functionality.[152a] It is formed by several ordered, captive water molecules that fill a vacant space in the substrate/inhibitor binding cavity. This would enable to incorporate some hydroxy- or oxo-substituents into the ABP, which could displace these ordered water molecules and increase the affinity of the ABP to the enzyme active site by hydrogen bonding.

Finally, the reporter tag should be attached at the distal position to the reactive group, preferably in *para* position to the warhead at the aromatic ring, *via* an alkyl, alkoxy or peptide linker. As we opted for a two-step 'tag-free' approach for labelling we decided to use small 'clickable' handles as azide or alkyne group at the end of a linker.

The above mentioned considerations, additionally supported by numerous SAR and experimental studies on MAO inhibitors,[245,246] enabled us to construct the desired ABP, which would combine the *N*-propargylamine group as a warhead, favourable structural features of the binding group and click chemistry compatible reporter tag (Figure 40 A). Subsequently, we collected several chemical scaffolds and analytical tags, fulfilling the aforementioned requirements. (Figure 40 B and 40 C).

A.

propargylamine group
for covalent binding to flavin cofactor

small CC compatible group (azide, alkyne)
attached at the distal position to reactive group
via alkyl or alkoxy linker

highly hydrophobic structure (aromatic or heteroaromatic)
to interact with the hydrophobic lining of the active site
hydrophilic groups only in the proximity of the warhead

B.

R=H, Me   R'=H, Me   R"=H, OH

C.

TAG = azide, alkyne, biotin, fluorophore

Figure 40. Possible chemical scaffolds for ABPs for MAOs (A) and analytical tags (B).

Consequently, the simplest scaffold based on pargyline inhibitor has been chosen as a model ABP. From a wide range of reporter tags available the latent 'clickable' azide group attached to an alkoxy linker has been selected. This resulted in the following chemical structure which represents the first ABP designed for MAO enzymes (Figure 41).

TAG   LINKER   BINDING REGION   WARHEAD

R = Me or H
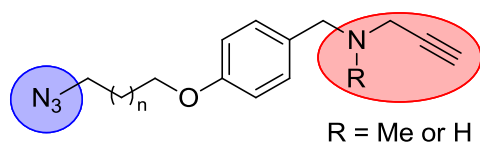
Figure 41. The first ABP designed for monoamine oxidases. The warhead is highlighted by a red circle, a reporter tag by a blue circle.

The first ABP for monoamine oxidases used a robust and unspecific aromatic scaffold as we wanted first to prove the concept of our approach and also be able to extend it to other flavin-dependent oxidases.

4.1.2 Development of synthetic strategies for activity-based probes

Once the first ABPP probe has been designed (Figure 41), retrosynthetic analysis was performed to plan the synthetic route (Scheme 3). The attachment of the propargylamine moiety should occur *via* substitution of the appropriate bromide **2** obtained from the *O*-substituted *p*-cresol (**3**) by the radical bromination at the benzylic position. Bromination should follow the substitution by sodium azide of (3-bromopropoxy)-4-cresol (**4**) to avoid the possible complications of double substitution when it would be performed at an earlier stage. Thus, the starting material turned out to be the commercially available *p*-cresol (**5**).
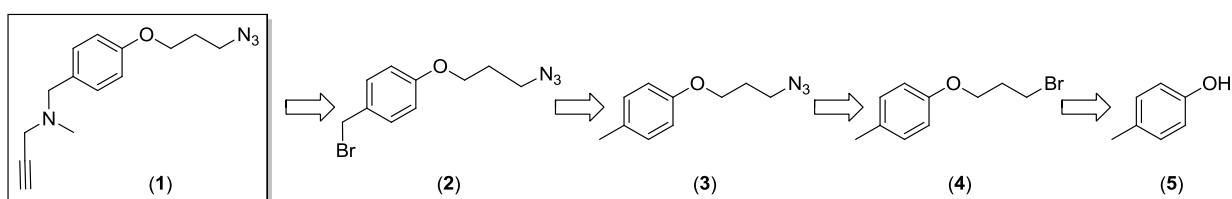
Scheme 3. Retrosynthetic analysis of the first ABPP probe.

4.1.2.1 First approaches

The synthesis started with the reaction of *p*-cresol (**5**) with 1,3-dibromopropane according to the protocol reported by Kubota et al.[247] To avoid the disubstitution by-product, high dilution conditions and 5-fold excess of 1,3-dibromopropane were used. However, the disubstituted

product was formed in approx. 20% (GC-MS) and it was difficult to separate it from the product either by flash column chromatography or distillation (only 60% yield in 83% purity). Also, the outcome of the alkylation of *p*-cresol with 1,3-dibromopropane was not improved when phase transfer catalysis conditions were applied using tetra-*n*-butylammonium bromide (TBAB) as catalyst as described by Reinholz and co-workers.[248] The most satisfactory results were obtained when a phenolic version of Mitsunobu reaction according to Bosanac and Wilcox[249] between *p*-cresol and 1-bromo-propanol was used furnishing the product **4** in 71% yield (Scheme 4).
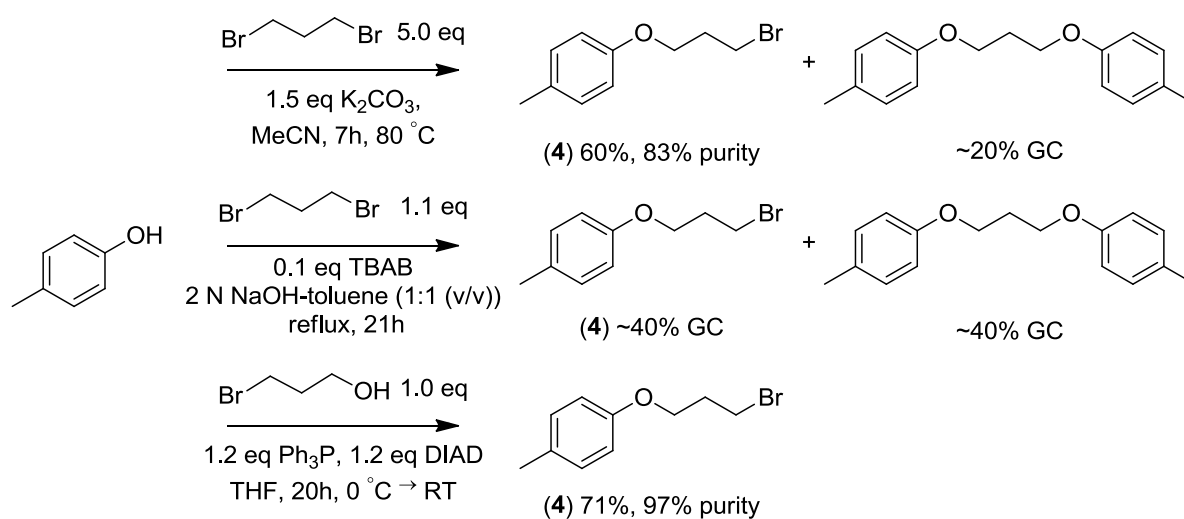
Scheme 4. Applied methods of substitution of *p*-cresol.

Subsequently, the nucleophilic substitution of product **4** with sodium azide, using procedures from Yilmaz et al.[250] and Wang et al.,[251] resulted in (3-bromopropoxy)-4-cresol (**3**) in good yield (89%) (Scheme 5 A). Next, the product was subjected to a radical bromination using *N*-bromosuccinimide (NBS) and dibenzoylperoxide as radical activator according to the general procedure used in the practical course.[252] Unfortunately, instead of the desired product **2** brominated at the benzylic position, the ring substituted product **6** was formed due to the strong activation effect from the alkoxy group present at the aromatic ring,[253] which was confirmed by NMR analysis of the reaction product (Scheme 5 B).

A.

B.
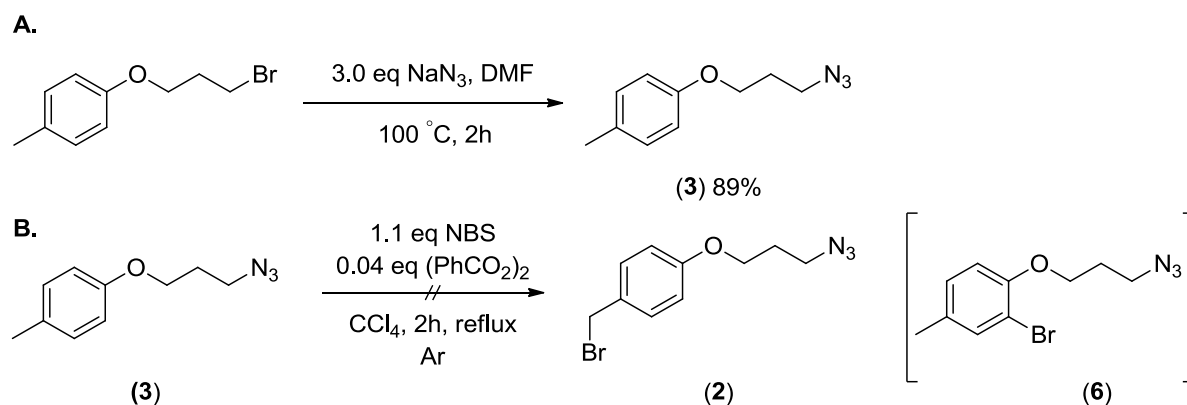
Scheme 5. A. Substitution of product **4** with sodium azide. B. Unsuccessful radical bromination of compound **3**.

This situation has led to the modification of the original synthetic plan. Previous successful application of Mitsunobu reaction gave the indication that compound **2** can be synthesized from azidoalcohol **7** and 4-hydroxybenzyl bromide (**8**), obtained by substitution with NaN_3 of 3-bromopropan-1-ol and bromination of 4-hydroxybenzyl alcohol, respectively (Scheme 6).
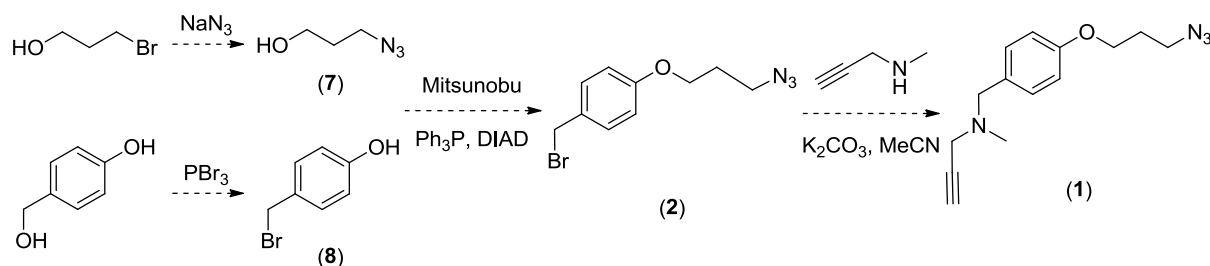
Scheme 6. Modified synthetic route leading to compound **1**.

The conversion of 3-bromopropan-1-ol to the corresponding 3-azidopropan-1-ol (**7**) proceeded smoothly by heating the substrate with sodium azide in water overnight (91% yield), using the procedure from Aucagne et al.[254] (Scheme 7A). On the other hand, considerable difficulties were encountered in converting 4-hydroxybenzyl alcohol to the corresponding bromide **8**. Neither traditional bromination by phosphorus tribromide reported by Wissner et al.[255] and also conducted under different conditions (see insert under Scheme 7 B) nor mild Appel reaction[256] allowed obtaining the bromide **8** (Scheme 7 B).

A.

B.
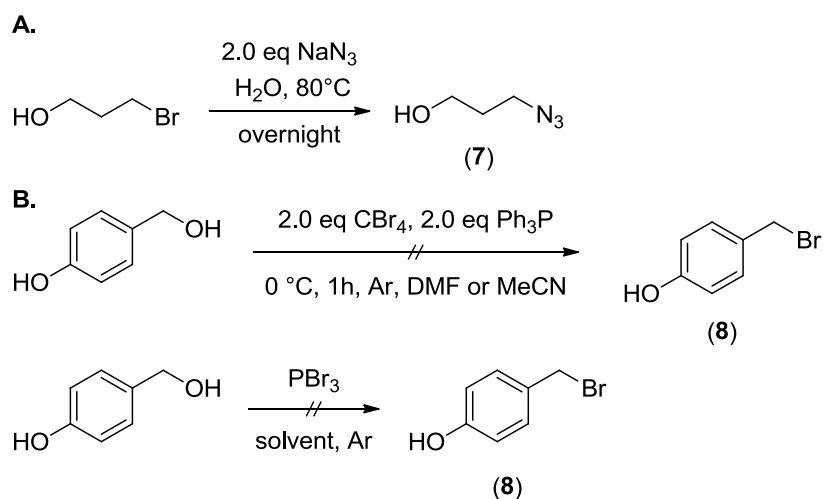
entry	PBr$_3$	solvent	Additives	T [°C]	Reference
1	0.33 eq	THF	Py 0.167 eq	-5 °C → RT	[255]
2	2.5 eq	-	-	80	-
3	1.0 eq	THF	-	-5 °C → RT	

Scheme 7. Application of the modified synthetic route. A. Synthesis of 3-azidopropan-1-ol (**7**). B. Unsuccesssful approaches to 4-hydroxybenzyl bromide (**8**).

Surprisingly and unfortunately, in both cases the substrate was completely consumed, however the formation of the product was not observed, in turn number of unidentified by-products could be identified both by GC-MS and TLC analysis.

4.1.2.2 Application of reductive amination and Mitsunobu reaction

Such unexpected complications in the synthesis of the first ABP afforded an extensive search for an alternative approach. As a result of these efforts, an elegant, convergent and relatively simple methodology combining a reductive amination and previously successful Mitsunobu reaction has been proposed (Scheme 8).

The key step of this synthesis turned out to be the reductive amination reaction, which is a powerful and robust method, enabling the preparation of a wide range of different amines when starting from aldehydes or ketones and primary or secondary amines and using sodium triacetoxyborohydride (STABH) as a reducing agent.[257-259] Sodium triacetoxyborohydride proved to be more efficient than another commonly used reducing

agent sodium cyanoborohydride in numerous challenging reactions, not giving cyanide by-products and being devoid of the toxicity of sodium cyanoborohydride.[260-261]
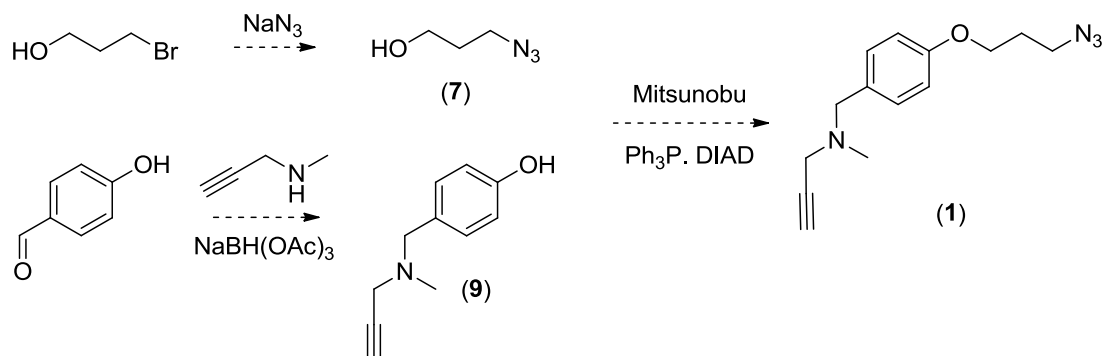
Scheme 8. The synthetic route leading to the first ABP, which employs a reductive amination and a Mitsunobu reaction.

This reaction allowed the preparation of the strategic intermediate aminophenol **9** from *p*-hydroxybenzaldehyde and *N*-methylpropargylamine using standard conditions reported by Abdel-Magid and co-workers.[257] (Scheme 9). However, the hint for such a synthetic strategy was found in two patents describing the development of *N*-benzyl-*N*-propargylamines[262] and propargyl- and indanyl nitroxides[263] for the treatment of obesity and neurological disorders, respectively.
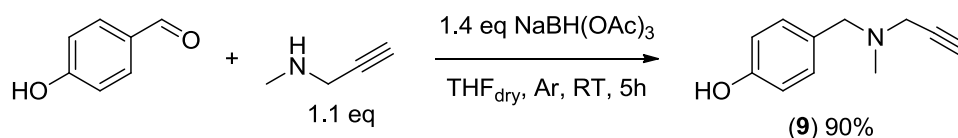
Scheme 9. Reductive amination leading to the key aminophenol **9**.

The reaction was carried out in THF under inert atmosphere of argon using an excess of amine (1.1 eq) and 1.4 eq sodium triacetoxyborohydride as a reducing agent and furnished the desired product **9** in very good yield (90%). The reaction has been also performed in 1,2-dichloroethane and gave satisfactory results as well (61% yield).

Mitsunobu reaction[264,265] between the aminophenol **9** and 3-azidopropan-1-ol allowed the attachment of an alkyl linker carrying an azide group under very mild conditions furnishing the appropriate probe **P1-N₃** (**1**) in good yield (73%) (Scheme 10 A). In order to avoid the reduction of azide moiety by triphenylphosphine in Staudinger reduction, first the

aminophenol **9** (1.0 eq), Ph_3P (1.0 eq) and diisopropyl azodicarboxylate (DIAD) (1.0 eq) were premixed (approx. 10 min) prior to the dropwise addition of slight excess of 3-azidopropan-1-ol (1.5 eq), according to the method reported by the group of Jacobsen.[266] The premixing guarantees that the betaine resulting from the reaction between Ph_3P and DIAD is stably and irreversibly formed, at least on the time scale of Mitsunobu reaction.[267] An equimolar ratio of these reagents assures that there is no free Ph_3P available in the reaction mixture, which could potentially reduce the azidoalcohol to the corresponding amine.

A.

B.
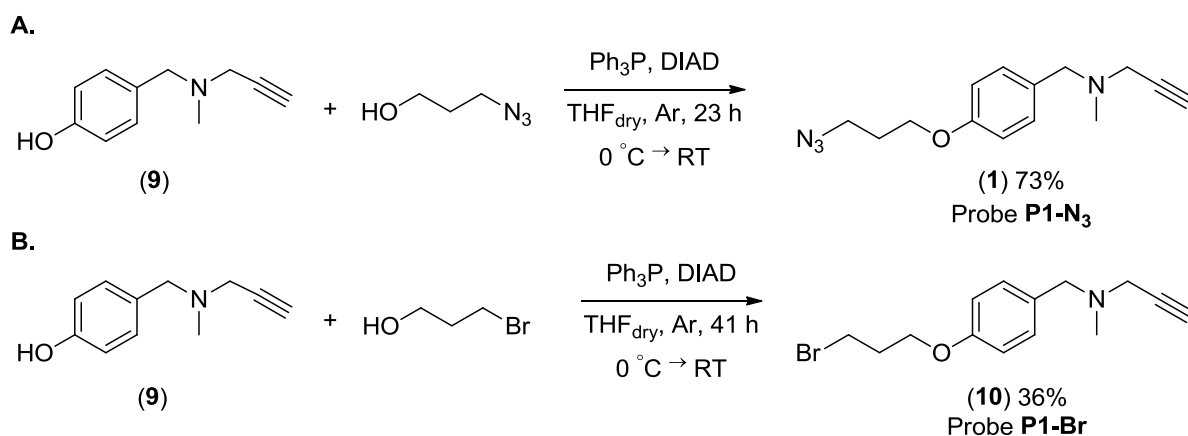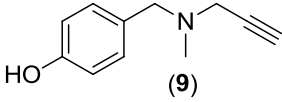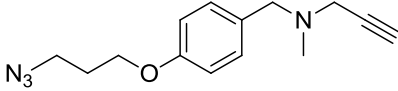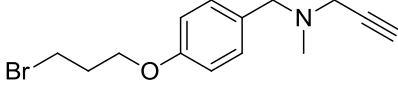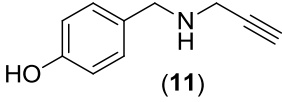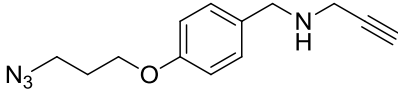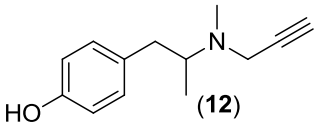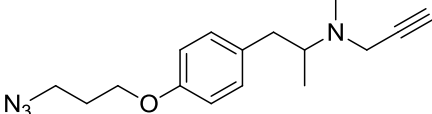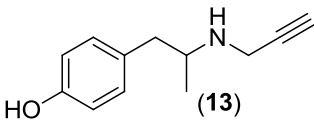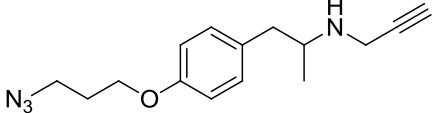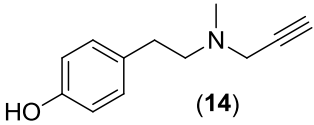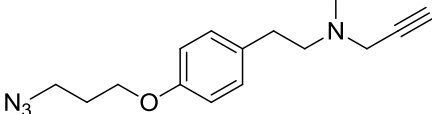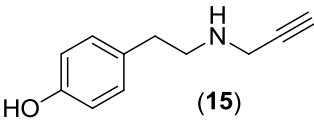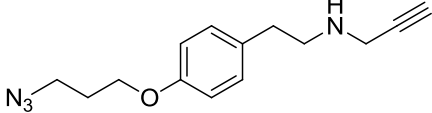
Scheme 10. Mitsunobu reaction between aminophenol **9** and 3-azidopropan-1-ol (A) and 3-bromopropan-1-ol (B).

As alternative, Mitsunobu reaction was also performed with 3-bromopropan-1-ol, furnishing the probe **P1-Br** (**10**) in moderate yield (36%) (Scheme 10 B), which could be subsequently substituted with sodium azide to afford the probe **P1-N3** (**1**). However, the much lower yield of this reaction, compared to the direct route, caused that this synthetic strategy was not further optimized.

Once the efficient synthetic methodology had been worked out for the first ABP, **P1-N3**, it was possible to synthesize other structurally related ABPs, only by using various aldehydes and ketones as well as propargyl amines with or without substituent at the nitrogen atom. This resulted in the first small set of ABPP probes, which are collected along with their aminophenol precursors and the corresponding yields in Table 2.

Table 2. Structure of activity-based probes **P1-N₃** - **P6-N₃** and **P1-Br** with their corresponding precursors and yields.

No.	Product of reductive amination – ABP precursor	Yield [%]	Product of Mitsunobu reaction - ABP	Yield [%]
1	(9)	90	(1) P1-N₃	73
			(10) P1-Br	36
2	(11)	55	(16) P2-N₃	34
3	(12)	68	(17) P3-N₃	70
4	(13)	78	(18) P4-N₃	73
5	(14)	53 (over 2 steps)	(19) P5-N₃	55
6	(15)	37 (over 2 steps)	(20) P6-N₃	63

The structural diversity was introduced by a different substitution pattern at the amino group and by the various lengths and structures of the carbon skeleton between reactive group and arene ring in the aminophenol precursors of activity-based probes.

Precursors **9** and **11** differ from each other only by the presence of methyl substituent at the amine group and were both obtained by the reductive amination starting with *p*-hydroxybenzaldehyde. Aminophenol **9** is based on the structure of the MAO inhibitor

pargyline, while aminophenol **12** is a racemic derivative of another MAO inhibitor – deprenyl (compare with Figure 33). Aminophenol **13** is its counterpart without the methyl substituent at the propargylamine moiety. Aminophenols **12** and **13** were obtained from ketone *p*-hydroxyphenylacetone and *N*-methylpropargylamine or propargylamine, respectively. In order to achieve satisfactory yields 2.0 eq sodium triacetoxyborohydride (STABH) were used along with 2.0 eq glacial acetic acid to accelerate the rate of these reactions. Aminophenols **14** and **15** were obtained in a two step procedure. First, 2-(*p*-hydroxyphenyl)ethanol was converted to its corresponding aldehyde under mild conditions of Parikh-Doering oxidation (Py-SO$_3$, DMSO, Et$_3$N)[268,269] as reported by Sunazuka and co-workers[270] (Scheme 11). Subsequently, this fairly unstable aldehyde **21** was immediately subjected to the reductive amination with *N*-methylpropargylamine or propargylamine, furnishing aminophenols **14** and **15** in moderate yields, 53% and 37%, respectively.
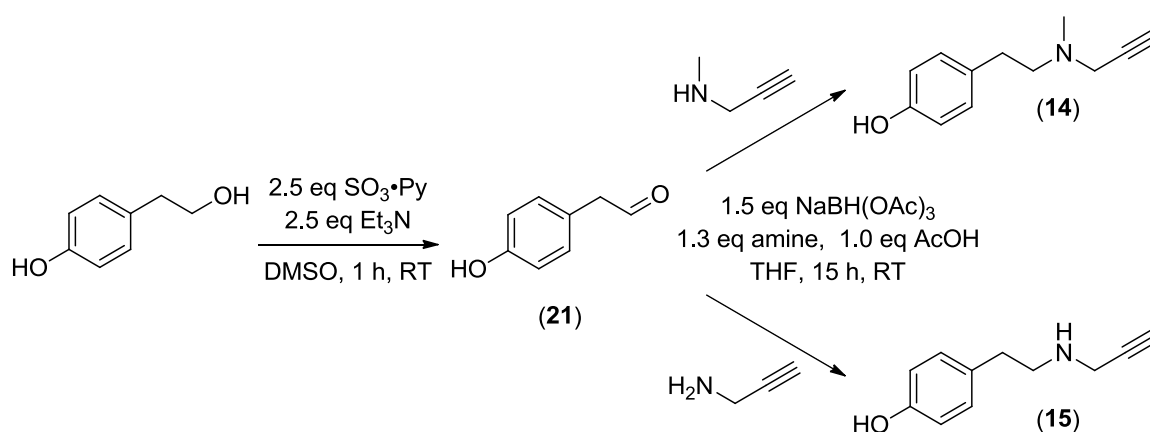
Scheme 11. Synthetic route leading to aminophenols **14** and **15**, which involves Parikh-Doering oxidation and reductive amination.

Although the first set of activity-based probes were equipped with the azide group attached *via* alkyl linker for the further attachment of a fluorescent tag under click chemistry conditions, the literature reports indicated that this direction of the bioconjugation reaction (azide group on the probe and alkyl tag on a fluorophore) can give rise to a high background of the labeling due to the unspecific association between a fluorescent alkyne with a protein.[80] Therefore, we decided to prepare the second generation of the activity-based probes

possessing an alkyne tag to compare both sets of probes and then choose the probes exhibiting better labeling properties.

This was easily feasible thanks to the modular nature of Mitsunobu reaction and availability of the probe precursors. Instead of the 3-azidopropan-1-ol, 4-pentyn-1-ol was reacted with all precursors (**9**, **11**-**15**) under Mitsunobu reaction furnishing the appropriate probes. In addition, optimization of the reaction conditions by applying high concentrations of the reagents as reported by Lepore et al.[271] led to the significant improvement of the reaction yields. The novel collection of the probes bearing an alkyne tag with the reaction yields is depicted in Figure 42.

(**22**) **P1** (85%) (**23**) **P2** (84%)
(**24**) **P3** (67%) (**25**) **P4** (46%)
(**26**) **P5** (70%) (**27**) **P6** (91%)
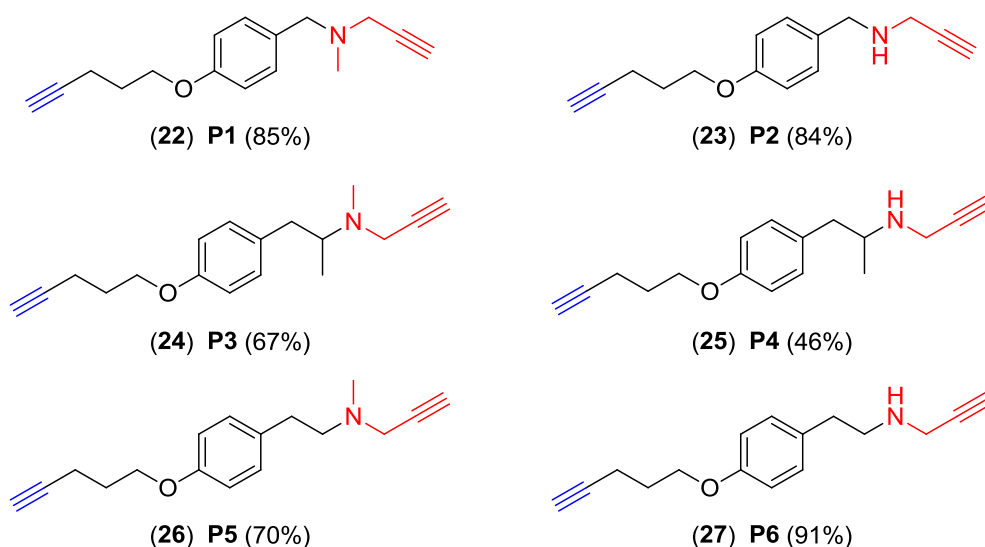
Figure 42. Structure of activity-based probes **P1**-**P6** and yields of the Mitsunobu reaction. Propargylamine warhead is highlighted in red whereas a reporter tag (alkyne group) in blue.

In conclusion, we developed a relatively simple and robust synthetic methodology involving a reductive amination and Mitsunobu reaction to access various activity-based probes dedicated to monoamine oxidases, which posses a propargylamine group as a warhead. The structural diversity of the small library could be easily extended if necessary, due to the modular nature of the key steps of the synthesis.

4.2 Assignment of inhibition properties of ABPP probes towards MAO enzymes

Once the activity-based probes dedicated to monoamine oxidases have been successfully prepared, it was important to assign their inhibitory properties towards MAO enzymes. As probes **P1** and **P3** were directly derived from MAO inhibitors, pargyline and deprenyl, respectively, we wanted to evaluate if the incorporation of a reporter tag (i.e. alkyne or azide handle) into these inhibitors alternates their MAO inhibition potency. The simplest way to test the inhibiton properties of the ABPs was to determine their IC_{50} values and compare them to the values obtained for parent inhibitors. However, first the development of an efficient activity assay for monoamine oxidase was necessary: in order to not only apply it in the determination of IC_{50} values but also to assign the intrinsic activity of the enzymes.

4.2.1 Development of activity assay for MAO enzymes

Activity-based probes target exclusively the active form of an enzyme excluding the immature or inhibitor bound form, hence, it was very important to establish first a simple and reliable activity assay for monoamine oxidases.

Several methods have been developed for the determination of MAO activity. The direct measurements comprise detection of oxygen consumption using an oxygen-sensitive electrode[272,273] or co-product H_2O_2 by measuring the absorbance of H_2O_2 at 230 nm,[274] HPLC[275] and/or radiochemical[276-278] detection of oxidized products, monitoring changes in absorbance or fluorescence of the oxidized substrates of formed products.[279-283] Polarographic measurement of oxygen consumption is a precise and reproducible method, however it requires a well controlled assay environment, hence it is not suitable for a rapid processing of large amount of samples. In monitoring of OD_{230} spectroscopic interference with most biological and synthetic compounds occurs, so this method is also not fully functional. HPLC or radiochemical methods are common, but expensive and time-

consuming. Direct spectrophotometric or fluorometric methods are rapid, quite sensitive, but limited to experiments with one substrate and spectroscopic interference often occurs. The indirect assays employ a horseradish peroxidase (HRP)-coupled reaction system.[284-288] Monoamine oxidase, catalyzing the oxidation of its substrates, generates hydrogen peroxide as a by-product, which then is detected by HRP-catalyzed oxidation of H_2O_2-sensitive fluorescent or chromophoric probes which typically absorb and emit light in higher wavelength range, avoiding spectral interference with biological sample. Most recently, also bioluminescent assays coupled with luciferase reaction were developed.[289,290]

For our purposes, we have chosen an indirect continous MAO activity assay, described by Zhou et al.[288] and modified by the group of Edmondson,[291] which is based on the detection of H_2O_2 in a horse radish peroxidase (HPR) coupled reaction (Scheme 12), employing 10-acetyl-3,7-dihydroxyphenoxazine (Amplex Red reagent). Amplex Red is a highly sensitive and stable probe for H_2O_2 and is oxidized with an exact stoichiometry (1 molecule H_2O_2 per 1 molecule of Amplex Red) to resorufin, a stable reaction product with the long wavelength spectra (absorption wavelength – 571 nm, emission wavelength – 585 nm). Due to that fact, there is little interference of absorption with most biological samples.

Activity of MAO A and MAO B was assayed spectrophotometrically by monitoring the rate of resorufin formation at 560 nm using kynuramine dihydrobromide and benzylamine hydrochloride as substrates for MAO A and MAO B, respectively. Prepared in advance chromogenic solution containing 3 mM substrate, 1 U/mL HRP, 50 μM Amplex Red in an appropriate buffer was mixed with the enzyme preparation (total volume 1 mL in a cuvette format), the mixture was mixed well and the absorbance change was followed at 560 nm for 3 min and 1 min for MAO A and MAO B, respectively, at ambient temperature. The amounts of the assay components were also accordingly adjusted to 96-well plate format (total volume 100 μL per well), which enabled reduction of time and amounts of reagents used and improved the assaying efficiency and reproducibility.
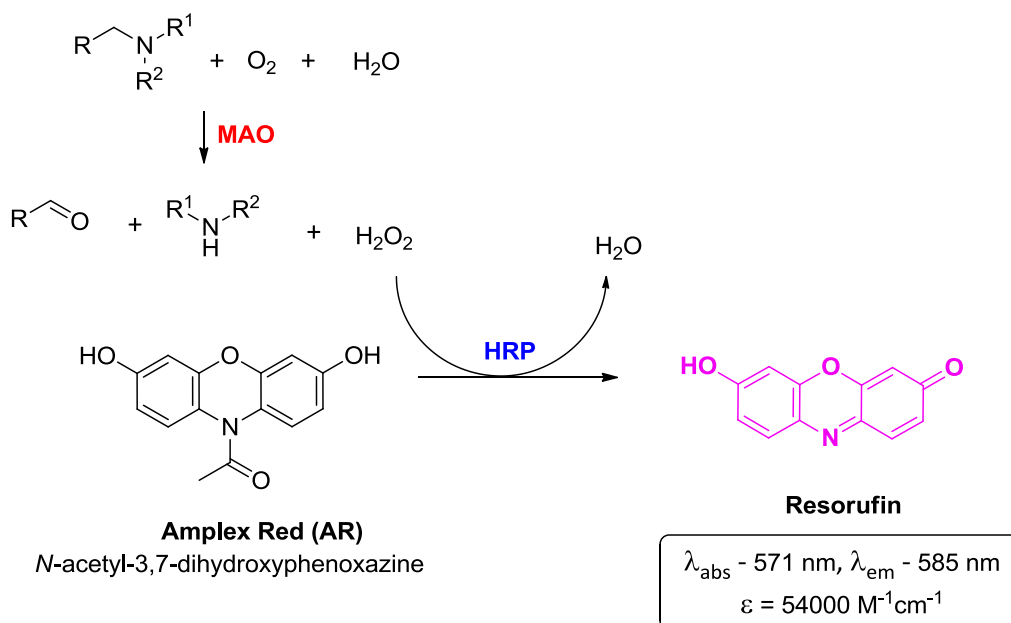
Scheme 12. HRP-coupled Amplex Red monoamine oxidase activity assay.

The representative results of the assay for MAO A and MAO B are depicted in Figure 43.

A.

substrate: **kynuramine**

B.

substrate: **benzylamine**
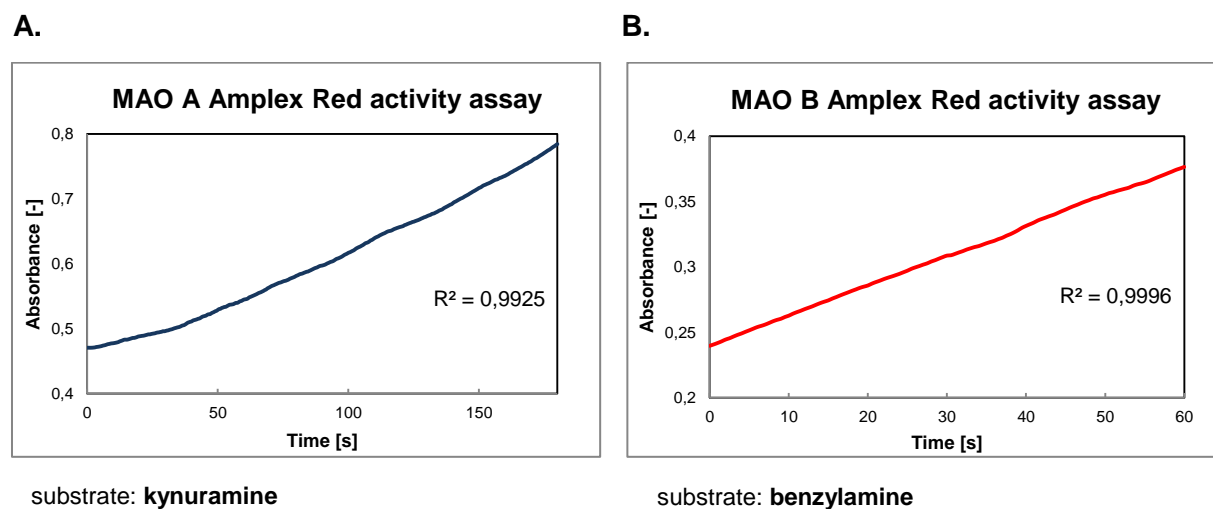
Figure 43. The change of the absorbance monitored in Amplex Red MAO activity assay for MAO A (A) and MAO B (B).

From the slope of the absorbance increase, the activity of the enzymes could be easily calculated as well as the specific activity of the enzymes when taking into the account the protein concentration.

4.2.2 Assignment of IC_{50} values of ABPP probes towards MAO enzymes

The developed activity assay for monoamine oxidases served as a basis for the assignment of inhibitory properties of selected activity-based probes. Probe **P1** derived from unspecific MAO inhibitor pargyline was used to assess the IC_{50} value towards MAO A whereas probe **P3**, which is a racemic derivative of MAO B specific inhibitor deprenyl, was involved in the assignment of IC_{50} towards MAO B.

Enzyme preparations were incubated in 50 mM potassium phosphate buffer (pH 7.5) with varying concentrations of the probes (range 1-400 µM) or DMSO, which was used as a blank control. After 1h incubation at ambient temperature, the chromogenic solution was added to the enzyme inubated with a probe or DMSO, the solution was well mixed and absorbance change was recorded in a 96-well plate at 560 nm at 25 °C. The sample incubated with DMSO was regarded as unaffected in terms of enzyme activity and the absorbance value obtained for that sample was arbitrarily assigned as 100% enzyme activity. The identical experiments under the same conditions were performed for the parent inhibitors pargyline and deprenyl in order to compare IC_{50} values between the probes and the inhibitors and assign only a fold of change and not an absolute value. IC_{50} values were calculated from curve fittings of a Boltzmann model using the Origin Pro 8.6 software (OriginLab Corporation). The obtained fittings and the IC_{50} values for the probes and their parent inhibitors are presented in Figure 44.

Fortunately, the structural modifications introduced to the probes did not affect significantly the inhibition of both isozymes. Probe **P3**, a racemic version of deprenyl equipped with an alkyne, showed approx. 16-fold decrease in inhibition of MAO B (IC_{50} = 1.76 µM for **P3** vs. 0.11 µM for deprenyl). This might be presumably a consequence of several factors such as lack of stereocontrol in the probe or an unfavorable conformation of the alkyne tag, however no further experimental work was accomplished (separation of enantiomers and performing activity assays with both enantiomers) which would elucidate this phenomenon. In contrast,

probe **P1**, based on pargyline revealed a slight improvement in the inhibition of MAO A, when compared to its parent inhibitor (IC$_{50}$ = 0.04 µM for **P1** vs. 0.93 µM for pargyline).
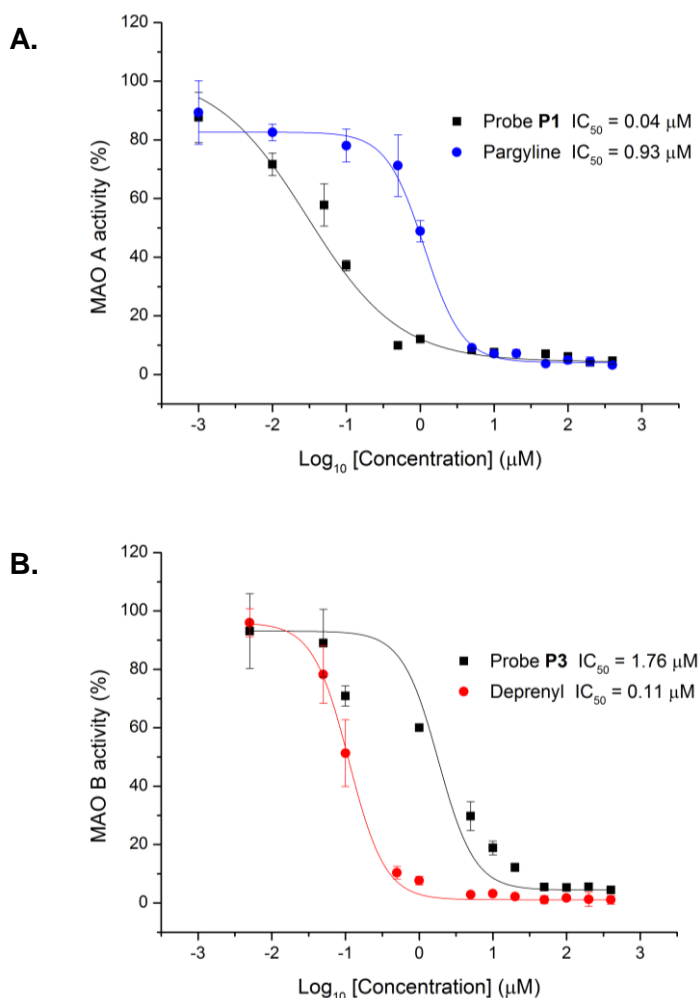
Figure 44. Inhibition of MAO A by probe **P1** and pargyline (A) and MAO B by probe **P3** and deprenyl (B). IC$_{50}$ values were determined using curve fittings (Boltzmann model) by Origin Pro 8.6 (OriginLab Corporation).

4.3 Synthesis of fluorescent tags

Having demonstrated that the designed activity-based probes meet the requirement of inhibition of monoamine oxidases we could set out for the preparation of custom fluorescent tags, which are compatible with click chemistry approach in tandem labeling.

Small molecule fluorophores are exceptionally powerful tools in Chemical Biology, which enable a precise interrogation of biological systems. They are widely used as macromolecule

labels, cellular stains, ion indicators, and enzyme substrates.[292-294] Selection of a suitable fluorophore to visualize a biological system of interest can be very difficult given a wide range of available molecules displaying various photophysical and structural properties[293] (Figure 45). Ideally, a fluorophore should match excellent spectral characteristics (high quantum yield Φ and extinction coefficient ϵ) and high chemical stability with facile synthesis and modular nature allowing preparation of many derivatives starting from a common set of intermediates.
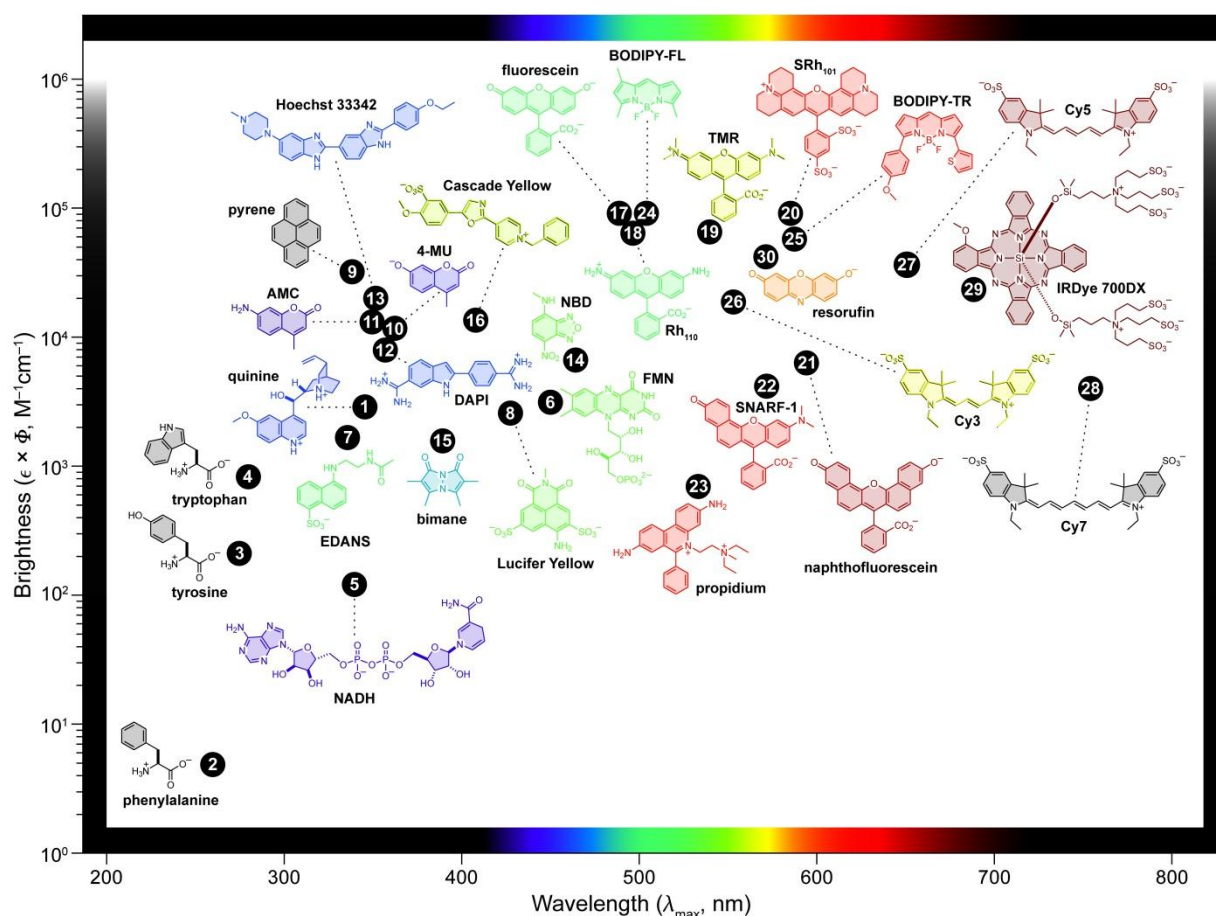
Figure 45. Plot of fluorophore brightness ($\epsilon \times \Phi$) *vs* the wavelength of maximum absorption (λ_{max}) for the major classes of fluorophores. The color of the structure indicates its wavelength of maximum emission (λ_{em}). Picture taken from Ref. [293].

In ABPP, the most commonly used fluorophores are rhodamine (Rh) and its tetramethyl-derivative (TAMRA), boron-dipyrromethene (BODIPY) and cyanines (Cy3, Cy5) as discussed in detail in the introductory section 2.1.2.4. For our ABPP studies we have chosen two

different fluorescent dyes as basis for our custom tags, namely yellow 4-nitrobenz-2-oxa-1,3-diazole (NBD) and purple 5(6)-carboxytetramethylrhodamine (TAMRA).

4.3.1 Synthesis of NBD-based fluorescent tags

For our initial studies we have selected a simple and inexpensive bright yellow 4-nitrobenz-2-oxa-1,3-diazole (4-chloro-7-nitrobenzofurazan, NBD) fluorophore, displaying decent photophysical properties (λ_{max} = 465 nm, λ_{max} = 535 nm, quantum yield =0.3 (MeOH)).[295] NBD was already used in ABPP as a reporter tag by the group of Hermetter to visualize the activity of lipolytic enzymes.[67,296,297]

The synthetic strategy (Scheme 13) started with the synthesis of aminocaproic acid derivative **28** containing NBD fluorophore *via* the substitution of NBD chloride with aminocaproic acid in methanol as reported by Ludolph et al.[298] The desired product was isolated by column chromatography and crystallization as a brown solid in very good yield (80%), which significantly exceeded the one published in the literature (57%). In the second step, the acid **28** was converted to the corresponding succinimide ester **29** by a direct coupling of the acid **28** with *N*-hydroxysuccinimide (1.5 eq) using EDC (1.2 eq) as a coupling agent, according to a modified procedure reported by the group of Kutateladze.[299] Reaction was carried out in THF due to the insolubiltity of the starting material in DCM and it afforded the desired product **29** as dark yellow solid in very good yield (80%). The water-soluble coupling reagent EDC was used in this synthesis instead of the common and cheaper counterpart DCC, because it was not possible to efficiently separate the urea side-product from the ester **29** during work-up and column chromatography. Finally, the active ester **29** was an ideal intermediate which could be easily transformed into diverse amides equipped with either alkyne or azide group depending on an amine used in the reaction. The substitution of the ester **29** with propargylamine (**30**) or a longer hex-5-yn-1-amine (**31**), carried out in DMF in the presence of triethylamine, afforded the appropriate amides **32** and **33**, carrying the alkyne group, in 91% and 44% yield, respectively. The analogous reaction

with 3-azidopropan-1-amine (**34**) furnished amide **35** in 79% yield, which possessed an azide

tag suitable for further modification *via* click chemistry.
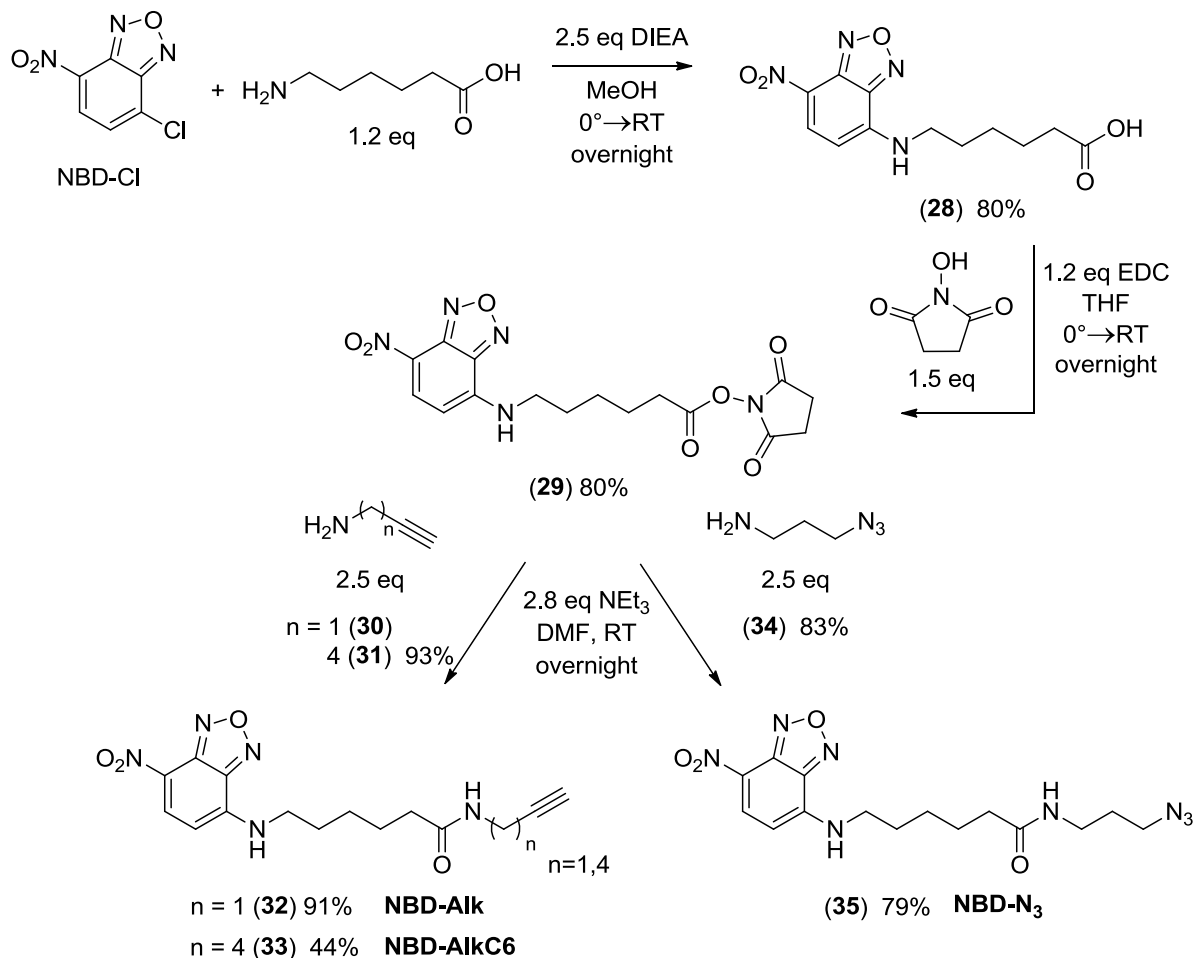
Scheme 13. Synthesis of NBD-based fluorescent tags.

Amine **31** was prepared by reduction of hex-5-ynenitrile with lithium aluminium hydride

according to a protocol described by Barglow et al.[35] and Tojino et al.[300] The reaction was

carried out in dry diethyl ether at RT and n-n-3n work up furnished 85% pure amine **31** in

91% yield which was directly used for the amidation reaction. 3-Azidopropan-1-amine (**34**)

was prepared by a substitution of 3-bromopropylamine hydrobromide with sodium azide with

the subsequent release of the free amine from its hydrobromide salt by treatment with KOH

in 83% yield, following the procedures reported by Carboni and Lampkins.[301]

4.3.2 Synthesis of TAMRA-based fluorescent tags

In the course of our studies we decided to prepare other fluorescent tags which employ a 5(6)-carboxytetramethylrhodamine (TAMRA) fluorophore, which is commonly used in numerous ABPP studies to visualize a wide range of active enzymes.[18c,23g,34a] In addition, this dye exhibits much better photophysical properties (λ_{max} = 540 nm, λ_{max} = 565 nm, quantum yield = 0.68) than the NBD dye.

4.3.2.1 Development of a direct coupling method

In the first approach, we planned to synthesize TAMRA derived reporter tags by converting 5(6)-carboxytetramethylrhodamine into its *N*-hydroxysuccinimidyl ester in an analogous coupling as applied for NBD derived acid **28**. TAMRA *N*-hydroxysuccinimidyl ester would be a convenient starting material for modular preparation of different amides carrying either azide or alkyne group as it has been already demonstrated by Cravatt et al.[80] Unfortunately, the simple, reliable and scalable synthesis of TAMRA *N*-hydroxysuccinimidyl ester was not successful mostly due to the decomposition of the active ester during the purification step, although protocols for such a transformation for a trifluoroacetic acid protected TAMRA were described in the literature.[302] Therefore, we seeked for an alternative synthetic route, which could produce the desired tags in a single step.

Direct couplings employing 5(6)-carboxytetramethylrhodamine used for instance a HATU/HOAt coupling system as reported by Singleton et al.[303] or BOP/HOBt as shown by Lyttle and co-workers.[304] Since our research group made good experience with PyBOP/HOBt coupling system, we developed a simple coupling between 5(6)-TAMRA and previously synthesized amines **31** and **34** using benzotriazol-1-yl-oxytripyrrolidinophosphonium hexafluorophosphate (PyBOP) as a coupling reagent. The reactions were carried out under mild conditions at RT in DMF and afforded amides **36** and **37** in 60% and 59% yield, respectively. The synthetic route leading to the amides **36** and **37**, bearing correspondingly an alkyne and azide reporter handle, is depicted in Scheme 14.
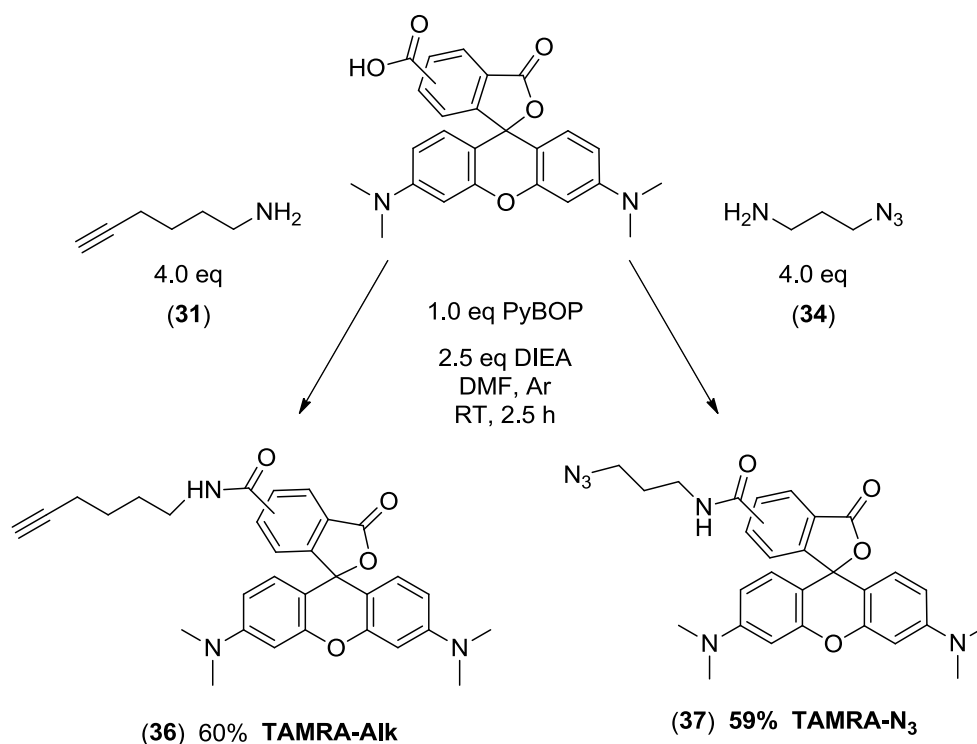
Scheme 14. Synthesis of TAMRA-based fluorescent tags.

4.3.2.2 Synthesis of 5- and 6-TAMRA and its derivatives

In the course of our synthetic efforts to obtain pure fluorescent reporter tags from inexpensive and easily available starting materials we set out for the preparation of isomerically pure 5- and 6-carboxytetramethylrhodamines, using a procedure reported by Kvach et al.[305] and their conversion to the corresponding click chemistry compatible amides applying the previously developed PyBOP coupling method.

We started the synthetic route with the acylation of inexpensive 3-dimethylaminophenol with 1,3-dioxo-2-benzofuran-5-carboxylic acid (trimellitic anhydride) in toluene under reflux (Scheme 15). The reaction afforded a mixture of 4-dimethylamino-2-hydroxy-2′,4′(5′)-dicarboxybenzophenones (**38**) and (**39**), which could be separated into individual compounds upon recrystallization from methanol and acetic acid, taking advantage of different solubility of both isomers in these solvents. Although, the yields were relatively low, 18% and 11%, respectively, they resembled the yields shown in the literature (16% and 10%, respectively).
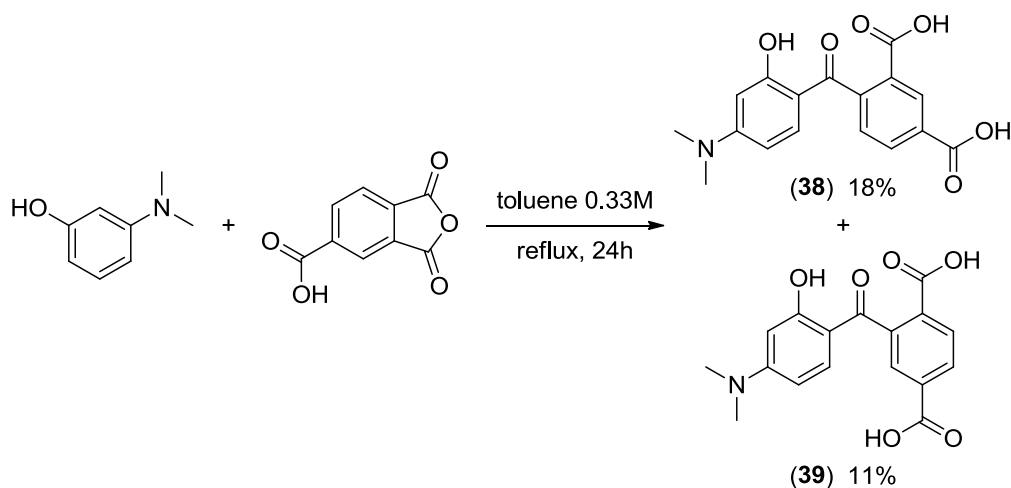
Scheme 15. Synthesis of 4-dimethylamino-2-hydroxy-2′,4′-dicarboxybenzophenone (**38**) and 4-dimethylamino-2-hydroxy-2′,5′-dicarboxybenzophenone (**39**).
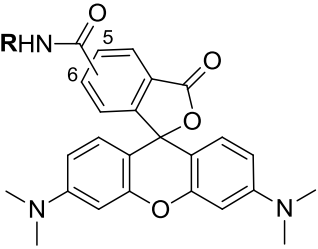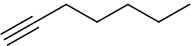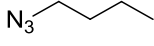
Subsequently, individual benzophenones **38** and **39** were reacted with additional portion of 3-dimethylaminophenol (1.3 eq) in DMF using trimethylsilylpolyphosphate (PPSE) as a dehydrating agent and weak acid catalyst[306] to furnish isomerically pure 5- and 6-carboxytetramethylrhodamines (**40** and **41**) (Scheme 16). The resulting pure isomers of tetramethylrhodamine were obtained in excellent yields (98 and 90% respectively) and were used without additional purification for further synthesis of isomerically pure amides.
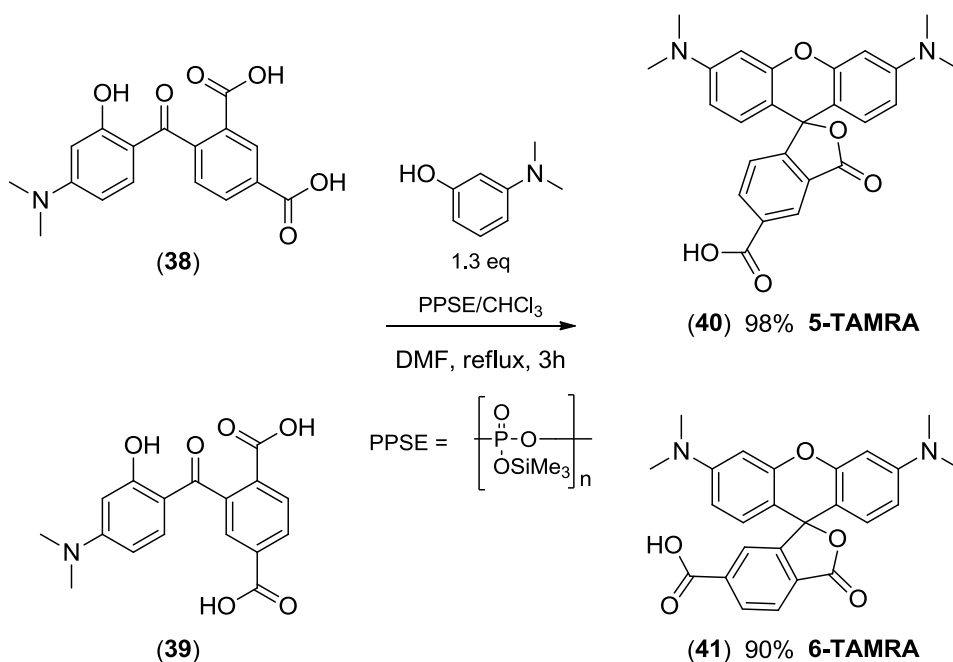
Scheme 16. Synthesis of 5-TAMRA **40** and 6-TAMRA **41**.

Finally, 5- and 6-carboxytetramethylrhodamines (**40** and **41**) were reacted with previously prepared amines **31** and **34** using the same coupling method, which was described for a mixture of both isomers. The results of these reactions are summarized in Table 3.

Table 3. The results of amidation of 5- and 6-TAMRA **40** and **41** with hex-5-yn-1-amine (**31**) and 3-azidopropan-1-amine (**34**).

TAMRA	R	Position	Compound	Yield [%]
		5	(**42**) 5-TAMRA-Alk	48
		6	(**43**) 6-TAMRA-Alk	32
		5	(**44**) 5-TAMRA-N$_3$	70
		6	(**45**) 6-TAMRA-N$_3$	40

In summary, we have developed simple, reliable and scalable synthetic methods for the preparation of custom fluorescent tags, which were based both on NBD and TAMRA fluorophores. The tags can be easily conjugated with enzyme-bound activity-based probe to visualize labeled enzymes by the in-gel fluorescence scanning.

4.3.3 Model click chemistry reaction

Before we evaluated the potential of the developed ABPP system in the enzyme labeling we wanted to make sure that the click chemistry reaction between the probe and a fluorescent tag works efficiently. Therefore we performed a series of reactions between the **NBD-Alk** tag **32** and a modified probe **P1-N$_3$ 46** (Scheme 17 A). The probe **46** was equipped with an azide group but it was devoid of an acetylenic substituent at the amine group, which was replaced by an ethyl group, in order to avoid the formation of a homocycloaddition product **47** (Scheme 17 B). The probe **46** was prepared according to the general procedure worked out previously. It consisted of a reductive amination between *p*-hydroxybenzaldehyde and *N*-ethyl-*N*-methylamine, which resulted in aminophenol **48**, to which 3-azidopropan-1-ol (**7**) was attached *via* Mitsunobu reaction (Scheme 18).

A.

B.
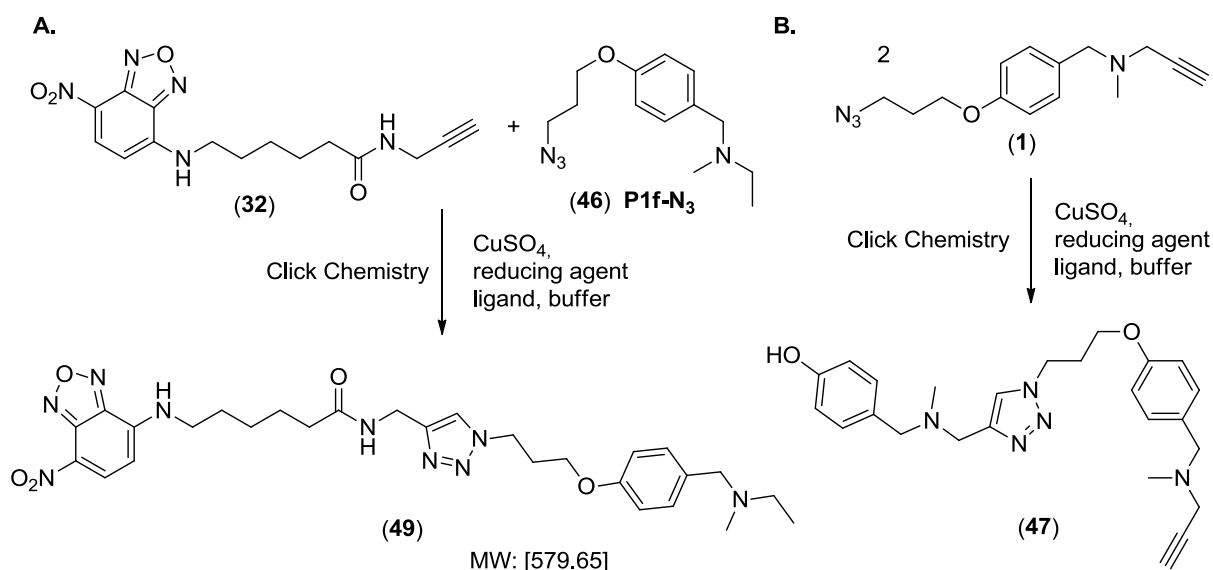
Scheme 17. A. Model click chemistry reaction between the NBD-tag **32** and modified probe **P1-N₃. 46** B. Plausible product of homocycloaddition reaction of two molecules of probe **P1-N₃**.

The reactions between alkyne **32** and azide **46**, mixed in a ratio 1:1 (mol/mol), were carried out under different conditions in 100 μL total volume for 24 h in 100 mM phosphate buffer pH 8.0. The formation of the cycloaddition product **49** was evaluated by MS-HPLC and UV-HPLC after quenching the reaction mixture with acetonitrile (Table 4).
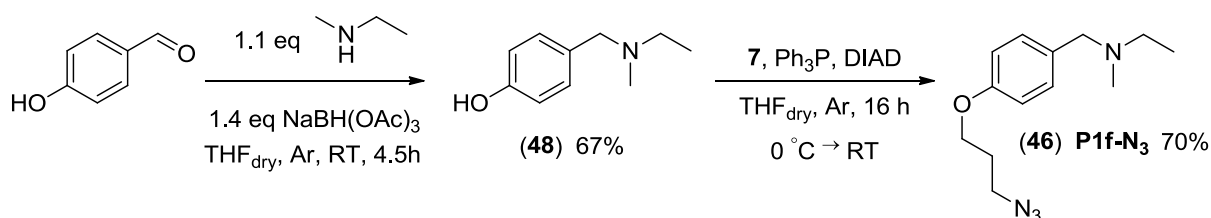
Scheme 18. Synthesis of probe **P1f-N₃**.

The reactions employed submolar amounts of copper(II) sulphate (1-25% mol) which was reduced to the catalytic copper(I) either by sodium ascorbate (NaAsc) (Table 4, entries 1-3) or tris(2-carboxyethyl)phosphine (TCEP) (Table 4, entries 4-7) in the presence (Table 4, entry 2-3 and 5-7) or absence (Table 4, entry 1 and 4) of tris-(benzyltriazolylmethyl)amine (TBTA) ligand. The application of TBTA significantly improved the amount of the formed product in both catalytic systems (68% to 78 % in NaAsc/TBTA vs. 27% to 54% in TCEP/TBTA system). The highest conversion 85% was achieved when 10% mol copper(II) sulphate, 20% mol NaAsc and 20% mol TBTA were applied (Table 4, entry 3).

Table 4. Results of model click chemistry reaction between the NBD alkyne tag **32** and modified azide probe P1f-N$_3$ **46**.

Entry	CuSO$_4$ % mol	NaAsc % mol	TCEP % mol	TBTA % mol	% product HPLC (210 nm trace)	% product HPLC (460 nm trace)
1	1	10	-	-	68	98
2	1	10	-	10	78	71
3	10	20	-	20	**85**	92
4	1	-	10	-	27	30
5	1	-	10	10	54	57
6	10	-	20	20	61	67
7	25	-	25	50	**71**	73

PB = 100 mM phosphate buffer pH 8.0, NaAsc = sodium ascorbate, TCEP = tris(2-carboxyethyl)phosphine, TBTA = tris-(benzyltriazolylmethyl)amine.
Reaction conditions: total volume 100 µL, alkyne **32** : azide **46** ratio = 1:1, alkyne and azide 8.0 mM, PB, 25.0 °C, 600 rpm, no exclusion of air or light.

The results of the model click chemistry experiments provided the proof that under conditions, which are present in a biological system (the presence of water and air) the cycloaddition product is cleanly formed in satisfying yield and the same outcomes are expected with enzyme-bound activity-based probes. In addition, in ABPP experiments the components of click chemistry reaction (copper(II) sulphate, reducing agent, TBTA ligand) are used in excess (here they were used in submolar quantities), which should assure even a higher conversion of the click chemistry bioconjugation.

4.4 Evaluation of labeling of monoamine oxidase *in vitro*

Having in hands all components, which are indispensible for ABPP: a target enzyme (membrane preparations of monoamine oxidases), activity-based probes (**P1-N$_3$-P6-N$_3$** and **P1**-**P6**) and fluorescent tags (NBD- or TAMRA-derivatives) we were able to perform a proof-of-concept experiment, which could demonstrate whether the designed strategy works or not (Figure 46).
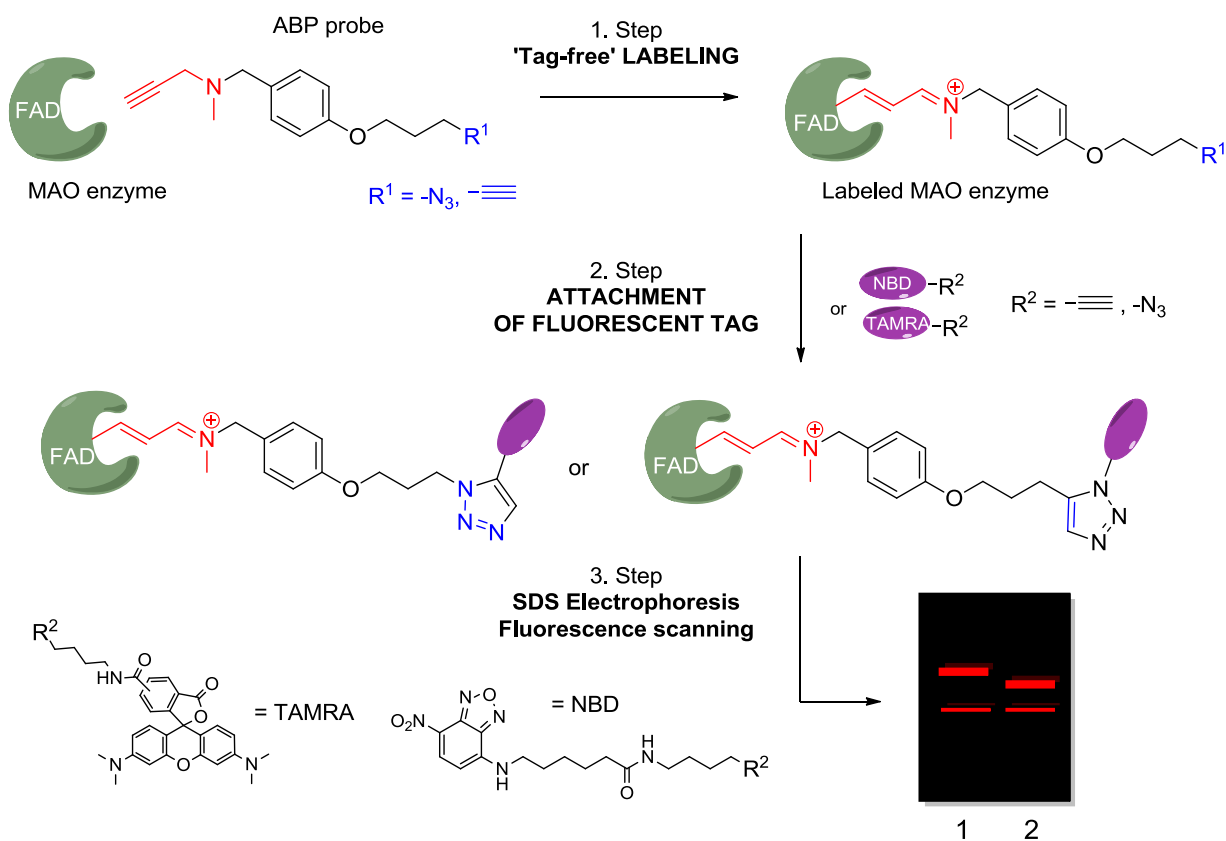
Figure 46. Proof-of-concept ABPP experiment for labeling of flavin-dependent oxidases.

4.4.1 Labeling of MAO enzymes *in vitro* using ABPP probes and NBD-based fluorescent tag

In our first experiments we focused mainly on two probes, **P1-N₃** and **P1**, based on known MAO inhibitor pargyline, and compatible NBD-based fluorescent tags, **NBD-Alk** and **NBD-N₃** for **P1-N₃** and **P1**, respectively. First of all, we intended to verify, whether the ABPP labeling of MAO enzymes occurs at all and if yes, whether the labeling is specific or not.

Also, we wanted to evaluate the influence of direction of click chemistry reaction on the labeling efectiveness as we found evidence in the literature,[80] indicating that a fluorescent tag carrying an alkyne group can unspecifically interact with a protein, contributing to high background level in fluorescence measurements. The formation of a stable connection between the probe labeled protein and a fluorescent tag *via* click chemistry can be accomplished in two different manners as depicted in Figure 47.
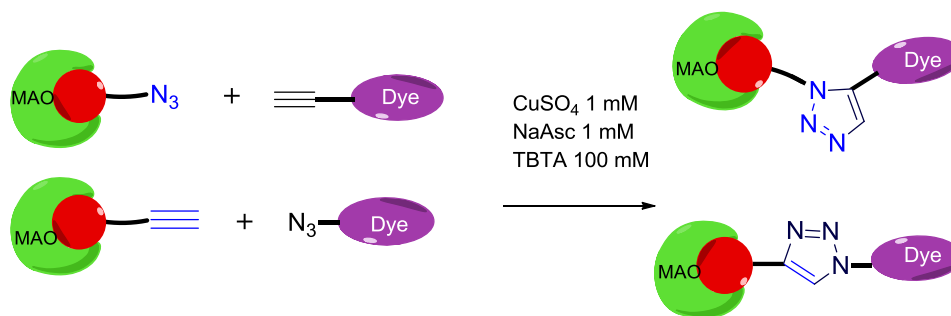
Figure 47. Directionality of click chemistry reaction used for the attachment of a fluorescent tag.

Consequently, we wanted to test these both reactions as we had already prepared two sets of probes as well as compatible fluorescent tags.

4.4.1.1 Development and optimization of the labeling method

In the initial experiments we employed a labeling procedure based on a method described by Speers et al.[80] In our modified protocol, monoamine oxidase preparations (2 mg/mL) were incubated with 5 µM probe (**P1-N₃** or **P1**) or DMSO as a blank control for 30 min at 37 °C. To test if the labeling occurs only with the active form of the enzyme in a specific manner a so called heat denaturation control was included, in which a protein sample was heated at 80 °C for 5 min and then cooled down to RT prior to the addition of a probe. Following the incubation, 100 µM appropriate NBD tag (**NBD-Alk** or **NBD-N₃**) was appended *via* click chemistry reaction (1 mM sodium ascorbate, 100 µM TBTA, 1 mM CuSO₄), which was carried out at RT for 1 h. Subsequently, proteins were separated by gel electrophoresis and visualized by in-gel fluorescence scanning.

Unfortunately, in the first labeling experiments we were not able to observe any fluorescent signals corresponding to a labeled MAO enzyme because of the very high background level, originating presumably from an excess of a fluorescent tag (20-fold escess). Hence, in the next experiments, the protein samples were centrifuged after click chemistry reaction to remove the supernatant with the excess of CC reagents. This method did not help much to improve the quality of the fluorescence scanning. However, finally some weak fluorescent bands in the range of 60 kDa could be detected. Consequently, two various protein

precipitation methods were used, which employed either trichloroacetic acid-acetone (TCA 50% aqueous solution (w/v)) or chloroform-methanol,[307] in order to precipitate proteins and remove the excess of fluorescent tag from the sample. Fortunately, both methods significantly decreased the background level so that clear fluorescent bands corresponding to labeled MAO enzymes could be visualized by fluorescence scanning (Figure 48 A).
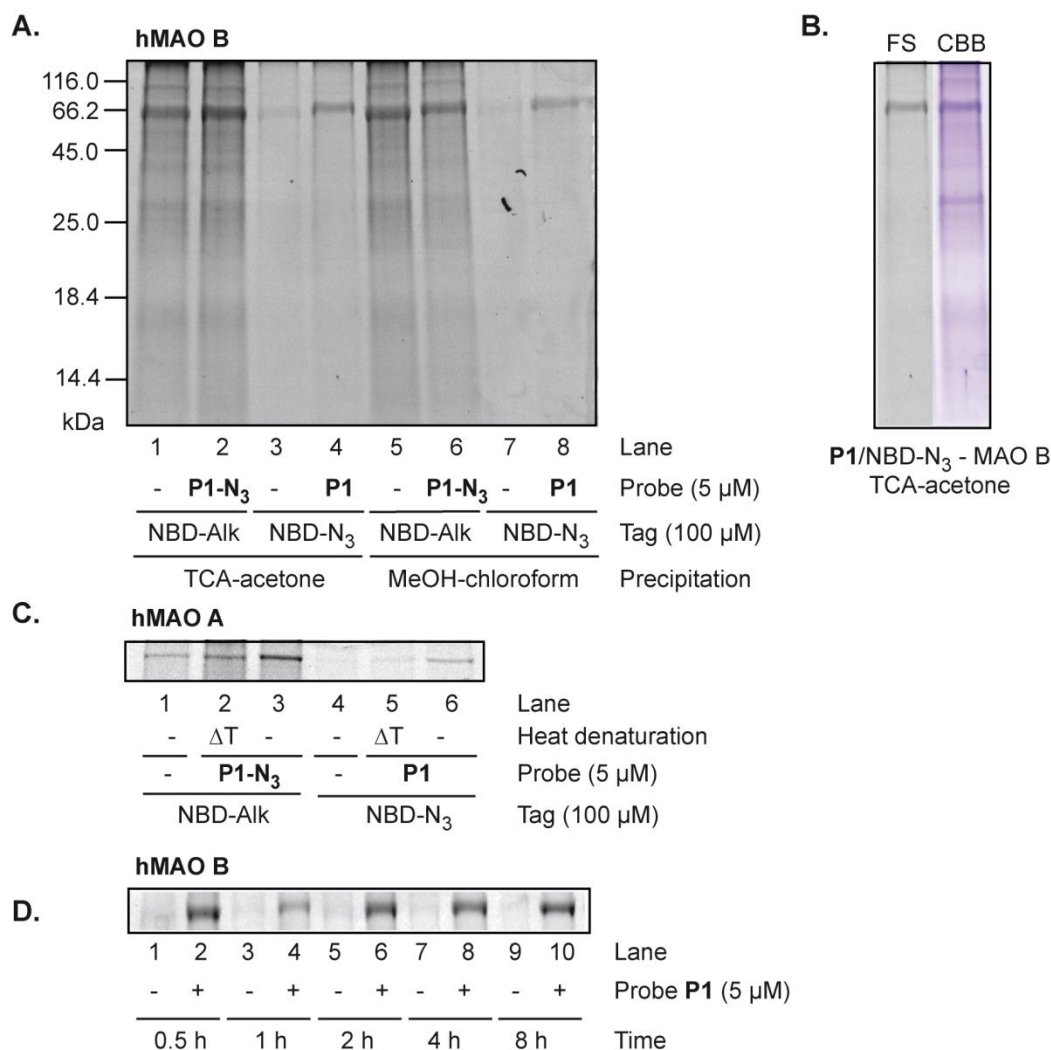
Figure 48. Fluorescent SDS-PAGE analysis of labeling of monoamines *in vitro* using NBD-based fluorescent tags. A. Comparison of TCA-acetone (lanes 1-4) and methanol-chloroform (lanes 5-8) precipitation method and influence of CC direction on background of labeling. B. Comparison of fluorescence scanning (FS) and Coomassie Brilliant Blue (CBB) staining of labeling of MAO B by the probe **P1**. C. Labeling of MAO A after heat denaturation (5 min at 80 °C) (lanes 2 and 5) and without heat denaturation (lanes 3 and 6) of the enzyme. D. Time-dependent labeling of MAO B by probe **P1**.

However, we have clearly seen distinct background levels for the two pairs of click chemistry reaction. In case of combination of probe **P1-N₃** with **NBD-Alk** fluorescent tag we observed a

high background level in labeling of MAO B, even when no probe was added to the sample and regardless the applied precipitation method (Figure 48 A, lanes 1-2 (TCA-acetone) and 5-6 (MeOH-chloroform)). This was probably due to the formation of unspecific but stable association between the protein and fluorescent alkyne tag **NBD-Alk** as it was previously reported.[80] Fortunately, we did not notice similar effects when the pair **P1** carrying alkyne group and **NBD-N₃** was employed (Figure 48 A, lanes 3-4 and 7-8). Blank controls (Figure 48 A, lanes 3 and 7) did not show any unspecific labeling with the fluorescent tag **NBD-N₃**.

Comparison of fluorescence scanning (FS) and total protein staining by Commassie Brilliant Blue (CBB) revealed that MAO B was labeled by probe **P1** as a main target and no other proteins were specifically tagged by probe **P1** (Figure 48 B).

We also performed heat denaturation controls as described above (Figure 48 C), which showed that the fluorescent signals for denatured protein (MAO A) (Figure 48 C, lanes 2 and 5) correspond to the respective blank controls (Figure 48 C, lanes 1 and 4, respectively) and are much weaker when compared to the non-denatured samples (Figure 48 C, lanes 3 and 6). This suggested that the labeling indeed occurs only with the active enzyme. On the other hand, the fluorescence signals were not abolished completely, indicating that the enzyme was either not fully deactivated by denaturation (5 min at 80 °C) or that there is some intrinsic background level of NBD fluorescent tag. This experiment also confirmed the previous observation that pair **P1**/**NBD-N₃** (Figure 48 C, lanes 4-6) displays much lower background level in comparison to pair **P1-N₃**/**NBD-Alk** (Figure 48 C, lanes 1-3).

Finally, we investigated in more detail the labeling of MAO with regard to time of incubation (Figure 48 D) required for efficient labeling of the target enzyme. We found that MAO can be effectively labeled within 30 min (Figure 48 D, lane 2). However, a bit prolonged incubation time improves significantly the intensity of the labeling (Figure 48 D, lanes 6, 8, 10).

4.4.1.2 Summary

From the first labeling experiments of recombinant MAO enzymes with the developed activity-based probes and compatible NBD-derived fluorescent tags we concluded that monoamine oxidases could be specifically labeled, when the probe **P1** and **NBD-Alk** fluorescent tag were used. The proof-of-concept experiment (Figure 46) was accomplished positively, providing a new method into the ABPP toolbox. However, further optimization of the labeling conditions (appropriate controls, protein precipitation protocol) is highly needed. The employment of another fluorophore displaying better photophysical properties (higher quantum yield) would be substantial in lowering the high intrinsic background level of NBD-based fluorescent markers.

4.4.2 Labeling of MAO enzymes *in vitro* using ABPP probes and TAMRA-based fluorescent tag

Our ABPP strategy based on NBD fluorescent tags served as an excellent training platform to establish the methodology for the labeling of MAO enzymes. However, in the course of our studies we decided to implement other fluorescent tags, built on TAMRA fluorophore, which exhibit very good photophysical properties and are commonly used in various biological studies. The tags were synthesized as described in the section 4.3.2. Using TAMRA-derived fluorescent tags we evaluated our ABPP strategy with respect to the scope of probes library, site and sensitivity of labelling, time of incubation required for efficient enzyme tagging as well as the direction of click chemistry reaction.

4.4.2.1 Scope of probes collection

At first, we decided to investigate the scope of the probes collection in labeling of monoamine oxidases. Membrane preparations of recombinant human MAO enzymes overexpressed in *Pichia pastoris* were incubated with the corresponding 10 µM probe (**P1**-**P6**) (Figure 42) or

DMSO as a blank control for 1 h at RT. The labeling was followed by the attachment of

TAMRA-N$_3$ tag (100 µM) under copper(I) catalyzed alkyne-azide cycloaddition (click

chemistry, CC) conditions (1 mM TCEP, 100 µM TBTA, 1 mM CuSO$_4$). SDS-gel

electrophoresis and in-gel fluorescence scanning were employed to detect labeling events

which are shown in Figure 49.
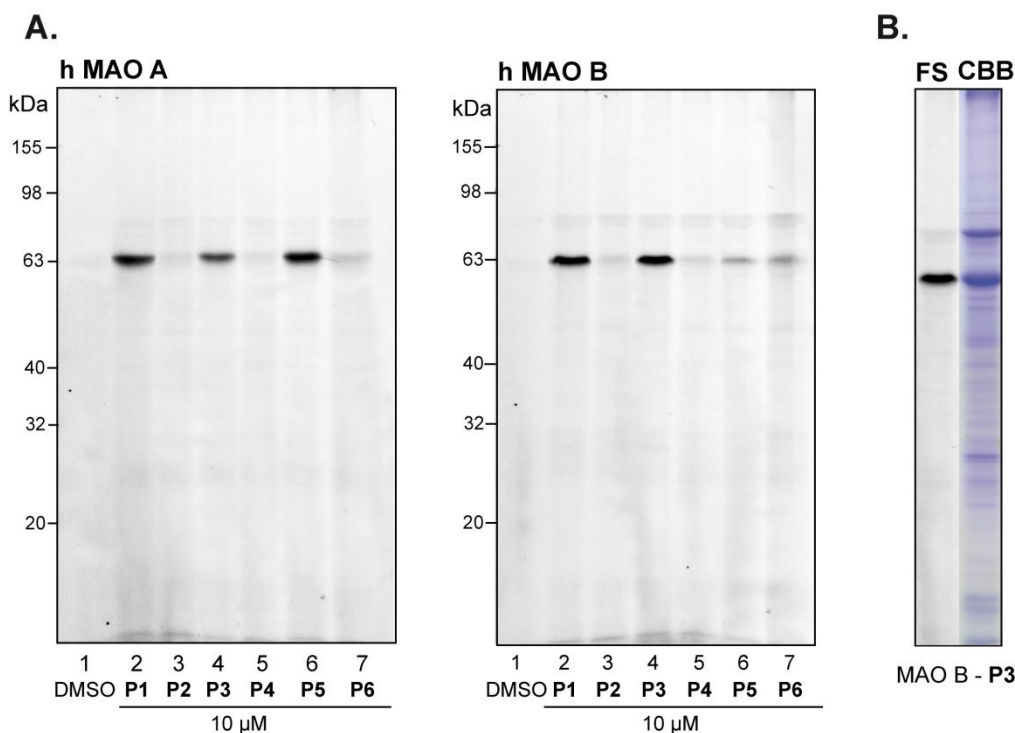
Figure 49. A. Screening of alkyne probes **P1**-**P6** with MAO A and MAO B. B. Comparison of fluorescence scanning (FS) and Coomassie Brilliant Blue (CBB) staining of labeling of MAO B by probe **P3**.

In these screening experiments we could demonstrate that both isoforms of MAO can be

efficiently labeled by three probes **P1**, **P3** and **P5** (Figure 49 A) as a main target, which

shows a direct comparison of total protein staining (CBB) with the fluorescence scanning

(FS) (Figure 49 B). Interestingly, all potent probes identified in the screening (**P1**, **P3**, **P5**)

include methyl substituted tertiary amines indicating that this feature might be important for

efficient labeling. Their structural counterparts without a methyl substituent at the amino

group (**P2**, **P4**, **P6**) exhibit very weak labeling suggesting that a secondary amino group is

decreasing the interactions between a probe and the protein or has unfavorable redox

behavior.

Incubation of the identified potent ABPs (**P1**, **P3**, **P5**) with the equimolar mixture of MAO A and MAO B revealed slightly different isoform preferences (Figure 50).

DMSO **P1** **P3** **P5**   10 µM

MAO A + MAO B (1 : 1)
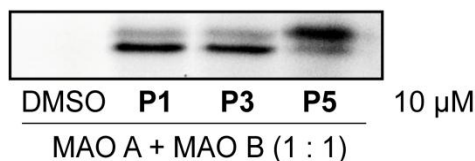
Figure 50. Labeling of mixture of both MAO isoforms with probe **P1**, **P3** and **P5**.

Probes **P1** and **P3** based on unspecific inhibitor pargyline and MAO B specific inhibitor deprenyl not surprisingly showed higher affinity towards MAO B, however in the absence of MAO B these probes were also able to efficiently label MAO A. Interestingly, probe **P5**, which is structurally related to probe **P3** only weakly labeled MAO B and exhibited the selectivity towards MAO A in the mixture of both isozymes.

4.4.2.2 Effect of click chemistry reaction directionality

As shown in Figure 49 A the background control (DMSO instead of a probe) revealed almost no unspecific interaction between the fluorescent tag (**TAMRA-N$_3$**) and the MAO enzyme. However, we wanted to check the effect of the opposite direction of click chemistry reaction on the labeling efficiency, as we had already prepared the appropriate probes and a fluorescent tag (**TAMRA-Alk**). The results of this comparison are presented in Figure 51.

hMAO A

1	2	3	4	5	6	Lane
-	**P1**	**P1**	-	**P1-N$_3$**	**P1-N$_3$**	Probe (10 µM)
-	ΔT	-	-	ΔT	-	Heat denaturation
TAMRA-N$_3$			TAMRA-Alk			Tag (100 µM)
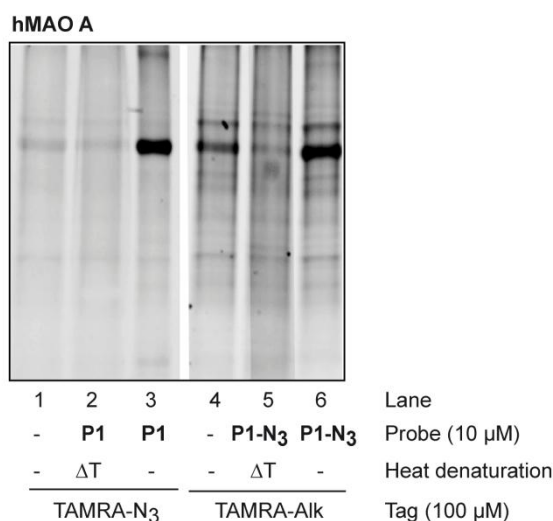
Figure 51. Comparison of click chemistry reaction between compatible pairs: **P1/TAMRA-N$_3$** and **P1-N$_3$/TAMRA-Alk**.

We could observe a similar trend for TAMRA-based fluorescent tags as we noticed previously for NBD-based tags. A fluorescent tag carrying alkyne group (**TAMRA-Alk**) gave rise to a significant background in the absence and presence (Figure 51, lanes 4-6) of activity-based probe **P1-N$_3$**, which was not the case when **TAMRA-N$_3$** tag was used (Figure 51, lanes 1-3). Such a high background can dramatically obscure weak fluorescent signals coming from low abundant proteins which is an undesirable factor in the labeling of complex proteomes. Therefore, in all other experiments we decided to use only probes carrying alkyne group (**P1**-**P6**) and **TAMRA-N$_3$**.

4.4.2.3 Specificity of labeling

One of the most important features of ABPP is that the labeling takes place exclusively with the active form of an enzyme and the covalent linkage is formed specifically in the active site. In order to test if the labeling of MAO enzymes is specific we performed a heat denaturation experiment, in which the enzyme sample was denatured by heat (6 min at 96 °C) and then cooled down to RT before adding the probe. The results are given in Figure 52.
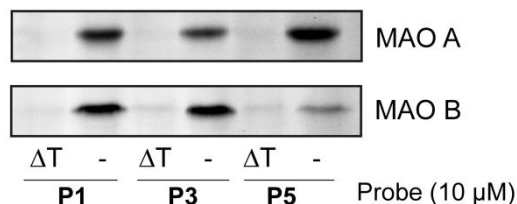
Figure 52. Labeling of MAO A and MAO B after heat denaturation (6 min at 96 °C) (right) and without heat denaturation (left) of the enzyme.

Importantly, the labeling of both isoforms MAO A and MAO B was completely abolished when the protein was deactivated by heat denaturation prior to incubation with the probe (Figure 52), suggesting that labeling occurs only with the active enzyme in a specific manner.

4.4.2.4 Site of labeling

To find out whether the labeling occurs on the same site as inhibition, we performed competetitive experiments in which the enzyme preparation was pre-incubated with various

concentrations of specific MAO inhibitors such as deprenyl for MAO B and clorgyline for MAO A prior to the addition of a probe. In case when a probe and inhibitor compete for the same site, one should expect that the fluorescence signal should be significantly decreased or lost. The results of such competitive experiments are shown in Figure 53.
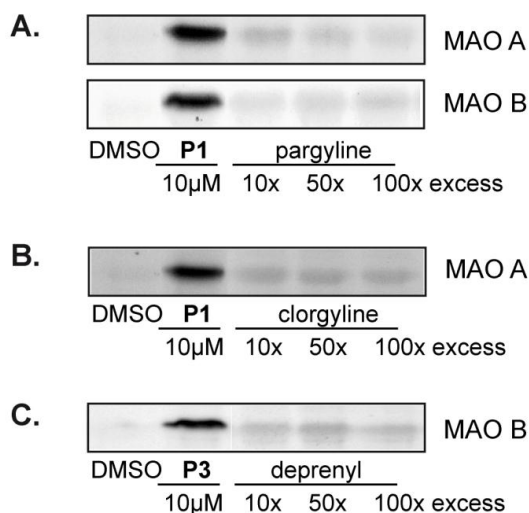
Figure 53. A. Competitive labeling of MAO A and MAO B with pargyline and **P1**, B. Competitive labeling of MAO A with clorgyline and **P1**. C. Competitive labeling of MAO B with deprenyl and **P3**.

Strikingly, the fluorescent signals were only present when no inhibitor was added to the enzyme sample and even a 10-fold excess of inhibitor (compared to a probe concentration) was able to abolish the enzyme labeling. Consequently, we could show in these competition experiments that our ABPP probes compete with MAO specific inhibitors for the same binding site (flavin cofactor) in the enzyme active site since for instance pargyline was able to efficiently block the enzyme labeling by probe **P1** (Figure 53 A). Similar outcome was observed also for all other combinations tested (clorgyline vs. **P1** or deprenyl vs. **P3** (Figure 53 B and C)).

4.4.2.5 Sensitivity of labeling

For the assignment of minimal probe concentration which was capable to efficiently label monoamine oxidases, we performed so called dose-down experiments for both MAO

isoforms with the most potent probes **P1**, **P3**, **P5** in labeling of MAO A (Figure 54 A) and **P1** and **P3** in labeling of MAO B (Figure 54 B).
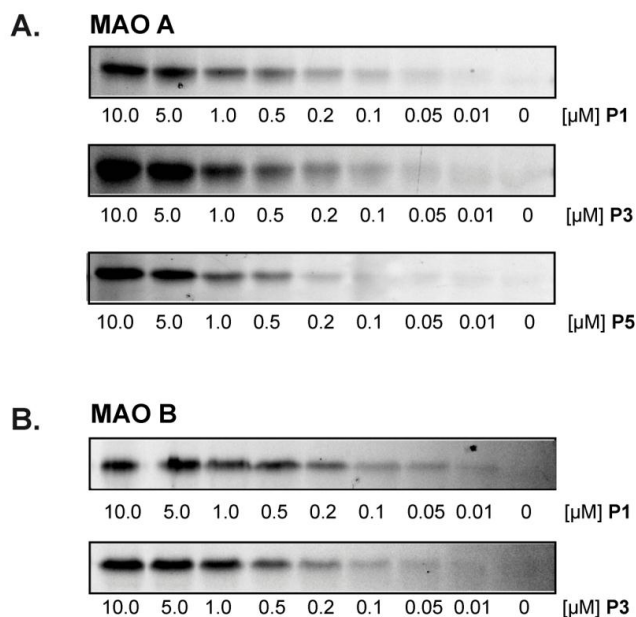
Figure 54. Concentration-dependent labeling of MAO A and MAO B by probe **P1**.

We found out that probes display dose-dependent labeling of MAO enzymes. MAO A could be yet efficiently labeled with probes **P1** or **P3** at the concentration as low as 100 nM, and with probe **P5** at the concentration as low as 200 nM. The labeling of MAO B with probe **P1** could be still observable at the concentration of 10 nM, whereas labeling by probe **P3** was efficient only up to the concentration of 100 nM.

In conclusion, the probes **P1**, **P3** and **P5** were able to label MAO enzymes in the nanomolar range, exhibiting a reasonable sensitivity, when compared to other ABPP studies.

4.4.2.6 Time of incubation

During *in vivo* studies, time of labeling is a crucial factor influencing its quality, since probes require a particular time to reach their targets and to accomplish this task they need to cross numerous cell membranes and cell compartments. Thus, we investigated the effect of time of incubation on the labeling efficacy (Figure 55). The incubation of MAO A and MAO B

membrane preparations with a given probe at the concentration of 10 µM was performed at

RT for a given period of time, followed by the attachment of **TAMRA-N$_3$** tag.
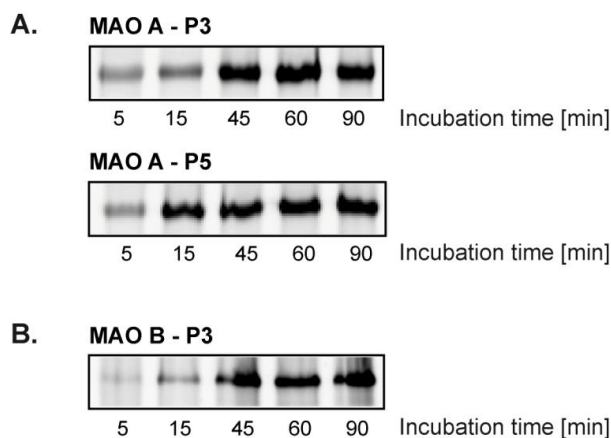
Figure 55. Time-dependent labeling of MAO A with probes **P3** and **P5** (A) and MAO B with **P3** (B).

In these experiments we could observe that labeling efficacy depends on the time of

incubation of a probe with the enzyme. Efficient labeling requires at least 15 min of

incubation, however a prolonged incubation time (45-90 min) improved the intensity of the

fluorescent signal. Hence, this experiment confirmed that 1 h incubation, used previously, is

an optimal time period that assures a proper balance between the time-performance of the

procedure and efficient labeling of the enzyme.

4.4.2.7 Optimization of the labeling

In further experiments we made an effort to optimize and simplify the labeling procedure.

First of all, we attempted to reduce the concentration of a fluorescent tag and eliminate the

protein precipitation procedure. Protein precipitation was not necessary when a more

sensitive fluorescent scanner was used (Fujifilm Life Science Las-4000 Luminescent Image

Analyzer). However, when Bio-Rad Molecular Imager FX was employed a high background

from a fluorescent tag very often concealed the labeled protein bands, making the

precipitation procedure indispensable under conditions used.

Fortunately, the decrease in fluorescent tag (**TAMRA-N$_3$**) concentration from 100 µM to 20

µM resulted in a low background (Figure 56 A, lanes 1-2 vs. lanes 3-8), so that even without

precipitation procedure the fluorescent bands were observable (Figure 56 A, lanes 4 and 6). Decreased concentration of TAMRA-N$_3$ fluorescent tag was sufficient for MAO labeling regardless the reducing agent used (Figure 56 A, lanes 3-4 and 5-6, respectively) or probe applied (**P3** and **P5**, Figure 56 A, lanes 5 and 6).
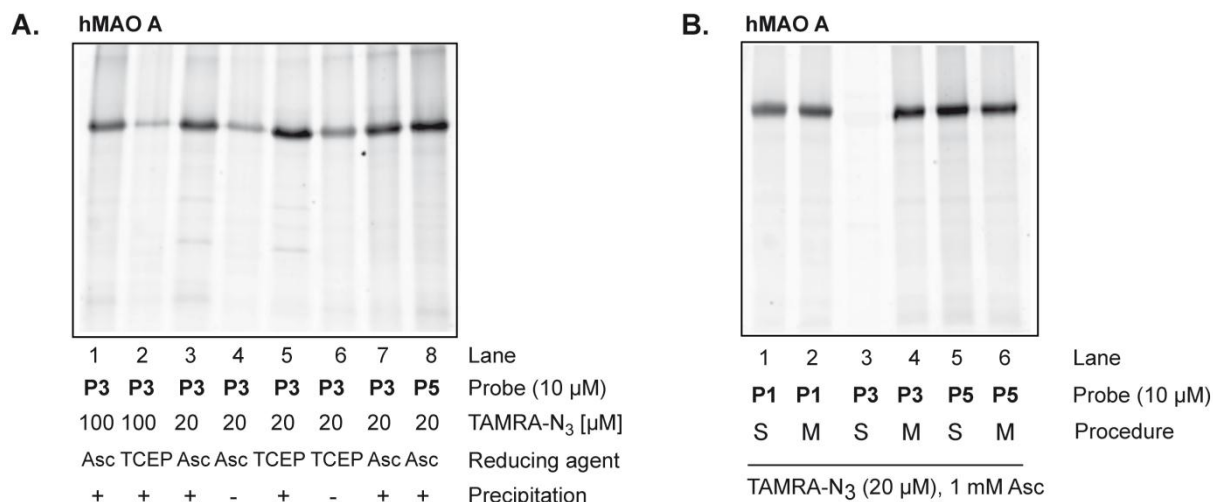
Figure 56. Optimization of the labeling procedure. (Asc = sodium ascorbate, TCEP = tris(2-carboxyethyl)phosphine, S = sequential procedure, M = master mix procedure).

Also, we attempted to improve the performance of click chemistry conjugation through the replacement of a successive addition of reaction components (S = sequential procedure) by preparing a master mix comprising fluorescent tag, reducing agent and TBTA ligand and adding it at once to the enzyme sample (M = master mix procedure), followed by the addition of copper catalyst (Figure 56 B). This procedure turned out to be not only time-saving, but also helped to avoid statistical mistakes resulting in some cases in the absence of a fluorescent signal (Figure 56 B, lane 3).

4.4.2.8 Labeling of other flavin-dependent enzymes

Finally, we investigated the developed ABPP strategy in terms of its selectivity. We wanted to find out whether it can be also extended to profiling of other flavin-dependent oxidases. For this purpose we used several other flavin-dependent enzymes such as berberine bridge enzyme (BBE, (*S*)-reticuline oxidase, bicovalently attached FAD, 56 kDa),[142,308] Lot6p (FMN-dependent reductase, non-covalently attached FMN, 21.2 kDa),[309] Dbv29 (H91A mutant,

oxidase, bicovalently attached FMN, 66 kDa),[310] YcnD (FMN-dependent oxidoreductase, non-covalently attached FMN, 29.1 kDa).[311] These enzymes were labeled (Figure 57) using the same procedure as for MAO A and MAO B. As a positive control MAO A was included and BSA (bovine serum albumin, 69 kDa) as a negative control.

MAO A			BBE			Lot6p			Dbv29 H91A			YcnD			BSA			
1	2	3	1	2	3	1	2	3	1	2	3	1	2	3	1	2	3	Lane
-	P3	P3	-	P3	P3	-	P3	P3	-	P3	P3	-	P3	P3	-	P3	P3	Probe (10 µM)
-	ΔT	-	-	ΔT	-	-	ΔT	-	-	ΔT	-	-	ΔT	-	-	ΔT	-	Heat denaturation
TAMRA-N$_3$			TAMRA-N$_3$			TAMRA-N$_3$			TAMRA-N$_3$			TAMRA-N$_3$			TAMRA-N$_3$			Tag (100 µM)
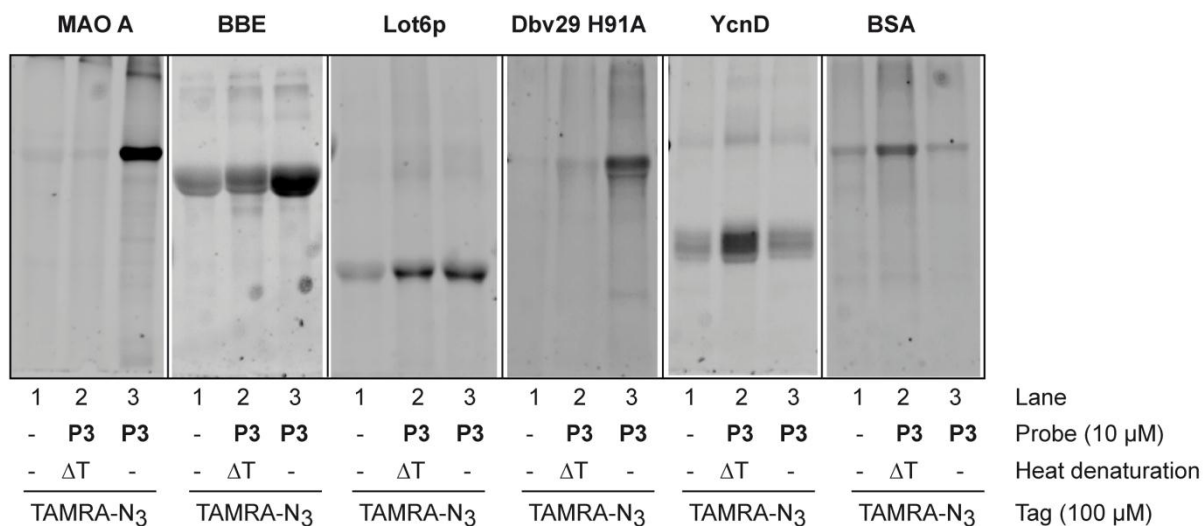
Figure 57. Labeling of different flavoenzymes and BSA (as negative control) with probe **P3**.

From those simple experiments we found out that also other flavoenzymes, which possess covalently linked flavin cofactor (BBE or Dbv29) can be labeled by developed activity-based probes (probe **P3** at 10 µM concentration), however, the labeling is not as efficient as for MAO enzymes and it required a further in-depth investigations. Other flavoenzymes which have the flavin cofactor non-covalently attached to the apoenzyme (Lot6p, YcnD) or BSA showed only unspecific binding of a fluorescent tag, suggesting that for such kind of enzymes incorporation of a photocrosslinker moiety could help to stabilize the linkage to the flavin cofactor.

4.4.2.9 Summary

The developed ABPP system was evaluated *in vitro* using human monoamine oxidase membrane preparations with respect to the scope of probes library, site and sensitivity of labeling, time of incubation as well as the direction of click chemistry reaction.

It was found that three probes **P1**, **P3** and **P5** are able to efficiently label MAO A and MAO B as a main target. Interestingly, all the probes comprise a methyl substituent within tertiary amino group, indicating this feature is essential for efficient labeling.

With respect to the direction of click chemistry reaction, the MAO labeling is effective and devoid of high background level only when a fluorescent tag containing an azido group (**TAMRA-N$_3$**) is employed.

We could observe that probes display dose- and time-dependent labeling. MAO A can be labeled effectively with probe **P1** at a concentration as low as 100 nM, whereas MAO B can be labeled with **P1** even at a concentration of 10 nM, within less than 1 h.

We also could prove that probes compete with MAO specific inhibitors for the same binding site (flavin cofactor) in the enzyme active site since even a slight excess of inhibitor concentration was able to efficiently block the enzyme labeling.

Concerning the selectivity of prepared activity-based probes, they are highly specific for both MAO enzymes, however, are not able to distinguish one from another. Also, other flavin-dependent enzymes, possessing covalently attached cofactor can be labeled by those probes, however the efficiency is much lower, when compared to MAO labeling. Nevertheless, it indicates that this system can be applied in profiling also other flavoenzymes.

Collectively, these results demonstrate that the developed ABPP system can serve as an effective chemical tool for profiling activity of both isoforms of monoamine oxidase *in vitro*.

4.5 Application of developed ABPP system in complex proteomes

The developed ABPP platform proved to be a very efficient tool in studying the activity of monoamine oxidases as well as showed a reasonable promiscuity in labeling of other flavin-dependent enzymes. Therefore, it was of utmost interest to investigate the applicability of this system in complex biological systems *in vivo.* We were very interested in evaluating the

potency, selectivity and scope of the most promising probes **P1** and **P3** (Figure 58) in profiling of monoamine oxidases in far more complex biological samples (cell lysates or in living cells). Additionally, we wanted to find out if these probes are able to target other flavin-dependent enzymes.
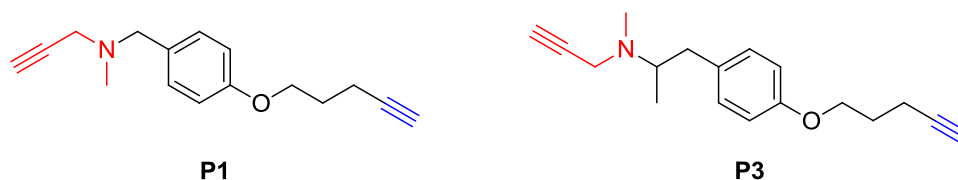
Figure 58. Structure of most potent activity-based probes **P1** and **P3**.

4.5.1 Labeling of mouse tissue homogenates *in vitro*

We started the evaluation of the ABPP strategy with *in vitro* screening of different mouse tissue homogenates. Samples of tissue lysates were diluted with PBS pH 7.4 to the total protein concentration ca. 1-2 mg/mL and then incubated with DMSO (blank control) or a given concentration of a probe (**P1** or **P3**) for 1 h at RT with gentle mixing. Subsequently, the samples were subjected to click chemistry reaction to append a fluorescent tag (**TAMRA-N₃**) in order to visualize the labeled proteins.

4.5.1.1 Scope of labeling

We screened three different mouse tissue proteomes: heart, lungs and brain to test how efficient and selective probes **P1** and **P3** are. The results of the labeling of mouse heart and lung tissue are presented in Figure 59.

These first labeling experiments have revealed only few fluorescent protein bands (e.g. bands of ca. 65, 45, and 30 kDa), which were found mostly in the soluble fraction of both proteomes, indicating a remarkable selectivity of probes **P1** and **P3** towards only very few protein targets. However, heat denaturation controls could not clearly determine whether these bands were specifically tagged or not. Unfortunately, the attempts to identify the

labeled proteins by analysis of tryptic peptides by tandem LC-MS/MS platform were not successful.
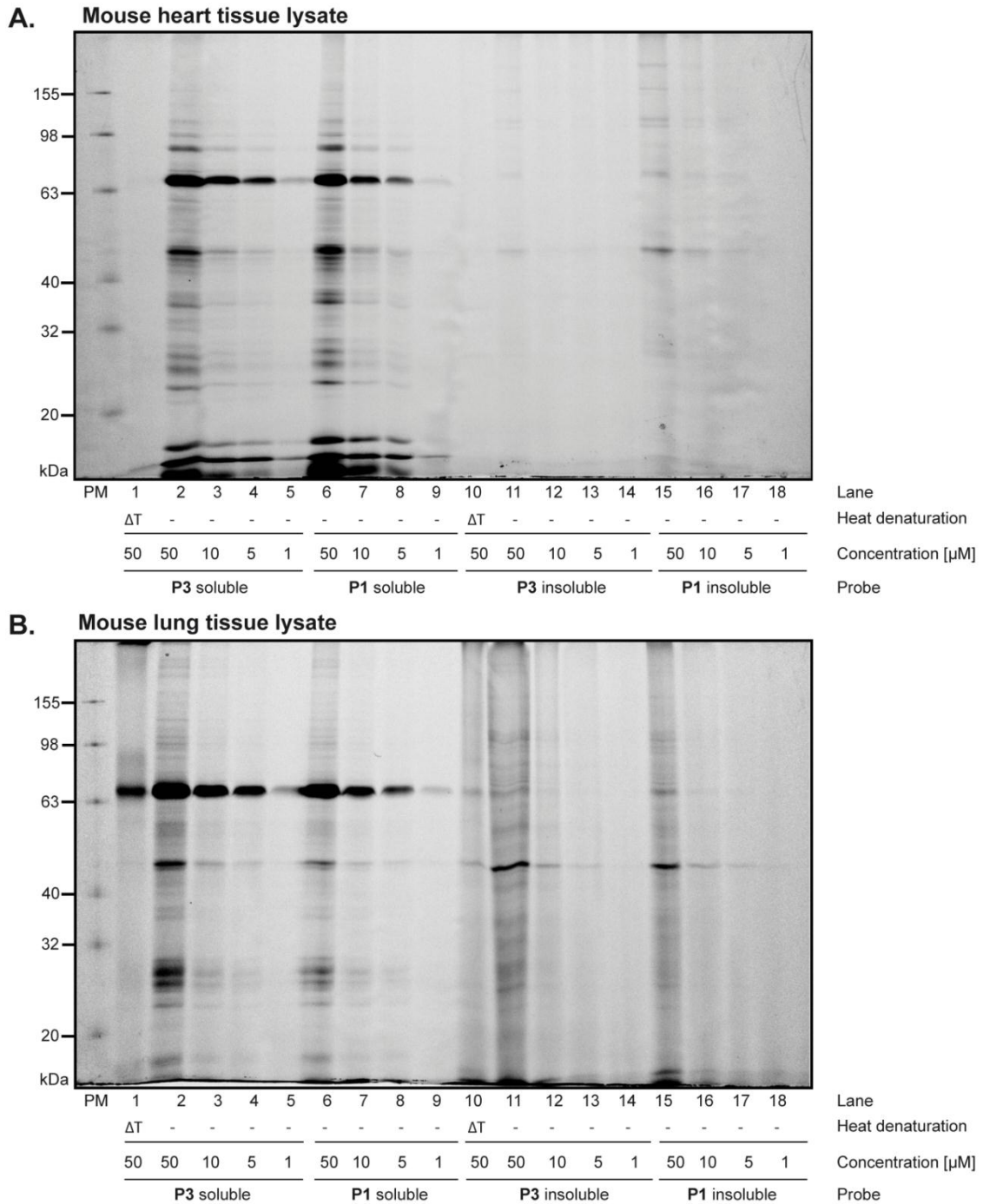
Figure 59. Labeling of mouse heart (A) and lung (B) tissue homogenate by probes **P1** and **P3** (PM = protein marker).

The standard protein identification workflow (Figure 60) employs first the attachment of a trifunctional reporter tag **TAMRA-biotin-N₃**[312] (Figure 61) to a protein-bound probe under click chemistry conditions. Then, labeled proteins are enriched on avidin beads thanks to the

strong binding to the biotin, which is a component of the reporter tag. Subsequently, they are separated by gel electrophoresis. Enriched proteins are then visualized by in-gel fluorescence scanning and proteins of interest are excised from the gel and subjected to the following in-gel tryptic digest.[29] Finally, tryptic peptides are analyzed by LC-MS/MS. Mass spectrometry results are searched against the corresponding databases using for instance the SEQUEST algorithm[90] in order to reveal the identity of a protein of interest.
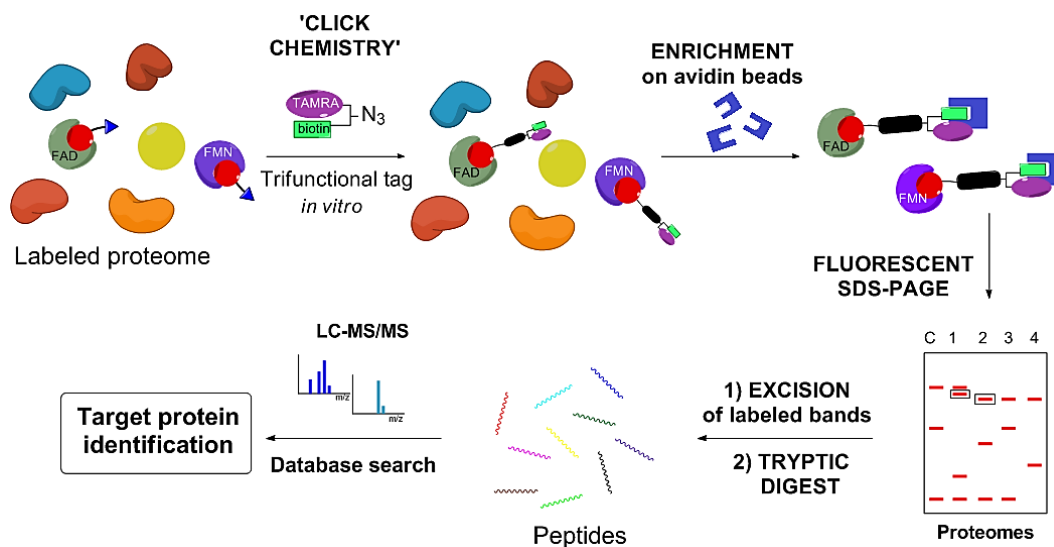
Figure 60. Workflow of protein identification by mass spectrometry platform.

In our case, we were not able to observe the efficient enrichment of labeled proteins in comparison to control samples, which did not involve a trifunctionaler linker, thus we could not proceed further with the identification protocol. Nevertheless, these difficulties enforced our investigations on optimization of labeling and enrichment procedure.
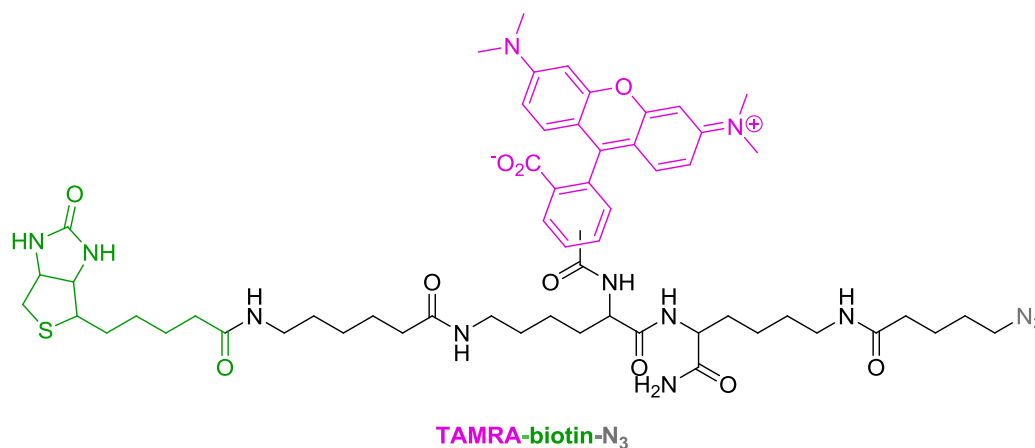
TAMRA-**biotin**-N$_3$

Figure 61. Structure of trifunctionaler reporter tag **TAMRA-biotin-N$_3$** used in our studies and kindly provided by the group of Sieber.[312]

The most promising and interesting results were obtained from the labeling of mouse brain lysate. Among many unspecific protein bands on the fluorescent gel (Figure 62) we were able to identify two relatively weak bands labeled by probe **P1** (Figure 62, lanes 2-4) and one band labeled by probe **P3** (Figure 62, lanes 14-15), which was compliant to the lower band labeled by probe **P1**.

Mouse lung tissue lysate

	PM	1	2	3	4	5	6	7	8	9	10	11	12	13	14	15	16	Lane
Heat denaturation		ΔT	-	-	-	ΔT	-	-	-	ΔT	-	-	-	ΔT	-	-	-	Heat denaturation
Concentration [µM]		10	10	50	100	10	10	50	100	10	10	50	100	10	10	50	100	Concentration [µM]
Probe		**P1** soluble				**P1** insoluble				**P3** soluble				**P3** insoluble				Probe
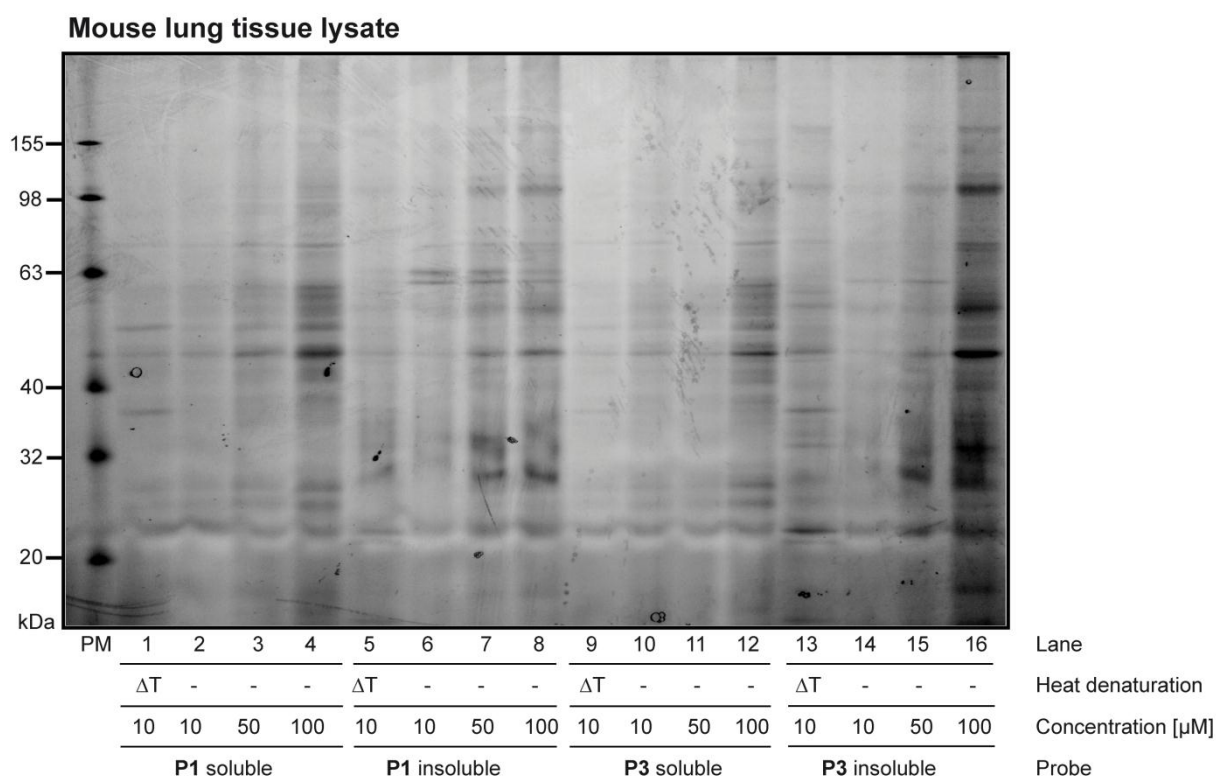
Figure 62. Labeling of mouse brain tissue lysate by probes **P1** and **P3** (PM = protein marker).

These protein bands were located in the range of 60 kDa in the insoluble fraction of the lysate and were not present in the heat denaturation control (Figure 62, lanes 1 and 13 and Figure 63 A). The localization of the labeled protein targets gave a hint that they could presumably correspond to monoamine oxidases A and B, hence we performed an in-depth ABPP investigation of insoluble fraction of mouse brain proteome (Figure 63).

Further dose-down experiments revealed that the labeling, although weak, was dose-dependent and was still observable at the concentration of 100 nM (Figure 63 B). Interestingly and importantly, molecular weights of the labeled bands matched up with those of MAO A (higher band) and MAO B (lower band) (Figure 63 C), when we performed a comparative labeling of mouse brain lysate (insoluble fraction) and MAO A and MAO B. Also,

102

the labeling was completely abolished when the lysate was first incubated with excess of

MAO inhibitors (Figure 63 D).
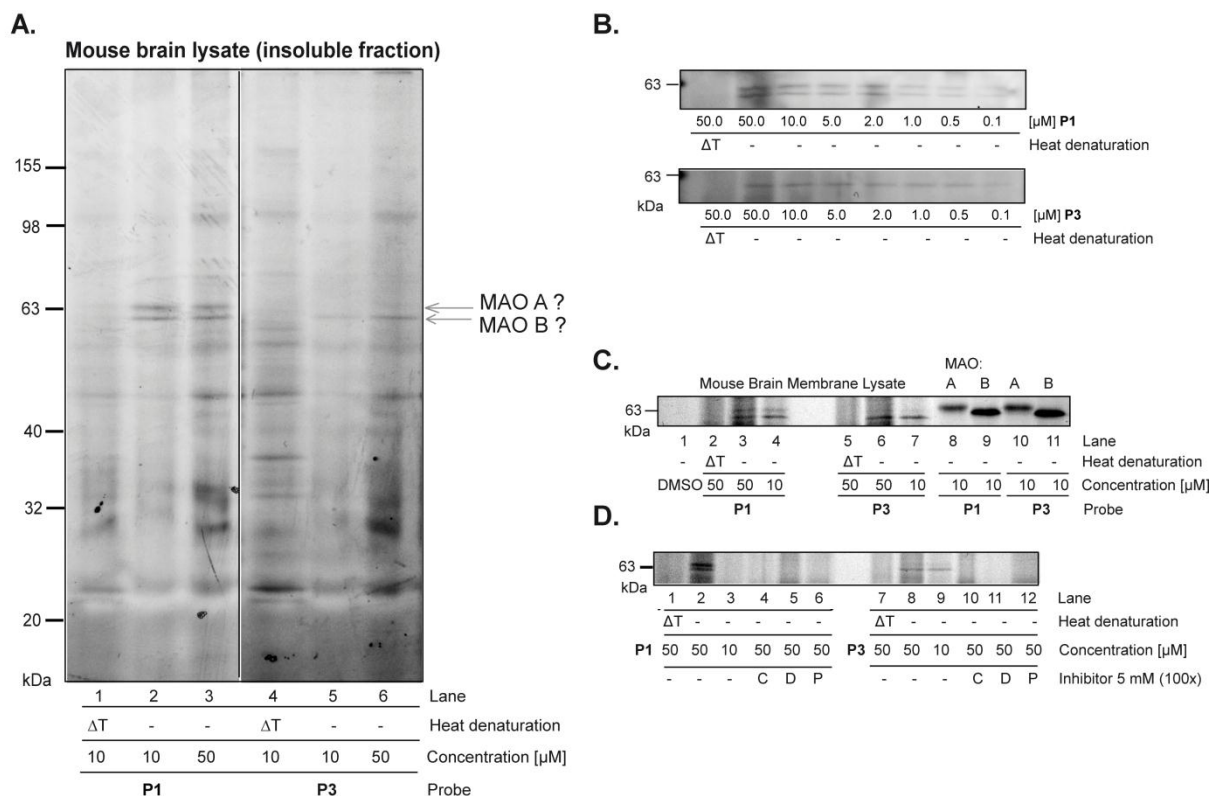
Figure 63. A. Labeling of mouse brain lysate (insoluble fraction) with **P1** and **P3**. B. Concentration-dependent labeling of mouse brain membrane lysate by probe **P1** and **P3**. C. Comparative labeling of mouse brain lysate (insoluble fraction) and MAO A and MAO B with **P1** and **P3**. D. Competitive labeling of mouse brain lysate with **P1** and **P3** and MAO specific irreversible inhibitors (C – clorgyline, D – deprenyl, P – pargyline).

Collectively, these results gave a strong but indirect indication that the labeled protein targets are MAO A and MAO B. Unfortunately, unambiguous identification of these targets by mass spectrometry was again not successful, probably due to the instability of protein samples enriched on avidin beads.

4.5.1.2 Development of photocrosslinker probes

In order to increase the stability of the covalent connection between the target protein and the activity-based probe, we decided to prepare new ABPs equipped with a photocrosslinker moiety which would form an unspecific but stable covalent bond to any proximal amino acid residue upon UV irradiation.

4.5.1.2.1 Design and synthesis of photocrosslinker probes

Using our previous observations that any structural modification on pargyline or deprenyl MAO inhibitors, which does not significantly changes their inhibitory properties, should be introduced in *para* position to the reactive group in the arene ring, we decided to incorporate a photoreactive benzophenone moiety exactly in this position. We intended to conjugate a photoreactive amino acid analog, *p*-benzoyl-L-phenylalanine[313] with the intermediate aminophenols **9** and **12** using standard direct coupling methods. The involvement of aminoacid residue would allow attaching the alkyne handle to the free amine group by a substitution with the appropriate alkyne derivative (e.g. chloride or succinimide ester). These considerations led to the design of structures presented in Figure 64.

Once the structure of the probes was designed, we could work on the development of a simple and reliable synthetic strategy.

(50) **P1-Phot**   (51) **P3-Phot**
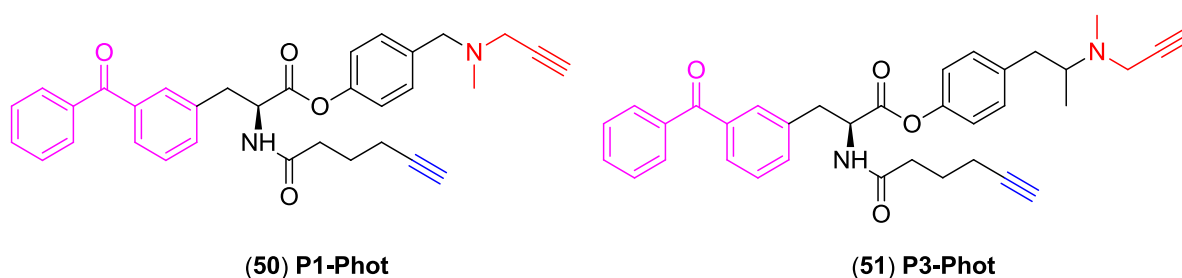
Figure 64. Design of the photocrosslinker probes based on probes **P1** and **P3**. A reactive group is highlighted in red, a photocrosslinker moiety in purple, and alkyne tag in blue.

At first, we performed a direct esterification between Fmoc-protected *p*-benzoyl-L-phenylalanine (Fmoc-Bpa-OH) and the intermediate aminophenols **9** and **12** using *N,N*-

diisopropylethylamine (DIEA) and PyBOP as a coupling agent in DCM, according to the reports of Kim and Patel[314] and Castro et al.[315] The corresponding esters **52** and **53** were obtained in 63% and 58% yield, respectively (Scheme 19).
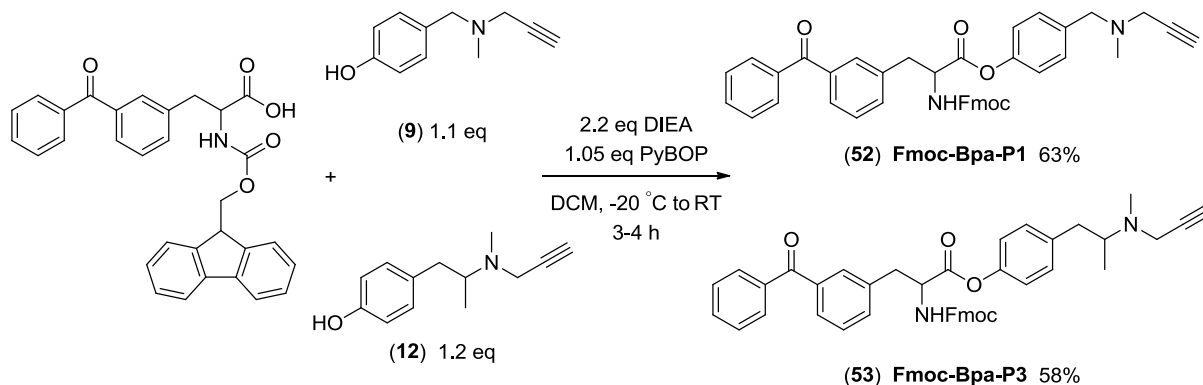
Scheme 19. Synthesis of Fmoc protected esters **52** and **53** by PyBOP coupling.

Unfortunately, the deprotection of Fmoc group to liberate the free amine group using several procedures (piperidine in DCM or DMF,[316] catalytic DBU in THF[317]) led only to the consumption of the starting material but deprotected amino acids could not be identified and isolated. This forced us to change the reaction sequence and start with the preparation of *N*-substituted p-benzoylphenylalanine.

In the modified approach, we prepared first *N*-substituted *p*-benzoylphenylalanine **54** by reacting *p*-benzoyl-L-phenylalanine (H-Bpa-OH) with 5-hexynoic acid succinimide ester (**55**) in DCM and using DIEA as a base as described by the group of Sieber.[121] The reaction proceeded smoothly delivering the product **54** (**Bpa-Alk**) as a yellowish foam in 96% yield (Scheme 20, upper reaction).
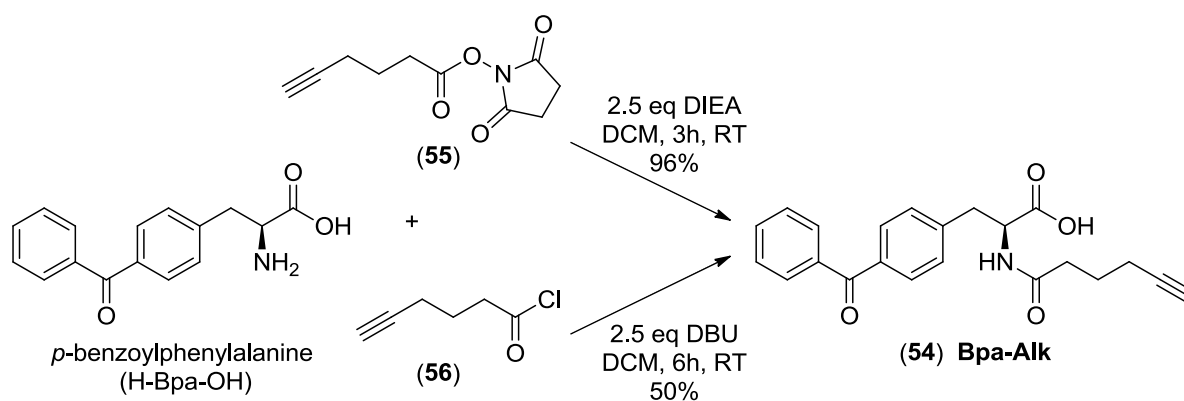
Scheme 20. Synthesis of (*S*)-3-(*p*-benzoylphenyl)-2-(hex-5-ynamido)propanoic acid (**54**).

5-Hexynoic acid succinimide ester (**53**) was prepared by coupling of 5-hexynoic acid with *N*-hydroxysuccinimide using either EDC (98% yield) or DIC (86% yield), aaccording to the procedures of Jagadish et al.[318] and Eirich and co-workers,[121] respectively (Scheme 21, upper reaction). Alternatively, *p*-benzoylphenylalanine was substituted by hex-5-ynoyl chloride (**56**) using DBU as a base to deliver product **54** as described by Staub,[319] however, this method turned out to be less efficacious (50% yield) (Scheme 20, lower reaction). Hex-5-ynoyl chloride (**56**) was synthesized by reacting 5-hexynoic acid with oxalyl chloride in DCM in the presence of catalytic amount of DMF. The product **56** was obtained in 64% yield after distillation (Scheme 21, lower reaction).
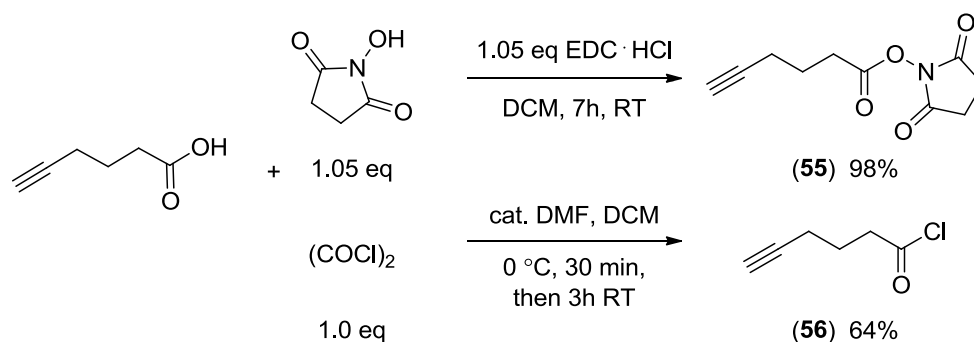
Scheme 21. Synthesis of 5-hexynoic acid succinimide ester (**53**) and hex-5-ynoyl chloride (**54**).

In the second step, the intermediate **54** was subjected to different coupling reactions using the previously applied DIEA/PyBOP system or a standard EDC esterification. Unfortunately, PyBOP coupling, performed under conditions decribed in the synthesis of esters **52** and **53** delivered the photocrosslinker probe **P1-Phot** only in 38% yield. On the other hand, a simple direct coupling in DCM at RT using EDC provided the desired product **51** in much higher yield (85%). Hence, this method was used for the preparation of the second photocrosslinker probe **P3-Phot**, which was obtained in moderate yield (62%). The final synthesis of photocrosslinker probes **51** and **52** is depicted in Scheme 22.
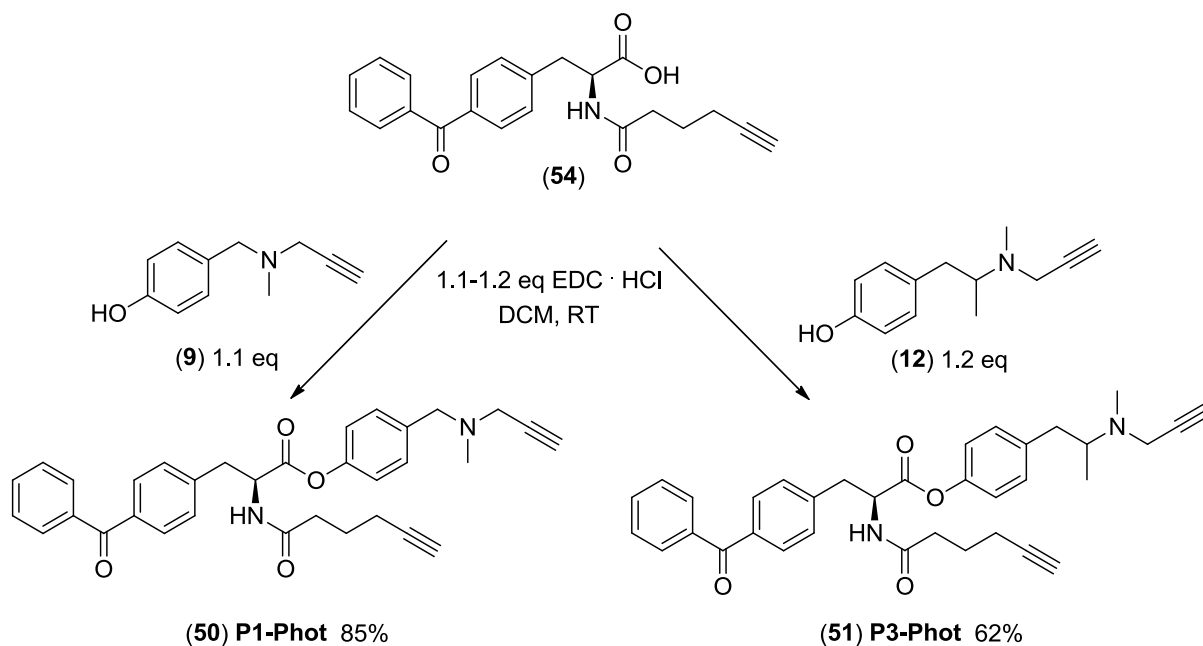
Scheme 22. Final step of the synthesis of photocrosslinker probes **50** and **51** based on probes **P1** and **P3**, respectively.

Subsequently, these probes could be evaluated with regard to their ability to label MAO enzymes and other related proteins in complex proteomes.

4.5.1.2.2 Evaluation of photocrosslinker probes with mouse tissue homogenates

In the first attempt, we wanted to evaluate whether prepared photocrosslinker probes **P1-Phot** and **P3-Phot** fit into the active site of monoamine oxidases and are able to label the MAO isoforms. When performing a photocrosslinking ABPP experiment, it is very important to include all necessary controls such as a blank control (it does not include the probe but it is exposed to UV light), heat denaturation control (it involves a heat inactivated sample, which is then incubated with a probe and illuminated by UV light) and a negative control (a sample which was not irradiated by UV light, but was labeled by a probe). Comparing these all controls with a sample, which is pre-incubated first with a photocrosslinker probe and then irradiated by UV light, helps to determine which protein targets are labeled in a specific manner. The pre-incubation enables the probe to find its protein target, whereas UV irradiation assures the formation of a covalent linkage to this protein. The results of such an experiment performed with MAO enzymes are presented in Figure 65.
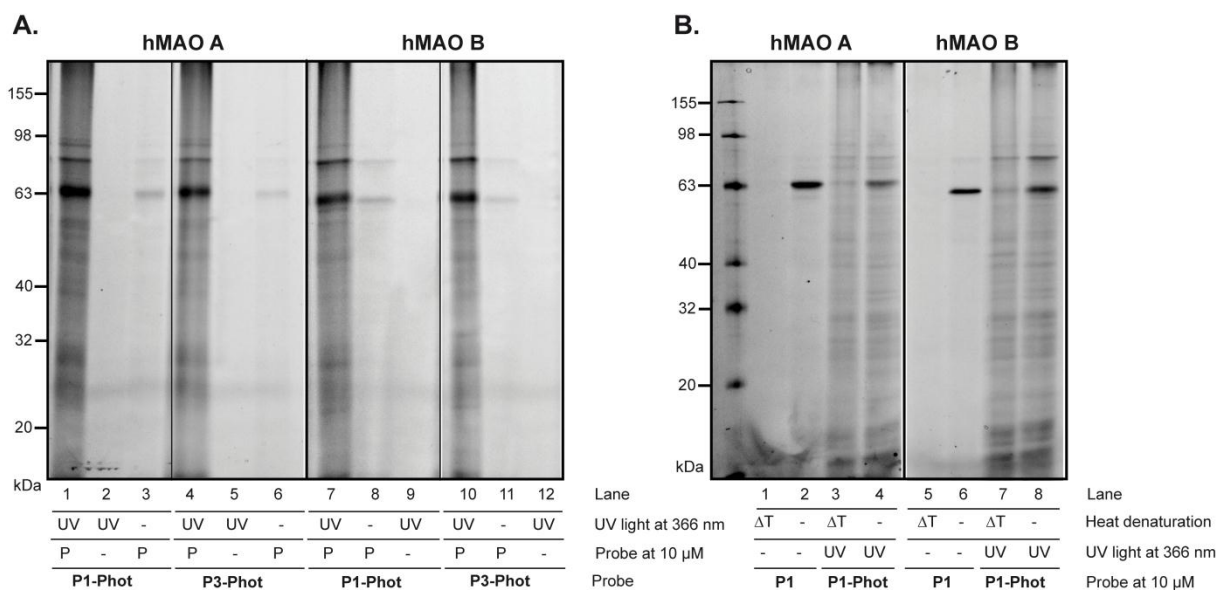
Figure 65. A. Fluorescent analysis of labeling of MAO A and MAO B with photoactive probes **P1-Phot** and **P3-Phot**. B. Comparison of labeling of MAO enzymes between probe **P1** and **P1-Phot**.

Upon UV irradiation at 366 nm both photocrosslinker probes **P1-Phot** and **P3-Phot** were able to efficiently label MAO A (Figure 65 A, lanes 1 and 4, respectively) and MAO B (Figure 65 A, lanes 7 and 10, respectively). Interestingly, the probes labeled both MAO enzymes also without UV irradiation (Figure 65 A, lanes 3, 6 and 8, 11, respectively) using only a covalent bond to FAD cofactor formed by a warhead. However, the intensity of the labeling was relatively weaker. The blank controls have shown very little background originating from the fluorescent tag **TAMRA-N$_3$** and UV illumination (Figure 65 A, lanes 2, 5 and 9, 12).

We also compared the efficiency in labeling of MAO A and B between the photocrosslinker probes **P1-Phot** and **P3-Phot** and their parent probes **P1** and **P3**. Probe **P1-Phot** labeled both isoforms of MAO in a specific manner as indicated from the heat denaturation controls (Figure 65 B, lanes 3-4 and 7-8). However, the intensity of that labeling was lower in a direct comparison with probe **P1** (Figure 65 B, lanes 1-2 and 5-6). In addition, probe **P1** gave much less background, compared to probe **P1-Phot** (Figure 65 B). Similar results were obtained for the probes **P3** and **P3-Phot** (data not shown). Collectively, these data demonstrate that prepared photocrosslinker probes **P1-Phot** and **P3-Phot** were capable of labeling of MAO A and B, although the introduced structural modifications were significant and resulted in

probes of a greater size when compared to probes **P1** and **P3**. The labeling seems to be dual and occurs presumably *via* a warhead and benzophenone moiety.

Next, we wanted to test whether the probes **P1-Phot** and **P3-Phot** are effective in labeling protein targets in more complex proteomes. Especially, we were interested if these probes are able to stably tag two proteins in the range of 60 kDa in mouse brain homogenate, which were previously labeled by probes **P1** and **P3**.

Surprisingly, only few protein bands were found in mouse brain lysate upon labeling by photoactive probes **P1-Phot** and **P3-Phot** (Figure 66). Probes **P1-Phot** and **P3-Phot** labeled several proteins, which were localized in the soluble fraction of mouse brain homogenate and exhibited various molecular weight (e.g. approx. 155, 65, 55, 45 kDa) (Figure 66, lanes 2 and 10). However, some of these bands (55, 45 kDa) were also present in the heat denaturation control, suggesting that these protein targets were labeled unspecifically. Unfortunately, in the insoluble fraction of the lysate we were not able to identify any significant and specific bands in the range of ca. 60 kDa, which could correspond to bands previously labeled by probes **P1** and **P3**.
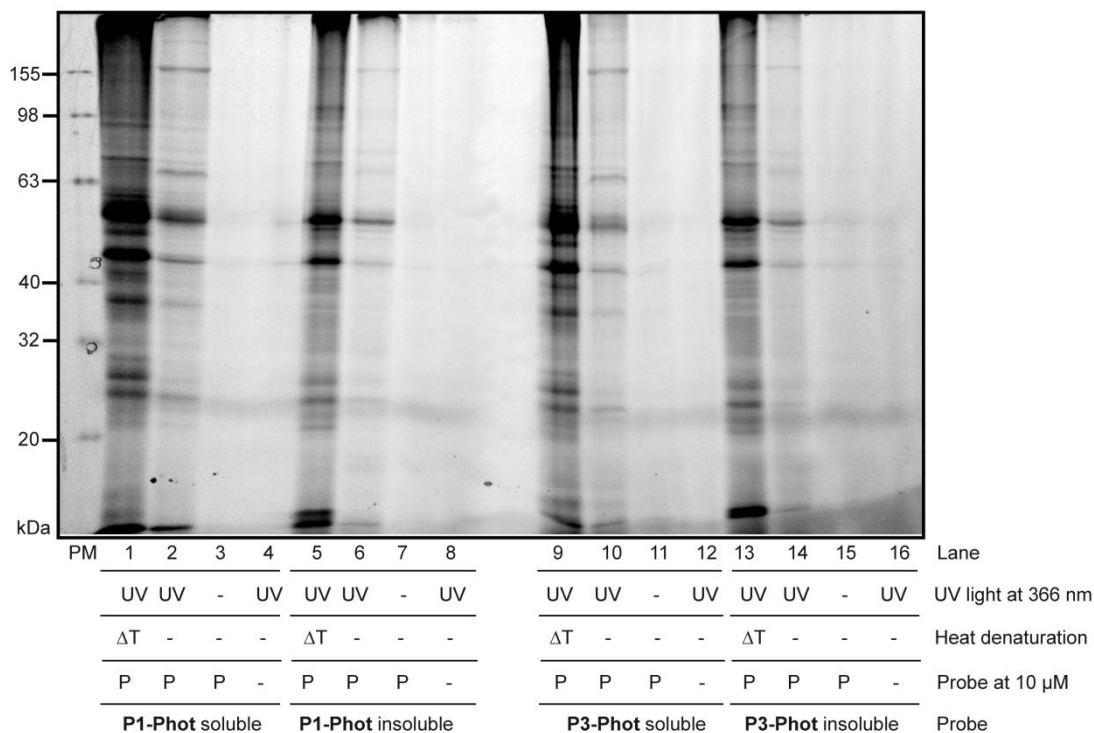
Figure 66. Labeling of mouse brain lysate by probes **P1-Phot** and **P3-Phot**.

Therefore, our assumption that photocrosslinker probes should stably label MAO enzymes, as it was shown in the preliminary experiments with recombinant enzymes, was not successful. As a consequence, we were also not able to identify these targets by mass spectrometry.

4.5.1.3 Summary

ABPP labeling of complex proteomes *in vitro* such as different mouse tissue homogenates turned out to be a very challenging and difficult task.

Although very potent in the first screenings probes **P1** and **P3** and newly prepared photoreactive probes **P1-Phot** and **P3-Phot** proved very effective ABPP tools in labeling of recombinant isoforms of monoamine oxidases, their efficacy in labeling of MAO enzymes in native samples was significantly reduced. One reason for such results might be that these proteins are unstable and lose rapidly their activity in a homogenate, hence they cannot be efficiently labeled by the probes. On the other hand, their intrinsic abundance in the lysate might be also scarce and therefore their visualization by a fluorescent tag might be obscured by some unspecific background signals.

Nevertheless, we found in the insoluble fraction of mouse brain lysate two protein bands, which presumably are MAO A and MAO B. We could not unambiguously assign the identity of the protein by mass spectrometry. However, indirect evidence from competitive and comparative ABPP experiments are in favour that we labeled MAO enzymes in this complex proteome. Doubtlessly, further investigation and optimization of methods (preparation of the tissue samples, enrichment protocols) is necessary to confirm these data.

4.5.2 Labeling of different human cells and human cell lysates

Labeling of native eukaryotic systems *in vivo* was a parallel direction in our investigations. We intended to perform the ABPP labeling by probes **P1** and **P3** in living cells as well as in cell lysates. This would provide an insight in differences in enzyme activities in intact cells and cell lysates after the discruption of cells integrity and complex interactions existing only *in vivo*.

First, we performed a random screening of three various human cell lines: HeLa (cervix adenocarcinoma, ATCC number: CCL-2™), MDA-MB-231 (breast adenocarcinoma, ATCC number: HTB-26™) and H460 (large cell lung carcinoma, ATCC number: HTB-177™). The most interesting differences and a distinctive labeling could be observable in HeLa cells. Unfortunately, labeling in two other cell lines was inconclusive and not reproducible. Therefore we did not investigate it further.

4.5.2.1 Labeling of HeLa cells

The HeLa cell line is the oldest, most widely distributed, immortal human cell line[320] established from a biopsy originated from a visible lesion on the cervix.[321] These cells are commonly used in laboratory research and medical investigations on HeLa cells made an enormous contribution in uncovering the genetics of cancer, cloning, gene mapping and the effects of radiation and toxic substances on human tissue. It also helped in developing the treatment for polio, herpes, leukemia, influenza, hemophilia and many other severe diseases.[320,322] Morphologically, HeLa are epithelial-like cells which grow very rapidly in monolayers (Figure 67).
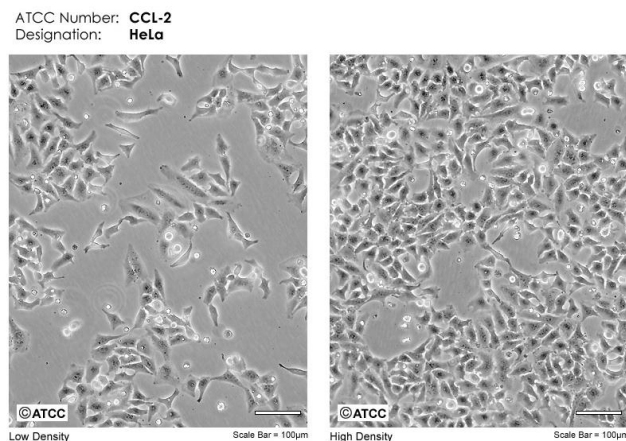
Figure 67. Morphology of HeLa cells. (Source: http://www.atcc.org/Attachments/1765.jpg)

First, we performed a typical ABPP labeling of HeLa cell lysate, by incubating both soluble and insoluble fraction of cell lysate samples with various concentrations of probes **P1** and **P3** or DMSO for 1 h at RT. The incubation was followed by the attachment of the fluorescent **TAMRA-N$_3$** tag to visualize the labeled protein targets (Figure 68).
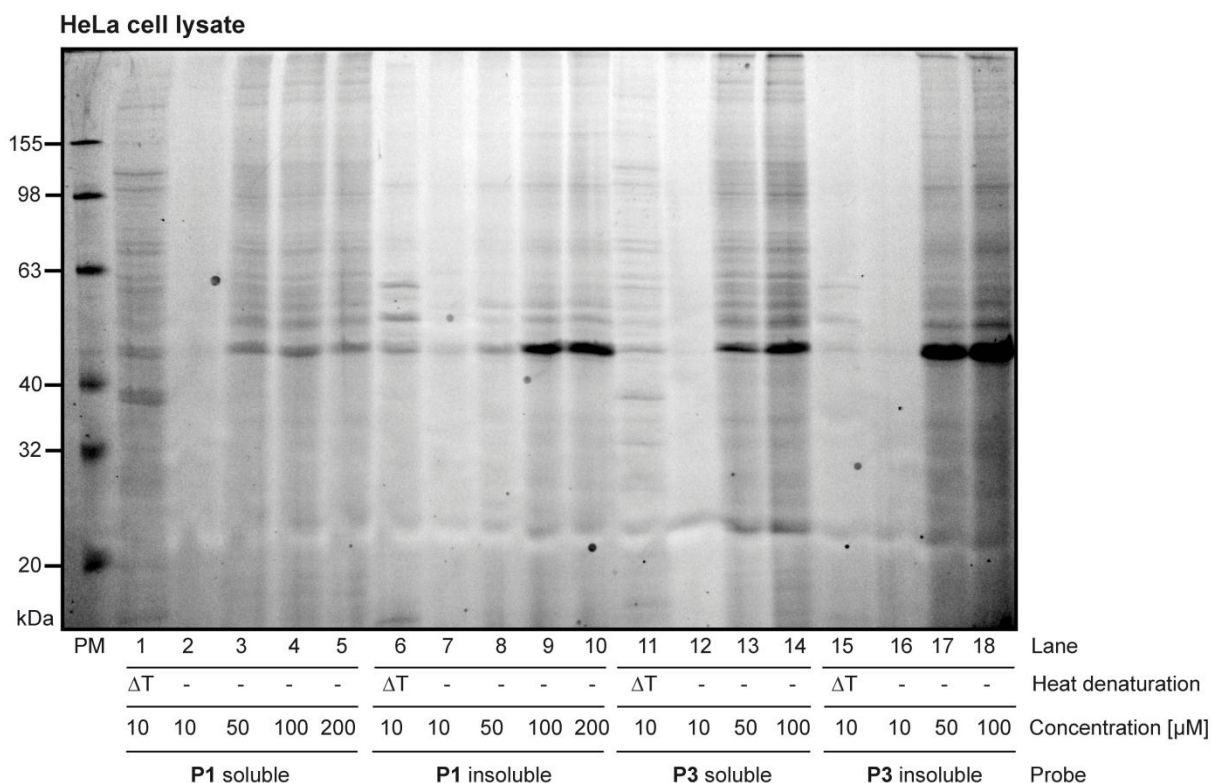
Figure 68. ABPP labeling of HeLa cervical cancer cells with probes **P1** and **P3**.

In the cell lysate we could identify several fluorescent protein bands in both soluble and insoluble fraction of the homogenate in the wide range of molecular weights (approx. 40-65 kDa), however from heat denaturation controls it was difficult to assign whether the labeling

112

was specific or not (Figure 68, lanes 1, 6, 11 and 15). The most prominent band, very well visible at high concentration of the probes (Figure 68, lanes 9-10, 13-14 and 17-18), exhibiting the mass of ca. 45 kDa was also present in the heat denaturation control, suggesting that it originated from some unspecific binding. Other bands were very weak and thus it would be difficult to identify them by MS.

Distinct image was obtained from *in situ* labeling in living cells. For *in situ* labeling experiments cells were grown to ca. 80-90% confluency in a complete medium on Petri dishes. Then fresh complete medium, containing either DMSO (as blank control) or probes **P1** or **P3**, was added in place of a standard medium. Cells were incubated with varying concentrations of probes **P1** and **P3** in a humidified 5% CO_2 incubator at 37 °C for 2 h. Subsequently, the cells were lysed by sonication, soluble and insoluble fractions were separated by ultracentrifugation and protein concentration in both fractions was determined using a Bradford or BCA protein concentration assay and adjusted to 2 mg/mL in PBS. The samples could be then subjected to click chemistry reaction to append a fluorescent **TAMRA-N₃** tag to visualize the labeled proteins (Figure 69).
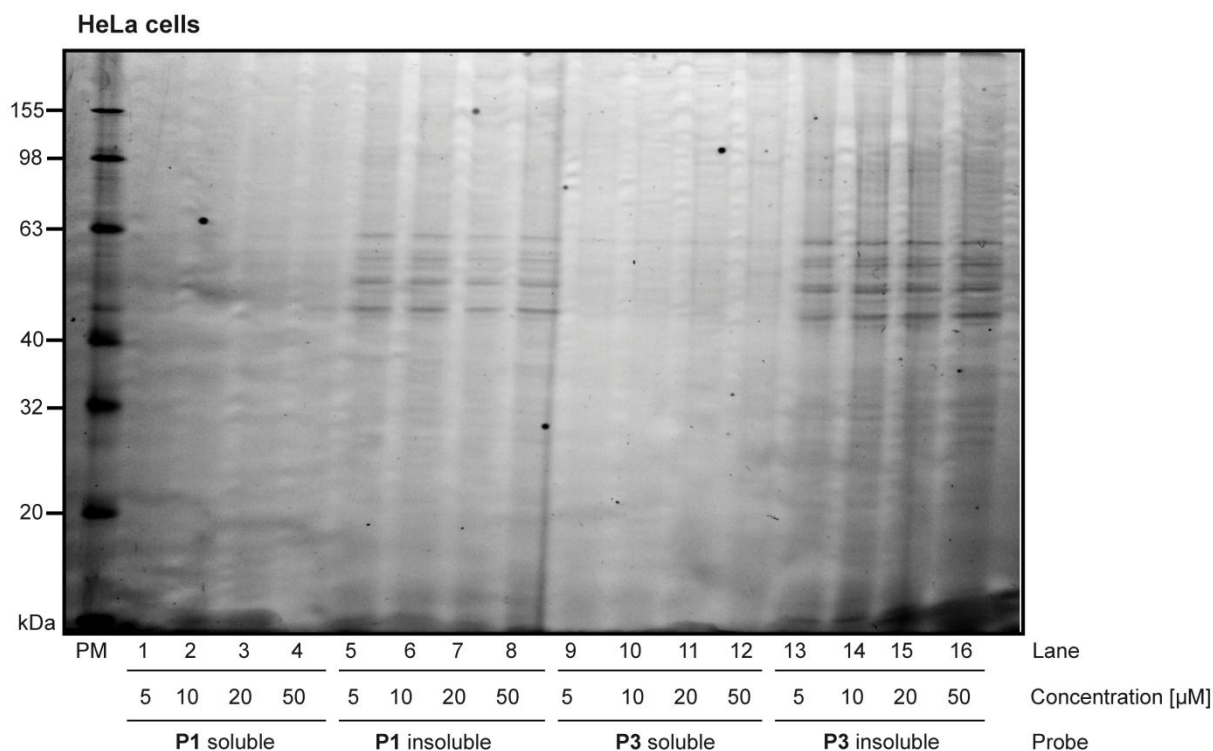
Figure 69. Labeling *in situ* of HeLa cells with probes **P1** and **P3**.

113

Four distinct protein bands in the range of 45-63 kDa could be clearly identified in the insoluble fraction of HeLa cells and the increasing concentration of probes **P1** and **P3** (5-50 µM) did not have a significant effect on the intensity of these bands (Figure 69, lanes 5-8 and 13-16). This was in contrast to *in vitro* labeling of HeLa cell lysate, in which the bands were mostly noticeable in the soluble part of the proteome and have revealed concentration-dependent labeling. Particularly, a protein band of approx. molecular mass of 63 kDa has drawn a special attention as it resembled, in terms of the localization and molecular weight, a protein target (possibly MAO enzyme) labeled specifically by both probes in the mouse brain lysate.

In order to shed light on the identity of the probe-bound proteins we performed a preparative quantitative proteomic analysis using a trifunctional reporter tag **TAMRA-biotin-N$_3$** (Fiigure 61) as described previously. Unfortunately, despite of careful performance of the procedure, we were not able to achieve the satisfying enrichment of the protein targets using avidin beads and to subject them to tryptic digest and MS analysis.

4.5.2.2 Summary

In conclusion, ABPP labeling experiment performed with the same proteome, but in two different ways: *in situ* with living HeLa cells and *in vitro* with HeLa cell lysate, revealed a remarkable difference in the pattern of labeled protein targets. The experiment reflects possible alterations in enzyme activity upon the disruption of cell membranes, which leads to significant changes in their native environment. Moreover, it underscores the impact of ABPP investigations *in vivo* as an excellent and simple tool in mirroring enzyme activity in their natural functional state.

Unfortunately, the identity of proteins, labeled by the developed ABPs, remained undisclosed. As a solution to this failure, we started to search for alternative identification methods such as Western Blotting. In addition, we decided to pursue our ABPP

investigations in the proteomes, in which the probability of discovering monoamine oxidases were relatively high in comparison to random biological samples.

4.5.3 Labeling of human brain cancer cell lines

Encouraged by the promising results obtained from the labeling of mouse brain lysate with the probes **P1** and **P3**, we rationalized that due to the application of their parent inhibitors pargyline and deprenyl in studying and treatment of CNS disorders (deprenyl is used as an antiparkinsonian drug) human brain cells would be a suitable biological system for target validation of probes **P1** and **P3**.

Unfortunately, immortal non-cancerous cells derived from human brain are not easily available for obvious ethical reasons. Hence, we decided to use diverse human brain cancer cell lines to perform our ABPP study.

4.5.3.1 Scope of labeling

For our ABPP investigations we used three different human brain tumors cell lines, generously provided by Prof. Walter Berger from Institute of Cancer Research, Medical University Vienna. They were: DBTRG-05MG (glioblastoma multiforme (GBM) model, treated with local brain irradiation and multidrug chemotherapy, ATCC number: CRL2020™), U373 MG (glioblastoma-astroglioma model, ATCC number: HTB-17™ or ICLC HTL99014), RAEW (glioblastoma multiforme model, cell line established from a patient isolate, donated by Prof. Berger (Institute of Cancer Research, Medical University of Vienna, Austria)).

The cells derived from a clinical material (RAEW) were included in our study because despite of potential changes in enzymes activity associated with the tumor incidence, they reflect a native state of human brain cells at the largest degree when compared to cells existing in the cell culture for a longer time. Comparative genomic hybridization (CGH) analysis (provided by Prof. W. Berger) showed no striking changes in levels of MAO A and MAO B genes in

these cells. Hence they resemble a healthy human brain with respect to activity of MAO enzymes.

Morphologically, all cells have elongated, epithelial-like shape and were grown as monolayers (Figure 70).

A. DBTRG-05MG   **B. U373 MG**   **C. RAEW**
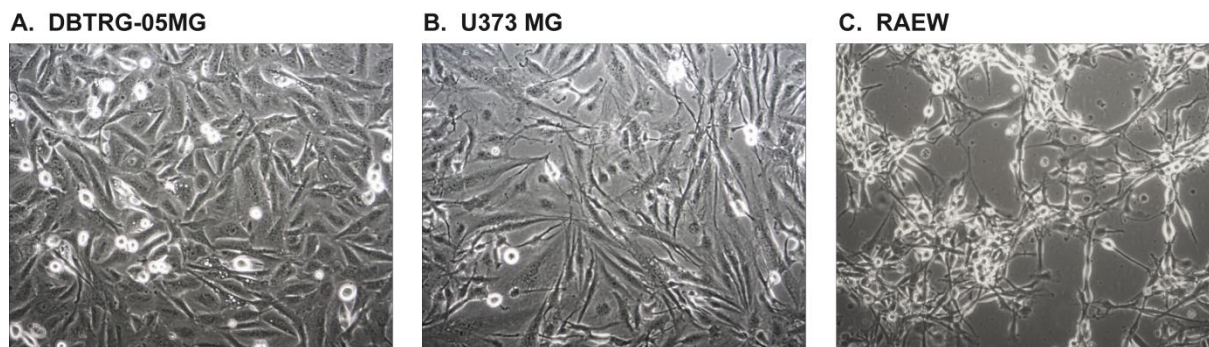
Figure 70. Morphology of human brain cancer cell lines used in the ABPP study. Images taken with VisiCam® camera 1.3 attached to the optical microscope at the 40x magnification.

4.5.3.2 Assignment of cytotoxicity using MTT assay

Prior to ABPP labeling we determined the cytotoxicity of probes **P1** and **P3** against two different human cell lines (DBTRG-05MG (GBM model) and HepG2 (hepatocellular carcinoma)) to test whether within the range of concentrations used for ABPP experiments cells were still viable.

We used a MTT metabolic activity assay which employs yellow MTT (3-(4,5-dimethylthiazol-2-yl)-2,5-diphenyltetrazolium bromide), which is reduced to purple formazan in the mitochondria of living cells (Figure 71).[323,324] The reduction takes place only when mitochondrial reductases are active, and therefore this process can be directly correlated to the number of viable cells. The amount of purple formazan (which can be measured spectrophotometrically by recording its absorbance at a particular wavelength) produced by cells treated with a compound in question can be compared with the amount of formazan produced by untreated control cells, and thus the efficiency of the compound in causing death of cells can be assigned by the determination of IC_{50} or EC_{50} values, through the construction of dose-response plots.
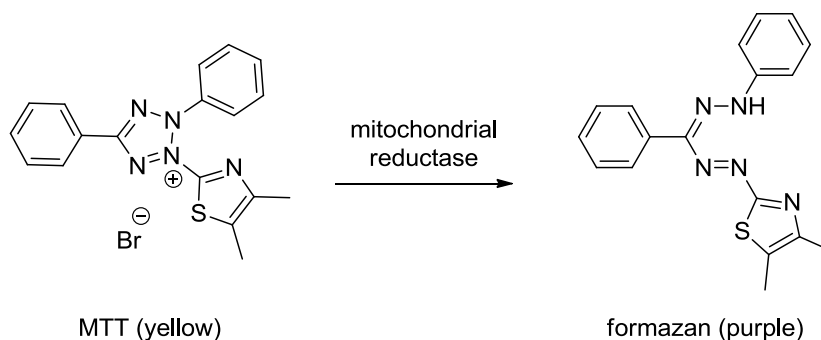
Figure 71. Reduction of MTT to formazan by mitochondrial reductases, which is a basis for MTT metabolic activity assay.

In the MTT assay, that we performed, cells, cultured in a 96-well plate, were incubated with DMSO or a given concentration of a probe (range 1 µM-1 mM) for 24 h. Then, MTT solution was added and incubated with cells for further 2 h. Subsequently, the medium was discarded and cells were lysed in DMSO, causing also the dissolution of formazan (metabolic product of MTT). Finally, optical density of the purple formazan solution was measured at 570 nm. This procedure enabled us to determine EC_{50} values for both probes **P1** and **P3**, exerted on both cell lines used in the cytotoxicity assignment (Figure 72).
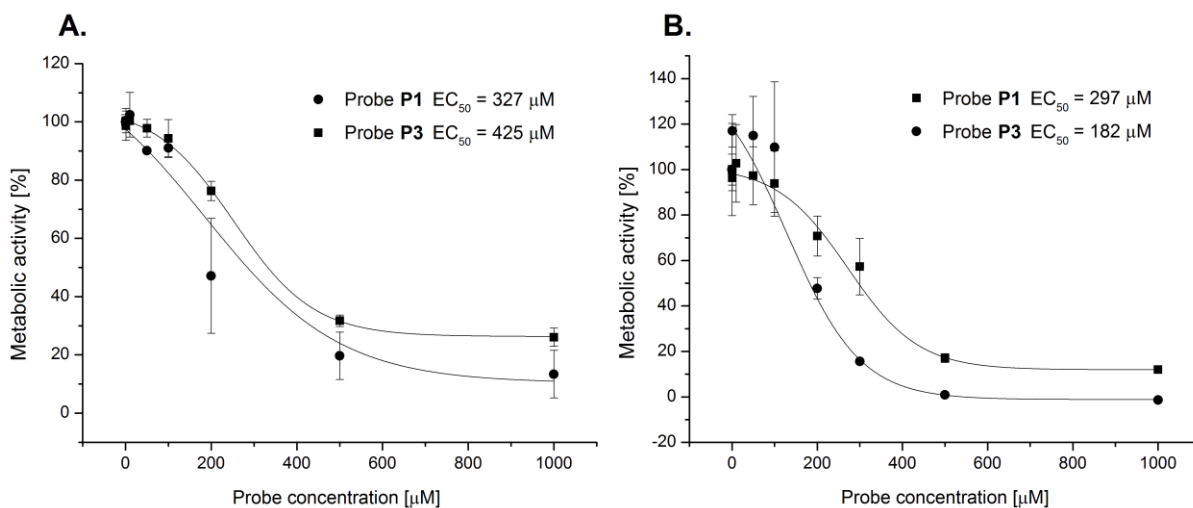
Figure 72. Cell toxicity assigned by MTT assay for metabolic activity on human brain GBM cell line DBTRG-05MG (A) and human hepatocellular carcinoma cell line HepG2 (B).

MTT assays revealed that probes were indeed toxic to cells but only at very high concentrations (EC_{50} at 327 and 425 µM for **P1** and **P3** in DBTRG-05MG cells, respectively and EC_{50} at 297 and 182 µM for **P1** and **P3** in HepG2 cells, respectively). However, at the highest concentration used in the ABPP experiment (200 µM) over 50% cells showed their

metabolic activity after 24 h treatment with the probes (Figure 72), indicating clearly that the cells were viable during the incubation with the probes.

4.5.3.3 Results of labeling of human brain tumor cells

We performed *in situ* labeling in three previously described human brain tumor cell lines in a time- (1-4 h) and concentration- (10-200 µM) dependent manner using a general procedure described for HeLa cells in Section 4.5.2.1. On the basis of several labeling experiments carried out in living cells we found out that the incubation lasting 2 h with a probe at the concentration between 50 and 100 µM are optimal conditions to balance the satisfying intensity of labeled bands and cell viability (typically, cells were observed under the microscope prior and after labeling) (data not shown). Also, competitive ABPP experiments with MAO irreversible inhibitors (pargyline and deprenyl) were included when it was reasonable to test whether probes compete with the inhibitor for the same protein target.

These experiments revealed that there are only few enzyme targets labeled by the probes **P1** and **P3** and only some of them seemed to be labeled in a specific fashion, as indicated from the comparison to DMSO blank controls. Interestingly, the labeling pattern significantly varies among different cell lines used in our ABPP experimentation. An overview of the labeling results received from three cell lines (DBTRG-05MG, RAEW, U373-MG) is presented in Figure 73.

The weakest and predominantly unspecific fluorescent bands were found in cells originating from glioblastoma-astroglioma brain tumor (U373-MG) (Figure 74). The bands were very indistinct (Figure 74), and even the increase in the probe concentration from 50 to 200 µM (Figure 73, lanes 7-9 and 14-15) did not improve their intensity. The most dominant band of ca. 45 kDa (Figure 74, lanes 3, 5, 10 and Figure 73, lanes 7-9 and 14-15) was unfortunately present in the background control, suggesting its origin in some unspecific binding with the fluorescent tag **TAMRA-N$_3$**.
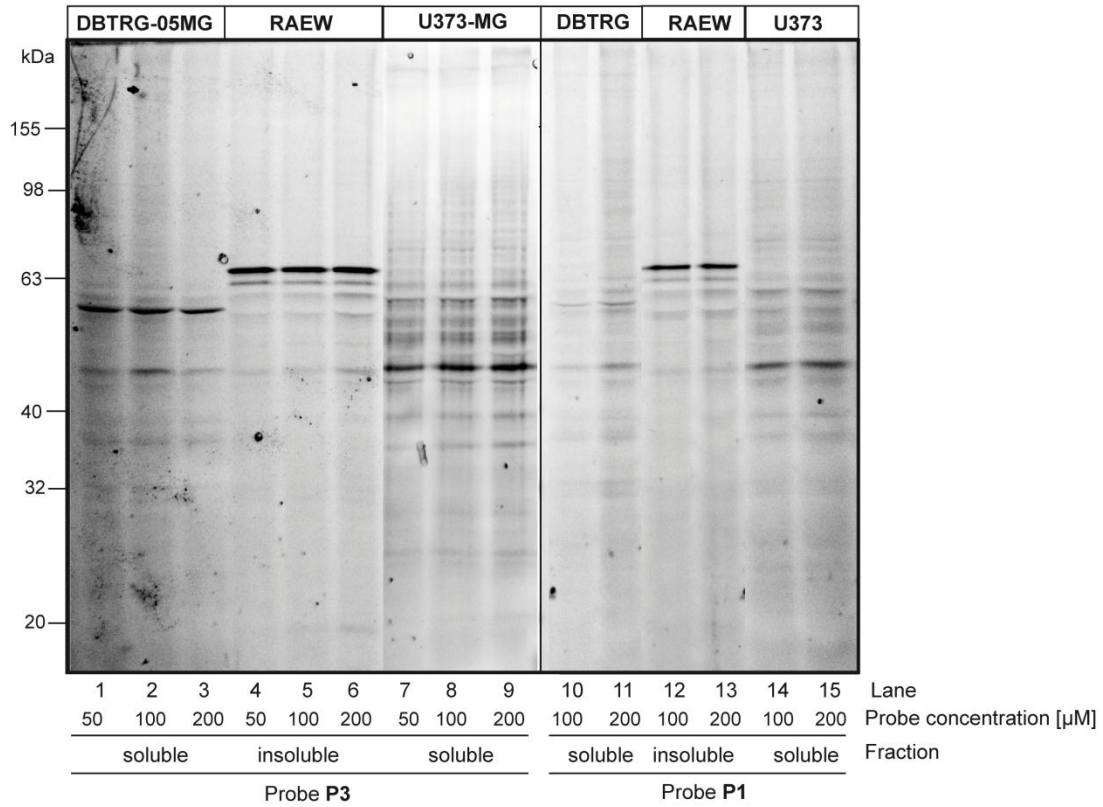
Figure 73. Comparison of *in situ* labeling of three human brain tumors cell lines: DBTRG-05MG (GBM), RAEW (GBM), U373-MG (astroglioma) with probes **P1** and **P3**.
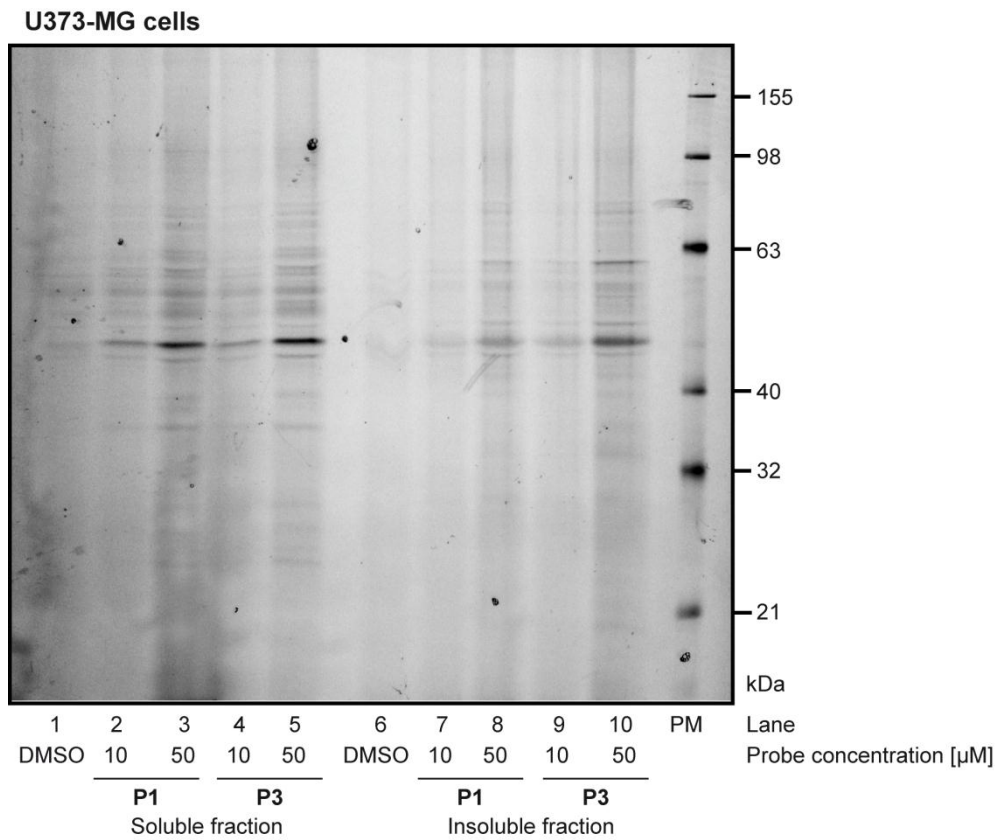
Figure 74. *In situ* labeling of human brain glioblastoma-astroglioma cell line U373-MG.

119

Different labeling pattern delivered the ABPP experiment with human glioblastoma multiforme cell line (DBTRG-05MG) shown in Figure 75.

A. DBTRG-05MG cells - soluble fraction

B. DBTRG-05MG cells - insoluble fraction
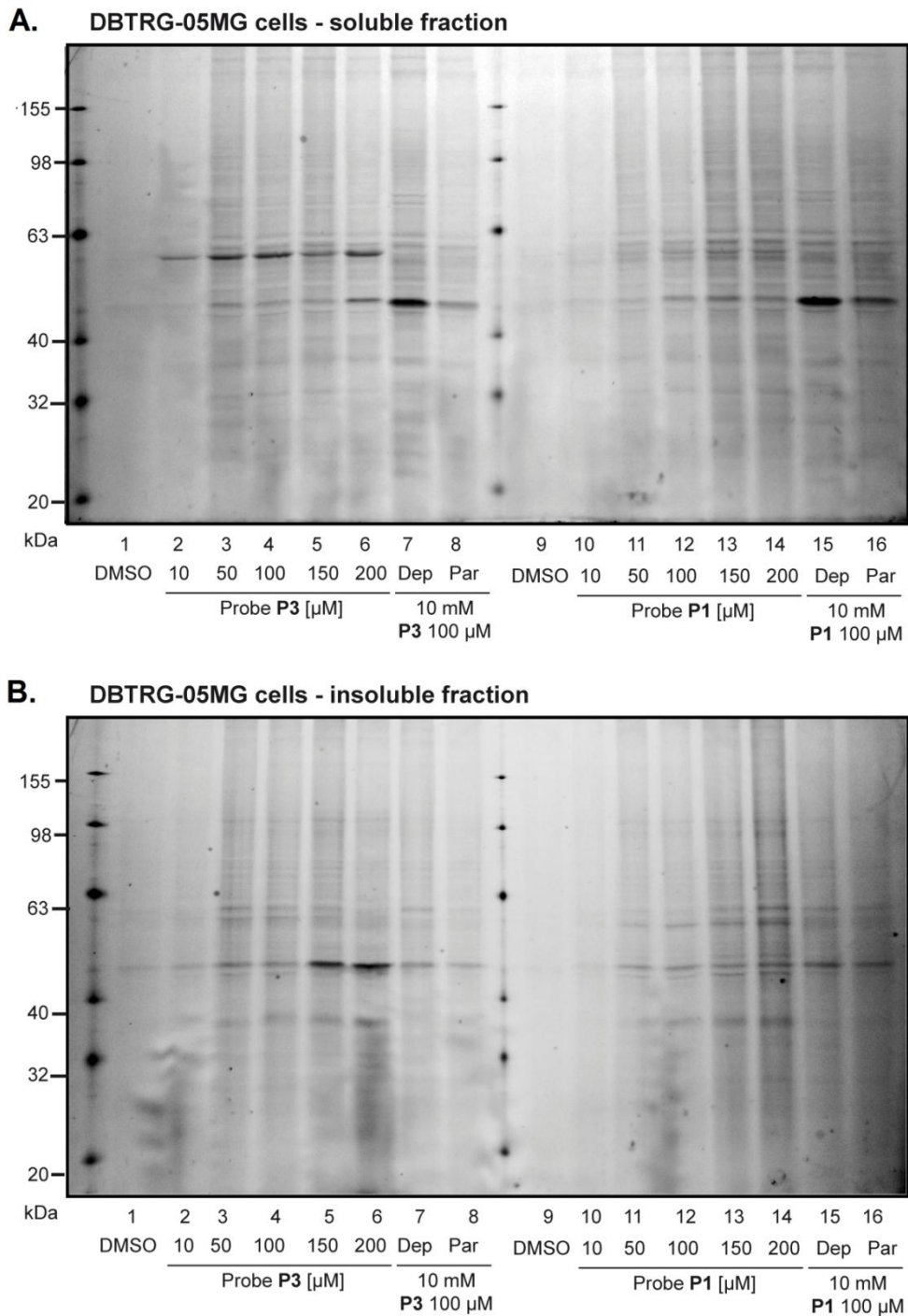
Figure 75. *In situ* labeling of soluble (A) and insoluble (B) fraction of human brain glioblastoma multiforme cell line DBTRG-05MG with probes **P1** and **P3**. (Par = pargyline, Dep = deprenyl).

In the soluble fraction of the cell lysate we could identify one distinct fluorescent protein band labeled by probe **P3** already at the concentration of 50 µM, which was located around 55 kDa

(Figure 75 A, lanes 2-6) and it was not noticeable in the background control (Figure 75 A, lane 1). Interestingly, this fluorescent band was completely outcompeted by 10-fold excess of inhibitors pargyline and deprenyl in the competitive labeling (Figure 75 A, lanes 7-8). However, this band was not equally pronounced in the labeling with the probe **P1**. (Figure 75 A, lanes 10-14).

On the other hand, very few protein targets were labeled by probes **P1** and **P3** in the insoluble fraction. Similarly to the soluble fraction as well as to the cells U373-MG, an unspecific band of ca. 45 kDa was a dominant fluorescent band. In addition, two weak bands of equal intensity could be identified in the range of ca. 63 kDa (Figure 75 B, lanes 3-4 and 13-14). Interestingly, higher concentration of probe **P3** resulted in the decrease of their intensity and unspecific labeling was more pronounced (Figure 75 B, lanes 5-6). However, they were not completely abolished in the competitive labeling with MAO inhibitors (Figure 75 B, lanes 7-8 and 15-16).

The most promising protein targets were found in the cell line established from a surgical specimen (RAEW) (Figure 76). *In situ* labeling with GBM cells revealed that both probes **P1** and **P3** labeled two bands in the range of 63 kDa (Figure 76 A, lanes 10-14) as main protein targets when compared to the total protein staining (Figure 76 B). The labeled proteins were clearly noticeable in the insoluble fraction. However, corresponding very weak bands were also present in the soluble portion of the proteome. The labeling by probe **P3** proved to be much more effective (Figure 76 A, lanes 10-12) than by probe **P1** (Figure 76 A, lanes 13-14). 50 µM concentration of probe **P3** was sufficient for achieving binding saturation as higher concentrations did not improve the labeling of the much weaker lower band. Importantly, inhibitors of monoamine oxidases outcompeted the labeling by probe **P3**, suggesting that these two proteins might be MAO A (60.5 kDa)[221] and MAO B (59.4 kDa).[221]
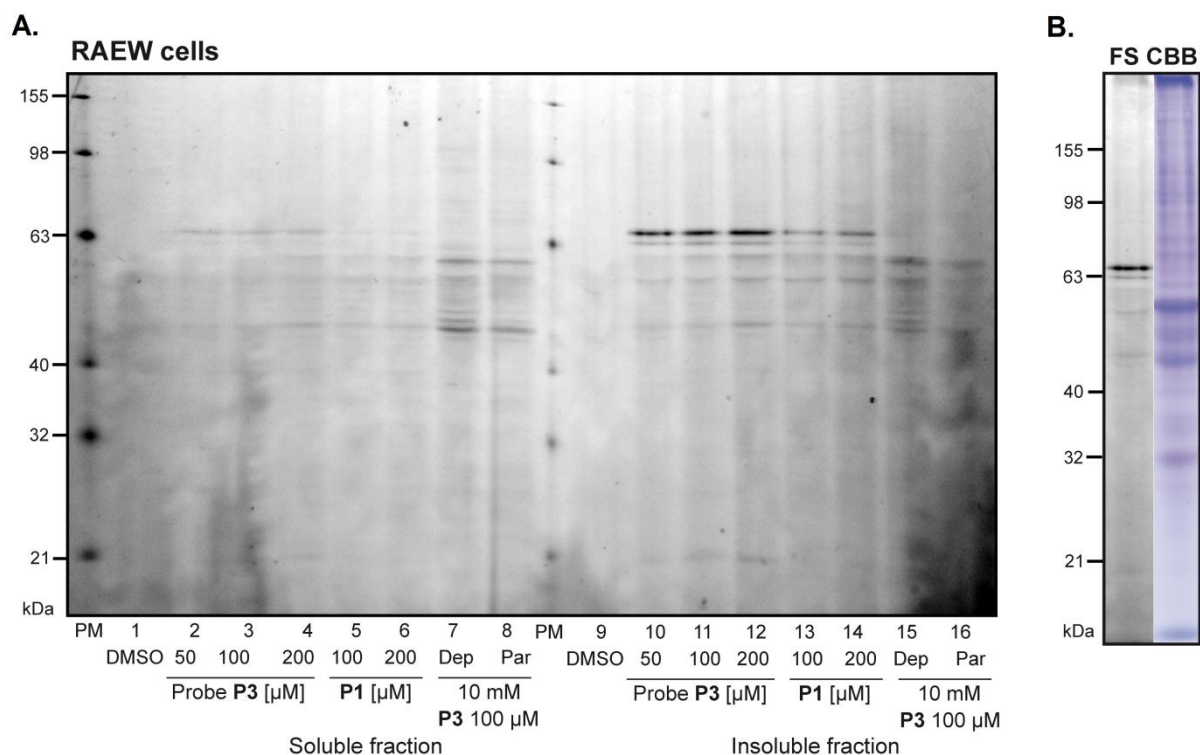
Figure 76. A. *In situ* ABPP labeling of human brain cancer cells RAEW with probes **P1** and **P3**. Competitive labeling with MAO inhibitors deprenyl (Dep) and pargyline (Par) and probe **P3** (lanes 7-8 and 15-16). B. Comparison of fluorescence scanning (FS) and Coomassie Brilliant Blue (CBB) staining of labeling by the probe **P3**.

4.5.3.3.1 Identification of protein targets

The major challenge was the unequivocal identification of the labeled targets as in several previous attempts we were not able to successfully enrich and identify the proteins of interest by mass spectrometry.

We performed a quantitative proteomic analysis of GBM cells (DBTRG-05MG and RAEW) using a trifunctional reporter tag **TAMRA-biotin-N$_3$** (Figure 61), which was attached to a protein-bound probe **P1** or **P3** under click chemistry conditions to allow visualization, enrichment and subsequent identification of proteins by mass spectrometry (Figure 60).[18g] Unfortunately, not all desired bands were efficiently enriched as compared to blank controls (Figure 77). Particularly, the enrichment of bands of interest from DBTRG-05MG cells was unsatisfying and it was not clear whether the enriched bands (Figure 77, lanes 6 and 8). correspond to the bands visible on an analytical gel (Figure 75). In RAEW cells, only upper

band could be effectively enriched (Figure 77, lane 2), whereas a lower band was only faintly visible in labeling by probe **P1** (Figure 77, lane 3). All cut bands, including some unspecific bands (numbered 1-10) are depicted in Figure 77.
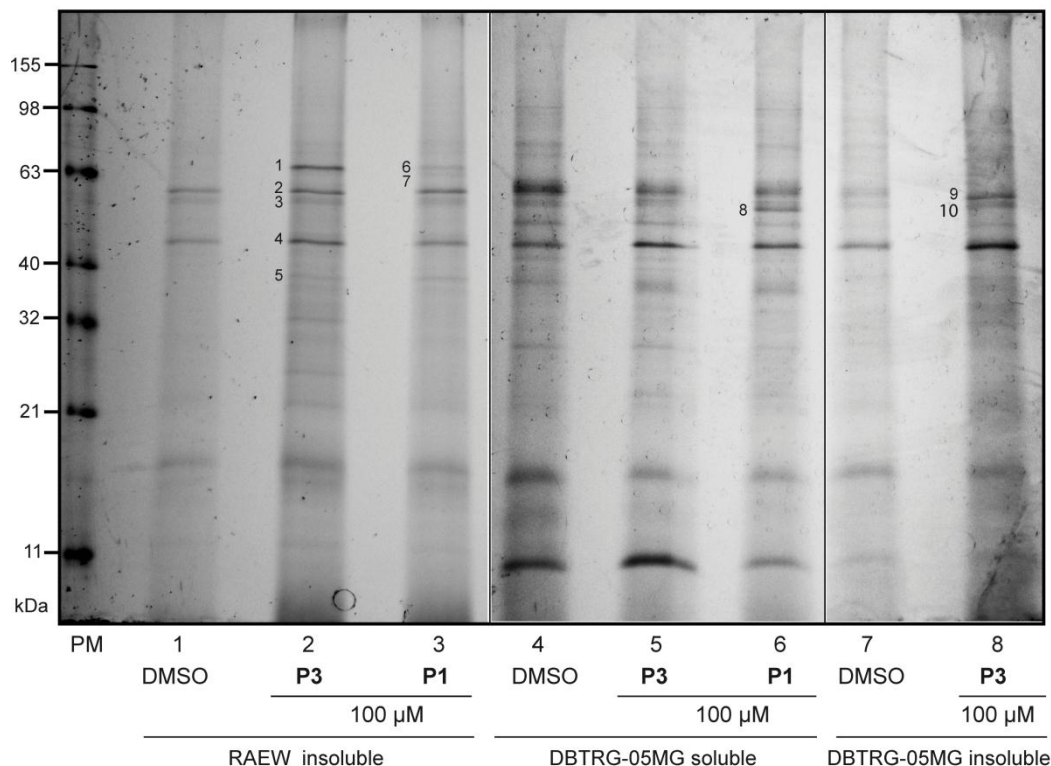
Figure 77. Preparative fluorescent gel from the labeling of RAEW (lanes 1-3) and DBTRG-05MG (lanes 4-7) cells.

As alternative, also Western Blotting for MAO enzymes was developed and applied to confirm or exclude the identity of labeled proteins as MAO A or MAO B.

Finally, all the above mentioned efforts resulted in the identification of labeled protein in RAEW cell line. Analysis of peptide fragments employing SEQUEST algorithms identified MAO A with nearly 40% protein coverage and 17 unique peptides (upper band on fluorescent SDS-PAGE). Unfortunately, the enrichment on avidin beads was insufficient for the lower protein band. However, this protein was unambiguously identified as MAO B by Western Blotting using specific anti-MAO B antibodies (Figure 78).

RAEW insoluble fraction
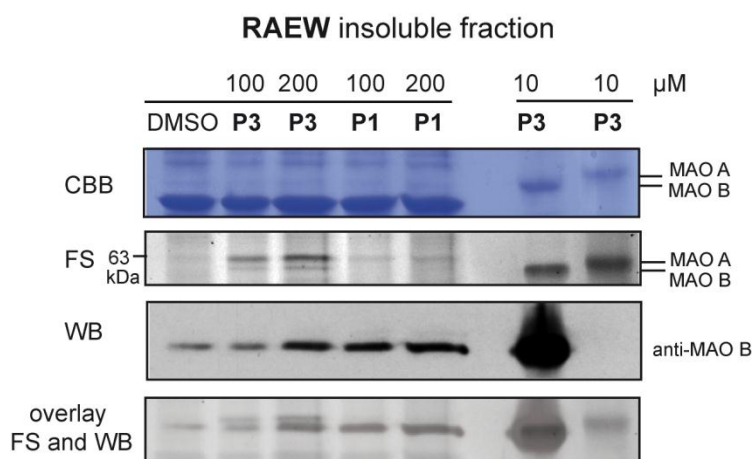
Figure 78. Identification of lower band in RAEW cells by Western Blotting using specific anti-MAO B antibodies (Abbreviations: CBB - Coomassie Brilliant Blue, FS – fluorescence scanning, WB – Western Blot).

Unfortunately, the identification of the target in the second GBM cell line (DBTRG-05MG) by MS failed. As anticipated, the enrichment of the cut bands over background controls was insufficient to identify the protein targets. On the other hand, Western Blotting with specific anti-MAO B specific antibodies excluded the identity of this protein as MAO B.

4.5.3.4 Discussion

The enzyme profiling in live human brain tumor cells using the established ABPP platform proved to be very challenging but also exceptionally interesting.

The results of labeling in live brain cells (RAEW) strikingly demonstrate that the covalently binding inhibitors pargyline and deprenyl, on which ABPs **P1** and **P3** were built on, act very selectively with MAO A and B but with no other protein targets. This outstanding selectivity is triggered by a unique 'suicide' inhibition mechanism that is customized for this enzyme family. This is in contrast to other ABPP studies which unraveled many off-targets of clinically used covalent drugs. Recently, Yao et al. could show that a marketed drug (tetrahydrolipstatin, Orlistat®) targeted multiple lipases within gastrointestinal tract as well as fatty acid synthase (FAS) and selectivity towards this latter target could not be significantly improved by structural modifications of Orlistat.[120a,120b]

Probe **P3** based on MAO B specific inhibitor deprenyl, showed distinct isozyme preference in *in vitro* and *in situ* labeling. In experiments with recombinant proteins, this probe labeled both isoforms of MAO in agreement with studies indicating loss of MAO B specificity at high concentrations.[325] However, it demonstrated higher binding affinity towards MAO B (Figure 50), which was also noticeable in mouse brain tissue, in which only the lower protein band, presumably MAO B, was labeled (Figure 62 A). Interestingly, in living human brain tumor cells, this probe was bound preferentially to MAO A. This important result can be explained by the fact that the activity of MAO A is much higher in intact cells than in the purified enzyme which is known to be particularly unstable at ambient temperatures and loses its activity rapidly.[154] Moreover, one could speculate that mitochondrial outer membrane (MOM) topology of both MAO isozymes can influence enzyme accessibility to the probe. Recent studies of the group of Edmondson[164] demonstrated that MAO A localizes to the cytosolic face in intact rat liver mitochondria and in intact human placental mitochondria,[165] while MAO B resides in the intermembrane space[164] what can pose some difficulties for the probe in MOM permeability.[166] On the other hand, a weak labeling of MAO B correlates with lower activity of MAO B found in some cultured brain cells,[326] although both isoforms of MAO A and MAO B are expressed in human brain at similar levels.[327]

Taken together, these results underscore the relevance of *in situ* studies on enzyme activity which is apparently not a simple function of enzyme abundance but is tightly regulated by many dynamic processes taking place exclusively in intact living cells.

4.5.4 Labeling of human hepatocellular carcinoma cell line HepG2

After the fruitful experience in labeling of human brain cancer cells, we decided to perform *in situ* ABPP labeling of human liver cancer HepG2 cells (hepatocellular carcinoma, ATCC number: HTB-177™). The cells served as a substitute of liver, which is a tissue where MAO enzymes are also abundant due to their role in deamination and detoxification of many exogenous dietary and toxic amines entering the human body.

Morphologically, HepG2 are adherent, epithelial-like cells growing as monolayers and in small aggregates (Figure 79).
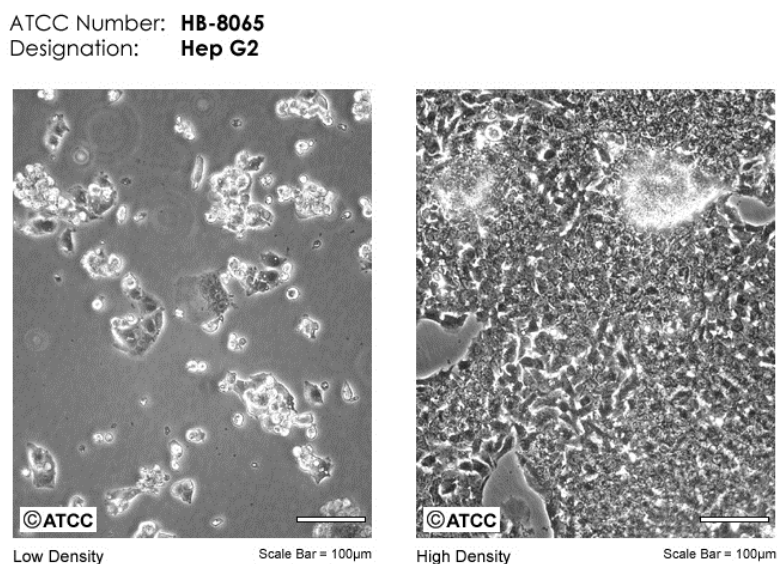
Figure 79. Morphology of HepG2 cells. (Source: http://www.atcc.org/Attachments/1967.jpg)

4.5.4.1 Results of the labeling

We carried out *in situ* labeling of HepG2 cells (hepatocellular carcinoma) using probes **P1** and **P3** as well as competitive experiments with pargyline and deprenyl inhibitors (Figure 80) using the same strategy, which was previously established for RAEW cells. The cytotoxicity assay performed on HepG2 cells revealed lower EC_{50} values (at 297 and 182 µM for **P1** and **P3**, respectively) than compared to brain cancer cells (327 and 425 µM for **P1** and **P3** in DBTRG-05MG cells, respectively), therefore we used the maximal concentration of probes at 100 µM.

We were very pleased to identify MAO A and MAO B in the insoluble fraction of HepG2 proteome (Figure 80 B, lanes 1-3) using mass spectrometry for MAO A and Western Blotting for MAO B (Figure 82 B, lanes 4-6), as previously established for RAEW cells.
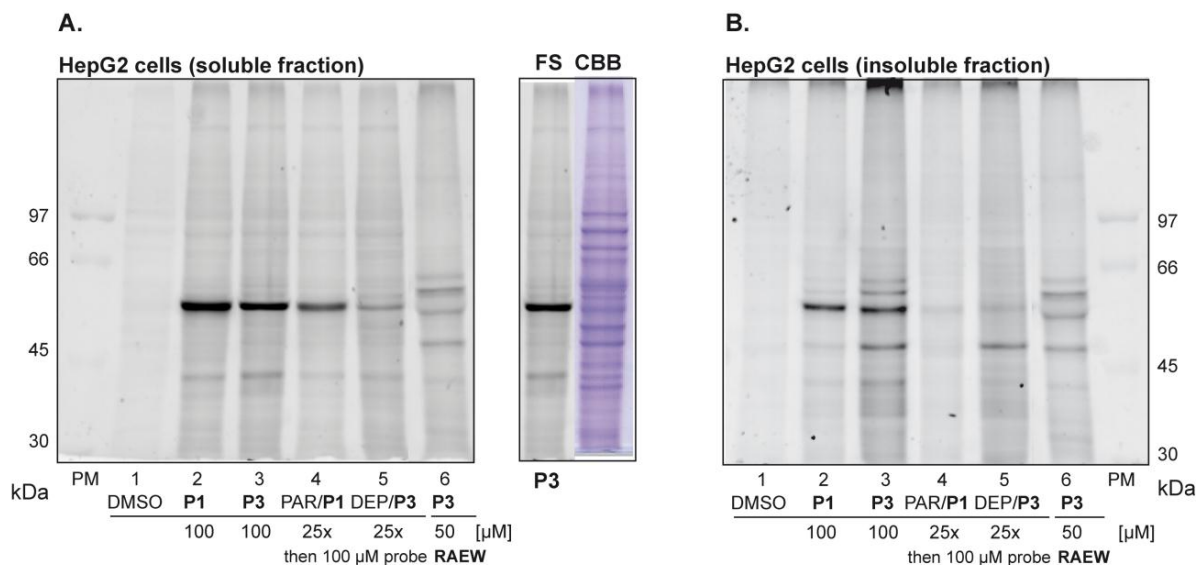
Figure 80. ABPP labeling of soluble (A) and insoluble (B) fraction of HepG2 cells with probes **P1** and **P3** (lanes 1-3) compared to RAEW cells (lane 6). Competitive labeling was carried out between probe **P1** and pargyline and probe **P3** and deprenyl (lanes 4-5).

These targets matched well with MAO A and B identified in RAEW cells (Figure 80 B, lane 6) and MAO enzymes itself (Figure 81, lanes 7-8).
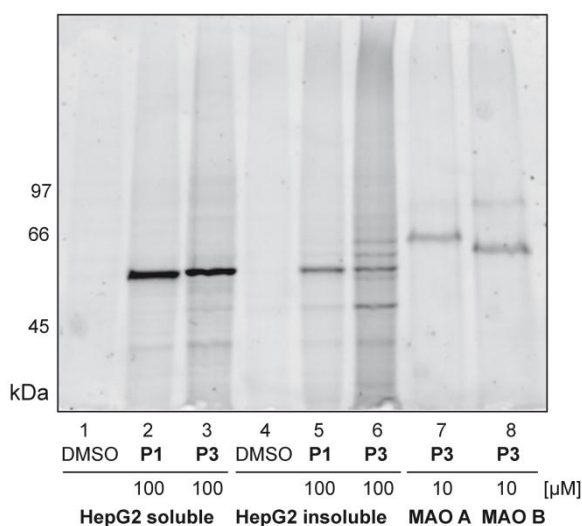
Figure 81. ABPP labeling of soluble (lanes 1-3) and insoluble (lanes 4-6) fraction of HepG2 cells with probes **P1** and **P3** compared to MAO A and MAO B (lanes 7-8).

Intriguingly, we were able to detect another very intensive protein band of ca. 55 kDa, which was not noticeable in the background control both in the soluble (Figure 80 A, lanes 1-3,

Figure 81, lanes 1-3) and insoluble fraction (Figure 80 B, lanes 1-3, Figure 81, lanes 4-6) of cells. Therefore it was very important and interesting for us to identify in an unambiguous manner this protein target.

4.5.4.2 Identification of targets

In order to identify the protein of ca. 55 kDa in the soluble fraction of HepG2 cells we performed a quantitative proteomic analysis of HepG2 cells (soluble fraction) using a trifunctional reporter tag **TAMRA-biotin-N$_3$** (Figure 61), which was attached to a protein-bound probe **P1** or **P3** under click chemistry conditions. Fortunately, the enrichment on avidin beads was efficient when compared to a background control (Figure 82 A). Then, this protein band was excised from the gel and processed further as described previously. Finally tryptic peptides were subjected to LC-MS/MS analysis and then the protein was searched using SEQUEST algorithm. Western Blotting using specific anti-MAO B antibodies served as a negative control and excluded the identitiy of this protein as MAO B (Figure 82 B).
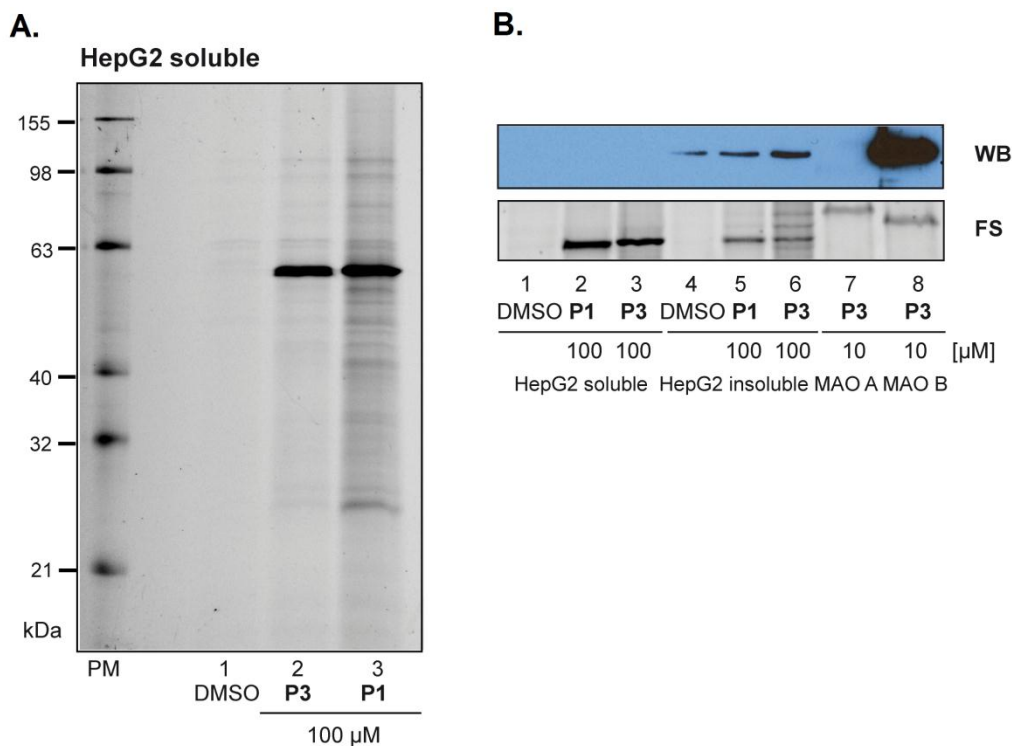
Figure 82. Identification of protein targets in HepG2 cells. A. Fluorescent SDS-PAGE after the enrichment of a protein target from soluble fraction of HepG2 cells on avidin beads. B. Western Blotting of HepG2 cells with specific anti-MAO B antibodies.

Initial data from MS identification suggest that this protein might correspond to retinal dehydrogenase 1 (20 unique peptides, 54% coverage), which is an important enzyme in metabolism of retinol.[328]

However further in-depth investigation of a mode of binding is required to provide information whether the labeling is specific and if it occurs at the cofactor or at any other nucleophilic residue in the active site. Unfortunately, these enzymes only rarely contain FAD cofactor[329] and typically involve NAD$^+$ cofactor[330-332] in the oxidation of an aldehyde, therefore the covalent linkage could be formed by another mechanism. The validation of the labeled enzyme and the elucidation of the mode of labeling is one of major aims of further investigations.

4.6 Development of MAO specific activity-based probes

Apart of the application of the developed ABPs in profiling MAOs and other related enzymes, in the course of our studies we got very much interested in the expansion of the probe collection. To this end, we developed new photocrosslinker probes **P1-Phot** and **P3-Phot** with the aim to extend the scope of protein targets labeled by these molecules. On the other hand, we strived to develop MAO A and MAO B specific probes, which would be able to distinguish between these two isoforms. In turn, this would allow identification and visualization of both MAO isozymes in biological samples where both isoforms coexist.

Probe **P3** was based on MAO B specific inhibitor deprenyl, however our experiments with the equimolar mixtures of MAO isozymes or tissues or living cells confirmed evidence from the literature, indicating loss of MAO B specificity in deprenyl when used at high concentrations.[325] Therefore, these original probes were not able to specifically label only one isozyme of MAO at the concentrations typically used in ABPP studies.

This motivated us to design and synthesize new probes which would be based on the differences in the shape and size of active sites of MAO A and MAO B. More bulky and less

flexible core structures provided the basis for MAO specific spin-labels described by Upadhyay et al.,[333] which inspired us to use a similar principle in our probes.

4.6.1 Design of MAO specific ABPs

We designed two probes based on the structure of specific spin-labeled pargyline analogues reported by Upadhyay et al.[333] and used as topological probes in EPR measurements. In place of a spin label we planned to incorporate an alkyne group attached *via* an alkyl linker. Further retrosynthetic analysis delivered two building blocks, which should be easily coupled furnishing the desired probes (Figure 83).
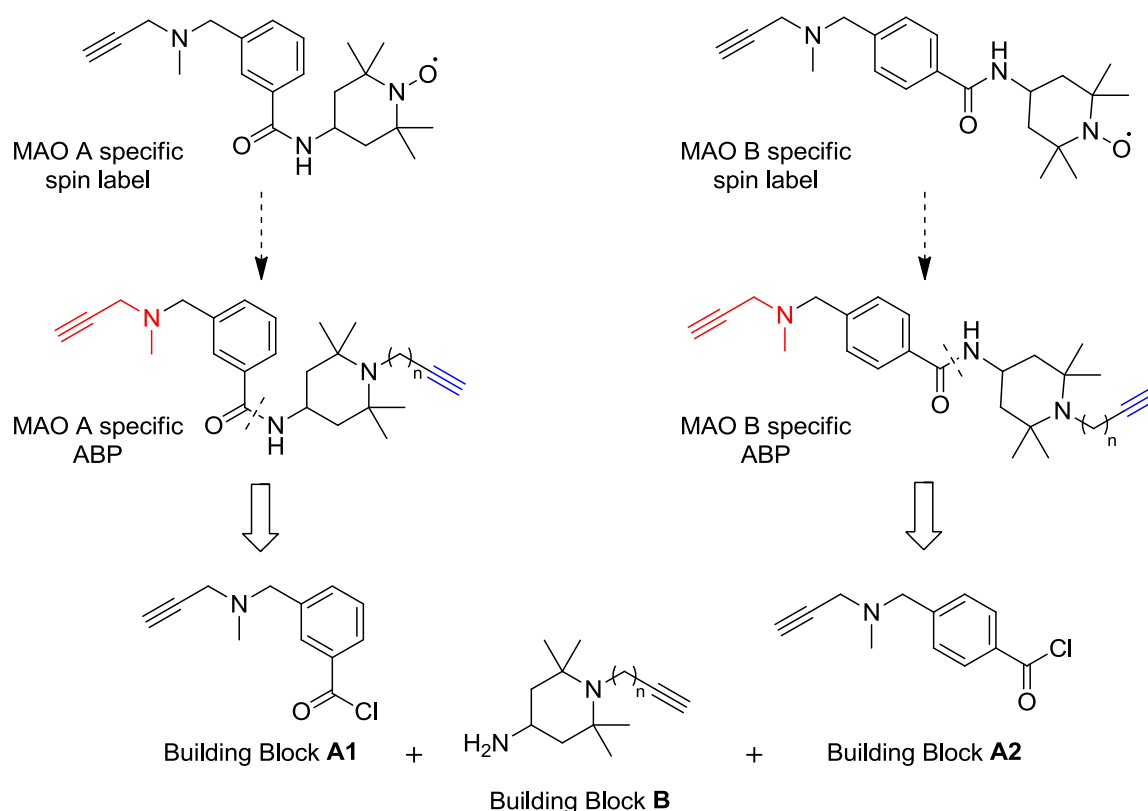
Figure 83. Structure of MAO specific spin labels (top) and MAO specific ABPP probes (middle) and their retrosynthetic analysis (bottom).

4.6.2 Efforts towards synthesis of isozyme specific ABPs

The two-step synthesis of building blocks **A1** and **A2** proceeded smoothly and involved a substitution of *m*- or *p*-(bromomethyl)benzoate with *N*-methylpropargylamine according to the

protocol of Upadhyay et al.[333] and the following mild hydrolysis of esters **57**-**a** and **57**-**b**, which furnished the corresponding carboxylic acids **58**-**a** (building block **A1'**) and **58**-**b** (building block **A2'**) in excellent yields (99%) (Scheme 23). The carboxylic acids could be easily transformed into their corresponding chlorides by reaction with thionyl chloride providing desired building blocks **A1** and **A2**.
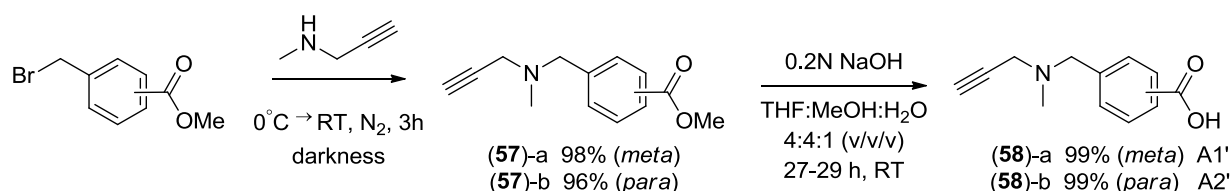
Scheme 23. Synthesis of building blocks **A1'** and **A2'**.

Preparation of building block B proved to be much more challenging. In the first approach we planned to synthesize it starting from the alkylation of 2,2,6,6-tetramethylpiperidine-4-one (**59**) at the *N*-position. Ketone moiety replaced the primary amine group in the starting material in order to avoid the favorable substitution at this position. Due to the steric hindrance caused by four methyl groups, compound **59** is considered basic, but not nucleophilic and hence reacts poorly in substitution reactions. Therefore, a Mannich condensation, seemed to be a good alternative to deliver intermediate **60**, which could be subsequently subjected to contrathermodynamic isomerization reaction to terminal alkyne **61** with potassium 3-aminopropylamide (KAPA). Final transformation of the ketone moiety of **61** to the corresponding oxime and its reduction would provide the desired building block **B1 62**. This synthetic plan is depicred in Scheme 24.
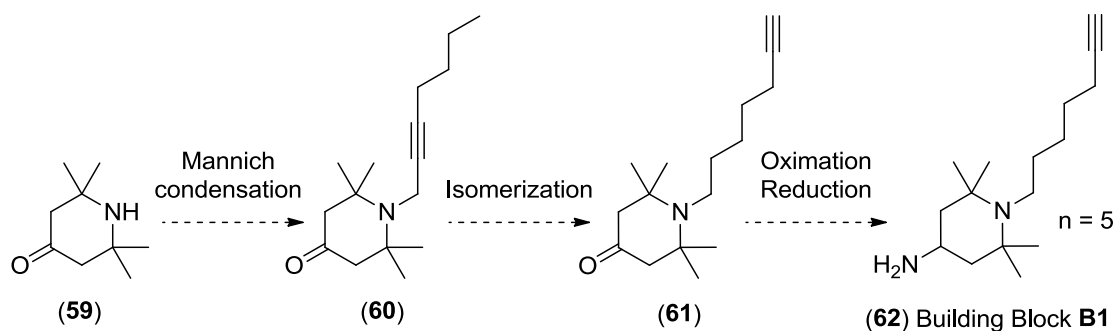
Scheme 24. Synthetic plan leading to building block **B1**.

In the first step we used a Mannich reaction, a robust condensation of an amine with formaldehyde and an active hydrogen compound, such as enolizable aldehydes, ketones or alkynes,[334] using the procedure reported by Karlen et al.[335] In this reaction (Scheme 25), AcOH was added to a suspension of amine **59**, paraformaldehyde, 1-hexyne and CuI (5% mol) in 1,4-dioxane and the suspension was heated at 90 °C for 1 h. Optimization of the reaction conditions provided the product **60** in only 25% yield, however it significantly exceeded that reported in the literature (ca. 10%) for similar compounds.[335]
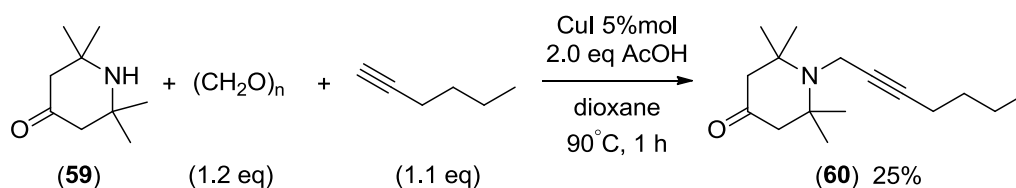
Scheme 25. Synthesis of *N*-substituted 2,2,6,6-tetramethylpiperidine-4-one **60**.

Contrathermodynamic migration of an internal triple bond to terminal alkyne using potassium 3-aminopropylamide (KAPA)[336] is a very powerful isomerization method, known also as an 'acetylenic zipper' reaction. It is often used in the total synthesis of natural products[337] or other complex molecules[338] as it proceeds smoothly under mild conditions within minutes.[336] To the freshly prepared solution of potassium 3-aminopropylamide by the treatment of potassium hydride with distilled 3-aminopropylamine (APA), intermediate **60** was injected at 0 °C and the reaction mixture was stirred for various periods of time and then quenched. Unfortunately, the analysis of the reaction mixture by GC-MS indicated the formation of all possible isomers. The conversion of the ketone **60** to its acetal **63**, carried out as described by Weerawarna and Jewell,[339] to avoid possible complications due to the presence of acidic protons, and the successive isomerization of ketal **63** reaction also did not deliver the desired product **64**, possessing the terminal alkyne. (Scheme 26).

These complications forced us to modify our synthetic plan and as well as the structure of the bulding block B. We wanted to use previously worked out Mannich condensation, but in place of 1-hexyne we planned to employ 5-hexyn-1-ol to to prepare a Mannich base with a terminal alcohol **65**, which next should be subjected to hydrogenation of the triple bond to

deliver the corresponding alkane **66**. Finally, the intermediate **66** would be substituted by a propargyl bromide to give the terminal alkyne **67**, which could be then transformed to the final amine **68** via oximation-reduction sequence.
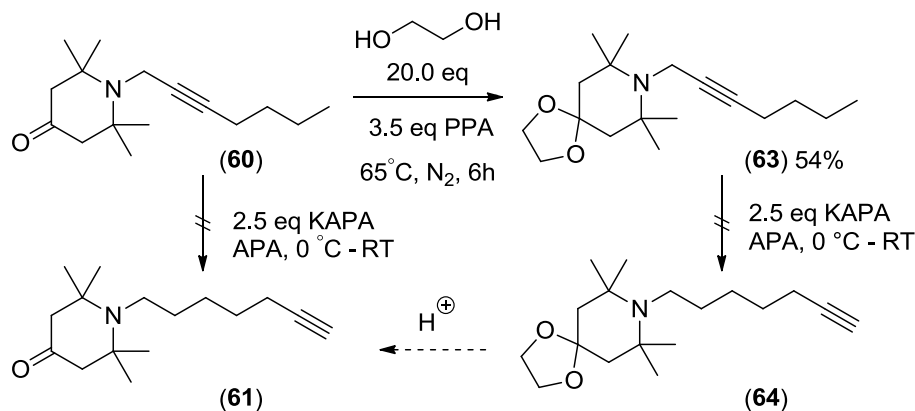
Scheme 26. Trials of isomerization of an internal triple bond to the terminal alkyne of ketone **60** or its corresponding ketal **63**.

The modified synthetic plan leading to the building block **B2** is presented in Scheme 27.
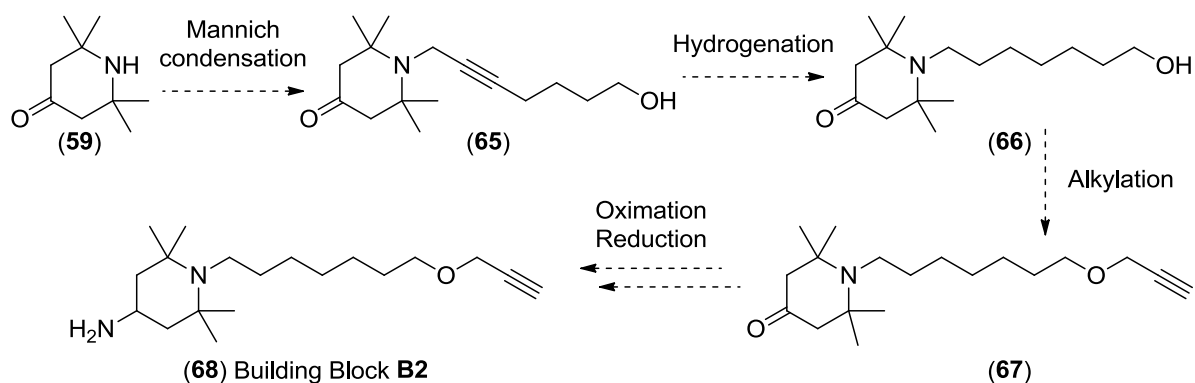
Scheme 27. Synthetic plan leading to building block **B2**.

In addition to our efforts to synthesize the final molecule **68**, the optimization of reaction conditions of this synthetic route was also performed by a bachelor student Lukas Schafzahl and is described in details in his bachelor thesis.[340] In short, 2,2,6,6-tetramethylpiperidine-4-one (**59**) was elongated to alcohol **66** through a Mannich condensation[335] and the following catalytic hydrogenation of a triple bond of alcohol **65**, using conditions described by Chen et al.[341] in moderate yield (24% after 2 steps). Hydrogenation of alkyne using Raney nickel (W-2)[342,343] as catalyst or methanol as solvent were much less effective and gave rise to hydrogenolysis, which is an important competitive reaction. Employing palladium on charcoal (10% wt) in ethanol led to the complete decomposition of the substrate within 90 min. Thus,

platinum dioxide and ethanol was the system of choice and gave the desired alcohol **66** in 50% yield. Subsequently, alcohol **66** was subjected to the well-known Williamson ether synthesis reaction. Sodium hydride was employed as a base to deprotonate the alcohol, which then nucleophilically attacks the propargyl bromide in an S_N2 reaction to furnish ether **67** in 43% yield (Scheme 28).
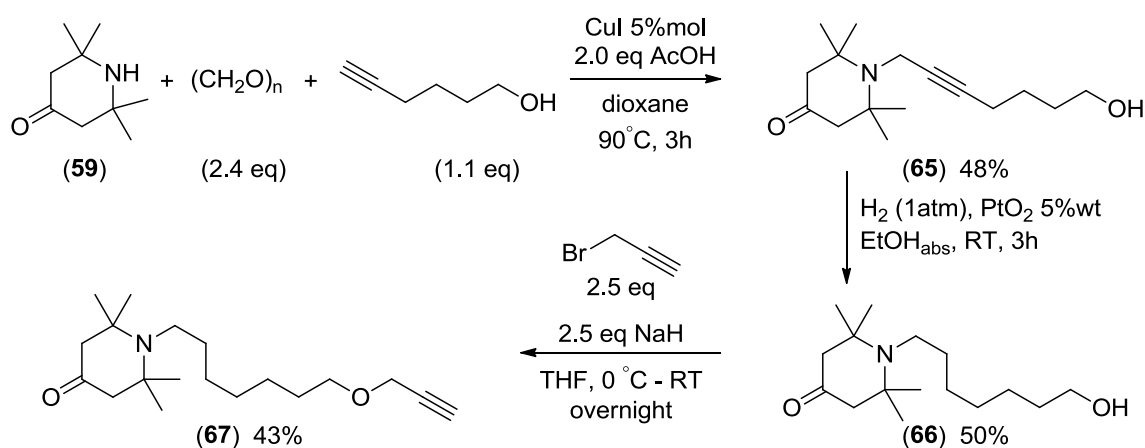
Scheme 28. Synthesis of intermediate **67** equipped with alkyne handle.

Furthermore, product **67** was subjected to the transformation of its ketone group to the corresponding oxime **69**, under modified conditions described by the group of Studer.[344] Reaction with hydroxylamine hydrochloride, using triethylamine as a base provided the oxime **69** in very good yield (95%). Subsequent reduction of oxime **69** in THF employing lithium aluminium hydride as a reducing agent furnished the final amine **68** in 58% yield (Scheme 29).
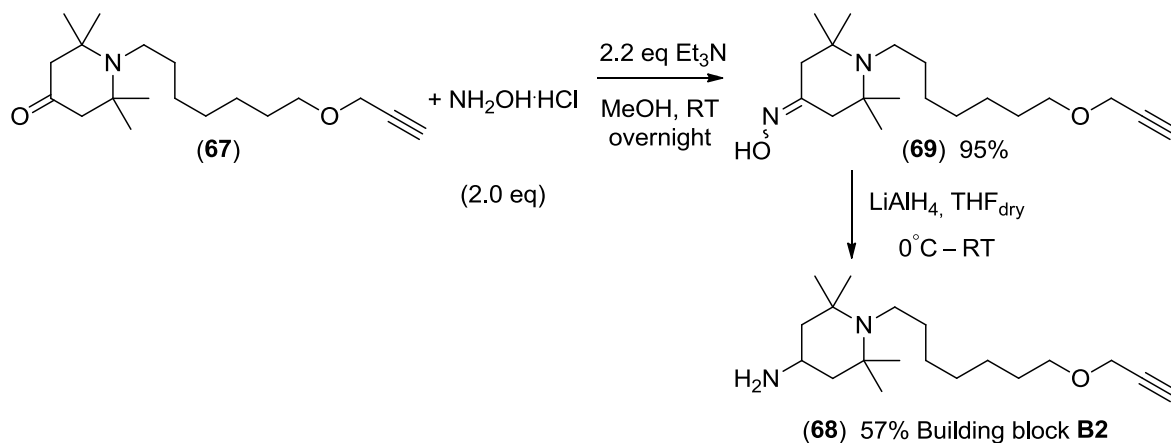
Scheme 29. Transformation of ketone **67** to the amine **68**.

Overall yield of the whole 5-step synthesis was very low (5%). Hence, we needed to develop a reliable and reproducible scale-up of this synthetic method to produce reasonable amounts of building block **B2**. Surprisingly, in the course of this process, we encounter unexpected problems in the preparation the intermediate ether **67**. We were not able to reproduce previous results and could observe only very low conversion of the starting material **66**. This caused that an alternative way to introduce an alkyne handle was investigated.

Having already prepared alcohol **66**, we pursued the idea that it can be converted to a terminal alkyne **70** by oxidizing it first to the corresponding aldehyde **71** which can then be transformed to the alkyne **70** using a Bestmann-Ohira reaction. Transformation of a ketone moiety in the alkyne **70** to the corresponding amine **72** would provide the building block **B3**.

First we examined different oxidation methods (i.e. Swern-like oxidation as well as oxidation by hypervalent iodine compounds such as 2-iodoxybenzoic acid (IBX) and Dess-Marin periodinane (DMP)) and finally employed mild conditions of Parikh-Doering oxidation[268] to furnish the appropriate aldehyde **71** in good yield (75%). For the conversion of the aldehyde **71** to terminal alkyne **70**, a Seyferth-Gilberth homologation[345] with the Bestmann-Ohira reagent, generated *in situ* from dimethyl-2-oxopropylphosphonate by a diazotation, was chosen as reported by the group of Bestmann.[346] Unfortunately, this reaction gave product **70** in unsatisfactory yield (22%) and low purity (78% according to GC-MS).
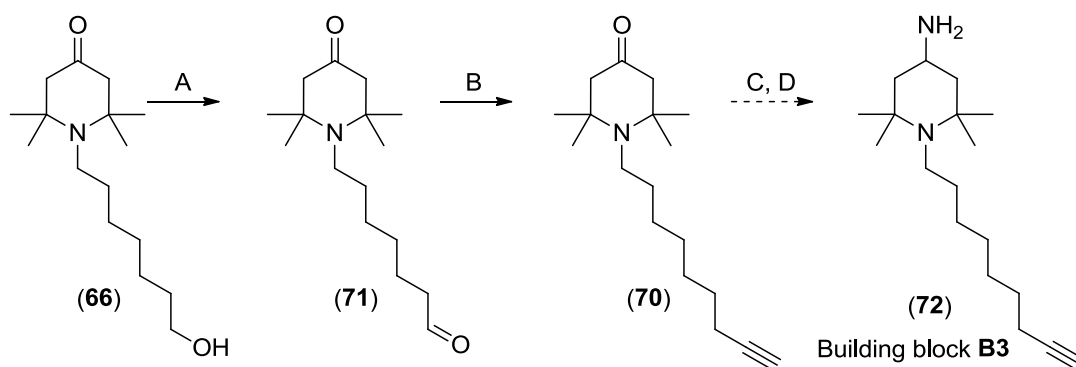
A: SO$_3$. Py (2.5 eq), Et$_3$N (2.5 eq), DCM, DMSO, RT, 1h (75%); **B**: (a) dimethyl-2-oxopropyl phosphonate (1.2 eq), p-TsN$_3$ (1.2 eq), K$_2$CO$_3$ (3.0 eq), MeCN, RT, 2h, (b) MeOH, RT, overnight (22%, 78% purity); **C**: NH$_2$OH, Et$_3$N, MeOH, RT; **D**: LiAlH$_4$, THF

Scheme 30. Attempts for the synthesis of the modified building block **B3**.

As a consequence, we decided to prepare an alternative building block **B4** with a shorter alkyl linker. The synthesis of building block **B4** started with a substitution of propargyl tosylate (**73**) with 4-hydroxy-2,2,6,6-tetramethylpiperidine as reported by Tanaka and Yagi.[347] The resulting *N*-substituted alcohol **74** was oxidized to the corresponding ketone **75** using Swern oxidation,[348] which was then converted to the final amine **77** *via* developed previously oximation[344] and a standard reduction of the oxime **76** with LiAlH₄ in dry THF (Scheme 31).

A: MeCN, reflux (78%); **B**: (COCl)₂, DMSO, Et₃N, DCM, 0 °C-RT, 1h (73%);
C: NH₂OH·HCl, Et₃N, MeOH, RT (97%) **D**: LiAlH₄, THF, 40 °C, 3d (50%)
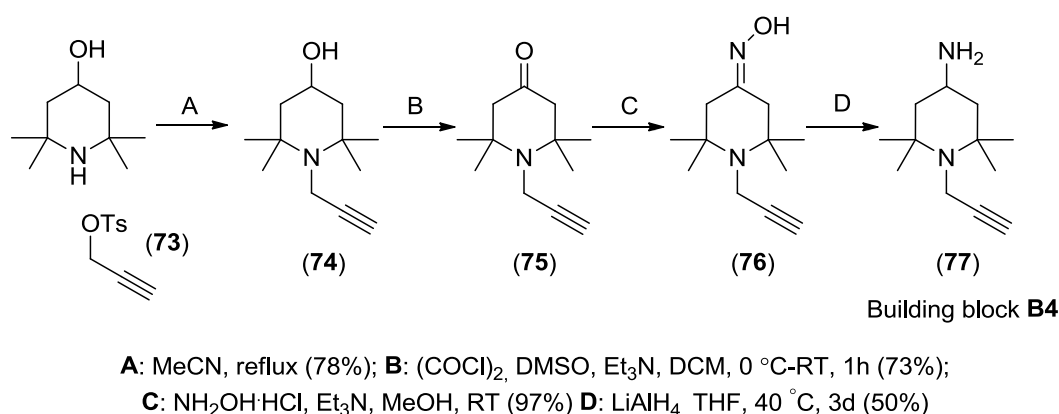
Scheme 31. Synthesis of a modified building block **B4** with a shorter alkyl linker.

The building blocks **A1'** and **A2'** were then converted *in situ* to the carboxylic acids chlorides **77**-**a** and **77**-**b** in a reaction with thionyl chloride,[333] and these reactive intermediates were subsequently substituted by the amine **76** to furnish final probes **78**-**a** and **78**-**b** (Scheme 32).

(**78**)-**a** (meta) 84% MAO A probe
(**78**)-**b** (para) 94% MAO B probe
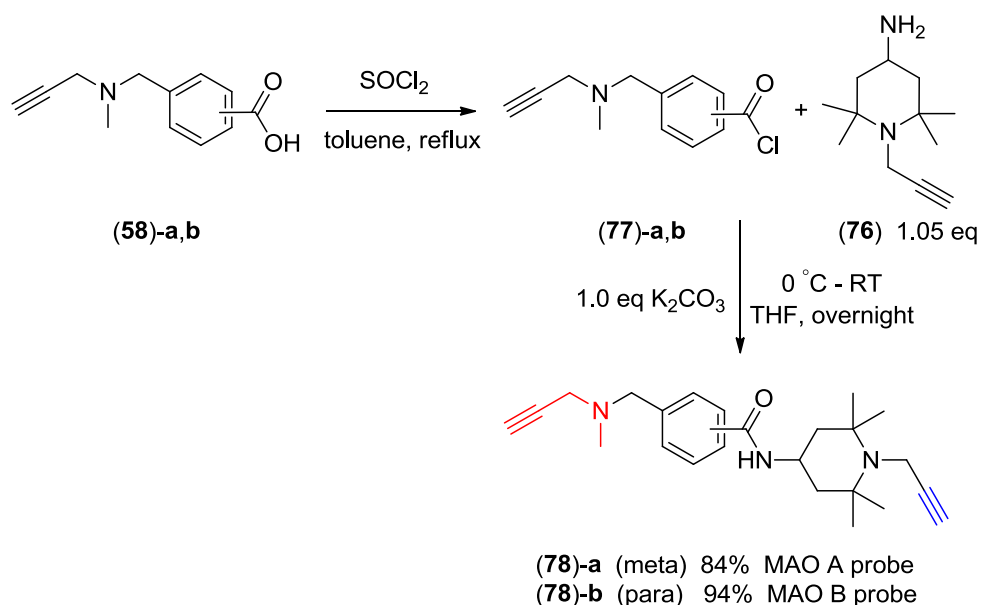
Scheme 32. Final synthesis of MAO A and MAO B specific probes **78**-**a** and **78**-**b**.

The final synthesis was carried out in toluene at reflux and provided the desired products in very good yields, 84% and 94% for *meta*- and *para*-substituted ABPs, respectively.

Prepared probes **78-a** and **78-b** will be evaluated in the further ABPP experiments with complex samples involving both MAO isozymes, with regard to their selectivity and sensitivity of labeling of MAO A and MAO B, respectively. When they display similar inhibitory properties as a parent spin labels due to the steric differences in the size and shape of active sites of MAO A and MAO B, we will receive a very specific ABPP tools to profile activity of both monoamine oxidases.

5 Summary and conclusions

In recent years Activity-Based Protein Profiling (ABPP) has become a well-established and exceptionally powerful chemical proteomic technology allowing dissection of complex proteins interactions in their native cellular environment[13,14] (Figure 84 A). One important challenge in ABPP is however expanding the pool of probe molecules to enzyme classes with more complex catalytic activities such as kinases, transferases and oxidoreductases to extend the proteome coverage. The aim of this PhD thesis was the development and biological evaluation of unprecedented activity-based probes targeting flavin-dependent oxidases. These enzymes represent an important group of oxidoreductases,[129-131] which oxidizes a broad spectrum of molecules by the employment of molecular oxygen as electron acceptor. Their intrinsic structural diversity, multiplicity of accepted substrates, and lack of conserved residues in the active-site make them elusive to functional annotation *via* established genomic, structural or proteomic analyses.[139,146,147] In contrast, ABPP could serve as a powerful and simple alternative for global profiling of these enzymes. Therefore, we envisioned that selective activity-based probes could be built on the simple principle of binding affinity of the oxidatively-activated probes towards the flavin cofactor (Figure 78 B), the only common and intrinsic feature of flavin-dependent oxidases, which is involved in the catalytic mechanism.

The ABPP strategy was examined using a monoamine oxidase enzyme, a representative example of flavin-dependent oxidases, to validate the new labeling mechanism on a well-known target. Monoamine oxidases[148] (MAO, EC 1.4.3.4) are FAD containing enzymes, localized in the mitochondrial outer membrane, which catalyze the oxidative deamination of several important neurotransmitters in the central nervous system (CNS), including serotonin, norepinephrine and dopamine as well as xenobiotic amines.

The methodology involves a 'tag-free' approach for *in situ* enzyme labeling within intact cells. Subsequent cell lysis followed by click chemistry provides the attachment of the fluorescent

tag, which visualizes enzyme activities by gel electrophoresis and fluorescence scanning. A LC-MS based platform and Western blotting finally reveals the identity of labeled enzymes.
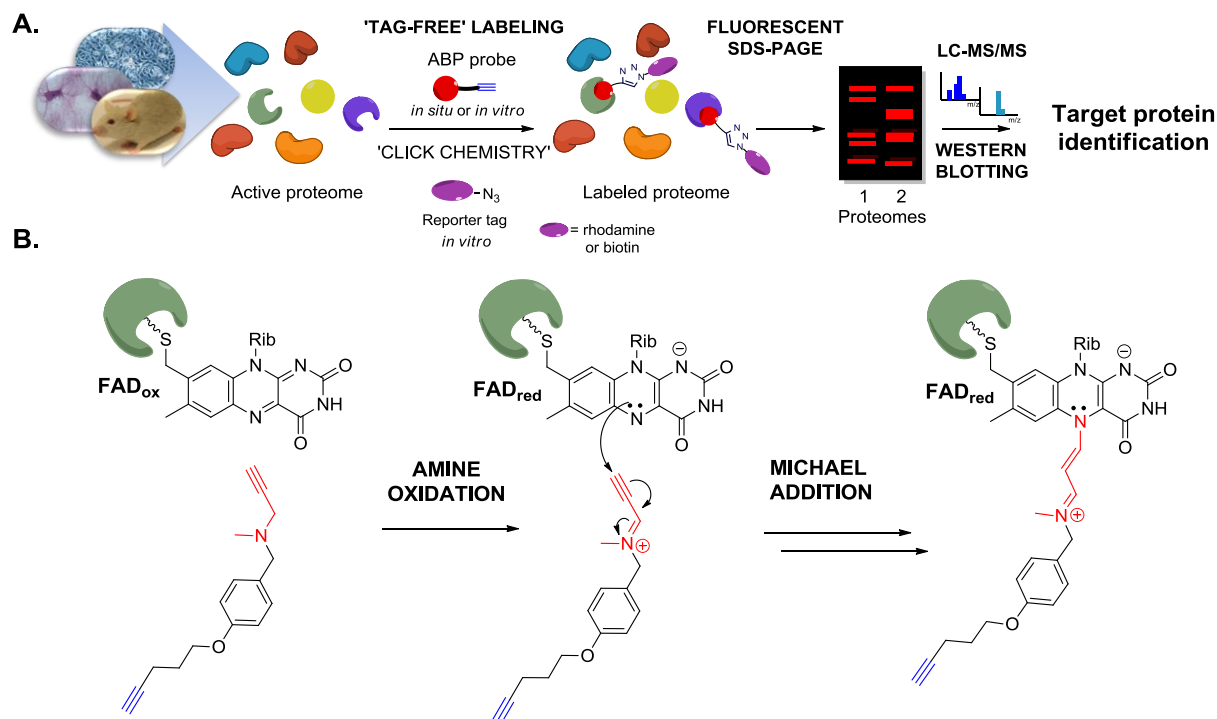
Figure 84. A. Identification of a target protein by the use of ABPP. B. Labeling of activity-based probes dedicated to monoamine oxidases (FAD-dependent oxidases).

First we designed and synthesized a small set of novel activity probes (Figure 85 A) based on the structure of the known irreversible MAO inhibitors pargyline and deprenyl (Figure 85 B). Both inhibitors feature a *N*-propargylamine group which is essentially involved in irreversible enzyme inhibition and formation of a stable covalent adduct, whose existence has been unambiguously assigned by crystal structures of MAO with acetylenic inhibitors such as deprenyl, clorgyline, or rasagiline.[151b,234] In the initial step of this inhibition mechanism, the amine group undergoes catalytic oxidation to an iminium cation mediated through the FAD cofactor, which delivers a reactive intermediate resembling a Michael acceptor, which promotes a nucleophilic attack by N(5) atom of the isoalloxazine ring leading finally to the formation of the covalent adduct. We anticipated that activity-based probes built on these inhibitors will employ the same labeling mechanism (Figure 84 B).

The probes were synthesized by using a simple and robust methodology involving reductive amination to introduce the desired propargylamine group. Subsequent Mitsunobu reaction

with 4-pentyn-1-ol or 3-azidopropan-1-ol allowed the attachment of an alkyl linker carrying an alkyne or azide group, respectively, under very mild conditions furnishing the appropriate probes (Figure 85 C). The structural diversity was introduced by a different substitution pattern at the amino group and by the various lengths and structures of the carbon skeleton between reactive group and arene ring (Figure 85 A).
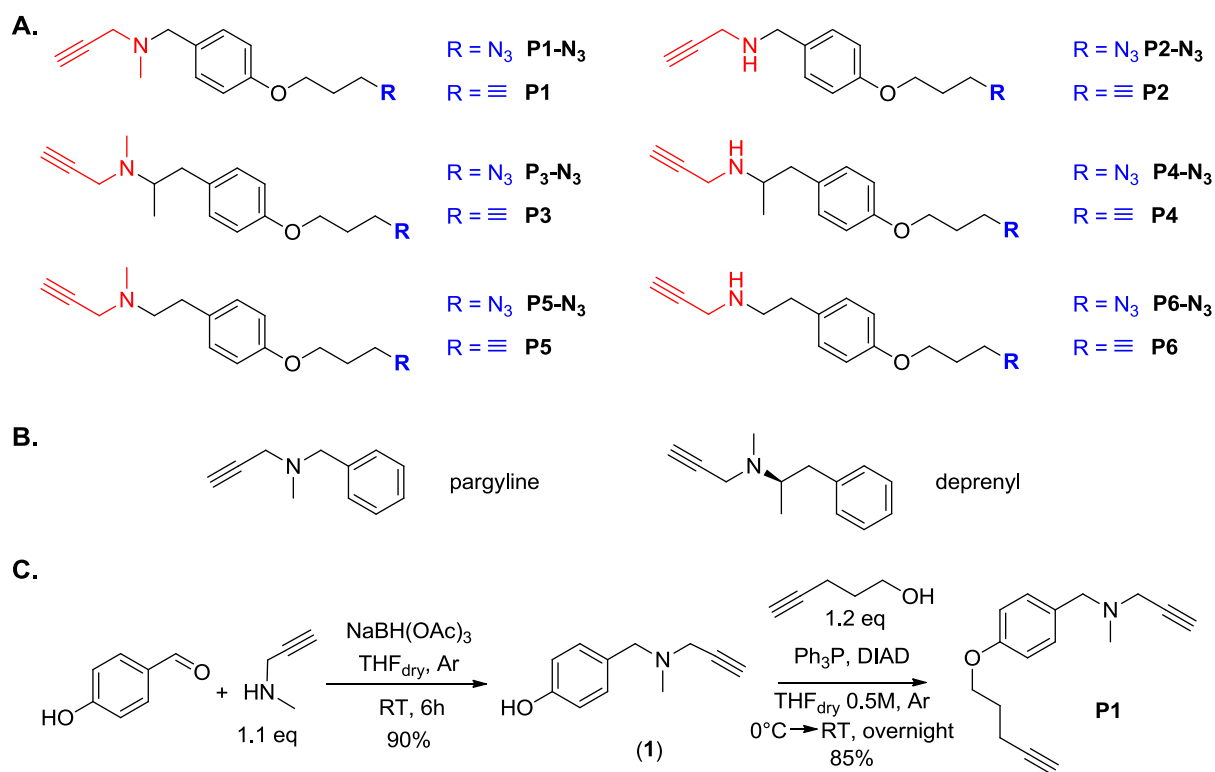
Figure 85. Design and synthesis of ABPP probes dedicated to monoamine oxidases (MAO). A. Structure of ABPs inspired by irreversible MAO inhibitors. B) Structure of irreversible MAO inhibitors: pargyline (unspecific), deprenyl (specific for MAO B). C) Synthetic route leading to probe **P1**.

We also prepared click chemistry compatible fluorescent tags, which employed either NBD or TAMRA fluorophores. Tags were equipped either with an azide (**NBD-N₃** or **TAMRA-N₃**) (Figure 86) or an alkyne group (**NBD-Alk** or **TAMRA-Alk**) (not shown). Initial studies have shown that tags with an azide group exhibited a significantly lower background in the labeling as well as TAMRA-based tag was more effective than the NBD-derived tag. As a result **TAMRA-N₃** tag was employed in the further investigations.
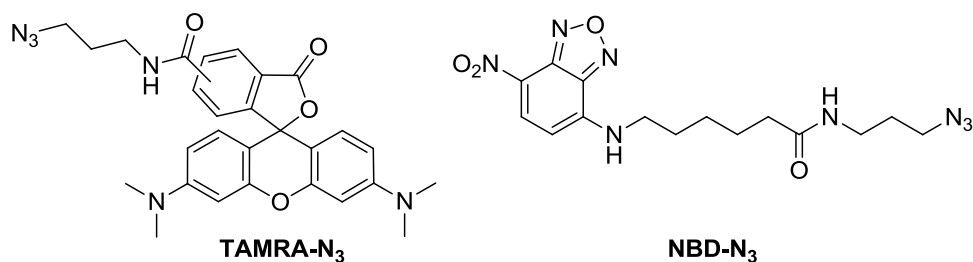
Figure 86. Structure of fluorescent tags **TAMRA-N$_3$** and **NBD-N$_3$** used in the ABPP study.

To test whether the incorporation of an alkyne handle into the pargyline and deprenyl alternates their inhibition potency towards MAO, we determined IC$_{50}$ values of the synthesized probes in a continuous Amplex® Red-peroxidase coupled assay and compared them to the parent inhibitors. Fortunately, the structural modifications introduced to the probes did not affect significantly the inhibition of both isozymes. Probe **P3**, a racemic version of deprenyl equipped with an alkyne, showed a decrease in inhibition of MAO B; whereas probe **P1** based on pargyline showed an improvement of its IC$_{50}$ value, compared to its parent inhibitor.

Having shown that the design of ABPs meets the requirement of MAO inhibition we examined then their use in *in vitro* labeling of *Pichia pastoris* membrane preparations overexpressing human monoamine oxidase. Recombinant human MAO preparations were incubated with the corresponding probe at 10 µM for 1 h at RT followed by the attachment of **TAMRA-N$_3$** tag (Figure 86) under copper(I) catalyzed alkyne-azide cycloaddition (click chemistry, CC) conditions. SDS-PAGE and in-gel fluorescence scanning were employed to detect labeling events. We evaluated the developed ABPP system with respect to the scope of probes collection, specificity and sensitivity of labeling as well as binding site of the probe to the enzyme. The results of this examination are collected in Figure 87.

In these initial 'proof-of-concept' experiments we could demonstrate that both isoforms of MAO can be efficiently labeled as a main target by three probes **P1**, **P3** and **P5** (Figure 87 A and 87 B) with slightly different isoform preferences (Figure 87 F) at concentrations as low as 100 nM (Figure 87 D). Interestingly, all potent probes identified in the screening (**P1**, **P3**, **P5**) include methyl substituted tertiary amines indicating that this feature is important for efficient

141

labeling. Their structural analogs without a methyl substituent at the amino group (**P2**, **P4**, **P6**) exhibited very weak labeling suggesting that a secondary amino group is decreasing the interactions between a probe and the protein or has unfavorable redox behavior.
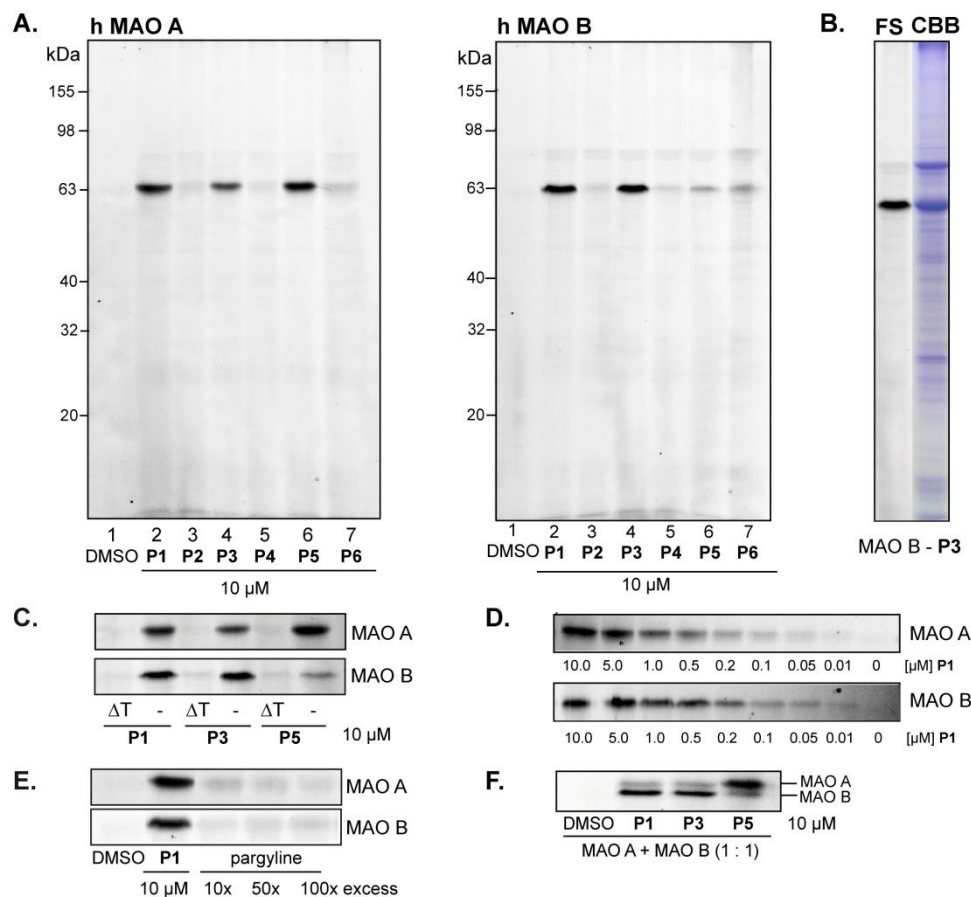
Figure 87. Fluorescent SDS-PAGE analysis of labeling of monoamine oxidase A and B *in vitro*. A. Screening of probes **P1**-**P6** with MAO A and B. B. Comparison of fluorescence scanning (FS) and Coomassie Brilliant Blue (CBB) staining of labeling of MAO B by the probe **P3**. C. Labeling of MAO A and B after heat denaturation (right) and without heat denaturation (left) of the enzyme. D. Concentration-dependent labeling of MAO A and B by **P1**. E. Competitive labeling of MAO A and B with pargyline and probe **P1**. F. Labeling of mixture of both MAO isoforms with probe **P1**, **P3** and **P5**.

Importantly, labeling was completely abolished when the protein was deactivated by heat denaturation prior to incubation with the probe (Figure 87 C), suggesting that labeling occurs only with the active enzyme in a specific manner. In competition experiments we could show that our ABPP probes compete with MAO specific inhibitors for the same binding site (flavin cofactor) in the enzyme active site since pargyline was able to efficiently block the enzyme labeling by probe **P1** (Figure 87 E). Collectively, these results demonstrate that the developed ABPP system can serve as an effective chemical tool for profiling activity of both

isoforms of MAO *in vitro*. To the best of our knowledge this is the first example of activity-based probes targeting a flavin-dependent oxidase.

These valuable results prompted us to examine further the efficiency of the best probes **P1** and **P3** in profiling activity of monoamine oxidases in far more complex biological samples (tissues, living cells). Additionally, we were interested to test whether these probes are able to target other flavin-dependent enzymes, including MAO off-targets.

First, we evaluated the general labeling properties of probes **P1** and **P3** with different mouse tissue homogenates (heart, lung, brain). Interestingly, the only specific bands were noticeable in the insoluble fraction of mouse brain lysate (Figure 88 A).
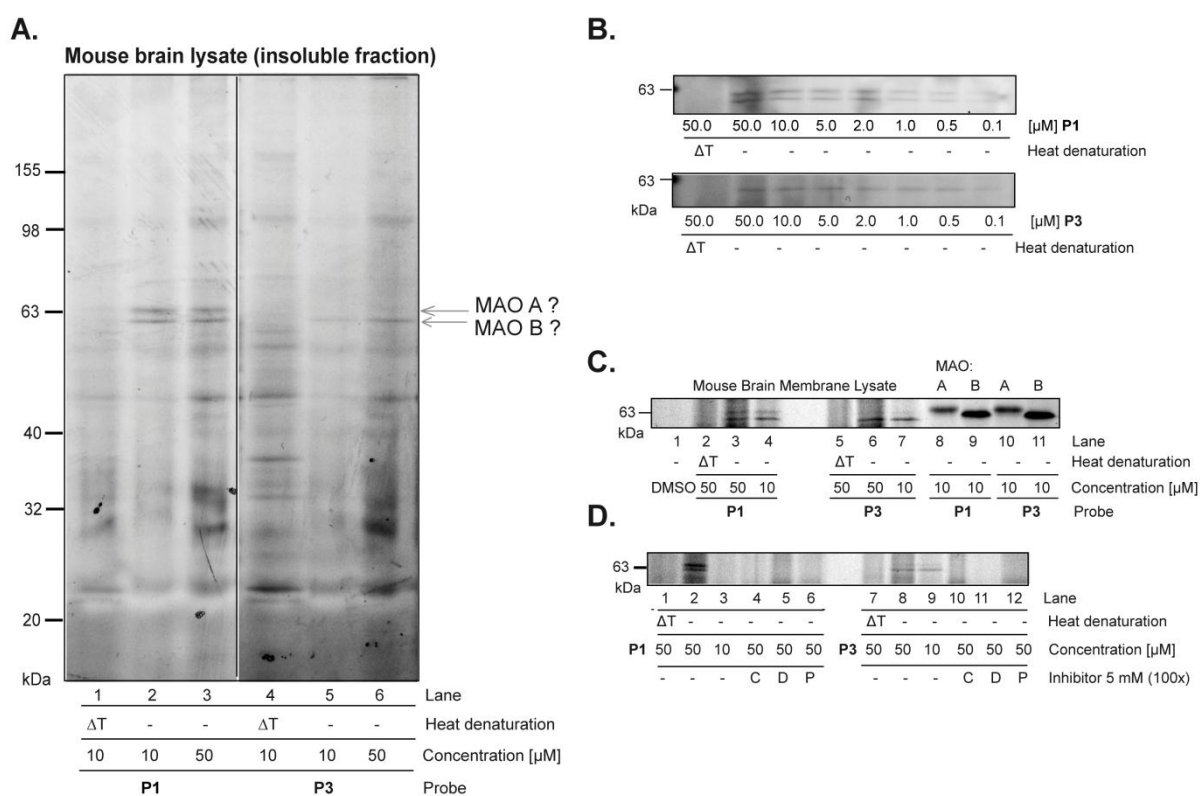
Figure 88. A. Labeling of mouse brain lysate (insoluble fraction) with probes **P1** and **P3**. B. Dose-dependent labeling of mouse brain membrane lysate by **P1** and **P3**. C. Comparative labeling of mouse brain lysate and MAO A and B with **P1** and **P3**. D. Competitive labeling of mouse brain lysate with **P1** and **P3** and MAO specific irreversible inhibitors (C - clorgyline, D - deprenyl, P - pargyline).

Probe **P1**, based on unspecific MAO inhibitor pargyline, labeled two proteins in the range of 60 kDa, whereas probe **P3**, based on MAO B specific inhibitor deprenyl, labeled only one target, compliant to the lower band labeled by probe **P1**. The labeling was dose-dependent

and was still observable at the concentration of 100 nM (Figure 88 B). Interestingly and importantly, molecular weights of the labeled bands matched up with those of MAO A (higher band) and MAO B (lower band) (Figure 88 C) as well as the labeling was completely abolished when the lysate was first incubated with excess of MAO inhibitors (Figure 88 D).

In parallel, we performed a random *in vivo* labeling of different human cells. Initial experiments with MAO naive HeLa cells unfortunately did not provide conclusive results. Therefore, we rationalized that due to the application of pargyline and deprenyl in studying and treatment of CNS disorders, human brain cancer cells (glioblastoma multiforme (GBM) and astroglioma cell lines) would be a more suitable biological system for target validation of probes **P1** and **P3**. Prior to ABPP labeling we determined the cytotoxicity of probes **P1** and **P3** against two eukaryotic cell lines (GBM model DBTRG-05MG and hepatocellular carcinoma HepG2) and validated that within the range of concentrations used for ABPP experiments the cells were still viable.

The most exciting and interesting results were obtained with cell line designated RAEW established from a patient isolate, who was suffering from a glioblastoma multiforme (GBM) tumor (Figure 89). *In situ* labeling with GBM cells revealed that both probes **P1** and **P3** labeled two bands in the range of 63 kDa as main protein targets (Figure 89 B), however the labeling by probe **P3** proved to be much more effective (Figure 89 A). 50 µM concentration of probe **P3** was sufficient for achieving binding saturation as higher concentrations did not improve the labeling of the much weaker lower band. Importantly, inhibitors of monoamine oxidases outcompeted the labeling by probe **P3**, suggesting that these two proteins are MAO A (60.5 kDa) and MAO B (59.4 kDa).

For unequivocal identification of the two probe-bound proteins we performed a quantitative proteomic analysis using a trifunctional reporter tag **TAMRA-biotn-N$_3$**, which was attached to a probe **P3** under CC conditions to allow visualization, enrichment and subsequent identification of proteins by mass spectrometry.[18g] Analysis of peptide fragments employing the SEQUEST algorithm identified MAO A with nearly 40% protein coverage (upper band on

a fluorescent SDS-PAGE). Unfortunately, the enrichment on avidin beads was insufficient for the lower protein band. However, this protein was unambiguously identified as MAO B by Western Blotting using specific anti-MAO B antibodies (Figure 89 C).
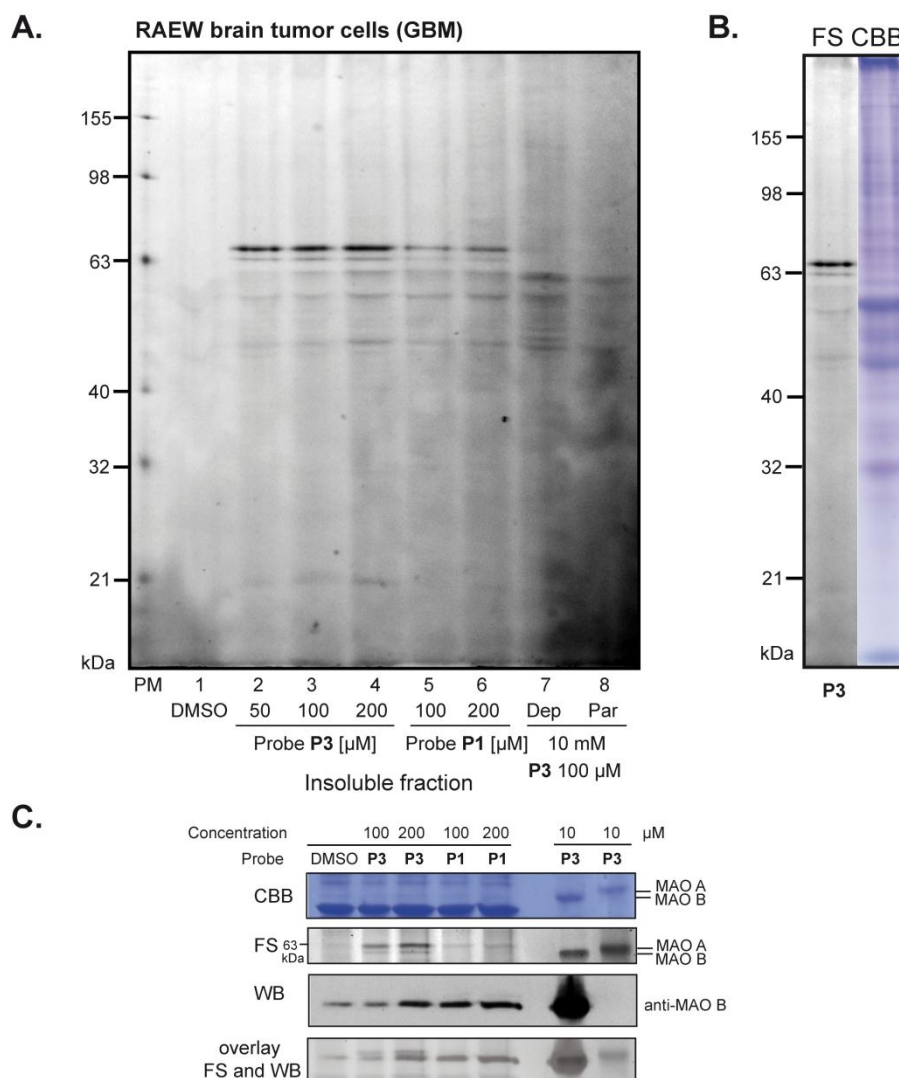
Figure 89. A. *In situ* ABPP labeling of human brain cancer cells (insoluble fraction) with probes **P1** (lanes 5-6) and **P3** (lanes 2-4). Competitive labeling with MAO inhibitors deprenyl (Dep) and pargyline (Par) and probe **P3** (lanes 7-8). B. Comparison of fluorescence scanning (FS) and Coomassie Brilliant Blue (CBB) staining of labeling by the probe **P3**. C. Identification of lower band by Western Blotting using specific anti-MAO B antibodies (Abbreviations: CBB - Coomassie Brilliant Blue, FS – fluorescence scanning, WB – Western Blot).

In conclusion, we have presented in this PhD thesis the successful development of activity-based probes targeting a flavin-dependent oxidase. We could demonstrate their utility in ABPP studies with both tissues and live cells, particularly in exploring the activity of monoamine oxidases. The unique labeling mechanism (Figure 84 B) assured outstanding

selectivity of the probe molecules in labeling of different proteomes. This allowed studying the potential off-target interactions of the clinically used drug deprenyl, for which we could show that it reacted exclusively with MAO A and B. We could also demonstrate the importance of *in vivo* studies on enzyme activity, which very often differs from corresponding *in vitro* studies as enzyme activity is strictly regulated by many dynamic processes taking place exclusively in living cells.

Until now, we were able to unequivocally identify only MAO enzymes as protein targets of novel ABPP probes **P1** and **P3**. However, we are convinced that the scope of our novel chemoproteomic approach can be extended by careful fine-tuning of the probe core structure which can result either in higher specificity of probes or a broader spectrum of targeted flavin oxidases.

6   Future directions

The established ABPP strategy provides an ideal starting point for detailed investigation of this system in the future.

6.1   Scope of protein targets

First of all, the developed activity-based profiling platform should be validated in other proteomes with regard to the scope of protein targets labeled by the best probes.

In the first place, cell lines, for which relatively high expression levels of MAO can be predicted using antibody-based proteomics approach (e.g. RT-4 (bladder cancer), MCF-7 (breast cancer), SH-SY5Y (neuroblastoma), and Hep G2 (hepatocellular carcinoma)), which can be searched in Human Protein Atlas database,[349-351] could be profiled for validation of MAO labeling.

As a first step in this direction, we performed *in situ* labeling of HepG2 cells (hepatocellular carcinoma, ATCC number: HTB-177™) using probes **P1** and **P3** as well as competitive experiments with pargyline and deprenyl inhibitors. Not surprisingly, we were able to identify in these cells both isozymes of monoamine oxidases as MAO enzymes are known to be abundant in liver due to their role in deamination and detoxification of many xenobiotic amines entering the human body.

Interestingly, we were also able to label another protein in the soluble fraction of HepG2 cells. Initial data suggest that this protein might correspond to retinal dehydrogenase 1, which plays a key role in metabolism of retinal and other aldehydes. However further in-depth investigation of a mode of binding is required to provide information whether the labeling is specific and if it occurs at the cofactor or at any other nucleophilic residue in the active site.

These enzymes only rarely contain FAD cofactor[329] and typically involve NAD$^+$ cofactor[330-332] in the oxidation of an aldehyde, therefore the covalent linkage probably is formed by

another mechanism. Nevertheless, this result show, that the scope of protein targets might be potentially extended to other oxidoreductases.

6.2 Optimization of identification platform

In all proteomes evaluated in the ABPP profiling, only few specific protein targets could be detected by comparing the protein bands with control samples, which either lack the probe (background control) or were deactivated by heat denaturation (heat denaturation control) giving strong evidence for an excellent selectivity of the labeling. The most challenging was however the uneqivocal identification of these targets. Obviously, identification of labeled proteins by mass spectrometry is the most robust and straightforward method, but in our studies this strategy proved to be very often limiting and difficult as in many cases we were not able to efficiently enrich the probe-bound proteins. The reason for that could be the instability of the covalent bond between the probe and the enzyme (*via* flavin cofactor) or the instability of the flavin cofactor itself. Therefore, the development of milder and reliable conditions for the release of proteins from avidin beads would be of special interest for such kind of covalent connections to a protein. An easily cleavable linker (by chemical, enzymatic or photo-cleavage as described in section 2.1.5.1) could be a good alternative to the heat release from the avidin resin as it can be carried out under mild conditions and can help diminishing high background originating from some unspecific binding.

For unequivocal identification of MAO enzymes in various proteomes further improvement of Western blotting is also required. We were able to establish a good and reproducible blotting method for the identification of MAO B. However, this method could not be easily transferred for the identification of MAO A by using anti-MAO A antibodies.

6.3 Development of new ABPP probes

In order to achieve either a higher specificity of labeling or a broader target spectrum, a careful fine-tuning of probe structure is necessary.

New probes possesing more general structural features or other warheads, which would also use mechanistic principles of the catalytic oxidation of a probe to deliver a reactive intermediate forming a covalent bond to the flavin cofactor, could tremendously expand the scope of labeled targets and provide tools for global profiling of flavin-dependent oxidases.

Also, the incorporation of a small and innocent photocrosslinker group such as aziridine into the probe core, would establish an additional unspecific covalent linkage to a protein upon UV irradiation. This is of special importance for the majority of flavin-dependent enzymes, which have non-covalently bound flavin cofactor (ca. 90% according to Mecharoux et al.[139]). Unfortunately, their labeling at the flavin cofactor by an ABP possessing only a warhead cannot be detected when proteins are separated by SDS-PAGE. We should also make an effort to improve labeling conditions and identification methods for already prepared photocrosslinker probes **P1-Phot** and **P3-Phot**, employing a benzophenone photoactive group.

Conversely, structural modifications leading to the development of MAO A and MAO B specific probes would deliver tools, which could distinguish between these two isoforms. This will allow identification and visualization of both MAO isozymes in biological samples where both isoforms coexist, serving a role of very sensitive and activity-driven 'fluorescent chemical antibodies'.

To this end, we designed and prepared two probes based on the structure of specific spin-labeled pargyline analogues described by Upadhyay et al.[333] and used as topological probes in EPR measurements. In place of a spin label we installed an alkyne group attached *via* a short alkyl linker (Figure 90).
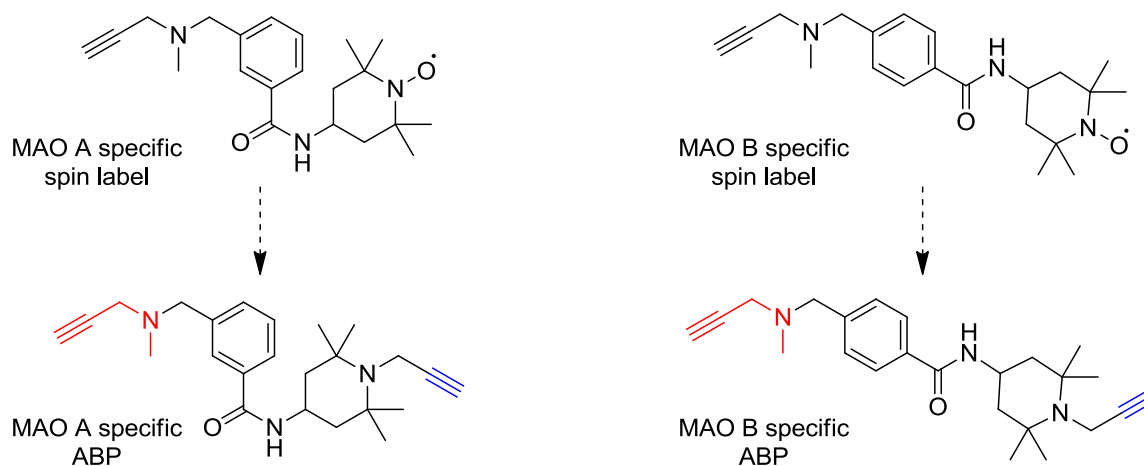
Figure 90. Structure of MAO specific spin labels (top) and MAO specific ABPP probes (middle) and their retrosynthetic analysis (bottom).

The prepared probes will be in the near future evaluated with regard to their selectivity in labeling of MAO A and MAO B. When they display similar inhibitory properties as a parent spin labels due to the steric differences in the size and shape of active sites of MAO A and MAO B, we will receive a very specific ABPP tools to profile activity of both monoamine oxidases.

6.4 Potential applications of ABPP probes

Beyond of the obvious application of the developed for monoamine oxidases activity-based probes in profiling activity of these enzymes, we anticipate that they could also be used for other purposes.

First of all, probes **P1** and **P3** along with newly prepared MAO specific probes could be applied as very simple and efficient tools for the ABPP inhibitor discovery platform (either by competitive ABPP or fluopol-ABPP) for new potent and specific irreversible MAO inhibitors. We estimate that it could be possible to use these probes to assign the inhibitory potency of candidate compounds either using a recombinant enzyme or using a cell or tissue lysate.

Moreover, the MAO specific probes could be used as tool compounds for rapid evaluation of expression levels of MAO in live *Pichia pastoris* cells. The comparison of total fluorescence between selected yeast strain or strains, producing MAO enzyme and grown under various

expression conditions, could provide a simple alternative to Western Blot in assessing the levels of the active expressed enzyme. However, a development of optimal labeling conditions along with the application of an internal standard and all necessary controls for a quantification of the active enzyme expressed in live *Pichia* cells is indispensable.

Also, the application of ABPs dedicated to MAO enzymes in visualization, detection and quantification of active fraction of the enzymes can be a useful tool in different medical studies, which investigate essential changes of MAO activity and not only abundance in different disease models (Parkison's disease,[214,216] heart failure,[213,215] and others). In other words, ABPs for monoamine oxidases could serve as sensitive and specific 'chemical antibodies' for MAO enzymes. In addition, it also could be possible to use the developed ABPs in localization studies, across different tissues of interest, as fluorescent covalent and selective labels, which could be observed using fluorescence microscopy.

In conclusion, the establishment of ABPP system for profiling FAD-dependent monoamine oxidases is just the first step in the enterprise of dissecting a rich world of other flavin-dependent enzymes. Despite of many challenges, it reveals a high potential which should be further studied in the future.

7 Experimental section

7.1 Chemistry section

7.1.1 General

All experiments were carried out using classical Schlenk techniques under an inert atmosphere of argon or nitrogen unless otherwise indicated. When applying Schlenk technique all solvents used were dry and degassed before use and kept under an inert atmosphere of argon or nitrogen.

Degassing of solvents or reaction mixtures was performed by subjecting the appropriate reaction vessel to vacuum until the solvent/reaction mixture started to boil and then purging it with an inert gas. This procedure was repeated at least three times, depending on the solvent volume (vacuum/gas cycles).

Molecular sieves (Sigma-Aldrich, beads, 8-12 mesh) were activated by heating them carefully in a Schlenk flask at 200 °C in a heating mantle under oil pump vacuum (10^{-2} – 10^{-3} mbar) for approx. 2 days until complete dryness was achieved. Subsequently, they were cooled down to RT under argon atmosphere. The activated molecular sieves were stored at RT under argon atmosphere.

Temperatures were measured externally. When working at a temperature of 0 °C, an ice-water bath served as the cooling agent. Temperatures of -5°C and -20°C were achieved with ice/MeOH and dry ice/acetone mixtures, respectively. Reactions carried out at higher temperatures than RT were heated up in a silicon oil bath on a hot plate (RCT basic IKAMAG® safety control) equipped with a temperature controller.

All the reactions were carried out on a hot plate (IKA® RCT basic safety control, 0-1500 rpm) with a magnetic stirrer. Teflon resin-coated, magnetic stir bars (VWR) were used to maintain uniform efficient stirring.

The workup of hydrogenation reactions using PtO_2 catalyst was performed by separating the pyrophoric catalyst from the reaction mixture by filtration through a Celite® pad under an inert atmosphere of nitrogen. The hydrogenation catalyst was washed with ethanol and H_2O and stored in a glass bottle covered with water. This slurry was then disposed of as hazardous waste.

7.1.1.1 Chemicals and solvents

7.1.1.1.1 Chemicals

All reagents and chemicals were purchased from ABCR, Aldrich, Alfa Aesar, Acros Organics, Bachem, Fisher Scientific, Fluka, Maybridge, Merck-Schuchardt, or Sigma-Aldrich. All chemicals were of reagent grade or better and used as received.

7.1.1.1.2 Solvents

Acetonitrile was purchased from Sigma Aldrich (99.5 %), dried over an aluminium oxide column (Pure Solv™ , Innovative Technology Inc.) under inert conditions, then distilled over calcium hydride under argon atmosphere and stored over 3 Å molecular sieves in an amber 1 L Schlenk bottle.

Chloroform was purchased from Acros Organics as extra dry solvent (99.9%, Extra Dry, over 4 Å molecular sieves, AcroSeal®).

1,2-Dichloroethane (DCE) was purchased from Acros Organics as extra dry solvent (99.8%, Extra Dry, AcroSeal®).

Dichloromethane (DCM) was distilled over phosphorus pentoxide and then over calcium hydride under argon atmosphere and stored over 4 Å molecular sieves in an amber 1 L Schlenk bottle under argon atmosphere. Alternatively, it was purchased from Sigma-Aldrich as anhydrous solvent (≥99.8%).

Diethyl ether was distilled over sodium under argon atmosphere and stored over 4 Å molecular sieves in an amber 1 L Schlenk bottle under argon atmosphere.

1,4-Dioxane was purchased from Acros Organics as extra dry solvent (99.8 %, over 4 Å molecular sieves, H_2O <50 ppm, AcroSeal®).

***N,N*-Dimethylformamide** (DMF) was purchased from Acros Organics as extra dry solvent (99.8%, over 3 Å molecular sieves, AcroSeal®) or from Sigma-Aldrich (99.8%).

Dimethylsulfoxide (DMSO) was purchased from Acros Organics as extra dry solvent (99.7+%, over 3 Å molecular sieves, AcroSeal®) and stored over 3 Å molecular sieves in an amber 1 L Schlenk bottle.

Ethanol was purchased was purchased from Merck (99 %, 1 % ethylmethylketone as poisoning agent), distilled over sodium and diethyl phthalate and stored over 3 Å molecular sieves in an amber 1 L Schlenk bottle under argon atmosphere. Alternatively, it was purchased from Sigma-Aldrich as anhydrous solvent (99.8%) and stored over 3 Å molecular sieves in an amber 1 L Schlenk bottle under argon atmosphere.

Methanol was distilled over magnesium turnings and iodine under argon atmosphere and stored over 3 Å molecular sieves in an amber 1 L Schlenk bottle under argon atmosphere. Alternatively, it was purchased from Sigma-Aldrich as anhydrous solvent (99.8%) and stored over 3 Å molecular sieves in an amber 1 L Schlenk bottle under argon atmosphere.

Pyridine was purchased from Acros Organics as extra dry solvent (99.5%, over 4 Å molecular sieves, AcroSeal®).

Tetrahydrofuran was dried over sodium at reflux under argon atmosphere until benzophenone indicated its dryness by turning into deep blue color. The dry THF was stored over 4 Å molecular sieves in an amber 1 L Schlenk bottle under argon atmosphere.

Toluene was purchased in dry quality from Sigma-Aldrich (99.7%), dried over an aluminium oxide column (Pure Solv, Innovative Technology) under inert conditions and stored in an amber 1 L Schlenk bottle over 4 Å molecular sieves under argon atmosphere.

Triethylamine was first distilled over KOH and then pre-dried triethylamine was distilled over calcium hydride under argon atmosphere and stored over 4 Å molecular sieves in an amber 1 L Schlenk bottle under argon atmosphere.

Solvents used for reactions which could be performed on air, flash column chromatography workup and recrystallization were generally of analytical grade.

Cyclohexane, **chloroform**, **dichloromethane**, **ethyl acetate** and **methanol** were purchased from Fisher Scientific as analytical grade (99.99 %) solvents and used directly without any purification. If needed, solvents were additionally distilled using a rotary evaporator to get rid of trace impurities or stabilizers.

Acetone was distilled using a rotary evaporator and stored in a dark bottle.

Diethyl ether and **tetrahydrofuran** were carefully distilled using a rotary evaporator and stored over KOH pellets in an amber 1 L bottle.

Acetic acid was purchased from Sigma-Aldrich (glacial, 99.8%) or Acros Organics (96%), **acetonitrile** was purchased from Alfa Aesar (99.9%), **ethanol** was purchased from Merck (1% ethylmethylketone as stabilizer), **toluene** was purchased from Sigma-Aldrich (99.7%) and were used directly without any purification.

For work-up purposes and quenching of reactions deionized **water** was used.

7.1.1.2 Analytical methods

7.1.1.2.1 Chromatography methods

Thin layer chromatography (TLC)

Analytical thin layer chromatography (TLC) was carried out on Merck TLC silica gel 60 F_{254} aluminium sheets and spots were visualized by UV light (λ = 254 and/or 366 nm) or by staining with iodide, ninhydrin (250.0 mg ninhydrin, 5 mL pyridine and 95 mL MeOH) or cerium ammonium molybdate (2.0 g cerium (IV) sulfate, 50.0 g ammonium molybdate and 50

mL conc. H_2SO_4 in 400 mL water) (CAM) solution followed by the development of the stains in the heat.

<u>Flash column chromatography</u>

Flash column chromatography was performed on silica gel 0.035-0.070 mm, 60Å (Acros Organics). A 50 to 100 fold excess of silica gel was used with respect to the amount of dry crude product, depending on the separation problem. The dimensions of the column were selected in such a way that the required amount of silica gel formed a pad between 10 cm and 25 cm.

Typically, the column was equilibrated first with the solvent or solvent mixture, and the crude product diluted with the eluent was applied onto the top of silica pad. In case when the crude product was insoluble in the eluent, the sample was dissolved in an appropriate solvent (MeOH, ethyl acetate or DCM), and the equal amount of silica gel was added, followed by removal of the solvent under reduced pressure and drying the sample *in vacuo* which was then directly loaded onto the top of silica pad. The mobile phase was forced through the column using a rubber bulb pump.

<u>Gas chromatography</u>

GC-MS analyses were carried out on two instruments; either Agilent Technologies HP 6890 GC system equipped with a 5972 mass selective detector (EI, 70 eV) or Agilent Technologies 7890A GC system equipped with a 5975C mass selective detector (inert MSD with Triple Axis Detector system, EI, 70 eV). In both systems samples were injected by employing autosampler 7683B in a split mode 1/175 (inlet temperature: 250°C; injection volume: 2.0 µL) and separated on an Agilent Technologies J&W GC HP-5MS capillary column ((5%-phenyl)-methylpolysiloxane; 30 m x 0.25 mm x 0.25 µm) at a constant helium flow rate (He 5.0 (Air Liquide), 1.085 mL/min, average velocity 41.6 cm/sec).

General gradient temperature method was used (JK_50_S28 or JK_50_S40) (initial temperature: 50 °C for 1 min, linear increase 40°C/min to 300 °C, hold for 5 min, 1 min post-

run at 300°C, detecting range: 50.0 to 550.0 amu, solvent delay of 2.80 or 4.00 min, respectively).

<u>High performance liquid chromatography (HPLC)</u>

Analytical HPLC-MS analyses were performed on a Shimadzu Nexera LCMS-2020 system (CBM-20A Prominence system controller, Nexera SIL-30AC autosampler, DGU-20A3 and DGU-20A5 on-line degassers, Nexera LC-30AD binary pump, FCV-20AH2 valve unit, CTO-20AC Prominence column oven, SPD-M20A Prominence photodiode array (PDA) detector (deuterium lamp, tungsten lamp, 190-800 nm)) equipped with single quadrupole ultra-fast LC/MS detector "LCMS-2020" using electrospray ionization source (ESI in positive and negative mode). The HPLC analyses were carried out on Agilent Poroshell 120 SB-C18 (100.0 x 3.0 mm, 2.7 µm) or Agilent Poroshell 120 EC-C18 (100.0 x 3.0 mm, 2.7 µm) columns equipped with Agilent ZORBAX Reliance Cartridge pre-column. Two general LC time methods were used:

JK_10to90: A: 5 mM $HCOONH_4$, B: MeCN, 30 °C, flow 0.7 mL/min; 0.0-3.0 min: 10% B constant, 3.0-7.9 min: linear gradient 10-90% B, 7.9-11.0 min: 90% B constant, 11.0-12.01: linear gradient 90-10% B, 13.0 min: stop).

JK_35to90: A: 5 mM $HCOONH_4$, B: MeCN, 30 °C, flow 0.7 mL/min; 0.0-3.0 min: 35% B constant, 3.0-7.9 min: linear gradient 35-90% B, 7.9-11.0 min: 90% B constant, 11.0-12.01: linear gradient 90-35% B, 13.0 min: stop).

Analytical HPLC-MS analyses (model click chemistry reactions) were performed on an Agilent Technologies 1200 Series instrument (G1379B Degasser, G1312B Binary Pump SL, G1367C High Performance Autosampler SL, G1330 FC/ALS Thermostat, G1316B Thermostated Column Compartment SL, G1365C Multiple Wavelength Detector SL) with an Agilent Technologies 6120 quadrupole LC/MS Detector with a G1918B Electrospray Ionization Source. Signals were detected at 210 and 460 nm. Merck Chromolith Performance Rp-18e (100.0 x 3.0 mm, Merck) column was used. Two LC time methods were applied:

157

Std_25Const_Pos_Atune: A: 10 mM CH_3COONH_4, pH 5.5, B: MeCN, 25 °C, flow 0.7 mL/min; 0.0-1.5 min: 10% B constant, 1.5-7.5 min: 25% B constant, 7.5-9.0 min: linear gradient 25-100% B, 9.0-12.01: linear gradient 100-10% B, 13.0 min: stop).

Std_23Const_TFA: A: 0.1% TFA in H_2O, B: MeCN, 25 °C, flow 0.7 mL/min; 0.0-6.0 min: 23% B constant, 6.0-7.0 min: linear gradient 23-100% B, 7.0-9.01: linear gradient 100-23% B, 10.0 min: stop).

HPLC analyses (model click chemistry reactions) were also conducted on an HP 1100 instrument (G1322A Degasser, G1313A Quaternary Pump, G1316A Thermostated Column Compartment) equipped with G1362A Refractive Index Detector and G1315A Diode Array detector (DAD) and Macherey & Nagel Nucleodur Rp-18e (150.0 x 4.6 mm, 5 µm) column. Signals were detected at 210 nm and 460 nm. The following LC time method was used:

Std_30Const_50_TFA: A: 0.05% TFA in H_2O, B: MeCN, 25 °C, flow 1.0 mL/min; 0.0-3.5 min: 30% B constant, 3.6-6.5 min: 50% B constant, 6.6-8.0 linear gradient 50-100% B, 8.0-10.01: linear gradient 100-30% B, 11.0 min: stop).

Demineralized water used for HPLC was additionally filtered through 0.2 µm cellulose nitrate membrane filter.

7.1.1.2.2 Nuclear magnetic resonance (NMR) spectroscopy

^{1}H NMR and ^{13}C NMR spectra were recorded on a Bruker AVANCE III 300 spectrometer ([1]H: 300.36 MHz; [13]C: 75.53 MHz) or Varian Unity Inova 500 ([1]H: 499.76 MHz; [13]C: 125.66 MHz) or Bruker AVANCE 360 ([1]H: 360 MHz; [13]C: 90 MHz) or Bruker AVANCE 500 ([1]H: 500 MHz; [13]C: 125 MHz). Chemical shifts were referenced to the residual proton and carbon signal of the deuterated solvent, respectively (DMSO-d_6: δ = 2.50 ppm (^{1}H), 39.52 ppm (^{13}C), CDCl$_3$: δ = 7.26 ppm (^{1}H), 77.16 ppm (^{13}C), MeOD-d_4: δ = 3.31 ppm (^{1}H), 49.00 ppm (^{13}C)). Signal multiplicities are abbreviated as s (singlet), brs (broad singlet), d (doublet), dd (doublet of doublet), dt (doublet of triplet), dtd (doublet of triplet of doublet), t (triplet), td (triplet of doublet), q (quadruplet), qd (quadruplet of dublets), p (pentet) and m (multiplet). Additionally,

quarternary carbon atoms are designated as C_q, aromatic carbon atoms as C_{Ar}. For differentiation of the carbon atoms APT spectra were recorded if necessary.

7.1.1.2.3 Infrared spectroscopy (IR)

IR spectra were recorded on a Bruker Tensor 37^{TM} FT-IR spectrophotometer equipped with integrated (Attenuated Total Reflectance) ATR module (zinc selenide crystal). The background air signal was automatically subtracted from the recorded spectra. The wavenumbers are reported in cm^{-1}.

7.1.1.2.4 High resolution mass spectrometry (HRMS)

High resolution mass spectrometry (HRMS) spectra were recorded on Waters® Micromass GCT Premier^{TM} mass spectrometer using a direct inlet electron impact ionization (DI-EI) (70 eV) and time-of-flight (TOF) mass analyzer in a positive mode (TOF MS EI+). For MALDI-TOF HRMS Waters® Micromass TofSpec 2E mass spectrometer was used and samples were ionized from α-cyano-4-hydroxycinnamic acid matrix analyzed by a time-of-flight (TOF) mass analyzer.

7.1.1.2.5 Melting points

Melting points were measured on Mel-Temp® melting point apparatus (Electrothermal) with an integrated microscopical support in open capillary tubes and were not corrected. The temperature was measured with a mercury-in-glass thermometer.

7.1.2 Synthesis of probes precursors

7.1.2.1 1-(3-Bromopropoxy)-4-methylbenzene (4)
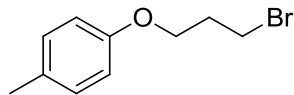
Method A: In a 100 mL round-bottom flask equipped with a condenser 1.08 g *p*-cresol (10.0 mmol, 1.0 eq) were dissolved in 25 mL MeCN. Then, 2.07 g potassium carbonate (15.0 mmol, 1.5 eq) were added, followed by addition of 10.1 g 1,3-dibromopropane (5.08 mL, 50.0 mmol, 5.0 eq). The reaction mixture was then stirred at reflux for 7 h. The reaction progress was followed by TLC and GC-MS analysis and once the starting material was no longer indicated the reaction mixture was cooled down to RT, inorganic salt was separated by filtration, washed with MeCN and the filtrate concentrated *in vacuo*. The residue was dissolved in 25 mL CHCl$_3$ and washed with 0.2 N NaOH (2 x 20 mL). The organic layer was dried over anhydrous sodium sulphate and concentrated *in vacuo. T*he product was purified by distillation (100-105 °C / 0.8 mbar) resulting in 1.65 g (7.20 mmol, 60%, 83% purity) 1-(3-bromopropoxy)-4-methylbenzene (**4**) as a yellowish oil.

Method B: In an oven dried, evacuated and argon purged 50 mL Schlenk flask 541 mg *p*-cresol (523 µL, 5.0 mmol, 1.0 eq), 764 mg 3-bromo-1-propanol (497 µL, 6.0 mmol, 1.1 eq) and 1.443 g triphenylphosphine (6.0 mmol, 1.1 eq) were dissolved in 15 mL dry and degassed THF under argon. The reaction mixture was cooled down to 0 °C in an ice-water bath and subsequently, 1.112 g diisopropyl azodicarboxylate (DIAD) (1.083 mL, 6.0 mmol, 1.1 eq) were added dropwise over the course of 15 min and the reaction mixture was stirred under inert atmosphere at RT for 20 h. After that time, when no more conversion of the starting materials was observed by GC-MS and TLC analysis, the mixture was cooled down in a water-ice bath and ca. 30 mL cold cyclohexane were added to precipitate triphenylphosphine oxide. The white solid was filtrated off, washed with cold cyclohaxane and the filtrate concentrated *in vacuo.* The residue was purified by flash column

chromatography (cyclohexane:ethyl acetate = 95:5 (v/v), 125 g silica gel, size: 23.0 x 4.0 cm) yielding 811 mg (3.54 mmol, 71%) 1-(3-bromopropoxy)-4-methylbenzene (**4**) as a yellowish oil.

$C_{10}H_{13}BrO$ [229.11 g/mol]

R_f = 0.66 (cyclohexane:ethyl acetate = 95:5 (v/v)).

GC-MS (EI) t_R = 5.76 min; m/z (%) 229.3 (36.6) [M$^+$], 120.7 (5.3), 107.7 (100.0), 90.8 (10.2), 76.8 (17.9), 64.8 (5.8), 50.8 (5.5).

^{1}H NMR (300 MHz, CDCl$_3$) δ: 7.09 (d, J = 8.4 Hz, 2H, arom.), 6.81 (d, J = 8.4 Hz, 2H, arom.), 4.08 (t, J = 5.7 Hz, 2H, OC**H**$_2$), 3.61 (t, J = 6.6 Hz, 2H, C**H**$_2$Br), 2.36 – 2.30 (m, 5H; 2.31 (p, J = 6.0 Hz, 2H, (CH$_2$C**H**$_2$CH$_2$)), 2.30 (s, 3H, (C**H**$_3$)).

^{13}C NMR (75 MHz, CDCl$_3$) δ 156.70 (**C**$_{Ar}$-1), 130.30 (**C**$_{Ar}$-4), 130.07 (**C**$_{Ar}$-3), 114.54 (**C**$_{Ar}$-2), 65.53 (O**C**H$_2$), 32.60 (**C**H$_2$Br), 30.25 (CH$_2$**C**H$_2$CH$_2$), 20.60 (**C**H$_3$).

The spectral data are identical to those published previously.[248]

7.1.2.2 1-(3-Azidopropoxy)-4-methylbenzene (3)
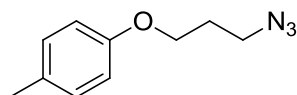
In an oven dried, evacuated and argon purged 50 mL Schlenk flask 895 mg 1-(3-bromopropoxy)-4-methylbenzene (**4**) (3.9 mmol, 1.0 eq) were dissolved in 22 mL dry and degassed DMF under argon. Subsequently, 761 mg sodium azide (11.7 mmol, 3.0 eq) were added and the reaction was stirred for 2 h at 100 °C. After that time, when full conversion of the starting material was observed by TLC analysis, the mixture was cooled down to RT, diluted with ca. 40 mL distilled water and extracted with DCM (1 x 40 mL, 2 x 30 mL). The combined organic layers were washed with brine (1 x 40 mL), dried over anhydrous sodium sulphate and concentrated *in vacuo*. The crude product was purified by flash column

chromatography (cyclohexane:ethyl acetate = 95:5 (v/v), 80 g silica gel, size: 24.0 x 3.5 cm) yielding 677 mg (89%) 1-(3-azidopropoxy)-4-methylbenzene (**3**) as a yellowish oil.

$C_{10}H_{13}BrN_3O$ [191.23 g/mol]

R_f = 0.43 (cyclohexane:ethyl acetate = 95:5 (v/v)).

GC-MS (EI) t_R = 5.76 min; m/z (%) 190.9 (54.4) [M$^+$], 162.0 (7.5), 147.8 (6.3), 134.2 (20.2), 120.0 (8.8), 107.0 (100.0), 90.8 (31.5), 76.8 (47.0), 64.8 (16.4), 55.8 (38.7), 50.8 (13.8).

^{1}H NMR (300 MHz, CDCl$_3$) δ: 7.09 (d, J = 8.4 Hz, 2H, arom.), 6.81 (d, J = 8.4 Hz, 2H, arom.), 4.03 (t, J = 6.0 Hz, 2H, OC**H**$_2$), 3.52 (t, J = 6.6 Hz, 2H, C**H**$_2$N$_3$), 2.30 (s, 3H, C**H**$_3$), 2.05 (p, J = 6.3 Hz, 2H, CH$_2$C**H**$_2$CH$_2$).

^{13}C NMR (75 MHz, CDCl$_3$) δ 156.68 (**C**$_{Ar}$-1), 130.29 (**C**$_{Ar}$-4), 130.06 (**C**$_{Ar}$-3), 114.49 (**C**$_{Ar}$-2), 64.69 (O**C**H$_2$), 48.44 (**C**H$_2$N$_3$), 28.99 (CH$_2$**C**H$_2$CH$_2$), 20.59 (**C**H$_3$).

7.1.2.3 4-((Methyl(prop-2-yn-1-yl)amino)methyl)phenol (9)
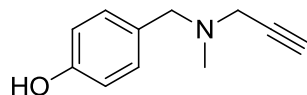
In an oven dried, evacuated and argon purged 100 mL Schlenk flask 610 mg 4-hydroxybenzaldehyde (5.0 mmol, 1.0 eq) were dissolved in 20 mL dry and degassed THF at RT resulting in a clear yellowish solution. Subsequently, 380 mg *N*-methylpropargylamine (464 µL, 5.5 mmol, 1.1 eq) were added at once to the reaction mixture giving a bright yellow solution. The mixture was stirred at RT for 30 min. Then 1.483 g sodium triacetoxyborohydride (7.0 mmol, 1.4 eq) were added at once. After addition of the reducing agent the mixture became thicker and cloudy. The reaction was monitored by GC-MS and TLC analysis and carried out for 5 h at RT until complete consumption of the aldehyde was indicated. After that time the reaction mixture was quenched with 25 mL saturated NaHCO$_3$. The solution was extracted with ethyl acetate (4 x 20 mL). The combined organic layers were

washed with water (2 x 20 mL) and brine (1 x 20 mL) and dried over anhydrous Na_2SO_4. The solvent was removed in *vacuo* and the crude product purified by flash column chromatography (cyclohexane:ethyl acetate = 7:3 (v/v), 40 g silica gel, size: 15.5 x 3.5 cm) furnishing 790 mg (4.50 mmol, 90%) 4-((methyl(prop-2-yn-1-yl)amino)methyl)phenol (**9**) as a pale yellowish solid.

$C_{11}H_{13}NO$ [175.23 g/mol]

R_f = 0.35 (cyclohexane:ethyl acetate = 1:1 (v/v)), 0.16 (cyclohexane:ethyl acetate = 7:3 (v/v)).

m.p. = 105-107 °C (pale yellowish solid)

GC-MS (EI): t_R = 5.81 min; m/z (%) 175.1 (38.6) [M^+], 158.2 (2.1), 148.1 (3.2), 134.0 (13.3), 107.0 (100.0), 82.1 (15.4), 78.1 (39.7), 68.1 (45.5), 51.0 (17.1).

^{1}H NMR (300 MHz, MeOD-d_4) δ: 7.14 (d, *J* = 8.7 Hz, 2H, arom.), 6.74 (d, *J* = 8.7 Hz, 2H, arom.), 3.50 (s, 2H, PhC**H**$_2$N), 3.24 (d, *J* = 2.1 Hz, 2H, C**H**$_2$C≡CH), 2.69 (t, *J* = 2.4 Hz, 1H, CH$_2$C≡C**H**), 2.30 (s, 3H, C**H**$_3$).

^{13}C NMR (75 MHz, MeOD-d_4) δ: 158.06 (**C**$_{Ar}$-1), 131.93 (**C**$_{Ar}$-3), 129.14 (**C**$_{Ar}$-4), 116.09 (**C**$_{Ar}$-2), 78.77 (**C**≡CH), 75.37 (C≡**C**H), 60.20 (Ph**C**H$_2$N), 44.98 (**C**H$_2$C≡CH), 41.69 (**C**H$_3$).

IR (neat) cm^{-1}: 3269, 2801, 1612, 1592, 1514, 1457, 1365, 1276, 1252, 1232, 1098, 1016, 824, 683, 645.

HRMS (DI-EI) calcd for $C_{11}H_{13}NO$ 175.0997 [M^+], found 175.0998.

7.1.2.4 4-((Prop-2-yn-1-ylamino)methyl)phenol (11)
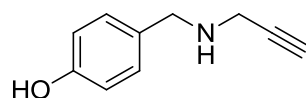
In an oven dried, evacuated and argon purged 100 mL Schlenk flask 733 mg 4-hydroxybenzaldehyde (6.0 mmol, 1.0 eq) were dissolved in 36 mL dry and degassed mixture of DCE:THF 5:1 (v/v) at RT forming a clear yellowish solution. Subsequently, a solution of

397 mg propargylamine (461 µL, 7.2 mmol, 1.2 eq) in 1 mL dry DCE was added at once resulting in a bright yellow solution. The mixture was stirred at RT for 30 min. Then 1.780 g sodium triacetoxyborohydride (8.4 mmol, 1.4 eq) were added at once. After addition of the reducing agent the mixture became thicker and cloudy. The reaction was monitored by GC-MS and TLC analysis and carried out overnight for 18 h at RT until nearly complete consumption of the aldehyde was indicated. After that time the reaction mixture was quenched with 20 mL saturated $NaHCO_3$. The solution was extracted with ethyl acetate (3 x 40 mL) and the combined organic layers were washed with water (2 x 50 mL) and brine (1 x 50 mL) and dried over anhydrous Na_2SO_4. The solvent was removed *in vacuo* and the crude product purified by flash column chromatography (cyclohexane:ethyl acetate = 7:3 (v/v) and 1% Et_3N, 150 g silica gel, size: 21.0 x 4.5 cm) resulting in 528 mg (3.27 mmol, 55%) 4-((prop-2-yn-1-ylamino)methyl)phenol (**11**) as a dark yellow solid.

$C_{10}H_{11}NO$ [161.20 g/mol]

R_f = 0.18 (cyclohexane:ethyl acetate = 7:3 (v/v) with 1% Et_3N), 0.13 (cyclohexane:ethyl acetate = 1:1 (v/v)), 0.06 (cyclohexane:ethyl acetate = 7:3 (v/v)).

m.p. = 100-102 °C (dark yellow solid)

GC-MS (EI): t_R = 5.84 min; m/z (%) 160.0 (100.0) $[M-H]^+$, 144.0 (12.6), 132.0 (44.8), 120.0 (39.9), 107.1 (94.5), 78.1 (45.8), 77.0 (57.7), 68.1 (13.6), 65.0 (16.9), 54.0 (28.9), 52.0 (30.2).

^{1}H NMR (500 MHz, MeOD-d$_4$) δ: 7.15 (d, *J* = 8.5 Hz, 2H, arom.), 6.74 (d, *J* = 8.5 Hz, 2H, arom.), 3.72 (s, 2H, PhC**H**$_2$N), 3.32 (d, *J* = 2.5 Hz, 2H, C**H**$_2$C≡CH), 2.64 (t, *J* = 2.5 Hz, 1H, CH$_2$C≡C**H**).

^{13}C NMR (75 MHz, MeOD-d$_4$) δ: 157.86 (**C**$_{Ar}$-1), 131.08 (**C**$_{Ar}$-3), 130.53 (**C**$_{Ar}$-4), 116.19 (**C**$_{Ar}$-2), 81.93 (**C**≡CH), 73.43 (C≡**C**H), 52.23 (Ph**C**H$_2$N), 37.22 (**C**H$_2$C≡CH).

IR (neat) cm^{-1}: 3276, 3250, 1591, 1516, 1454, 1388, 1248, 1170, 1070, 984, 813, 777, 706, 676.

HRMS (DI-EI) calcd for $C_{10}H_{11}NO$ 160.0762 $[M-H]^+$, found 160.0763.

7.1.2.5 4-(2-(Methyl(prop-2-yn-1-yl)amino)propyl)phenol (12)
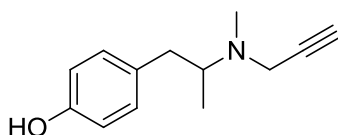
In an oven dried, evacuated and argon purged 50 mL Schlenk flask 601 mg 4-hydroxyphenylacetone (4.0 mmol, 1.0 eq) were dissolved in 20 mL dry and degassed THF at RT resulting in a clear yellow solution. Subsequently, a solution of 553 mg *N*-methylpropargylamine (675 µL, 8.0 mmol, 2.0 eq) in 3 mL dry THF was added at once to the reaction mixture resulting in a dark yellow solution. The mixture was stirred at RT for 30 min. Then 1.696 g sodium triacetoxyborohydride (8.0 mmol, 2.0 eq) were added at once, followed by addition of 448 mg glacial acetic acid (458 µL, 8.0 mmol, 2.0 eq). After addition of the reducing agent the mixture became thicker and cloudy. The reaction was monitored by GC-MS and TLC analysis and carried out for 92 h at RT until nearly complete consumption of the ketone was indicated. After that time the reaction mixture was quenched with 20 mL saturated $NaHCO_3$. The solution was extracted with ethyl acetate (3 x 20 mL). The combined organic layers were washed with water (2 x 20 mL) and brine (1 x 20 mL) and dried over anhydrous Na_2SO_4. The solvent was removed in *vacuo* and the crude product purified by flash column chromatography (cyclohexane:ethyl acetate = 7:3 (v/v), 45 g silica gel, size: 18.0 x 3.0 cm) furnishing 555 mg (2.73 mmol, 68%) 4-(2-(methyl(prop-2-yn-1-yl)amino)propyl) phenol (**12**) as a light yellow solid.

$C_{13}H_{17}NO$ [203.28 g/mol]

R_f = 0.27 (cyclohexane:ethyl acetate = 1:1 (v/v)), 0.14 (cyclohexane:ethyl acetate = 7:3 (v/v).

m.p. = 113-115 °C (light yellow solid)

GC-MS (EI): t_R = 6.39 min; m/z (%) 202.0 (0.2) [M-H]$^+$, 107.0 (19.1), 96.1 (100.0), 77.1 (15.5), 70.1 (5.5), 56.0 (30.3).

^{1}H NMR (300 MHz, MeOD-d$_4$) δ: 6.99 (d, J = 8.4 Hz, 2H, arom.), 6.70 (d, J = 8.4 Hz, 2H, arom.), 3.44 (m, 2H, C**H**$_2$C≡CH), 2.95 (dd, J = 13.5, 2.8 Hz, 1H, C**H**$_a$H$_b$CH and m, 1H, C**H**), 2.68 (t, J = 2.4 Hz, 1H, CH$_2$C≡C**H**), 2.39 (s, 3H, NC**H**$_3$), 2.28 (dd, J = 13.7, 11.1 Hz, 1H, CH$_a$**H**$_b$CH), 0.94 (d, J = 6.5 Hz, 3H, C**H**$_3$).

^{13}C NMR (75 MHz, MeOD-d$_4$) δ: 156.75 (**C**$_{Ar}$-1), 131.83 (**C**$_{Ar}$-4), 131.17 (**C**$_{Ar}$-3), 116.15 (**C**$_{Ar}$-2), 80.29 (**C**≡CH), 74.66 (C≡**C**H), 60.71 (C$_q$), 43.69 (**C**H$_2$C≡CH), 39.08 (Ph**C**H$_2$CH), 37.67 (N**C**H$_3$), 14.97 (**C**H$_3$).

IR (neat) cm^{-1}: 3285, 2965, 1611, 1513, 1463, 1273, 1249, 1146, 1100, 1035, 824, 804, 679, 639, 614.

HRMS (DI-EI) calcd for C$_{13}$H$_{17}$NO 203.1310 [M$^+$], found 203.1314.

7.1.2.6 4-(2-(Prop-2-yn-1-ylamino)propyl)phenol (13)
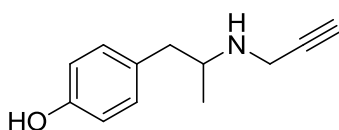
In an oven dried, evacuated and argon purged 50 mL Schlenk flask 300 mg 4-hydroxyphenylacetone (2.0 mmol, 1.0 eq) were dissolved in 5 mL dry and degassed THF at RT resulting in a clear light orange solution. Subsequently, a solution of 132 mg propargylamine (154 µL, 2.4 mmol, 1.2 eq) in 1 mL THF was added at once resulting in a yellow solution. The mixture was stirred at RT for 30 min. Then 848 mg sodium triacetoxyborohydride (4.0 mmol, 2.0 eq) were added at once, followed by addition of 240 mg glacial acetic acid (229 µL, 4.0 mmol, 2.0 eq). After addition of the reducing agent the mixture became thicker and cloudy. The reaction was monitored by GC-MS and TLC analysis and carried out for 46 h at RT until nearly complete consumption of the ketone was indicated. After that time the reaction mixture was quenched with 15 mL saturated NaHCO$_3$. The solution was extracted with ethyl acetate (4 x 10 mL). The combined organic layers were washed with water (2 x 20 mL) and brine (1 x 20 mL) and dried over anhydrous Na$_2$SO$_4$. The

solvent was removed in *vacuo* and the crude product purified by flash column chromatography (cyclohexane:ethyl acetate = 7:3 to 5:5 (v/v), 125 g silica gel, size: 14.0 x 2.5 cm) furnishing 293 mg (1.55 mmol, 78%) 4-(2-(prop-2-yn-1-ylamino)propyl)phenol (**13**) as a yellow solid.

$C_{12}H_{15}NO$ [189.25 g/mol]

R_f = 0.15 (cyclohexane:ethyl acetate = 1:1 (v/v)), 0.06 (cyclohexane:ethyl acetate = 7:3 (v/v)).

 m.p. = 107-108 °C (yellow solid)

GC-MS (EI): t_R = 6.18 min; m/z (%) 188.1 (0.3) [M-H]$^+$, 107.0 (25.6), 82.1 (100.0), 77.1 (19.2), 56.1 (5.7), 52.1 (7.7).

^{1}H NMR (300 MHz, MeOD-d$_4$) δ: 7.01 (d, *J* = 8.4 Hz, 2H, arom.), 6.72 (d, *J* = 8.4 Hz, 2H, arom.), 3.41 (qd, *J* = 17.0 Hz, 2.4 Hz, 2H, C**H**$_2$C≡CH), 3.08 (m, 1H, C**H**), 2.68 (dd, *J* = 13.2, 6.3 Hz, 1H, C**H**$_a$H$_b$CH), 2.58 (t, *J* = 2.4 Hz, 1H, CH$_2$C≡C**H**), 2.45 (dd, *J* = 13.2, 7.2 Hz, 1H, CH$_a$**H**$_b$CH), 1.00 (d, *J* = 6.3 Hz, 3H, C**H**$_3$).

^{13}C NMR (75 MHz, MeOD-d$_4$) δ: 156.99 (**C**$_{Ar}$-1), 131.22 (**C**$_{Ar}$-3), 130.85 (**C**$_{Ar}$-4), 116.27 (**C**$_{Ar}$-2), 81.88 (**C**≡CH), 73.20 (C≡**C**H), 54.18 (C$_q$), 42.90 (Ph**C**H$_2$CH), 35.84 (**C**H$_2$C≡CH), 18.97 (**C**H$_3$).

IR (neat) cm^{-1}: 3269, 1613, 1517, 1465, 1379, 1347, 1252, 1172, 1109, 1039, 998, 943, 824, 772, 677, 651.

HRMS (DI-EI) calcd for $C_{12}H_{15}NO$ 189.1154 [M$^+$], found 189.1152.

7.1.2.7 4-(2-(Methyl(prop-2-yn-1-yl)amino)ethyl)phenol (14)
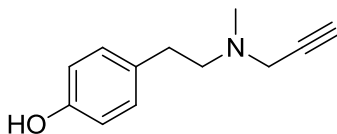
In an oven dried, evacuated and argon purged 100 mL Schlenk flask 691 mg (5.0 mmol, 1.0 eq) 4-(2-hydroxyethyl)phenol were dissolved at RT in 10 mL dry and degassed DMSO forming a clear light yellow solution. Subsequently, 1.265 g dry triethylamine (1.742 mL, 12.5 mmol, 2.5 eq) were added to the mixture, followed by a dropwise addition of solution of 1.989 g sulfur trioxide pyridine complex (12.5 mmol, 2.5 eq) in 10 mL dry DMSO. The resulting dark yellow mixture was let to react at RT for 1 h. Then, the reaction mixture was poured onto ice-cold water (200 mL) and extracted with ethyl acetate (4 x 50 mL). The combined organic layers were washed with 10% solution of citric acid (2 x 50 mL), water (1 x 50 mL) and brine (1 x 50 mL) and dried over anhydrous sodium sulfate. The organic solvent was removed under reduced pressure resulting in a yellow oil used without further purification for the next step. Crude 2-(4-hydroxyphenyl)acetaldehyde (**21**) was dissolved in 15 mL of dry THF in a 50 mL Schlenk flask and 360 mg *N*-methylpropargylamine (438 µL, 6.5 mmol, 1.3 eq) were added and the mixture stirred at RT for 15 min. Then, 1.590 g sodium triacetoxyborohydride (7.5 mmol, 1.5 eq) were added at once followed by addition of 300 mg glacial acetic acid (290 µL, 5.0 mmol, 1.0 eq). After addition of the reducing agent the mixture became thicker and cloudy. The reaction was monitored by GC-MS and TLC analysis and carried out overnight for 15 h at RT until full conversion of starting material was indicated. After that time the reaction mixture was quenched with 10 mL saturated $NaHCO_3$. The solution was extracted with ethyl acetate (3 x 10 mL). The combined organic layers were washed with water (2 x 20 mL) and brine (1 x 20 mL) and dried over anhydrous Na_2SO_4. The solvent was removed *in vacuo* and the crude product purified by column chromatography (cyclohexane:ethyl acetate = 7:3 (v/v) to 5:5 (v/v), 35 g silica gel, size: 19.5 x 2.5 cm)

furnishing 500 mg (2.64 mmol, 53% after two steps) 4-(2-(methyl(prop-2-yn-1-yl)amino)ethyl)phenol (**14**) as a yellowish solid.

$C_{12}H_{15}NO$ [189.25 g/mol]

R_f = 0.26 (cyclohexane:ethyl acetate = 1:1 (v/v)), 0.13 (cyclohexane:ethyl acetate = 7:3 (v/v)).

m.p. = 116-118 °C (yellow solid)

GC-MS (EI): t_R = 6.18 min; m/z (%) 189.1 (0.3) [M$^+$], 107.0 (16.4), 91.1 (5.1), 82.1 (100.0), 77.0 (18.2), 53.1 (4.3).

^{1}H NMR (300 MHz, MeOD-d$_4$) δ: 7.02 (d, J = 8.4 Hz, 2H, arom.), 6.70 (d, J = 8.4 Hz, 2H, arom.), 3.43 (d, 2H, J = 2.4 Hz, C**H**$_2$C≡CH), 2.69 (t, 1H, J = 2.4 Hz, CH$_2$C≡C**H**), 2.67 (brs, 4H, C**H**$_2$C**H**$_2$), 2.38 (s, 3H, C**H**$_3$).

^{13}C NMR (75 MHz, MeOD-d$_4$) δ: 156.84 (**C**$_{Ar}$-1), 131.54 (**C**$_{Ar}$-4), 130.55 (**C**$_{Ar}$-3), 116.26 (**C**$_{Ar}$-2), 78.44 (**C**≡CH), 75.38 (C≡**C**H), 58.89 (CH$_2$**C**H$_2$N), 45.94 (**C**H$_2$C≡CH), 41.93 (**C**H$_3$), 33.66 (Ph**C**H$_2$CH).

IR (neat) cm^{-1}:3279, 3224, 1638, 1513, 1451, 1251, 1101, 929, 826, 714, 653, 609.

HRMS (DI-EI) calcd for $C_{12}H_{15}NO$ 189.1154 [M$^+$], found 189.1153.

7.1.2.8 4-(2-(Prop-2-yn-1-ylamino)ethyl)phenol (15)
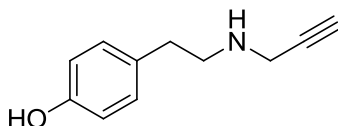
The reaction sequence was performed in an analogous manner as described for 4-(2-(methyl(prop-2-yn-1-yl)amino)ethyl)phenol (**14**), only 358 mg propargylamine (416 µL, 6.5 mmol, 1.3 eq) was used in place of *N*-methylpropargylamine. Flash column chromatography (cyclohexane:ethyl acetate = 8:2 (v/v) to 5:5 (v/v), 36 g silica gel, size: 20.0 x 2.5 cm) yielded

320 mg (1.83 mmol, 37% after two steps) 4-(2-(prop-2-yn-1-ylamino)ethyl)phenol as a yellow solid (**15**).

$C_{11}H_{13}NO$ [175.23 g/mol]

R_f = 0.09 (cyclohexane:ethyl acetate = 1:1 (v/v)), 0.04 (cyclohexane:ethyl acetate = 7:3 (v/v).

m.p. = 89-91 °C (yellow solid)

GC-MS (EI): t_R = 6.135 min; m/z (%) 175.1 (2.8) [M$^+$], 107.0 (23.3), 91.0 (4.4), 77.0 (21.4), 68.1 (100.0), 53.0 (4.7).

^{1}H NMR (300 MHz, MeOD-d$_4$) δ: 7.03 (d, J = 8.4 Hz, 2H, arom.), 6.71 (d, J = 8.4 Hz, 2H, arom.), 3.38 (d, 2H, J = 2.4 Hz, C**H**$_2$C≡CH), 2.85 (m, 2H, CH$_2$C**H**$_2$N), 2.69 (m, 2H, C**H**$_2$CH$_2$N), 2.59 (t, J = 2.4 Hz, 1H, CH$_2$C≡C**H**).

^{13}C NMR (75 MHz, MeOD-d$_4$) δ: 156.90 (**C**$_{Ar}$-1), 131.49 (**C**$_{Ar}$-4), 130.58 (**C**$_{Ar}$-3), 116.31 (**C**$_{Ar}$-2), 81.93 (**C**≡CH), 73.23 (C≡**C**H), 51.07 (CH$_2$**C**H$_2$N), 38.29 (**C**H$_2$C≡CH), 35.61 (Ph**C**H$_2$CH).

IR (neat) cm^{-1}: 3269, 1590, 1516, 1462, 1279, 1249, 1171, 1120, 1010, 916, 837, 677, 639.

HRMS (DI-EI) calcd for $C_{11}H_{13}NO$ 175.0997 [M$^+$], found 175.0997.

7.1.2.9 4-((Ethyl(methyl)amino)methyl)phenol (48)
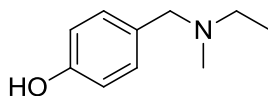
In an oven dried, evacuated and argon purged 50 mL Schlenk flask 366 mg 4-hydroxybenzaldehyde (3.0 mmol, 1.0 eq) were dissolved in 10 mL dry and degassed THF at RT resulting in a clear yellowish solution. Subsequently, 195 mg *N*-ethylmethylamine (283 µL, 3.3 mmol, 1.1 eq) were added at once resulting in a yellow solution. The mixture was stirred at RT for 15 min. Then 0.890 mg sodium triacetoxyborohydride (4.2 mmol, 1.4 eq) were added at once. After addition of the reducing agent the mixture became thicker and cloudy. The reaction was monitored by GC-MS analysis and carried out for 4.5 h at RT until

complete consumption of the aldehyde was indicated. After that time the reaction mixture was quenched with 10 mL saturated NaHCO$_3$. The solution was extracted with ethyl acetate (2 x 15 mL). The combined organic layers were washed with water (2 x 15 mL) and brine (1 x 15 mL) and dried over anhydrous Na$_2$SO$_4$. The solvent was removed in *vacuo* yielding 332 mg (2.0 mmol, 67%) 4-((ethyl(methyl)amino)methyl)phenol (**48**) as a yellowish oil, which was used for the next step without further purification.

C$_{10}$H$_{15}$NO [165.23 g/mol]

GC-MS (EI): t$_R$ = 5.56 min; m/z (%) 165.1 (29.2) [M$^+$], 150.1 (29.8), 107.1 (100.0), 77.0 (17.2), 58.0 (4.9), 51.0 (5.3).

^{1}H NMR (300 MHz, MeOD-d$_4$) δ: 7.12 (d, *J* = 8.4 Hz, 2H, arom.), 6.74 (d, *J* = 8.4 Hz, 2H, arom.), 3.43 (s, 2H, PhC**H**$_2$N), 2.46 (q, *J* = 7.2 Hz, 2H, C**H**$_2$CH$_3$), 2.17 (s, 3H, NC**H**$_3$), 1.11 (t, *J* = 7.2 Hz, 3H, CH$_2$C**H**$_3$).

^{13}C NMR (75 MHz, MeOD-d$_4$) δ: 158.04 (**C**$_{Ar}$-1), 132.12 (**C**$_{Ar}$-3), 129.01 (**C**$_{Ar}$-4), 116.06 (**C**$_{Ar}$-2), 61.93 (Ph**C**H$_2$N), 51.68 (N**C**H$_2$CH$_3$), 41.36 (N**C**H$_3$), 11.97 (CH$_2$**C**H$_3$).

7.1.3 Synthesis of probes with azide group

7.1.3.1 3-Azidopropan-1-ol (7)
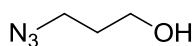
1.390 g 3-Bromopropan-1-ol (904 µL, 10.0 mmol, 1.0 eq) were dissolved in 20 mL distilled water in a 100 mL round-bottom flask equipped with a condenser. Subsequently, a solution of 1.300 g (20.0 mmol, 2.0 eq) sodium azide in 10 mL distilled water was added at once and the colorless clear mixture was warmed up to 80 °C. The reaction mixture was stirred at 80 °C for 14 h. After complete consumption of the starting material the mixture was cooled down and extracted with diethyl ether (4 x 20 mL). The combined organic layers were washed with brine (20 mL) and dried over anhydrous Na$_2$SO$_4$. Organic solvent was removed under

reduced pressure resulting in 920 mg (91%) 3-azidopropan-1-ol (**7**) as a colorless liquid which was used in subsequent step without further purification.

$C_3H_7N_3O$ [101.11 g/mol]

GC-MS (EI): t_R = 3.35 min; m/z (%) 101.1 (0.4) [M$^+$], 72.0 (100.0), 56.0 (67.1), 54.0 (97.8).

^{1}H NMR (300 MHz, CDCl$_3$) δ: 3.75 (t, J = 6.0 Hz, 2H, C**H**$_2$OH), 3.45 (t, J = 6.6 Hz, 2H, C**H**$_2$N$_3$), 1.83 (p, ^3J = 6.3 Hz, 2H, CH$_2$C**H**$_2$CH$_2$), 1.77-1.66 (m, 1H, O**H**).

^{13}C NMR (75 MHz, CDCl$_3$) δ: 59.88 (O**C**H$_2$), 48.46 (**C**H$_2$N$_3$), 31.40 (CH$_2$**C**H$_2$CH$_2$).

IR (film) cm^{-1}: 3325, 2947, 2882, 2360, 2092, 1738, 1455, 1259, 1046, 955, 901.

The spectral data are identical to those published previously.[254]

7.1.3.2 *N*-(4-(3-Azidopropoxy)benzyl)-*N*-methylprop-2-yn-1-amine (1) (P1-N$_3$)
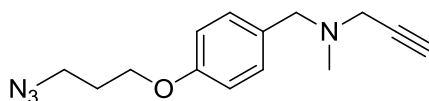
In an oven dried, evacuated and nitrogen purged 10 mL Schlenk flask 87.6 mg 4-((methyl(prop-2-yn-1-yl)amino)methyl)phenol (**9**) (0.50 mmol, 1.0 eq) were dissolved in 1 mL dry and degassed THF resulting in a clear yellowish solution. The solution was cooled down to 0 °C in an ice-water bath and 131 mg triphenylphosphine (0.50 mmol, 1.0 eq) were added, followed by a dropwise addition of 101 mg diisopropyl azodicarboxylate (DIAD) (98 µL, 0.50 mmol, 1.0 eq) over the course of 10 min. After 10 min of stirring the mixture, 76 mg 3-azido-1-propanol (0.75 mmol, 1.5 eq) were added dropwise and the reaction mixture was stirred under inert atmosphere at RT for 23 h. After that time, the solvent was removed under reduced pressure and the crude product was triturated with cold cyclohexane to precipitate triphenylphosphine oxide and diisopropyl hydrazodicarboxylate. The solid was filtrated off and washed with cold cyclohexane. The filtrate was concentrated *in vacuo* and crude product was purified by flash column chromatography (cyclohexane:ethyl acetate = 8:2 (v/v), 12 g

silica gel, size: 12.0 x 2.0 cm) yielding 95 mg (0.37 mmol, 73%) *N*-(4-(3-azidopropoxy) benzyl)-*N*-methylprop-2-yn-1-amine (**1**) (probe **P1-N$_3$**) as a colorless oil.

C$_{14}$H$_{18}$N$_4$O [258.32 g/mol]

R$_f$ = 0.42 (cyclohexane:ethyl acetate = 6:4 (v/v)), 0.31 (cyclohexane:ethyl acetate = 7:3 (v/v)), 0.22 (cyclohexane:ethyl acetate = 8:2 (v/v)).

HPLC-MS (EI+): t$_R$ = 6.762 min (JK_35to90); m/z (%) 259.2 (100.0) [M+H]$^+$, 233.4 (9.1), 223.7 (8.8), 205.0 (10.0), 190.3 (19.8), 167.0 (9.3), 2, 141.0 (11.1), 135.0 (8.1), 109.0 (6.6), 107.2 (3.0).

GC-MS (EI): t$_R$ = 7.18 min; m/z (%) 258.2 (1.8) [M$^+$], 229.2 (8.0) [M-H-N$_2$]$^+$, 190.1 (8.2) 175.1 (49.4), 174.1 (57.5). 162.1 (13.5), 134.1 (14.9), 108.1 (12.8), 107.1 (100.0), 82.1 (23.8), 77.1 (21.8), 68.1 (31.2), 56.1 (48.1).

^{1}H NMR (300 MHz, MeOD-d$_4$) δ: 7.24 (d, *J* = 8.4 Hz, 2H, arom.), 6.89 (d, *J* = 8.4 Hz, 2H, arom.), 4.05 (t, *J* = 6.0 Hz, 2H, OC**H**$_2$), 3.53 (s, 2H, PhC**H**$_2$N), 3.49 (t, *J* = 6.6 Hz, 2H, N$_3$C**H**$_2$), 3.25 (d, *J* = 2.4 Hz, 2H, NC**H**$_2$C≡CH), 2.70 (t, *J* = 2.4 Hz, 1H, NCH$_2$C≡C**H**), 2.31 (s, 3H, C**H**$_3$), 2.02 (p, ^{3}*J* = 6.4 Hz, 2H, CH$_2$C**H**$_2$CH$_2$).

^{13}C NMR (75 MHz, MeOD-d$_4$) δ: 159.80 (**C**$_{Ar}$-1), 131.89 (**C**$_{Ar}$-3), 130.77 (**C**$_{Ar}$-4), 115.42 (**C**$_{Ar}$-2), 78.78 (**C**≡CH), 75.40 (C≡**C**H), 65.85 (O**C**H$_2$), 60.13 (Ph**C**H$_2$N), 49.37 (**C**H$_2$N$_3$), 45.09 (N**C**H$_2$C≡CH), 41.75 (**C**H$_3$), 29.88 (OCH$_2$**C**H$_2$).

IR (film) cm^{-1}: 3295, 2939, 2874, 2792, 2095 (RN$_3$), 1611, 1510, 1455, 1236, 1172, 1106, 1029, 845, 817.

HRMS (DI-EI) calcd for C$_{14}$H$_{18}$N$_4$O 258.1481 [M$^+$], found 258.1475.

7.1.3.3 *N*-(4-(3-Bromopropoxy)benzyl)-*N*-methylpropargyl-1-amine (10) (P1-Br)
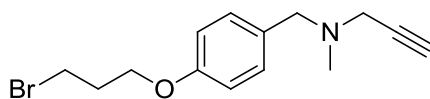
In an oven dried, evacuated and nitrogen purged 10 mL Schlenk flask 100 mg 4-((methyl(prop-2-yn-1-yl)amino)methyl)phenol (**9**) (0.57 mmol, 1.0 eq) were dissolved in 3 mL dry and degassed THF resulting in a clear yellow solution. Then the solution was cooled down to 0 °C in an ice-water bath and 150 mg triphenylphosphine (0.57 mmol, 1.0 eq) were added, followed by dropwise addition of 115 mg diisopropyl azodicarboxylate (DIAD) (112 µL, 0.57 mmol, 1.0 eq) over the course of 5 min. After 10 min of stirring the mixture, 95 mg 3-bromopropan-1-ol (64 µL, 0.68 mmol, 1.2 eq) were added dropwise and the reaction mixture was stirred under inert atmosphere at 0 °C for 1 h. After that time the reaction was stirred at RT for 41h. Then the solvent was removed under reduced pressure and the crude product was purified by flash column chromatography (cyclohexane:ethyl acetate = 9:1 (v/v), 25 g silica gel, size: 15.0 x 2.5 cm) yielding 61 mg (36%) *N*-(4-(3-bromopropoxy)benzyl)-N-methylpropargyl-1-amine (**10**) (**P1-Br**) as a yellowish oil.

$C_{14}H_{18}BrNO$ [296.20 g/mol]

R_f = 0.25 (cyclohexane:ethyl acetate = 8:2 (v/v)), 0.20 (cyclohexane:ethyl acetate = 9:1 (v/v)).

HPLC-MS (EI+): t_R = 8.028 min (JK_10to90); m/z (%) 296.0 (100.0) [M+H]+, 295.1 (3.9) [M+], 228.9 (29.7), 226.9 (30.5).

GC-MS (EI): t_R = 7.15 min; m/z (%) 295.4 (43.4) [M+], 294.5 (41.9), 252.5 (14.4), 228.6 (91.3), 227.5 (100.0), 174.1 (5.0), 134.2 (5.7), 107.0 (71.6), 89.3 (5.4), 81.9 (10.5), 77.2 (8.2), 68.0 (3.4).

^{1}H NMR (300 MHz, MeOD-d$_4$) δ: 7.25 (d, *J* = 8.7 Hz, 2H, arom.), 6.90 (d, *J* = 8.7 Hz, 2H, arom.), 4.10 (t, *J* = 6.0 Hz, 2H, OC**H**$_2$), 3.62 (t, *J* = 6.6 Hz, 2H, BrC**H**$_2$) 3.53 (s, 2H, PhC**H**$_2$N), 3.25 (d, *J* = 2.4 Hz, 2H, C**H**$_2$C≡CH), 2.70 (t, *J* = 2.4 Hz, 1H, CH$_2$C≡C**H**), 2.31 (s, 3H, C**H**$_3$), 2.28 (p, *J* = 6.3 Hz, 2H, CH$_2$C**H**$_2$CH$_2$).

^{13}C NMR (75 MHz, MeOD-d$_4$) δ: 159.79 (**C**$_{Ar}$-1), 131.90 (**C**$_{Ar}$-3), 130.80 (**C**$_{Ar}$-4), 115.42 (**C**$_{Ar}$-2), 78.76 (**C**≡CH), 75.39 (C≡**C**H), 66.56 (O**C**H$_2$), 60.12 (Ph**C**H$_2$N), 45.09 (N**C**H$_2$C≡CH), 41.74 (**C**H$_3$), 33.63 (**C**H$_2$Br), 30.60 (OCH$_2$**C**H$_2$).

IR (film) cm^{-1}: 3293, 2939, 2792, 2360, 1611, 1510,1468, 1236, 1172, 1105 1028, 845, 811.

7.1.3.4 *N*-(4-(3-Azidopropoxy)benzyl)prop-2-yn-1-amine (16) (P2-N$_3$)
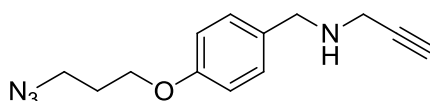
In an oven dried, evacuated and nitrogen purged 10 mL Schlenk flask 38 mg 4-((prop-2-yn-1-ylamino)methyl)phenol (**11**) (0.24 mmol, 1.0 eq) were dissolved in 0.5 mL dry and degassed THF resulting in a clear yellow solution. Then the solution was cooled down to 0 °C in an ice-water bath and 63 mg triphenylphosphine (0.24 mmol, 1.0 eq) were added, followed by dropwise addition of 49 mg diisopropyl azodicarboxylate (DIAD) (47 µL, 0.24 mmol, 1.0 eq) over the course of 5 min. After 10 min of stirring the mixture, 36 mg 3-azido-1-propanol (0.36 mmol, 1.5 eq) were added dropwise and the reaction mixture was stirred under inert atmosphere at RT for 38 h. After that time, the solvent was removed under reduced pressure and the crude product was triturated with cold cyclohexane to precipitate triphenylphosphine oxide and diisopropyl hydrazodicarboxylate. The solid was filtrated off and washed with cold cyclohexane. The filtrate was concentrated *in vacuo* and crude product was purified by flash column chromatography (cyclohexane:ethyl acetate = 6:4 (v/v), 5 g silica gel, size: 8.0 x 1.0 cm) yielding 20 mg (0.08 mmol, 34%) *N*-(4-(3-azidopropoxy)benzyl)prop-2-yn-1-amine (**16**) (probe **P2-N$_3$**) as a yellow oil. Analytically pure sample was prepared by saturation of the solution of crude product in diethyl ether with gaseous HCl and precipitation of the amine as its hydrochloric salt. The yellowish solid was collected by filtration and dried under vacuum.

C$_{13}$H$_{16}$N$_4$O [244.29 g/mol]

R$_f$ = 0.18 (cyclohexane:ethyl acetate = 6:4 (v/v), 0.11 (cyclohexane:ethyl acetate = 7:3 (v/v)).

HPLC-MS (EI+): t_R = 5.246 min (JK_35to90); m/z (%) 245.2 (31.7) [M+H]$^+$, 235.0 (0.1), 212.9 (0.2), 191.2 (14.2), 190.2 (100.0), 156,8 (0.2), 143,3 (0.2), 107.2 (0.8).

GC-MS (EI): t_R = 7.22 min; m/z (%) 244.1 (0.6) [M]$^+$, 215.1 (17.3) [M-H-N$_2$]$^+$, 187.1 (9.2). 160.1 (100.0), 144.1 (16.6), 132.1 (33.6), 120.0 (26.9), 107.1 (80.1), 94.1 (5.5), 77.1 (29.0), 68.1 (15.7), 56.1 (46.5).

^{1}H NMR (300 MHz, MeOD-d$_4$) δ: 7.25 (d, J = 8.4 Hz, 2H, arom.), 6.89 (d, J = 8.4 Hz, 2H, arom.), 4.05 (t, J = 6.0 Hz, 2H, OC**H**$_2$), 3.76 (s, 2H, PhC**H**$_2$N), 3.50 (t, J = 6.6 Hz, 2H, N$_3$C**H**$_2$), 3.33 (d, J = 2.4 Hz, 2H, NC**H**$_2$C≡CH), 2.64 (t, J = 2.4 Hz, 1H, NCH$_2$C≡C**H**), 2.02 (p, ^3J = 6.3 Hz, 2H, CH$_2$C**H**$_2$CH$_2$), 1.29 (d, J = 6.0 Hz, 1H, N**H**).

^{1}H NMR (300 MHz, D$_2$O) δ: 7.42 (d, J = 8.7 Hz, 2H, arom.), 7.06 (d, J = 8.4 Hz, 2H, arom.), 4.27 (s, 2H, PhC**H**$_2$N), 4.16 (t, J = 6.0 Hz, 2H, OC**H**$_2$), 3.87 (d, J = 2.4 Hz, 2H, NC**H**$_2$C≡CH), 3.51 (t, J = 6.6 Hz, 2H, N$_3$C**H**$_2$), 3.01 (t, J = 2.4 Hz, 1H, NCH$_2$C≡C**H**), 2.04 (p, ^3J = 6.3 Hz, 2H, CH$_2$C**H**$_2$CH$_2$) (hydrochloric salt).

^{13}C NMR (75 MHz, MeOD-d$_4$) δ: 159.62 (**C**$_{Ar}$-1), 132.17 (**C**$_{Ar}$-4), 131.05 (**C**$_{Ar}$-3), 115.53 (**C**$_{Ar}$-2), 81.97 (**C**≡CH), 73.39 (C≡**C**H), 65.85 (O**C**H$_2$), 52.17 (Ph**C**H$_2$N), 49.37 (**C**H$_2$N$_3$), 37.30 (N**C**H$_2$C≡CH), 29.88 (OCH$_2$**C**H$_2$) (free amine).

^{13}C NMR (75 MHz, D$_2$O) δ: 159.14 (**C**$_{Ar}$-1), 131.68 (**C**$_{Ar}$-3), 122.73 (**C**$_{Ar}$-4), 115.40 (**C**$_{Ar}$-2), 78.27 (**C**≡CH), 73.06 (C≡**C**H), 65.58 (O**C**H$_2$), 49.35 (Ph**C**H$_2$N), 48.06 (**C**H$_2$N$_3$), 35.31 (N**C**H$_2$C≡CH), 27.78 (OCH$_2$**C**H$_2$) (hydrochloric salt).

IR (film) cm^{-1}: 3294, 2929,2875, 2095, 1737, 1611, 1510, 1452, 1238, 1173, 1104, 1043, 826.

HRMS (DI-EI) calcd for C$_{13}$H$_{16}$N$_4$O 244.1324 [M$^+$], found 244.1316.

7.1.3.5 *N*-(1-(4-(3-Azidopropoxy)phenyl)propan-2-yl)-*N*-methylprop-2-yn-1-amine (17) (P3-N₃)
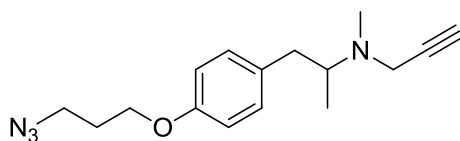
In an oven dried, evacuated and nitrogen purged 10 mL Schlenk flask 56 mg 4-(2-(methyl(prop-2-yn-1-yl)amino)propyl)phenol (**12**) (0.27 mmol, 1.0 eq) were dissolved in 0.55 mL dry and degassed THF resulting in a clear yellow solution. The solution was cooled down to 0 °C in an ice-water bath and 72 mg triphenylphosphine (0.27 mmol, 1.0 eq) were added, followed by dropwise addition of 56 mg diisopropyl azodicarboxylate (DIAD) (54 µL, 0.27 mmol, 1.0 eq) over the course of 5 min. After 10 min of stirring the mixture, 42 mg 3-azido-1-propanol (0.41 mmol, 1.5 eq) were added dropwise and the reaction mixture was stirred under inert atmosphere at RT for 39 h. After that time, the solvent was removed under reduced pressure and the crude product was treated with an excess of 20% aqueous hydrochloric acid (10 mL) to pH 1. The aqueous phase was extracted with diethyl ether (3 x 15 mL) to remove diisopropyl hydrazodicarboxylate. The aqueous phase was then basified with concentrated sodium hydroxide solution to pH 10 and extracted with ethyl acetate (3 x 20 mL). The organic extract was dried over anhydrous $MgSO_4$. The solvent was removed *in vacuo* and the crude product purified by flash column chromatography (cyclohexane:ethyl acetate = 8:2 to 7:3 (v/v), 5 g silica gel, size: 5.0 x 2.0 cm) yielding 57 mg (0.20 mmol, 70%) *N*-(1-(4-(3-azidopropoxy)phenyl)propan-2-yl)-*N*-methylprop-2-yn-1-amine (**17**) (probe **P3-N₃**) as a yellowish oil.

$C_{16}H_{22}N_4O$ [286.37 g/mol]

R_f = 0.33 (cyclohexane:ethyl acetate = 6:4 (v/v), 0.23 (cyclohexane:ethyl acetate = 7:3 (v/v)), 0.17 (cyclohexane:ethyl acetate = 8:2 (v/v)).

HPLC-MS (EI+): t_R = 6.762 min (JK_35to90); m/z (%) 287.2 (100.0) [M+H]$^+$, 259.3 (1.5), 246.2 (17.3), 218.2 (2.2), 167.40 (0.2), 163.2 (0.1), 146.9 (0.1), 135.3 (0.3), 105.1 (0.4).

GC-MS (EI): t_R = 7.62 min; m/z (%) 258.0 (0.2) [M-N$_2$]$^+$, 207.0 (4.1), 107,1 (5.0), 96.1 (100.0), 77.1 (3.2), 56.1 (14.1).

^{1}H NMR (300 MHz, MeOD-d$_4$) δ: 7.09 (d, J = 8.4 Hz, 2H, arom.), 6.85 (d, J = 8.4 Hz, 2H, arom.), 4.02 (t, J = 6.0 Hz, 2H, OC**H**$_2$), 3.49 (t, J = 6.6 Hz, 2H, N$_3$C**H**$_2$), 3.43 (brs, 2H, NC**H**$_2$C≡CH), 3.03 – 2.90 (m, 2H, C**H**$_a$H$_b$CH, CH$_a$H$_b$C**H**), 2.67 (t, J = 2.4 Hz, 1H, NCH$_2$C≡C**H**), 2.39 (s, 3H, NC**H**$_3$), 2.32 (dd, J = 13.7, 11.1 Hz, 1H, CH$_a$**H**$_b$CH), 2.01 (p, J = 6.3 Hz, 2H, CH$_2$C**H**$_2$CH$_2$), 0.94 (d, J = 6.6 Hz, 2H, C**H**$_3$).

^{13}C NMR (125 MHz, MeOD-d$_4$) δ: 158.70 (**C**$_{Ar}$-1), 133.38 (**C**$_{Ar}$-4), 131.22 (**C**$_{Ar}$-3), 115.52 (**C**$_{Ar}$-2), 80.35 (**C**≡CH), 74.62 (C≡**C**H), 65.84 (O**C**H$_2$), 60.62 (**C**$_q$), 49.38 (**C**H$_2$N$_3$), 43.70 (N**C**H$_2$C≡CH), 39.09 (Ph**C**H$_2$CH), 37.66 (N**C**H$_3$), 29.91 (OCH$_2$**C**H$_2$), 15.03 (**C**H$_3$).

IR (film) cm^{-1}: 3296, 2932, 2874, 2792, 2095, 1728, 1611, 1510, 1454, 1241, 1147, 1113, 826, 796.

HRMS (DI-EI) calcd for C$_{16}$H$_{22}$N$_4$O 286.1794 [M$^+$], found 286.1801.

7.1.3.6 *N*-(1-(4-(3-Azidopropoxy)phenyl)propan-2-yl)prop-2-yn-1-amine (18) (P4-N$_3$)
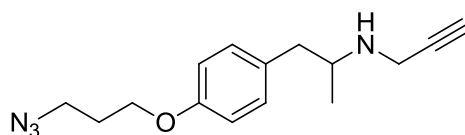
In an oven dried, evacuated and nitrogen purged 10 mL Schlenk flask 94.6 mg 4-(2-(prop-2-yn-1-ylamino)propyl)phenol (**13**) (0.5 mmol, 1.0 eq) were dissolved in 1 mL dry and degassed THF resulting in a clear yellow solution. Then the solution was cooled down to 0 °C in an ice-water bath and 131 mg triphenylphosphine (0.5 mmol, 1.0 eq) were added, followed by dropwise addition of 101 mg diisopropyl azodicarboxylate (DIAD) (98 µL, 0.5

178

mmol, 1.0 eq) over the course of 10 min. After 10 min of stirring the mixture, 76 mg 3-azido-1-propanol (0.75 mmol, 1.5 eq) were added dropwise over 10 min and the reaction mixture was stirred under inert atmosphere at RT for 23 h. After that time, the solvent was removed under reduced pressure and the crude product was triturated with cold cyclohexane to precipitate triphenylphosphine oxide and diisopropyl hydrazodicarboxylate. The yellowish solid was filtrated off and washed with cold cyclohexane. The filtrate was concentrated *in vacuo* and crude product was purified by flash column chromatography (cyclohexane:ethyl acetate = 7:3 (v/v), 12 g silica gel, size: 11.0 x 2.0 cm) yielding 99 mg (0.36 mmol, 73%) *N*-(1-(4-(3-azidopropoxy)phenyl)propan-2-yl)prop-2-yn-1-amine (**18**) (probe **P4-N₃**) as a yellowish oil.

$C_{15}H_{20}N_4O$ [272.34 g/mol]

R_f = 0.19 (cyclohexane:ethyl acetate = 6:4 (v/v), 0.12 (cyclohexane:ethyl acetate = 7:3 (v/v)).

HPLC-MS (EI+): t_R = 6.027 min (JK_35to90); m/z (%) 273.2 (100.0) [M+H]⁺, 246.2 (1.5), 218.2 (5.4), 162.8 (0.1), 100.20 (0.2).

GC-MS (EI): t_R = 7.45 min, m/z (%) 207.0 (3.3), 163.10 (8.8), 135.0 (1.2), 107.0 (10.3), 82.1 (100.0), 67.0 (2.3), 56.1 (7.6).

¹H NMR (300 MHz, MeOD-d₄) δ: 7.10 (d, *J* = 8.4 Hz, 2H, arom.), 6.87 (d, *J* = 8.4 Hz, 2H, arom.), 4.03 (t, *J* = 6.0 Hz, 2H, OC**H₂**), 3.50 (t, *J* = 6.6 Hz, 2H, N₃C**H₂**), 3.42 (m, 2H, NC**H₂**C≡CH), 3.18 – 3.01 (m, 1H, C**H**), 2.72 (dd, *J* = 13.4, 6.3 Hz, 1H, C**H**ₐH_bCH), 2.58 (t, *J* = 2.4 Hz, 1H, NCH₂C≡C**H**), 2.48 (dd, *J* = 13.4, 7.5 Hz, 1H, CHₐ**H**_bCH), 2.01 (p, *J* = 6.6 Hz, 2H, CH₂C**H₂**CH₂), 1.00 (d, J = 6.3 Hz, 1H, NC**H₃**).

¹³C NMR (75 MHz, MeOD-d₄) δ: 158.90 (**C**_Ar-1), 132.40 (**C**_Ar-4), 131.28 (**C**_Ar-3), 115.61 (**C**_Ar-2), 81.92 (**C**≡CH), 73.19 (C≡**C**H), 65.85 (O**C**H₂), 54.12 (C_q), 49.39 (**C**H₂N₃), 42.87 (Ph**C**H₂CH), 35.85 (N**C**H₂C≡CH), 29.90 (OCH₂**C**H₂), 19.01 (**C**H₃).

IR (film) cm⁻¹: 3295, 2961, 2927, 2873, 2095, 1737, 1611, 1510, 1470, 1240, 1176, 1114, 1043, 808, 751.

HRMS (EI) calcd for $C_{15}H_{20}N_4O$ 272.1637 [M+], found 272.1639.

7.1.3.7 *N*-(4-(3-Azidopropoxy)phenethyl)-*N*-methylprop-2-yn-1-amine (19) (P5-N3)
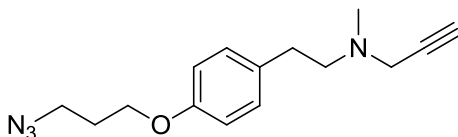
In an oven dried, evacuated and nitrogen purged 10 mL Schlenk flask 94.6 mg 4-(2-(methyl(prop-2-yn-1-yl)amino)ethyl)phenol (**14**) (0.5 mmol, 1.0 eq) were dissolved in 1 mL dry and degassed THF resulting in a clear yellowish solution. Then the solution was cooled down to 0 °C in an ice-water bath and 131 mg triphenylphosphine (0.5 mmol, 1.0 eq) were added, followed by dropwise addition of 101 mg diisopropyl azodicarboxylate (DIAD) (98 µL, 0.5 mmol, 1.0 eq) over the course of 5 min. After 10 min of stirring the mixture, 76 mg 3-azido-1-propanol (0.75 mmol, 1.5 eq) were added dropwise over 5 min and the reaction mixture was stirred under inert atmosphere at RT for 39 h. After that time, the solvent was removed under reduced pressure and the crude product was treated with excess of 20% aqueous hydrochloric acid (ca. 10 mL) to pH 1. The aqueous phase was extracted with ethyl acetate (2 x 15 mL) to remove diisopropyl hydrazodicarboxylate. The aqueous phase was then basified with concentrated sodium hydroxide solution to pH 10 and extracted with ethyl acetate (3 x 20 mL). The organic extract was dried over anhydrous $MgSO_4$. The solvent was removed *in vacuo* and the crude product was purified by flash column chromatography (cyclohexane:ethyl acetate = 6:4 (v/v), 24 g silica gel, size: 15.0 x 2.5 cm) yielding 75 mg (0.28 mmol, 55%) *N*-(4-(3-azidopropoxy)phenethyl)-*N*-methylprop-2-yn-1-amine (**19**) (probe **P5-N3**) as a yellowish oil.

$C_{15}H_{20}N_4O$ [272.34 g/mol]

R_f = 0.19 (cyclohexane:ethyl acetate = 6:4 (v/v), 0.12 (cyclohexane:ethyl acetate = 7:3 (v/v)).

HPLC-MS (EI+): t_R = 3.240 min (JK_35to90); m/z (%) 273.2 (100.0) [M+H]$^+$, 260.1 (0.2), 246.1 (1.3), 233.2 (0.1), 204.2 (0.8), 176.2 (0.1), 121.1 (0.1), 100.3 (0.1).

GC-MS (EI): t_R = 7.44 min, m/z (%) 244.2 (1.5) [M-N$_2$]$^+$, 207.0 (0.4), 149.1 (0.8), 121.1 (2.2), 107.1 (4.0), 91.1 (1.9), 82.1 (100.0), 77.1 (4.2), 65.1 (1.1), 55.1 (3.0).

^{1}H NMR (300 MHz, MeOD-d$_4$) δ: 7.12 (d, J = 8.4 Hz, 2H, arom.), 6.85 (d, J = 8.4 Hz, 2H, arom.), 4.02 (t, J = 6.0 Hz, 2H, OC**H**$_2$), 3.49 (t, J = 6.6 Hz, 2H, N$_3$C**H**$_2$), 3.39 (d, J = 2.1 Hz, 2H, NC**H**$_2$C≡CH), 2.76 – 2.59 (m, 5H, PhC**H**$_2$C**H**$_2$, NCH$_2$C≡C**H**), 2.36 (s, 3H, NC**H**$_3$), 2.00 (p, J = 6.3 Hz, 2H, CH$_2$C**H**$_2$CH$_2$).

^{13}C NMR (75 MHz, MeOD-d$_4$) δ: 158.75 (**C**$_{Ar}$-1), 133.22 (**C**$_{Ar}$-4), 130.60 (**C**$_{Ar}$-3), 115.63 (**C**$_{Ar}$-2), 78.65 (**C**≡CH), 75.17 (C≡**C**H), 65.84 (O**C**H$_2$), 58.78 (**C**H$_2$CH$_2$N), 49.38 (**C**H$_2$N$_3$), 45.96 (N**C**H$_2$C≡CH), 41.99 (N**C**H$_3$), 33.75 (Ph**C**H$_2$CH$_2$), 29.90 (OCH$_2$**C**H$_2$).

IR (film) cm^{-1}: 3295, 2937, 2868, 2796, 2095, 1738, 1611, 1510, 1239, 1176, 1122, 1048, 823.

HRMS (DI-EI) calcd for C$_{15}$H$_{20}$N$_4$O 272.1637 [M$^+$], found 272.1642.

7.1.3.8 *N*-(4-(3-Azidopropoxy)phenethyl)prop-2-yn-1-amine (20) (P6-N$_3$)
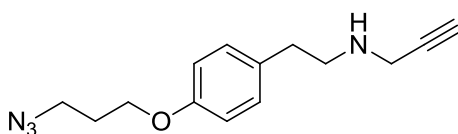
In an oven dried, evacuated and nitrogen purged 10 mL Schlenk flask 103 mg 4-(2-(prop-2-yn-1-ylamino)ethyl)phenol (**15**) (0.59 mmol, 1.0 eq) were dissolved in 1.2 mL dry and degassed THF resulting in a clear yellow solution. Then the solution was cooled down to 0 °C in an ice-water bath and 154 mg triphenylphosphine (0.59 mmol, 1.0 eq) were added, followed by dropwise addition of 119 mg diisopropyl azodicarboxylate (DIAD) (116 µL, 0.59 mmol, 1.0 eq) over the course of 5 min. After 10 min of stirring the mixture, 89 mg 3-azido-1-propanol (0.89 mmol, 1.5 eq) were added dropwise and the reaction mixture was stirred

under inert atmosphere at RT for 38 h. After that time, the solvent was removed under reduced pressure and the crude product was triturated with cold cyclohexane to precipitate triphenylphosphine oxide and diisopropyl hydrazodicarboxylate. The solid was filtrated off and washed with cold cyclohexane. The filtrate was concentrated *in vacuo*, and the crude product was purified by flash column chromatography (cyclohexane:ethyl acetate = 6:4 (v/v), 12 g silica gel, size: 11.5 x 2.0 cm) yielding 63 mg (0.24 mmol, 41%) *N*-(4-(3-azidopropoxy)phenethyl)prop-2-yn-1-amine (**20**) (probe **P6-N$_3$**) as a yellowish oil.

$C_{14}H_{18}N_4O$ [258.32 g/mol]

R_f = 0.14 (cyclohexane:ethyl acetate = 6:4 (v/v), 0.09 (cyclohexane:ethyl acetate = 7:3 (v/v)).

HPLC-MS (EI+): t_R = 1.621 min (JK_35to90); m/z (%) 259.2 (100.0) [M+H]$^+$, 245.3 (0.1), 232.0 (0.6), 218.2 (3.5), 204.2 (2.2), 188.2 (0.1), 158.1 (0.1), 140.2 (0.1), 121.4 (0.3), 100.1 (0.4).

GC-MS (EI): t_R = 7.43 min, m/z (%) 230.1 (0.4) [M-N$_2$]$^+$, 188.1 (0.2), 175.1 (4.0), 163.1 (34.1), 146.1 (10.3), 120.1 (3.6), 107.1 (22.7), 91.1 (5.8), 77.1 (12.8), 68.1 (100.0), 56.1 (21.8).

^{1}H NMR (300 MHz, MeOD-d$_4$) δ: 7.13 (d, *J* = 8.4 Hz, 2H, arom.), 6.86 (d, *J* = 8.4 Hz, 2H, arom.), 4.03 (t, *J* = 6.0 Hz, 2H, OC**H$_2$**), 3.49 (t, *J* = 6.6 Hz, 2H, N$_3$C**H$_2$**), 3.38 (brs, 2H, NC**H$_2$**C≡CH), 2.86 (m, 2H, CH$_2$C**H$_2$**N), 2.73 (m, 2H, C**H$_2$**CH$_2$N), 2.59 (d, *J* = 2.2 Hz, 1H, NCH$_2$C≡C**H**), 2.01 (p, ^{3}*J* = 6.3 Hz, 2H, CH$_2$C**H$_2$**CH$_2$).

^{13}C NMR (75 MHz, MeOD-d$_4$) δ: 158.83 (**C**$_{Ar}$-1), 133.05 (**C**$_{Ar}$-4), 130.64 (**C**$_{Ar}$-3), 115.68(**C**$_{Ar}$-2), 81.95 (**C**≡CH), 73.24 (C≡**C**H), 65.85 (O**C**H$_2$), 50.98 (CH$_2$**C**H$_2$N), 49.38 (**C**H$_2$N$_3$), 38.31(N**C**H$_2$C≡CH), 35.62 (Ph**C**H$_2$CH$_2$), 29.90 (OCH$_2$**C**H$_2$).

IR (film) cm^{-1}: 3294, 2927, 2095, 1738, 1611, 1510, 1470, 1238, 1176, 1113, 1044, 826.

HRMS (DI-EI) calcd for $C_{14}H_{18}N_4O$ 258.1481 [M$^+$], found 258.1486.

7.1.3.9 *N*-(4-(3-Azidopropoxy)benzyl)-N-methylethanamine (46) (P1f-N₃)
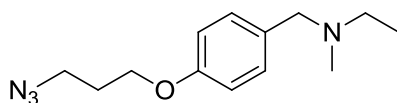
In an oven dried, evacuated and nitrogen purged 10 mL Schlenk flask 189 mg 4-((ethyl(methyl)amino)methyl)phenol (**48**) (1.15 mmol, 1.0 eq) were dissolved in 1.5 mL dry and degassed THF resulting in a clear yellowish solution. Then the solution was cooled down to 0 °C in an ice-water bath and 300 mg triphenylphosphine (1.15 mmol, 1.0 eq) were added, followed by dropwise addition of 232 mg diisopropyl azodicarboxylate (DIAD) (226 µL, 1.15 mmol, 1.0 eq) over the course of 10 min. After 10 min of stirring the mixture, 151 mg 3-azido-1-propanol (1.5 mmol, 1.3 eq) were added dropwise and the reaction mixture was stirred overnight at RT under inert atmosphere. After that time, the solvent was removed under reduced pressure and the crude product was triturated with cold cyclohexane to precipitate triphenylphosphine oxide and diisopropyl hydrazodicarboxylate. The solid was filtrated off and washed with cold cyclohexane. The filtrate was concentrated *in vacuo* and the crude product was purified by flash column chromatography (cyclohexane:ethyl acetate = 7:3 to 6:4 (v/v), 20 g silica gel, size: 15.5 x 2.0 cm) yielding 200 mg (0.81 mmol, 70%) *N*-(4-(3-azidopropoxy)benzyl)-*N*-methylethanamine (**46**) (probe **P1f-N₃**) as a yellowish oil.

$C_{13}H_{20}N_4O$ [248.32 g/mol]

R_f = 0.10 (cyclohexane:ethyl acetate = 1 : 1 (v/v))

GC-MS (EI): t_R = 6.85 min; m/z (%) 220.2 (5.7) $[M-N_2]^+$, 165.1 (17.6), 162.1 (25.6), 150.1 (19.7), 107.1 (100.0), 77.0 (23.1), 72.1 (12.6), 56.0 (35.4), 51.0 (8.8).

HPLC-MS (EI+): t_R = 5.993 min (JK_35to90); m/z (%) 249.1 (100.0) $[M+H]^+$, 248.0 (0.8) $[M^+]$, 222.0 (1.3), 190.0 (12.4).

^{1}H NMR (300 MHz, MeOD-d₄) δ: 7.22 (d, *J* = 8.7 Hz, 2H, arom.), 6.89 (d, *J* = 8.7 Hz, 2H, arom.), 4.06 (t, *J* = 6.0 Hz, 2H, OC**H₂**), 3.51 (t, *J* = 6.6 Hz, 2H, N₃C**H₂**), 3.46 (s, 2H, PhC**H₂**N),

2.46 (q, J = 7.2 Hz, 2H, C**H**$_2$CH$_3$), 2.17 (s, 3H, NC**H**$_3$), 2.03 (p, J = 6.3 Hz, 2H, CH$_2$C**H**$_2$CH$_2$), 1.11 (t, J = 7.2 Hz, 3H, CH$_2$C**H**$_3$).

^{13}C NMR (75 MHz, MeOD-d$_4$) δ: 159.69 (**C**$_{Ar}$-1), 132.06 (**C**$_{Ar}$-3), 130.84 (**C**$_{Ar}$-4), 115.33 (**C**$_{Ar}$-2), 65.85 (O**C**H$_2$), 61.89 (Ph**C**H$_2$N), 51.76 (N**C**H$_2$CH$_3$), 49.38 (**C**H$_2$N$_3$), 41.47 (N**C**H$_3$), 29.88 (O**C**H$_2$CH$_2$), 12.04 (CH$_2$**C**H$_3$).

IR (film) cm^{-1}: 2969, 2875, 2787, 2360, 2095, 1738, 1611, 1510, 1470, 1365, 1237, 1172, 1107.

7.1.4 Synthesis of probes with alkyne group

7.1.4.1 *N*-Methyl-*N*-(4-(pent-4-yn-1-yloxy)benzyl)prop-2-yn-1-amine (22) (P1)
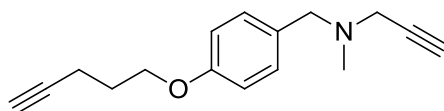
Method A: In an oven dried, evacuated and argon purged 10 mL Schlenk flask 87.6 mg 4-((methyl(prop-2-yn-1-yl)amino)methyl)phenol (**9**) (0.5 mmol, 1.0 eq) were dissolved in 1 mL dry and degassed THF at 0 °C (ice-water bath) resulting in a clear yellowish solution. Subsequently, 157 mg triphenylphosphine (0.6 mmol, 1.2 eq) were added, followed by dropwise addition of 121 mg diisopropyl azodicarboxylate (DIAD) (118 µL, 0.6 mmol, 1.2 eq) over the course of 5 min. Then, 50.5 mg 4-pentyn-1-ol (56 µL, 0.6 mmol, 1.2 eq) were added and the reaction mixture was stirred under inert atmosphere at RT for 22 h. After that time, the solvent was removed under reduced pressure and the crude product was purified by flash column chromatography (cyclohexane:ethyl acetate = 95:5 to 90:10 (v/v), 25 g silica gel, size: 14.5 x 2.5 cm) yielding 102 mg (85%) *N*-methyl-*N*-(4-(pent-4-yn-1-yloxy)benzyl)prop-2-yn-1-amine (**22**) (probe **P1**) as a yellowish oil.

Method B: In an oven dried, evacuated and argon purged 10 mL Schlenk flask 87.6 mg aminophenol (**1**) (0.5 mmol, 1.0 eq), 50.5 mg 4-pentyn-1-ol (46 µL, 0.6 mmol, 1.2 eq) and

157 mg triphenylphosphine (0.6 mmol, 1.2 eq) were dissolved in 0.5 mL dry and degassed THF under argon. The mixture was then sonicated for 5 min. Subsequently, 121 mg diisopropyl azodicarboxylate (DIAD) (125 µL, 0.6 mmol, 1.2 eq) were added dropwise over the course of 5 min. The mixture was then sonicated at RT for 45 min. After that time, when no more conversion of the starting materials was observed by GC-MS and TLC analysis, the solvent was removed under reduced pressure and the crude product was purified by flash column chromatography (cyclohexane:ethyl acetate = 95:5 to 90:10 (v/v), 22 g silica gel, size: 13.5 x 2.5 cm) yielding 97 mg (0.40 mmol, 80%) *N*-methyl-*N*-(4-(pent-4-yn-1-yloxy)benzyl)prop-2-yn-1-amine (**22**) (probe **P1**) as a yellowish oil.

$C_{16}H_{19}NO$ [241.33 g/mol]

R_f = 0.36 (cyclohexane:ethyl acetate = 7:3 (v/v), 0.13 (cyclohexane:ethyl acetate = 9:1 (v/v)).

HPLC-MS (EI+): t_R = 6.714 min (JK_35to90); m/z (%) 242.2 (100.0) [M+H]$^+$, 241.5 (2.2) [M$^+$], 173.2 (38.7), 107.2 (2.6).

GC-MS (EI): t_R = 6.75 min; m/z (%) 241.2 (22.6) [M$^+$], 240.1 (21.1) [M-H]$^+$, 198.1 (13.5), 174.1 (18.8), 173.1 (94.0), 158.1 (3), 134.0 (8.0), 107.0 (100.0), 82.1 (11.6), 77.1 (9.4), 65.1 (4.8), 51.1 (2.3).

^{1}H NMR (300 MHz, CDCl$_3$) δ: 7.24 (d, *J* = 8.7 Hz, 2H, arom.), 6.85 (d, *J* = 8.7 Hz, 2H, arom.), 4.05 (t, *J* = 6.0 Hz, 2H, OC**H**$_2$), 3.51 (s, 2H, Ph-C**H**$_2$N), 3.29 (d, *J* = 2.4 Hz, 2H, -NC**H**$_2$C≡CH), 2.40 (td, *J* = 7.0 Hz, 2.7 Hz, 2H, C**H**$_2$C≡CH), 2.33 (s, 3H, C**H**$_3$), 2.27 (t, *J* = 2.4 Hz, 1H, NCH$_2$C≡C**H**), 1.99 (p, *J* = 6.6 Hz, 2H, CH$_2$C**H**$_2$CH$_2$), 1.96 (t, *J* = 2.7 Hz, 1H, CH$_2$C≡C**H**).

^{13}C NMR (75 MHz, CDCl$_3$) δ: 158.31 (**C**$_{Ar}$-1), 130.55 (**C**$_{Ar}$-4), 130.50 (**C**$_{Ar}$-3), 114.47 (**C**$_{Ar}$-2), 83.66 (CH$_2$**C**≡CH), 78.72 (NCH$_2$**C**≡CH), 73.45 (C≡**C**H), 68.96 (C≡**C**H), 66.29 (O**C**H$_2$), 59.41 (Ph**C**H$_2$N), 44.73 (N**C**H$_2$C≡CH), 41.77 (N**C**H$_3$), 28.37 (OCH$_2$**C**H$_2$), 15.33 (**C**H$_2$C≡CH).

IR (film) cm^{-1}: 3293, 2938, 2873, 2794, 2359, 1738, 1611, 1510, 1468, 1240, 1107, 845, 811.

HRMS (DI-EI) calcd for $C_{16}H_{19}NO$ 241.1467 [M$^+$], found 241.1463.

7.1.4.2 *N*-(4-(Pent-4-yn-1-yloxy)benzyl)prop-2-yn-1-amine (23) (P2)
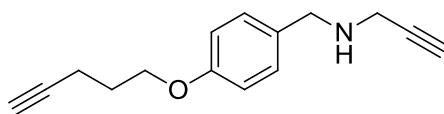
In an oven dried, evacuated and argon purged 10 mL Schlenk flask 162 mg 4-((prop-2-yn-1-ylamino)methyl)phenol (**11**) (1.0 mmol, 1.0 eq) and 101 mg 4-pentyn-1-ol (112 µL, 1.2 mmol, 1.2 eq) were dissolved in 2 mL dry and degassed THF at RT. Subsequently, 315 mg triphenylphosphine (1.2 mmol, 1.2 eq) were added and the mixture cooled to 0 °C in an ice-water bath. Then 243 mg diisopropyl azodicarboxylate (DIAD) (236 µL, 1.2 mmol, 1.2 eq) were added dropwise over the course of 5 min and the reaction mixture was stirred under argon at RT for 25 h. After that time the solvent was removed under reduced pressure and the crude product was purified by flash column chromatography (cyclohexane:ethyl acetate = 3:2 (v/v), 50 g silica gel, size: 16.0 x 3.5 cm) yielding 190 mg (0.84 mmol, 84%) *N*-(4-(pent-4-yn-1-yloxy)benzyl)prop-2-yn-1-amine (**23**) (probe **P2**) as a yellow oil.

$C_{15}H_{17}NO$ [227.30 g/mol]

R_f = 0.29 (cyclohexane:ethyl acetate = 1:1 (v/v), 0.20 (cyclohexane:ethyl acetate = 3:2 (v/v)).

HPLC-MS (EI+): t_R = 5.631 min (JK_35to90); m/z (%) 228.2 (14.1) [M+H]+, 173.2 (100.0), 107.3 (3.2).

GC-MS (EI): t_R = 6.79 min; m/z (%) 226.1 (94.8) [M-H]+, 198.1 (87.5), 173.1 (29.8), 160.1 (38.2), 144.1 (24.6), 131.1 (12.1), 120.1 (19.0), 107.1 (100.0), 89.1 (8.9), 77.1 (18.9), 68.1 (13.3), 51.1 (5.4).

^{1}H NMR (300 MHz, MeOD-d_4) δ: 7.24 (d, *J* = 8.7 Hz, 2H, arom.), 6.88 (d, *J* = 8.7 Hz, 2H, arom.), 4.06 (t, *J* = 6.1 Hz, 2H, OC**H**$_2$), 3.76 (s, 2H, Ph-C**H**$_2$N), 3.33 (d, *J* = 2.4 Hz, 2H, NC**H**$_2$C≡CH), 2.64 (t, *J* = 2.4 Hz, 1H, NCH$_2$C≡C**H**), 2.40 (td, *J* = 7.0 Hz, 2.4 Hz, 2H, C**H**$_2$CH$_2$C≡CH), 2.24 (t, *J* = 2.4 Hz, 1H, CH$_2$C≡C**H**), 1.95 (p, *J* = 6.6 Hz, 2H, CH$_2$C**H**$_2$CH$_2$).

^{13}C NMR (125 MHz, MeOD-d$_4$) δ: 159.76 (**C**$_{Ar}$-1), 132.00 (**C**$_{Ar}$-4), 131.03 (**C**$_{Ar}$-3), 115.51 (**C**$_{Ar}$-2), 84.13 (CH$_2$**C**≡CH), 81.97 (NCH$_2$**C**≡CH), 73.41 (C≡**C**H), 69.98 (**C**≡CH), 67.32 (O**C**H$_2$), 52.17 (Ph**C**H$_2$N), 37.29 (N**C**H$_2$C≡CH), 29.51 (OCH$_2$**C**H$_2$), 15.74 (**C**H$_2$C≡CH).

IR (film) cm^{-1}: 3292, 2937, 2875, 1738, 1611, 1511, 1468, 1241, 1173, 1101, 1045, 823, 790.

HRMS (DI-EI) calcd for C$_{15}$H$_{17}$NO 226.1232 [M-H]$^+$, found 226.1228.

7.1.4.3 *N*-Methyl-*N*-(1-(4-(pent-4-yn-1-yloxy)phenyl)propan-2-yl)prop-2-yn-1-amine (24) (P3)
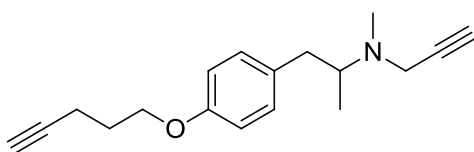
In an oven dried, evacuated and argon purged 10 mL Schlenk flask 203 mg 4-(2-(methyl(prop-2-yn-1-yl)amino)propyl)phenol (**12**) (1.0 mmol, 1.0 eq) were dissolved in 2 mL dry and degassed THF at 0 °C (ice-water bath) resulting in a clear yellow solution. Subsequently, 315 mg triphenylphosphine (1.2 mmol, 1.2 eq) were added, followed by dropwise addition of 243 mg diisopropyl azodicarboxylate (DIAD) (236 µL, 1.2 mmol, 1.2 eq) over the course of 5 min. Then, 101 mg 4-pentyn-1-ol (112 µL, 1.2 mmol, 1.2 eq) were added and the reaction mixture was stirred under inert atmosphere at RT for 16 h. After that time, the solvent was removed *in vacuo* and the crude product was purified by flash column chromatography (cyclohexane:ethyl acetate = 9:1 to 3:2 (v/v), 65 g silica gel, size: 22.0 x 3.5 cm) furnishing 181 mg (0.67 mmol, 67%) *N*-methyl-*N*-(1-(4-(pent-4-yn-1-yloxy)phenyl)propan-2-yl)prop-2-yn-1-amine (**24**) (probe **P3**) as a yellow oil.

C$_{18}$H$_{23}$NO [269.38 g/mol]

R$_f$ = 0.27 (cyclohexane:ethyl acetate = 7:3 (v/v)), 0.07 (cyclohexane:ethyl acetate = 9:1 (v/v)).

HPLC-MS (EI+): t$_R$ = 7.183 min (JK_35to90); m/z (%) 270.2 (100.0) [M+H]$^+$, 269.5 (2.9) [M$^+$], 246.3 (1.2), 201.2 (3.9) 176.3 (0.2).

GC-MS (EI): t_R = 7.24 min; m/z (%) 268.2 (0.1) [M-H]$^+$, 229.1 (0.7), 201.1 (0.6), 173.1 (0.9), 144.1 (0.2), 133.1 (0.7), 107.1 (7.1), 96.1 (100.0), 77.1 (2.4), 56.1 (14.2).

^{1}H NMR (500 MHz, MeOD-d$_4$) δ: 7.08 (d, J = 8.5 Hz, 2H, arom.), 6.84 (d, J = 8.5 Hz, 2H, arom.), 4.04 (t, J = 6.0 Hz, 2H, OC**H**$_2$), 3.44 (m, 2H, **CH**$_2$C≡CH), 3.02 – 2.91 (m, 2H, CH$_a$**H**$_b$CH, CH$_a$H$_b$**CH**), 2.67 (t, J = 2.4 Hz, 1H, CH$_2$C≡C**H**), 2.40 (s, 3H, NC**H**$_3$), 2.37 (td, J = 7.1 Hz, 2.6 Hz, 2H, CH$_2$**CH**$_2$C≡CH) 2.32 (dd, J = 11.5 Hz, 8.8 Hz,1H, CH$_a$**H**$_b$CH), 2.24 (t, J = 2.7 Hz, 1H), 1.94 (p, J = 6.6 Hz, 2H, CH$_2$**CH**$_2$CH$_2$), 0.94 (d, J = 6.6 Hz, 3H, C**H**$_3$).

^{13}C NMR (125 MHz, MeOD-d$_4$) δ: 158.84 (**C**$_{Ar}$-1), 133.22 (**C**$_{Ar}$-4), 131.19 (**C**$_{Ar}$-3), 115.50 (**C**$_{Ar}$-2), 84.17 (CH$_2$**C**≡CH), 80.33 (NCH$_2$**C**≡CH), 74.64 (C≡**C**H), 69.96 (**C**≡CH), 67.32 (O**C**H$_2$), 60.63 (**C**$_q$), 43.67 (N**C**H$_2$C≡CH), 39.08 (Ph**C**H$_2$CH), 37.66 (N**C**H$_3$), 29.55 (OCH$_2$**C**H$_2$), 15.76 (**C**H$_2$C≡CH), 15.02 (**C**H$_3$).

IR (film) cm^{-1}: 3294, 2935, 2873, 2792, 1726, 1611, 1510, 1243, 1176, 1044, 825, 794.

HRMS (DI-EI) calcd for C$_{18}$H$_{23}$NO 269.1780 [M$^+$], found 269.1774.

7.1.4.4 *N*-(1-(4-(pent-4-yn-1-yloxy)phenyl)propan-2-yl)prop-2-yn-1-amine (25) (P4)
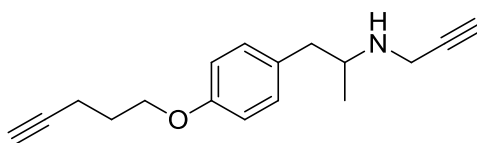
In an oven dried, evacuated and argon purged 10 mL Schlenk flask 189 mg 4-(2-(prop-2-yn-1-ylamino)propyl)phenol (**13**) (1.0 mmol, 1.0 eq) were dissolved in 2 mL dry and degassed THF at 0 °C (ice-water bath) resulting in a clear yellow solution. Subsequently, 315 mg triphenylphosphine (1.2 mmol, 1.2 eq) were added, followed by dropwise addition of 243 mg diisopropyl azodicarboxylate (DIAD) (236 µL, 1.2 mmol, 1.2 eq) over the course of 5 min. Then, 101 mg 4-pentyn-1-ol (112 µL, 1.2 mmol, 1.2 eq) were added and the reaction mixture was stirred under inert atmosphere at RT for 24 h. After that time, the solvent was removed

in vacuo and the crude product was purified by flash column chromatography (cyclohexane:ethyl acetate = 7:3 (v/v), 35 g silica gel, size: 20.0 x 2.5 cm) furnishing 117 mg (0.46 mmol, 46%) *N*-(1-(4-(pent-4-yn-1-yloxy)phenyl)propan-2-yl)prop-2-yn-1-amine (**25**) (probe **P4**) as a yellow oil.

$C_{17}H_{21}NO$ [255.35 g/mol]

R_f = 0.25 (cyclohexane:ethyl acetate = 3:2 (v/v), 0.17 (cyclohexane:ethyl acetate = 7:3 (v/v)).

HPLC-MS (EI+): t_R = 6.381 min (JK_35to90); m/z (%) 256.2 (100.0) [M+H]$^+$, 255.6 (4.1) [M$^+$], 201.2 (9.3), 135.2 (0.4).

GC-MS (EI): t_R = 7.05 min; m/z (%) 254.2 (0.2) [M-H]$^+$, 201.1 (0.5), 174.1 (5.9), 145.1 (0.7), 133.1 (0.9), 107.1 (11.5), 82.1 (100.0), 77.1 (3.6), 65.1 (2.3), 51.1 (1.0).

^{1}H NMR (300 MHz, MeOD-d$_4$) δ: 7.10 (d, *J* = 8.4 Hz, 2H, arom.), 6.86 (d, *J* = 8.4 Hz, 2H, arom.), 4.04 (t, *J* = 6.0 Hz, 2H, OC**H**$_2$), 3.42 (qd, *J* = 17.1 Hz, 1.8 Hz, 2H, NC**H**$_2$C≡CH), 3.16 – 3.03 (m, 1H, C**H**), 2.72 (dd, *J* = 13.2, 6.3 Hz, 1H, C**H**$_a$H$_b$CH), 2.59 (t, *J* = 2.4 Hz, 1H, NCH$_2$C≡C**H**), 2.48 (dd, *J* = 13.4, 7.6 Hz, 1H, CH$_a$**H**$_b$CH), 2.37 (td, *J* = 7.0 Hz, 2.4 Hz, 2H, CH$_2$C**H**$_2$C≡CH), 2.24 (t, *J* = 2.4 Hz, 1H, CH$_2$CH$_2$C≡C**H**), 1.95 (p, *J* = 6.6 Hz, 2H, CH$_2$C**H**$_2$CH$_2$), 1.00 (d, *J* = 6.3 Hz, 3H, NC**H**$_3$).

^{13}C NMR (75 MHz, MeOD-d$_4$) δ: 159.05 (**C**$_{Ar}$-1), 132.24 (**C**$_{Ar}$-4), 131.25 (**C**$_{Ar}$-3), 115.58 (**C**$_{Ar}$-2), 84.16 (CH$_2$**C**≡CH), 81.91 (NCH$_2$**C**≡CH), 73.20 (C≡**C**H), 69.96 (C≡**C**H), 67.32 (O**C**H$_2$), 54.12 (**C**$_q$), 42.86 (N**C**H$_2$C≡CH), 35.84 (Ph**C**H$_2$CH), 29.55 (OCH$_2$**C**H$_2$), 18.99 (**C**H$_3$), 15.76 (**C**H$_2$C≡CH).

IR (film) cm^{-1}: 3293, 2961, 2924, 2873, 1726, 1611, 1510, 1242, 1176, 1047, 808.

HRMS (DI-EI) calcd for $C_{17}H_{21}NO$ 255.1623 [M$^+$], found 255.1626.

7.1.4.5 *N*-Methyl-*N*-(4-(pent-4-yn-1-yloxy)phenethyl)prop-2-yn-1-amine (26) (P5)
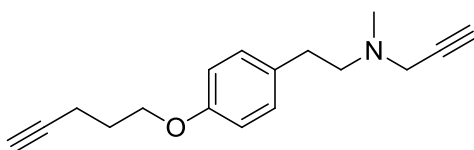
In an oven dried, evacuated and argon purged 10 mL Schlenk flask 189 mg 4-(2-(methyl(prop-2-yn-1-yl)amino)ethyl)phenol (**14**) (1.0 mmol, 1.0 eq) and 101 mg 4-pentyn-1-ol (112 µL, 1.2 mmol, 1.2 eq) were dissolved in 2 mL dry and degassed THF at RT. Subsequently, 315 mg triphenylphosphine (1.2 mmol, 1.2 eq) were added and the mixture cooled to 0 °C in an ice-water bath. Then 243 mg diisopropyl azodicarboxylate (DIAD) (236 µL, 1.2 mmol, 1.2 eq) were added dropwise over the course of 5 min and the reaction mixture was stirred under argon at RT for 26 h. After that time the solvent was removed under reduced pressure and the crude product was purified by flash column chromatography (cyclohexane:ethyl acetate = 3:2 (v/v), 50 g silica gel, size: 16.0 x 3.5 cm) yielding 178 mg (0.70 mmol, 70%) *N*-methyl-*N*-(4-(pent-4-yn-1-yloxy)phenethyl)prop-2-yn-1-amine (**26**) (probe **P5**) as a yellowish oil.

$C_{17}H_{21}NO$ [255.35 g/mol]

R_f = 0.27 (cyclohexane:ethyl acetate = 3:2 (v/v)), 0.22 (cyclohexane:ethyl acetate = 7:3 (v/v)).

HPLC-MS (EI+): t_R = 7.183 min (JK_35to90); m/z (%) 256.2 (100.0) [M+H]$^+$, 218.2 (0.1), 187.2 (2.3).

GC-MS (EI): t_R = 7.06 min; m/z (%) 255.2 (0.4) [M$^+$], 187.1 (0.7), 173.1 (0.7), 121.1 (1.6), 107.1 (5.9), 91.1 (2), 82.1 (100.0), 77.1 (2.9), 65.1 (1.8), 51.1 (0.8).

^{1}H NMR (300 MHz, MeOD-d$_4$) δ: 7.13 (d, *J* = 8.7 Hz, 2H, arom.), 6.86 (d, *J* = 8.7 Hz, 2H, arom.), 4.05 (t, *J* = 6.0 Hz, 2H, OC**H**$_2$), 3.42 (d, 2H, *J* = 2.4 Hz, C**H**$_2$C≡CH), 2.70 (m, 5H, C**H**$_2$C**H**$_2$, C**H**$_2$C≡CH), 2.45-2.33 (m, 5H: 2.38 (s, 3H, C**H**$_3$), 2.37 (td, *J* = 7.0 Hz, 2.7 Hz, 2H, C**H**$_2$CH$_2$C≡CH)), 2.26 (t, *J* = 2.7 Hz, 1H, CH$_2$CH$_2$C≡C**H**), 1.96 (p, *J* = 6.6 Hz, 2H, CH$_2$C**H**$_2$CH$_2$).

^{13}C NMR (75 MHz, MeOD-d$_4$) δ: 158.90 (**C**$_{Ar}$-1), 133.07 (**C**$_{Ar}$-4), 130.57 (**C**$_{Ar}$-3), 115.61 (**C**$_{Ar}$-2), 84.16 (CH$_2$**C**≡CH), 78.65 (NCH$_2$**C**≡CH), 75.17 (C≡**C**H), 69.95 (**C**≡CH), 67.33 (O**C**H$_2$), 58.80 (**C**H$_2$CH$_2$N), 45.95 (N**C**H$_2$C≡CH), 41.99 (N**C**H$_3$), 33.76 (Ph**C**H$_2$CH$_2$), 29.54 (OCH$_2$**C**H$_2$), 15.75 (**C**H$_2$C≡CH).

IR (film) cm^{-1}: 3293, 2867, 2797, 1726, 1612, 1510, 1467, 1241, 1176, 1122, 823.

HRMS (DI=EI) calcd for C$_{17}$H$_{21}$NO 255.1623 [M$^+$], found 255.1625.

7.1.4.6 *N*-(4-(Pent-4-yn-1-yloxy)phenethyl)prop-2-yn-1-amine (27) (P6)
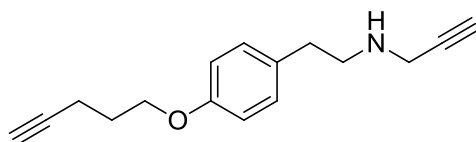
In an oven dried, evacuated and argon purged 10 mL Schlenk flask 175 mg 4-(2-(prop-2-yn-1-ylamino)ethyl)phenol (**15**) (1.0 mmol, 1.0 eq) and 101 mg 4-pentyn-1-ol (112 µL, 1.2 mmol, 1.2 eq) were dissolved in 2 mL dry and degassed THF at RT. Subsequently, 315 mg triphenylphosphine (1.2 mmol, 1.2 eq) were added and the mixture cooled down to 0 °C in an ice-water bath. Then 243 mg diisopropyl azodicarboxylate (DIAD) (236 µL, 1.2 mmol, 1.2 eq) were added dropwise over the course of 5 min and the reaction mixture was stirred under argon at RT for 26 h. After that time the solvent was removed under reduced pressure and the crude product was purified by flash column chromatography (cyclohexane:ethyl acetate = 3:2 to 1:1 (v/v), 50 g silica gel, size: 16.0 x 3.5 cm) yielding 220 mg (0.91 mmol, 91%) *N*-(4-(pent-4-yn-1-yloxy)phenethyl)prop-2-yn-1-amine (**27**) (probe **P6**) as a yellowish oil.

C$_{16}$H$_{19}$NO [241.33 g/mol]

R$_f$ = 0.21 (cyclohexane:ethyl acetate = 1:1 (v/v)), 0.13 (cyclohexane:ethyl acetate = 3:2 (v/v)).

HPLC-MS (EI+): t$_R$ = 7.183 min (JK_35to90); m/z (%) 242.2 (100.0) [M+H]$^+$, 241.5 (2.7), [M$^+$], 187.2 (5.7).

GC-MS (EI): t_R = 7.03 min; m/z (%) 241.2 (0.2) [M$^+$], 187.1 (0.5), 174.1 (56.1), 159.1 (0.7), 146.1 (3.5), 134.1 (0.8), 107.1 (20.2), 91.1 (3.9), 77.1 (6.9), 68.1 (100.0), 53.1 (0.9), 51.1 (1.7).

^{1}H NMR (300 MHz, MeOD-d$_4$) δ: 7.12 (d, J = 8.7 Hz, 2H, arom.), 6.85 (d, J = 8.7 Hz, 2H, arom.), 4.03 (t, J = 6.0 Hz, 2H, OC**H**$_2$), 3.38 (d, 2H, J = 2.1 Hz, C**H**$_2$C≡CH), 2.87 (m, 2H, C**H**$_2$NH), 2.72 (m, 2H, C**H**$_2$CH$_2$NH), 2.60 (t, 1H, J = 2.4 Hz, CH$_2$C≡C**H**), 2.36 (td, J = 7.1, 2.7 Hz, 2H, CH$_2$C**H**$_2$C≡CH), 2.24 (t, J = 2.7 Hz, 1H, CH$_2$CH$_2$C≡C**H**), 1.94 (p, J = 6.6 Hz, 2H, CH$_2$C**H**$_2$CH$_2$).

^{13}C NMR (75 MHz, MeOD-d$_4$) δ: 158.94 (**C**$_{Ar}$-1), 132.88 (**C**$_{Ar}$-4), 130.60 (**C**$_{Ar}$-3), 115.66 (**C**$_{Ar}$-2), 84.17 (CH$_2$**C**≡CH), 81.95 (NCH$_2$**C**≡CH), 73.24 (C≡**C**H), 69.97 (C≡**C**H), 67.32 (O**C**H$_2$), 50.98 (**C**H$_2$CH$_2$N), 38.30 (N**C**H$_2$C≡CH), 35.61 (Ph**C**H$_2$CH$_2$), 29.52 (OCH$_2$**C**H$_2$), 15.75 (**C**H$_2$C≡CH).

IR (film) cm^{-1}: 3291, 3029, 2923, 1611, 1510, 1469, 1241, 1176, 1113, 1048, 825.

HRMS (DI-EI) calcd for C$_{16}$H$_{19}$NO 241.1467 [M$^+$], found 241.1471.

7.1.5 Synthesis of photocrosslinker probes

7.1.5.1 2,5-Dioxopyrrolidin-1-yl hex-5-ynoate (5-hexynoic acid succinimide ester) (55)
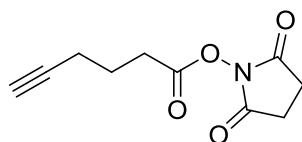
Method A:[318] In an oven dried, evacuated and argon purged 50 mL Schlenk flask 352 mg 5-hexynoic acid (347 µL, 3.14 mmol, 1.0 eq) were dissolved in 14 mL dry dichloromethane forming a clear colorless solution to which 380 mg N-hydroxysuccinimide (3.3 mmol, 1.05 eq) were added at RT. Subsequently, 633 mg 1-ethyl-3-(3-dimethylaminopropyl)carbodiimide hydrochloride (EDC HCl) (3.3 mmol, 1.05 eq) were added at once at RT. The reaction

progress was monitored by TLC analysis and carried out for 7 h at RT under inert atmosphere until complete consumption of the substrate was indicated. Then, the reaction mixture was diluted with dichloromethane, washed with distilled H_2O (3 x 15 mL), brine (1 x 15 mL) and dried over anhydrous Na_2SO_4. The solvent was removed *in vacuo* and pure product dried under vacuum furnishing 648 mg (3.10 mmol, 98%) 2,5-dioxopyrrolidin-1-yl hex-5-ynoate (5-hexynoic acid succinimide ester) (**x**) as a colorless oil.

Method B:[121] In an oven dried, evacuated and argon flushed 100 mL Schlenk flask 561 mg 5-hexynoic acid (552 µL, 5.0 mmol, 1.0 eq) were dissolved in 20 mL dry dichloromethane forming a clear colorless solution to which 604 mg *N*-hydroxysuccinimide (5.25 mmol, 1.05 eq) were added at RT. Subsequently, 662 mg *N,N'*-diisopropylcarbodiimide (DIC) (5.25 mmol, 1.05 eq) were added at once at RT and the reaction mixture was stirred overnight (ca. 15 h) under argon atmosphere. After a certain time a precipitate appeared due to formation of *N,N'*-diisopropylurea. The reaction progress was monitored by TLC analysis and the reaction was stopped when there was no more starting material indicated. Urea was filtered off under vacuum, the filtrate was concentrated under reduced pressure, cooled on water-ice bath to 0 °C and triturated with cold hexane causing some further precipitation of urea which was then filtrated off and washed with hexane. Furthermore, the organic phase was washed with distilled water (2 x 15 mL), brine (1 x 15 mL) and dried over anhydrous Na_2SO_4. The solvent was removed *in vacuo* and the crude product purified by flash column chromatography (hexane:ethyl acetate = 6:4 (v/v), 58 g silica gel, size: 12.0 x 4.0 cm) furnishing 900 mg (4.30 mmol, 86%) 2,5-dioxopyrrolidin-1-yl hex-5-ynoate (5-hexynoic acid succinimide ester)(**55**) as a colorless oil.

$C_{10}H_{11}NO_4$ [209.20 g/mol]

R_f = 0.13 (hexane:ethyl acetate = 4:1 (v/v)), 0.33 (hexane:ethyl acetate = 3:2 (v/v)), 0.48 (hexane:ethyl acetate = 1:1 (v/v)).

^{1}H NMR (500 MHz, CDCl$_3$) δ: 2.84 (d, J = 5.5 Hz, 4H, 2 x **CH**$_2$ NHS), 2.78 (t, J = 7.5 Hz, 2H, **CH**$_2$COO), 2.35 (td, J = 6.9, 2.5 Hz, 2H, **CH**$_2$C≡CH), 2.02 (t, J = 2.5 Hz, 1H, CH$_2$C≡C**H**), 1.97 (p, J = 7.0 Hz, 2H, CH$_2$**CH**$_2$CH$_2$).

^{13}C NMR (125 MHz, CDCl$_3$) δ: 169.07 (**C**=O NHS), 168.15 (**C**=O), 82.38 (**C**≡CH), 69.82 (C≡**C**H), 29.63 (**C**H$_2$CO), 25.56 (**C**H$_2$ NHS), 23.29 (**C**H$_2$CH$_2$CO), 17.57 (**C**H$_2$C≡CH).

The spectral data are identical to those published previously.[121,318]

7.1.5.2 Hex-5-ynoyl chloride (56)
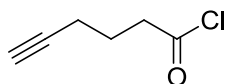
An oven dried, evacuated and argon purged 50 mL Schlenk flask was charged with 20 mL dry dichloromethane, then two drops dry DMF were added and the solvent mixture was cooled down to 0 °C in an ice-water bath. Subsequently, 1.121 g 5-hexynoic acid (1.104 mL, 10.0 mmol, 1.0 eq) were dissolved, followed by a dropwise addition of 1.269 g oxalyl chloride (0.859 mL, 10.0 mmol, 1.0 eq) over 10 min at 0 °C. Then the reaction mixture was stirred for 30 min at 0 °C followed by 3 h at RT. The solvent was removed under reduced pressure, resulting in a red liquid which was directly purified by distillation under atmospheric pressure (ca. 158 °C) yielding 840 mg (6.4 mmol, 64%) hex-5-ynoyl chloride (**56**) as a colorless liquid.

C$_6$H$_7$ClO [130.57 g/mol]

b.p. = 156-158 °C / atm.

^{1}H NMR (500 MHz, CDCl$_3$) δ: 3.06 (t, J = 7.5 Hz, 2H, **CH**$_2$CO), 2.29 (td, J = 6.8, 2.5 Hz, 2H, **CH**$_2$C≡CH), 2.01 (t, J = 2.5 Hz, 1H, CH$_2$C≡C**H**), 1.90 (p, J = 7.0 Hz, 2H, CH$_2$**CH**$_2$CH$_2$).

^{13}C NMR (125 MHz, CDCl$_3$) δ: 173.43 (**C**=O), 82.11 (**C**≡CH), 69.97 (C≡**C**H), 45.53 (**C**H$_2$CO), 23.55 (**C**H$_2$CH$_2$CO), 17.16 (**C**H$_2$C≡CH).

The spectral data are identical to those published previously.[352]

7.1.5.3 (*S*)-3-(4-Benzoylphenyl)-2-(hex-5-ynamido)propanoic acid (54) (Bpa-Alk)
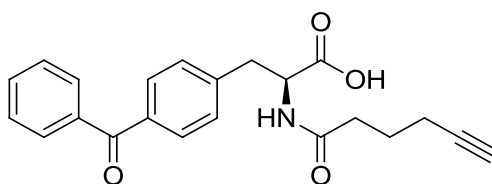
Method A: In an oven dried, evacuated and argon flushed 25 mL Schlenk flask 242 mg (*S*)-2-amino-3-(4-benzoylphenyl)propanoic acid (L-*p*-benzoylphenylalanine, H-*p*-Bz-Phe-OH, H-Bpa-OH) (0.9 mmol, 1.0 eq) were dissolved in 3 mL dry dichloromethane forming a white suspension. Then, 291 mg *N,N'*-diisopropylethylamine (392 µL, 2.25 mmol, 2.5 eq) were added at once at RT, followed by dropwise addition 245 mg (1.17 mmol, 1.3 eq) of 5-hexynoic acid succinimide ester at RT. The reaction was stirred for 3 h at RT, within this time the suspension turned into a clear yellowish solution. The reaction progress was monitored by TLC analysis and once it did not indicate the presence of the starting material, the reaction mixture was acidified with ca. 0.2 mL of 2N aqueous hydrochloric acid (pH 1), and diluted with ca. 10 mL dichloromethane. Then the organic phase was washed with distilled H_2O (1 x 15 mL), brine (1x15 mL) and dried over anhydrous Na_2SO_4. The solvent was removed under reduced pressure and the crude product was purified by flash column chromatography (DCM:MeOH = 97:3 (v/v) with 1% formic acid, 23 g silica gel, size: 13.0 x 2.5 cm) yielding 315 mg (0.87 mmol, 96%) 3-(4-benzoylphenyl)-2-(hex-5-ynamido)propanoic acid (**54**) (**Bpa-Alk**) as a yellowish foam.

Method B: In an oven dried, evacuated and argon flushed 10 mL Schlenk flask 135 mg 2-amino-3-(4-benzoylphenyl)propanoic acid (0.5 mmol, 1.0 eq) were dissolved in 2 mL dry dichloromethane forming a white suspension. Then, 190 mg diazabicyclo[5.4.0]undec-7-ene (DBU) (187 µL, 1.25 mmol, 2.5 eq) were added at once at RT which caused that the reaction mixture turned clear. The mixture was then cooled down to 0 °C in an ice-water bath and 85 mg hex-5-ynoyl chloride (1.17 mmol, 1.3 eq) were added dropwise. The reaction mixture was stirred vigorously for 6 h at RT. The reaction progress was monitored by TLC analysis and

once the presence of the starting material was not indicated, the reaction mixture was acidified with ca. 0.2 mL of 2N aqueous hydrochloric acid (pH 1) and diluted with ca. 10 mL dichloromethane. Then the organic phase was washed with distilled H_2O (2 x 10 mL), brine (1 x 10 mL) and dried over anhydrous Na_2SO_4. Then the solvent was removed under reduced pressure and the crude product was purified by flash column chromatography (DCM:MeOH:formic acid = 97:3:1 (v/v/v), 11 g silica gel, size: 10.0 x 2.0 cm) yielding 91 mg (0.25 mmol, 50%) 3-(4-benzoylphenyl)-2-(hex-5-ynamido)propanoic acid (**54**) as a yellowish foam.

$C_{22}H_{21}N_2O_4$ [363.41 g/mol]

R_f = 0.29 (DCM:MeOH:formic acid = 97:3:1 (v/v/v)), 0.32 (DCM:MeOH:formic acid = 97:3:1 (v/v/v)), 0.64 (DCM:MeOH:acetic acid = 90:10:1 (v/v/v)).

HPLC-MS (EI+): t_R = 5.597 min (JK_10to90); m/z (%) 402.0 (49.9) [M+K]$^+$, 386.0 (71.1) [M+Na]$^+$, 364.(100.0) [M+H]$^+$, 342.1 (1.2), 320.1 (3.7).

^{1}H NMR (500 MHz, CDCl$_3$) δ 9.97 (s, 1H, COO**H**), 7.76 (d, *J* = 7.0 Hz, 2H, arom. (Bz)), 7.72 (d, *J* = 8.0 Hz, 2H, arom. (Phe)), 7.58 (t, *J* = 7.5 Hz, 1H, arom. (Bz)), 7.46 (t, *J* = 7.5 Hz, 2H, arom. (Bz)), 7.29 (d, *J* = 8.0 Hz, 2H, arom. (Phe)), 6.45 (d, *J* = 7.5 Hz, 1H, N**H**), 4.95 (dd, *J* = 13.5, 6.5 Hz, 1H, C**H**), 3.33 (dd, *J* = 14.0, 5.5 Hz, 1H, C**H**$_a$CH$_b$), 3.18 (dd, *J* = 14.0, 6.5 Hz, 1H, CH$_a$C**H**$_b$), 2.36 (t, *J* = 7.5 Hz, 2H, NHCOC**H**$_2$), 2.17 (m, 2H, C**H**$_2$C≡CH), 1.93 (t, *J* = 2.5 Hz, 1H, CH$_2$C≡C**H**), 1.79 (m, 2H, CH$_2$C**H**$_2$CH$_2$).

^{13}C NMR (125 MHz, CDCl$_3$) δ 196.84 (**C**=O Bz), 173.74 (**C**=O), 173.22 (**C**=O), 140.97 (**C**$_{Ar}$), 137.23 (**C**$_{Ar}$), 136.27 (**C**$_{Ar}$), 132.63 (**C**$_{Ar}$), 130.42 (**C**$_{Ar}$), 130.05 (**C**$_{Ar}$), 129.35 (**C**$_{Ar}$), 128.31 (**C**$_{Ar}$), 83.12 (**C**≡CH), 69.51 (C≡**C**H), 52.92 (**C**$_q$), 37.26 (Phe**C**H$_2$), 34.68 (**C**H$_2$CO), 23.95 (**C**H$_2$CH$_2$CO), 17.64 (**C**H$_2$C≡CH).

The spectral data are identical to those published previously.[121]

7.1.5.4 (*S*)-4-((Methyl(prop-2-yn-1-yl)amino) methyl)phenyl 3-(4-benzoylphenyl)-2-(hex-5- ynamido)propanoate (50) (P1-Phot)
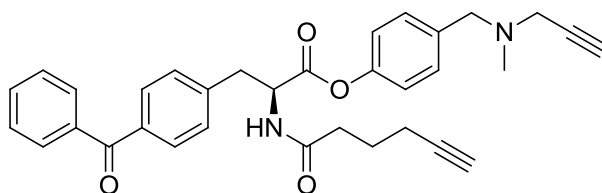
Method A: In an oven dried, evacuated and argon flushed 25 mL Schlenk flask 148 mg 3-(4-benzoylphenyl)-2-(hex-5-ynamido)propanoic acid (**54**) (0.4 mmol, 1.0 eq) and 77 mg 4-((methyl(prop-2-yn-1-yl)amino)methyl)phenol (**9**) (0.44 mmol, 1.1 eq) were dissolved in 2 mL dry dichloromethane forming a clear solution. Subsequently, 84 mg 1-ethyl-3-(3-dimethylaminopropyl)carbodiimide hydrochloride (EDC·HCl) (0.44 mmol, 1.1 eq) were added at once at RT and stirred for 3.5 h under argon atmosphere. The reaction progress was followed by TLC analysis and once there was no starting material indicated the reaction mixture was diluted with ca. 15 mL DCM, the organic phase was washed with distilled water (2 x 10 mL) and brine (1 x 10 mL) and dried over anhydrous Na_2SO_4. Then the solvent was removed *in vacuo* and the crude product purified by flash column chromatography (hexane:ethyl acetate = 3:2 to 2:3 (v/v), 15 g silica gel, size: 13.0 x 2.5 cm), furnishing 178 mg (0.34 mmol, 85%) 4-((methyl(prop-2-yn-1-yl)amino) methyl)phenyl (*S*)-3-(4-benzoylphenyl)-2-(hex-5-ynamido) propanoate (**50**) (probe **P1-Phot**) as an oily yellowish solid.

Method B: In an oven dried, evacuated and argon flushed 25 mL Schlenk flask 102 mg 3-(4-benzoylphenyl)-2-(hex-5-ynamido)propanoic acid (**54**) (0.28 mmol, 1.0 eq) and 52 mg 4-((methyl(prop-2-yn-1-yl)amino)methyl)phenol (**9**) (0.29 mmol, 1.05 eq) were dissolved in 5 mL dry dichloromethane forming a clear solution. The mixture was cooled down to ca. -5 °C and then 73 mg *N,N'*-diisopropylethylamine (98 µL, 0.56 mmol, 2.0 eq) were added and stirred for 15 min under argon atmosphere. Subsequently, 153 mg benzotriazol-1-yl-oxytripyrrolidinophosphonium hexafluorophosphate (PyBOP) (0.29 mmol, 1.05 eq) were

added and the reaction mixture stirred for 3.5 h letting the temperature to reach RT. The reaction progress was followed by TLC analysis and once there was no starting material indicated the reaction mixture was diluted with ca. 15 mL DCM. The organic phase was washed with 5% HCl$_{aq}$ (2 x 15 mL), brine (2 x 15 mL), saturated NaHCO$_3$ (1 x 15 mL), brine (1 x 15 mL) and dried over anhydrous Na$_2$SO$_4$. Then the solvent was removed *in vacuo* and the crude product was purified by flash column chromatography (hexane:ethyl acetate = 3:2 to 1:1 (v/v), 14 g silica gel, size: 12.5 x 2.5 cm), furnishing 56 mg (0.11 mmol, 38%) (*S*)-4-((methyl(prop-2-yn-1-yl)amino) methyl)phenyl 3-(4-benzoylphenyl)-2-(hex-5-ynamido) propanoate (**50**) (probe **P1-Phot**) as an oily yellowish solid.

C$_{33}$H$_{32}$N$_2$O$_4$ [520.62 g/mol]

R$_f$ = 0.42 (hexane:ethyl acetate = 1:1 (v/v), 0.27 (hexane:ethyl acetate = 3:2 (v/v)).

m.p. = 83-85 °C (yellowish solid)

HPLC-MS (EI+): t$_R$ = 7.161 min (JK_35to90); m/z (%) 559.2 (11.5) [M+K]$^+$, 543.2 (39.9) [M+Na]$^+$, 521.2 (100.0) [M+H]$^+$, 520.2 (3.0) [M$^+$], 346.0 (0.5), 224.1 (0.5), 216.9 (0.4), 111.8 (0.9).

^{1}H NMR (500 MHz, CDCl$_3$) δ 7.78 (m, 4H, arom. (Bz, Phe)), 7.59 (t, *J* = 7.5 Hz, 1H, arom. (Bz)), 7.49 (t, *J* = 7.5 Hz, 2H, arom. (Bz)), 7.35 (d, *J* = 8.5 Hz, 4H; arom, (Phe, Ph)), 6.98 (d, *J* = 8.5 Hz, 2H, arom. (Ph)), 6.08 (d, *J* = 8.0 Hz, 1H, N**H**), 5.18 (dd, *J* = 13.5, 6.5 Hz, 1H, C**H**), 3.56 (s, 2H, PhC**H$_2$**N), 3.40 (dd, *J* = 14.0, 6.0 Hz, 1H, C**H$_a$**H$_b$), 3.35 (dd, *J* = 14.0, 6.0 Hz, 1H, CH$_a$**H$_b$**), 3.30 (d, *J* = 2.0 Hz, 2H, NC**H$_2$**C≡CH), 2.39 (t, *J* = 7.5 Hz, 2H, NHCOC**H$_2$**), 2.33 (s, 3H, NC**H$_3$**), 2.28 (t, *J* = 2.0 Hz, 1H, NCH$_2$C≡C**H**), 2.24 (m, 2H, C**H$_2$**C≡CH), 1.97 (t, *J* = 2.5 Hz, 1H, CH$_2$C≡C**H**), 1.86 (m, 2H, CH$_2$C**H$_2$**CH$_2$).

^{13}C NMR (125 MHz, CDCl$_3$) δ: 196.21 (**C**=O Bz), 171.95 (**C**=O), 170.04 (**C**=O), 149.19 (**C**$_{Ar}$), 140.53 (**C**$_{Ar}$), 137.43 (**C**$_{Ar}$), 136.59 (**C**$_{Ar}$), 132.48 (**C**$_{Ar}$), 130.50 (**C**$_{Ar}$), 130.21 (**C**$_{Ar}$), 129.96 (**C**$_{Ar}$), 129.40 (**C**$_{Ar}$), 128.30 (2 x **C**$_{Ar}$), 120.92 (**C**$_{Ar}$), 83.24 (**C**≡CH), 78.24 (**C**≡CH), 73.53 (C≡**C**H),

69.44 (C≡**C**H), 59.09 (Ph**C**H$_2$N), 52.94 (**C**$_q$), 44.79 (N**C**H$_2$C≡CH), 41.73 (N**C**H$_3$), 37.93 (Phe**C**H$_2$), 34.67 (**C**H$_2$CO), 23.83(**C**H$_2$CH$_2$CO), 17.68 (**C**H$_2$C≡CH).

HRMS (EI) calcd for C$_{33}$H$_{32}$N$_2$O$_4$ 521.2440 [M+H]$^+$, found 521.2451.

7.1.5.5 (*S*)-4-(2-(Methyl(prop-2-yn-1-yl)amino) propyl)phenyl 3-(4-benzoylphenyl)-2-(hex-5-ynamido)propanoate (51) (P3-Phot)
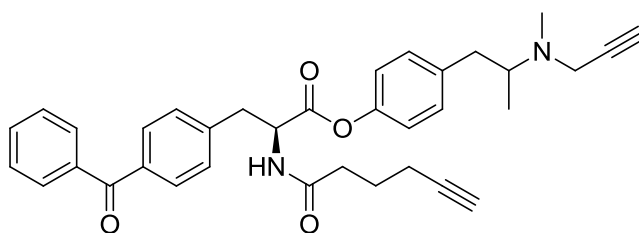
In an oven dried, evacuated and argon flushed 25 mL Schlenk flask 158 mg 3-(4-benzoylphenyl)-2-(hex-5-ynamido)propanoic acid (**54**) (0.43 mmol, 1.0 eq) and 106 mg 4-(2-(methyl(prop-2-yn-1-yl)amino)propyl)phenol (**12**) (0.52 mmol, 1.2 eq) were dissolved in 2.5 mL dry dichloromethane forming a clear solution. Subsequently, 100 mg 1-ethyl-3-(3-dimethylaminopropyl)carbodiimide hydrochloride (EDC HCl) (0.52 mmol, 1.2 eq) were added at once at RT and stirred overnight under argon atmosphere. The reaction progress was followed by TLC analysis and once there was no starting material indicated, the reaction mixture was diluted with ca. 15 mL DCM. The organic phase was washed with distilled water (2 x 15 mL) and brine (1 x 15 mL) and dried over anhydrous Na$_2$SO$_4$. Then the solvent was removed *in vacuo* and the crude product purified by flash column chromatography (hexane:ethyl acetate = 1:1 to 2:3 (v/v), 16 g silica gel, size: 14.0 x 2.5 cm), furnishing 148 mg (0.27 mmol, 62%) 4-(2-(methyl(prop-2-yn-1-yl)amino)propyl)phenyl 3-(4-benzoylphenyl)-2-(hex-5-ynamido) propanoate (**51**) (probe **P3-Phot**) as a yellow oil.

C$_{35}$H$_{36}$N$_2$O$_4$ [548.67 g/mol]

R$_f$ = 0.55 (ethyl acetate), 0.30 (hexane:ethyl acetate = 2:3 (v/v)).

HPLC-MS (EI+): t_R = 7.407 min (JK_35to90); m/z (%) 587.2 (9.5) [M+K]⁺, 571.2 (13.8) [M+Na]⁺, 549.3 (100.0) [M+H]⁺, 529.2 (2.2), 501.3 (1.3), 500.4 (3.6), 419.0 (0.9), 415.4 (1.9), 378.9 (1.5), 149.2 (1.0).

¹H NMR (500 MHz, CDCl₃) δ 7.79 (m, 4H, arom. (Bz, Phe)), 7.59 (t, *J* = 7.5 Hz, 1H, arom. (Bz)), 7.48 (t, *J* = 7.5 Hz, 2H, arom. (Bz)), 7.35 (d, *J* = 8.0 Hz, 2H, arom.(Phe)), 7.18 (d, *J* = 8.5 Hz, 2H (Ph)), 6.93 (d, *J* = 8.5 Hz, 2H (Ph)), 6.10 (d, *J* = 8.0 Hz, 1H, N**H**), 5.18 (dd, *J* = 13.5, 6.0 Hz, 1H, C**H**), 3.42 (m, 2H, NC**H₂**C≡CH), 3.40 (dd, *J* = 14.0, 6.0 Hz, 1H, C**H**ₐ**H**₆CHCO), 3.35 (dd, *J* = 14.0, 6.0 Hz, 1H, CHₐ**H**₆CHCO), 3.03 − 2.94 (m, 2H, C**H**ₐ**H**₆CHN), 2.43 − 2.36 (m, 6H: 2.41 (s, 3H, NC**H₃**), 2.39 (t, *J* = 7.5 Hz, 2H, NHCOC**H₂**), 1H (NCH₂C≡C**H**)), 2.26 − 2.22 (m, 3H: 2H (CH₂C**H₂**C≡CH), 1H (CHₐ**H**₆CH)), 1.97 (t, *J* = 2.5 Hz, 1H, CH₂C≡C**H**), 1.86 (dtd, *J* = 14.0, 7.0, 2.5 Hz, 2H, CH₂C**H₂**CH₂), 0.96 (d, *J* = 6.5 Hz, 3H, C**H₃**).

¹³C NMR (125 MHz, CDCl₃) δ: 196.21 (**C**=O Bz), 171.94 (**C**=O), 170.09 (**C**=O), 148.29 (**C**ₐᵣ), 140.57 (**C**ₐᵣ), 138.38 (**C**ₐᵣ), 137.42 (**C**ₐᵣ), 136.56 (**C**ₐᵣ), 132.47 (**C**ₐᵣ), 130.48 (**C**ₐᵣ), 130.29 (**C**ₐᵣ), 129.96 (**C**ₐᵣ), 129.40 (**C**ₐᵣ), 128.29 (**C**ₐᵣ), 120.80 (**C**ₐᵣ), 83.24 (**C**≡CH), 80.11 (**C**≡CH), 72.69 (C≡**C**H), 69.42 (C≡**C**H), 59.17 (**C**q), 52.93 (**C**q), 43.11 (N**C**H₂C≡CH), 39.13 (Ph**C**H₂CH), 37.92 (N**C**H₃), 37.34 (Phe**C**H₂), 34.66 (**C**H₂CO), 23.84 (**C**H₂CH₂CO), 17.68 (**C**H₂C≡CH), 14.94 (**C**H₃).

HRMS (EI) calcd for C₃₅H₃₆N₂O₄ 549.2753 [M+H]⁺, found 549.2775.

7.1.5.6 (*S*)-4-((Methyl(prop-2-yn-1-yl)amino) methyl)phenyl 2-((Fmoc)amino))-3-(4-benzoylphenyl)propanoate (52) (Fmoc-Bpa-P1)
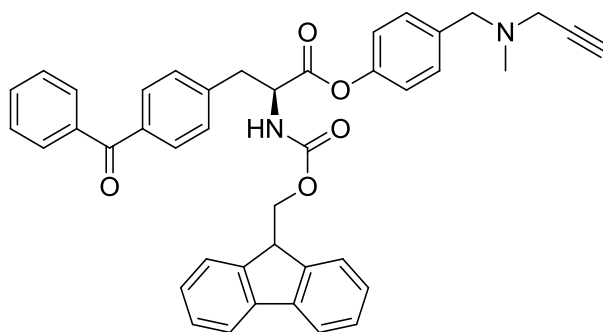
In an oven dried, evacuated and argon flushed 25 mL Schlenk flask 393 mg (S)-2-((Fmoc)amino)-3-(4-benzoylphenyl)propanoic acid (0.80 mmol, 1.0 eq) were dissolved in 15 mL dry dichloromethane, followed by 154 mg 4-((methyl(prop-2-yn-1-yl)amino)methyl)phenol (**9**) (0.88 mmol, 1.1 eq) forming a clear solution. the mixture was cooled down to ca. -20 °C in an acetone/dry ice bath and then 228 mg *N,N'*-diisopropylethylamine (397 µL, 1.76 mmol, 2.2 eq) were added and stirred for 15 min at -20 °C. Subsequently, 437 mg benzotriazol-1-yl-oxytripyrrolidinophosphonium hexafluorophosphate (PyBOP) (0.84 mmol, 1.05 eq) were added and the reaction mixture stirred for 4 h allowing the temperature to reach RT. The reaction progress was followed by TLC analysis and once there were no starting materials indicated the reaction mixture was diluted with ca. 10 mL DCM. The organic phase was washed with 5% HCl_{aq} (2 x 15 mL), brine (2 x 15 mL), saturated $NaHCO_3$ (1 x 15 mL), brine (1 x 15 mL) and dried over anhydrous Na_2SO_4. Then the solvent was removed *in vacuo* and the crude product was purified by flash column chromatography (hexane:ethyl acetate = 55:45 to 50:50 (v/v), 40 g silica gel, size: 19.0 x 3.0 cm), furnishing 321 mg (0.49 mmol, 63%) (*S*)-4-((methyl(prop-2-yn-1-yl)amino) methyl)phenyl 2-((Fmoc)amino))-3-(4-benzoylphenyl) propanoate (**52**) (**Fmoc-Bpa-P1**) as a white solid.

$C_{42}H_{36}N_2O_5$ [648.75 g/mol]

R_f = 0.39 (hexane:ethyl acetate = 1:1 (v/v)).

m.p. = 140-142 °C (white solid)

HPLC-MS (EI+): t_R = 8.680 min (JK_35to90); m/z (%) 687.2 (9.7) [M+K]$^+$, 671.25 (18.0) [M+Na]$^+$, 649.2 (100.0) [M+H]$^+$, 621.7 (0.9), 412.9 (0.8), 282.1 (0.5), 280.0 (1.1).

^{1}H NMR (500 MHz, CDCl$_3$) δ: 7.77 (m, 6H, arom.; 2H (Bz), 2H (Phe), 2H (Fmoc)), 7.64 – 7.55 (m, 3H, arom.; 2H (Fmoc), 1H (Bz)), 7.48 (t, J = 7.5 Hz, 2H, arom. (Bz)), 7.43 – 7.27 (m, 8H, arom,; 4H (Fmoc), 2H (Phe), 2H (Ph)), 6.98 (d, J = 8.5 Hz, 2H (Ph)), 5.37 (d, J = 8.0 Hz, 1H, N**H**), 4.96 (dd, J = 14.0, 6.0 Hz, 1H, C**H**COO), 4.53 (dd, J = 10.5, 7.0 Hz, 1H, OC**H**$_a$H$_b$), 4.43 (dd, J = 10.5, 7.0 Hz, 1H, OCH$_a$**H**$_b$), 4.23 (t, J = 7.0 Hz, 1H, C**H** (Fmoc)), 3.56 (s, 2H, PhC**H**$_2$N), 3.36 (dd, J = 5.5, 3.2 Hz, 2H, C**H**$_2$CHCO), 3.30 (d, J = 2.5 Hz, 2H, C**H**$_2$C≡CH), 2.34 (s, 3H, C**H**$_3$), 2.27 (t, J = 2.5 Hz, 1H, CH$_2$C≡C**H**).

^{13}C NMR (125 MHz, CDCl$_3$) δ: 196.21 (**C**=O), 169.84 (**C**=O), 155.50 (**C**=O), 149.18 (**C**$_{Ar}$ Ph), 143.66 (**C**$_{Ar}$ Fmoc), 143.55 (**C**$_{Ar}$ Fmoc), 141.33 (**C**$_{Ar}$ Fmoc), 141.29 (**C**$_{Ar}$ Fmoc), 140.39 (**C**$_{Ar}$ Bpa), 137.48 (**C**$_{Ar}$ Bpa), 136.66 (**C**$_{Ar}$ Ph), 136.56 (**C**$_{Ar}$ Bpa), 132.44 (**C**$_{Ar}$ Bpa), 130.51 (**C**$_{Ar}$ Bpa), 130.20 (**C**$_{Ar}$ Ph), 129.96 (**C**$_{Ar}$ Bpa), 129.47 (**C**$_{Ar}$ Bpa), 128.30 (**C**$_{Ar}$ Bpa), 127.77 (**C**$_{Ar}$ Fmoc), 127.07 (**C**$_{Ar}$ Fmoc), 125.00 (**C**$_{Ar}$ Fmoc), 124.92 (**C**$_{Ar}$ Fmoc), 120.93 (**C**$_{Ar}$ Ph), 120.03 (**C**$_{Ar}$ Fmoc), 78.30 (**C**≡CH), 73.49 (C≡**C**H), 66.96 (**C**$_q$ Fmoc), 59.12 (Ph**C**H$_2$N), 54.64 (**C**$_q$ Bpa), 47.13 (O**C**H$_2$), 44.81 (N**C**H$_2$C≡CH), 41.76 (N**C**H$_3$), 38.21 (Phe**C**H$_2$CH).

HRMS (EI) calcd for C$_{42}$H$_{36}$N$_2$O$_5$ 649.2703 [M+H]$^+$, found 649.2733.

7.1.5.7 (*S*)-4-(2-(Methyl(prop-2-yn-1-yl) amino)propyl)phenyl 2-((Fmoc)amino)-3-(4-benzoylphenyl)propanoate (53) (Fmoc-Bpa-P3)
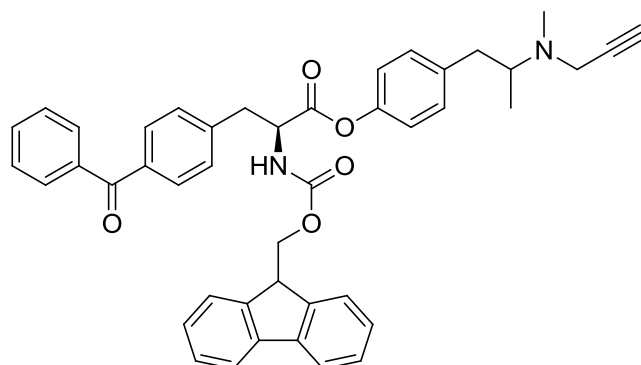
In an oven dried, evacuated and argon flushed 25 mL Schlenk flask 393 mg (*S*)-2-((Fmoc)amino)-3-(4-benzoylphenyl)propanoic acid (0.80 mmol, 1.0 eq) were dissolved in 15 mL dry dichloromethane, followed by 179 mg 4-(2-(methyl(prop-2-yn-1-yl)amino)propyl)phenol (**12**) (0.88 mmol, 1.1 eq) forming a clear yellowish solution. The mixture was cooled down to ca. -20 °C on acetone/dry ice bath and then 228 mg *N,N'*-diisopropylethylamine (397 μL, 1.76 mmol, 2.2 eq) were added and stirred for 15 min at -20° C. Subsequently, 437 mg benzotriazol-1-yl-oxytripyrrolidinophosphonium hexafluorophosphate (PyBOP) (0.84 mmol, 1.05 eq) were added and the reaction mixture stirred for 3 h allowing the temperature to achieve RT. The reaction progress was followed by TLC analysis and once there were no starting materials indicated the reaction mixture was diluted with ca. 10 mL DCM, the organic phase was washed with 5% HCl_{aq} (2 x 15 mL), brine (2 x 15 mL), saturated $NaHCO_3$ (1 x 15 mL), brine (1 x 15 mL) and dried over anhydrous Na_2SO_4. Then the solvent was removed *in vacuo* and the crude product was purified by flash column chromatography (hexane:ethyl acetate = 2:3 to 3:7 (v/v), 60 g silica gel, size: 40.0 x 2.5 cm), furnishing 317 mg (0.47 mmol, 58%) (2S)-4-(2-(methyl(prop-2-yn-1-yl) amino)propyl)phenyl 2-((Fmoc)amino)-3-(4-benzoylphenyl)propanoate (**53**) (**Fmoc-Bpa-P3**) as a yellowish solid.

$C_{44}H_{40}N_2O_5$ [676.80 g/mol]

R_f = 0.32 (hexane:ethyl acetate = 2:3), 0.35 (hexane:ethyl acetate = 2:3), 0.40 (hexane:ethyl acetate = 3:7 (v/v)).

m.p. = 116-119 °C.

HPLC-MS (EI+): t_R = 8.919 min (JK_35to90); m/z (%) 699.25 (10.7) $[M+Na]^+$, 677.3 (100.0) $[M+H]^+$, 675.7 (0.2), 649.4 (0.3), 631.8 (0.2), 512.4 (0.2), 500.1 (0.3), 272.2 (0.2), 265.9 (0.4), 249.1 (0.2), 242.9 (0.2).

^{1}H NMR (500 MHz, CDCl$_3$) δ: 7.77 (m, 6H, arom.; 2H (Bz), 2H (Phe), 2H (Fmoc)), 7.63 – 7.56 (m, 3H, arom.; 2H (Fmoc), 1H (Bz)), 7.48 (t, J = 7.5 Hz, 2H, arom. (Bz)), 7.39 (m, 2H, arom.(Fmoc)), 7.30 (m, 4H, arom.; 2H (Fmoc), 2H (Phe)), 7.19 (d, J = 8.5 Hz, 2H, arom. (Ph)), 6.93 (d, J = 8.5 Hz, 2H, arom. (Ph)), 5.36 (d, J = 8.0 Hz, 1H, N**H**), 4.95 (dd, J = 14.0, 5.5 Hz, 1H, C**H**COO), 4.53 (dd, J = 11.0, 7.0 Hz, 1H, OC**H**$_a$H$_b$), 4.43 (dd, J = 10.5, 7.0 Hz, 1H, OCH$_a$**H**$_b$), 4.23 (t, J = 7.0 Hz, 1H, C**H** (Fmoc)), 3.42 (m, 2H, NC**H**$_2$C≡CH), 3.36 (d, J = 6.0 Hz, 2H C**H**$_2$CHCO), 3.10 – 2.87 (m, 2H, C**H**$_a$H$_b$CHN), 2.49 – 2.33 (m, 4H: NC**H**$_3$ (s, 3H), CH$_a$**H**$_b$CHN (1H)), 2.24 (t, J = 2.5 Hz, 1H), 0.96 (d, J = 6.5 Hz, 3H, C**H**$_3$).

^{13}C NMR (125 MHz, CDCl$_3$) δ 196.23 (**C**=O Bpa), 169.88 (**C**=O), 155.49 (**C**=O), 148.28 (**C**$_{Ar}$ Ph), 143.67 (**C**$_{Ar}$ Fmoc), 143.55 (**C**$_{Ar}$ Fmoc), 141.33 (**C**$_{Ar}$ Fmoc), 141.29 (**C**$_{Ar}$ Fmoc), 140.41 (**C**$_{Ar}$ Bpa), 138.46 (**C**$_{Ar}$ Ph), 137.49 (**C**$_{Ar}$ Bpa), 136.55 (**C**$_{Ar}$ Bpa), 132.45 (**C**$_{Ar}$ Bpa), 130.51 (**C**$_{Ar}$ Bpa), 130.30 (**C**$_{Ar}$ Ph), 129.96 (**C**$_{Ar}$ Bpa), 129.49 (**C**$_{Ar}$ Bpa), 128.29 (**C**$_{Ar}$ Bpa), 127.77 (**C**$_{Ar}$ Fmoc), 127.07 (**C**$_{Ar}$ Fmoc), 125.00 (**C**$_{Ar}$ Fmoc), 124.93 (**C**$_{Ar}$ Fmoc), 120.81 (**C**$_{Ar}$ Ph), 120.03 (**C**$_{Ar}$ Fmoc), 80.25 (**C**≡CH), 72.60 (C≡**C**H), 66.95 (**C**$_q$ Fmoc), 59.17 (**C**$_q$), 54.63 (**C**$_q$ Bpa), 47.13 (OC**H**$_2$), 43.15 (N**C**H$_2$C≡CH), 39.19 (Ph**C**H$_2$CH), 38.22 (N**C**H$_3$), 37.38 (Phe**C**H$_2$CH), 14.99 (**C**H$_3$).

HRMS (EI) calcd for $C_{44}H_{40}N_2O_5$ 677.3016 $[M+H]^+$, found 677.3031.

7.1.6 Synthesis of NBD-based fluorescent tags

7.1.6.1 *N*-(4-Nitrobenz-2-oxa-1,3-diazol-7-yl)aminocaproic acid (28)
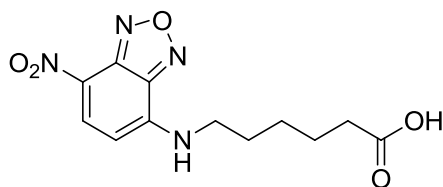
To a bright yellow solution of 1.996 g 4-chloro-7-nitrobenz-2-oxa-1,3-diazole (4-chloro-7-nitrobenzofurazan, NBD chloride) (10.0 mmol, 1.0 eq) in 100 mL dry, degassed and argon purged methanol 3.231 g *N,N'*-diisopropylethylamine (DIEA) (4.35 mL, 25.0 mmol, 2.5 eq) were added at once followed by a slow, over an hour addition of 1.574 mg 6-aminohexanoic acid (aminocaproic acid) (12.0 mmol, 1.2 eq) at 0 °C (ice-water bath) and under argon atmosphere. The color of the reaction mixture changed from yellow to dark brown. The reaction mixture was stirred overnight (ca. 20 h) at RT under inert atmosphere. The reaction progress was controlled by a TLC analysis. When TLC control indicated the full consumption of the starting material the solvent was removed *in vacuo* and the crude product (brown oil) was purified by gradient flash column chromatography (cyclohexane ethyl acetate = 1:1 (v/v), ethyl acetate and ethyl acetate:MeOH 10:1 (v/v), 350 g silica gel, size: 31.0 x 5.0 cm). The product was recrystallized from methanol-water mixture to give 2.355 g (8.0 mmol, 80%) *N*-(4-nitrobenz-2-oxa-1,3-diazol-7-yl)aminocaproic acid (**28**) as brown crystals.

$C_{12}H_{14}N_4O_5$ [294.26 g/mol]

R_f = 0.05 (ethyl acetate:cyclohexane = 3:1 (v/v)), 0.38 (ethyl acetate), 0.61 (ethyl acetate:MeOH = 10:1 (v/v)) (yellow fluorescent spots under 366 nm UV).

m.p. = 159-161 °C (brown crystals)

HPLC-MS (EI+): t_R = 5.199 min (JK_35to90); m/z (%): 333.1 (33.4) $[M+K]^+$, 317.1 (32.5) $[M+Na]^+$, 295.1 (100.0) $[M+H]^+$, 284.2 (6.4), 259. 2 (8.0), 193.0 (3.3), 105.1 (2.1).

^{1}H NMR (300 MHz, DMSO-d$_6$): δ = 12.00 (s, 1H; COO**H**), 9.54 (s, 1H, N**H**), 8.49 (d, *J* = 8.7 Hz, 1H; C**H** NBD), 6.40 (d, *J* = 9.0 Hz, 1H; C**H** NBD), 3.45 (s, 2H, NHC**H**$_2$), 2.22 (t, *J* = 7.2 Hz, 2H, C**H**$_2$CO), 1.68 (m, 2H, NHCH$_2$C**H**$_2$), 1.55 (m, 2H, C**H**$_2$CH$_2$CO), 1.38 (m, 2H, NHCH$_2$CH$_2$C**H**$_2$).

^{13}C NMR (75 MHz, DMSO-d$_6$): δ = 174.43 (**C**=O), 145.19 (**C**$_{NBD}$), 144.44 (**C**$_{NBD}$), 144.18 (**C**$_{NBD}$), 137.86 (**C**$_{NBD}$), 120.45 (**C**$_{NBD}$), 99.08 (**C**$_{NBD}$), 48.59 (NH**C**H$_2$), 33.61 (**C**H$_2$COOH), 27.38 (**C**H$_2$ Aca), 25.97 (**C**H$_2$ Aca), 24.18 (**C**H$_2$ Aca).

The spectral data are identical to those published previously.[298]

Synonyms: 6-(7-Nitrobenzofurazan-4-ylamino)hexanoic   acid,   6-(7-Nitro-2,1,3-benzoxadiazol-4-ylamino)hexanoic acid

7.1.6.2 *N*-(4-Nitrobenz-2-oxa-1,3-diazol-7-yl)aminocaproic acid *N*-hydroxysuccimidyl ester (29)
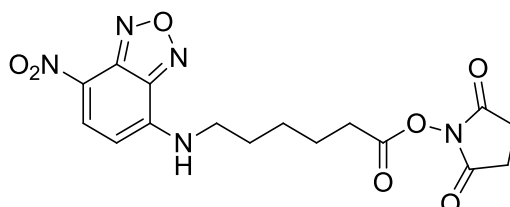
2.355 g *N*-(4-Nitrobenz-2-oxa-1,3-diazol-7-yl) aminocaproic acid (**28**) (8.0 mmol, 1.0 eq) were dissolved in 200 mL dry, degassed and argon purged THF forming a yellow solution, which was cooled down to 0 °C. 1.381 g *N*-Hydroxysuccinimide (NHS) (12.0 mmol, 1.5 eq) were then added followed by 1.106 g *N*-(3-dimethylaminopropyl)-*N*'-ethylcarbodiimide (EDC) (1.261 mL, 9.6 mmol, 1.2 eq). The reaction was allowed to reach RT and stirred overnight (ca. 17 h) at RT under inert atmosphere. The reaction progress was controlled by a TLC analysis. When a TLC control indicated the full consumption of the starting material, the solvent was removed under reduced pressure and the residue was dissolved in 250 mL ethyl acetate and washed with water (2 x 150 mL), saturated NaHCO$_3$ (1 x 150 mL), brine (1 x 150 mL) and dried over anhydrous Na$_2$SO$_4$. The solvent was then removed *in vacuo* and crude

product was purified by flash column chromatography (cyclohexane:ethyl acetate = 3:2 to 1:4 (v/v), 200 g silica gel, size: 26.0 x 4.0 cm) yielding 2.451 g (6.26 mmol, 80%) *N*-(4-nitrobenz-2-oxa-1,3-diazol-7-yl)aminocaproic acid *N*-hydroxysuccimidyl ester (**29**) as a dark yellow solid.

$C_{16}H_{17}N_4O_7$ [391.33 g/mol]

R_f = 0.29 (cyclohexane:ethyl acetate = 2:3 (v/v)), 0.46 (cyclohexane:ethyl acetate = 1:3 (v/v)), 0.16 (cyclohexane:ethyl acetate = 1:1 (v/v)) (yellow fluorescent spots under 366 nm UV).

m.p. = 180-183 °C (dark yellow solid).

HPLC-MS (EI+): t_R = 6.879 min (JK_35to90); m/z (%) 392.20 (100.0) [M]$^+$, 356.15 (4.9), 354.20 (3.9), 346.20 (12.1), 284.25 (4.1), 282.30 (2.6), 259.10 (3.6), 105.05 (2.3).

^{1}H NMR (300 MHz, DMSO-d$_6$): δ = 9.54 (s, 1H, N**H**), 8.50 (d, *J* = 8.7 Hz, 1H; C**H** NBD), 6.41 (d, *J* = 9.0 Hz, 1H; C**H** NBD), 3.47 (s, 2H, NHC**H**$_2$), 2.80 (s, 4H, 2 x C**H**$_2$ NHS), 2.69 (t, ^{3}*J* = 7.2 Hz, 2H, C**H**$_2$CO), 1.70 (m, 4H, NHCH$_2$C**H**$_2$, C**H**$_2$CH$_2$CO), 1.49 (m, 2H, NHCH$_2$CH$_2$C**H**$_2$).

^{13}C NMR (75 MHz, DMSO-d$_6$): δ = 170.20 (**C**=O NHS), 168.90 (**C**=O), 145.14 (**C**$_{NBD}$), 144.41 (**C**$_{NBD}$), 144.13 (**C**$_{NBD}$), 137.86 (**C**$_{NBD}$), 120.52 (**C**$_{NBD}$), 99.09 (**C**$_{NBD}$), 43.07 (NH**C**H$_2$), 30.07 (**C**H$_2$CO), 27.06 (**C**H$_2$ Aca), 25.42 (**C**H$_2$ Aca, **C**H$_2$ NHS), 23.87 (**C**H$_2$ Aca).

HRMS (DI-EI) calcd for $C_{16}H_{17}N_5O_7$ [M$^+$] 391.1128 found 391.1129.

Synonyms: 6-(7-Nitrobenzofurazan-4-ylamino)hexanoic acid *N*-hydroxysuccimidyl ester, 6-(7-Nitro-2,1,3-benzoxadiazol-4-ylamino)hexanoic acid *N*-hydroxysuccimidyl ester.

7.1.6.3 *N*-(4-Nitrobenz-2-oxa-1,3-diazol-7-yl) aminocaproic *N'*-propargylamide

(32) NBD-Alk
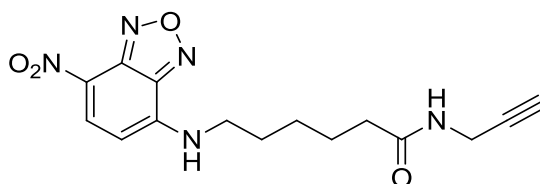
To a yellow solution of 391 mg *N*-(4-nitrobenz-2-oxa-1,3-diazol-7-yl)aminocaproic acid *N*-hydroxysuccimidyl ester (**29**) (1.0 mmol, 1.0 eq) and 138 mg propargylamine (160 µL, 2.5 mmol, 2.5 eq) in 15 mL dry DMF 283 mg triethylamine (390 µL, 2.8 mmol, 2.8 eq) were added. The color of the reaction mixture changed from yellow to orange. The reaction mixture was stirred for 4h at RT under argon atmosphere. The reaction progress was controlled by a TLC analysis. When a TLC control indicated the full consumption of the starting material the reaction mixture was concentrated *in vacuo* and the resulting residue dissolved in 50 mL ethyl acetate and washed with water (3 x 20 mL) and brine (10 mL). The organic phase was dried over anhydrous Na_2SO_4. The solvent was removed under reduced pressure and the crude product was purified by flash column chromatography (cyclohexane:ethyl acetate = 3:2 to 1:3 (v/v), 30 g silica gel, size: 18.5 x 2.5 cm) yielding 301 mg (0.91 mmol, 91%) *N*-(4-nitrobenz-2-oxa-1,3-diazol-7-yl)aminocaproic *N'*-propargylamide (**32**) (**NBD-Alk**) as an orange solid.

$C_{15}H_{17}N_5O_4$ [331.32 g/mol]

R_f = 0.30 (cyclohexane:ethyl acetate = 3:1 (v/v)) (yellow fluorescent spots under 366 nm UV).

m.p. = 136-138 °C (orange solid).

HPLC-MS (EI+): t_R = 6.218 min (JK_35to90); m/z (%) 370.1 (11.0) $[M+K]^+$, 354.2 (38.2) $[M+Na]^+$, 332.2 (100.0) $[M]^+$, 286.2 (9.1), 231.1 (1.1).

^{1}H NMR (300 MHz, DMSO-d_6): δ = 9.54 (s, 1H, N**H**CH$_2$), 8.49 (d, *J* = 8.7 Hz, 1H; C**H** NBD), 8.22 (m, 1H, CON**H**), 6.39 (d, *J* = 8.7 Hz, 1H, C**H** NBD), 3.83 (d, *J* = 2.7 Hz, 2H, C**H**$_2$C≡CH),

3.44 (s, 2H, NHC**H**$_2$ Aca), 3.07 (s, 1H, CH$_2$C≡C**H**), 2.09 (t, J = 6.9 Hz, 2H, C**H**$_2$CO), 1.66 (m, 2H, NHCH$_2$C**H**$_2$ Aca), 1.54 (m, 2H, C**H**$_2$CH$_2$CO), 1.35 (m, 2H, NHCH$_2$CH$_2$C**H**$_2$ Aca).

^{1}H NMR (500 MHz, DMSO-d$_6$): δ = 9.54 (s, 1H, N**H**CH$_2$), 8.50 (d, ^3J = 9.0 Hz, 1H; C**H** NBD), 8.22 (t, J = 5.5 Hz, 1H, CON**H**), 6.40 (d, J = 9.0 Hz, 1H; C**H** NBD), 3.82 (dd, J = 5.5, 2.5 Hz, 2H, C**H**$_2$C≡CH), 3.45 (s, 2H, NHC**H**$_2$ Aca), 3.06 (t, J = 2.5 Hz 1H, CH$_2$C≡C**H**), 2.09 (t, J = 7.0 Hz, 2H, C**H**$_2$CO), 1.67 (dt, J = 14.7, 7.3 Hz, 2H, NHCH$_2$C**H**$_2$ Aca), 1.54 (dt, 2H, J = 15.1, 7.5 Hz, C**H**$_2$CH$_2$CO), 1.34 (m, 2H, NHCH$_2$CH$_2$C**H**$_2$ Aca).

^{13}C NMR (75 MHz, DMSO-d$_6$): δ = 171.74 (**C**=O), 145.12 (**C**$_{NBD}$), 144.39 (**C**$_{NBD}$), 144.14 (**C**$_{NBD}$), 137.89 (**C**$_{NBD}$), 120.49 (**C**$_{NBD}$), 99.06 (**C**$_{NBD}$), 81.32 (**C**≡CH), 72.76 (C≡**C**H), 43.23 (NH**C**H$_2$), 34.91 (**C**H$_2$CO), 27.70 (**C**H$_2$ Aca), 27.38 (**C**H$_2$C≡CH), 26.02 (**C**H$_2$ Aca), 24.75 (**C**H$_2$ Aca).

HRMS (DI-EI) calcd for C$_{15}$H$_{17}$N$_5$O$_4$ [M$^+$] 331.1281 found 331.1293.

Synonyms: 6-(7-Nitrobenzofurazan-4-ylamino)-*N*-(prop-2-ynyl)hexanamide, 6-(7-Nitro-2,1,3-benzoxadiazol-4-ylamino)-*N*-(prop-2-ynyl)hexanamide.

7.1.6.4 *N*-(4-Nitrobenz-2-oxa-1,3-diazol-7-yl) aminocaproic *N'*-(hex-5-ynyl)amide (33) NBD-AlkC6
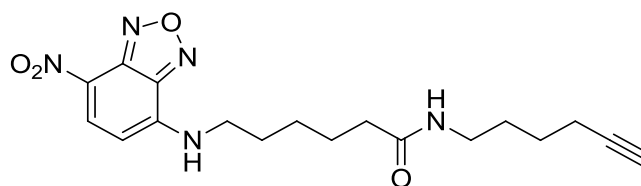
To a yellow solution of 156 mg *N*-(4-nitrobenz-2-oxa-1,3-diazol-7-yl)aminocaproic acid *N*-hydroxysuccimidyl ester (**29**) (0.40 mmol, 1.0 eq) and 93 mg 6-amino-hexyne (0.96 mmol, 2.5 eq) in 6 mL dry DMF 114 mg triethylamine (156 µL, 1.12 mmol, 2.8 eq) were added. The color of the reaction mixture changed from yellow to orange. The reaction mixture was stirred for 3 h at RT under argon atmosphere. The reaction progress was controlled by a TLC analysis. When a TLC control indicated the full consumption of the starting material the

reaction mixture was concentrated *in vacuo* and the resulting residue dissolved in 25 mL ethyl acetate and washed with water (3 x 15 mL) and brine (10 mL). The organic phase was dried over anhydrous Na_2SO_4. The solvent was removed under reduced pressure and the crude product was purified by flash column chromatography (cyclohexane:ethyl acetate = 3:2 to 1:3 (v/v), 7 g silica gel, size: 9.0 x 1.5 cm) yielding 65 mg (0.17 mmol, 44%) *N*-(4-nitrobenz-2-oxa-1,3-diazol-7-yl)aminocaproic *N'*-(hex-5-ynyl)amide (**33**) (**NBD-AlkC6**) as a red solid.

$C_{18}H_{23}N_5O_4$ [373.41 g/mol]

R_f = 0.20 (cyclohexane:ethyl acetate = 3:1 (v/v)) (yellow fluorescent spots under 366 nm UV).

m.p. = 140-142 °C (red solid)

HPLC-MS (EI+): t_R = 6.848 min (JK_35to90); m/z (%) 396.2 (50.8) $[M+Na]^+$, 374.2 (100.0) $[M]^+$, 328.2 (19.8), 311.3 (0.9), 246.3 (0.6), 100.3 (0.2).

^{1}H NMR (300 MHz, DMSO-d$_6$): δ = 9.54 (s, 1H, N**H**CH$_2$ Aca), 8.50 (d, *J* = 8.4 Hz, 1H; C**H** NBD), 7.75 (s, 1H, CON**H**), 6.40 (d, *J* = 9.0 Hz, 1H; C**H** NBD), 3.45 (s, 2H, NHC**H**$_2$ Aca), 3.01 (d, *J* = 5.7 Hz, 2H, CONHC**H**$_2$), 2.73 (s, 1H, CH$_2$C≡C**H**), 2.13 (s, 2H, C**H**$_2$C≡CH), 2.05 (t, *J* = 7.2 Hz, 2H, CH$_2$C**H**$_2$CO Aca), 1.67 (m, 2H, NHCH$_2$C**H**$_2$ Aca), 1.60-1.26 (m, 8H, C**H**$_2$CH$_2$CO Aca, NHCH$_2$CH$_2$C**H**$_2$ Aca, C**H**$_2$C**H**$_2$CH$_2$C≡CH).

^{1}H NMR (500 MHz, DMSO-d$_6$): δ = 9.54 (s, 1H, N**H**CH$_2$ Aca), 8.50 (d, *J* = 9.5 Hz, 1H; C**H** NBD), 7.75 (s, 1H, CON**H**), 6.40 (d, *J* = 9.0 Hz, 1H; C**H** NBD), 3.45 (s, 2H, NHC**H**$_2$ Aca), 3.01 (dd, *J* = 12.5, 6.0 Hz, 2H, CONHC**H**$_2$), 2.74 (t, *J* = 2.5 Hz, 1H, CH$_2$C≡C**H**), 2.14 (dt, 2H, *J* = 6.5, 2.5 Hz C**H**$_2$C≡CH), 2.05 (t, *J* = 7.5 Hz, 2H, CH$_2$C**H**$_2$CO Aca), 1.67 (m, 2H, NHCH$_2$C**H**$_2$ Aca), 1.53 (m, 2H, C**H**$_2$CH$_2$CO Aca), 1.42 (m, 4H, C**H**$_2$C**H**$_2$CH$_2$C≡CH), 1.34 (m, 2H, NHCH$_2$CH$_2$C**H**$_2$ Aca).

^{13}C NMR (75 MHz, DMSO-d$_6$): δ = 171.78 (**C**=O), 145.16 (**C**$_{NBD}$), 144.42 (**C**$_{NBD}$), 144.18 (**C**$_{NBD}$), 137.92 (**C**$_{NBD}$), 120.50 (**C**$_{NBD}$), 99.08 (**C**$_{NBD}$), 84.35 (**C**≡CH), 71.21 (C≡**C**H), 43.26

(NBD-NH**C**H$_2$), 37.74 (CONH**C**H$_2$), 35.27 (**C**H$_2$CO), 28.29 (**C**H$_2$), 27.42 (**C**H$_2$), 26.06 (**C**H$_2$), 25.38 (**C**H$_2$), 24.96 (**C**H$_2$), 17.34 (**C**H$_2$C≡CH).

HRMS (DI-EI) calcd for C$_{18}$H$_{23}$N$_5$O$_4$ [M$^+$] 373.1750 found 373.1737.

Synonyms: 6-(7-Nitrobenzofurazan-4-ylamino)- *N*-(hex-5-ynyl)hexanamide, 6-(7-Nitro-2,1,3-benzoxadiazol-4-ylamino)-*N*-(hex-5-ynyl)hexanamide.

7.1.6.5 *N*-(4-Nitrobenz-2-oxa-1,3-diazol-7-yl) aminocaproic *N'*-(3-azidopropyl) amide (35) NBD-N$_3$
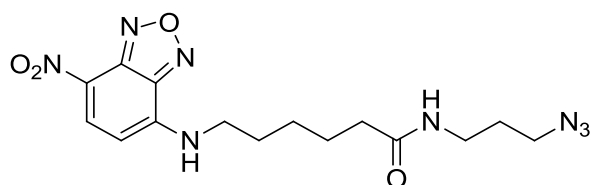
To a yellow solution of 117 mg *N*-(4-nitrobenz-2-oxa-1,3-diazol-7-yl)aminocaproic acid *N*-hydroxysuccimidyl ester (**29**) (0.30 mmol, 1.0 eq) and 75 mg propargylamine (0.75 mmol, 2.5 eq) in 5 mL dry DMF 85 mg triethylamine (62 µL, 0.84 mmol, 2.8 eq) were added. The color of the reaction mixture has changed from yellow to orange. The reaction mixture was stirred overnight at RT under argon atmosphere. The reaction progress was controlled by a TLC analysis. When a TLC control indicated the full consumption of the starting material the reaction mixture was concentrated *in vacuo* and the resulting residue dissolved in 10 mL ethyl acetate and washed with water (3 x 10 mL) and brine (10 mL). The organic phase was dried over anhydrous Na$_2$SO$_4$. The solvent was removed under reduced pressure and the crude product was purified by flash column chromatography (cyclohexane:ethyl acetate = 3:2 to 1:3 (v/v), 20 g silica gel, size: 14.0 x 2.5 cm) yielding 89 mg (0.24 mmol, 79%) *N*-(4-nitrobenz-2-oxa-1,3-diazol-7-yl)aminocaproic *N'*-(3-azidopropyl)amide (**35**) (**NBD-N$_3$**) as an orange solid.

$C_{15}H_{20}N_8O_4$ [376.37 g/mol]

R_f = 0.13 (cyclohexane:ethyl acetate = 3:1 (v/v)) (yellow fluorescent spots under 366nm UV).

m.p. = 95-97 °C (orange solid)

HPLC-MS (EI+): t_R = 6.673 min (JK_35to90); m/z (%) 399.2 (44.5) $[M+Na]^+$, 377.1 (100.0) $[M+H]^+$, 349.2 (2.7), 331.3 (11.2), 320.3 (0.9), 248.1 (0.8).

^{1}H NMR (300 MHz, DMSO-d$_6$): δ = 9.53 (s, 1H, N**H**CH$_2$ Aca), 8.49 (d, J = 8.7 Hz, 1H; C**H** NBD), 7.81 (t, J = 5.1 Hz, 1H, CON**H**), 6.39 (d, J = 9.0 Hz, 1H; C**H** NBD), 3.45 (s, 2H, NHC**H**$_2$CH$_2$ Aca), 3.31 (t, J = 6.6 Hz, 2H, C**H**$_2$N$_3$), 3.07 (dd, J = 12.6 Hz, 6.6 Hz, 2H, CONHC**H**$_2$), 2.06 (t, J = 7.2 Hz, 2H, C**H**$_2$CO), 1.75 – 1.45 (m, 6H), (m, 6H, NHCH$_2$C**H**$_2$ Aca, C**H**$_2$CH$_2$CO Aca, C**H**$_2$CH$_2$N$_3$), 1.36 (m, 2H, NHCH$_2$CH$_2$C**H**$_2$ Aca).

^{13}C NMR (75 MHz, DMSO-d$_6$): δ = 171.98 (**C**=O), 145.16 (**C**$_{NBD}$), 144.41 (**C**$_{NBD}$), 144.16 (**C**$_{NBD}$), 137.92 (**C**$_{NBD}$), 120.52 (**C**$_{NBD}$), 99.07 (**C**$_{NBD}$), 48.41 (**C**H$_2$N$_3$), 43.24 (NH**C**H$_2$ Aca), 35.73 (CONH**C**H$_2$), 35.24 (**C**H$_2$CO), 28.44 (**C**H$_2$), 27.42 (**C**H$_2$), 26.05 (**C**H$_2$), 24.89 (**C**H$_2$).

HRMS (DI-EI) calcd for $C_{15}H_{20}N_8O_4$ $[M^+]$ 376.1608 found 376.1583.

Synonyms: 6-(7-Nitrobenzofurazan-4-ylamino)-*N*-(3-azidopropyl)hexanamide, 6-(7-Nitro-2,1,3-benzoxadiazol-4-ylamino)-*N*-(3-azidopropyl)hexanamide.

7.1.6.6 6-Amino-hexyne (31)
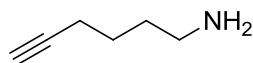
A solution of 15 mL lithium aluminium hydride (LAH, 1.0 M in diethyl ether, 15.0 mmol, 1.5 eq) in 20 mL dry, freshly distilled diethyl ether was prepared under argon atmosphere and allowed to cool down to 0 °C in an ice-water bath with stirring for 20 min. A solution of 931 mg hex-5-ynenitrile (1.05 mL, 10 mmol, 1.0 eq) in 5 mL diethyl ether was prepared under argon atmosphere and added dropwise, over an hour, to the LAH solution at 0 °C. The addition of hex-5-ynenitrile caused change from a clear colorless solution to a white slurry.

The reaction was kept for 15 min at 0 °C and subsequently left to warm up to RT and stirred overnight. After that, the reaction mixture was again cooled down to 0 °C and 0.57 mL distilled water was slowly added to the reaction mixture, followed by 0.57 mL 15% sodium hydroxide solution (w/w) and 1.71 mL distilled water to hydrolyze any remaining LAH (n-n-3n work-up). The mixture was left on stirring for 1 h and formed inorganic salts were separated by vacuum filtration through a Celite® pad, which was then washed well with diethyl ether. The organic filtrate was dried over anhydrous Na_2SO_4 and diethyl ether was carefully removed under reduced pressure yielding 900 mg 6-amino-hex-1-yne (**31**) (9.26 mmol, 93%, 85% purity) as colorless oil which was used for the next step without any further purification. Analytically pure sample was prepared by saturation of the solution of crude product in diethyl ether with gaseous HCl and precipitation of the amine as its hydrochloric salt. The white solid was collected by filtration and dried under vacuum.

$C_6H_{11}N$ [97.16 g/mol], hydrochloric salt $C_6H_{12}ClN$ [133.62 g/mol]

m.p. = 175-177 °C (white solid as hydrochloric salt).

GC-MS (EI): t_R = 3.09 min; m/z (%) 97.0 (1.6) [M$^+$], 96.0 (14.3) [M-H]$^+$, 82.0 (8.2), 77.0 (6.2), 69.0 (100.0), 56.0 (85.3) (free amine).

^{1}H NMR (300 MHz, CDCl$_3$): δ = 2.71 (m, 2H, C**H**$_2$NH$_2$), 2.20 (m, 2H, C**H**$_2$C≡CH), 1.94 (t, J = 2.6 Hz, 1H, C≡C**H**), 1.56 (m, 4H, C**H**$_2$C**H**$_2$CH$_2$C≡CH), 1.42 (brs, 2H, N**H**$_2$) (free amine).

^{1}H NMR (500 MHz, DMSO-d$_6$): δ = 8.00 (s, 3H, N**H**$_3$$^+$), 2.82 (t, J = 2.5 Hz, 1H, C≡C**H**), 2.77 (t, ^3J = 7.5 Hz, 2H, H$_3$NC**H**$_2$), 2.18 (td, J = 7.0, 2.5 Hz, 2H, C**H**$_2$C≡CH), 1.64 (m, 2H, CH$_2$C**H**$_2$CH$_2$), 1.49 (m, 2H, C**H**$_2$CH$_2$C≡CH) (hydrochloric salt).

^{13}C NMR (75 MHz, DMSO-d$_6$): δ = 84.02 (**C**≡CH), 71.58 (C≡**C**H), 38.19 (H$_3$N**C**H$_2$), 26.12 (H$_3$NCH$_2$**C**H$_2$), 24.88 (**C**H$_2$CH$_2$C≡CH), 17.31 (**C**H$_2$C≡CH) (hydrochloric salt).

IR (film) cm^{-1}: 3295, 2936, 2862, 2360, 2341, 1738, 1592, 1455, 1433. 1366, 1229, 1071 (free amine).

The spectral data are identical to those published previously.[35,300]

7.1.6.7 3-Azido-propylamine (34)

$$H_2N\diagdown\diagup N_3$$
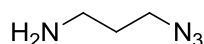
To a solution of 2.189 g 3-bromopropylamine hydrobromide (10.0 mmol, 1.0 eq) in 15 mL distilled H_2O a solution (10 mL) of 1.95 g NaN_3 (30.0 mmol, 3.0 eq) in 10 mL distilled H_2O was added dropwise over 15 min. The resulting colorless solution was stirred overnight at 80 °C. After cooling to RT most of the water was removed *in vacuo* (ca. 2/3 of the total volume). The remaining solution was diluted with 35 mL diethyl ether. This biphasic mixture was cooled down to 0 °C in an ice-water bath and 2.75 g KOH pellets were added slowly over 15 min with vigorous stirring. Then the phases were separated and the water phase was additionally extracted with diethyl ether (2 x 20 mL). All organic layers were combined and dried over anhydrous Na_2SO_4. The solvent was then carefully removed under reduced pressure yielding 815 mg (83%) 3-azido-propylamine (**34**) as a yellowish liquid which was used in the next step without further purification.

$C_3H_8N_4$ [100.12 g/mol]

GC-MS (EI): t_R = 3.24 min; m/z (%) 100.9 (0.2) [M$^+$], 71.0 (100.0), 56.0 (50.1).

^{1}H NMR (300 MHz, CDCl$_3$): δ = 3.36 (t, *J* = 6.9 Hz, 2H, C**H**$_2$NH$_2$), 2.79 (t, *J* = 6.9 Hz, 2H, C**H**$_2$N$_3$), 1.73 (dd, *J* = 13.5, 6.9 Hz, 2H, CH$_2$C**H**$_2$CH$_2$), 1.33 (d, *J* = 1.0 Hz, 2H, N**H**$_2$).

^{13}C NMR (75 MHz, CDCl$_3$): δ = 49.27 (**C**H$_2$NH$_2$), 39.44 (**C**H$_2$N$_3$), 32.54 (**C**H$_2$).

IR (film) cm^{-1}: 3369, 2941, 2870, 2360, 2091, 1738, 1594, 1456, 1349, 1257, 1069.

The spectral data are identical to those published previously.[301]

7.1.7 Synthesis of TAMRA-based fluorescent tags

7.1.7.1 4-(Dimethylamino)-2-hydroxy-2',4'-dicarboxy-benzophenone (38) and 4-(dimethylamino)-2-hydroxy-2',5'-dicarboxy-benzophenone (39)
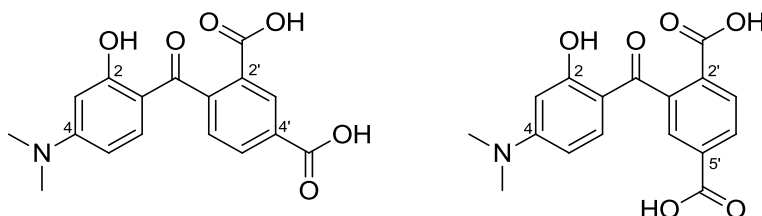
An oven dried, evacuated and argon flushed two-neck 250 mL round-bottom flask equipped with a condenser was charged with 5.49 g 3-dimethylaminophenol (40.0 mmol, 1.0 eq) and 140 mL dry toluene resulting in a dark brown solution, which was heated up to 60 °C. Then, pounded 9.22 g 1,3-dioxo-2-benzofuran-5-carboxylic acid (trimellitic anhydride) (48.0 mmol, 1.2 eq) were added portionwise with magnetic stirring and the reaction mixture was refluxed then for 24 h (oil bath ca. 130 °C). After cooling down to RT, the purple crystalline solid formed was collected by filtration, washed with toluene (3 x 30 mL), dissolved in 120 mL MeOH and refluxed for 10 min. Then, the mixture was cooled down to RT and glacial acetic acid (40 mL) was added and the mixture was concentrated under reduced pressure to dryness and dried under vacuum. Subsequently, the solid residue was dissolved in 80 mL MeOH, refluxed for 2 h and cooled down and kept at 4°C overnight. The crystals formed were collected by filtration and washed with 30 mL MeOH, dried under vacuum to yield 2.37 g (7.20 mmol, 18%) 4-(dimethylamino)-2-hydroxy-2',4'-dicarboxy-benzophenone (**38**) as purple solid. The mother liquid was concentrated *in vacuo* to dryness, refluxed with 60 mL concentrated acetic acid for 1 h and after cooling it down to RT, stored overnight at RT. The precipitated crystalline solid was collected by filtration and dried *in vacuo* at 120 °C to give a mixture of both isomers in ratio 1:2 = (**38**):(**39**). This was then recrystallized twice from boiling concentrated acetic acid, resulting in 1.45 g (4.40 mmol, 11%) 4-(dimethylamino)-2-hydroxy-2',5'-dicarboxy-benzophenone as orange crystalline solid (**39**) (purity 95% according to NMR).

4-(dimethylamino)-2-hydroxy-2',4'-dicarboxy-benzophenone (**38**):

$C_{17}H_{15}NO_6$ [329.30 g/mol]

R_f = 0.30 (Et_3N:MeOH:DCM = 5:10:85 (v/v/v)).

Decomp. > 240 °C (purple solid)

HPLC-MS (EI+): t_R = 1.896 min (JK_10to90); m/z (%) 368.0 (31.3) $[M+K]^+$, 352.0 (68.9) $[M+Na]^+$, 330.0 (100.0) $[M+H]^+$, 329.1 (2.8) $[M^+]$, 270.1 (5.4), 256.1 (5.8).

^1H NMR (300 MHz, DMSO-d_6) δ: 13.41 (brs, 2H, 2 x CO$_2$**H**), 12.36 (s, 1H, O**H**), 8.48 (s, 1H, H-3'), 8.20 (d, J = 6.6 Hz, 1H, H-5'), 7.53 (d, J = 7.2 Hz, 1H, H-6'), 6.80 (d, J = 8.7 Hz, 1H, H-6), 6.21 (d, J = 8.4 Hz, 1H, H-5), 6.11 (s, 1H, H-3), 3.01 (s, 6H, 2 x C**H**$_3$).

^{13}C NMR (75 MHz, DMSO-d_6) δ: 197.64 (**C**=O), 166.12 (2 x **C**=O, CO$_2$H), 164.23 (**C**$_{Ar}$-2), 155.84 (**C**$_{Ar}$-4), 143.75 (**C**$_{Ar}$-1'), 133.81 (**C**$_{Ar}$-6), 132.68 (**C**$_{Ar}$-5'), 131.67 (**C**$_{Ar}$-2' or **C**$_{Ar}$-4'), 130.71 (**C**$_{Ar}$-3'), 130.04 (**C**$_{Ar}$-2' or **C**$_{Ar}$-4'), 128.26 (**C**$_{Ar}$-6'), 109.48 (**C**$_{Ar}$-1), 104.51 (**C**$_{Ar}$-5), 97.03 (**C**$_{Ar}$-3), 39.59 (2 x C**H**$_3$).

The spectral data are identical to those published previously.[305]

(4-(dimethylamino)-2-hydroxy-2',5'-dicarboxy-benzophenone (**39**):

$C_{17}H_{15}NO_6$ [329.30 g/mol]

R_f = 0.38 (Et_3N:MeOH:DCM = 5:10:85 (v/v/v)).

Decomp. > 240 °C (yellow solid)

HPLC-MS (EI+): t_R = 0.951 min (JK_10to90); m/z (%) 361.2 (29.2) $[M+K]^+$, 352.0 (59.3) $[M+Na]^+$, 329.9 (100.0) $[M+H]^+$, 329.1 (4.2) $[M^+]$, 270.1 (5.7), 256.1 (5.4).

^1H NMR (300 MHz, DMSO-d_6) δ: 13.43 (brs, 2H), 12.40 (s, 1H), 8.13 (d, J = 8.1 Hz, 1H, H-4'), 8.05 (d, J = 8.1 Hz, 1H, H-3'), 7. 82 (s, 1H, H-6'), 6.86 (d, J = 9.0 Hz, 1H, H-6), 6.23 (d, J = 9.0, 1H, H-5), 6.12 (s, 1H, H-3), 3.01 (s, 6H, 2 x C**H**$_3$).

^{13}C NMR (75 MHz, DMSO-d$_6$) δ: 197.36 (**C**=O), 166.48 (2'-**C**O$_2$H), 166.06 (5'-**C**O$_2$H), 164.36 (**C**$_{Ar}$-2), 155.86 (**C**$_{Ar}$-4), 140.07 (**C**$_{Ar}$-1'), 133.89 (**C**$_{Ar}$-6), 133.70 (**C**$_{Ar}$-2'), 133.62 (**C**$_{Ar}$-5'), 130.38 (**C**$_{Ar}$-3'), 130.19 (**C**$_{Ar}$-4'), 128.21 (**C**$_{Ar}$-6'), 109.41 (**C**$_{Ar}$-1), 104.54 (**C**$_{Ar}$-5), 97.06 (**C**$_{Ar}$-3), 39.59 (2 x **CH**$_3$).

The spectral data are identical to those published previously.[305]

7.1.7.2 5-Carboxytetramethylrhodamine (5-TAMRA) (40)
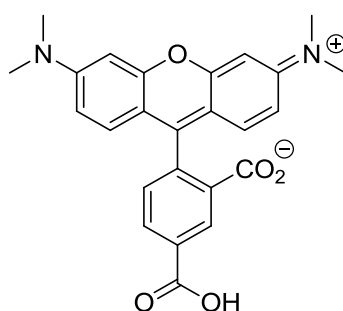
An oven dried, evacuated and argon flushed two-neck 100 mL round-bottom flask equipped with a condenser was charged with 659 mg 4-(dimethylamino)-2-hydroxy-2',4'-dicarboxy-benzophenone (**38**) (2.0 mmol, 1.0 eq) and 357 mg 3-dimethylaminophenol (2.6 mmol, 1.3 eq). By addition of 16 mL dry DMF a purple solution formed. Subsequently, trimethylsilylpolyphosphate (PPSE) solution (4.72 g, 4 mL) in 4 mL dry CHCl$_3$ was added under argon atmosphere and the reaction mixture was refluxed for 3 h. After that time the reaction mixture was cooled down to RT and solvents removed under reduced pressure and the residue dried *in vacuo*. Then, the residue was dissolved in 20 mL 5% NaHCO$_3$ and stirred at RT overnight. After that time, the solution was diluted with 40 mL distilled water and the product was precipitated with ca. 2 mL concentrated HCl. The product was collected by filtration and washed with water (ca. 20 mL). The product was dried *in vacuo* at 150 °C resulting in 847 mg (1.97 mmol, 98%) 5-carboxytetramethylrhodamine (5-TAMRA) (**40**) as a purple solid. The product was used in the next step without further purification.

$C_{25}H_{22}N_2O_5$ [430.45 g/mol]

R_f = 0.42 (Et_3N:MeOH:$CHCl_3$ = 5:20:75 (v/v/v), 0.39 (Et_3N:MeOH:DCM = 5:15:80 (v/v/v), 0.22 (Et_3N:MeOH:DCM = 5:10:85 (v/v/v)).

HPLC-MS (EI+): t_R = 5.111 min (JK_10to90); m/z (%) 431.1 (100.0) $[M+H]^+$, 430.2 (2.9), 417.1 (0.4), 316.6 (0.7), 256.0 (0.3).
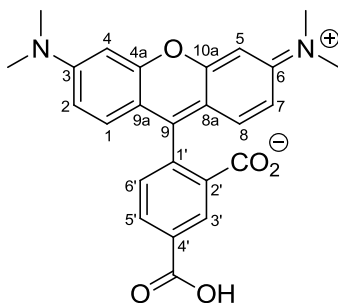
^{1}H NMR (300 MHz, MeOD-d_4, open chain numbering) δ: 8.88 (d, J = 1.2 Hz, 1H, H-3'), 8.39 (dd, J = 8.1, 1.2 Hz, 1H, H-5'), 7.50 (d, J = 8.1 Hz, 1H, H-6'), 7.12 (d, J = 9.6 Hz, 2H, H-1,8), 7.03 (dd, J = 9.6 Hz, 1.8 Hz, 2H, H-2,7), 6.91 (d, J = 1.8 Hz, 2H, H-4,5), 3.27 (s, 12H overlapping with MeOD-d_4, 4 x NC**H**$_3$).

^{13}C NMR (75 MHz, MeOD-d_4) δ: 168.06 (**C**=O, 4'-**C**O$_2$H), 167.59 (**C**=O, 2'-**C**O$_2^-$), 160.68 (**C**$_{Ar}$-9), 159.04 (2**C**, **C**$_{Ar}$-4a,10a), 158.96 (2**C**, **C**$_{Ar}$-3,6), 139.29 (**C**$_{Ar}$), 134.34 (**C**$_{Ar}$), 134.27 (**C**$_{Ar}$), 133.45 (2**C**, **C**$_{Ar}$-1,8), 133.41 (**C**$_{Ar}$), 131.98 (**C**$_{Ar}$), 131.94 (**C**$_{Ar}$), 115.57 (2**C**, **C**$_{Ar}$-2,7), 114.66 (2**C**, **C**$_{Ar}$-8a,9a), 97.45 (2**C**, **C**$_{Ar}$-4,5), 40.94 (4 x **C**H$_3$).

The spectral data are identical to those published previously.[305]

7.1.7.3 6-Carboxytetramethylrhodamine (6-TAMRA) (41)
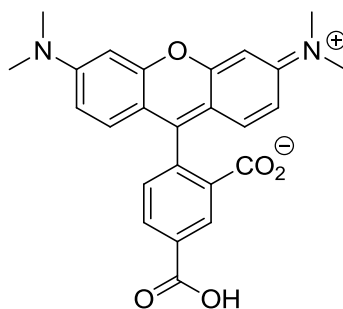
The reaction was performed in an analogous manner as described for 5-carboxytetramethylrhodamine (5-TAMRA) (**40**), only 4-(dimethylamino)-2-hydroxy-2',5'-dicarboxy-benzophenone (**39**) was used in place of 4-(dimethylamino)-2-hydroxy-2',4'-dicarboxy-benzophenone (**38**) resulting in 763 mg (1.77 mmol, 90%) 6-carboxytetramethylrhodamine (6-TAMRA) (**41**) as a purple solid.

$C_{25}H_{22}N_2O_5$ [430.45 g/mol]

R_f = 0.51 (Et_3N:MeOH:$CHCl_3$ = 5:20:75 (v/v/v) 0.57 (Et_3N:MeOH:DCM = 5:15:80 (v/v/v), 0.30 (Et_3N:MeOH:DCM = 5:10:85 (v/v/v)).

HPLC-MS (EI+): t_R = 5.111 min (JK_10to90); m/z (%) 431.1 (100.0) $[M+H]^+$, 429.7 (0.2), 416.3 (0.2), 270.0 (0.6), 256.0 (0.4).
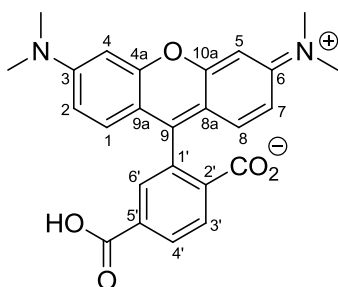
^{1}H NMR (300 MHz, MeOD-d_4) δ: 8.37 (brs, 2H, H-3', H-4'), 7.95 (brs, 1H, H-6'), 7.13 (d, J = 9.6 Hz, 2H, H-1,8), 7.02 (dd, J = 9.6 Hz, 2.1 Hz, 2H, H-2,7), 6.93 (d, J = 2.1 Hz, 2H, H-4,5), 3.25 (s, 12H, overlapping with MeOD-d_4, 4 x N**C**H$_3$).

^{13}C NMR (75 MHz, MeOD-d_4) δ: δ 167.82 (**C**=O, 5'-CO_2H) , 167.65 (**C**=O, 2'-CO_2H), 160.50 (**C**$_{Ar}$-9), 159.07 (2**C**, **C**$_{Ar}$-4a,10a), 158.94, (2**C**, **C**$_{Ar}$-3,6), 136.53 (**C**$_{Ar}$), 135.89 (**C**$_{Ar}$), 135.26

($\mathbf{C}_{Ar}$), 132.72 (2**C**, $\mathbf{C}_{Ar}$-1,8), 132.31 ($\mathbf{C}_{Ar}$), 132.25 ($\mathbf{C}_{Ar}$), 132.00 ($\mathbf{C}_{Ar}$), 115.57 (2**C**, $\mathbf{C}_{Ar}$-2,7), 114.89 (2**C**, $\mathbf{C}_{Ar}$-8a,9a), 97.48 (2**C**, $\mathbf{C}_{Ar}$-4,5), 40.94 (4 x **CH**$_3$).

The spectral data are identical to those published previously.[305]

7.1.7.4 5(6)-*N*-(3-Azidopropyl)-carboxamidotetramethylrhodamine (37) (TAMRA-N$_3$)
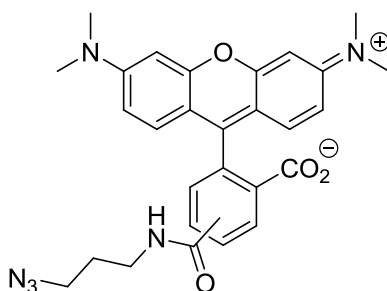
An oven dried, evacuated and argon flushed two-neck 25 mL round-bottom flask was charged with 35.5 mg 5(6)-carboxytetramethylrhodamine (5(6)-TAMRA) (0.07 mmol, 1.0 eq, 85% purity). Addition of 1.4 mL dry DMF resulted in a dark purple solution (0.05 M). Subsequently, 36.5 mg benzotriazol-1-yl-oxytripyrrolidinophosphonium hexafluorophosphate (PyBOP) (0.07 mmol, 1.0 eq) were added, followed by 18.1 mg *N,N'*-diisopropylethylamine (DIEA) (0.14 mmol, 23.2 μL, 2.0 eq) giving a deep red solution. After 10 min stirring at RT, 28.2 mg 3-azidopropan-1-amine (**34**) (0.28 mmol, 4.0 eq) were added at once and the reaction mixture was stirred for 3 h at RT in the dark. The reaction progress was monitored by TLC analysis and when the consumption of the starting material was indicated, the solvent was removed *in vacuo* and the residue dried under vacuum. Then, the dark purple solid was dissolved in 10 mL DCM and washed with 10 mL saturated NaHCO$_3$. Then the water phase was extracted with DCM (2 x 5 mL). The combined organic layers were washed with brine (10 mL) and then dried over anhydrous Na$_2$SO$_4$. The solvent was removed *in vacuo* and the crude product purified by flash column chromatography on neutral alumina previously wetted with 7 wt % water. The crude product was dissolved in a minimal volume DCM and loaded on a column packed in CH$_2$Cl$_2$ (5 g neutral alumina, size: 7.0 x 1.2 cm). The

gradient up to 20% MeOH in DCM was used to elute the mixture of both isomers yielding 20 mg (0.04 mmol, 59%) 5(6)-*N*-(3-azidopropyl)-carboxamidotetramethylrhodamine (**37**) (**TAMRA-N₃**) as a deep red solid.

$C_{28}H_{28}N_6O_4$ [512.56 g/mol]

R_f = 0.50 and 0.29 (DCM:MeOH = 9:1 (v/v)), 0.32 and 0.15 (DCM:MeOH = 97:3 (v/v)) on silica TLC plate.

HPLC-MS (EI+): t_R = 6.404 and 6.491 min (JK_10to90); m/z (%) 532.2 (2.4) $[M+Na]^+$, 510.2 (100.0) $[M+H]^+$, 496.1 (1.6), 375.7 (1.2), 307.0 (1.4), 228.9 (1.2).

6-TAMRA-N₃   5-TAMRA-N₃
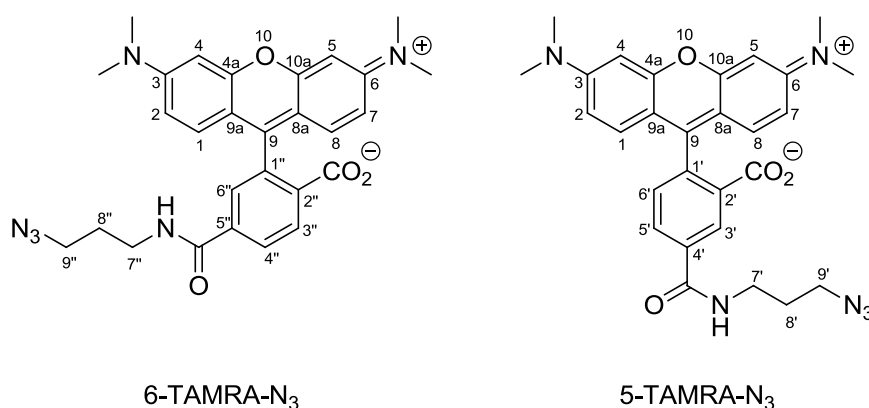
^{1}H NMR (500 MHz, MeOD-d₄, assignment includes both isomers) δ: 8.51 (d, *J* = 1.5 Hz, 1H, H-3'), 8.14 (d, *J* = 8.0 Hz, 1H, H-4''), 8.08 (dd, *J* = 8.0, 2.0 Hz, 1H, H-3''), 8.05 (dd, *J* = 8.0, 2.0 Hz, 1H, H-5'), 7.71 (d, *J* = 1.5 Hz, 1H, H-6''), 7.37 (d, *J* = 7.5 Hz, 1H, H-6'), 7.27 – 7.25 (2 x d, *J* = 9.5 Hz, 4H, H-1,8), 7.02 (dd, *J* = 9.5, 2.5 Hz, 4H, H-2,7), 6.93 (s, 4H, H-4,5), 3.54 (t, *J* = 7.0 Hz, 2H, NH**CH₂** (7')), 3.49 – 3.45 (m, 4H; 2H (N₃**CH₂** (9')), 2H, (NH**CH₂** (7''))), 3.40 (t, *J* = 7.0 Hz, 2H, N₃**CH₂** (9'')), 3.28 (s, 24H, 8 x N**CH₃**), 1.94 (m, 2H, CH₂**CH₂**CH₂ (8')), 1.89 (m, 2H, CH₂**CH₂**CH₂ (8'')).

^{13}C NMR (125 MHz, MeOD-d₄) δ: 172.49 (**C**=O, 2'-**CO₂⁻** or 2''-**CO₂⁻**), 172.41 (**C**=O, 2'-**CO₂⁻** or 2''-**CO₂⁻**), 169.25 (**C**=O, 4'-**C**ONH or 5''-**C**ONH), 168.75 (**C**=O, 4'-**C**ONH or 5''-**C**ONH), 162.18 (**C**$_{Ar}$-9), 162.04 (**C**$_{Ar}$-9), 159.11 (2**C**, **C**$_{Ar}$-4a,10a), 159.06 (2**C**, **C**$_{Ar}$-4a,10a), 158.75 (2**C**, **C**$_{Ar}$-3,6), 158.73 (2**C**, **C**$_{Ar}$-3,6), 144.57 (**C**$_{Ar}$), 142.14 (**C**$_{Ar}$), 137.11 (**C**$_{Ar}$), 136.93 (**C**$_{Ar}$), 136.32 (**C**$_{Ar}$), 134.03 (**C**$_{Ar}$), 132.73 (2**C**, **C**$_{Ar}$-1,8), 132.61 (2**C**, **C**$_{Ar}$-1,8), 131.03 (**C**$_{Ar}$), 130.85 (**C**$_{Ar}$), 129.58

(C_{Ar}), 129.44 (C_{Ar}), 129.39 (C_{Ar}), 129.35 (C_{Ar}), 115.04 (2**C**, C_{Ar}-2,7), 115.00 (2**C**, C_{Ar}-2,7), 114.82 (4**C**, C_{Ar}-8a,9a), 97.30 (4**C**, C_{Ar}-4,5), 50.24 (2**C**, **C**H$_2$N$_3$ (9' and 9'')), 40.81 (8 x **C**H$_3$), 38.58 (NH**C**H$_2$ (7' or 7'')), 38.53 (NH**C**H$_2$ (7' or 7'')), 29.83 (CH$_2$**C**H$_2$CH$_2$ (8' or 8'')), 29.71 (CH$_2$**C**H$_2$CH$_2$ (8' or 8'')).

The spectral data are identical to those published previously.[80]

7.1.7.5 5(6)-*N*-(Hex-5-yn-1-yl)-carboxamidotetramethylrhodamine (36)
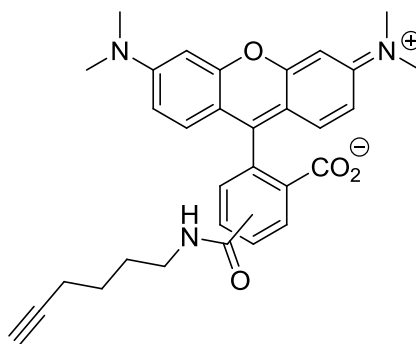
(TAMRA-Alk)

An oven dried, evacuated and argon flushed two-neck 25 mL round-bottom flask was charged with 35.5 mg 5(6)-carboxytetramethylrhodamine (5(6)-TAMRA) (0.07 mmol, 1.0 eq, 85% purity). Addition of 1.4 mL dry DMF resulted in a dark purple solution (0.05 M). Subsequently, 36.5 mg benzotriazol-1-yl-oxytripyrrolidinophosphonium hexafluorophosphate (PyBOP) (0.07 mmol, 1.0 eq) were added, followed by 18.1 mg *N,N'*-diisopropylethylamine (DIEA) (0.14 mmol, 23.2 µL, 2.0 eq) giving a deep red solution. After 10 min stirring at RT, 97.2 mg 5-hexyn-1-amine (**31**) (0.28 mmol, 4.0 eq) were added at once and the reaction mixture was stirred for 3 h at RT in the dark. The reaction progress was monitored by TLC analysis and when the consumption of the starting material was indicated, the solvent was removed *in vacuo* and the residue dried under vacuum. Then, the dark purple solid was dissolved in 10 mL DCM and washed with 10 mL saturated NaHCO$_3$. Then the water phase was extracted with DCM (2 x 5 mL). The combined organic layers were washed with brine (10 mL) and then dried over anhydrous Na$_2$SO$_4$. The solvent was removed *in vacuo* and the

crude product purified by flash column chromatography on neutral alumina previously wetted with 7 wt % water. The crude product was dissolved in a minimal volume DCM and loaded on a column packed in CH_2Cl_2 (5 g neutral alumina, size: 7.5 x 1.2 cm). The gradient up to 20% MeOH in DCM was used to elute the mixture of both isomers yielding 21 mg (0.04 mmol, 60%) 5(6)-N-(hex-5-yn-1-yl)-carboxamidotetramethylrhodamine (**36**) (**TAMRA-Alk**) as a deep red solid.

$C_{31}H_{31}N_3O_4$ [509.60 g/mol]

R_f = 0.46 and 0.27 (DCM:MeOH = 9:1 (v/v)), 0.29 and 0.12 (DCM:MeOH = 97:3 (v/v)) on silica TLC plate.

HPLC-MS (EI+): t_R = 6.109 and 6.201 min (JK_10to90); m/z (%) 535.1 (2.4) $[M+Na]^+$, 513.2 (100.0) $[M+H]^+$, 499.2 (43.0), 485.2 (3.0), 266.2 (6.4), 261.1 (13.3).

6-TAMRA-Alk   5-TAMRA-Alk
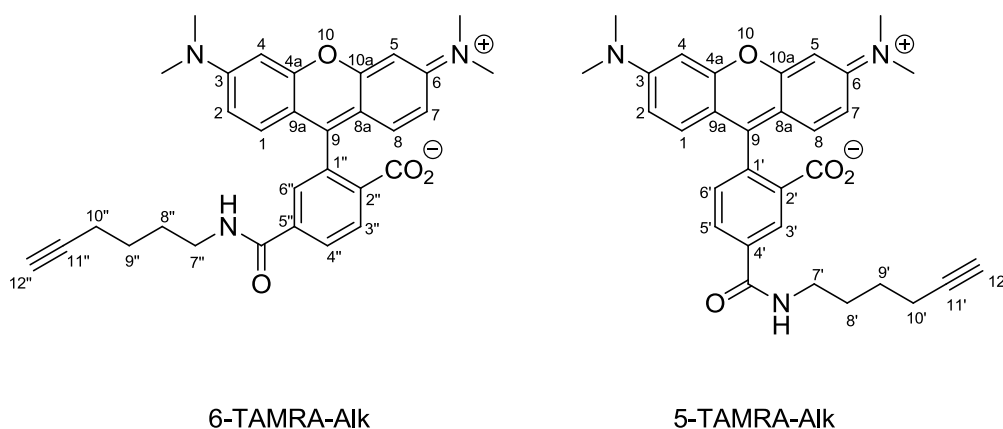
^{1}H NMR (500 MHz, MeOD-d_4, assignment includes both isomers) δ: 8.50 (d, J = 1.5 Hz, 1H, H-3'), 8.14 (d, J = 8.0 Hz, 1H, H-4''), 8.07 (dd, J = 8.0, 2.0 Hz, 1H, H-3''), 8.04 (dd, J = 8.0, 1.5 Hz, 1H, H-5'), 7.70 (d, J = 1.5 Hz, 1H, H-6''), 7.36 (d, J = 8.0 Hz, 1H, H-6'), 7.27 – 7.25 (2 x d, J = 9.5 Hz, 4H, H-1,8), 7.02 (dd, J = 9.5, 2.5 Hz, 4H, H-2,7), 6.92 (s, 4H, H-4,5), 3.48 (t, J = 7.0 Hz, 2H, NH**CH$_2$** (7')), 3.40 (t, J = 7.0 Hz, 2H, NH**CH$_2$** (7'')), 3.28 (s, 24H, 8 x **CH$_3$**), 2.28 (td, J = 7.0, 3.0 Hz, 2H, **CH$_2$**C≡CH (10')), 2.25 – 2.20 (m, 4H; 2H (**CH$_2$**C≡CH (10'')), 2 x 1H (**CH$_2$**C≡**CH**)), 1.80 (p, J = 7.5 Hz, 2H, NHCH$_2$**CH$_2$** (8')), 1.73 (p, J = 7.0 Hz, 2H, NHCH$_2$**CH$_2$** (8'')), 1.65 (p, J = 7.0 Hz, 2H, **CH$_2$**CH$_2$C≡CH (9')), 1.58 (p, J = 7.0 Hz, 2H, **CH$_2$**CH$_2$C≡CH (9'')).

^{13}C NMR (125 MHz, MeOD-d$_4$) δ: 172.50 (**C**=O, 2'-**C**O$_2^-$ or 2''-**C**O$_2^-$), 172.46 (**C**=O, 2'-**C**O$_2^-$ or 2''-**C**O$_2^-$), 169.11 (**C**=O, 4'-**C**ONH or 5''-**C**ONH), 168.59 (**C**=O, 4'-**C**ONH or 5''-**C**ONH), 162.21 (**C**$_{Ar}$-9), 162.04 (**C**$_{Ar}$-9), 159.09 (2**C**, **C**$_{Ar}$-4a,10a), 159.04 (2**C**, **C**$_{Ar}$-4a,10a), 158.73 (2**C**, **C**$_{Ar}$-3,6), 158.71 (2**C**, **C**$_{Ar}$-3,6), 144.48 (**C**$_{Ar}$), 142.13 (**C**$_{Ar}$), 137.26 (**C**$_{Ar}$), 136.83 (**C**$_{Ar}$), 136.45 (**C**$_{Ar}$), 134.01 (**C**$_{Ar}$), 132.74 (2**C**, **C**$_{Ar}$-1,8), 132.62 (2**C**, **C**$_{Ar}$-1,8), 131.02 (**C**$_{Ar}$), 130.84 (**C**$_{Ar}$), 129.57 (**C**$_{Ar}$), 129.40 (**C**$_{Ar}$), 129.38 (**C**$_{Ar}$), 129.31 (**C**$_{Ar}$), 115.03 (2**C**, **C**$_{Ar}$-2,7), 115.00 (2**C**, **C**$_{Ar}$-2,7), 114.82 (4**C**, **C**$_{Ar}$-8a,9a), 97.31 (4**C**, **C**$_{Ar}$-4,5), 84.70 (**C**≡**C**H (11' or 11'')), 84.65 (**C**≡**C**H (11' or 11'')), 69.83 (C≡**C**H (12' or 12'')), 69.82 (C≡**C**H (12' or 12'')), 40.82 (8 x **C**H$_3$), 40.57 (NH**C**H$_2$ (7' and 7'')), 29.64 (NHCH$_2$**C**H$_2$ (8' or 8'')), 29.52 (NHCH$_2$**C**H$_2$ (8' or 8'')), 27.13 (**C**H$_2$CH$_2$C≡CH (9' or 9'')), 27.10 (**C**H$_2$CH$_2$C≡CH (9' or 9'')), 18.79 (**C**H$_2$C≡CH (10' or 10'')), 18.73 (**C**H$_2$C≡CH (10' or 10'')).

7.1.7.6 5-*N*-(3-Azidopropyl)-carboxamidotetramethylrhodamine (44) (5-TAMRA-N$_3$) and 6-*N*-(3-azidopropyl)-carboxamidotetramethylrhodamine (45) (6-TAMRA-N$_3$)
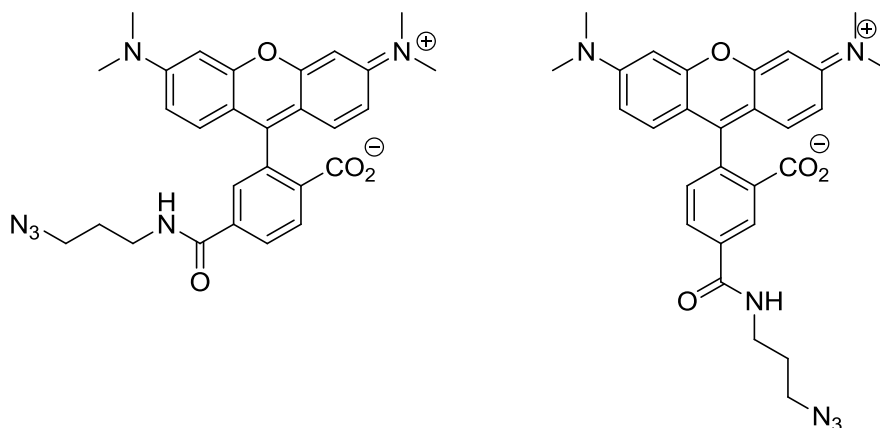
An oven dried, evacuated and argon flushed two-neck 25 mL round-bottom flask was charged with 107.6 mg 5-carboxytetramethylrhodamine (5-TAMRA) (**40**) or 6-carboxytetramethylrhodamine (6-TAMRA) (**41**) (0.25 mmol, 1.0 eq). Addition of 5 mL dry DMF resulted in a dark purple solution (0.05 M). Subsequently, 130.1 mg benzotriazol-1-yl-oxytripyrrolidinophosphonium hexafluorophosphate (PyBOP) (0.25 mmol, 1.0 eq) were

added, followed by 64.6 mg *N,N'*-diisopropylethylamine (DIEA) (82.6 µL, 0.50 mmol, 2.0 eq).

After 5 min of stirring at RT, 100.4 mg 3-azidopropan-1-amine (**34**) (1.0 mmol, 4.0 eq) were

added at once and the reaction mixture was stirred for 3 h at RT in the dark. The reaction

progress was monitored by TLC analysis and when the consumption of the starting material

was indicated, the solvent was removed *in vacuo* and the residue dried under vacuum. Then,

the dark purple solid was dissolved in 30 mL DCM and washed with 30 mL saturated

$NaHCO_3$. Then the water phase was extracted with DCM (2 x 10 mL). The combined organic

layers were washed with brine (30 mL) and then dried over anhydrous Na_2SO_4. The solvent

was removed *in vacuo* and the crude product purified by flash column chromatography on

neutral alumina previously wetted with 7 wt % water. The crude product was dissolved in a

minimal volume DCM and loaded on a column packed in CH_2Cl_2 (30 g neutral alumina, size:

18.0 x 2.5 cm (**44**) and 13 g neutral alumina, size: 14.0 x 2.0 cm (**45**)). The gradient up to

20% MeOH in DCM was used to elute the product yielding 90 mg (0.18 mmol, 70%) 5-*N*-(3-

azidopropyl)-carboxamidotetramethylrhodamine (**44**) (**5-TAMRA-N₃**) as a purple red solid

and 51 (0.10 mmol, 40%) mg 5-*N*-(3-azidopropyl)-carboxamidotetramethylrhodamine (**45**) (**6-

TAMRA-N₃**) as a purple solid.

$C_{28}H_{28}N_6O_4$ [512.56 g/mol]

5-*N*-(3-azidopropyl)-carboxamidotetramethylrhodamine (**44**):

R_f = 0.36 (DCM:MeOH = 9:1 (v/v), on silica TLC plate).

HPLC-MS (EI+): t_R = 6.265 min (JK_10to90); m/z (%) 551.1 (0.6) $[M+K]^+$, 535.1 (5.2)
$[M+Na]^+$, 513.2 (100.0) $[M+H]^+$, 512.4 (6.4) $[M^+]$, 485.2 (2.3), 458.2 (0.4), 442.1 (1.5), 430.0
(0.3).

^{1}H NMR (500 MHz, MeOD-d₄) δ: 8.51 (d, *J* = 1.5 Hz, 1H, H-3'), 8.05 (dd, *J* = 8.0, 1.5 Hz, 1H,

H-5'), 7.36 (d, *J* = 8.0 Hz, 1H, H-6'), 7.25 (d, *J* = 9.5 Hz, 2H, H-1,8), 7.02 (dd, *J* = 9.5, 2.5 Hz,

2H, H-2,7), 6.93 (d, *J* = 2.5 Hz, 2H, H-4,5), 3.54 (t, *J* = 7.0 Hz, 2H, NHC**H₂**), 3.47 (t, *J* = 7.0

Hz, 2H N₃C**H₂**), 3.28 (s, 12H, 4 x C**H₃**), 1.94 (p, *J* = 7.0 Hz, 2H, CH₂C**H₂**CH₂).

HRMS (EI) calcd for $C_{28}H_{29}N_6O_4$ 513.2250 [M+H]$^+$, found 513.2286.

6-N-(3-azidopropyl)-carboxamidotetramethylrhodamine (**45**):

R_f = 0.13 (DCM:MeOH = 9:1 (v/v) on silica TLC plate).

HPLC-MS (EI+): t_R = 6.124 min (JK_10to90); m/z (%) 551.2 (1.1) [M+K]$^+$, 535.2 (4.8) [M+Na]$^+$, 513.2 (100.0) [M+H]$^+$, 485.1 (2.4), 458.2 (0.2), 442.1 (1.2), 430.0 (0.2).

^{1}H NMR (500 MHz, MeOD-d$_4$) δ: 8.14 (d, J = 8.0 Hz, 1H, H-4'), 8.08 (d, J = 8.0 Hz, 1H, H-3'), 7.71 (s, 1H, H-6'), 7.27 (d, J = 9.5 Hz, 2H, H-1,8), 7.02 (dd, J = 9.5, 2.0 Hz, 2H, H-2,7), 6.93 (d, J = 2.0 Hz, 2H, H-4,5), 3.46 (t, J = 6.5 Hz, 2H, NHCH_2), 3.40 (t, J = 6.5 Hz, 2H, N$_3$CH_2), 3.28 (s, 12H, 4 x NCH_3), 1.87 (p, J = 6.5 Hz, 2H, CH$_2$CH_2CH$_2$).

HRMS (EI) calcd for $C_{28}H_{29}N_6O_4$ 513.2250 [M+H]$^+$, found 513.2296.

7.1.7.7 5-N-(Hex-5-yn-1-yl)-carboxamidotetramethylrhodamine (42) (5-TAMRA-Alk) and 6-N-(hex-5-yn-1-yl)-carboxamidotetramethylrhodamine (43) (6-TAMRA-Alk)
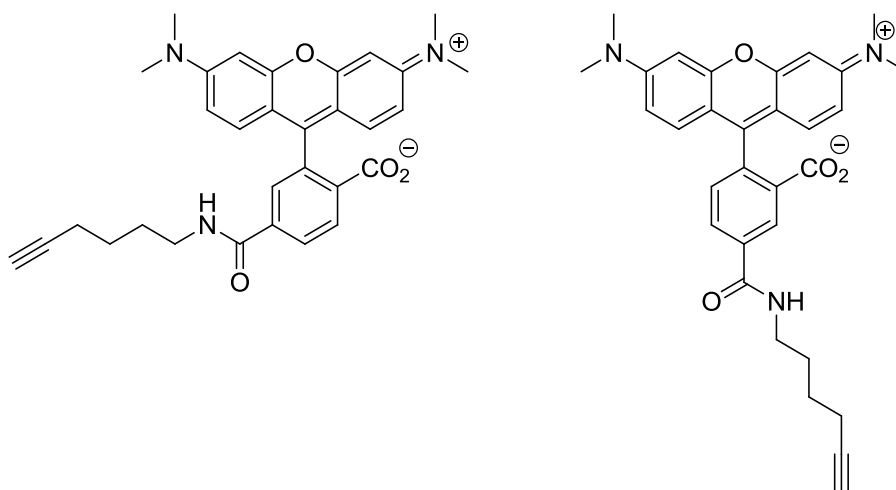

An oven dried, evacuated and argon flushed two-neck 25 mL round-bottom flask was charged with 107.6 mg 5-carboxytetramethylrhodamine (5-TAMRA) (**40**) or 6-carboxytetramethylrhodamine (6-TAMRA) (**41**) (0.25 mmol, 1.0 eq). Addition of 5 mL dry DMF resulted in a dark purple solution (0.05 M). Subsequently, 130.1 mg benzotriazol-1-yl-

oxytripyrrolidinophosphonium hexafluorophosphate (PyBOP) (0.25 mmol, 1.0 eq) were added, followed by 64.6 mg *N,N'*-diisopropylethylamine (DIEA) (82.6 µL, 0.50 mmol, 2.0 eq). After 5 min of stirring at RT, 97.2 mg 5-hexyn-1-amine (**x**) (1.0 mmol, 4.0 eq) were added at once and the reaction mixture was stirred for 3 h at RT in the dark. The reaction progress was monitored by TLC analysis and when the consumption of the starting material was indicated, the solvent was removed *in vacuo* and the residue dried under vacuum. Then, the dark purple solid was dissolved in 30 mL DCM and washed with 30 mL saturated $NaHCO_3$. Then the water phase was extracted with DCM (2 x 10 mL). The combined organic layers were washed with brine (30 mL) and then dried over anhydrous Na_2SO_4. The solvent was removed *in vacuo* and the crude product purified by flash column chromatography on neutral alumina previously wetted with 7 wt % water. The crude product was dissolved in a minimal volume DCM and loaded on a column packed in CH_2Cl_2 (both 17 g neutral alumina, size: 14.0 x 2.5 cm). The gradient up to 20% MeOH in DCM was used to elute the product yielding 61 mg (0.12 mmol, 48%) 5-*N*-(hex-5-yn-1-yl)-carboxamidotetramethylrhodamine (**42**) (**5-TAMRA-Alk**) as red solid and 40 mg (0.08 mmol, 32%) 5-*N*-(hex-5-yn-1-yl)-carboxamidotetramethylrhodamine (**43**) (**6-TAMRA-N₃**) as red solid.

$C_{31}H_{31}N_3O_4$ [509.60 g/mol]

5-*N*-(hex-5-yn-1-yl)-carboxamidotetramethylrhodamine (**42**):

R_f = 0.40 (DCM:MeOH = 9:1 (v/v) on silica TLC plate).

HPLC-MS (EI+): t_R = 6.258 min (JK_10to90); m/z (%) 548.0 (1.6) $[M+K]^+$, 532.2 (6.1) $[M+Na]^+$, 510.2 (100.0) $[M+H]^+$, 458.1 (0.2), 379.2 (0.3).

^{1}H NMR (500 MHz, MeOD-d₄) δ: 8.51 (d, *J* = 1.5 Hz, 1H, H-3'), 8.04 (dd, *J* = 8.0, 1.5 Hz, 1H, H-5'), 7.36 (d, *J* = 8.0 Hz, 1H, H-6'), 7.25 (d, *J* = 9.5 Hz, 2H, H-1,8), 7.01 (dd, *J* = 9.5, 2.5 Hz, 2H, H-2,7), 6.91 (d, *J* = 2.5 Hz, 2H, H-4,5), 3.48 (t, *J* = 7.0 Hz, 2H, NHC**H₂**), 3.28 (s, 12H, 4 x C**H₃**), 2.28 (td, *J* = 7.0, 2.5 Hz, 2H, C**H₂**C≡CH), 2.24 (d (pst), *J* = 2.5 Hz, 1H, CH₂C≡C**H**), 1.80 (p, *J* = 7.5 Hz, 2H, NHCH₂C**H₂**), 1.65 (p, *J* = 7.0 Hz, 2H, C**H₂**CH₂C≡CH).

HRMS (EI) calcd for $C_{31}H_{32}N_3O_4$ 510.2393 $[M+H]^+$, found 510.2347.

6-*N*-(hex-5-yn-1-yl)-carboxamidotetramethylrhodamine (**43**):

R_f = 0.27 (DCM:MeOH = 9:1 (v/v) on silica TLC plate).

HPLC-MS (EI+): t_R = 6.341 min (JK_10to90); m/z (%) 548.0 (2.3) $[M+K]^+$, 532.2 (8.0) $[M+Na]^+$, 510.2 (100.0) $[M+H]^+$, 509.0 (0.9) $[M^+]$, 458.2 (0.3).

^{1}H NMR (500 MHz, MeOD-d$_4$) δ: 8.13 (d, *J* = 8.0 Hz, 1H, H-4'), 8.07 (d, *J* = 8.0 Hz, 1H, H-3'), 7.70 (s, 1H, H-6'), 7.26 (d, *J* = 9.5 Hz, 2H, H-1,8), 7.02 (d, *J* = 9.5, 2H, H-2,7), 6.92 (s, 2H, H-4,5), 3.40 (t, *J* = 7.0 Hz, 2H, NHC**H**$_2$), 3.28 (s, 12H, 4 x NC**H**$_3$), 2.25 - 2.19 (m, 2H, C**H**$_2$C≡CH), 2.16 (s, 1H, CH$_2$C≡C**H**), 1.73 (p, *J* = 7.5 Hz, 2H, NHCH$_2$C**H**$_2$), 1.56 (p, *J* = 7.0 Hz, 2H, C**H**$_2$CH$_2$C≡CH).

HRMS (EI) calcd for calcd for $C_{31}H_{32}N_3O_4$ 510.2393 $[M+H]^+$, found 510.2426.

7.1.8 Synthesis of MAO-isozyme specific probes

7.1.8.1 Synthesis of building block A1 and A2

7.1.8.1.1 Methyl 3-((methyl(prop-2-yn-1-yl)amino)methyl)benzoate (57)-a and methyl 4-((methyl(prop-2-yn-1-yl)amino)methyl)benzoate (57)-b
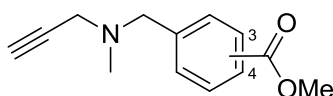
An oven dried, evacuated and nitrogen flushed two-neck 25 mL round-bottom flask was charged with 0.687 g methyl 3- or 4-(bromomethyl)benzoate (3.0 mmol, 1.0 eq) under nitrogen stream and cooled in an ice-water bath. Addition of ice cold 2.334 g *N*-methylpropargylamine (2.85 mL, 33.7 mmol, 11.2 eq) under nitrogen stream resulted in a clear dark yellow solution. The reaction mixture was stirred for 3 h in the dark, letting the temperature to reach RT. After that time, the conversion of starting material was complete as indicated by TLC and GC-MS analysis. Subsequently, the solvent was removed under

reduced pressure and the residue was dried *in vacuo.* The brown oil was dissolved in ca. 30 mL chloroform and washed with water (3 x 20 mL). The organic phase was dried over anhydrous $MgSO_4$. The solvent was removed under reduced pressure and the crude product (thick brownish oil) purified by flash column chromatography on silica (cyclohexane:ethyl acetate = 4:1 (v/v), 45 g silica gel, size: 12.0 x 3.5 cm) furnishing 0.636 g (2.93 mmol, 98%) methyl 3-((methyl(prop-2-yn-1-yl)amino)methyl) benzoate (**57**)-**a** and 0.626 g (2.88 mmol, 96%) methyl 4-((methyl(prop-2-yn-1-yl)amino) methyl)benzoate, respectively as a yellowish oil.

$C_{13}H_{15}NO_2$ [217.26 g/mol]

Methyl 3-((methyl(prop-2-yn-1-yl)amino)methyl)benzoate (**57**)-**a**:

R_f = 0.35 (cyclohexane:ethyl acetate = 4:1 (v/v))

GC-MS (EI): t_R = 6.23 min; m/z (%) 217.1 (35.0) $[M]^+$, 216.1 (25.7), 186.1(7.3), 176.1 (8.6), 158.1 (7.6), 149.1 (33.3), 119.1 (25.5), 91.1 (28.9), 89.1 (16.2), 82.1 (100.0), 77.1 (5.8), 68.1 (42.1).

^{1}H NMR (300 MHz, $CDCl_3$) δ: 8.01 (s, 1H, arom.), 7.94 (d, *J* = 7.5 Hz, 1H, arom.), 7.57 (d, *J* = 7.8 Hz, 1H, arom.), 7.40 (t, *J* = 7.5 Hz, 1H, arom.), 3.91 (s, 3H, OC**H**$_3$), 3.63 (s, 2H, PhC**H**$_2$N), 3.33 (d, *J* = 2.1 Hz, 2H, C**H**$_2$C≡CH), 2.35 (s, 3H, NC**H**$_3$), 2.30 (t, *J* = 2.1 Hz,1H, CH$_2$C≡C**H**).

^{13}C NMR (75 MHz, $CDCl_3$) δ: 167.04 (**C**=O), 138.56 (**C**$_{Ar}$-1), 133.70 (**C**$_{Ar}$-2), 130.27 (**C**$_{Ar}$-3), 130.20 (**C**$_{Ar}$-6), 128.62 (**C**$_{Ar}$-4), 128.46 (**C**$_{Ar}$-5), 78.04 (**C**≡CH), 73.71 (C≡**C**H), 59.45 (Ph**C**H$_2$N), 52.06 (O**C**H$_3$), 44.95 (**C**H$_2$C≡CH), 41.58 (N**C**H$_3$).

Methyl 4-((methyl(prop-2-yn-1-yl)amino)methyl)benzoate (**57**)-**b**:

R_f = 0.35 (cyclohexane:ethyl acetate = 4:1 (v/v))

GC-MS (EI): t_R = 6.31 min; m/z (%) 217.1 (58.4) $[M]^+$, 216.1 (41.6), 190.1 (13.2), 186.1 (15.7), 176.1 (15.9), 158.1 (9.8), 149.1 (42.0), 121.1 (22.2), 118.1 (13.7), 91.1 (23.1), 89.1 (20.9), 82.1 (100.0), 68.1 (46.1).

^{1}H NMR (300 MHz, CDCl$_3$) δ: 7.99 (d, J = 8.4 Hz, 2H, arom.), 7.42 (d, J = 8.4 Hz, 2H, arom.), 3.90 (s, 3H, OC**H**$_3$), 3.63 (s, 2H, PhC**H**$_2$N), 3.31 (d, J = 2.4 Hz, 2H, C**H**$_2$C≡CH), 2.34 (s, 3H, NC**H**$_3$), 2.29 (t, J = 2.4 Hz, 1H, CH$_2$C≡C**H**).

^{13}C NMR (75 MHz, CDCl$_3$) δ: 166.95 (**C**=O), 143.55 (**C**$_{Ar}$-1), 129.65 (**C**$_{Ar}$-2), 129.18 (**C**$_{Ar}$-3) 128.99 (**C**$_{Ar}$-4), 78.04 (**C**≡CH), 73.67 (C≡**C**H), 59.52 (Ph**C**H$_2$N), 52.01 (O**C**H$_3$), 45.00 (**C**H$_2$C≡CH), 41.70 (N**C**H$_3$).

7.1.8.1.2 3-((Methyl(prop-2-yn-1-yl)amino)methyl)benzoic acid (58)-a and 4-((methyl(prop-2-yn-1-yl)amino)methyl)benzoic acid (58)-b
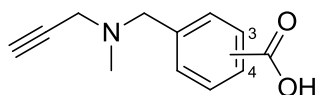
In an oven dried 50 mL round-bottom flask 215 mg 3-((methyl(prop-2-yn-1-yl)amino)methyl)benzoate (**57**)-**a** (0.99 mmol, 1.0 eq) were dissolved in 9.0 mL of a solvent mixture (THF:MeOH:H$_2$O = 4:4:1 (v/v/v)) resulting in a clear yellowish solution. Then 1.0 mL solution of 2N sodium hydroxide in MeOH was added at once so that the final concentration of NaOH was 0.2N. The reaction progress was monitored by TLC analysis and the reaction mixture was stirred for 27 h at RT. When there was no starting material indicated, the reaction mixture was quenched with ca. 10 mL water, acidified with minimal volume of 6N aqueous HCl until pH ca. 3. The solvent was removed under reduced pressure and the residue was dried *in vacuo.* Then the crude product (sticky pale solid) was purified by gradient flash column chromatography on silica (ethyl acetate:MeOH (0-50%) (v/v), 20 g silica gel, size: 12.0 x 2.0 cm) yielding 200 mg (0.98 mmol, 99%) 3-((methyl(prop-2-yn-1-yl)amino)methyl) benzoic acid (**58**)-**a** as a beige solid.

For 4-((methyl(prop-2-yn-1-yl)amino)methyl)benzoic acid (**58**)-**b** the reaction was carried out in an analogous manner as described above only 292 mg 4-((methyl(prop-2-yn-1-yl)amino)methyl)benzoate (**57**)-**b** (1.35 mmol, 1.0 eq) were dissolved in 12.1 mL solvent, followed by the addition of 1.3 mL 2N NaOH in MeOH. Flash column chromatography on

silica (ethyl acetate:MeOH (0-50%) (v/v), 22 g silica gel, size: 13.0 x 2.0 cm) furnished 270 mg (1.33 mmol, 99%) 4-((methyl(prop-2-yn-1-yl)amino)methyl)benzoic acid (**58**)-**b** as a sticky beige solid.

$C_{12}H_{13}NO_2$ [203.24 g/mol]

3-((methyl(prop-2-yn-1-yl)amino)methyl)benzoic acid (**58**)-**a**:

R_f = 0.05 (cyclohexane:ethyl acetate = 4:1 (v/v)).

HPLC-MS (EI+): t_R = 5.777 min (JK_10to90); m/z (%) 204.0 (100.0).

^{1}H NMR (300 MHz, D_2O) δ: 8.06 (s, 1H, arom.), 8.03 (s, 1H, arom.), 7.71 (d, J = 7.8 Hz, 1H, arom.), 7.59 (t, J = 7.8 Hz, 1H, arom.), 4.49 (s, 2H, PhC**H**$_2$N), 4.00 (d, J = 2.1 Hz, 2H, C**H**$_2$C≡CH), 3.18 (t, J = 2.4 Hz, 1H, CH$_2$C≡C**H**), 2.94 (s, 3H, NC**H**$_3$).

^{13}C NMR (75 MHz, D_2O) δ: 172.29 (**C**=O), 135.56 (**C**$_{Ar}$-1), 134.19 (**C**$_{Ar}$-6), 132.26 (**C**$_{Ar}$-2), 131.71 (**C**$_{Ar}$-3), 130.26 (**C**$_{Ar}$-4), 129.60 (**C**$_{Ar}$-5), 81.16 (**C**≡CH), 72.05 (C≡**C**H), 58.86 (Ph**C**H$_2$N), 45.03 (**C**H$_2$C≡CH), 40.06 (N**C**H$_3$).

4-((methyl(prop-2-yn-1-yl)amino)methyl)benzoic acid (**58**)-**b**:

R_f = 0.05 (cyclohexane:ethyl acetate = 4:1 (v/v)).

HPLC-MS (EI+): t_R = 5.647 min (JK_10to90); m/z (%) 204.0 (100.0).

^{1}H NMR (300 MHz, D_2O) δ: 8.01 (d, J = 8.1 Hz, 2H, arom.), 7.60 (d, J = 8.1 Hz, 2H, arom.), 4.48 (s, 2H, PhC**H**$_2$N), 4.00 (d, J = 1.8 Hz, 2H, C**H**$_2$C≡CH), 3.18 (s, 1H, CH$_2$C≡C**H**), 2.94 (s, 3H, NC**H**$_3$).

^{13}C NMR (75 MHz, D_2O) δ: 171.36 (**C**=O), 133.63 (**C**$_{Ar}$-1), 133.00 (**C**$_{Ar}$-4), 131.09 (**C**$_{Ar}$-3), 130.18 (**C**$_{Ar}$-2), 80.61 (**C**≡CH), 71.39 (C≡**C**H), 58.06 (Ph**C**H$_2$N). 44.53 (**C**H$_2$C≡CH), 39.59 (N**C**H$_3$).

7.1.8.2 Synthesis of building block B

7.1.8.2.1   1-(Hept-2-yn-1-yl)-2,2,6,6-tetramethylpiperidin-4-one (60)
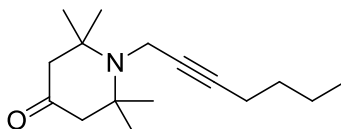
In an oven dried, evacuated and nitrogen purged 100 mL Schlenk tube 1.552 g 2,2,6,6-tetramethylpiperidin-4-one (10.0 mmol, 1.0 eq) were dissolved in 10.0 mL dry dioxane forming a clear orange solution. Subsequently, 0.360 g paraformaldehyde (12.0 mmol, 1.2 eq), 0.904 g hex-1-yne (1.273 mL, 11.0 mmol, 1.1 eq), 100 mg copper(I) iodide (0.5 mmol, 0.05 eq) were added under a nitrogen stream, followed by 1.201 g glacial acetic acid (1.150 mL, 20.0 mmol, 2.0 eq). The orange suspension was stirred at RT for 5 min, then heated up to 90°C and stirred at 90°C for 1 h. After that time, the reaction mixture was cooled down to RT and quenched with 150 mL distilled H_2O. The mixture was acidified to pH approx. 1 using 6N aqueous HCl and extracted with diethyl ether (3 x 70 mL). The water phase was basified with saturated Na_2CO_3 solution to pH approx. 9 and then extracted with chloroform (4 x 50 mL). Product was identified both in ethereal and chloroform phase by TLC and GC-MS analysis. The chloroform and ethereal phases were dried over anhydrous $MgSO_4$. The organic phases were combined and the solvent was removed under reduced pressure. The crude product (thick brownish oil) was purified by flash column chromatography on silica (cyclohexane:ethyl acetate = 96 : 4 (v/v), 150 g silica gel, size: 21.0 x 4.5 cm) yielding 614 mg (2.46 mmol, 25%) 1-(hept-2-yn-1-yl)-2,2,6,6-tetramethylpiperidin-4-one (**60**) as a light orange oil.

$C_{16}H_{27}NO$ [249.39 g/mol]

R_f = 0.33 (cyclohexane:ethyl acetate = 9:1 (v/v)), 0.18 (cyclohexane : ethyl acetate = 95:5 (v/v)), 0.14 (cyclohexane : ethyl acetate = 96:4 (v/v)).

GC-MS (EI): t_R = 6.64 min, m/z = 249.2 (2.2) $[M]^+$, 234.2 (100.0) $[M-CH_3]^+$, 178.1 (2.5), 152.2 (8.8), 150.1 (3.7), 136.1 (2.9), 108.1 (2.5), 95.1 (9.3), 83.1 (32.9), 67.1 (8.2), 55.1 (9.1).

IR: 2964, 2932, 1716, 1462, 1381, 1368, 1315, 1252, 1218, 1148, 1012, 914, 847, 734.

^{1}H NMR (300 MHz, CDCl$_3$) δ: 3.46 (s, 2H, NC**H**$_2$), 2.38 (s, 4H, C**H**$_2$C(O)C**H**$_2$), 2.15 (m, 2H, C≡CC**H**$_2$), 1.52 – 1.29 (m, 4H, 2 x C**H**$_2$), 1.24 (s, 12H, 4 x C**H**$_3$), 0.89 (t, J = 7.2 Hz, 3H, C**H**$_3$).

^{13}C NMR (75 MHz, CDCl$_3$) δ: 209.96 (**C**=O), 81.98 (C$_q$), 81.57 (C$_q$), 59.28 (2 x C$_q$), 55.82 (**C**H$_2$C(O)**C**H$_2$), 32.94 (N**C**H$_2$), 30.87 (**C**H$_2$), 28.52 (4 x **C**H$_3$), 21.94 (**C**H$_2$), 18.53 (**C**H$_2$), 13.57 (**C**H$_3$).

7.1.8.2.2   8-(Hept-2-yn-1-yl)-7,7,9,9-tetramethyl-1,4-dioxa-8-azaspiro[4.5]decane (63)
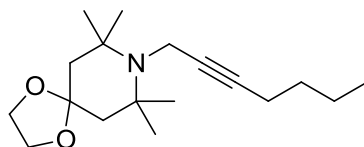
In an oven dried, evacuated and nitrogen purged 50 mL round-bottom Schlenk flask 363 mg 1-(hept-2-yn-1-yl)-2,2,6,6-tetramethylpiperidin-4-one (**60**) (1.45 mmol, 1.0 eq) were dissolved in 1.62 mL ethylene glycol (1.800 g, 29.0 mmol, 20.0 eq). Then, 425 mg polyphosphoric acid (PPA) (206 µL, 5.08 mmol, 3.5 eq) were added at once. The reaction mixture was stirred at 65°C for 6 h. The reaction progress was monitored by TLC analysis and carried out until no starting material was indicated. Then, the reaction mixture was cooled down to RT, basified with saturated Na$_2$CO$_3$ to pH ca. 8-9 and diluted with 10 mL H$_2$O. The aquous phase was extracted with chloroform (4 x 10 mL). The combined organic layers were washed with saturated Na$_2$CO$_3$ (2 x 15 mL), water (2 x 15 mL) and dried over anhydrous MgSO$_4$. The solvent was removed *in vacuo* and the crude product purified by flash column chromatography on silica (cyclohexane:ethyl acetate = 96 : 4 (v/v), 16 g silica gel, size: 14.0 x 2.0 cm) yielding 234 mg (0.79 mmol, 54%) 8-(hept-2-yn-1-yl)-7,7,9,9-tetramethyl-1,4-dioxa-8-azaspiro[4.5]decane (**63**) as a light yellow liquid.

$C_{18}H_{31}NO_2$ [293.44 g/mol]

R_f = 0.44 (cyclohexane:ethyl acetate = 9:1 (v/v)), 0.39 (cyclohexane:ethyl acetate = 95:5 (v/v)).

GC-MS (EI): t_R = 7.11 min, m/z = 293.3 (1.2) $[M]^+$, 278.2 (100.0) $[M-CH_3]^+$, 192.2 (20.9), 152.1 (2.9), 136.1 (3.1), 127.1 (33.0), 109.1 (2.9), 95.1 (9.0), 83.1 (6.6), 67.1 (6.8), 55.1 (8.3).

^{1}H NMR (300 MHz, CDCl$_3$) δ: 3.91 (s, 4H, 2 x O**C**H$_2$), 3.35 (t, J = 2.1 Hz, 2H, N**C**H$_2$), 2.13 (m, 2H, C≡CC**H**$_2$), 1.68 (s, 4H, **C**H$_2$C(O)**C**H$_2$), 1.49 – 1.32 (m, 4H, 2 x **C**H$_2$), 1.20 (s, 12H, 4 x **C**H$_3$), 0.88 (t, J = 7.2 Hz, 2H, **C**H$_3$)

^{13}C NMR (75 MHz, CDCl$_3$) δ: 107.62 (spiro-C$_q$), 82.64 (C$_q$), 80.81 (C$_q$), 63.60 (2 x O**C**H$_2$), 56.01 (2 x C$_q$), 47.56 (2 x **C**H$_2$), 32.51 (N**C**H$_2$), 30.99 (**C**H$_2$), 27.91 (4 x **C**H$_3$), 21.92 (**C**H$_2$), 18.61 (**C**H$_2$), 13.60 (**C**H$_3$).

7.1.8.2.3 1-(7-Hydroxyhept-2-yn-1-yl)-2,2,6,6-tetramethylpiperidin-4-one (65)
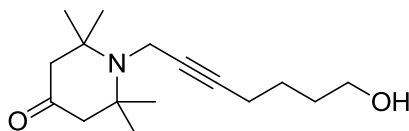
In an oven dried, evacuated and nitrogen purged 100 mL Schlenk tube, 1.552 g 2,2,6,6,-tetramethylpiperidin-4-one (10.0 mmol, 1.0 eq) were dissolved in 10 mL dry 1,4-dioxane. Subsequently, 720 mg paraformaldehyde (24.0 mmol, 2.4 eq), 1.080 g hex-5-yn-1-ol (1.213 mL, 11.0 mmol, 1.1 eq), 100 mg copper(I) iodide (0.5 mmol, 0.05 eq) were added under a nitrogen stream, followed by 1.201 g glacial acetic acid (1.150 mL, 20.0 mmol, 2.0 eq). The orange suspension was stirred at RT for 5 min, then heated up quickly to 90°C and stirred at 90°C for 2 h. After that time, the reaction mixture was cooled down to RT and quenched with 100 mL distilled H$_2$O. The suspension was acidified to pH ca. 1 using 6 N HCl. The water phase was washed with Et$_2$O (3 x 50 mL) to remove unreacted hex-5yn-1-ol and other by-products, and then basified with saturated Na$_2$CO$_3$ solution to pH ca. 9. The aqueous solution was extracted with CHCl$_3$ (3 x 50 mL). The combined organic layers were dried over

anhydrous $MgSO_4$ and the solvent was removed *in vacuo*. The crude product was purified by flash column chromatography on silica (cyclohexane:ethyl acetate = 3:2 to 1:1 (v/v), 115 g silica, size: 35.5 x 3.0 cm) furnishing 1.258 g (4.75 mmol, 48% yield) 1-(7-hydroxyhept-2-yn-1-yl)-2,2,6,6-tetramethylpiperidin-4-one (**65**) as a yellowish solid.

$C_{16}H_{27}NO_2$ [265.39 g/mol]

R_f = 0.44 (cyclohexane:ethyl acetate = 1:1 (v/v))

m.p. = 73-75 °C (yellowish solid).

GC-MS (EI): t_R = 7.41 min; m/z (%) 265.2 (1.3) $[M]^+$, 250.2 (100.0) $[M-CH_3]^+$, 168.1 (6.7), 150.1 (2.0), 97.1 (1.9), 91.1 (4.2), 83.1 (23.6), 77.1 (4.9), 70.1 (2.5), 55.1 (6.6).

^{1}H NMR (300 MHz, $CDCl_3$): δ = 3.66 (q, *J* = 6.0 Hz, 2H, C**H**$_2$OH), 3.44 (t, *J* = 2.1 Hz, 2H, NC**H**$_2$), 2.37 (s, 4H, C**H**$_2$C(O)C**H**$_2$), 2.20 (m, 2H, C≡CC**H**$_2$), 1.67 – 1.53 (m, 5H, 2 x C**H**$_2$, O**H**), 1.23 (s, 12H, 4 x C**H**$_3$).

^{13}C NMR (75 MHz, $CDCl_3$) δ: = 209.91 (**C**=O), 82.01 (C_q), 81.61 (C_q), 62.22 (**C**H$_2$OH), 59.35 (2 x C_q), 55.71 (**C**H$_2$C(O)**C**H$_2$), 32.93 (N**C**H$_2$), 31.88 (**C**H$_2$CH$_2$OH), 28.45 (4 x **C**H$_3$), 24.98 (**C**H$_2$), 18.60 (**C**H$_2$).

7.1.8.2.4   1-(7-Hydroxyheptyl)-2,2,6,6-tetramethylpiperidin-4-one (66)
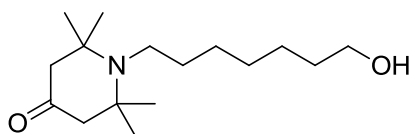
An oven dried, evacuated and nitrogen purged 100 mL three-neck round bottom flask equipped with a hydrogen inlet and a gas/vacuum inlet was charged with 600 mg 1-(7-hydroxyhept-2-yn-1-yl)-2,2,6,6-tetramethylpiperidin-4-one (**65**) (2.26 mmol, 1.0 eq). Addition of 25 mL dry EtOH resulted in a clear yellowish solution, which was degassed and flushed with nitrogen twice. Then, 30 mg platinum dioxide (0.13 mmol, 0.06 eq, 5% wt) were added under nitrogen stream and the resulting blackish suspension was degassed and flushed with

nitrogen twice. Then, the reaction mixture was saturated with hydrogen, followed by a short opening of the vacuum, while a hydrogen inlet was closed. This gas-vacuum cycle was repeated three times, and then the reaction mixture was vigorously stirred for 2 h under a hydrogen atmosphere. When TLC analysis indicated only small amounts of partially reduced alkene by-product, the reaction was stopped by closing the hydrogen inlet and purging the suspension with nitrogen. The reaction mixture was filtered through a Celite® pad under nitrogen stream (as used catalyst is highly flammable) and washed with EtOH. The solvent was removed under reduced pressure and the crude product purified by flash chromatography on silica (cyclohexane:ethyl acetate = 3:2, 30 g silica gel, size: 18.0 x 2.5 cm) yielding 305 mg (1.13 mmol, 50%) 1-(7-hydroxyheptyl)-2,2,6,6-tetramethylpiperidin-4-one (**66**) as a yellow oil.

$C_{16}H_{31}NO_2$ [269.42 g/mol]

R_f = 0.36 (cyclohexane:ethyl acetate = 1:1 (v/v)), 0.28 (cyclohexane:ethyl acetate = 3:2 (v/v)).

GC-MS (EI): t_R = 7.41 min; m/z (%) 269.2 (3.7) $[M]^+$, 254.2 (100.0) $[M-CH_3]^+$, 198.2 (7.4), 172.2 (8.1), 168.1 (55.7), 112.1 (21.7), 97.1 (8.8), 83.1 (29.8), 70.1 (20.0), 55.1 (15.7).

^{1}H NMR (300 MHz, CDCl$_3$) δ: 3.62 (m, 2H, C**H**$_2$OH), 2.42 (m, 2H, NC**H**$_2$), 2.31 (s, 4H, C**H**$_2$C(O)C**H**$_2$), 1.59 -1.20 (m, 11H, 5 x C**H**$_2$, -O**H**), 1.10 (s, 12H, 4 x C**H**$_3$)

^{13}C NMR (75 MHz, CDCl$_3$) δ: 210.26 (**C**=O), 62.89 (**C**H$_2$OH), 59.79 (2 x C$_q$), 55.82 (**C**H$_2$C(O)**C**H$_2$), 44.60 (N**C**H$_2$), 35.48 (**C**H$_2$), 32.68 (**C**H$_2$), 29.30 (**C**H$_2$), 28.25 (4 x **C**H$_3$), 27.34 (**C**H$_2$), 25.81 (**C**H$_2$).

7.1.8.2.5 2,2,6,6-Tetramethyl-1-(7-(prop-2-yn-1-yloxy)heptyl)piperidin-4-one (67)
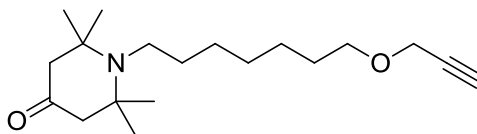
In an oven dried, evacuated and nitrogen purged two-neck 50 mL round-bottom flask was charged with 90 mg sodium hydride (3.75 mmol, 2.5 eq, washed with *n*-pentane and stored under argon) under a nitrogen stream. The addition of 3.0 mL dry THF resulted in a white suspension which was cooled to ca. 0 °C in an ice-water bath. Then, a solution of 405 mg 1-(7-hydroxyheptyl)-2,2,6,6-tetramethylpiperidin-4-one (**66**) (1.5 mmol, 1.0 eq) in 2.0 mL dry THF was added slowly *via* a syringe over 20 min. Then, the yellowish suspension was additionally stirred for 60 min at 0 °C. After that time 557.6 mg propargyl bromide (404 µL, 2.5 eq, 80% wt in toluene) were added dropwise at 0 °C over 30 min. The reaction mixture changed color from yellow through orange to reddish. The reaction mixture was stirred overnight letting the temperature to reach RT. The reaction progress was followed by TLC and GC-MS analysis. Due to formation of some by-products, after 20 h the reaction was quenched with 25 mL ice-cold water, which was slowly added to the reaction mixture. Then the water phase was extracted with diethyl ether (5 x 20 mL). The combined organic layers were dried over anhydrous $MgSO_4$. The solvent was removed *in vacuo* and the crude product purified by flash column chromtography on silica (cyclohexane : ethyl acetate = 9 : 1 (v/v), 28 g silica gel, size: 17.0 x 2.5 cm) furnishing 200 mg (0.65 mmol, 43%) 2,2,6,6-tetramethyl-1-(7-(prop-2-yn-1-yloxy)heptyl)piperidin-4-one (**67**) as a yellowish liquid.

$C_{19}H_{33}NO_2$ [307.47 g/mol]

R_f = 0.78 (cyclohexane:ethyl acetate = 1:1 (v/v)), 0.68 (cyclohexane:ethyl acetate = 3:2 (v/v)), 0.44 (cyclohexane:ethyl acetate = 4:1 (v/v)), 0.24 (cyclohexane:ethyl acetate = 9:1 (v/v)).

GC-MS (EI): t_R = 7.73 min; m/z (%) 307.3 (2.2) $[M]^+$, 292.3 (100.0) $[M-CH_3]^+$, 210.2 (7.3), 168.2 (87.1), 112.1 (29.5), 97.1 (14.0), 83.1 (38.5), 70.1 (31.1), 69.1 (15.2), 55.1 (21.8).

^{1}H NMR (300 MHz, CDCl$_3$) δ: 4.12 (d, J = 2.1 Hz, 2H, C**H**$_2$C≡CH), 3.50 (t, J = 6.6 Hz 2H, CH$_2$C**H**$_2$O), 2.53 – 2.36 (m, 3H, NC**H**$_2$ and CH$_2$C≡C**H**), 2.31 (s, 4H, C**H**$_2$C(O)C**H**$_2$), 1.63 - 1.17 (m, 10H, 5 x C**H**$_2$), 1.11 (s, 12H, 4 x C**H**$_3$).

^{13}C NMR (75 MHz, CDCl3) δ: 210.14 (**C**=O), 80.00 (C$_q$), 74.01 (C$_q$), 70.18 (**C**H$_2$OH), 59.78 (2 x C$_q$), 57.97 (**C**H$_2$C≡CH), 55.86 (**C**H$_2$C(O)**C**H$_2$), 44.61 (N**C**H$_2$), 35.48 (**C**H$_2$), 29.40 (**C**H$_2$), 29.30 (**C**H$_2$), 28.27 (4 x **C**H$_3$), 27.30 (**C**H$_2$), 26.14 (**C**H$_2$).

7.1.8.2.6   2,2,6,6-Tetramethyl-1-(7-(prop-2-yn-1-yloxy)heptyl)piperidin-4-one oxime (69)
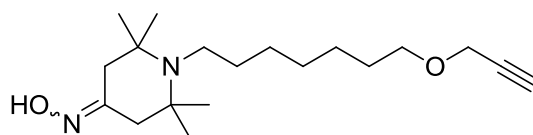
In an oven dried, evacuated and nitrogen purged two-neck 25 mL round-bottom flask 175 mg 2,2,6,6-tetramethyl-1-(7-(prop-2-yn-1-yloxy)heptyl)piperidin-4-one (**67**) (0.57 mmol, 1.0 eq) were dissolved in 2.0 mL dry MeOH forming a clear yellowish solution. Then, 79 mg hydroxylamine hydrochloride (1.14 mmol, 2.0 eq) were dissolved, followed by the addition of 127 mg dry triethylamine (175 µL, 1.25 mmol, 2.2 eq) under a nitrogen stream. The reaction mixture was stirred overnight at RT. The reaction progress was monitored by TLC analysis. When TLC analysis indicated the complete consumption of the starting material, the solvent was removed under reduced pressure. The residue was dissolved in 30 mL diethyl ether and washed with water (3 x 10 mL). Then the organic phase was dried over anhydrous MgSO$_4$. The solvent was removed *in vacuo* and the crude product purified by flash column chromatography on silica (DCM:methanol = 98:2 to 95:5 (v/v), 12 g silica gel, size: 12.0 x 2.0 cm) yielding 175 mg 2,2,6,6-tetramethyl-1-(7-(prop-2-yn-1-yloxy)heptyl)piperidin-4-one oxime (**69**) (0.54 mmol, 95%) as a yellowish crystallizing oil.

C$_{19}$H$_{34}$N$_2$O$_2$ [322.49 g/mol]

R$_f$ = 0.44 (DCM:MeOH = 9:1 (v/v)), 0.26 (cyclohexane:ethyl acetate = 3:2 (v/v)).

GC-MS (EI): t_R = 8.20 min, m/z (%) 322.3 (2.0) [M]$^+$, 307.3 (100.0) [M-CH$_3$]$^+$, 210.2 (11.7), 207.1 (18.4), 183.1 (66.8), 154.1 (6.2), 98.1 (6.7), 70.1 (11.8), 58.1 (10.9), 55.1 (17.5).

^{1}H NMR (300 MHz, CDCl$_3$) δ: 4.12 (d, J = 2.4 Hz, 2H, C**H**$_2$C≡CH), 3.50 (t, J = 6.6 Hz, 2H, C**H**$_2$CH$_2$O), 2.48- 2.29 (m, 5H, NC**H**$_2$, C≡C**H** and C**H**$_2$C(O)), 2.13 (s, 2H, C**H**$_2$C(O)) 1.74 (brs, 1H, N=O**H**), 1.64 - 1.19 (m, 10H, 5 x C**H**$_2$), 1.07 (s, 12H, 4 x C**H**$_3$).

^{13}C NMR (75 MHz, CDCl$_3$) δ: 157.59 (**C**=NOH), 80.01 (C$_q$), 74.03 (C$_q$), 70.22 (**C**H$_2$OH), 57.98 (**C**H$_2$C≡CH), 57.76 (C$_q$), 57.66 (C$_q$), 46.21 (**C**H$_2$C(N)**C**H$_2$), 44.76 (N**C**H$_2$), 39.48 (**C**H$_2$), 35.46 (**C**H$_2$), 29.41 (2 x CH$_3$), 29.30 (2 x CH$_3$), 27.82 (**C**H$_2$), 27.33 (**C**H$_2$), 26.14 (**C**H$_2$).

7.1.8.2.7   2,2,6,6-Tetramethyl-1-(7-(prop-2-yn-1-yloxy)heptyl)piperidin-4-amine (68)
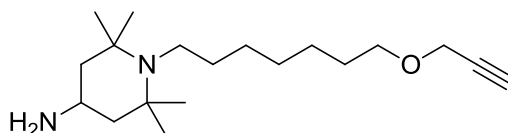
An oven dried, evacuated and nitrogen purged 10 mL Schlenk tube was charged with 100 mg lithium aluminium hydride (2.375 mmol, 5.0 eq) under a nitrogen stream. Addition of 2.0 mL dry THF resulted in a grey suspension which was then cooled to ca. 0 °C in an ice-water bath. Subsequently, a solution of 153 mg 2,2,6,6-tetramethyl-1-(7-(prop-2-yn-1-yloxy)heptyl) piperidin-4-one oxime (**69**) (0.475 mmol, 1.0 eq) in 2.0 mL dry THF was added slowly *via* a syringe over 30 min. The mixture was stirred vigorously overnight letting the temperature to reach RT. The reaction progress was monitored by TLC analysis after a mini-work-up. The reaction was stopped after 41 h when TLC analysis did not indicate any remaining starting material. The reaction mixture was diluted with 2 mL diethyl ether and cooled to ca. 0°C in an ice-water bath. Subsequently, 100 μL ice cold water, 100 μL 15% aqueous NaOH solution and 300 μL ice cold water were added dropwise (n-n-3n work-up). The mixture was then stirred for 30 min. The formed white solid was filtrated off, washed with diethyl ether. The ether phase was dried over anhydrous MgSO$_4$. The solvent was removed *in vacuo* and the crude product purified by flash column chromatography on silica (DCM:methanol = 4:1 with

1% Et$_3$N (v/v)) furnishing 84 mg 2,2,6,6-tetramethyl-1-(7-(prop-2-yn-1-yloxy)heptyl)piperidin-4-amine (**68**) (0.27 mmol, 58%) as a yellowish oil.

C$_{19}$H$_{36}$N$_2$O [308.50 g/mol]

R$_f$ = 0.28 (DCM:MeOH = 4:1 and 1% Et$_3$N (v/v)).

GC-MS (EI): t$_R$ = 7.71 min; m/z (%) 308.3 (2.3) [M]$^+$, 293.3 (100.0) [M-CH$_3$]$^+$, 276.3 (11.1), 250.2 (5.8), 210.2 (19.4), 169.2 (40.8), 97.1 (12.2), 84.1 (11.4), 70.1 (10.4), 58.1 (15.0), 55.1 (6.6).

^{1}H NMR (300 MHz, CDCl$_3$) δ: 4.11 (d, *J* = 2.4 Hz, 2H, **CH$_2$**C≡CH), 3.65 (t, *J* = 5.7 Hz, 2H, N**H$_2$**), 3.48 (t, J = 6.6 Hz, 2H, CH$_2$**CH$_2$**O), 3.02 (tt, J = 12.0, 3.6 Hz, 1H, C**H**), 2.40 (t, *J* = 2.4 Hz, 1H, CH$_2$C≡C**H**), 2.38 – 2.30 (m, 2H, NC**H$_2$**), 1.71 – 1.61 (m, 2H, 2 x C**H$_a$**H$_b$CH), 1.61 – 1.50 (m, 2H, 2 x CH$_a$**H$_b$**CH), 1.47 – 1.14 (m, 10H, 5 x CH$_2$), 1.09 (s, 6H, 2 x CH$_3$), 1.00 (s, 6H, 2 x CH$_3$).

^{13}C NMR (75 MHz, CDCl$_3$) δ: 79.99 (C$_q$), 74.00 (C$_q$), 70.20 (**CH$_2$**OH), 62.43 (C$_q$), 57.93 (**CH$_2$**C≡CH), 55.87 (2 x C$_q$), 44.53 (N**CH$_2$**), 42.63 (**CH$_2$**), 35.37 (**CH$_2$**), 33.88 (**CH$_2$**), 30.02 (**CH$_2$**), 29.37 (2 x **C**H$_3$), 29.26 (2 x **C**H$_3$), 27.32 (**CH$_2$**), 26.11 (**CH$_2$**), 21.68 (**CH$_2$**).

7.1.8.2.8   7-(2,2,6,6-Tetramethyl-4-oxopiperidine-1-yl)heptanal (71)
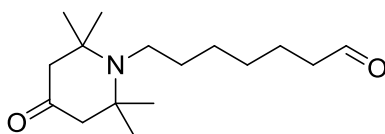
In an oven dried, evacuated and nitrogen purged 100 mL Schlenk tube 738 mg 1-(7-hydroxyheptyl)-2,2,6,6-tetramethylpiperidin-4-one (**66**) (2.74 mmol, 1.0 eq) was dissolved in 5.5 mL dry DCM. Subsequently, 1.40 mL dry DMSO, 693 mg triethylamine (962 µL, 6.84 mmol, 2.5 eq) and 1.09 g Py•SO$_3$ (6.84 mmol, 2.5 eq) were added under a nitrogen stream. The reaction mixture was stirred for 1 h at RT until the color changed to orange and TLC analysis showed a full conversion. Then, the mixture was quenched with 80 mL ice cold

water, neutralized using saturated Na_2CO_3 solution and extracted with ethyl acetate (3 x 80 mL) and $CHCl_3$ (3 x 50 mL). The combined organic layers were dried over anhydrous $MgSO_4$. The solvent was removed under reduced pressure and the crude product was purified by flash column chromatography on silica (cyclohexane:ethyl acetate = 9:1 to 8:2, 40 g silica, size: 24.0 x 2.5 cm) yielding 547 mg 7-(2,2,6,6-tetramethyl-4-oxopiperidine-1-yl)heptanal (**71**) (2.04 mmol, 75%) as a yellow oil.

$C_{16}H_{29}NO_2$ [267.41 g/mol]

R_f = 0.62 (cyclohexane:ethyl acetate = 1:1 (v/v)), 0.23 (cyclohexane:ethyl acetate = 9:1 (v/v)).

GC-MS (EI): t_R = 7.22 min; m/z (%) 267.2 (2.1) [M]$^+$, 252.2 (100.0) [M-CH$_3$]$^+$, 170.1 (15.4), 168.1 (68.6), 126.1 (23.5), 112.1 (35.3), (98.1) (11.6), 95.1 (25.1), 83.1 (79.7), 70.1 (64.3), 69.1 (27.1), 55.1 (42.9).

^{1}H NMR (300 MHz, CDCl$_3$) δ: 9.76, (t, *J* = 1.5 Hz, 1H, **C**H**O**), 2.44 (m, 4H, **C**H$_2$CHO, N**C**H$_2$), 2.32 (s, 4H, **C**H$_2$C(O)**C**H$_2$), 1.69 – 1.57 (m, 2H, **C**H$_2$), 1.54 – 1.42 (m, 2H, **C**H$_2$), 1.38-1.19 (m, 4H, **C**H$_2$), 1.11 (s, 12H, 4 x **C**H$_3$).

^{13}C NMR (75 MHz, CDCl$_3$) δ: 210.07 (**C**=O), 202.71 (**C**HO), 59.79 (2 x C$_q$), 55.84 (**C**H$_2$C(O)**C**H$_2$), 44.53 (N**C**H$_2$), 43.82 (**C**H$_2$CHO), 35.34 (**C**H$_2$), 29.06 (**C**H$_2$), 28.30 (4 x **C**H$_3$), 27.14 (**C**H$_2$), 22.10 (**C**H$_2$).

7.1.8.2.9   2,2,6,6-Tetramethyl-1-(oct-7-yn-1-yl)piperidin-4-one (70)
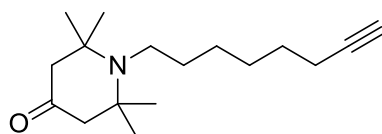
An oven dried, evacuated and nitrogen purged 50 mL two-neck round-bottom flask with a vacuum/gas inlet was charged with 402 mg K_2CO_3 (2.91 mmol, 3.0 eq) in 15 mL dry MeCN. Subsequently, 1.53 g *p*-toluenesulfonylazide (1.16 mmol, 1.2 eq, 15% in toluene), 161 µL dimethyl (2-oxopropyl)phosphonate (1.16 mmol, 1.2 eq) were added under a nitrogen

stream. The resulting mixture was stirred at RT for 2 h, then 259 mg 7-(2,2,6,6-tetramethyl-4-oxopiperidine-1-yl)heptanal (**71**) (0.97 mmol, 1.0 eq) in 3.5 mL dry MeOH were added. The reaction mixture was stirred for 20 h at RT. The reaction progress was monitored by TLC analysis and the reaction was stopped when TLC indicated almost full conversion of the starting material. The solvent was removed under reduced pressure and the residue re-dissolved in 10 mL H_2O and 10 mL Et_2O. The phases were separated and the aqueous phase was additionally extracted with Et_2O (2 x 10 mL). The combined organic layers were dried over anhydrous $MgSO_4$. The solvent was removed under reduced pressure and the crude product purified by flash column chromatography on silica (cyclohexane:ethyl acetate = 95:5, 30 g silica, size: 8.5 x 3.5 cm) yielding 61 mg 2,2,6,6-tetramethyl-1-(oct-7-yn-1-yl)piperidin-4-one (**70**) (0.21 mmol, 24%, 78% purity according to GC-MS.) as yellowish oil.

$C_{17}H_{29}NO_2$ [263.42 g/mol]

R_f = 0.60 (cyclohexane:ethyl acetate = 7:3 (v/v)), 0.44 (cyclohexane:ethyl acetate = 4:1 (v/v)), 0.27 (cyclohexane:ethyl acetate = 9:1 (v/v)).

GC-MS (EI): t_R = 6.93 min; m/z (%) 263.2 (3.4) $[M]^+$, 248.2 (100.0) $[M-CH_3]^+$, 168.1 (79.0), 166.1 (11.4), 126.1 (16.2), 112.1 (36.8), 83.1 (73.4), 69.1 (23.2), 67.1 (22.9), 55.1 (41.0).

^{1}H NMR (300 MHz, $CDCl_3$) δ: 2.45 (m, 2H, NC**H**$_2$), 2.33 (s, 4H, C**H**$_2$C(O)C**H**$_2$), 2.19 (td, *J* = 6.9, 2.7 Hz, 2H, C**H**$_2$C≡CH), 1.95 (t, *J* = 2.7 Hz, 1H, CH$_2$C≡C**H**), 1.58 – 1.39 (m, 6H, 3 x C**H**$_2$), 1.24 (m, 2H, C**H**$_2$), 1.12 (s, 12H, 4 x C**H**$_3$).

^{13}C NMR (76 MHz, $CDCl_3$) δ: 210.16 (**C**=O), 84.64 (**C**≡CH), 68.14 (C≡**C**H), 59.81 (2 x C_q), 55.88 (**C**H$_2$C(O)**C**H$_2$), 44.58 (N**C**H$_2$), 35.39 (**C**H$_2$), 28.62 (**C**H$_2$), 28.54 (**C**H$_2$), 28.30 (4 x **C**H$_3$).

7.1.8.2.10   Prop-2-yn-1-yl 4-methylbenzenesulfonate (propargyl tosylate) (73)
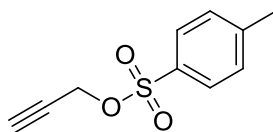
In an oven dried 50 mL round-bottom flask 9.90 g 4-methylbenzene-1-sulfonyl chloride (tosyl chloride) (3.0 mL, 51.9 mmol, 1.0 eq) were dissolved in 10 mL DCM forming a white suspension which was cooled down to 0 °C in an ice-water bath. Subsequently, 2.91 g prop-2-yn-1-ol (propargyl alcohol) (51.9 mmol, 1.0 eq) dissolved in 4.5 mL H_2O were added at 0 °C, followed by dropwise addition of 2.28 g NaOH (57.1 mmol, 1.1 eq) dissolved in 4.4 mL H_2O. The reaction mixture was stirred overnight, letting the temperature to reach RT. After 17 h 30 mL DCM and 25 mL H_2O were added to the reaction mixture and the phases were separated. The organic phase was washed with H_2O (2 x 25 mL) and dried over anhydrous $MgSO_4$. The solvent was removed *in vacuo.* As according to GC-MS analysis the crude product was >99% pure therefore it was used in the subsequent step without further purification. After drying under vacuum, 10.25 g prop-2-yn-1-yl 4-methylbenzenesulfonate (propargyl tosylate) (**73**) (48.8 mmol, 94%) was obtained as a colorless oil.

$C_{10}H_{10}O_3S$ [210.25 g/mol]

GC-MS (EI): t_R = 6.11 min; m/z (%) 210.0 (3.8) [M]$^+$, 155.0 (15.2), 139.0 (18.9), 130.0 (41.2), 118.1 (24.2), 117.1 (16.3), 115.0 (14.3), 91.0 (100.0), 89.0 (16.7), 77.0 (11.2), 65.0 (40.7), 63.0 (14.3), 51.0 (6.9).

^{1}H NMR (300 MHz, CDCl$_3$) δ: 7.81 (d, *J* = 8.4 Hz, 2H, arom.), 7.35 (d, *J* = 8.4 Hz, 2H, arom.), 4.69 (d, *J* = 2.7 Hz, 2H, C**H**$_2$C≡CH), 2.47 (t, *J* = 2.7 Hz, 1H, CH$_2$C≡C**H**), 2.45 (s, 3H, C**H**$_3$).

^{13}C NMR (75 MHz, CDCl$_3$) δ: 145.20 (**C**$_{Ar}$-1), 132.87 (**C**$_{Ar}$-4), 129.84 (**C**$_{Ar}$-3), 128.10 (**C**$_{Ar}$-2), 77.27 (**C**≡CH), 75.32 (C≡**C**H), 57.31 (**C**H$_2$C≡CH), 21.65 (**C**H$_3$).

The spectral data are identical to those published previously.[339]

7.1.8.2.11   2,2,6,6-Tetramethyl-1-(prop-2-yn-1-yl)piperidin-4-ol (74)
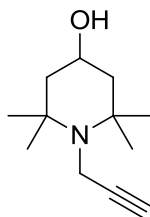
In an oven dried, evacuated and nitrogen flushed three-neck 100 mL round-bottom flask equipped with a condenser 1.258 g 2,2,6,6-tetramethylpiperidin-4-ol (8.0 mmol, 2.0 eq) was dissolved in 14.4 mL dry MeCN. Subsequently, 841 mg propargyl tosylate (**73**) (4.0 mmol, 1.0 eq) was added to the solution *via* a syringe forming a white suspension. The reaction mixture was then carried out at reflux for 5 h. Within the first minutes of heating the suspension became clear and the color changed from white to yellowish. When no further conversion of starting materials was observed using GC-MS analysis, the reaction mixture was cooled down to RT and quenched with 20 mL H_2O. The water phase was extracted with ethyl acetate (3 x 20 mL). The combined organic layers were dried over anhydrous $MgSO_4$. The mixture was then cooled down in an ice-water bath. This facilitated the crystallization of the product. The product was collected by filtration and dried *in vacuo.* This provided 607 mg 2,2,6,6-trimethyl-1-(prop-2-yn-1-yl)piperidin-4-ol (**74**) (3.11 mmol, 78%) as a white crystalline solid.

$C_{12}H_{21}NO$ [195.30 g/mol]

R_f = 0.13 (cyclohexane:ethyl acetate = 4:1 (v/v)).

GC-MS (EI): t_R = 5.51 min; m/z (%) 195.1 (1.3) $[M]^+$, 180.1 (100.0) $[M-CH_3]^+$, 162.0 (6.0), 124.0 (22.9), 108.1 (3.3), 96.0 (14.7), 94.0 (6.1), 85.0 (4.7), 80.0 (14.5), 79.0 (4.4), 67.0 (3.5), 55.9 (4.7).

^{1}H NMR (300 MHz, CDCl$_3$) δ: 3.96 (m, 1H, C**H**), 3.33 (d, *J* = 2.1 Hz, 2H, C**H$_2$**C≡CH), 2.11 (s, 1H, CH$_2$C≡C**H**), 1.82 (dd, *J* = 12.0, 3.6 Hz, 2H, C**H$_2$**CH), 1.61 (brs, 1H, O**H**), 1.41 (t, *J* = 11.7 Hz, 2H, C**H$_2$**CH), 1.26 (s, 7H), 1.07 (s, 6H).

^{13}C NMR (75 MHz, CDCl$_3$) δ: 86.96 (**C**≡CH), 68.89 (C≡**C**H), 63.83 (C$_q$ **C**HOH), 56.35 (C$_q$), 49.93 (2 x **C**H$_2$), 33.57 (**C**H$_2$C≡CH), 32.39 (2 x **C**H$_3$), 22.31 (2 x **C**H$_3$).

The spectral data are identical to those published previously.[339]

7.1.8.2.12   2,2,6,6-Tetramethyl-1-(prop-2-yn-1-yl)piperidin-4-one (75)
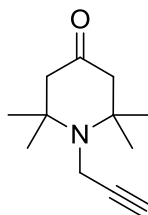
An oven dried, evacuated and nitrogen purged 250 mL Schlenk flask was cooled down to -78 °C in an acetone-dry ice bath. Subsequently, 1.133 g oxalyl chloride (8.93 mmol, 1.1 eq) were dissolved in 95 mL dry DCM under a nitrogen stream. Then, 1.395 g dry DMSO (1.27 mL, 17.90 mmol, 2.2 eq) were added slowly *via* a syringe resulting in a slightly yellowish mixture, which was stirred at -78 °C for 10 min. Subsequently, 1.586 g 2,2,6,6-trimethyl-1-(prop-2-yn-1-yl)piperidin-4-ol (**74**) (8.12 mmol, 1.0 eq) in 15 mL dry DCM were added dropwise, followed by dropwise addition of 4.927 g triethylamine (6.791 mL, 48.70 mmol, 6.0 eq). The reaction mixture was then stirred at -78 °C for 30 min. After that time the cooling was removed and the reaction mixture was stirred for 1 h, letting the temperature to reach RT. The reaction was quenched with 90 mL saturated NaHCO$_3$ solution and neutralized with 9 mL 1M HCl. The phases were separated and the aqueous phase was extracted with DCM (3 x 110 mL). The combined organic layers were dried over anhydrous MgSO$_4$. The solvent was removed under reduced pressure and the crude product was purified by flash column chromatography on silica (cyclohexane:ethyl acetate = 9:1 to 8:1, 100 g silica, size: 34.0 x 2.5 cm) yielding 1.140 g 2,2,6,6-tetramethyl-1-(prop-2-yn-1-yl)piperidin-4-one (**75**) (5.90 mmol, 73%) as colorless crystals.

$C_{12}H_{19}NO$ [193.29 g/mol]

R_f = 0.50 (cyclohexane:ethyl acetate = 4:1 (v/v)), 0.28 (cyclohexane:ethyl acetate = 9:1 (v/v)).

GC-MS (EI): t_R = 5.40 min; m/z (%) 193.2 (2.9) [M]$^+$, 178.1 (100.0) [M-CH$_3$]$^+$, 122.0 (9.9), 96.0 (11.6), 94.1 (5.4), 83.0 (52.5), 80.0 (42.7), 70.0 (4.5), 55.0 (16.3).

^{1}H NMR (300 MHz, CDCl$_3$) δ: 3.47 (d, J = 1.8 Hz, 2H, **CH$_2$**C≡CH), 2.39 (s, 2H, **CH$_2$**C(O)**CH$_2$**), 2.17 (brs, 1H, CH$_2$C≡C**H**), 1.25 (s, 12H, 4 x **CH$_3$**).

^{13}C NMR (75 MHz, CDCl$_3$) δ: 209.50 (**C**=O), 86.01 (**C**≡CH), 69.89 (C≡**C**H), 59.51 (2 x C$_q$), 55.65 (**C**H$_2$C(O)**C**H$_2$), 32.73 (**C**H$_2$C≡CH), 28.40 (4 x **C**H$_3$).

7.1.8.2.13 2,2,6,6-Tetramethyl-1-(prop-2-yn-1-yl)piperidin-4-one oxime (76)
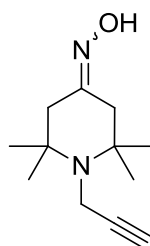
In an oven dried, evacuated and nitrogen purged 100 mL Schlenk flask 1.140 g 2,2,6,6-tetramethyl-1-(prop-2-yn-1-yl)piperidin-4-one (**75**) (5.9 mmol, 1.0 eq) were dissolved in 18.0 mL dry MeOH forming a colorless solution. Then, 819 mg hydroxylamine hydrochloride (11.8 mmol, 2.0 eq) were dissolved, followed by the addition of 1.312 g dry triethylamine (1.81 mL, 13.00 mmol, 2.2 eq) under a nitrogen stream. The yellow solution turned to a yellowish suspension. The reaction mixture was stirred overnight at RT. The reaction progress was monitored by TLC analysis. When TLC analysis indicated the complete consumption of the starting material, the solvent was removed under reduced pressure. The residue was dissolved in 100 mL ethyl acetate and washed with water (3 x 50 mL). Then the organic phase was dried over anhydrous MgSO$_4$. The solvent was removed *in vacuo* to furnish analytically pure 1.190 g 2,2,6,6-tetramethyl-1-(prop-2-yn-1-yl)piperidin-4-one oxime (**76**) (5.71 mmol, 97%) as white to yellowish crystals.

$C_{12}H_{20}N_2O$ [208.30 g/mol]

R_f = 0.75 (cyclohexane:ethyl acetate = 1:1 (v/v)), 0.54 (cyclohexane:ethyl acetate = 2:1 (v/v)), 0.26 (cyclohexane:ethyl acetate = 4:1 (v/v)).

GC-MS (EI): t_R = 5.98 min; m/z (%) 208.2 (2.3) [M]$^+$, 193.1 (100.0) [M-CH$_3$]+, 96.1 (16.7), 94.0 (12.0), 81.9 (6.2), 80.0 (37.0), 55.1 (12.5), 53.0 (9.6).

^{1}H NMR (300 MHz, DMSO-d$_6$) δ: 3.32 (2H, C**H**$_2$C≡CH, overlay with H$_2$O from DMSO-d$_6$) 2.88 (s, 1H, CH$_2$C≡C**H**), 2.34 (s, 2H, C**H**$_2$C(O)), 2.08 (s, 2H, C**H**$_2$C(O)), 1.56 (s, 1H, N=O**H**), 1.08 (s, 12H, 4 x C**H**$_3$).

7.1.8.2.14   2,2,6,6-Tetramethyl-1-(prop-2-yn-1-yl)piperidin-4-amine (77)
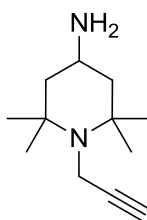
An oven dried, evacuated and argon purged 100 mL Schlenk flask was charged with 1.080 g lithium aluminium hydride (28.5 mmol, 5.0 eq) under an argon stream. Addition of 40.0 mL dry THF resulted in a grey suspension which was then cooled to ca. 0 °C in an ice-water bath. Subsequently, 1.190 g 2,2,6,6-tetramethyl-1-(prop-2-yn-1-yl)piperidin-4-one oxime (**76**) (5.71 mmol, 1.0 eq) in 10.0 mL dry THF were added slowly *via* a syringe over 20 min. The reaction mixture was then stirred vigorously at 40 °C for 3 d. When TLC analysis indicated the full conversion of the starting material, the reaction mixture was cooled to 0°C in an ice-water bath. Subsequently, 1.080 mL ice cold water, 1.080 mL 15% aqueous NaOH solution and 3.240 mL ice cold water were added dropwise (n-n-3n work-up). The mixture was then stirred for 5 min at 0 °C, The formed white solid was filtrated off through a Celite® pad and washed with 130 mL diethyl ether. The ether phase was dried over anhydrous MgSO$_4$. The solvent was removed *in vacuo* and the crude product purified by flash column chromatography on silica (DCM:methanol = 19:1 with 1% Et$_3$N (v/v), 60 g silica, size: 29.0 x

2.5 cm) furnishing 515 mg 2,2,6,6-tetramethyl-1-(prop-2-yn-1-yl)piperidin-4-amine (**77**) (2.65 mmol, 42%) as colorless crystals.

$C_{12}H_{22}N_2$ [194.32 g/mol]

R_f = 0.53 (DCM:MeOH = 5:1 with 1% Et_3N (v/v)), 0.45 (DCM:MeOH = 10:1 with 1% Et_3N (v/v)).

GC-MS (EI): t_R = 5.42 min; m/z (%) 194.1 (1.7) $[M]^+$, 179.1 (100.0) $[M-CH_3]^+$, 162.1 (20.9), 136.1 (21.7), 123.0 (21.7), 96.0 (35.2), 84.1 35.2, 82.0 (9.5), 80.0 (67.9), 70.1 (12.4), 56.0 (17.5), 53.0 (9.7).

^{1}H NMR (300 MHz, $CDCl_3$) δ: 3.31 (d, J = 2.1 Hz, 2H, **CH**$_2$C≡CH), 3.02 (tt, J = 12.0, 3.6 Hz, 1H, **CH**), 2.09 (t, J = 2.1 Hz, 1H, CH$_2$C≡C**H**), 1.87 (brs, 2H, N**H**$_2$), 1.68 (dd, J = 12.3, 3.6 Hz, 2H, 2 x C**H**$_a$H$_b$CH), 1.27 (d, J = 12.0 Hz, 2H, 2 x CH$_a$**H**$_b$CH), 1.23 (s, 6H, 2 x C**H**$_3$), 1.04 (s, 6H, 2 x C**H**$_3$).

^{13}C NMR (75 MHz, $CDCl_3$) δ 87.09 (**C**≡CH), 68.77 (C≡**C**H), 55.97 (2 x C$_q$), 51.05 (2 x **C**H$_2$), 42.57 (C$_q$ **C**HNH$_2$), 33.60 (**C**H$_2$C≡CH), 32.54 (2 x **C**H$_3$), 21.92 (2 x **C**H$_3$).

7.1.8.2.15 3-((Methyl(prop-2-yn-1-yl)amino)methyl)-*N*-(2,2,6,6-tetramethyl-1-(prop-2-yn-1-yl)piperidin-4-yl)benzamide (78)-a
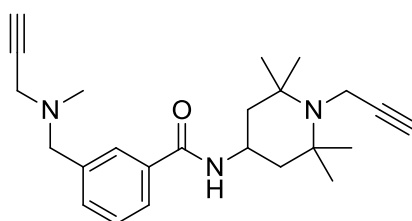
An oven dried, evacuated and nitrogen purged 50 mL Schlenk tube was charged with 185 mg 3-((methyl(prop-2-yn-1-yl)amino)methyl)benzoic acid (**58**)-**a** (0.91 mmol, 1.0 eq) under a nitrogen stream. Addition of 4.0 mL dry toluene and 4.0 mL thionyl chloride resulted in a whitish suspension. The reaction mixture was stirred vigorously at 100 °C for 90 min leading to the formation of a clear yellowish solution. The reaction mixture was cooled down to RT

and the solvent was removed *in vacuo*. The crude product (3-((methyl(prop-2-yn-1-yl)amino)methyl)benzoyl chloride) was dried under vacuum in a Schlenk flask. Subsequently, the crude product was cooled down to ca. -10 °C and 195 mg 2,2,6,6-tetramethyl-1-(prop-2-yn-1-yl)piperidin-4-amine (**77**) (1.0 mmol, 1.05 eq) dissolved in 15.0 mL dry THF and 126 mg K_2CO_3 (0.91 mmol,1.0 eq) were added under a nitrogen stream. The reaction mixture was stirred overnight, letting the temperature to reach RT. After 20 h, TLC analysis indicated the complete consumption of the starting materials. The solvent was removed in vacuo, the residue re-dissolved in 50 mL chloroform and washed with 0.1 M K_2CO_3 solution (2 x 50 mL) and H_2O (1 x 50 mL). The organic phase was then dried over anhydrous $MgSO_4$. The solvent was removed *in vacuo* and the crude product purified by flash column chromatography on silica (cyclohexane:ethyl acetate = 2:1 to 3:2 (v/v), 22 g silica, size: 15.0 x 2.0 cm) furnishing 290 mg 3-((methyl(prop-2-yn-1-yl)amino)methyl)-*N*-(2,2,6,6-tetramethyl-1-(prop-2-yn-1-yl) piperidin-4-yl)benzamide (**78**)-**a** (0.76 mmol, 84%) as a yellowish crystallizing oil.

$C_{24}H_{33}N_3O$ [379.54 g/mol]

R_f = 0.38 (cyclohexane:ethyl acetate = 1:1 (v/v)).

HPLC-MS (EI+): t_R = 5.529 min (JK_10to90); m/z (%) 380.3 (100.0).

^{1}H NMR (300 MHz, CDCl$_3$) δ: 7.70 (s, 1H, arom.), 7.66 (s, 1H, arom.), 7.46 (d, *J* = 7.5 Hz, 1H, arom.), 7.37 (t, *J* = 7.5 Hz, 1H, arom.), 5.99 (d, *J* = 7.5 Hz, 1H, N**H**), 4.49 – 4.28 (m, 1H, C**H**), 3.62 (brs, 2H, PhC**H**₂N), 3.37 (d, *J* = 2.1 Hz, 2H, N(CH₃)**CH**₂C≡CH), 3.31 (d, *J* = 2.1 Hz, 2H, **CH**₂C≡CH), 2.34 (s, 3H, NC**H**₃), 2.29 (t, *J* = 2.1 Hz, 1H, C≡C**H**), 2.13 (s, 1H, C≡C**H**), 1.90 (dd, *J* = 12.0, 3.3 Hz, 2H, 2 x C**H**ₐH$_b$CH), 1.52 – 1.44 (m, 2H, 2 x CHₐ**H**$_b$CH), 1.28 (s, 6H, 2 x C**H**₃), 1.18 (s, 6H, 2 x C**H**₃).

^{13}C NMR (75 MHz, CDCl₃) δ: 166.69 (**C**=O), 138.63 (**C**$_{Ar}$-1), 134.93 (**C**$_{Ar}$-3), 132.11 (**C**$_{Ar}$-6), 128.63 (**C**$_{Ar}$-5), 127.27 (**C**$_{Ar}$-2), 126.14 (**C**$_{Ar}$-4), 78.07 (2 x **C**≡CH), 73.73 (2 x C≡**C**H), 59.60 (Ph**C**H₂N), 47.06 (2 x C$_q$), 44.94 (**C**H₂C≡CH pargyline), 42.01 (2 x **C**H₂), 41.66 (N**C**H₃), 33.37 (**C**$_q$HNH), 32.65 (**C**H₂C≡CH piperidine), 21.81 (4 x **C**H₃).

7.1.8.2.16   4-((Methyl(prop-2-yn-1-yl)amino)methyl)-*N*-(2,2,6,6-tetramethyl-1-(prop-2-yn-1-yl)piperidin-4-yl)benzamide (78)-b
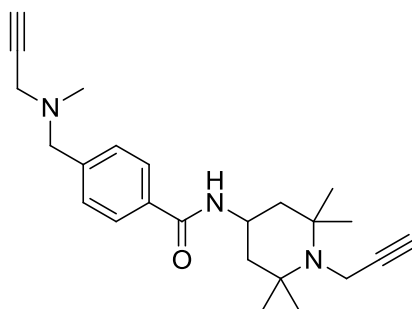
An oven dried, evacuated and nitrogen purged 50 mL Schlenk tube was charged with 209 mg 4-((methyl(prop-2-yn-1-yl)amino)methyl)benzoic acid (**58**)-**b** (1.03 mmol, 1.0 eq) under a nitrogen stream. Addition of 4.0 mL dry toluene and 4.0 mL thionyl chloride resulted in a yellow solution. The reaction mixture was then stirred vigorously at 100 °C for 60 min. The reaction mixture was cooled down to RT and the solvent was removed *in vacuo*. The crude product (4-((methyl(prop-2-yn-1-yl)amino)methyl)benzoyl chloride) was dried under vacuum in a Schlenk flask. Subsequently, the crude product was cooled down to ca. -10 °C and 220 mg 2,2,6,6-tetramethyl-1-(prop-2-yn-1-yl)piperidin-4-amine (**77**) (1.13 mmol, 1.1 eq) dissolved in 15.0 mL dry THF and 142 mg K_2CO_3 (1.03 mmol,1.0 eq) were added under a nitrogen stream. The reaction mixture was stirred overnight, letting the temperature to reach RT. After 20 h, TLC analysis indicated the complete consumption of the starting materials. The solvent was removed *in vacuo*, the residue re-dissolved in 80 mL chloroform and washed with 0.1 M K_2CO_3 solution (2 x 50 mL) and H2O (1 x 50 mL). The organic phase was then dried over anhydrous $MgSO_4$. The solvent was removed *in vacuo* and the crude product purified by flash column chromatography on silica (cyclohexane:ethyl acetate = 2:1 to 3:2 (v/v), 30 g silica, size: 15.0 x 2.5 cm) furnishing 367 mg 4-((methyl(prop-2-yn-1-yl)amino) methyl)-*N*-(2,2,6,6-tetramethyl-1-(prop-2-yn-1-yl)piperidin-4-yl)benzamide (**78**)-**a** (0.97 mmol, 94%) as a crystallizing yellowish oil.

$C_{24}H_{33}N_3O$ [379.54 g/mol]

R_f = 0.34 (cyclohexane:ethyl acetate = 1:1 (v/v)).

HPLC-MS (EI+): t_R = 5.433 min (JK_10to90); m/z (%) 380.2 (100.0).

^{1}H NMR (300 MHz, CDCl$_3$) δ: 7.69 (d, J = 8.1 Hz, 2H, arom.), 7.40 (d, J = 8.0 Hz, 2H, arom.), 5.90 (d, J = 7.4 Hz, 1H, N**H**), 4.48 – 4.27 (m, 1H, C**H**), 3.60 (brs, 2H, PhC**H**$_2$N), 3.37 (d, J = 1.8 Hz, 2H, N(CH$_3$)C**H**$_2$C≡CH), 3.29 (d, J = 2.1 Hz, 2H, C**H**$_2$C≡CH), 2.33 (s, 3H, NC**H**$_3$), 2.27 (t, J = 2.2 Hz, 1H, C≡C**H**), 2.14 (s, 1H, C≡C**H**), 1.90 (dd, J = 12.0, 3.3 Hz, 2H, 2 x C**H**$_a$H$_b$CH), 1.52 – 1.40 (m, 2H, 2 x CH$_a$**H**$_b$CH), 1.28 (s, 6H, 2 x C**H**$_3$), 1.19 (s, 6H, 2 x C**H**$_3$).

^{13}C NMR (76 MHz, CDCl$_3$) δ: 166.58 (**C**=O), 142.07 (**C**$_{Ar}$-1), 133.69 (**C**$_{Ar}$-4), 129.19 (**C**$_{Ar}$-2), 126.87 (**C**$_{Ar}$-3), 78.21 (2 x **C**≡CH), 73.53 (2 x C≡**C**H), 59.48 (Ph**C**H$_2$N), 47.05 (2 x C$_q$), 44.96 (**C**H$_2$C≡CH pargyline), 41.92 (2 x **C**H$_2$), 41.72 (N**C**H$_3$), 33.32 (**C**HNH), 32.67 (**C**H$_2$C≡CH piperidine), 21.84 (4 x **C**H$_3$).

7.1.9 Synthesis of clorgyline

7.1.9.1 1-(3-Bromopropoxy)-2,4-dichlorobenzene
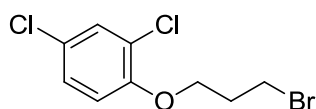
Method A: A mixture of 1.63 g 2,4-dichlorophenol (10.0 mmol, 1.0 eq), 4.04 g 1,3-dibromopropane (20.0 mmol, 2.0 eq) and a solution of 400 mg sodium hydroxide (10.0 mmol, 1.0 eq) in 1.6 mL distilled water were placed to a 10 mL two-neck round-bottom flask equipped with a condenser and stirred at reflux (oil bath temperature ca. 150°C) for 90 min. Then, a solution of 400 mg NaOH (10.0 mmol, 1.0 eq) in 2.4 mL distilled water was added and the reaction mixture was stirred at reflux for another 90 min. After being cooled to room temperature, the reaction mixture was extracted with 20 mL CHCl$_3$ and the organic layer was washed with water (3 x 10 mL) and dried over anhydrous Na$_2$SO$_4$. The solvent was removed

under reduced pressure and the product was purified by flash column chromatography (cyclohexane, 440 g silica, 30.0 x 8.0 cm) resulting in 1.836 g (47%, 73% purity) 1-(3-bromopropoxy)-2,4-dichlorobenzene as a colorless oil.

Method B: In a 50 mL round-bottom flask equipped with condenser 1.63 g 1,4-dichlorophenol (10.0 mmol, 1.0 eq) were dissolved in 25 mL MeCN. Subsequently, 2.764 g potassium carbonate (20.0 mmol, 2.0 eq) were added forming a suspension, followed by the addition of 8.08 g 1,3-dibromopropane (40.0 mmol, 4.0 eq). The resulting reaction mixture was stirred at reflux (oil bath temperature ca. 95°C) for 2 h. The reaction progress was followed by TLC and GC-MS analysis and once the starting material was no longer indicated the mixture was cooled down to RT, the inorganic salt was filtrated off and the organic phase concentrated in *vacuo*. The residue was taken up in 30 mL CHCl$_3$ and the organic phase was washed with 0.2 N NaOH solution (2 x 25 mL), brine (1 x 25 mL) and dried over anhydrous Na$_2$SO$_4$. The solvent was removed under reduced pressure and the product was purified by distillation (85-110°C / 1 mbar) resulting in 1.878 g (6.61 mmol, 66%) as a colorless oil.

C$_9$H$_9$BrCl$_2$O [283.98 g/mol]

R$_f$ = 0.36 (cyclohexane), 0.58 (cyclohexane:ethyl acetate = 9:1 (v/v)).

GC-MS (EI): t$_R$ = 5.32 min; m/z (%) 281.8 (6.4) [M$^+$], 163.9 (61.5), 161.9 (100.0), 133.0 (10.3), 123.0 (8.0), 120.9 (8.3), 97.9 (7.7), 73.0 (10.4), 63.0 (22.2).

^{1}H NMR (500 MHz, CDCl$_3$) δ: 7.36 (d, *J* = 2.0 Hz, 1H, arom.), 7.18 (dd, *J* = 8.5 Hz, *J* = 2.0 Hz, 1H, arom.), 6.87 (d, *J* = 8.5 Hz, 1H, arom.), 4.15 (t, *J* = 5.5 Hz, 2H, OC**H**$_2$), 3.65 (t, *J* = 6.0 Hz, 2H, C**H**$_2$Br), 2.36 (p, *J* = 6.0 Hz, 2H, CH$_2$C**H**$_2$CH$_2$).

^{13}C NMR (125 MHz, CDCl$_3$) δ: 153.20 (**C**$_{Ar}$-1), 130.17 (**C**$_{Ar}$-3), 127.75 (**C**$_{Ar}$-5), 126.18 (**C**$_{Ar}$-4), 124.03 (**C**$_{Ar}$-2), 114.40 (**C**$_{Ar}$-6), 66.89 (O**C**H$_2$), 32.29 (**C**H$_2$Br), 29.95 (CH$_2$**C**H$_2$CH$_2$).

7.1.9.2 *N*-(3-(2,4-Dichlorophenoxy)propyl)-*N*-methylprop-2-yn-1-amine (Clorgyline)
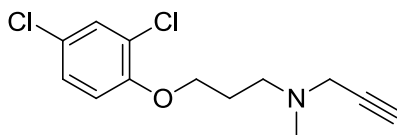
In a 50 mL round-bottom flask 1.863 g 1-(3-bromopropoxy)-2,4-dichlorobenzene (6.56 mmol, 1.0 eq) were dissolved in 16 mL MeCN. Then, 1.088 g potassium carbonate (7.87 mmol, 1.2 eq) dissolved in 2.3 mL distilled water were added, followed by dropwise addition of 907 mg *N*-methylpropargylamine (1.09 mL, 13.12 mmol, 2.0 eq). The resulting clear yellow mixture was stirred at RT for 40 h. The reaction progress was monitored by TLC and GC-MS analysis and once the starting material was no longer indicated the acetonitrile solution was separated from the inorganic solid, which was additionally washed with MeCN and then organic solution was concentrated *in vacuo*. The residue was dissolved in 40 mL diethyl ether and washed with water (3 x 30 mL). The organic layer was dried over anhydrous sodium sulphate and concentrated *in vacuo*. The product was purified by flash column chromatography (diethyl ether) yielding 1.439 g (5.60 mmol, 81%) *N*-(3-(2,4-dichlorophenoxy)propyl)-*N*-methylprop-2-yn-1-amine as a yellowish oil. For convenience of product manipulation, the amine was converted to its hydrochloric salt by saturation of the solution of the product in diethyl ether with gaseous HCl to cause the precipitation of the hydrochloric salt. The white solid was collected by filtration and dried under vacuum.

$C_{12}H_{12}Cl_2NO$ [257.13 g/mol]

R_f = 0.10 (cyclohexane:ethyl acetate = 9:1 (v/v)).

GC-MS (EI): t_R = 6.93 min; m/z (%) 271.0 (0.2) [M+], 132.9 (4.1), 110.0 (2.8), 94.1 (1.4), 82.1 (100.0), 73.0 (2.2), 68.0 (5.4), 63.0 (4.6).

^{1}H NMR (500 MHz, CDCl$_3$) δ: 7.35 (d, *J* = 2.5 Hz, 1H, arom. H-3), 7.16 (dd, *J* = 9.0, 2.5 Hz, 1H, arom. H-5), 6.85 (d, *J* = 9.0 Hz, 1H, arom. H-6), 4.07 (t, *J* = 6.5 Hz, 2H, OC**H**$_2$), 3.38 (d, *J*

= 2.0 Hz, 2H, NC**H**$_2$C≡CH), 2.66 (t, J = 7.0 Hz, 2H, CH$_2$C**H**$_2$N), 2.35 (s, 3H, C**H**$_3$), 2.23 (s, 1H, C≡C**H**), 1.99 (p, J = 6.5 Hz, 2H, CH$_2$C**H**$_2$CH$_2$).

^{13}C NMR (125 MHz, CDCl$_3$) δ: 153.49 (**C**$_{Ar}$-1), 130.05 (**C**$_{Ar}$-3), 127.65 (**C**$_{Ar}$-5), 125.70 (**C**$_{Ar}$-4), 123.86 (**C**$_{Ar}$-2), 114.25 (**C**$_{Ar}$-6), 78.38 (**C**≡CH), 73.48 (C≡**C**H), 67.52 (OC**H**$_2$), 52.15 (CH$_2$**C**H$_2$N), 45.82 (**C**H$_2$C≡CH), 41.84 (**C**H$_3$), 27.23 (CH$_2$**C**H$_2$CH$_2$).

The spectral data are identical to those published previously.[353]

7.2 Biology section

7.2.1 Materials for Biological Experiments

Cell lines DBTRG-05MG (ATCC code CRL2020[TM]), U373 MG (ATCC code HTB-17[TM] or ICLC HTL99014), H460 (ATCC code HTB-177[TM]), HeLa (ATCC code CCL-2[TM]), MDA-MB-231 (ATCC code HTB-26[TM]) and HepG2 (ATCC code HB-8065[TM]) were obtained from American Type Culture Collection (ATCC, Manassas, VA, USA). Cell line RAEW was generously donated by Prof. Walter Berger (Institute of Cancer Research, Medical University of Vienna, Austria).

All cell culture media and supplements were obtained from PAA, Gibco or Sigma-Aldrich.

Human recombinant MAO A and MAO B were generously provided by Prof. Dale E. Edmondson (Department of Biochemistry and Chemistry, Emory University, Atlanta, USA). All other recombinant flavin-dependent enzymes (BBE, Dbv29, Lot6p, YcnD) were kindly provided by the group of Prof. Peter Macheroux (Institute of Biochemistry, Graz University of Technology, Graz, Austria).

Anti-MAO A (ab90675) and anti-MAO B (ab67297) antibodies were purchased from Abcam.

Amplex® Red MAO assay kit (A12214) was purchased from Invitrogen.

Kynuramine·2HBr, benzylamine·HCl, deprenyl·HCl, pargyline·HCl, avidin-agarose beads and Thiazolyl Blue Tetrazolium Bromide were obtained from Sigma-Aldrich. TBTA and TCEP were purchased from Aldrich. Formic acid (MS grade) was purchased from Fluka (94318) and DMSO for molecular biology from Sigma (D8418).

Roti®-Quant universal BCA Protein Assay Kit (0120.1) was purchased from Carl Roth, BCA Protein Assay Kit (23225) was purchased from Thermo Scientific Pierce® and Protein Assay Kit II (Cat. No. 500-0002) was purchased from Bio-Rad.

Sequencing grade modified trypsin (V542A) was purchased from Promega (Madison, WI, USA).

Common salts and reagents used for preparation of buffers and solutions for SDS-PAGE were purchased from Acros Organics, Carl Roth, Fisher Scientific, Fluka, Merck or Sigma-Aldrich.

7.2.2 Equipment

SDS-PAGE were performed on different types of **electrophoresis apparatus**: Bio-Rad Criterion™ Cell or Mini-PROTEAN® Tetra Cell (small gels 10 x 10 cm) (at TUG), Peqlab PerfectBlue Dual Gel System Twin L (45-2020-I) (big gels 20 x 20 cm), Peqlab PerfectBlue Dual Gel System Twin S (45-1010-I) (small gels 10 x 10 cm) (at TUM).

Western Blots were carried out using two types of **electrophoretic blotting apparatus**: either Bio-Rad Mini Trans-Blot Electrophoretic Transfer Cell (for a wet transfer) (at TUG) or Bio-Rad Trans-Blot® SD Semi-Dry Electrophoretic Transfer Cell (for a semi-dry transfer) (at TUM).

For in-gel fluorescence scanning two **fluorescence scanners** were used: Bio-Rad Molecular Imager FX System (at TUG) using two settings with regard to laser and emission filter combination (for NBD fluorophore - laser: 488 nm laser, emission filter wheel A: 530 nm BP, emission filter wheel B: Blank, for TAMRA fluorophore - laser: 532 nm laser, emission filter wheel A: Blank, emission filter wheel B: 555 nm LP) and Fujifilm Life Science Las-4000 Luminescent Image Analyzer equipped with a Fujinon VRF43LMD3 Lens and a 575DF20 Cy3 Filter (at TUM).

SPECORD® 205 UV VIS **spectrophotometer** (Analytik Jena AG) was used to perform Amplex Red MAO activity assay and BCA protein concentration assays (at TUG).

For protein activity, protein concentration or MTT assays two **microplate readers** were used: TECAN Infinite® M200 Pro microplate reader (at TUM) and Amersham Biosciences Biotrak™ II Visible Plate Reader (at University of Graz).

For cell lysis, tissue homogenization or protein/lysate resuspension by **sonication** two types of **ultrasonic homogenizers** were in use: Bandelin Sonoplus HD2070 (at TUM) or Misonix Q125 Sonicator Ultrasonic Cell Disrupter (at University of Graz).

7.2.3 Cell culture

The human glioblastoma multiforme cells (RAEW (established from a surgical specimen and analysed in early passage number) or DBTRG-05MG) and the human large cell lung carcinoma cells H460 (ATCC number: HTB-177™) were cultured in RPMI 1640 medium containing 2 mM L-glutamine, 100 µM penicillin/streptomycin supplemented with 10% FCS in a humidified 5% CO_2 incubator at 37 °C.

The human glioblastoma-astrocytoma cell line U373 MG was maintained in MEME medium (Minimum Essential Medium with Earle's salts) containing 2 mM L-glutamine, 1% (v/v) non-essential amino acids (NEAA), 1 mM sodium pyruvate, 100 µM penicillin/streptomycin supplemented with 10% FCS in a humidified 5% CO_2 incubator at 37 °C.

The human cervix adenocarcinoma cell line HeLa was cultured in MEME medium containing 2 mM L-glutamine, 100 µM penicillin/streptomycin supplemented with 10% FCS in a humidified 5% CO_2 incubator at 37 °C.

The human breast adenocarcinoma cells MDA-MB-231 were cultured in Leibovitz's L-15 medium containing 2 mM L-glutamine, 100 µM penicillin/streptomycin supplemented with 10% FCS in a humidified 5% CO_2 incubator at 37 °C.

The human hepatocellular carcinoma cells HepG2 were grown in DMEM (Dulbecco's Modified Eagle Medium) medium containing 4 mM L-glutamine, 1 mM sodium pyruvate, 100 µM penicillin/streptomycin, high glucose (4.5 g/L) supplemented with 10% FCS in a humidified 5% CO_2 incubator at 37 °C.

7.2.4 Labeling of human monoamine oxidase *in vitro*

Method A: *Pichia pastoris* membrane preparations overexpressing human monoamine oxidase MAO A and MAO B were diluted with 50 mM potassium phosphate buffer, pH 7.5, up to the concentration of ca. 1 mg/mL. Protein samples (43 µL) were incubated with DMSO (blank control) or 10 µM probe (1 µL of 500 µM stock in DMSO) for 1 h at RT with gentle mixing at 750 rpm. For heat denaturation controls, protein samples were denaturated at 96 °C for 6 min and then cooled down to RT prior to the addition of a probe. The samples (44 µL) were then subjected to CC and SDS-PAGE analysis as described below (7.2.9). In competitive ABPP labeling experiments 42 µL protein sample were incubated for 30 min at RT with 1 µL given MAO inhibitor (10-100 fold probe excess, 0.1-1.0 mM, 5-50 mM stock in water), followed by addition of 1 µL 10 µM probe which was incubated as described above.

Method B: *Pichia pastoris* membrane preparations overexpressing human monoamine oxidase MAO A and MAO B were diluted with 50 mM potassium phosphate buffer, pH 7.5 and 50 mM HEPES buffer, pH 7.5, respectively, up to the concentration of ca. 1 mg/mL. Protein samples (43 µL) were incubated with DMSO (blank control) or 10 µM probe (1 µL of 500 µM stock in DMSO) for 1 h at 37 °C with gentle mixing at 350 rpm. For heat controls, protein samples were denaturated at 80 °C for 5 min (denaturation not complete) or at 95 °C for 15 min and then cooled down to RT prior to the addition of a probe. The samples (44 µL) were then subjected to CC and SDS-PAGE analysis as described below (7.2.9). In competitive ABPP labeling experiments 42 µL protein sample were incubated for 30 min at RT with 1 µL given MAO inhibitor (10-100 fold probe excess, 0.1-1.0 mM, 5-50 mM stock in water), followed by addition of 1 µL 10 µM probe which was incubated as described above.

7.2.5 Labeling of an enzyme or tissue or cell lysate *in vitro*

Tissue or cell lysate prepared as described below (7.2.18 and 7.2.19) were diluted with PBS pH 7.4 or a suitable buffer to an appropriate total protein concentration (typically 1 or 2

mg/mL). Protein samples (43 µL) were incubated with DMSO (blank control) or a given concentration of a probe (1 µL of an appropriate 50 x stock in DMSO) for 1 h at RT with gentle mixing at 400-500 rpm. For heat denaturation controls, 41 µL protein samples were mixed with 2 µL 21.5% SDS in PBS and denatured at 96 °C for 6 min and then cooled down to RT prior to the addition of a probe. Alternatively, the samples (43 µL) were heated for ca. 10-15 min at 96 °C and then cooled down to RT and resuspended well by vortexing prior to the addition of a probe. The samples (44 µL) were then subjected to CC and SDS-PAGE analysis as described below (7.2.9). In competitive ABPP labeling experiments 42 µL protein sample were incubated for 30 min at RT with 1 µL given MAO inhibitor (10-100 fold probe excess), followed by addition of 1 µL probe which was incubated as described above.

7.2.6 Labeling of tissue lysates with photocrosslinker probes *in vitro*

Tissue or cell lysate prepared as described below (7.2.18 and 7.2.19) were diluted with PBS pH 7.4 to 2 mg/mL total protein concentration. Protein samples (49 µL) were dispensed into opened 96-microwell polystyrene plates. Then, DMSO (1 µL, as blank control) or a probe (1 µL of an appropriate 50 x stock in DMSO) was added, the plate was gently shaken to assure equal distribution of a probe and the samples were incubated for 30 min at RT. Subsequently, they were irradiated for 60 min with 366 nm UV light (Benda UV hand lamp NU-15 W) under ice cooling. For heat denaturation controls the tissue lysate was denatured at 96 °C for 6 min and cooled down to RT and transferred to the plate before the probe was applied. The samples which were not irradiated with UV light were allowed to incubate with a probe for 90 min at RT on a separate plate. The samples (44 µL) were then subjected to CC and SDS-PAGE analysis as described below (7.2.9).

7.2.7 Labeling *in situ*

Method A: For analytical and preparative *in situ* labeling experiments cells were grown to ca. 80-90% confluency in a complete medium on Petri dishes (150 x 25 mm). Then the medium

was aspirated, cells were washed with prewarmed PBS (10 mL), followed by removal of PBS by suction. Then, 20 mL fresh medium containing either DMSO (as blank control) or probes **P1** or **P3** at the appropriate concentration (10-200 µM) were added. DMSO content in the medium did not exceed 0.1%. Cells were incubated for 2 h with varying concentrations of probes **P1** and **P3** at 37 °C and 5% CO_2 for analytical studies and with concentration of 100 µM for preparative studies. Subsequently, the medium was carefully aspirated, cells were washed with PBS (2 x 10 mL) to remove the excess of the probe and then harvested in 20 mL fresh PBS by scraping. Cell pellets were isolated by centrifugation (1200 rpm, 5 min, 4 °C), resuspended in 500 µL PBS and lysed by sonication under ice cooling. Soluble and insoluble fractions were separated by centrifugation at 14800 rpm for 60 min at 4 °C. (Alternatively, ultracentrifugation at 45000 rpm for 30 min at 4 °C was done). Insoluble pellets were resuspended in 500 µL PBS by sonication under ice cooling. Protein concentration was determined using Bradford or BCA protein concentration assay (Bio-Rad or Carl Roth, respectively) and adjusted to 2 mg/mL in PBS.

Method B: Cells were grown to ca. 80-90% confluency in a complete medium on Petri dishes (150 x 25 mm). Then the medium was aspirated and cells were washed with 10 mL PBS and then harvested in 20 mL fresh PBS by scraping. Cell pellets were isolated by centrifugation (800 g, 5 min), resuspended in 500 µL complete medium containing probes **P1** or **P3** at the appropriate concentration (10-200 µM, from 50 mM DMSO stock) and cells were incubated for 2 h at 37 °C at 900 rpm. Subsequently, cell pellets were spun for 5 min at 800 g at RT to remove the medium with excess of the probe, washed twice with 500 µL PBS, resuspended in 500 µL PBS and processed further as described for Method A. Method B allowed using smaller volumes of media as well as of DMSO stocks of probes giving results identical to Method A.

7.2.8 Competitive labeling *in situ*

Method A: Cells were grown to ca. 80-90% confluency in a complete medium on Petri dishes (150 x 25 mm). Then the medium was aspirated, cells were washed with prewarmed PBS (10 mL), followed by removal of PBS by suction. Then, 20 mL fresh medium containing 2.5 mM pargyline hydrochloride or 2.5 mM deprenyl hydrochloride (25-fold excess compared to a 100 µM probe) were added. Cells were incubated with inhibitors for 1 h at 37 °C and 5% CO_2. After that time, 20 µL probe (100 mM stock in DMSO to give 100 µM probe concentration) were added to medium, gently mixed into medium and the cells were incubated for additional 1 h at 37 °C and 5% CO_2. Further, the competitive labeling was performed as described for labeling *in situ* (see 7.2.7 Method A).

Method B: Cells were grown to ca. 80-90% confluency in a complete medium on Petri dishes (150 x 25 mm). Then the medium was aspirated and cells were washed with 10 mL PBS and then harvested in 20 mL fresh PBS by scraping. Cell pellets were isolated by centrifugation (800 g, 5 min), resuspended in 500 µL complete medium containing 10 mM pargyline hydrochloride or deprenyl hydrochloride (5 µL, 1 M stock in water, 100-fold excess) and incubated for 1 h at 37 °C at 900 rpm. Then, 100 µM probe **P1** or **P3** (1 µL, 50 mM stock in DMSO) was added to the medium and cells were incubated for 1 h at 37 °C at 900 rpm. Subsequently, cell pellets were spun for 5 min at 800 g at RT to remove the medium with excess of the inhibitor and the probe, washed twice with 500 µL PBS, resuspended in 500 µL PBS and lysed by sonication under ice cooling. Soluble and insoluble fractions were separated by centrifugation at 14800 rpm for 60 min at 4 °C. Insoluble pellets were resuspended in 500 µL PBS by sonication under ice cooling. Protein concentration was determined using Bradford or BCA protein concentration assay (Bio-Rad or Carl Roth, respectively) and adjusted to 2 mg/mL in PBS.

7.2.9 Cycloaddition Reactions (CC), Protein Electrophoresis (SDS-PAGE) and In-Gel Fluorescence Scanning (IG-FS)

7.2.9.1 Protocol without protein precipitation

In analytical experiments 44 µL probe-bound protein, tissue or cell lysate (ca. 2 mg/mL total protein concentration) was used to append a fluorescent reporter tag *via* click chemistry (CC) reaction. 100 µM Fluorescent tag (TAMRA-N$_3$ or TAMRA-Alk) (1 µL/reaction, 5 mM stock in DMSO) was added to each lysate sample followed by 1 mM TCEP (1 µL/reaction, 50 mM stock in water) and 100 µM TBTA ligand (3 µL/reaction, 1.7 mM stock in DMSO:*tert*-BuOH 1:4 (v/v)). Samples were gently vortexed and 1 mM CuSO$_4$ (1 µL/reaction, 50 mM stock in water) was added to initiate the 1,3-cycloaddition reaction, giving the total reaction volume of 50 µL. Samples were incubated at RT (25 °C) for 1 h at 350-500 rpm in the dark. Then, the reaction was quenched with 50 µL 2 x SDS loading buffer and samples denatured for 5 min at 95 °C. Proteins were separated by SDS-PAGE on 10% polyacrylamide gels (20 x 20 cm) (50 µL protein sample loading, ca. 40 µg protein/lane) using for first 20-30 min 180 V, then 300 V voltage (ca. 3-4 h). Fluorescence was recorded using Fujifilm Las-4000 Luminescent Image Analyzer with a Fujinon VRF43LMD3 Lens and a 575DF20 filter. Gels were then subjected to Coomassie Brilliant Blue staining to verify equivalent protein loading.

7.2.9.2 Protocol with protein precipitation by trichloroacetic acid (TCA)

The appending of a fluorescent tag *via* click chemistry was performed as described above (7.2.9.1). After click chemistry reaction, protein precipitation procedure was carried out to remove the excess of click chemistry reagents. First, all samples were diluted up to volume 400 µL with an appropriate buffer (350 µL buffer) and then 100 µL (1/4 volume) 50% (w/w) aqueous solution of trichloroacetic acid (TCA) were added, the samples were gently vortexed and left on ice for 1 hour. Then, samples were centrifuged at 13000 rpm for 15 min at 4 °C. Supernatant was discarded and the protein pellets were washed with 200 µL pre-chilled

acetone, resuspended by sonication, centrifuged at 13000 rpm for 5 min at 4 °C and supernatant removed (repeated twice if necessary). After removal of acetone the samples were left to dry for 5-10 min. Then, samples were redissolved in 24 µL of an appropriate buffer, 8 µL 4 x SDS-PAGE loading buffer (reducing) were added, samples were vortexed and denaturated at 95 °C for 5 min. Proteins were separated by 1D SDS-PAGE on 12.5% polyacrylamide gels (ca. 10 x 8 cm) (ca. 7-10 µL protein sample loading, ca. 20-25 µg of protein/gel lane) using for first 30 min 130 V, then 180 V voltage (ca. 1 h). After running a SDS-PAGE the gels were kept in a fixing solution (10% EtOH, 7% AcOH in deionized water) for approximately 1 h and then visualized in-gel using a fluorescence scanner (Bio-Rad Molecular Imager FX, Method: TAMRA (low intensity sample), excitation – 532 nm (blank), emission LP 555 nm). After fluorescence scanning the gels were stained with Commassie staining solution for approx. 30 min and then destained with the destaining solution overnight allowing the visualization of all protein bands and its relative intensity (reflecting the protein amount) in the sample.

7.2.9.3 Protocol with protein precipitation by acetone and premixing of CC reagents

To 44 µL probe-bound protein, tissue or cell lysate (ca. 2 mg/mL total protein concentration) 5 µL of a freshly prepared master mix containing 1 µL TAMRA-N_3 fluorescent tag (5 mM stock in DMSO), 1 µL TCEP (50 mM stock in water) and 3 µL TBTA ligand (1.7 mM stock in DMSO:*tert*-BuOH 1:4 (v/v)) was added. The samples were gently vortexed and 1 µL $CuSO_4$ (50 mM stock in water) was added to initiate the 1,3-cycloaddition reaction, giving the total reaction volume of 50 µL. The final concentrations were as follows: 100 µM TAMRA-N_3, 1 mM TCEP, 100 µM TBTA and 1 mM $CuSO_4$. Samples were incubated at RT (25 °C) for 1 h at 500 rpm in the dark. After click chemistry reaction, 200 µL pre-chilled acetone were added, the samples were gently vortexed and left on ice for 1 h. Then, samples were centrifuged at 15000 rpm for 30 min at 4 °C. Supernatant was discarded and the protein pellets were

washed with 200 µL pre-chilled methanol, resuspended by sonication, centrifuged at 13000 rpm for 15 min at 4 °C and supernatant removed (repeated twice if necessary). After removal of acetone, the samples were left to warm up to RT. Then, samples were redissolved in 30 µL 0.2% SDS in PBS, 10 µL 4 x SDS-PAGE loading buffer (reducing) were added, samples were vortexed and denatured at 95 °C for 5 min. Proteins were separated by 1D SDS-PAGE on 12.5% polyacrylamide gels (ca. 10 x 8 cm) (ca. 10-12 µL protein sample loading, ca. 20-25 µg of protein/gel lane) applying 90 V for 10 min, then 60 min 130 V, then 180 V voltage (ca. 1.5 h). Further, the proteins were fixed in a gel and visualized as described above (7.2.9.2).

7.2.10   Protein enrichment for MS identification

Reactions for preparative enrichment were carried out together with a control lacking the probe to subtract the background unspecific protein binding on avidin-agarose beads from the specifically biotin-avidin enriched protein samples. For preparative scale click chemistry reactions 955 µL probe-bound cell lysates were mixed with 50 µM TAMRA-biotin-N$_3$[312] (Figure 61) (5 µL, 10 mM stock in DMSO), 500 µM TCEP (10 µL, 50 mM stock in water), 50 µM TBTA ligand (30 µL, 1.7 mM stock in DMSO:*tert*-BuOH 1:4 (v/v)) and 500 µM CuSO$_4$ (10 µL, 50 mM stock in water). Samples were gently vortexed and incubated for 1 h at RT in the dark under constant mixing. After CC, proteins were precipitated using three volumes of pre-chilled acetone. Samples were stored at -21 °C overnight and centrifuged at 14800 rpm for 20 min at 4 °C. The supernatant was discarded, and the pellet was washed twice with pre-chilled methanol (200 µL) and resuspended by sonication (Bandelin Sonopuls, 5 sec, 10% intensity) under ice cooling. After removal of supernatant, the pellet was warmed up to RT and dissolved in 0.4% SDS in PBS (800 µL) by sonication (Bandelin Sonopuls, 6 x 10 sec, 30% intensity) and incubated under gentle mixing with 60 µL of pre-equilibrated (60 µL beads resuspended in 1 mL 0.2% SDS in PBS, spun down for 1 min at 2000 rpm, supernatant discarded carefully, repeated 2 times) avidin-agarose beads for 1 h at RT. Thereafter, the

beads were washed with 0.2% SDS in PBS (3 x 1 mL), with urea (2 x 1 mL, 6 M) and with PBS (3 x 1 mL). After each washing, the beads were spun for 1 min at 2000 rpm and supernatant carefully discarded. 60 µL of 2 x SDS loading buffer was added to the beads and the proteins were released from the beads for the preparative SDS-PAGE by incubation for 6 min at 90 °C. The beads were spun down for 2 min at 13000 rpm and supernatant containing released proteins were subjected to SDS-PAGE and in-gel fluorescence scanning.

7.2.11 In-gel digest with trypsin

After SDS-PAGE gel bands with proteins of interest were excised, washed, and tryptically digested as described previously.[29a]

7.2.11.1 Washing gel pieces

The excised gel pieces were cut into ca. 1 mm^3 cubes and placed in a 50 µL Eppendorf tube, washed with 100 µL ddH$_2$O for 15 min at RT, 550 rpm, followed by removal of the supernatant. Subsequently, the gel pieces were washed with 200 µL of a mixture MeCN:50 mM ammonium bicarbonate (ABC) 1:1 (v/v) for 15 min at RT, 550 rpm, then supernatant was discarded. 100 µL MeCN were added to cover completely gel particles and left for 10 min, at RT, 550 rpm. The gel plugs shrunk and sticked together (dehydratation of gel pieces). Acetonitrile was then removed and gel pieces were rehydrated in 100 µL 50 mM ABC for 5 min at RT. Then, 100 µL acetonitrile were added, gel pieces were incubated for 15 min. After that time all liquids were removed. Then, 100 µL acetonitrile were added to cover gel particles and left for 10 min at RT, 550 rpm. After the gel pieces have shrunk, acetonitrile was removed and gel pieces were dried down for 15 min at 40 °C in a vacuum centrifuge (SpeedVac).

7.2.11.2   Reduction and alkylation

100 µL 10 mM dithiothreitol (DTT) in 50 mM ABC (freshly prepared) were added to dried gel pieces and they were incubated for 45 min at 56 °C, 550 rpm. Then the supernatant was discarded, 100 µL acetonitrile were added and gel pieces incubated for 10 min at RT to remove DTT completely. Supernatant was discarded and 100 µL 55 mM iodacetamide (IAA) in 50 mM ABC (freshly prepared) were added and gel pieces incubated for 30 min at RT, with light exclusion, 550 rpm. The supernatant was then removed and gel pieces washed 3 times with 100 µL of a mixture MeCN:50 mM ABC 1:1 (v/v) for 15 min at RT, 550 rpm. After removal of the supernatant, 100 µL acetonitrile were added to cover gel particles and left for 10 min at RT, 550 rpm. After the gel pieces have shrunk, acetonitrile was discarded and gel pieces were dried down for 15 min at 40 °C in a vacuum centrifuge (SpeedVac).

7.2.11.3   Protein digest

Solution of trypsin was prepared freshly by diluting trypsin solution (Promega) with 25 mM ABC 1:100 (1 µLTrypsin per 100 µL 25 mM ABC), and cooling it on ice. Then, 100 µL of trypsin solution in 25 mM ABC were added to each sample containing gel pieces, samples were kept for 10 min on ice or in the fridge until the gel pieces were rehydrated and completely covered by digest solution. If necessary, additional volume of 25 mM ABC was added to cover the particles completely. Then, samples were incubated overnight at 37 °C with gentle mixing at 225 rpm.

7.2.11.4   Peptides extraction

Digest solution (supernatant) was transferred to a fresh 1.5 mL Eppendorf tube. Gel pieces were extracted with 100 µL 25 mM ABC for 15 min in an ultrasonic bath. Then, 100 µL acetonitrile was added and incubated for 15 min in an ultrasonic bath. Supernatant was removed and combined with the digest solution. Gel pieces were subsequently extracted with

100 μL 5 % formic acid (FA) for 15 min in an ultrasonic bath. Then, 100 μL acetonitrile was added and incubated for 15 min in an ultrasonic bath. Supernatant was removed and combined with the digest solution. 100 μL acetonitrile was added and incubated for 15 min in an ultrasonic bath. Finally, supernatant was removed and combined with the digest solution. The combined digest solution was completely dried for 2-3 h at 40 °C in a vacuum centrifuge (SpeedVac). The samples were then resuspended in 20 μL 5 % FA. The centrifuge filters were equilibrated with 20 μL 1 % formic acid (FA) at 13000 rpm for 1 min. The digest solution (ca. 20 μL) was transferred onto the centrifuge filter and eluted 1 - 2 min at 13000 rpm and the samples were measured in the following LC-MS/MS system as described below.

7.2.12   Mass spectrometry and bioinformatics

ESI-MS spectra were recorded by a Thermo LTQ Orbitrap XL coupled to a Dionex UltiMate 3000 RSLC nano. The peptides were loaded on a Dionex Acclaim® PepMap 100 75 μm x 2 cm, C18 (3 μm) and subsequently eluted and separated by a Dionex Acclaim® PepMap RLSC 75 μm x 15 cm, C18 (2 μm).

Mass spectrometry data was searched against the corresponding databases *via* the software Proteome Discoverer 1.3 (Thermo Scientific) using the SEQUEST algorithm.[90] The search was limited to only tryptic peptides, two missed cleavage sites, precursor mass tolerance of 10 ppm and fragment mass tolerance of 0.8 Da. Filters were set to further refine the search results. The X_{corr} vs. charge state filter was set to X_{corr} values of 1.5, 2.0, 2.25 and 2.5 for charge states +1, +2, +3 and +4, respectively. The number of different peptides had to be ≥ 2 and the peptide confidence filter was set to at least medium. These filter values are similar to others previously reported for SEQUEST analysis. X_{corr} values (Score) of each run, the peptide spectrum matches (PSM) as well as the total number of obtained peptides and unique peptides are reported in Table 5.

Table 5. Protein identified by mass spectrometry.

Protein	Protein ID	MW	Score	Coverage [%]	Peptides	Unique Peptides	PSM
RAEW cells (insoluble)							
Amine oxidase [flavin-containing] A	IPI00008483.1	59.6435	158.79	40.0	17	17	52
HepG2 cells (soluble)							
Retinal dehydrogenase 1	Pf00171; Pf05893; Pf07368	54,8269	196.64	54.1	20	20	58
HepG2 cells (insoluble)							
Amine oxidase [flavin-containing] A	Pf01593	59.6435	6.90	6.5	2	2	2

7.2.13 Protein concentration assay

7.2.13.1 BCA assay

7.2.13.1.1 Procedure for 1 mL cuvette format protein concentration assay

For protein concentration assignment Thermo Scientific Pierce® BCA Protein Assay Kit (23225) was used. Bovine serum albumin (BSA) standards (0 – 2.0 mg/mL range: 0, 25, 125, 250, 500, 750, 1000, 1500, 2000 µg/mL) were prepared from the 2.0 mg/mL stock solution in order to establish protein concentration standard curve. BCA working agent (WR) was prepared by mixing in ratio 50:1 (v/v) alkaline solution pH 11.25 containing BCA (A) (40 mL) and copper sulphate solution (B) (0.8 mL). Dilutions of protein sample of unknown concentration were prepared (typically 20, 50, 100, 200-fold diluted). Assay samples were prepared by mixing well 50 µL each BSA standard or unknown protein sample with 1.0 mL BCA working reagent. Then all samples were incubated for 30 min at 37°C and subsequently cooled down to RT and transferred to disposable plastic cuvettes and absorbance at 562 nm

was measured within 10 min. As blank sample water was used. All samples were measured in duplicate.

7.2.13.1.2 Procedure for plate reader format protein concentration assay

For protein concentration assignment Carl Roth Roti®-Quant universal BCA Protein Assay Kit (0120.1) was used. Bovine serum albumin (BSA) standards (0 – 400 µg/mL range: 0, 25, 50, 100, 200, 400 µg/mL) were prepared from the 2.0 mg/mL stock solution in order to establish protein concentration standard curve. BCA working agent was prepared by mixing in ratio 15:1 (v/v) alkaline solution pH 11.25 containing BCA (R1) (300 µL) and copper sulphate solution (R2) (4.5 mL). Dilutions of protein sample of unknown concentration were prepared (typically 50 and 100-fold diluted). Assay samples were prepared samples in a 96-well Flat Bottom Nunclon Surface (Brand) plate by mixing well 50 µL each BSA standard or unknown protein sample with 100 µL BCA working reagent. Then all samples were incubated for 30 min at 37°C and subsequently cooled down to RT and absorbance was measured at 562 nm by a TECAN Infinite® M200 Pro. All samples were measured in triplicate.

7.2.13.2 Bradford assay

For protein concentration assignment Bio-Rad Protein Assay Kit II (Cat. No. 500-0002) was used. Bovine serum albumin (BSA) standards (0 – 400 µg/mL range: 0, 25, 50, 100, 150, 200 µg/mL) were prepared from the 2.0 mg/mL stock solution in order to establish protein concentration standard curve. Assay working reagent (WR) was prepared by diluting dye reagent concentrate in ratio 4:1 (v/v) with deionized water. Dilutions of protein sample of unknown concentration were prepared (typically 50 and 100-fold diluted). Assay samples were prepared in a 96-well microtiter plate by mixing well 20 µL each BSA standard or unknown protein sample with 200 µL WR. Then all samples were incubated for 5 min at RT and absorbance was measured at 562 or 595 nm by Amersham Biosciences Biotrak^{TM} II plate reader. All samples were measured in triplicate.

7.2.14   MAO activity assay

Activity of MAO A and MAO B was assigned in the indirect continuous Amplex® Red – HRP (horse radish peroxidase) coupled assay using kynuramine dihydrobromide and benzylamine hydrochloride as substrates for MAO A and MAO B, respectively. The assay was based on the detection of H_2O_2 in a HRP coupled reaction, which employs 10-acetyl-3,7-dihydroxyphenoxazine (Amplex Red reagent). The activity was assayed spectrophotometrically by monitoring the rate of resorufin formation at 560 nm (product of Amplex Red oxidation).

7.2.14.1   Procedure for 1 mL cuvette format activity assay

7.2.14.1.1   MAO A Amplex Red activity assay

Prepared in advance chromogenic solution (990 µL) containing 3 mM kynuramine hydrochloride (30 µL 100 mM stock in H_2O), 1 U/mL HRP (10 µL 100 U/mL stock in 50 mM phosphate buffer, pH 7.5), 50 µM Amplex Red (10 µL 5 mM stock in DMSO) in 940 µL 50 mM potassium phosphate buffer, pH 7.5, was mixed with 10 µL WT hMAO A, the mixture was vortexed well and absorbance change was followed at 560 nm for 3 min at ambient temperature.

7.2.14.1.2   MAO B Amplex Red activity assay

Prepared in advance chromogenic solution (995 µL) containing 3 mM benzylamine hydrochloride (30 µL 100 mM stock in H_2O), 1 U/mL HRP (10 µL 100 U/mL stock in 50 mM phosphate buffer, pH 7.5), 50 µM Amplex Red (10 µL 5 mM stock in DMSO) in 945 µL 50 mM HEPES buffer, pH 7.5, was mixed with 5 µL WT hMAO B, the mixture was vortexed well and absorbance change was followed at 560 nm for 1 min at ambient temperature.

7.2.14.2   Procedure for plate reader format activity assay

To 3.5 µg MAO A or 2.5 µg MAO B in 50 µL 50 mM potassium phosphate buffer (pH 7.5) were added 50 µL chromogenic solution containing 3 µL 100 mM stock of kynuramine dihydrobromide (for MAO A) or benzylamine hydrochloride (for MAO B), 1 µL 100 U/mL stock horse radish peroxidase, 1 µL 5 mM stock Amplex® Red (10-acetyl-3,7-dihydroxyphenoxazine) and 45 µL 50 mM potassium phosphate buffer, pH 7.5. The samples were mixed thoroughly and absorbance change was recorded at 560 nm at 25 °C for 40-60 min in a 96-well Flat Bottom Nunclon Surface (Brand) plate by a TECAN Infinite® M200 Pro. All measurements were performed in triplicates.

7.2.15   Inhibition assay (IC$_{50}$ assignment)

IC$_{50}$ values for the inhibition of MAO A and MAO B by probes **P1**, **P3** as well as by pargyline and deprenyl and were measured by the Amplex® Red – peroxidase coupled assay described above. 3.5 µg MAO A or 2.5 µg MAO B were incubated in 50 µL 50 mM potassium phosphate buffer (pH 7.5) with varying concentrations of probes **P1**, **P3**, MAO inhibitors (range 1-400 µM) or DMSO (blank control) for 1 h at 25 °C under gentle shaking (750 rpm). Then 50 µL chromogenic solution described above were added to give a total volume of 100 µL, the solution well mixed and absorbance change was recorded in a 96-well Flat Bottom Nunclon Surface (Brand) plate at 560 nm at 25 °C for 60 min by a TECAN Infinite® M200 Pro. All measurements were performed in triplicates. IC$_{50}$ values were calculated from curve fittings (Boltzmann model) by Origin Pro 8.6 (OriginLab Corporation).

7.2.16   Cytotoxicity assay (MTT assay)

7.2.16.1   DBTRG-05MG cell line

DBTRG-05MG cell line was cultured in RPMI 1640 medium (2 mM L-glutamine) supplemented with 10% FCS. Cells from subconfluent cultures were used for the assay.

Precisely, 7.5 x 10^3 DBTRG-05MG cells were plated in 96 well flat-bottom plates (Nunclon, Nunc) in 100 µL medium and cultured for 24 h to obtain 30-40% confluent cultures. Probes **P1** and **P3** were diluted 1:100 from 100 x DMSO stocks in 100 µL of the appropriate culture medium and added to the cells after careful removal of the blank culture medium. After 24 h incubation 20 µL MTT substrate solution (5 mg/mL in PBS) were added and mixed well into the medium by gentle shaking at 300 rpm for 5 min. Following 2 h incubation, the medium was discarded and cells were lysed in 200 µL DMSO. The complete dissolution of the formazan salt (metabolic product of MTT) was checked under the microscope and the optical density was measured at 570 nm (background subtraction at 630 nm) by a TECAN Infinite® M200 Pro. All measurements were performed in triplicates. EC$_{50}$ values were calculated from curve fittings by Origin Pro 8.6 (OriginLab Corporation).

7.2.16.2   HepG2 cell line

HepG2 cell line was cultured in DMEM medium (4 mM L-glutamine) supplemented with 10% FCS. Cells from subconfluent cultures were used for the assay. Precisely, 5.0, 7.5 and 10.0 x 10^3 HepG2 cells were plated in 96-well flat-bottom plates (Nunclon, Nunc) in 100 µL medium and cultured for 24 h to obtain 30-40% confluent cultures. Probes **P1** and **P3** were diluted 1:100 from 100 x DMSO stocks in 100 µL of the appropriate culture medium and added to the cells after careful removal of the blank culture medium. After 24 h incubation 20 µL MTT substrate solution (5 mg/mL in PBS) were added by a multichannel pipette and mixed well into the medium by gentle shaking at 300 rpm for 5 min. Following 2 h incubation, the medium was carefully discarded and cells were lysed in 200 µL DMSO. To facilitate dissolution of formazan black crystals in DMSO the plate was gently shaken at 400 rpm until formazan was fully resuspended. The complete dissolution of the formazan salt (metabolic product of MTT) was checked under the microscope and the optical density was measured at 562 nm (background subtraction at 620 nm) by a Amersham Biosciences Biotrak^{TM}

microplate reader. All measurements were performed in triplicates. EC_{50} values were calculated from curve fittings by Origin Pro 8.6 (OriginLab Corporation).

7.2.17 Western Blotting

7.2.17.1 Semi-dry blotting

For MAO B detection, the cell lysate samples were prepared in the identical way as for in-gel fluorescence scanning. The proteins separated by 10% SDS-PAGE were transferred to a nitrocellulose membrane (VWR) with a Bio-Rad semi-dry blotter for 1 h at 140 mA (approx. 1.2 mA/cm^2 membrane). Prior to transfer, gel as well as the membrane was incubated for ca. 10 min in the Towbin transfer buffer. Then, the transfer sandwich was assembled by placing three pieces of soaked in the transfer buffer Watman paper cut in the size of a gel on top of the anode (platinum). Then, the equilibrated gel was placed on top of the transfer membrane, aligning the gel on the center of the membrane. Finally, three pieces of Watman paper were located on the top of the stack and air bubbles were rolled out. Then, the cathode (stainless steel) closed the apparatus. After the transfer, its efficiency was checked by reversible Ponceau staining. After destaining in deionized water, the blots were saturated with 5% non-fat dried milk in TBS-T (TBS with 0.05% Tween 20®, pH 8.0) for 1 h at 4 °C, incubated with primary rabbit polyclonal anti-MAO B antibody (1:20000 dilution in 1% milk in TBST) overnight at 4 °C, washed five times 5 min with TBST and detected with goat anti-rabbit IgG HRP-conjugated secondary antibody (1:20000 dilution in 1% milk in TBST, 45 min at RT). Signals were detected using Amersham ECL Plus Western Blotting Detection reagents (GE Healthcare) and exposure to light-sensitive film (Kodak or Agfa).

7.2.17.2 Wet blotting

For MAO B detection, the cell lysate samples were prepared in the identical way as for in-gel fluorescence scanning. The proteins separated by 10% SDS-PAGE were transferred to a

nitrocellulose membrane (VWR) with a Bio-Rad Mini Trans-Blot for 90 min at 100 V. Prior to transfer, gel as well as the membrane was incubated for ca. 10 min in a pre-chilled transfer buffer. Then, the gel sandwich assembly was prepared prior to transfer, gel as well as the membrane was incubated for ca. 10 min in the transfer buffer. Then, the transfer sandwich was assembled by placing on the black side of the cassette pre-wetted fiber pad and one sheet of soaked in the transfer buffer Watman paper. Then, the equilibrated gel was placed followed by the membrane. Finally, the sandwich was completed by placing one sheet of filter paper and wetted fiber pad. Then, air bubbles were rolled out and the cassette was closed up firmly and placed in a cassette holder in a transfer chamber. A cooling block was placed into the transfer tank to facilitate the heat dissipation. After the transfer, its efficiency was checked by reversible Ponceau staining. After destaining in deionized water, the blots were blocked with 5% non-fat dried milk in TBS-T (TBS with 0.05% Tween 20®, pH 8.0) for 1 h at 4 °C, incubated with primary rabbit polyclonal anti-MAO B antibody (1:20 000 dilution in 1% milk in TBST) overnight at 4 °C, washed five times 5 min with TBS-T and detected with goat anti-rabbit IgG HRP-conjugated secondary antibody (1:20 000 dilution in 1% milk in TBST, 45 min at RT). Signals were detected using SuperSignal® West Pico Chemiluminescent Substrate (Thermo Scientific) and exposure to light-sensitive film (Kodak or Agfa).

7.2.18   Tissue preparation

<u>Method A:</u> The frozen (-80 °C) mouse tissues (brain, liver) were cut into ca. 50-80 mg fragments and then each tissue slice was cut into smaller pieces. Subsequently, the tissue pieces were transferred to a chilled vial containing cold ceramic beads and ca. 700 µL chilled on ice PBS buffer (pH 7.4) were added. The tissue was homogenized using a Precellys 24 homogenizator (PEQLAB), for approximately 10-20 sec at 5000 rpm. The tissue lysate was additionally sonicated under ice cooling with a sonication beamer (Bandelin Sonoplus) for 10-15 sec (5 pulses, 10-20% intensity) depending on tissue and homogenization state. The

lysate was then centrifuged for 30 min at 4 °C at 13000 rpm and soluble fraction was transferred to a fresh precooled 1.5 mL vial. The insoluble fraction was resuspended in ca. 800 µL chilled PBS buffer by sonication (10-20 sec). The protein concentration was assigned in both fractions using either BCA or Bradford assay and then diluted with PBS to 2 mg/mL. The lysate samples were shock frozen in liquid nitrogen and stored at -80 °C until use.

Method B: The frozen brain tissue was cut into approx. 300 mg pieces and weighed. On ice, 6.5 mL homogenization buffer/g tissue was added and tissue was ground 15 times using a Teflon-pestle. The tissue homogenate was then transferred to 15 mL tubes and centrifuged for 10 min at 4°C at 1000 g. Supernatant was transferred to new 15 mL tubes. 3.5 mL Homogenization buffer was added to the pellet and ground again 15 times. The tissue homogenate was transferred to 15 mL tubes and centrifuged for 10 min at 4°C at 1000 g. Supernatant was collected and pooled with the first supernatant in tubes for ultracentrifugation (ca. 15 mL) and spun down at 40000 rpm (100000 g) for 20 min, at 4°C. The pellets (tissue debris and nuclei) were discarded. After centrifugation, supernatant (cytosolic fraction) was aspirated to new 15 mL tubes while the pellet was resuspended in 15 mL homogenization buffer and spun down at 40000 rpm (100000 g) for 20 min, at 4°C. Supernatant was discarded and the pellet was reconstituted in 2 mL aliquot buffer (membrane fraction). Protein concentration in both fractions (cytosol and membrane) was assigned by Bradford assay and and then diluted with aliquot buffer to 2 mg/mL. The lysate samples were shock frozen in liquid nitrogen and stored at -80 °C until use.

7.2.19 Cell lysate preparation

Method A: Cells were grown to ca. 80-90% confluency in a complete medium on Petri dishes (150 x 25 mm). Then the medium was aspirated, cells were washed with chilled on ice PBS (10 mL), followed by removal of PBS by suction. Then, cells were harvested in 20 mL cold PBS by scraping. Cell pellets were isolated by centrifugation (1200 rpm, 10 min, 4 °C), resuspended in 500 µL PBS and lysed by sonication under ice cooling. Soluble and insoluble

fraction were separated by centrifugation at 14800 rpm for 60 min at 4 °C. (Alternatively, ultracentrifugation at 45000 rpm for 30 min at 4 °C was done). Insoluble pellets were resuspended in 500 μL PBS by sonication under ice cooling. Protein concentration was determined using Bradford or BCA protein concentration assay (Bio-Rad or Thermo Scientific Pierce, respectively) and adjusted to 2 mg/mL in PBS.

Method B: Cells were grown to ca. 80-90% confluency in a complete medium in 175 cm^3 culture flask. Then the medium was aspirated, cells were washed with PBS (20 mL), followed by removal of PBS by suction. Then, the cells were trypsinized with 2 mL trypsin-EDTA for approx. 1-2 min. The detachment of cells was stopped by addition of 10 mL complete medium. Cells were resuspended in medium and subsequently cell pellets were isolated by centrifugation (1200 rpm, 10 min, 4 °C), resuspended in 500 μL cold PBS supplemented with proteinase inhibitors (Roche) and lysed by sonication under ice cooling. Further, the procedure was carried out as described in Method A.

7.2.20 Recipes for buffers, solutions

7.2.20.1 Common buffers

1 x PBS (phosphate buffered saline):

136.9 mM NaCl	8.00 g/L
10.1 mM Na$_2$HPO$_4$	1.44 g/L
2.7 mM KCl	0.20 g/L
1.8 mM KH$_2$PO$_4$	0.24 g/L

Dissolved in 1 L deionized H$_2$O, pH adjusted to 7.4 with conc. HCl.

10 x PBS (phosphate buffered saline):

1.37 M NaCl	80.0 g/L
101 mM Na$_2$HPO$_4$	14.4 g/L

27 mM KCl 2.0 g/L

18 mM KH_2PO_4 2.4 g/L

Dissolved in 1L deionized H_2O, pH adjusted to 7.4 with conc. HCl.

50 mM phosphate buffer (PB) pH 7.5

81.5 mL 100 mM KH_2PO_4 13.6 g/L

418.5 mL 100 mM Na_2HPO_4 14.2 g/L

were mixed and the volume was brought up to ca. 980 mL with deionized H_2O. pH was adjusted to 7.5 with 100 mM KH_2PO_4 solution and the final volume brought to 1 L with deionized H_2O.

50 mM HEPES buffer pH 7.5

11.91 g HEPES (2-[4-(2-hydroxyethyl)piperazin-1-yl]ethanesulfonic acid) was dissolved in ca. 980 mL deionized H_2O, pH was adjusted to 7.5 with 1 M NaOH and the final volume brought to 1 L with deionized H_2O.

7.2.20.2 SDS-PAGE

4 x SDS loading buffer:

2.5 mL 1 M Tris-HCl pH 6.8 (250 mM final concentration)

4 mL glycerol (40% (v/v) final concentration)

0.8 g SDS (8% (w/v) final concentration)

2 mL β-Mercaptoethanol (20% (v/v) final concentration)

1 mg Bromphenol blue (0.01% (w/v) final concentration)

Filled up to 10 mL with deionized H_2O

APS solution (10% (w/v))

100 g/L ammonium peroxide sulphate dissolved in deionized H_2O

SDS solution (10% (w/v))

100 g/L sodium dodecyl sulphate dissolved in deionized H_2O

SDS solution (20% (w/v))

200 g/L sodium dodecyl sulphate dissolved in deionized H_2O

1.5 M Tris- HCl pH 8.8

181.71 g/L Tris base

Dissolved in 1L deionized H_2O, pH adjusted to 8.8 with conc. HCl.

0.5 M Tris- HCl pH 6.8

60.57 g/L Tris base

Dissolved in 1L deionized H_2O, pH adjusted to 6.8 with conc. HCl.

SDS-PAGE: big (20 x 20 cm) gels; resolving gels (10, 12.5%) and stacking gel (3.75%)

% Acrylamide	H_2O_{deion}	Rotiphorese Gel 30	Tris-HCl pH 8.8	Tris-HCl pH 6.8	10% SDS	10% APS	TEMED
10	14.4 mL	12 mL	9 mL	-	360 µL	150 µL	15 µL
12.5	11.4 mL	15 mL	9 mL	-	360 µL	150 µL	15 µL
3.75	**7.35 mL**	**1.5 mL**	**-**	**3 mL**	**120 µL**	**60 µL**	**12 µL**

SDS-PAGE: small (10 x 10 cm, 1.5 mm thick) gels; resolving gels (10, 12.5%) and stacking gel (5.0%)

% Acrylamide	H_2O_{deion}	Rotiphorese Gel 30	Tris-HCl pH 8.8	Tris-HCl pH 6.8	20% SDS	10% APS	TEMED
10	4.0 mL	2.5 mL	3.3 mL	-	50 µL	48 µL	10 µL
12.5	2.99 mL	3.12 mL	3.75 mL	-	50 µL	48 µL	10 µL
5	**3.69 mL**	**0.625 mL**	**-**	**0.625 mL**	**25 µL**	**25 µL**	**5 µL**

1 x SDS-PAGE running buffer

192 mM Glycine   14.4 g/L

25 mM Tris-base   3.0 g/L

0.1% (w/v) SDS   1.0 g/L

Filled up to 1 L with deionized H_2O, pH ca. 8.3

Coomassie Staining solution:

0.25% (w/v) Coomassie Brilliant Blue R250   2.5 g/L

7.5% (v/v) Acetic acid (concentrated)   75 mL/L

50% (v/v) Ethanol (absolute)   500 mL/L

Dissolved in deionized H_2O

Coomassie Destaining solution:

7.5% (v/v) Acetic acid (concentrated)   75 mL/L

20% (v/v) Ethanol (absolute)   200 mL/L

Dissolved in deionized H_2O

Fixing solution

10% (v/v) EtOH (absolute) 100 mL/L

7% (v/v) AcOH 70 mL/L

 Dissolved in deionized H_2O

7.2.20.3   Western Blotting

1 x TBS (Tris-buffered saline)

50 mM Tris base   6.06 g/L

150 mM NaCl   8.77 g/L

Dissolved in 800 mL deionized H_2O, pH adjusted to 8.0 with conc. HCl, H_2O added to 1 L.

1 x TBS-T

50 mM Tris base	6.06 g/L
150 mM NaCl	8.77 g/L
0.05% Tween-20®	0.5 ml/L

Dissolved in 800 mL deionized H2O, pH adjusted to 8.0 with HCl, H_2O added to 1 L.

Towbin transfer buffer

192 mM Glycine	14.4 g/L
25 mM Tris-base	3.0 g/L
0.1% SDS	0.1 g/L
20% MeOH (100%)	200 mL/L

Filled up to 1 L with deionized H_2O

Transfer buffer

192 mM Glycine	14.4 g/L
25 mM Tris-base	3.0 g/L
20% MeOH (100%)	200 mL/L

Filled up to 1 L with deionized H_2O

Ponceau S staining solution (0.1% (w/v) Ponceau S in 5%(v/v) acetic acid)

1 g Ponceau S

50 mL acetic acid

Filled up to 1 L with deionized H_2O

Ponceau S staining solution (0.2%(w/v) Ponceau S in 3%(v/v) TCA)

2 g Ponceau S

30 g TCA

Filled up to 1 L with deionized H_2O

7.2.20.4 Tissue fractionation

Homogenization buffer

320 mM sucrose

10 mM Tris-HCl (pH 7.4)

Protease inhibitor tablet (Roche; 1 tablet / 50 mL)

Aliquot buffer

50 mM Tris/Cl (pH 7,4)

1 mM EDTA

3 mM $MgCl_2$

Protease inhibitor tablet (Roche; 1 tablet / 50 mL)

7.2.20.5 In-gel digest

50 mM ammonium bicarbonate (ABC)

118.6 mg NH_4HCO_3 in 30 mL ddH_2O

10 mM dithiothreitol (DTT) in 50 mM ABC

3.1 mg DDT in 2 mL 50 mM ABC

55 mM iodacetamide (IAA) in 50 mM ABC

20.3 mg IAA in 2 mL 50 mM ABC

8 References

1. J. C. Venter et al. *Science* **2001**, *291*, 1304-1351.

2. D. Hanahan, R. A. Weinberg, *Cell* **2000**,*100*, 57-70.

3. B. Vogelstein, K. W. Kinzler, *Nat. Med.* **2004**, *10*, 789-99.

4. Y. Kang, P. M. Siegel, W. Shu, M. Drobnjak, S. M. Kakonen, C. Cordon-Cardo, T. A. Guise, J. Massague, *Cancer Cell* **2003**, *3*, 537-49.

5. J. Daily, K. Le Roch, O. Sarr, X. Fang, Y. Zhou, O. Ndir, S. Mboup, A. Sultan, E. A. Winzeler, D. F. Wirth, *Malar. J.* **2004**, *3*, 30-37.

6. V. K. Mootha, C. M. Lindgren, K. F. Eriksson, A. Subramanian, S. Sihag, J. Lehar, P. Puigserver, E. Carlsson, M. Ridderstråle, E. Laurila, N. Houstis, M. J. Daly, N. Patterson, J. P. Mesirov, T. R. Golub, P. Tamayo, B. Spiegelman, E. S. Lander, J. N. Hirschhorn, D. Altshuler, L. C. Groop, *Nat. Genet.* **2003**, *34*, 267-273.

7. a) J. Peng, J. E. Elias, C. C. Thoreen, L. J. Licklider, S. P. Gygi, *J. Proteome Res.* **2003**, *2*, 43-50; b) M. P. Washburn, D. Wolters, J. R. Yates 3rd, *Nat. Biotechnol.* **2001**, *19*, 242-247; c) S. P. Gygi, B. Rist, S. A. Gerber, F. Turecek, M. H. Gelb, R. Aebersold, *Nat. Biotechnol.* **1999**, *17*, 994-999.

8. T. Ito, K. Ota, H. Kubota, Y. Yamaguchi, T. Chiba, K. Sakuraba, M. Yoshida, *Mol. Cell. Proteomics* **2002**, *1*, 561-566.

9. G. MacBeath, *Nat. Genetics* **2002**, *32*, 526-532.

10. H. Waldmann, P. Janning, *Chemical Biology: Learning through Case Studies*, Wiley VCH, Weinheim, **2009**.

11. Y. Liu, M. P. Patricelli, B. F. Cravatt, *Proc. Natl. Acad. Sci. U. S. A.* **1999**, *96*, 14694-14699.

12. D. Greenbaum, K. F. Medzihradszky, A. Burlingame, M. Bogyo, *Chem Biol.* **2000**, *7*, 569-581.

13. W. P. Heal, T. H. Tam Dang, E. W. Tate, *Chem. Soc. Rev.* **2011**, *40*, 246–257.

14. For reviews, see: a) N. Li, H. S. Overkleeft, B. I. Florea, *Curr. Opin. Chem. Biol.* **2012**, *16,* 227-233; b) B. F. Cravatt, A. T. Wright, J. W. Kozarich, *Annu. Rev. Biochem.* **2008**, *77*, 383-414; c) K. T. Barglow, B. F. Cravatt, *Nature Meth.* **2007**, *4*, 822-827; d) M. J. Evans, B. F. Cravatt, *Chem. Rev.* **2006**, *106*, 3279-3301.

15. a) D. K. Nomura, M. M. Dix, B. F. Cravatt, *Nat. Rev. Cancer* **2010**, *10*, 630-638; b) M. G. Paulick, M. Bogyo, *Curr. Opin. Genet. Dev.* **2008**, *18,* 97-106.

16. C. H. S. Lu, K. Liu, L. P. Tan, S. Q. Yao, *Chem. Eur. J.* **2012**, *18*, 28-39.

17. D. Kato, K. M. Boatright, A. B. Berger, T. Nazif, G. Blum, C. Ryan, K. A. Chehade, G. S. Salvesen, M. Bogyo, *Nat. Chem. Biol.* **2005**, *1*, 33-38.

18. a) W. P. Heal, E. W. Tate *Top. Curr. Chem.* **2012**, *324*, 115-135; b) A. W. Puri, P. J. Lupardus, E. Deu, V. E. Albrow, K. C. Garcia, M. Bogyo, A. Shen, *Chem. Biol.* **2010**, *17*, 1201-1211; c) T. Boettcher, S. A. Sieber, *J. Am. Chem. Soc.* **2010**, *132*, 6964-6972; d) T. H. Dang, L. de la Riva, R. P. Fagan, E. M. Storck, W. P. Heal, C. Janoir, N. F. Fairweather, E. W. Tate, *ACS Chem. Biol.* **2010**, *5*, 279-285; e) A. W. Puri, M. Bogyo, *ACS Chem. Biol.* **2009**, *4*, 603-616; f) I. Staub, S. A. Sieber, *J. Am. Chem. Soc.* **2008**, *130,* 13400-13409; g) T. Boettcher, S. A. Sieber, *Angew. Chem. Int. Ed.* **2008**, *47*, 4600-4603.

19. D. R. Blais, N. Nasheri, C. S. McKay, M. C. Legault, J. P. Pezacki, *Trends Biotechnol.* **2012**, *30*, 89-99.

20. a) G. M. Simon, B. F. Cravatt, *J. Biol. Chem.* **2010**, *285*, 11051-11055; b) J. L. Blankman, G. M. Simon, B. F. Cravatt, *Chem. Biol.* **2007**, *14*, 1347-1356; c) D. Kidd, Y. Liu, B. F. Cravatt, *Biochemistry* **2001**, *40*, 4005-4015.

21. a) B. I. Florea, M. Verdoes, N. Li, W. A. van der Linden, P. P. Geurink, H. van den Elst, T. Hofmann, A. de Ru, P. A. van Veelen, K. Tanaka, K. Sasaki, S. Murata, H. den Dulk, J. Brouwer, F. A. Ossendorp, A. F. Kisselev, H. S. Overkleeft, *Chem. Biol.* **2010**, *17*, 795-801; b) J. Clerc, B. I. Florea, M. Kraus, M. Groll, R. Huber, A. S. Bachmann, R. Dudler, C. Driessen, H. S. Overkleeft, M. Kaiser, *Chembiochem* **2009**, *10*, 2638-2643.

22. a) M. D. Witte, G. A. van der Marel, J. M. Aerts, H. S. Overkleeft, *Org Biomol. Chem.* **2011**, *9*, 5908-5926; b) M. D. Witte, M. T. Walvoort, K. Y. Li, W. W. Kallemeijn, W. E. Donker-Koopman, R. G. Boot, J. M. Aerts, J. D. Codée, G. A. van der Marel, H. S. Overkleeft, *Chembiochem* **2011**, *12*, 1263-1269.

23. a) A. Koch, H. B. Rode, A. Richters, D. Rauh, S. Hauf, *ACS Chem. Biol.* **2012**, *7*, 723-73; b) H. Shi, X. M. Cheng, S. K. Sze, S. Q. Yao, *Chem. Commun.* **2011**, *47*, 11306-11308; c) K. A. Kalesh, D. S. Sim, J. Wang, K. Liu, Q. Lin, S. Q. Yao, *Chem. Commun.* **2010**, *46*, 1118-1120; d) M. P. Patricelli, A. K. Szardenings, M. Liyanage, T. K. Nomanbhoy, M. Wu, H. Weissig, A. Aban, D. Chun, S. Tanner, J. W. Kozarich, *Biochemistry* **2007**, *46*, 350-358; e) M. S. Cohen, H. Hadjivassiliou, J. Taunton, *Nat. Chem. Biol.* **2007**, *3*, 156-160; f) M. C. Yee, S. C. Fas, M. M. Stohlmeyer, T. J. Wandless, K. A. Cimprich, *J. Biol. Chem.* **2005**, *280*, 29053-29059; g) Y. Liu, K. R. Shreder, W. Gai, S. Corral, D. K. Ferris, J. S. Rosenblum, *Chem. Biol.* **2005**, *12*, 99-107.

24. a) K. A. Kalesh, L. P. Tan, K. Lu, L. Gao, J. Wang, S. Q. Yao, *Chem. Commun.* **2010**, *46*, 589-91; b) D. Krishnamurthy, A. M. Barrios, *Curr. Opin. Chem. Biol.* **2009**, *13*, 375-381; c) K. R. Shreder, Y. Liu, T. Nomanhboy, S. R. Fuller, M. S. Wong, W. Z. Gai, J. Wu, P. S. Leventhal, J. R. Lill, S. Corral, *Bioconjug. Chem.* **2004**, *15*, 790-798.

25. a) D. Rotili, M. Altun, A. Kawamura, A. Wolf, R. Fischer, I. K. H. Leung, M. M. Mackeen, Y. Tian, P. J. Ratcliffe, A. Mai, B. M. Kessler, C. J. Schofield, *Chem. Biol.* **2011**, *18*, 642-654; b) A. T. Wright, J. D. Song, B. F. Cravatt, *J. Am. Chem. Soc.* **2009**, *131*, 10692-10700; c) A. T. Wright, B. F. Cravatt, *Chem. Biol.* **2007**, *14*, 1043-1051.

26. a) K. Tsuboi, D. A. Bachovchin, A. E. Speers, T. P. Spicer, V. Fernandez-Vega, P. Hodder, H. Rosen, B. F. Cravatt, *J. Am. Chem. Soc.* **2011**, *133*, 16605-16616; b) O. Obianyo, C. P. Causey, J. E. Jones, P. R. Thompson, *ACS Chem. Biol.* **2011**, *6*, 1127-1135; c) G. C. Adam, E. J. Sorensen, B. F. Cravatt, *Nat. Biotechnol.* **2002**, *20*, 805-809.

27. P. P. Geurink, L. M. Prely, G. A. van der Marel, R. Bischoff, H. S. Overkleeft, *Top. Curr. Chem.* **2012**, *324*, 85-113.

28. E. W. S. Chan, S. Chattopadhaya, R. C. Panicker, X. Huang, S. Q. Yao, *J. Am. Chem. Soc.* **2004**, 126, 14435-14446.

29. a) S. A. Sieber, S. Niessen, H. S. Hoover, B. F. Cravatt, *Nat. Chem. Biol.* **2006**, *2*, 274-281; b) A. Saghatelian, N. Jessani, A. Joseph, M. Humphrey, B. F. Cravatt, *Proc. Natl. Acad. Sci. U. S. A.* **2004**, *101*, 10000-10005.

30. a) C. M. Salisbury, B. F. Cravatt, *J. Am. Chem. Soc.* **2008**, *130*, 2184-2194; b) C. M. Salisbury, B. F. Cravatt, *Proc. Natl. Acad. Sci. U. S. A.* **2007**, *104*, 1171-1176.

31. M. C. Hagenstein, J. H. Mussgnug, K. Lotte, R. Plessow, A. Brockhinke, O. Kruse, N. Sewald, *Angew. Chem. Int. Ed.* **2003**, *42*, 5635-5638.

32. H. Shi, C. J. Zhang, G. Y. Chen, S. Q. Yao, *J. Am. Chem. Soc.* **2012**, *34*, 3001-3114.

33. Y. Hwang, P. R. Thompson, L. Wang, L. Jiang, N. L. Kelleher, P. A. Cole, *Angew. Chem. Int. Ed.* **2007**, *46*, 7621-7624.

34. a) S. Kumar, B. Zhou, F. Liang, H. Yang, W. Q. Wang, Z. Y. Zhang, *J. Proteome Res.* **2006**, 5, 1898-1905; b) S. Kumar, B. Zhou, F. Liang, W. Q. Wang, Z. Huang, Z. Y. Zhang, *Proc. Natl. Acad. Sci. U. S. A.* **2004**, *101*, 7943-7948.

35. K. T. Barglow, B. F. Cravatt, *Angew. Chem. Int. Ed.* **2006**, *45*, 7408-7411.

36. K. E. Wilke, S. Francis, E. E. Carlson, *J. Am. Chem. Soc.* **2012**, *134*, 9150-9153.

37. a) Q. Zhu, X. Huang, G. Y. J. Chen, S. Q. Yao, *Tetrahedron Lett.* **2003**, *44*, 2669-2672; b) L. C. Lo, T. L. Pang, C. H. Kuo, Y. L. Chiang, H. Y. Wang, J. J. Lin, *J. Proteome Res.* **2002**, *1*, 35-40.

38. a) T. H. Shie, Y. L. Chiang, J. J. Lin, Y. K. Li, L. C. Lo, *Carbohydr. Res.* **2006**, *341*, 443-456; b) C. P. Lu, C. T. Ren, Y. N. Lai, S. H. Wu, W. M. Wang, J. Y. Chen, L. C. Lo, *Angew. Chem. Int. Ed.* **2005**, *44*, 6888-6892; c) C. S.Tsai, Y. K. Li, L. C. Lo, *Org. Lett.* **2002**, *4*, 3607-3610; d) M. Ichikawa, Y. Ichikawa, *Bioorg. Med. Chem. Lett.* **2001**, *11*, 1769-1773.

39. C. P. Lu, C. T. Ren, S. H. Wu, C. Y. Chu, L. C. Lo, *Chembiochem* **2007**, *8*, 2187-2190.

40. Q. Zhu, A. Girish, S. Chattopadhaya, S. Q. Yao, *Chem. Commun.* **2004**, 1512-1513.

41. a) K. P. Chiang, S. Niessen, A. Saghatelian, B. F. Cravatt, *Chem. Biol.* **2006**, *13*, 1041-1050; b) N. Jessani, Y. Liu, M. Humphrey, B. F. Cravatt, *Proc. Natl. Acad. Sci. U. S. A.* **2002**, *99*, 10335-10340.

42. D. K. Nomura, J. Z. Long, S. Niessen, H. S. Hoover, S. W. Ng, B. F. Cravatt, *Cell* **2010**, *140*, 49-61.

43. D. J. Shields, S. Niessen, E. A. Murphy, A. Mielgo, J. S. Desgrosellier, S. K. Lau, L. A. Barnes, J. Lesperance, M. Bouvet, D. Tarin, B. F. Cravatt, D. A. Cheresh, *Proc. Natl. Acad. Sci. U. S. A.* **2010**, *107*, 2189-2194.

44. D. J. Vocadlo, C. R. Bertozzi, *Angew. Chem. Int. Ed.* **2004**, *43*, 5338-5342.

45. a) S. J. Williams, O. Hekmat, S. G. Withers *Chembiochem* **2006**, *7*, 116-124; b) O. Hekmat, Y. W. Kim, S. J. Williams, S. He, S. G. Withers, *J. Biol. Chem.* **2005**, *280*, 35126-35135.

46. a) A. T. Wright, B. F. Cravatt, *Chem. Biol.* **2007**, *14*, 1043-1051; b) A. T. Wright, J. D. Song, B. F. Cravatt, *J. Am. Chem. Soc.* **2009**, *131*, 10692-10700.

47. a) J. L. Slack, C. P. Causey, Y. Luo, P. R. Thompson, *ACS Chem. Biol.* **2011**, *6*, 466-476; b) Y. Luo, B. Knuckley, M. Bhatia, P. J. Pellechia, P. R. Thompson, *J. Am. Chem. Soc.* **2006**, *128*, 14468-14469.

48. J. Clardy, C. Walsh, *Nature* **2004**, *432*, 829-837.

49. C. Drahl, B. F. Cravatt, E. J. Sorensen, *Angew. Chem. Int. Ed.* **2005**, *44*, 5788-5809.

50. N. Dixon, L. S. Wong, T. H. Geerlings, J. Micklefield, *Nat. Prod. Rep.* **2007**, 24, 1288-1310.

51. E. E. Carlson, *ACS Chem. Biol.* **2010**, *5*, 639-653.

52. T. Böttcher, M. Pitscheider, S. A. Sieber, *Angew. Chem. Int. Ed.* **2010**, *49*, 2680-2698.

53. M. Gersch, J. Kreuzer, S. A. Sieber, *Nat. Prod. Rep.* **2012**, *29*, 659-682.

54. J. Krysiak, R. Breinbauer, *Top. Curr. Chem.* **2012**, *324*, 43-84.

55. a) D. Greenbaum, A. Baruch, L. Hayrapetian, Z. Darula, A. Burlingame, K. F. Medzihradszky, M. Bogyo, *Mol. Cell. Proteomics* **2002**, *1*, 60-68; b) D. Greenbaum, K. F. Medzihradszky, A. L. Burlingame, M. Bogyo, *Chem. Biol.* **2000**, *7*, 569-581.

56. F. Kaschani, S. H. L. Verhelst, P. F. van Swieten, M. Verdoes, C-S. Wong, Z. Wang, M. Kaiser, H. S. Overkleeft, M. Bogyo, R. A. L. van der Hoorn, *Plant J.* **2009**, *57*, 373-385; b) R. A. L. van der Hoorn, M. A. Leeuwenburgh, M. Bogyo, M. H. Joosten, S. C. Peck, *Plant Physiol.* **2004**, *135*, 1170-1178.

57. H. C. Hang, J. Loureiro, E. Spooner, A. W. van der Velden, Y. M. Kim, A. M. Pollington, R. Maehr, M. N. Starnbach, H. L. Ploegh, *ACS Chem. Biol.* **2006**, *1*, 713-723.

58. I. Kolodziejek, J. C. Misas-Villamil, F. Kaschani, J. Clerc, C. Gu, D. Krahn, S. Niessen, M. Verdoes, L. I. Willems, H. S. Overkleeft, M. Kaiser, R. A. L. van der Hoorn, *Plant Physiol.* **2011**, *155*, 477-489.

59. G. Fenteany, R. F. Standaert, W. S. Lane, S. Choi, E. J. Corey, S. L. Schreiber *Science* **1995**, *268*, 726-731.

60. E. Zeiler, N. Braun, T. Böttcher, A. Kastenmüller, S. Weinkauf, S. A. Sieber, *Angew. Chem. Int. Ed.* **2011**, *50*, 11001-11004.

61. M. B. Nodwell, H. Menz, S. F. Kirsch, S. A. Sieber, *Chembiochem* **2012**, *13*, 1439-1446.

62. T. Wirth, K. Schmuck, L. F. Tietze, S. A. Sieber, *Angew. Chem. Int. Ed.* **2012**, *51*, 2874-2877.

63. a) C. Gu, I. Kolodziejek, J. Misas-Villamil, T. Shindo, T. Colby, M. Verdoes, K. H. Richau, J. Schmidt, H. S. Overkleeft, R. A. L. van der Hoorn, *Plant J.* **2010**, *62*, 160-170; b) M. Verdoes, B. I. Florea, V. Menendez-Benito, C. J. Maynard, M. D. Witte, W. A. van der Linden, A. M. van den Nieuwendijk, T. Hofmann, C. R. Berkers, F. W. van Leeuwen, T. A. Groothuis, M. A. Leeuwenburgh, H. Ovaa, J. J. Neefjes, D. V.

Filippov, G. A. van der Marel, N. P. Dantuma, H. S. Overkleeft, *Chem. Biol.* **2006**, *13*, 1217-1226.

64. A. Borodovsky, H. Ovaa, W. J. Meester, E. S. Venanzi, M. S. Bogyo, B. G. Hekking, H. L. Ploegh, B. M. Kessler, H. S. Overkleeft, *Chembiochem* **2005**, *6*, 287-291.

65. G. C. Adam, B. F. Cravatt, E. J. Sorensen, *Chem. Biol.* **2001**, *8*, 81-95.

66. A. M. Sadaghiani, S. H. Verhelst, M. Bogyo, *Curr. Opin. Chem. Biol.* **2007**, *11*, 20-28.

67. H. Schmidinger, R. Birner-Gruenberger, G. Riesenhuber, R. Saf, H. Susani-Etzerodt, A. Hermetter, *Chembiochem* **2005**, *6*, 1776-1781.

68. C. R. Berkers, F. W. van Leeuwen, T. A. Groothuis, V. Peperzak, E. W. van Tilburg, J. Borst, J. J. Neefjes, H. Ovaa, *Mol. Pharm.* **2007**, *4*, 739-748.

69. a) A. Borodovsky, H. Ovaa, N. Kolli, T. Gan-Erdene, K. D. Wilkinson, H. L. Ploegh, B. M. Kessler *Chem. Biol.* **2002**, *9*, 1149-1159; b) A. Borodovsky, B. M. Kessler, R. Casagrande, H. S. Overkleeft, K. D. Wilkinson, H. L. Ploegh, *EMBO J.* **2001**, *20*, 5187-5196.

70. E. S. Okerberg, J. Wu, B. Zhang, B. Samii, K. Blackford, D. T. Winn, K. R. Shreder, J. J. Burbaum, M. P. Patricelli, *Proc. Natl. Acad. Sci. U. S. A.* **2005**, *102*, 4996-5001.

71. a) N. Winssinger, J. L. Harris, *Expert Rev. Proteomics* **2005**, *2*, 937-947; b) N. Winssinger, R. Damoiseaux, D. C. Tully, B. H. Geierstanger, K. Burdick, J. L. Harris, *Chem. Biol.* **2004**, *11*, 1351-1360.

72. G. Blum, G. von Degenfeld, M. J. Merchant, H. M. Blau, M. Bogyo, *Nat. Chem. Biol.* **2007**, *3*, 668-677.

73. a) G. Ren, G. Blum, M. Verdoes, H. Liu, S. Syed, L. E. Edgington, O. Gheysens, Z. Miao, H. Jiang, S. S. Gambhir, M. Bogyo, Z. Cheng, *PLoS One* **2011**, *6*, e28029; b) M. B. Skaddan, L. Zhang, D. S. Johnson, A. Zhu, K. R. Zasadny, R. V. Coelho, K. Kuszpit, G. Currier, K. H. Fan, E. M. Beck, L. Chen, S. E. Drozda, G. Balan, M. Niphakis, B. F. Cravatt, K. Ahn, T. Bocan, A. Villalobos, *Nucl. Med. Biol.* **2012** May 7. [Epub ahead of print]

74. L. I. Willems, W. A. van der Linden, N. Li, K. Y. Li, N. Liu, S. Hoogendoorn, G. A. van der Marel, B. I. Florea, H. S. Overkleeft, *Acc. Chem. Res.* **2011**, *44*, 718-29.

75. V. V: Rostovtsev, L. G. Green, V. V. Fokin, K. B. Sharpless, *Angew. Chem. Int. Ed.* **2002**, *41*, 2596-2599.

76. C. W. Tornøe, C. Christensen, M. Meldal, *J. Org. Chem.* **2002**, *67*, 3057-3064.

77. M. Meldal, C. W. Tornøe, *Chem. Rev.* **2008**, *108*, 2952-3015.   .

78. R. Breinbauer, M. Köhn, *Chembiochem* **2003**, *4*, 1147-1149.

79. A. E. Speers, G. C. Adam, B. F. Cravatt, *J. Am. Chem. Soc.* **2003**, *125*, 4686-4687.

80. A. E. Speers, B. F. Cravatt, *Chem. Biol.* **2004**, *11*, 535-546.

81. K. A. Kalesh, H. Shi, J. Ge, S. Q. Yao, *Org. Biomol. Chem.* **2010**, *8*, 1749-1762.

82. N. J. Agard, J. A. Prescher, C. R. Bertozzi, *J. Am. Chem. Soc.* **2004**, *126*, 15046-15047.

83. W. A. van der Linden, N. Li, S. Hoogendoorn, M. Ruben, M. Verdoes, J. Guo, G. J. Boons, G. A. van der Marel, B. I. Florea, H. S. Overkleeft, *Bioorg. Med. Chem.* **2012**, 20, 662-666.

84. a) S. S. van Berkel, M. B. van Eldijk, J. C. van Hest, *Angew. Chem. Int. Ed.* **2011**, *50*, 8806-8827; b) M. Köhn, R. Wacker, C. Peters, H. Schröder, L. Soulère, R. Breinbauer, C. M. Niemeyer, H. Waldmann, *Angew. Chem. Int. Ed.* **2003**, *42*, 5830-5834.

85. H. Ovaa, P. F. van Swieten, B. M. Kessler, M. A. Leeuwenburgh, E. Fiebiger, A. M. van den Nieuwendijk, P. J. Galardy, G. A. van der Marel, H. L. Ploegh, H. S. Overkleeft, *Angew. Chem. Int. Ed.* **2003**, *42*, 3626-3629.

86. M. Verdoes, B. I. Florea, U. Hillaert, L. I. Willems, W. A. van der Linden, M. Sae-Heng, D. V. Filippov, A. F. Kisselev, G. A. van der Marel, H. S. Overkleeft, *Chembiochem* **2008**, *9*, 1735-1738.

87. L. I. Willems, M. Verdoes, B. I. Florea, G. A. van der Marel, H. S. Overkleeft, *Chembiochem* **2010**, *11*, 1769-1781.

88. a) M. R. Karver, R. Weissleder, S. A. Hilderbrand, *Bioconjug. Chem.* **2011**, *22*, 2263-2270; b) N. K. Devaraj, R. Upadhyay, J. B. Haun, S. A. Hilderbrand, R. Weissleder, *Angew. Chem. Int. Ed.* **2009**, *48*, 7013-7016.

89. N. K. Devaraj, S. Hilderbrand, R. Upadhyay, R. Mazitschek, R. Weissleder, *Angew. Chem. Int. Ed.* **2010**, *49*, 2869-2872.

90. S. P. Mirza, B. D. Halligan, A. S. Greene, M. Olivier, *Physiol. Genomics* **2007**, 30, 89-94.

91. G. C. Adam, J. Burbaum, J. W. Kozarich, M. P. Patricelli, B. F. Cravatt, *J. Am. Chem. Soc.* **2004**, *126*, 1363-1368.

92. a) A. E. Speers, B. F. Cravatt, *J. Am. Chem. Soc.* **2005**, *127*, 10018-10019; b) E. Weerapana, A. E. Speers, B. F. Cravatt, *Nat. Protoc.* **2007**, *2*, 1414-1425.

93. S. A. Sieber, T. S. Mondala, S. R. Head, B. F. Cravatt, *J. Am. Chem. Soc.* **2004**, *126*, 15640-15641.

94. a) C. A. Gartner, J. E. Elias, C. E. Bakalarski, S. P. Gygi, *J. Proteome Res.* **2007**, *6*, 1482-1491; b) P. A. Everley, C. A. Gartner, W. Haas, A. Saghatelian, J. E. Elias, B. F. Cravatt, B. R. Zetter, S. P. Gygi, *Mol. Cell Proteomics* **2007**, *6*, 1771-1777.

95. A. Dirksen, S. Yegneswaran, P. E. Dawson, *Angew. Chem. Int. Ed.* **2010**, *49*, 2023-2027.

96. K. D. Park, R. Liu, H. Kohn, *Chem. Biol.* **2009**, *16*, 763-772.

97. S. H. Verhelst, M. Fonović, M. Bogyo, *Angew. Chem. Int. Ed.* **2007**, *46*, 1284-1286.

98. a) F. Landi, C. M. Johansson, D. J. Campopiano, A. N. Hulme, *Org. Biomol. Chem.* **2009**, *7*, 56-59; b) Y. Y. Yang, M. Grammel, A. S. Raghavan, G. Charron, H. C. Hang, *Chem. Biol.* **2010**, *17*, 1212-1222; c) G. Leriche, G. Budin, L. Brino, A. Wagner, *Eur. J. Org. Chem.* **2010**, 4360-4364.

99. P. P. Geurink, B. I. Florea, N. Li, M. D. Witte, J. Verasdonck, C. L. Kuo, G. A. van der Marel, H. S. Overkleeft, *Angew. Chem. Int. Ed.* **2010**, *49*, 6802-6805.

100. R. Orth, S. A. Sieber, *J. Org. Chem.* **2009**, *74*, 8476-8479.

101. G. Leriche, L. Chisholm, A. Wagner, *Bioorg. Med. Chem.* **2012**, *20*, 571-582.

102. A. Baruch, D. A. Jeffery, M. Bogyo, *Trends Cell Biol.* **2004**, *14*, 29-35.

103. G. Blum, S. R. Mullins, K. Keren, M. Fonovic, C. Jedeszko, M. J. Rice, B. F. Sloane, M. Bogyo, *Nat. Chem. Biol.* **2005**, *1*, 203-209.

104. L. E. Edgington, A. B. Berger, G. Blum, V. E. Albrow, M. G. Paulick, N. Lineberry, M. Bogyo *Nat. Med.* **2009**, *15*, 967-973.

105. D. Cavallo-Medved, D. Rudy, G. Blum, M. Bogyo, D. Caglic, B. F. Sloane, *Exp. Cell Res.* **2009**, *315*, 1234-1246.

106. S. H. Chang, K. Kanasaki, V. Gocheva, G. Blum, J. Harper, M. A. Moses, S. C. Shih, J. A. Nagy, J. Joyce, M. Bogyo, R. Kalluri, H. F. Dvorak, *Cancer Res.* **2009**, *69*, 4537-4544.

107. J. Lee, M. Bogyo, *ACS Chem. Biol.* **2010**, *5*, 233-243.

108. A. M. Boutte, D. B. Friedman, M. Bogyo, Y. Min, L. Yang, P. C. Lin, *FASEB J.* **2011**, *25*, 2626-2637.

109. a) D. A. Bachovchin, T. Ji, W. Li, G. M. Simon, J. L. Blankman, A. Adibekian, H. Hoover, S. Niessen, B. F. Cravatt, *Proc. Natl. Acad. Sci. U. S. A.* **2010**, *107*, 20941-20946; b) W. Li, J. L. Blankman, B. F. Cravatt, *J. Am. Chem. Soc.* **2007**, *129*, 9594-9595.

110. D. Leung, C. Hardouin, D. L. Boger, B. F. Cravatt, *Nat. Biotechnol.* **2003**, *21*, 687-691.

111. D. A. Bachovchin, S. J. Brown, H. Rosen, B. F. Cravatt, *Nat. Biotechnol.* **2009**, *27*, 387-394.

112. D. A. Bachovchin, M. R. Wolfe, K. Masuda, S. J. Brown, T. P. Spicer, V. Fernandez-Vega, P. Chase, P. S. Hodder, H. Rosen, B. F. Cravatt, *Bioorg. Med. Chem. Lett.* **2010**, *20*, 2254-2258.

113. A. M. Lone, D. A. Bachovchin, D. B. Westwood, A. E. Speers, T. P. Spicer, V. Fernandez-Vega, P. Chase, P. S. Hodder, H. Rosen, B. F. Cravatt, A. Saghatelian, *J. Am. Chem. Soc.* **2011**, *133*, 11665-11674.

114. B. Knuckley, J. E. Jones, D. A. Bachovchin, J. Slack, C. P. Causey, S. J. Brown, H. Rosen, B. F. Cravatt, P. R. Thompson, *Chem. Commun.* **2010**, *46*, 7175-7177.

115. a) D. A. Bachovchin, J. T. Mohr, A. E. Speers, C. Wang, J. M. Berlin, T. P. Spicer, V. Fernandez-Vega, P. Chase, P. S. Hodder, S. C. Schürer, D. K. Nomura, H. Rosen, G. C. Fu, B. F. Cravatt, *Proc. Natl. Acad. Sci. U. S. A.* **2011**, *108*, 6811-6816; b) D. A. Bachovchin, A. M. Zuhl, A. E. Speers, M. R. Wolfe, E. Weerapana, S. J. Brown, H. Rosen, B. F. Cravatt, *J. Med. Chem.* **2011**, *54*, 5229-5236.

116. P. F. van Swieten, R. Maehr, A. M. C. H. van den Nieuwendijk, B. M. Kessler, M. Reich, C. S. Wong, H. Kalbacher, M. A. Leeuwenburgh, C. Driessen, G. A. van der Marel, H. L. Ploegh, H. S. Overkleeft, *Bioorg. Med. Chem. Lett.* **2004**, *14*, 3131- 3134.

117. S. E. Ong, B. Blagoev, I. Kratchmarova, D. B. Kristensen, H. Steen, A. Pandey, M. Mann, *Mol. Cell. Proteomics* **2002**, *1*, 376-386.

118. A. Adibekian, B. R. Martin, C. Wang, K. L. Hsu, D. A. Bachovchin, S. Niessen, H. Hoover, B. F. Cravatt, *Nat. Chem. Biol.* **2011**, *7*, 469-478.

119. E. Weerapana, C. Wang, G. M. Simon, F. Richter, S. Khare, M. B. Dillon, D. A. Bachovchin, K. Mowen, D. Baker, B. F. Cravatt, *Nature* **2010**, *468*, 790-795.

120. a) P-Y. Yang, K. Liu, C. Zhang, G. Y. J. Chen, Y. Shen, M. H. Ngai, M. J. Lear, S. Y. Yao, *Chem. Asian J.* **2011**, *6*, 2762-2775; b) P-Y. Yang, K. Liu, M. H. Ngai, M. J. Lear, M. R. Wenk, S. Y. Yao, *J. Am. Chem. Soc.* **2010**, *132*, 656-666; c) M. H. Ngai, P-Y. Yang, K. Liu, Y. Shen, M. R. Wenk, S. Y. Yao, *Chem. Commun.* **2010**, *46*, 8335-8337.

121. J. Eirich, R. Orth, S. A. Sieber, *J. Am. Chem. Soc.* **2011**, *133*, 12144-12153.

122. K. A. Kalesh, D. S. Sim, J. Wang, K. Liu, Q. Lin, S. Q. Yao, *Chem. Commun.* **2010**, *46*, 1118-1120.

123. J. M. Krysiak, J. Kreuzer, P. Macheroux, A. Hermetter, S. A. Sieber, R. Breinbauer, *Angew. Chem. Int. Ed.* **2012**, *51*, 7035-7040.

124. R. E. Moellering, B. F. Cravatt, *Chem. Biol.* **2012**, *19*, 11-22.

125. M. P. Patricelli, T. K. Nomanbhoy, J. Wu, H. Brown, D. Zhou, J. Zhang, S. Jagannathan, A. Aban, E. Okerberg, C. Herring, B. Nordin, H. Weissig, Q. Yang, J. D. Lee, N. S. Gray, J. W. Kozarich, *Chem. Biol.* **2011**, *18*, 699-710.

126. M. Hu, L. Li, H. Wu, Y. Su, P. Y. Yang, M. Uttamchandani, Q. Q. H. Xu, S. Q. Yao, *J. Am. Chem. Soc.* **2011**, *133*, 12009-12020.

127. M. D. Witte, W. W. Kallemeijn, J. Aten, K. Y. Li, A. Strijland, W. E. Donker-Koopman, A. M. van den Nieuwendijk, B. Bleijlevens, G. Kramer, B. I. Florea, B. Hooibrink, C. E. Hollak, R. Ottenhoff, R. G. Boot, G. A. van der Marel, H. S, Overkleeft, J. M. Aerts, *Nat. Chem. Biol.* **2010**, *6*, 907-913.

128. a) D. R. Blais, R. K. Lyn, M. A. Joyce, Y. Rouleau, R. Steenbergen, N. Barsby, L. F. Zhu, A. F. Pegoraro, A. Stolow, D. L. Tyrrell, J. P. Pezacki, *J. Biol. Chem.* **2010**, *285*, 25602-25612; b) D. R. Blais, M. Brûlotte, Y. Qian, S. Bélanger, S. Q. Yao, J. P. Pezacki, *J. Proteome Res.* **2010**, *9*, 912-923; c) R. Singaravelu, D. R. Blais, C. S. McKay,J. P. Pezacki, *Proteome Sci.* **2010**, *8*, 5-19.

129. V. Joosten W. J. H. van Berkel, *Curr. Opin. Chem. Biol.* **2007**, *11*, 195-202

130. L. de Colibus, A. Mattevi, *Curr. Opin. Struct. Biol.* **2006**, *16*, 722-728

131. V. Massey, *FASEB J.* **1995**, *9*, 473-475

132. P. Sampathkumar, S. Turley, J. E. Ulmer, H. G. Rhie, C. H. Sibley, W. G. Hol, *J. Mol. Biol.* **2005**, *352*, 1091-1104.

133. E. Gross, D. B. Kastner, C. A. Kaiser, D. Fass, *Cell* **2004**, *117*, 601-610.

134. K. R. Marshall, M. Gong, L. Wodke, J. H. Lamb, D. J. Jones, P. B. Farmer, N. S. Scrutton, A. W. Munro, *J. Biol. Chem.* **2005**, *280*, 30735-30740.

135. J. R. Terman, T. Mao, R. J. Pasterkamp, H. H. Yu, A. L. Kolodkin, *Cell* **2002**, *109*, 887-900.

136. a) F. Forneris, C. Binda, M. A. Vanoni, A. Mattevi, E. Battaglioli, *FEBS Lett.* **2005**, 579, 2203-2207; b) Y. Shi, F. Lan, C. Matson, P. Mulligan, J. R. Whetstine, P. A. Cole, R. A. Casero, Y. Shi, *Cell* **2004**, *119*, 941-953.

137. S. W. LinWu, A. H. Wang, F. C. Peng *Expert Opin. Drug Metab. Toxicol.* **2010**, *6*, 967-981.

138. a) S. O. Mansoorabadi, C. J. Thibodeaux, H. Liu, *J. Org. Chem.* **2007**, *72*, 6329-6342; b) V. Massey, *Biochem. Soc. Trans.* **2000**, *28*, 283-296.

139. P. Macheroux, B. Kappes, S. E. Ealick, *FEBS J.* **2011**, *278*, 2625-2634.

140. D. P. H. M. Heuts, N. S. Scrutton, W. S. McIntire, M. W. Fraaije, *FEBS J.* **2009**, *276*, 3405-3427.

141. C. H. Huang, W. L. Lai, M. H. Lee, C. J. Chen, A. Vasella, Y. C. Tsai, S. H. Liaw, *J. Biol. Chem.* **2005**, *280*, 38831-38838.

142. A. Winkler, A. Lyskowski, S. Riedl, M. Puhl, T. M. Kutchan, P. Macheroux, K. Gruber, *Nat. Chem. Biol.* **2008**, *4*, 739-741.

143. A. Mattevi, *Trends Biochem. Sci.* **2006**, *5*, 276-283.

144. W. J. H. van Berkel, N. M. Kamerbeek, M. W. Fraaije, *J. Biotechnol.* **2006**, *124*, 670-689.

145. McDonald CA, Fagan RL, Collard F, Monnier VM, Palfey BA. *J. Am. Chem. Soc.* **2011**, *133*, 16809-16811.

146. O. Dym, D. Eisenberg, *Prot. Sci.* **2001**, *10*, 1712-1728.

147. M. W. Fraaije, A. Mattevi *Trends Biochem. Sci.* **2000**, *25*, 126-131.

148. a) C. Binda, A. Mattevi, D. E. Edmondson, *Int. Rev. Neurobiol.* **2011**, *100*, 1-11; b) D. E. Edmondson, C. Binda, J. Wang, A. K. Upadhyay, A. Mattevi, *Biochemistry* **2009**, *48*, 4220-4230; c) T. Nagatsu, *Neurotoxicology* **2004**, *25*, 11-20; c) J. C. Shih, K. Chen, M. J. Ridd, *Annu. Rev. Neurosci.* **1999**, *22*, 197-217; d) E. A. Zeller, *Helv. Chim. Acta*, **1938**, *21*, 881-890; e) M. L. Hare, *Biochem. J.* **1928**, *22*, 968-979.

149. J.P. Johnston, *Biochem. Pharmacol.* **1968**, *17*, 1285-1297.

150. A. W. Bach, N. C. Lan, D. L. Johnson, C. W. Abell, M. E. Bembenek, S. W. Kwan, P. H. Seeburg, J. C. Shih, *Proc. Natl. Acad. Sci. U. S. A.* **1988**, *85*, 4934-4938.

151. a) S. Y. Son, J. Ma, Y. Kondou, M. Yoshimura, E. Yamashita, T. Tsukihara, *Proc. Natl. Acad. Sci. U.S.A.* **2008**, *105*, 5739-5744; b) L. De Colibus, M. Li, C. Binda, A.

Lustig, D. E. Edmondson, A. Mattevi, *Proc. Natl. Acad. Sci. U. S. A.* **2005**, *102*, 12684-12689.

152. a) C. Binda, M. Li, F. Hubálek, N. Restelli, D. E. Edmondson, A. Mattevi, *Proc. Natl. Acad. Sci. U.S.A.* **2003**, *98*, 9750-9755; b) C. Binda, P. Newton-Vinson, F. Hubálek, D. E. Edmondson, A. Mattevi, *Nat. Struct. Biol.* **2002**, *9*, 22-26.

153. F. Hubálek, C. Binda, A. Khalil, M. Li, A. Mattevi, N. Castagnoli, D. E. Edmondson, *J. Biol. Chem.* **2005**, *280*, 15761-15766.

154. M. Li, F. Hubálek, P. Newton-Vinson, D. E. Edmondson, *Protein Expr. Purif.* **2002**, *24*, 152-162.

155. P. Newton-Vinson, F. Hubálek, D. E. Edmondson, *Protein Expr. Purif.* **2000**, *20*, 334-345.

156. a) J. Wang, D. E. Edmondson, *Protein Expr. Purif.* **2010**, *70*, 211-217; b) A. K. Upadhyay, D. E. Edmondson, *Protein Expr. Purif.* **2008**, *59*, 349-356.

157. B. K. Arslan, D. E. Edmondson, *Protein Expr. Purif.* **2010**, *70*, 290-297.

158. H. Gaweska, P. F. Fitzpatrick, *Biomol. Concepts* **2011**, *2*, 365-377.

159. A. K. Upadhyay, P. Borbat, J. Wang, J. Freed, D. E. Edmondson, *Biochemistry* **2008**, *47*, 1554-1566.

160. A. M. Andres, M. Soldevila, A. Navarro, K. K Kidd, B. Olivia, J. Bertranpetit, *Hum. Genet.* **2004**, *115*, 377-386.

161. a) K. Chen, H. F. Wu, J. C. Shih, *J. Neurochem.* **1996**, *66*, 797-803; b) J. Gottowik, P. Malherbe, G. Lang, M. DaPrada, A. M. Cesura, *Eur. J. Biochem.* **1995**, *230*, 934-942.

162. I. Rebrin, R. M. Geha, K. Chen, J. C. Shih, *J. Biol. Chem.* **2001**, *276*, 29499-29506.

163. C. Binda, F. Hubálek, M. Li, D. E. Edmondson, A. Mattevi, *FEBS Lett.* **2004**, *564*, 225-228.

164. J. Wang, D. E. Edmondson, *Biochemistry* **2011**, *50*, 2499-2505.

165. T. D. Buckman, M. S. Sutphin, S. Eiduson, *Mol. Pharmacol.* **1984**, *25*, 165-170.

166. O. Schmidt, N. Pfanner, C. Meisinger, *Nat. Rev. Mol. Cell Biol.* **2010**, *11*, 655-667.

167. a) J. Nagy, J. I. Salach, *Arch. Biochem. Biophys.* **1981**, *208*, 388-394. b) E. B. Kearney, J. I. Salach, W. H. Walker, R. L. Seng, W. Kenney, E. Zeszotek, T. P. Singer, *Eur. J. Biochem.* **1971**, *24*, 321-327.

168. D. E. Edmondson, C. Binda, A. Mattevi, *Neurotoxicology* **2004**, *25*, 63-72.

169. E. M. Milczek, C. Binda, S. Rovida, A. Mattevi, D. E. Edmondson, *FEBS J.* **2011**, *278*, 4860-4869.

170. R. M. Geha, I. Rebrin, K. Chen, J. C. Shih, *J. Biol. Chem.* **2001**, *276*, 9877-98782.

171. M. Li, C. Binda, A. Mattevi, D. E. Edmondson, *Biochemistry* **2006**, *45*, 4775-4784.

172. M. B. Youdim, Z. S. Bakhle, *Br. J. Pharmacol.* **2006**, *147*, S287-S296.

173. R. B. Silverman, S. J. Hoffman, W. B. Catus, *J. Am. Chem. Soc.* **1980**, *102*, 7126-7128.

174. J. R. Miller, D. E. Edmondson, *Biochemistry* **1999**, *38*, 13670-13683.

175. R. K. Nandigama, D. E. Edmondson, *Biochemistry* **2000**, *39*, 15258-15265.

176. M. C. Walker, D. E. Edmondson, *Biochemistry* **1994**, *33*, 7088-7098.

177. J. R. Miller, D. E. Edmondson, C. B. Grissom, *J. Am. Chem. Soc.* **1995**, *117*, 7830-7831.

178. L. A. Hull, G. T. Davis, D. H. Rosenblatt, C. K. Mann, *J. Phys. Chem.* **1969**, *73*, 1389-1393.

179. P. Newton-Vinson, D. E. Edmondson in *Flavins and Flavoproteins*, (Eds.: S. Ghisla, P. Kroneck, P. Macheroux, H. Sund), Agency for Scientific Publications, Berlin, **1999**, pp.431-438.

180. a) A. P. B. Vintem, N. T. Price, R. B. Silverman, R. R. Ramsay, *Bioorg. Med. Chem.* **2005**, *13*, 3487-3495. b) B. Zhong, R. B. Silverman, *J. Am. Chem. Soc.* **1997**, *119*, 6690-6691.

181. a) R. B. Silverman *Acc. Chem. Res.* **1995**, *28*, 335-342 (and citations thereof); b) R. B. Silverman, P. A. Zieske, *Biochemistry* **1985**, *24*, 2128-2138; c) M. L. Vazquez, R. B. Silverman, *Biochemistry* **1985**, *24*, 6538-6543.

182. a) P. Bissel, A. Khalil, J. M. Rimoldi, K. Igarashi, D. E. Edmondson, A. Miller, N. Castagnoli Jr., *Bioorg. Med. Chem.* **2008**, *16*, 3557-3564; b) J. M. Rimoldi, S. G. Puppali, E. Isin, P. Bissel, A. Khalil, N. Castagnoli Jr., *Bioorg. Med. Chem.* **2005**, *13*, 5808-5813.

183. D.E. Edmondson, A.K. Bhattacharrya, J. Xu, *Biochim. Biophys. Acta* **2000**, *1479*, 52-58.

184. H. Reterjans, G. Fleischmann, M. Knauf, F. Loehr, M. Bluemel, F. Lederer, S.G. Mayhew, F. Mueller, *Biochem. Soc. Trans.* **1996**, 116-121.

185. P. Macheroux, S. Ghisla, C. Sanner, H. Rueterjans, F. Mueller, *BMC Biochem.* **2005**, *6*, 26-36.

186. F.G. Bordwell, J-P. Cheng, A.V. Satish, C.L. Twyman, *J. Org. Chem.* **1992**, *57*, 6542-6546.

187. S. MacMillar, D. E. Edmondson, O. Matsson, *J. Am. Chem. Soc.* **2011**, *133*, 12319-12321.

188. Oral communication by D. E. Edmondson at 15th Amine Oxidase Congress 2012, Toulouse, France.

189. S. Umhau, L. Pollegioni, G. Molla, K. Diederichs, W. Welte, M. Pilone, S. Ghisla, *Proc. Natl. Acad. Sci. U. S. A.* **2000**, *97*, 2463-12468.

190. S. S. Erdem, B. Büyükmenekşe, *J. Neural Transm.* **2011**, *118*, 1021-1029.

191. R. Borštnar, M. Repič, M. Kržan, J. Mavri, R. Vianello, *Eur. J. Org. Chem.* **2011**, 6419-6433.

192. S. S. Erdem, O. Karahan, I. Yildiz, K. Yelekçi, *Org. Biomol. Chem.* **2006**, *4*, 646-658.

193. M. Bortolato, J. C. Shih, *Int. Rev. Neurobiol.* **2011**, *100*, 13-42.

194. M. Bortolato, K. Chen, J. C. Shih, *Adv. Drug Deliv. Rev.* **2008**, *60*, 1527-1533.

195. M. B. H. Youdim, D. E. Edmondson, K. F. Tipton, *Nat. Rev. Neurosci.* **2006**, *7*, 295-309.

196. M. C. Anderson, F. Hasan, J. M. McCrodden, K. F. Tipton, *Neurochem. Res.* **1993**, *18*, 1145-1149.

197. E. Klann, E. Thiels, *Prog. Neuropsychopharmacol. Biol. Psychiatry* **1999**, *23*, 359-376.

198. Jouvet, M. *Science* **1969**, *163*, 32-41.

199. a) P. J. O'Brien, A. G. Siraki, N. Shangari, *Crit. Rev. Toxicol.* **2005**, *35*, 609-662; b) L. Yang, K. Omori, J. Suzukawa, C. Inagaki, *Neurosci. Lett.* **2004**, *357*, 73-75; c) I. Lamensdorf, G. Eisenhofer, J. Harvey-White, A. Nechustan, K. Kirk, I. J. Kopin, *Brain Res.* **2000**, *868*, 191-201; d) B. J. Halliwell, *J. Neurochem.* **1992**, *59*, 1609-1623.

200. H. G. Brunner, M. Nelen, X. O, Breakefield, H. H. Ropers, B. A. van Oost, *Science* **1993**, *262*, 578-580.

201. a) R. McDermott, D. Tingley, J. Cowden, G. Frazetto, D. D. P. Johnson, *Proc. Natl. Acad. Sci. U. S. A.* **2009**, *106*, 2118-2123; b) N. Alia-Klein, R. Z. Goldstein, A. Kriplani, J. Logan, D. Tomasi, B. Williams, F. Telang, E. Shumay, A. Biegon, I. W. Craig, F. Henn, G. J. Wang, N. D. Volkow, J. S. Fowler, *J. Neurosci.* **2008**, *28*, 5099-5104.

202. a) A. L. Scott, M. Bortolato, K. Chen, J. C. Shih, *Neuroreport* **2008**, *19*, 739-743; b) O. Cases, I. Seif, J. Grimsby, P. Gaspar, K. Chen, S. Pournin, U. Muller, M. Aguet, C. Babinet, J. C. Shih, *Science* **1995**, *268*, 1763-1766.

203. M. Bortolato, K. Chen, S. C. Godar, G. Chen, W. Wu, I. Rebrin, M. R. Farrell, A. L. Scott, C. L. Wellman, J. C. Shih, *Neuropsychopharmacol.* **2011**, *36*, 2674-2688.

204. S. C. Godar, M. Bortolato, R. Frau, M. Dousti, K. Chen, J. C. Shih, *Int. J. Neuropsychopharmacol.* **2011**, *14*, 1195-1207.

205. a) V. V. Ruchkin, R. A. Koposov, B. af Klinteberg, L. Oreland, E. L. Grigorenko, *J. Abnorm. Psychol.* **2005**, *114*, 477-482; b) L. Oreland, *Neurotoxicology* **2004**, *25*, 79-89; c) J. S. Fowler, J. Logan, G. J. Wang, N. D. Volkow, F. Telang, W. Zhu, D. Franceschi, N. Pappas, R. Ferrieri, C. Shea, V. Garza, Y. Xu, D. Schlyer, S. J. Gatley, Y. S. Ding, D. Alexoff, D. Warner, N. Netusil, P. Carter, M. Jayne, P. King, P. Vaska, *Proc. Natl. Acad. Sci. U. S. A.* **2003**, *100*, 11600-11605; d) J. C. Fowler, L. von Knorring, L. Oreland, *Psychiatry Res.* **1980**, *3*, 273-279.

206. J. Grimsby, M. Toth, K. Chen, T. Kumazawa, L. Klaidman, J. D. Adams, F. Karoum, J. Gal, J. C. Shih, *Nat. Genet.* **1997**, *17*, 206-210.

207. M. Bortolato, S. C. Godar, S. Davarian, K. Chen, J. C. Shih, *Neuropsychopharmacol.* **2009**, *34*, 2746-2757.

208. M. Lee, K. Chen, J. C. Shih, N. Hiroi, *Genes Brain Behav.* **2004**, *3*, 216-227.

209. N. A. Garrick, D. L. Murphy, *Psychopharmacology (Berlin)* **1980**, *72*, 27-33.

210. A. Whibley, J. Urquhart, J. Dore, L. Willatt, G. Parkin, L. Gaunt, G. Black, D. Donnai, F. L. Raymond, *Eur. J. Hum. Genet.* **2010**, *18*, 1095-1099.

211. K. Chen, D. P. Holschneider, W. Wu, I. Rebrin, J. C. Shih, *J. Biol. Chem.* **2004**, *279*, 39645-39652.

212. R. E. O'Leary, J. C. Shih, K. Hyland, N. Kramer, Y. J. Tavyev Asher, J. M. Graham Jr., *Eur. J. Med. Genet.* **2012**, *55*, 349-353.

213. A. Maurel, C. Hernandez, O. Kunduzova, G. Bompart, C. Cambon, A. Parini, B. Frances, *Am. J. Physiol.* **2003**, *284*, H1460-H1467.

214. J. S. Fowler, J. Logan, N. D. Volkow, G. J. Wang, *J. Mol. Imaging Biol.* **2005**, *7*, 377-387.

215. a) N. Kaluderic, A. Carpi, R. Menabò, F. Di Lisa, N. Paolocci, *Biochim. Biophys. Acta* **2011**, *1813*, 1323-1332; b) P. Bianchi, O. Kunduzova, E. Masini, C. Cambon, D. Bani, L. Raimondi, M. H. Seguelas, S. Nistri, W. Colucci, N. Leducq, A. Parini, *Circulation* **2005**, *112*, 3297-3305.

216. J. K. Mallajosyula, D. Kaur, S. J.Chinta, S. Rajagopalan, A. Rane, D. G. Nicholls, D. A. Di Monte, H. Macarthur, J. K. Andersen, *PloS One* **2008**, *3*, e1616.

217. W. J. Burke, V. B. Kumar, N. Pandey, W. M. Panneton, Q. Gan, M. W. Franko, M. O'Dell, S. W. Li, Y. Pan, H. D. Chung, J. Galvin, *Acta Neuropathol.* **2008**, *115*, 193-203.

218. a) R. E. Heikkila, L. Manzino, F. S. Cabbat, R. C. Duvoisin, *Nature* **1984**, *311*, 467-469; b) K. Chiba, A. Trevor, N. Castagnoli Jr., *Biochem. Biophys. Res. Commun.* **1984**, *120*, 574-578.

219. D. M. Bosworth, J. W. Fielding, M. G. Acosta, L. M. Demarest, *J. Am. Med. Assoc.* **1955**, *157*, 132-136.

220. C. Binda, E. M. Milczek, D. Bonivento, J. Wang, A. Mattevi, D. E. Edmondson, *Curr. Top. Med. Chem.* **2011**, *11*, 2788-2796.

221. C. Binda, J. Wang, M. Li, F. Hubálek, A. Mattevi, D. E. Edmondson, *Biochemistry* **2008**, *47*, 5616-5625.

222. a) T. M. Polasek, D. J. Elliot, A. A. Somogyi, E. M. Gillam, B. C. Lewis, J. O. Miners, *Br. J. Clin. Pharmacol.* **2006**, *61*, 570-584. b) A. Holt, M. D. Berry, A. A. Boulton, *Neurotoxicology*, **2004**, *25*, 251-266.

223. a) W. Heydendael, L. Jacobson, *Brain Res.* **2008**, *1238*, 93-107; b) J. Vallejo, C. Gasto, R. Catalan, M. Salamero, *Br. J. Psychiatry* **1987**, *151*, 639-642.

224. H. Mirchandani, L. E. Reich *J. Forensic Sci.* **1985**, *30*, 217-220.

225. a) H. Frieling, S. Bleich, *Eur. Arch. Psychiatry Clin. Neurosci.* **2006**, *256*, 268-273; b) J. D. Amsterdam, N. J. Berwish, *Pharmacopsychiatry* **1989**, 22,21-25.

226. a) J. E. Oltman, S. Friedman, *Am. J. Psychiatry* **1963**, *120*, 493-494; b) J. C. Shee, *Br. Med. J.* **1964**, *1*, 1441.

227. J. Knoll, K. Magyar, *Adv. Biochem. Psychopharmacol.* **1972**, *5*, 393-408.

228. a) W. Z. Potter, D. L. Murphy, T. A. Wehr, M. Linnoila, F. K. Goodwin, *Arch. Gen. Psychiatry* **1982**, *39*, 505-510; b) D. Pickar, D. L. Murphy, R. M. Cohen, I. C. Campbell, S. Lipper, *Arch. Gen. Psychiatry* **1982**, *39*, 535-540.

229. Parkinson Study Group, *Ann. Neurol.* **1996***, 39*, 29-36.

230. W. Birkmayer, P. Riederer, M. B. H. Youdim, W. Linauer, *J. Neural Transm.* **1975**, *36*, 303-326.

231. E. H. Tobe, *J. Am. Osteopath. Assoc.* **2008**, *108*, 85-86.

232. J. P. Finberg, M. Tenne, M. B. Youdim, *Br. J. Pharmacol.* **1981**, *73*, 65-74.

233. a) F. Blandini, *CNS Drug. Rev.* **2005**, *11*, 183-194; b) O. Rascol, D. J. Brooks, E. Melamed, W. Oertel, W. Poewe, F. Stocchi, E. Tolosa, *Lancet* **2005**, *365*, 947-954; c)

J. M. Rabey, I. Sagi, M. Huberman, E. Melamed, A. Korczyn, N. Giladi, R. Inzelberg, R. Djaldetti, C. Klein, G. Berecz, *Clin. Neuropharmacol.* **2000**, *23*, 324-330.

234. C. Binda, M. Li, Y. Herzig, J. Sterling, D. E. Edmondson, A. Mattevi, *J. Med. Chem.* **2004**, *47,* 1767-1774.

235. a) M. B. Youdim, M. Weinstock, *Neurotoxicology* **2004**, *25*, 243-250; b) U. Bonnet, *CNS. Drug. Rev.* **2003**, *9*, 97-140; c) W. Haefely, W. P. Burkard, A. M. Cesura, R. Kettler, H. P. Lorez, J. R. Martin, J. G. Richards, R. Scherschlicht, M. Da Prada, *Psychopharmacology (Berlin)* **1992**, *106* (Suppl), S6-S14.

236. J. R. Davidson, *Acta Psychiatr. Scand.* **2003**, *417* (Suppl), 65-71.

237. a) P. A. LeWitt, D. C. Taylor, *Neurotherapeutics* **2008**, *5,* 210-225; b) R. P. Mason, E. G. Olmstead, R. F. Jacob, *Biochem. Pharmacol.* **2000**, *60*, 709-716.

238. R. G. Fariello, *Neurotherapeutics* **2007**, *4*, 110-116; b) C. Caccia, R. Maj, M. Calabresi, S. Maestroni, L. Faravelli, L. Curatolo, P. Salvati, R. G. Fariello, *Neurology* **2006**, *67*, S18-S23.

239. M. Murata, *DrugsToday* **2010**, *46*, 251- 258.

240. a) S. Mandel, O. Weinreb, T. Amit, M. B. Youdim, *Brain. Res. Rev.* **2005**, *48*, 379-387; b) Y. Sagi, N. Drigues, M. B. H. Youdim, *Br. J. Pharmacol.* **2005**, *146*, 553-560.

241. I. Bolea, J. Juarez-Jimenez, C. de los Rios, M. Chioua, R. Pouplana, F. J. Luque, M. Unzeta, J. Marco-Contelles, A. Samadi, *J. Med. Chem.* **2011**, *54*, 8251-8270.

242. a) H. Zheng, S. Gal, M. Fridkin, R. L. Weiner, M. B. H. Youdim, *J. Neurochem.* **2005**, 95, 68-78; b) S. Gal, H. Zheng, M. Fridkin, M. B. H. Youdim, *J. Neurochem.* **2005**, *95*, 79-88.

243. a) D. van den Berg, K. R. Zoellner, M. O. Ogunrombi, S. F. Malan, G. Terre'Blanche, N. Castagnoli Jr., J. J. Bergh, J. P. Petzer, *Bioorg. Med. Chem.* **2007**, *15*, 3692-3702; b) F. Hubálek, C. Binda, M. Li, A. Mattevi, D. E. Edmondson, D. E. *Acta Crystallogr. Sect. D* **2003***, 59,* 1874-1876.

244. T. Herraiz, C. Chaparro, *Life Sci.* **2006**, *78*, 795-802.

245. a) W. T. Harkcom, D. R. Bevan, *Biochem. Biophys. Res. Commun.* **2007**, *360*, 401-406; b) F. Chimenti, A. Bolasco, F. Manna, D. Secci, P. Chimenti, A. Granese, O. Befani, P. Turini, R. Cirilli, F. La Torre, S. Alcaro, F. Ortuso, T. Langer, *Curr. Med. Chem.* **2006,** *13,* 1411-1428; c) M Toprakçi, K. Yelekçi, *Bioorg. Med. Chem. Lett.* **2005**, *15*, 4438-4446.

246. a) A. Carotti, M. Catto, F. Leonetti, F. Campagna, R. Soto-Otero, E. Mendez-Alvarez, U. Thull, B. Testa, C. Altomare, *J. Med. Chem.* **2007,** *50,* 5364-5371; b) F. Leonetti, C. Capaldi, L. Pisani, O. Nicolotti, G.Muncipinto, A. Stefanachi, S. Cellamare, C. Caccia, A. Carotti, *J. Med. Chem.* **2007,** *50,* 4909-4916; c) R. Silvestri, G. La Regina, G. De Martino, M. Artico, O. Befani, M. Palumbo, E. Agostinelli, P. Turini, *J. Med. Chem.* **2003,** *46,* 917-920.

247. H. Kubota, A. Kakefuda, T. Watanabe, N. Ishii, K. Wada, N. Masuda, S. Sakamoto, S. Tsukamoto, *J. Med. Chem.* **2003**, *46*, 4728-4740.

248. E. Reinholz, A. Becker, B. Hagenbruch, S. Schaefer, A. Schmitt, *Synthesis* **1990**, 1069-1071.

249. T. Bosanac, C. S. Wilcox, *Org. Lett.* **2004**, *6*, 2321-2324.

250. M. D. Yilmaz, O. A. Bozdemir, E. U. Akkaya, *Org. Lett.* **2006**, *8*, 2871-2873.

251. C. Wang, D. Zhang, D. Zhu, *Langmuir* **2007**, *23*, 1478-1482.

252. Practical course of Organic Chemistry, Skriptum, TU Graz

253. G.-J. M. Gruter, O. S. Akkerman, F. Bickelhaupt, *J. Org. Chem.* **1994**, *59*, 4473-4481.

254. V. Aucagne, K. D. Haenni, D. A. Leigh, P. J. Lusby, D. B. Walker, *J. Am. Soc. Chem.* **2006**, *128*, 2186-2187.

255. A. Wissner, M. L. Carroll, K. E. Green, S. S. Kerwar, W. C. Pickett, R. E. Schaub, L. W. Torley, S. Wrenn, C. A. Kohler, *J. Med. Chem.* **1992**,*35*, 1660-1662.

256. R. Appel, *Angew. Chem. Int. Ed.* **1975**, *14*, 801-811.

257. A. F. Abdel-Magid, S. J. Mehrman, *Org. Process Res. Dev.* **2006**, *10*, 971-1031.

258. A. F. Abdel-Magid, K. G. Carson, B. D. Harris, C. A. Maryanoff, R. D. Shah, *J. Org. Chem.* **1996**, *61*, 3849-3862.

259. G. W. Gribble, *Org. Process Res. Dev.* **2006**, *10*, 1062-1075.

260. R. F. Borch, M. D. Bernstein, H. Dupont Durst, *J. Am. Chem. Soc.* **1971**, *93*, 2897-2904.

261. C. F. Lane, *Synthesis*, **1975**, 135-146.

262. J. F. Mcelroy, R. J. Chorvat (JENRIN Discovery), WO 2008/092091 A2, **2008**.

263. J. Sterling, B. Sklarz, Y. Herzig, D. Lerner, E. Falb, H. Ovadia (TEVA Pharmaceuticals USA Inc.), WO 2006/014968 A2, **2006**.

264. K. C. Kumara Swamy, N. N. Bhuvan Kumar, E. Balaraman, K. V. P. Pavan Kumar, *Chem. Rev.* **2009**, *109*, 2551-2651.

265. O. Mitsunobu, *Synthesis* **1981**, 1-28.

266. D. A. Annis, O. Helluin, E. N. Jacobsen, *Angew. Chem. Int. Ed.* **1998**, *37*, 1907-1909.

267. D. Crich, H. Dyker, R. J. Harris, *J. Org. Chem.* **1989**, *54*, 257-259.

268. J. P. Parikh, W. E. Doering, *J. Am. Chem. Soc.* **1967**, *89*, 5505-5507.

269. T. T. Tidwell, *Synthesis* **1990**, 857-870.

270. a) T. Sunazuka, N.Tabata, T. Nagamitsu, H. Tomoda, S. Omura, A. B. Smith III, *Tetrahedron Lett.* **1993**, *34*, 6659-6660; b) T. Sunazuka, T. Hirose, T. Zhi-Ming, R. Uchida, K. Shiomi, Y. Harigaya, S. Omura, *J. Antib.* **1997**, *50*, 453-455.

271. S. D. Lepore, Y. He, *J. Org. Chem.* **2003**, *68*, 8261-8263.

272. D. A. Averill-Bates, E. Agostinelli, E. Przybytkowski, M. A. Mateescu, B. Mondovi, *Arch. Biochem. Biophys.* **1993**, *300*, 75-79.

273. M. J. Krueger, T. P. Singer, *Anal. Biochem.* **1993**, *214*, 116-123.

274. R. Stevanato, F. Vianello, A. Rogo, *Arch. Biochem. Biophys.* **1995**, *324*, 374-378.

275. Z. Yan, G. W. Caldwell, B. Zhao, A. B. Reitz, *Rapid Commun. Mass Spectrom.* **2004,** *18*, 834-840.

276. a) G. Tufvesson, *Scand. J. Clin. Lab. Invest.* **1969**, *23*, 71-77; b) G. Tufvesson, *Scand. J. Clin. Lab. Invest.* **1970**, *25*, 231-235.

277. G. A. Lyles, B. A. Callingham, A. *Biochem. Pharmacol.* **1982**, *31*, 1417-1424.

278. M. E. May, *J. Neurochem.* **1989**, *35*, 1453-1454.

279. H. Weissbach, T. E. Smith, J. W. Daly, B. Witkop, S. Udenfriend, *J. Biol. Chem.* **1960**, *245*, 1160-1163.

280. C. M. McEwen Jr, J. D. Cohen, *J. Lab Clin. Med.* **1963**, *62*, 766-776.

281. O. Suzuki, E. Noguchi, K. Yagi, *J. Biochem.* **1976**, 1297-1299.

282. T. Matsumoto, O. Suzuki, T. Furuta, M. Asai, Y. Kurokawa, Y. Nimura, Y. Katsumata, I. Takahashi, *Clin. Biochem.* **1985**, *18*, 126-129.

283. J. P. Zhou, B. Zhong, R. B. Silverman, *Anal. Biochem.* **1996**, *234*, 9-12.

284. A. Szutowicz, R. D. Kobes, P. J. Orsulak, *Anal. Biochem.* **1984**, *138*, 86-94.

285. L. Morpurgo, E. Agostinelli, J. Muccigrosso, F. Martini, B. L. Mondovi, L. Avigliano, *Biochem. J.* **1989**, *260,* 19-25.

286. A. Holt, D. F. Sharman, G. B. Baker, M. M. Palcic, *Anal. Biochem.* **1997**, *244*, 384-392.

287. A. Holt, M. M. Palcic, *Nat. Protocols* **2006**, *1*, 2498-2505.

288. M. Zhou, N. Panchuk-Voloshina, *Anal. Biochem.* **1997**, *253*, 169-174.

289. M. P. Valley, W. Zhou, E. M. Hawkin, J. Shultz, J. J. Cali, T. Worzella, L. Bernad, T. Good, D. Good, T. L. Riss, D. K. Klaubert, K. V. Wood, *Anal. Biochem.* **2006**, *359*, 238-246.

290. W. Zhou, M. P. Valley, J. Shultz, E. M. Hawkins, L. Bernad, T. Good, D. Good, T. L. Riss, D. H. Klaubert, K. V. Wood, *J. Am. Chem. Soc.* **2006**, *128*, 3122-3123.

291. M. Li, M. Aldeco, D. E. Edmondson, Amplex Red peroxidase coupled assay, **2004**.

292. N. Johnsson, K. Johnsson, *ACS Chem. Biol.* **2007**, *2*, 31-38.

293. L. D. Lavis, R. T. Raines, *ACS Chem. Biol.* **2008**, *3*, 142-155.

294. L. M. Wysocki, L. D. Lavis, *Curr. Opin.Chem. Biol.* **2011**, *15*, 752-759.

295. P. B. Ghosh, M. W. Whitehouse, *Biochem. J.* **1968**, *108*, 155-156.

296. O. V. Oskolkova, R. Saf, E. Zenzmaier, A. Hermetter, *Chem. Phys. Lipids* **2003**, *125*, 103-114.

297. R. Birner-Gruenberger, H. Susani-Etzerodt, M. Kollroser, G. N. Rechberger, A. Hermetter, *Proteomics* **2008**, *8*, 3645-3656.

298. B. Ludolph, H. Waldmann, *Chem. Eur. J.* **2003**, *9*, 3683-3691.

299. K. Majjigapu, J. R. R. Majjigapu, A. G. Kutateladze, *Angew. Chem. Int. Ed.* **2007**, *46*, 6137-6140.

300. M. Tojino, Y. Uenoyama, T. Fukuyama, I. Ryu, *Chem. Commun.* **2004**, 2482-2483.

301. a) B. Carboni, A. Benalil, M. Vaultier, *J. Org. Chem.* **1993**, *58*, 3736-3741; b) A. J. Lampkins, E. J. O'Neil, B. D. Smith, *J. Org. Chem.* **2008**, *73*, 6053-6058.

302. R. D. Damoiseaux, J. L. Harris (IRM LLC), WO 2005/007678 A2, **2005**.

303. D. H. Singleton, H. Boyd, J. V. Steidl-Nichols, M. Deacon, M. J. de Groot, D. Price, D. O. Nettleton, N. K. Wallace, M. D. Troutman, C. Williams, J. G. Boyd, *J. Med. Chem.* **2007**, *50*, 2931-2941.

304. M. H. Lyttle, T. G. Carter, D. J. Dick, R. M. Cook, *J. Org. Chem.* **2000**, *65*, 9033-9038.

305. M. V. Kvach, I. A. Stepanova, I. A. Prokhorenko, A. P. Stupak, D. A. Bolibrukh, V. A. Korshun, V. V. Shmanai, *Bioconjugate Chem.* **2009,** *20,* 1673-1682.

306. M. Yokoyama, S. Yoshida, T. Imamoto, *Synthesis*, **1982**, 591-592.

307. Protocol from Dr. Ute Stemmer, Institute of Biochemistry, Graz University of Technology, **2009**.

308. a) A. Winkler, F. Hartner, T. M. Kutchan, A. Glieder, P. Macheroux, *J. Biol. Chem.* **2006**, *281*, 21276-21285; b) A. Winkler, M. Puhl, H. Weber, T. M. Kutchan, K. Gruber, P.Macheroux, *Phytochemistry* **2009**, *70*, 1092-1097.

309. S. Sollner, R. Nebauer, H. Ehammer, A. Prem, S. Deller, B. A. Palfey, G. Daum, P. Macheroux, *FEBS J.* **2007**, *274*, 1328-1339.

310. Y. S. Li, J. Y. Ho, C. C. Huang, S. Y. Lyu, C. Y. Lee, Y. T. Huang, C. J. Wu, H. C. Chan, C. J.Huang, N. S. Hsu, M. D. Tsai, T. L. Li, *J. Am. Chem. Soc.* **2007**, *129*, 13384-13385.

311. A. Morokutti, A. Lyskowski, S. Sollner, E. Pointner, T. B. Fitzpatrick,C. Kratky, K. Gruber, P. Macheroux, *Biochemistry* **2005,** *44,* 13724-13733.

312. J. Eirich, J. L. Burkhart, A. Ullrich, A. Vollmar, S. Zahler, U. Kazmaier, S. A. Sieber, *Mol Biosyst.* **2012**, *8*, 2067-2075.

313. J. C. Kauer, S. Erickson-Viitanen, H. R. Wolfe Jr, W. F. DeGrado, *J. Biol. Chem.* **1986**, *261*, 10695-10700.

314. M. H. Kim, D. V. Patel, *Tetrahedron Lett.* **1994**, *35*, 56403-5606.

315. B. Castro, G. Evin, C. Selve, R. Seyer, *Synthesis* **1977**, 413.

316. P. G. M. Wuts, T. W. Greene, *Greene's Protective Groups in Organic Synthesis*, 4th Ed., J. Wiley & Sons, **2006**, pp.712-713.

317. J. E. Sheppeck II, H.Kar, H. Hong, *Tetrahedron Lett.* **2000**, *41*, 5329-5333.

318. B. Jagadish, R. Sankaranarayanan, L. Xu, R. Richards, J. Vagner, V. J. Hruby, R. J. Gillies, E. A. Masha, *Bioorg. Med. Chem. Lett.* **2007**, *17*, 3310-3313.

319. Isabelle Staub, PhD Dissertation, Technische Universität München, **2010**.

320. B. P. Lucey, W. A. Nelson-Rees, G. M. Hutchins, *Arch. Pathol. Lab. Med.* **2009**, *133*, 1463-1467.

321. W. F. Scherer, J. T. Syverton, G. O. Gey, *J. Exp. Med.* **1953**, *97*, 695-710.

322. J. R. Masters, *Nat. Rev. Cancer* **2002**, *2*, 315-319.

323. T. F. Slater, B. Sawyer, U. Straeuli, *Biochim. Biophys. Acta* **1963**, *77*, 383-393.

324. M. C. Alley, D. A. Scudiero, A. Monks, M. L. Hursey, M. J. Czerwinski, D. L. Fine, B. J. Abbott, J. G. Mayo, R. H. Shoemaker, M. R. Boyd, *Cancer Res.* **1988**, *48*, 589-601.

325. B. Ekstedt, K. Magyar, J. Knoll, *Biochem. Pharmacol.* **1979**, *28*, 919-923.

326. a) T. Nakano, T. Nagatsu, H. Higashida, *J. Neurochem.* **1985**, *44*, 755-758; b) M. Hawkins Jr., X. O. Breakefield, *J. Neurochem.* **1978**, *30*, 1391-1397.

327. J. S. Fowler, R. R. MacGregor, A. P. Wolf, C. D. Arnett, S. L. Dewey, D. Schlyer, D. Christman, J. Logan, M. Smith, H. Sachs, *Science* **1987**, *235*, 481-485.

328. a) X. Parés, J. Farrés, N. Kedishvili, G. Duesterc, *Cell Mol. Life Sci.* **2008**, *65*, 3936-3949; b) G. Duester, *Eur. J. Biochem.* **2000**, *267*, 4315-4324.

329. D. J. Moffa, F. J. Lotspeich, R. F. Krause, *J. Biol. Chem.* **1970**, *245*, 439-447.

330. N. E. Sladek, *J. Biochem. Mol. Toxicol.* **2003**, *17*, 7-23.

331. J. S. Moreb, A. Gabr, G. R. Vartikar, S. Gowda, J. R. Zucali, D. J. Mohuczy, *J. Pharmacol. Exp. Ther.* **2005**, *312*, 339-345.

332. S. A. Marchitti, R. A. Deitrich, V. Vasiliou, *Pharmacol. Rev.* **2007**, *59*, 125-150.

333. A. K. Upadhyay, D. E. Edmondson, *Biochemistry* **2009**, *48*, 3928-3935.

334. M. Tramontini, L. Angiolini, *Tetrahedron* **1990**, *46*, 1791-1837.

335. B. Karlén, B. Lindeke, S. Lindgren, K.-G. Svensson, R. Dahlbom, *J. Med. Chem.* **1970**, *13*, 651-657.

336. C. A. Brown, A. Yamashita, *J. Am. Chem. Soc.* **1975**, *97*, 891-892.

337. a) C. H. Heathcock, J. C. Kath, R. B. Ruggeri, *J. Org. Chem.* **1995**, *60*, 1120-130; b) J. Cossy, D. Belotti, J.-P. Pete, *Tetrahedron* **1990**, *46*, 185-1870.

338. a) J. Blanchet, M. Bonin, L. Micouin, H. P. Husson, *Eur. J. Org. Chem.* **2002**, 2598-2602; b) W. Fitz, D. Arigoni, *J. Chem. Soc.*, *Chem. Commun.* **1992**, 1533-1534.

339. S. A. Weerawarna, R. A. Jewell (Weyerhauser Company Federal Way), EP1457491A1, **2004**.

340. L. Schafzahl, Bachelor thesis, Graz University of Technology, **2012**.

341. B. L. Chen, B. Wang, G. Q. Lin, *J. Org. Chem.* **2010**, *75*, 941-944.

342. M. G. Stanton, J. Hubbs, D, Sloman, C. Hamblett, P. Andrade, M. Angagaw, G. Bi, R. M. Black, J. Crispino, J. C. Cruz, E. Fan, G. Farris, B. L. Hughes, C. M. Kenific, R. E. Middleton, G. Nikov, P. Sajonz, S. Shah, N. Shomer, A. A. Szewczak, F. Tanga, M. T. Tudge, M. Shearman, B. Munoz, *Bioorg. Med. Chem. Lett.* **2010**, *20*, 755-758.

343. R. Mozingo, *Org. Synth.*, Coll. Vol. 3, **1955**, 181.

344. C. C. Chang, K. O. Siegenthaler, A. Studer, *Helv. Chim. Acta* **2006**, *89*, 2200-2210.

345. a) J. C. Gilbert, U. Weerasooriya, *J. Org. Chem.* **1982**, *47*, 1837-1845; b) D. G. Brown, E. J. Velthuisen, J. R. Commerford, R. G. Brisbois, T. H. Hoye, *J. Org. Chem.* **1996**, *61*, 2540-2541.

346. a) S. Müller, B. Liepold, G. Roth, H. J. Bestmann, *Synlett* **1996**, *6*, 521-522; b) G. J. Roth, B. Liepold, S. G. Müller, H. J. Bestmann, *Synthesis* **2004**, 1, 59-62.

347. M. Tanaka, K. Yagi (Toray Industries, Inc.), US4386127, **1983**.

348. K. Omura, D. Swern, *Tetrahedron* **1978**, *34*, 1651-1660.

349. M. Uhlén, P. Oksvold, L. Fagerberg, E. Lundberg, K. Jonasson, M. Forsberg, M. Zwahlen, C. Kampf, K. Wester, S. Hober, H. Wernérus, L. Björling, F. Pontén, *Nat. Biotechnol.* **2010**, *28*, 1248-1250.

350. F. Pontén, M. Gry, L. Fagerberg, E. Lundberg, A. Asplund, L. Berglund, P. Oksvold, E. Björling, S. Hober, C. Kampf, S. Navani, P. Nilsson, J. Ottosson, A. Persson, H. Wernérus, K. Wester, M. Uhlén, *Mol. Syst. Biol.* **2009**, *5*, 337.

351. Human Protein Atlas - http://proteinatlas.org

352. R. Luxenhofer, R. Jordan, *Macromolecules* **2006**, *39*, 3509-3516.

353. a) Y. Ohmomo, M. Hirata, K. Murakami, Y. Magata, C. Tanaka, A. Yokoyama, *Pharm. Soc. Jap.* **1991**, *39*, 1038-40; b) R. R. MacGregor, J. S. Fowler, A. P. Wolf, *J. Labelled Compd. Radiopharm.* **1988**, *25*, 1-9.

9 Abbreviations list

A	Ampere
aa	amino acid
ABC	ammonium bicarbonate / ammonium hydrocarbonate
ABPP	Activity-Based Protein Profiling
ABP	activity-based probe
A*f*BP	affinity-based probe
Aca	aminocaproic
AD	Alzheimer's disease
ALDH1 A1	aldehyde dehydrogenase 1
ASPP	active site peptide profiling
APS	ammonium peroxide sulphate
ATCC	American Type Culture Collection
ATR	attenuated total reflectance
BCA	bicinchoninic acid
BODIPY	boron-dipyrromethene
BSA	bovine serum albumin
Bpa	benzoylphenylalanine
Bz	benzoyl
CAM	cerium ammonium molybdate
CC	click chemistry
CES 1	carboxylesterase 1
CGH	comparative genomic hybridization
CoA	coenzyme A
Cy	cyanine (polymethine)
Cys (C)	cysteine
DA	Diels-Alder
DBU	diazabicyclo[5.4.0]undec-7-ene

DCE	1,2-dichloroethane
DCM	dichloromethane
DMSO	dimethyl sufoxide
DI	direct inlet
DIAD	diisopropyl azodicarboxylate
DIC	*N,N'*-diisopropylcarbodiimide
DIEA	*N,N'*-diisopropylethylamine
DIFP	diisopropyl fluorophosphate
DMF	*N,N*-dimethylformamide
DMEM	Dulbecco's Modified Eagle Medium
DNS	dansyl, 5-dimethylaminonaphthalene-1-sulfonamide
DTT	dithiothreitol
EDC	*N*-(3-dimethylaminopropyl)-*N'*-ethylcarbodiimide
e.g.	lat. *exempli gratia* (for example)
EI	electron impact
EPR-DEER	electron paramagnetic resonance-double electron–electron resonance
ESI	electrospray ionization
et al.	lat. *et alli* (and the others)
etc.	lat. *et cetera* (and the others)
FA	formic acid
FAD	flavin adenine dinucleotide
FCS	fetal calf serum
fluopol ABPP	fluorescence polarization ABPP
Fmoc	fluorenylmethyloxycarbonyl
FMN	flavin mononucleotide
FP	fluorophosphonate
FS	fluorescence scanning
g	relative centrifugal force
GBA	glucocerebrosidase

GBM	glioblastoma multiforme
GC	gas chromatography
GOOX	glucooligosaccharide oxidase
GSTO-1	glutathione S-transferase omega 1
h	hour(s)
i.e.	lat. *id est* (that is)
isoTOP-ABPP	isotopic tandem orthogonal proteolysis ABPP
HATU	O-(7-Azabenzotriazol-1-yl)-*N,N,N,N*-tetramethyl uronium hexafluorophosphate
HCV	Hepatitis C virus
HDAC	histone deacetylase
hMAO A	human MAO A
hMAO B	human MAO B
HOAt	*N*-Hydroxy-7-azabenzotriazole
HOBt	*N*-Hydroxy-1,2,3-benzotriazole
HPLC	high performance liquid chromatography
HRP	horse radish peroxidase
HRMS	high resolution mass spectrometry
IAA	iodoacetamide
ICAT	isotope-coded affinity tag
ICLC	Interlab Cell Lines Collection
Ile (I)	isoleucine
KIE	kinetic isotope effect
LAAO	L-amino acid oxidase
LAH	lithium aluminium hydride
LC	liquid chromatography
LSD 1	lysine specific demethylase 1
Lys (K)	lysine
MALDI	matrix assisted laser desorption ionization

MAO	monoamine oxidase
MCF7	breast cancer cell line
MeOH	methanol
MeCN	acetonitrile
min	minute(s)
MOM	mitochondrial outer membrane
MPTP	1-methyl-4-phenyl-1,2,3,6-tetrahydropyridine
MPP$^+$	1-methyl-4-phenylpyridine
MS	mass spectrometry
MTT	3-(4,5-dimethylthiazol-2-yl)-2,5-diphenyltetrazolium bromide, Thiazolyl Blue Tetrazoliumbromide
MudPIT	multidimensional protein identification technology
m/z	mass to charge ratio
NBD	7-nitrobenzo-2,1,3-oxadiazole/ 4-chloro-7-nitrobenzofurazan
NBS	*N*-bromosuccinimide
NHS	*N*-hydroxysuccinimide
NGP	neutrophilic granule protein
PAD4	protein arginine deiminase 4
PAO	polyamine oxidase
PBS	phosphate buffered saline
PD	Parkinson's disease
PDB	Protein Data Bank
PET	positron electron tomography
Ph	phenyl
PHBH	p-hydroxybenzoate hydroxylase
Phe	phenylalanine
PME-1	protein phosphatase methylesterase 1
PPSE	trimethylsilylpolyphosphate
PRMT-1	protein arginine methyltransferase 1

PSM	peptide spectrum match
PTM	post-translational modification
PTP	protein tyrosine phosphatase
PyBOP	benzotriazol-1-yl-oxytripyrrolidinophosphonium hexafluorophosphate
qABP	fluorescently quenched activity-based probe
QSAR	quantitative structure-activity relationship
RBBP9	retinoblastoma-binding protein 9
Rh	rhodamine
rMAO A/B	rat MAO A/B
RNA	ribonucleic acid
ROS	reactive oxygen species
rpm	revolutions per minute
RPMI	Roswell Park Memorial Institute
RT	room temperature
SAR	structure-activity relationship
SDS-PAGE	sodium dodecyl polyacrylamide electrophoresis
Ser (S)	serine
SET	single electron transfer
SILAC	stable isotope labeling of amino acids in cell culture
siRNA	small interfering RNA (ribonucleic acid)
SOX	sulfhydryl oxidases
SSRI	selective-serotonin re-uptake inhibitors
STABH	sodium triacetoxyborohydride
Su	succinimide
TAMRA	carboxytetramethylrhodamine
TEMED	*N,N,N',N'*-tetramethylethylendiamine
TBTA	tris[(1-benzyl-1*H*-1,2,3-triazol-4-yl)methyl] amine
TBS	tris buffered saline
TCA	trichloroacetic acid

TCEP	tris(2-carboxyethyl)phosphine
TEV	*Tobacco etch virus*
TLC	thin layer chromatography
TOF	time-of-flight
TOP	tandem orthogonal proteolysis
THF	tetrahydrofuran
Tyr (Y)	tyrosine
UV	ultraviolet (light)
V	Volt
VAO	vanillyl alcohol oxidase
VS	vinyl sulfones
v	wavenumber
v/v	volume per volume
VIS	visible (light)
W	watt
WT	wild type
w/v	weight per volume
w/w	weight per weight

10 Appendix

10.1 Bibliographic data

This work contains 314 pages, 90 figures, 32 schemes, 5 tables, 353 references.

10.2 CV

Resume of Joanna Krysiak, M. Sc., born in Poland, 31.05.1983

Education and research experience:

2008-2012	PhD studies within PhD program DK _Molecular Enzymology_ at Graz University of Technology with Prof. Rolf Breinbauer
01-07. 2011	Research stay with Prof. Stephan Sieber, Technische Universität München, Garching, Germany
10. 2002-03. 2008	Undergraduate education from Warsaw University of Technology, Faculty of Chemistry, Warsaw, Poland, master thesis with Prof. Jan Plenkiewicz
03-07. 2007	Erasmus research project at Twente University, Faculty of Science and Technology, Enschede, The Netherlands, with Dr. Albert Ruggi and Dr. Aldrik Velders
09. 2006	Research internship at the Institute of Biophysics and Biochemistry, Polish Academy of Sciences, Department of Lipid Biochemistry, Warsaw, Poland, with Prof. Ewa Kula-Świeżewska
03. 2004-12. 2005	Research internship at the Institute of Organic Chemistry, Polish Academy of Sciences, Warsaw, Poland, with Prof. Ryszard Ostaszewski

Conferences:

09.2012 EMBO Conference Series 'Chemical Biology 2012', Heidelberg, Germany (poster presentation) (awarded by EMBO conference fee fellowship)

07.2012 15th Amine Oxidase Congress AOC2012, Toulouse, France (oral presentation)

07.2012 3rd European Chemical Biology Symposium ECBS2012, Vienna, Austria (poster presentation)

06. 2012 ISACS 7 "Challenges in Organic Chemistry and Chemical Biology", Edinburgh, UK (poster presentation) (awarded by RSC bursary)

03. 2012 4th International Graz Symposium on Lipid and Membrane Biology, Graz, Austria

09. 2011 CIPSM - Fest of Biological Chemistry 2011, Munich, Germany

07. 2011 ISACS 5 "Challenges in Chemical Biology", Manchester, UK (poster presentation)

10. 2010 YoungChem 2010, International Congress of Young Chemists, Reda, Poland (oral and poster presentation)

06. 2010 60th Nobel Laureate Meeting, 3rd Interdisciplinary Nobel Laureate Meeting, Lindau and Isle of Mainau, Germany

Awards:

2012 EMBO conference fellowship

2012 RSC travel grant for ISACS7 conference

2010 Best oral presentation prize at YoungChem 2010, International Congress of Young Chemists, Reda, Poland

10.3 Publications list

1. J. M. Krysiak, J. Kreuzer, P. Macheroux, A. Hermetter, S. A. Sieber, R. Breinbauer, Activity-based probes for studying the activity of flavin-dependent oxidases and for the protein target profiling of monoamine oxidase inhibitors. *Angew. Chem. Int. Ed.* **2012**, *51*, 7035-7040. doi: 10.1002/anie.201201955

2. J. Krysiak, R. Breinbauer, Activity-Based Protein Profiling for Natural Product Target Discovery. *Top. Curr. Chem.* **2012**, *324*, 43-84. doi: 10.1007/128_2011_289

3. D. Koszelewski, W. Szymanski, J. Krysiak, R. Ostaszewski, Solvent-Free Passerini Reactions. *Synth. Commun.* **2008**, *38*, 1120-1127. doi: 10.1080/00397910701863608